DE GRUYTER

Juan H. Vera,
Grazyna Wilczek-Vera (Eds.)

IONIC SURFACTANTS AND AQUEOUS SOLUTIONS

BIOMOLECULES, METALS AND NANOPARTICLES

Ionic Surfactants and Aqueous Solutions

Also of interest

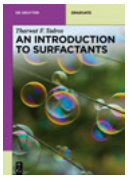

An Introduction to Surfactants.
Tadros, 2014
ISBN 978-3-11-031212-6,
e-ISBN 978-3-11-031213-3

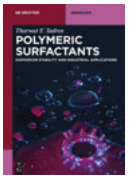

Polymeric Surfactants.
Dispersion Stability and Industrial Applications
Tadros, 2017
ISBN 978–3-11–048722-0,
e-ISBN 978–3-11–048728-2

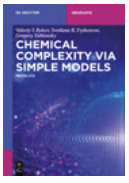

Chemical Complexity via Simple Models.
MODELICS
Bykov, Tsybenova, Yablonsky, 2018
ISBN 978–3-11–046491-7,
e-ISBN 978–3-11–046494-8

Chemical Product Technology.
Murzin, 2018
ISBN 978–3-11–047531-9,
e-ISBN 978–3-11–047552-4

Ionic Surfactants and Aqueous Solutions

Biomolecules, Metals and Nanoparticles

Edited by
Juan H. Vera, Grazyna Wilczek-Vera

DE GRUYTER

Editors
Prof. Dr. Juan H. Vera
Professor Emeritus
Department of Chemical Engineering,
McGill University
Wong Building, 3610 Rue University #3060, Montréal, QC H3A 0C5
Canada
juan.vera@mcgill.ca

Dr. Grazyna Wilczek-Vera
Retired Faculty Lecturer
Department of Chemistry
McGill University
801 Sherbrooke St W, Montreal, QC H3A 0B8
Canada
grazyna.wilczek@mcgill.ca

ISBN 978-3-11-056336-8
e-ISBN (PDF) 978-3-11-056480-8
e-ISBN (EPUB) 978-3-11-056375-7

Library of Congress Cataloging-in-Publication Data
Names: Vera, Juan H., 1936- editor. | Wilczek-Vera, Grazyna, 1952- editor.
Title: Ionic surfactants and aqueous solutions : biomolecules, metals, and nanoparticles.
Description: Berlin ; Boston : Walter de Gruyter, GmbH, 2018. | Edited by Juan H. Vera and Grazyna Wilczek-Vera. | Includes bibliographical references and index.
Identifiers: LCCN 2018012437| ISBN 9783110563368 (hardcover : alk. paper) | ISBN 9783110563757 (e-book (epub) : alk. paper) | ISBN 9783110564808 (e-book (pdf) : alk. paper)
Subjects: LCSH: Surface chemistry. | Surface active agents. | Ionic solutions. | Solution (Chemistry) | Chemistry, Inorganic. | Nanostructured materials.
Classification: LCC QD506 .I59 2018 | DDC 541/.3422–dc23 LC record available at https://lccn.loc.gov/2018012437

Bibliographic information published by the Deutsche Nationalbibliothek
The Deutsche Nationalbibliothek lists this publication in the Deutsche Nationalbibliografie; detailed bibliographic data are available on the Internet at http://dnb.dnb.de.

Typesetting: Integra Software Services Pvt. Ltd.
Printing and binding: CPI books GmbH, Leck
Cover image: Digital Vision. / Getty Images Plus

www.degruyter.com

In Memory of Professor Martin E. Weber
(August 4, 1937–November 24, 2008)

Preface

This book presents an overview of published research on aqueous systems and ionic surfactants, which started with the idea of using reverse micelles as separation agents. Reverse micelles are self-organizing structures in which surfactants can suspend considerable amount of water in an organic media by orienting their polar heads toward microdrops of water and their hydrocarbon tails toward the organic phase. When using ionic surfactants, the suspended aqueous phase has special properties that could be used to extract ions and biomolecules from a bulk aqueous phase. Two-tailed ionic surfactants were found to be particularly suitable for the formation of reverse micelles.

The organization of the presentation of material in this monograph does not necessarily follow the chronological order of the publication of results. An attempt is made to present a logical evolution of acquired knowledge in this field, independent of when, in the sequence of studies, the understanding of the matter was attained.

Thus, studies presented in Chapter 1 discuss the ways of forming reverse micelles as well as the potential of reverse micelles formed with ionic surfactants to serve as separation agents for ions or charged biomolecules diluted in aqueous solutions. The results obtained using a number of ionic surfactants are included in this chapter. The studies presented in Chapter 2 were oriented to gather information on the factors affecting the behavior of the microemulsions formed with ionic surfactants and to model the experimental results. In addition to the studies on reverse micelles, it was considered equally important to gain some understanding of the interactions between biomolecules and ions in aqueous solutions, and to gather and model data on the activity coefficients of the biomolecules in aqueous electrolyte solutions. Amino acids, which are the building blocks of peptides and proteins, were chosen for these studies. These two kinds of experimental studies are presented in Chapters 3 and 4, respectively. Chapter 5 discusses the modeling of the activity coefficients of biomolecules in aqueous electrolyte solutions. Studies of extraction of biomolecules from aqueous solutions using reverse micelles followed and are presented in Chapter 6.

Similar studies to extract heavy metals from aqueous solutions were initiated, and the breakthrough came when Dr Jamaladdin Esalah, a PhD student at the time, observed that the surfactants initially forming the reverse micelles in fact formed a solid phase with the metal ions. This solid phase accumulated in the interface of the organic and aqueous phases and could be directly removed. It was concluded that for the extraction of heavy metals from aqueous solutions there was no need to form reverse micelles; the ionic surfactant could be directly added to the aqueous phase containing metals in solution. Chapter 7 presents the results of studies in which the surfactant was directly added to the aqueous solution and removed the heavy metals. As the PhD thesis of Esalah took time to finish, his publications came after another faster study was finished and published, using the same basic idea. Thus, in

https://doi.org/10.1515/9783110564808-201

Chapter 7, complexation of lead using sodium caprate comes before the complexation of other metal ions with sodium phosphinate.

It did not take long to realize that a solid phase was also formed in the organic aqueous interface when using reverse micelles to extract biomolecules from aqueous solutions. Thus, it was clear that, instead of using reverse micelles, the same procedure of direct complexation with surfactants could also be used for the extraction of biomolecules. These studies are presented in Chapter 8.

As it occurred in the two situations described earlier, when attention is paid to details, serendipity is a powerful tool in research. It so happened that when an ionic surfactant was left in contact with a precipitate in an aqueous phase overnight, the next day it was found that the precipitate had vanished. Repeating the experiment under controlled conditions, it was clear that the ionic surfactant was taking one of the ions out of the solid phase and forming a water-soluble compound. This observation led to the idea of forming nanoparticles from macroscopic precipitates, which is described in Chapter 9.

After getting familiar with the potential uses of ionic surfactants, it was natural to think about their application as auxiliary media for nucleophilic sulfonation of organic halides, which involves an oil-soluble compound and a hydrophilic ionic reactant. Chapter 10 covers studies of sulfonation in microemulsions.

Finally, Chapter 11 presents the details and history of the two patents that were obtained, but not maintained, based on this work.

While the results of the studies included here have been in the literature for quite some time, it was thought that it was time to present an overview with additional information on the connections between them which was not available in the bits and pieces shown in the refereed publications. The authors of the different chapters of this book are the researchers who did the work and they have taken time of their present duties to brush up the material contained in their publications. An effort has been made to include up-to-date material published by other researchers on the topics included in this compilation. In each of the original publications, all authors had to agree in the text before their names could be included. In this compilation, the contributors are responsible for the text included under their name. As editors, we have just made sure that the format agrees with the requirements from the publisher and, in a minor way, offered suggestions for improvement.

All our efforts to contact two of the previous researchers, Dr Wayne Wang and Dr Jamaladdin Esalah failed, so the presentation of their work was taken by those with the closest research topic.

We decided to dedicate this compilation in the memory of Prof. Martin Edmund Weber, who was one of the main motors of the whole research program.

Grazyna Wilczek-Vera and Juan H. Vera
Montreal, March 2018

List of contributing authors

Dr. Remy Dumortier
Biopharmaceutical procurement and production expert
7 Chaucer Ct,
West Windsor, New Jersey, 08550
USA
rdumortier@hotmail.com

Dr. Maen M. Husein
Professor
Department of Chemical and Petroleum Engineering
Schulich School of Engineering
University of Calgary
2500 University Drive N.W.
Calgary, Alberta T2 N 1N4
Canada
mhusein@ucalgary.ca

Dr. Mohammad K. Khoshkbarchi
Process Ecology Inc.
Calgary, Alberta
Canada
khashayar_k@yahoo.com

Dr. Younok Dumortier Shin
Executive Pharmaceutical Professional
7 Chaucer Court, Princeton Junction, NJ 08550
USA
younok@hotmail.com

Dr. Ana Soto
Professor
Department of Chemical Engineering
Universidade de Santiago de Compostela
E-15782 Santiago de Compostela
Spain
ana.soto@usc.es

Dr. Hamid R. Rabie
President HMT Technologies Inc.
725 Queensway West
Mississauga, ON L5 C 1A7
Canada
hrabie@hmt-technologies.com

Dr. Eva Rodil
Associate Professor
Department of Chemical Engineering
Universidade de Santiago de Compostela
E-15782 Santiago de Compostela
Spain
eva.rodil@usc.es

Dr. Juan H. Vera
Professor Emeritus
Department of Chemical Engineering,
McGill University
Wong Building, 3610 Rue University #3060,
Montréal, QC H3A 0C5
Canada
juan.vera@mcgill.ca

Dr. Grazyna Wilczek
Retired Faculty Lecturer
Department of Chemistry
McGill University
801 Sherbrooke St W, Montreal, QC H3A 0B8
Canada
grazyna.wilczek@mcgill.ca

https://doi.org/10.1515/9783110564808-202

Contents

Abbreviations

AOT	sodium bis-(ethylhexyl) sulfo succinate
CMC	critical micelle concentration
CTAB	cetyl trimethylammonium bromide, hexadecyltrimethylammonium bromide
DODAB	dioctyldimethyl ammonium bromide
DODAC	dioctyldimethyl ammonium chloride
DODMAB	dimethyl dioctadecyl ammonium bromide
DODMAC	dimethyl dioctadecyl ammonium chloride
DOLPA	dioleyl phosphoric acid
ePC-SAFT	electrolyte perturbed-chain statistical association fluid theory
HD	dinonylnaphtalene sulfonic acid
HPLC	high-performance liquid chromatography
HSAB	hard and soft acids and bases
ICP-AES	inductively coupled plasma atomic emission spectroscopy
ISE	ion selective electrode
LLPTC	liquid–liquid phase transfer catalysis
MCC	minimum cosurfactant concentration
MESH	Medical Subject Heading
MSA	mean spherical approximation
NaPOO	Sodium bis(2,2,4-trimethylpenthyl) phosphinate
NaPSO	Sodium bis(2,2,4-trimethylpenthyl) monothiophosphinate
NaPSS	Sodium bis(2,2,4-trimethylpenthyl) dithiophosphinate
NP	nanoparticles
NRTL	non-random two-liquid
NRTL-NRF	NRTL non random factor
OTT	Office of Technology Transfer
OPA	o-phthaldialdehyde
PBE	Poisson–Boltzmann equation
PC-SAFT	Perturbed-Chain Statistical Associating Fluid Theory
p*I*	isoelectric point
PIE	pseudophase ion exchange
PS	pseudophase separation
SAFT	statistical associating fluid theory
SAFT-VR	statistical associating fluid theory for potentials of variable range
SLPTC	solid–liquid phase transfer catalysis
SPHS	simplified perturbed hard-sphere
TOMAC	trioctyl methyl ammonium chloride
TMPD	N,N,N',N'-tetramethyl-p-phenylenediamine

https://doi.org/10.1515/9783110564808-203

Juan H. Vera and Grazyna Wilczek-Vera

1 Exploratory Studies

1.1 Introduction

Ionic surfactants are amphiphilic compounds formed by one or more hydrocarbon chains attached to a polar group. In common jargon, the hydrocarbon chains are referred to as "tails" and the polar group is referred to as "head." In an anionic surfactant, the head group is negatively charged and has a cation as counterion. In a cationic surfactant, the head group is positively charged and has an anion as counterion. In aqueous solution, ionic surfactants can exchange the counterion. Figure 1.1(a) shows the chemical structure of the anionic surfactant sodium bis-2-(ethylhexyl) sulfosuccinate (commonly called aerosol OT or simply AOT). Figure 1.1(b) shows the chemical structure of the cationic surfactant dioctyldimethyl ammonium chloride, abbreviated in this work as DODAC.

Briefly stated, if an ionic surfactant is added to a two-phase liquid system of a nonpolar organic liquid in contact with water, the surfactant molecules go to the interface with their tails facing the upper organic liquid and their heads facing the water. At a certain concentration of surfactant, the interface is saturated with surfactant molecules and any excess of surfactant added migrates to aqueous phase with their heads facing the water and their tails forming micro-organic drops. These self-organizing structures are called *micelles* and the concentration of surfactant at which micelles appear is called the *critical micelle concentration* (CMC). Addition of an electrolyte to the aqueous phase will cause the surfactant molecules to migrate to the organic phase, but this time with their tails out, facing the organic liquid, and their heads facing small droplets of water. These different self-organizing structures are referred to as *reverse micelles* and their *water uptake* is normally expressed as the molar ratio of water to surfactant in the organic phase (W_O). Some surfactants, especially the cationic ones, need the presence of a *cosurfactant* to form reverse micelles. The cosurfactant is an amphiphilic compound, usually a long hydrocarbon chain *n*-alcohol. It participates in the interfacial surface of the surfactant heads and the water pool, screening the repulsive forces between the equal electrical sign charged heads. The physical properties of micellar and reverse micellar systems do not change with time, so these two types of microemulsions, in contrast with macroscopic emulsions, are thermodynamically stable. Another important difference between macroscopic emulsions and microemulsions is that the latter are optically isotropic, so they are translucent, while macroemulsions are milky.

Winsor classification of microemulsions [3] distinguishes four types of systems. A Winsor I system is the case of an organic liquid in contact with an aqueous phase

https://doi.org/10.1515/9783110564808-001

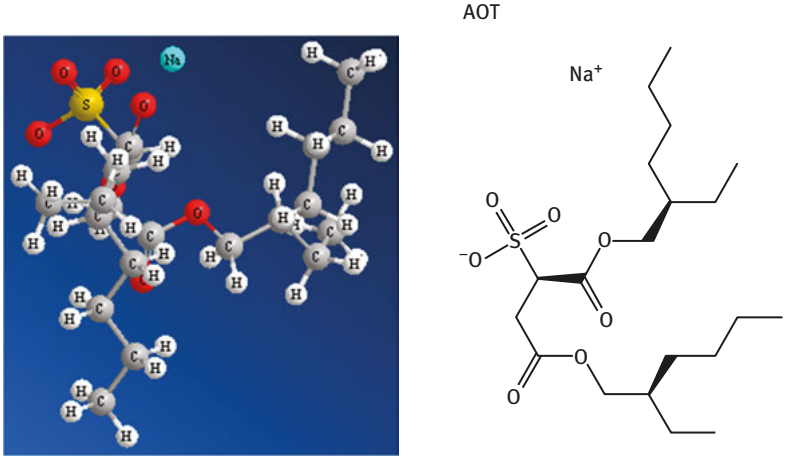

(a)

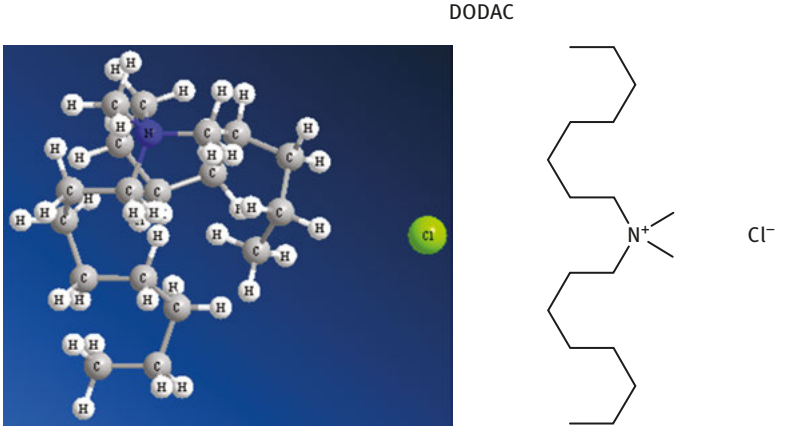

(b)

Figure 1.1: (a) Chemical structure of sodium bis-2-(ethylhexyl) sulfosuccinate (AOT) [1]. (b) Chemical formula of dioctyldimethyl ammonium chloride (CAS: 5538-94-3, DODAC) [2]. Figures done by the authors using CHem3D by Perkin Elmer.

containing micelles. An aqueous phase in contact with an organic phase containing reverse micelles corresponds to a Winsor II system. In a Winsor III system, a surfactant, water, and organic liquid form an intermediate microemulsion phase between the upper organic liquid and the lower water phase. In a Winsor IV system, a surfactant, water, and organic liquid form a microemulsion phase by itself, and there is no contact with excess water or excess organic liquid.

The purpose of the research discussed in this chapter was to explore the use of ionic surfactants to form reverse micelles that can be used to extract metals or biomolecules from dilute aqueous solutions. Thus, only Winsor I and Winsor II

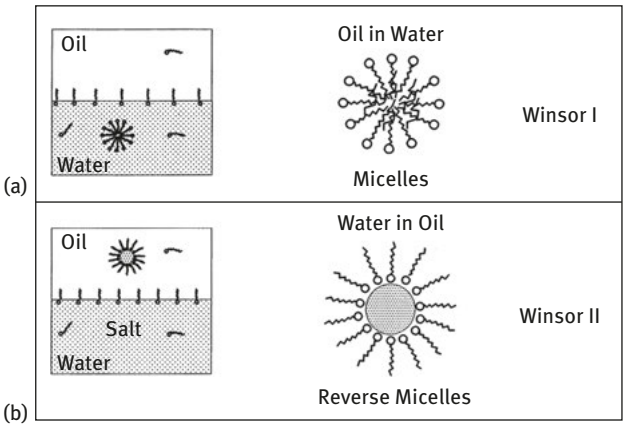

Figure 1.2: Graphical representation of Winsor I and II systems.

systems depicted in Figure 1.2 are of interest. As described above, these systems are obtained by contacting an organic liquid with water in the presence of a surfactant and with the help of an electrolyte in the case of reverse micelles. Winsor III and Winsor IV systems are of interest in the tertiary recovery of oil from the ground and they can be reproduced in the laboratory by titrating water in an organic phase containing a surfactant. For completeness, a brief presentation of the formation of microemulsions by both the contact method and the titration method is given below before centering the attention on the use of the contact method. The presentation of experimental results given in this chapter is rather qualitative. Quantitative values, and elaboration on the reasons for their trends, are given in the original publications.

1.2 Comparison of the Contact and Titration Methods to Form Microemulsions

As our studies in the formation of microemulsions progressed, we observed that there were discrepancies between our experimental observations and results reported in the literature. We soon realized that the discrepancies were due to the use of the contact method in our case and the use of the titration method in the results published by other authors (see Figure 1.3).

The same discrepancies had been previously found by other authors, Leodidis and Hatton [4] with respect to Eike [5] and Ashrafizadeh and Demopoulos [6] with respect to Leung and Shah [7], but the cause was not identified. Thus, we presented a comparison of the results obtained using the contact method and the titration

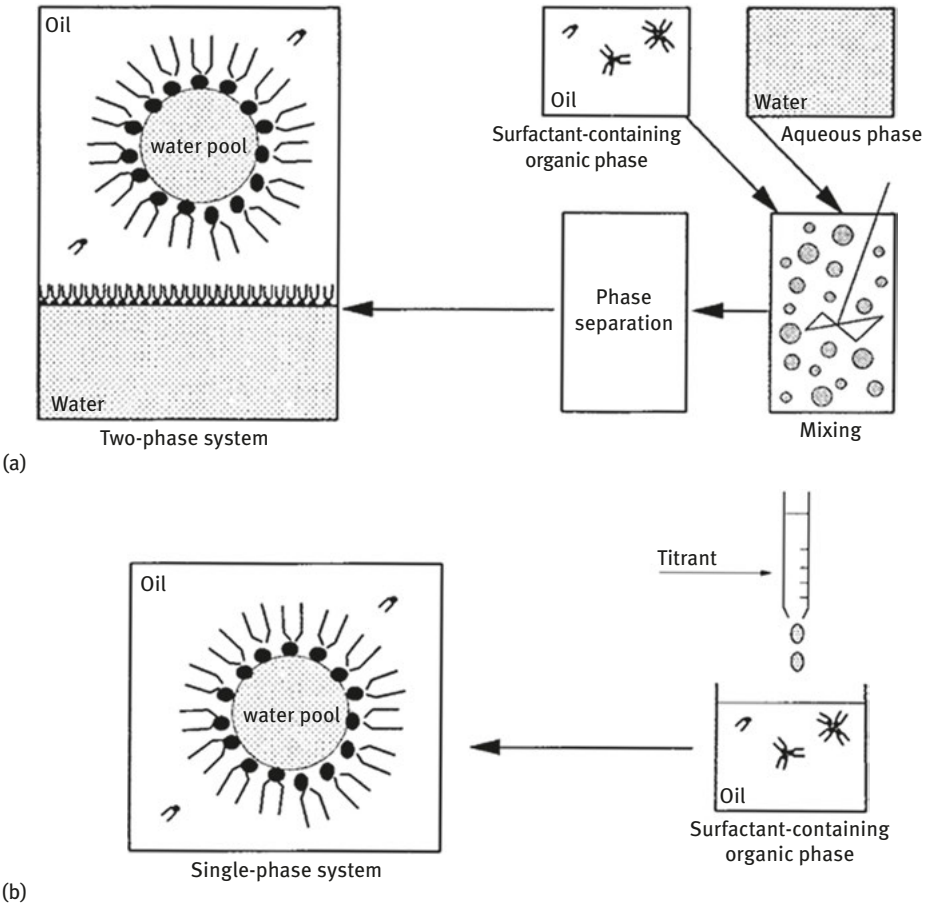

Figure 1.3: Comparison of the contact (a) and titration methods (b). Reprinted from [8]. Copyright (2018), with permission from Elsevier.

method for the case of sodium bis-2-(ethylhexyl) sulfosuccinate surfactant with the same organic phase in both methods [8].

This comparison is better seen in graphical form in Figures 1.4 and 1.5.

Figure 1.4 shows the effect of the concentration of heptanol cosurfactant on the water uptake of reverse micelles formed by AOT in decane using the contact method, while Figure 1.5 shows the effect of the same variable in the case of microemulsions formed with AOT in decane using the titration method. While the contact method requires the use of NaCl in the aqueous phase to form the reverse micelles in the organic phase, the titration method does not require any addition of salt. AOT reverse micelles form without addition of alcohol. Any addition of alcohol using the contact method decreases the water uptake. This decrease in the water uptake shown in Figure 1.4 has been explained [9] arguing that heptanol in decane

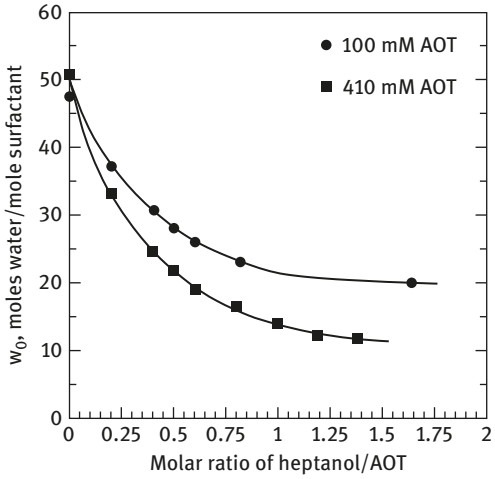

Figure 1.4: Effect of the concentration of heptanol cosurfactant on the water uptake, w_0, of reverse micelles formed by AOT in decane at 25 °C using the contact method. Initial organic phase ■ 410 mM AOT and ● 100 mM AOT. Initial aqueous phase 97 mM NaCl. Reprinted from [8]. Copyright (2018), with permission from Elsevier.

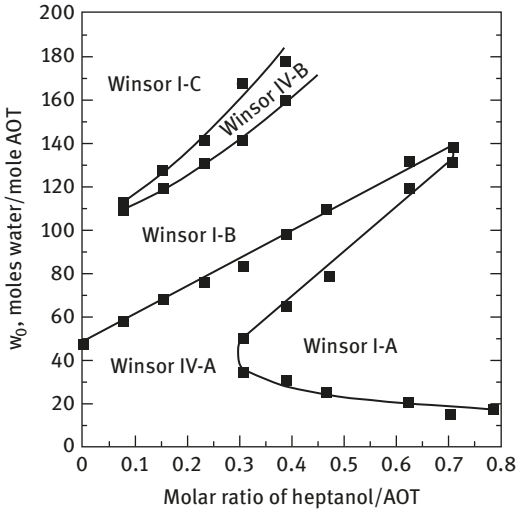

Figure 1.5: Effect of the concentration of heptanol cosurfactant on the water uptake, w_0, of reverse micelles formed by AOT in decane using the titration method at 25 °C. Initial organic phase 410 mM AOT. Initial aqueous phase distilled water, no salt. Reprinted from [8]. Copyright (2018), with permission from Elsevier.

helps dissolving undissociated surfactant in the organic phase thus effectively acting as cosolvent and decreasing the surfactant available to form reverse micelles. The effect of heptanol in the case of microemulsions formed by titration is quite impressive. Different zones of Winsor I systems exist, and different zones of Winsor IV systems appear. The water content of microemulsions formed by titration increases with the addition of heptanol and it is much higher than the water uptake of reverse micelles formed by contact of the organic and aqueous phases. The Winsor IV systems formed are not thermodynamically stable and separate into two liquid phases after some time.

1.3 Use of Dinonylnaphtalenesulfonic Acid Reverse Micelles as Liquid Ion Exchangers

The idea of using ionic surfactants as ionic exchangers was not new. More than 40 years ago, Kunin [10] had shown that solutions of dinonylnaphtalenesulfonic acid (HD) in nonpolar liquids acted as liquid ionic exchangers similar to solid ion-exchange resin beads. Figure 1.6 presents the structure of dinonylnaphtalenesulfonic acid. Thus, our first work in this field [11] consisted in a systematic study of the performance of reverse micelles of HD as ion exchangers for potassium and magnesium. As the main objective was the exchange of the cation H^+ either with the cation K^+ or with the cation Mg^{2+}, experiments were carried out for the three-binary systems H^+/K^+, H^+/Mg^{2+}, and K^+/Mg^{2+} and for the ternary system $H^+/K^+/Mg^{2+}$. For these experiments, in addition to the HD reverse micelles, microemulsions containing reverse micelles with only K^+ cation or only Mg^{2+} cation (KD or MgD_2 reverse micelles) were prepared by repeated contact of the HD microemulsions with concentrated aqueous solutions of KCl or $MgCl_2$. The three kinds of reverse micelles were contacted with aqueous solutions of the cations having the common anion chloride.

As can be expected, the same experimental results were obtained using a KD reverse micellar phase in contact with an $MgCl_2$ aqueous solution or an MgD_2 reverse micellar phase in contact with a KCl aqueous solution. The water uptake of the three reverse micellar systems was low and decreased in the order HD, MgD_2, and KD. In all cases, it decreased with an increase in the concentration of salt. The concentration of surfactant in the aqueous phase was always less than 2 mM and decreased as the concentration of an electrolyte increased in that phase. The relative concentrations of the cations in the aqueous phase and in the water pools of the reverse micelles were expressed in terms of their

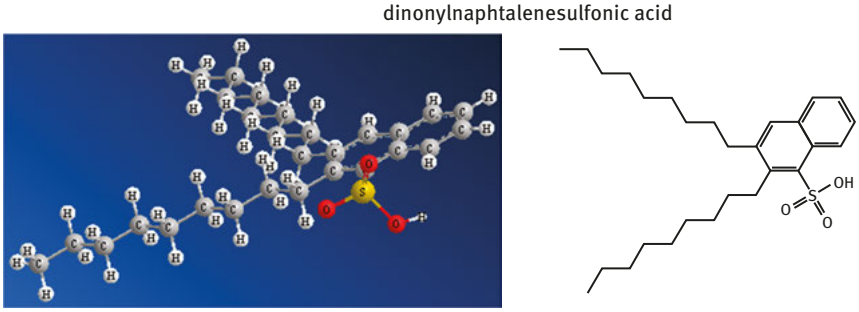

Figure 1.6: Structure of dinonylnaphtalenesulfonic acid (DH). Figure done by the authors using CHem3D by Perkin Elmer.

equivalent ionic fractions. The equivalent ionic fractions for the cations in the aqueous phase are given by

$$X_i = \frac{z_i\, C_i}{\sum_k z_k\, C_k}$$

where z_i is the charge of cation i and C_i is its molarity in the aqueous phase in mol/L. The equivalent ionic fractions for the cations in the water pools of the reverse micellar phase are given by

$$Y_i = \frac{z_i\, \overline{C_i}}{\sum_k z_k\, \overline{C_k}}$$

where $\overline{C_i}$ is the molarity of cation i in the reverse micellar water pools.

As in the original publication [11], the thermodynamic modeling was presented in a compact form; we give here a more detailed explanation. When a cation $M_i^{z_i+}$(aq) in the aqueous phase replaces a cation $M_j^{z_j+}$(rm) in the active sites of the reverse micelles formed by a cationic surfactant, the reaction takes the form

$$z_j\, M_i^{z_i+}\,(aq) + z_i\, M_j\,(rm) \leftrightarrow z_j\, M_i\,(rm) + z_i\, M_j^{z_j+}\,(aq)$$

The thermodynamic equilibrium constant for this reaction is

$$K_j^i = \frac{\bar{a}_i^{z_j}\, a_j^{z_i}}{\bar{a}_j^{z_i}\, a_i^{z_j}} = \frac{\left(Y_i\bar{\gamma}_i\right)^{z_j}\left(C_j\gamma_j\right)^{z_i}}{\left(Y_j\bar{\gamma}_j\right)^{z_i}\left(C_i\gamma_i\right)^{z_j}} = \left(\frac{Y_i\bar{\gamma}_i}{C_i\gamma_i}\right)^{z_j}\left(\frac{C_j\gamma_j}{Y_j\bar{\gamma}_j}\right)^{z_i}$$

or

$$Y_i = \left(K_j^i\right)^{1/z_j}\,\frac{C_i\gamma_i}{\bar{\gamma}_i}\left(\frac{Y_j\bar{\gamma}_j}{C_j\gamma_j}\right)^{z_i/z_j}$$

where the activities of the individual cations in the aqueous phase were expressed in the usual convention as the product of the molarity of the ion times the activity coefficient of the individual ion, while in the reverse micellar phase they were expressed as the product of the equivalent ionic fraction of the cation in the water pools of the reverse micellar phase times a corresponding activity coefficient identified by an upper bar. For the reverse micellar phase in a binary cation system,

$$Y_i + Y_j = 1$$

or

$$(K_j^i)^{1/z_j} \frac{C_i \gamma_i}{\bar{\gamma}_i} \left(\frac{Y_j \bar{\gamma}_j}{C_j \gamma_j} \right)^{z_i/z_j} + Y_j - 1 = 0$$

The experimental data collected in binary systems gave information on Y_j as a function of C_i and C_j. Thus, this equation was used to fit the value of the binary equilibrium constants plus the values of any other parameter introduced for the calculations of the activity coefficients of the individual ions in the aqueous and reverse micellar phases. Activities of the individual ions in the aqueous phase were not available, so it was necessary to estimate them from mean ionic activity coefficients of the electrolytes in aqueous solutions. Still, mean ionic activity coefficients in aqueous electrolyte solutions with more than one electrolyte were not available. Thus, for the aqueous phase, Haghtalab equations [12] for binary electrolytes were used. For binary systems of two 1:1 electrolytes, these equations are given as follows:

$$\ln \gamma_{\pm 1} = \ln \gamma_{\pm 1}^0 - \frac{m_2}{2I} [\ln \gamma_{\pm 1}^0 - \ln \gamma_{\pm 2}^0]$$

$$\ln \gamma_{\pm 2} = \ln \gamma_{\pm 2}^0 - \frac{m_1}{2I} [\ln \gamma_{\pm 2}^0 - \ln \gamma_{\pm 1}^0]$$

For a 1:1 electrolyte 1 and a 2:1 electrolyte 2, they take the form

$$\ln \gamma_{\pm 1} = \ln \gamma_{\pm 1}^0 - \frac{m_2}{I} [2 \ln \gamma_{\pm 1}^0 - \ln \gamma_{\pm 2}^0]$$

$$\ln \gamma_{\pm 2} = \ln \gamma_{\pm 2}^0 - \frac{m_1}{2I} [\ln \gamma_{\pm 2}^0 - 2 \ln \gamma_{\pm 1}^0]$$

with the ionic strength I given by

$$I = \sum_k^{c,a} m_k z_k^2$$

where the sum considers all anions and cations present and the superscript 0 indicates the mean ionic activity coefficient of the pure electrolyte in an aqueous solution. These values were calculated using Bromley's equation [13] with values of the Bromley parameter 0.1433 for HCl, 0.0240 for KCl, and 0.1129 kg/mol for $MgCl_2$.

For the ternary system of electrolytes 1 and 2 of type 1:1 and electrolyte 3 of type 2:1, the extension of these equations gave:

$$\ln \gamma_{\pm 1} = \ln \gamma^0_{\pm 1} - \frac{m_2}{2I}\left[\ln \gamma^0_{\pm 1} - \ln \gamma^0_{\pm 2}\right] - \frac{m_3}{I}\left[2 \ln \gamma^0_{\pm 1} - \ln \gamma^0_{\pm 3}\right]$$

$$\ln \gamma_{\pm 2} = \ln \gamma^0_{\pm 2} - \frac{m_1}{2I}\left[\ln \gamma^0_{\pm 2} - \ln \gamma^0_{\pm 1}\right] - \frac{m_3}{I}\left[2 \ln \gamma^0_{\pm 2} - \ln \gamma^0_{\pm 3}\right]$$

$$\ln \gamma_{\pm 3} = \ln \gamma^0_{\pm 3} - \frac{m_1}{2I}\left[\ln \gamma^0_{\pm 3} - 2 \ln \gamma^0_{\pm 1}\right] - \frac{m_2}{2I}\left[\ln \gamma^0_{\pm 3} - \ln \gamma^0_{\pm 2}\right]$$

The activity of the individual cations was then obtained assuming the validity of a Debye–Hückel type of relation:

$$\ln \gamma_+ = \frac{z_+^2}{|z_+ z_-|} \ln \gamma_\pm$$

The reverse micelles were assumed not to contain the anion Cl^-. Notably, these equations do not require the use of adjustable parameters. For the activity of the individual ions in the water pool of the reverse micelles, Wilson equation [14], introducing two additional adjustable parameters Λ_{ij} and Λ_{ji}, was used:

$$\ln \overline{\gamma_i} = 1 - \ln\left(\sum_k^c Y_k \Lambda_{ik}\right) - \sum_k \frac{Y_k \Lambda_{ki}}{\sum_j Y_j \Lambda_{kj}}$$

Thus, three adjustable parameters were fitted for each binary system and no new parameter was introduced to predict the ternary system.

Table 1.1 gives an idea of the selectivity of the HD reverse micelles for magnesium and the quality of the predictions given by the model. We have selected two rows to show these two aspects. In the first row, the molarity of potassium in the aqueous phase is more than double the molarity of magnesium, while in the reverse micellar phase this is reversed. In the second row, the molarities of these two ions are almost the same in the aqueous phase, while in the reverse micellar phase the molarity of magnesium is much larger than the molarity of potassium. The values of the molarities in the ternary systems predicted from binary data only are quite satisfactory and show the proper trends. Perhaps, the most important conclusion of this study was that the selectivity of the HD reverse micelles was comparable for H^+ and K^+ but it was greater for Mg^{2+} than for K^+, suggesting that these systems could be used to separate ions of different charges. Another important conclusion was that the prediction of the ternary system starting from data for the three binary systems was possible using a thermodynamic model with activity coefficients for the individual ions in both the

Table 1.1: Comparison of experimental and predicted results for the ternary system $H^+/K^+/Mg^{2+}$ with dinonylnaphtalenesulfonic acid (HD) as a reverse-micelles-forming agent [11].

X (exp)			Y(Mg^{2+})		Y(K^+)		Y(H^+)	
Mg^{2+}	K^+	H^+	Exp	Pred	Exp	Pred	Exp	Pred
0.21	0.54	0.25	0.37	0.40	0.16	0.18	0.47	0.42
0.38	0.37	0.25	0.45	0.48	0.09	0.13	0.46	0.39

Note: X = equivalent ionic fractions for the cations in the aqueous phase; Y = equivalent ionic fractions for the cations in the reverse micellar phase; exp = experimental value; pred = value predicted by the model.

aqueous phase and the water pool, or more properly in the charged inside surface, of the reverse micelles.

The conclusions of this first study influenced strongly the research program that followed. First, the possibility of separating heavy metals using ionic surfactants was immediately apparent from the selectivity of an ion with double charge with respect to an ion with single charge. In addition, as under certain conditions biomolecules are electrically charged, reverse micellar systems formed with ionic surfactants had a clear potential for their extraction from dilute aqueous solutions.

From the beginning it was considered interesting to explore the formation of reverse micelles using other ionic surfactants, both anionic and cationic. As there was the idea that the size of the water pool in the reverse micelles would be a factor in their solubilization capacity of ions and biomolecules, studies of the variables affecting the water uptake in reverse micelles formed by different ionic surfactants were planned.

In addition, the success of a simple thermodynamic model for the prediction of the ternary system based on data of binary systems suggested the idea of gathering information on the activity coefficients of biomolecules in aqueous solutions in the presence of electrolytes and on the activity coefficients of individual ions in aqueous electrolyte solutions. Studies on the activity coefficients of individual ions have been reported elsewhere [15, 16]. For the studies of activity coefficients of biomolecules in aqueous electrolyte solutions, it was decided to start with amino acids that are the building blocks of peptides and proteins. The first step was to gather experimental data and then attempt to model it. In the chapters that follow, we present an overview of the results of all these studies and, up to where possible, give references to work done by other researchers continuing work on these topics. The detailed results are given in peer-reviewed publications indicated in the references of each chapter. In what follows of this chapter, we present the results of exploratory studies of formation of microemulsions with three sodium alkyl phosphinate anionic surfactants and one alkyl ammonium chloride cationic surfactant.

1.4 Formation of Microemulsions with Three Dialkyl Sodium Phosphinates

The success obtained using reverse micelles of dinonylnaphtalenesulfonic acid (HD) as liquid ionic exchangers in association with the idea that the sodium salt AOT surfactant, i.e., sodium bis-2-(ethylhexyl) sulfosuccinate, formed reverse micelles with high water uptake suggested using sodium salts of other anionic ion exchangers for the formation of reverse micelles. After purification, three commercial liquid acids used as metal extractants were used to prepare the corresponding sodium salts. These were bis (2,2,4-trimethylpentyl) phosphinic acid (CYANEX 272), bis(2,2,4-trimethylpentyl) monothiophosphinic acid (CYANEX 302), and bis(2,2,4-trimethylpentyl) dithiophosphinic acid (CYANEX 301) donated by Cyanamid Canada Inc. The three purified acids had negligible solubility in water and did not produce any water uptake when dissolved in a nonpolar liquid and contacted with an aqueous phase. Their structure is presented in Figure 1.7.

The three corresponding dialkyl sodium phosphinates, designated by short names as NaPOO, NaPSO, and NaPSS, were then used as anionic surfactants to prepare water in oil microemulsions. Isooctane was used as a nonpolar organic liquid phase with either pentanol, octanol, or decanol as cosurfactant. The aqueous phase was a NaCl solution.

The behavior of these three ionic surfactants was quite similar. The three needed a minimum concentration of cosurfactant in the organic phase and of salt in the aqueous phase in order to form reverse micelles. At the minimum required concentration of cosurfactant or salt, the water uptake was a maximum. Increasing the cosurfactant or the salt concentration above the minimum required consistently decreased the water uptake. Below the minimum concentrations of salt or cosurfactant, most of the anionic surfactant is in the aqueous phase and the system is an oil in water microemulsion. Under the same conditions, the water uptake of the three anionic surfactants decreases in the order NaPOO > NaPSS > NaPSO. It was believed that this effect was due to the asymmetry of the head of the NaPSO anionic surfactant that may decrease the head group repulsion at the inside surface of the reverse micelles allowing the heads to pack closer and form smaller reverse micelles.

The most notable effect was caused by the length of the hydrocarbon chain of the alcohol used as cosurfactant. Water in oil microemulsions formed at a lower minimum cosurfactant concentration (MCC) as the hydrocarbon chain of the alcohol became longer. Once the water in oil microemulsion is formed, the water uptake is less for the longer chain alcohols and this effect becomes smaller as the alcohol hydrocarbon chain becomes longer. As suggested by Winsor [3], the formation of water in oil microemulsions is the result of a balance between the net cohesive energy of the surfactants and cosurfactants with the organic phase and the water at the interface of the reverse micelles. The OH groups of the different alcohols have

bis(2,2,4-trimethylpentyl) phosphinic acid

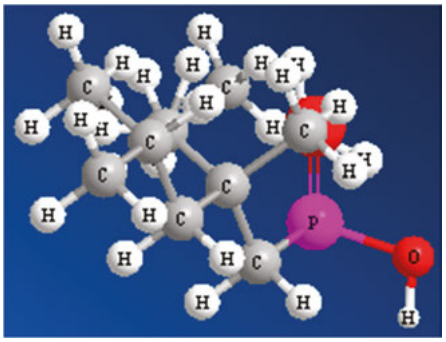

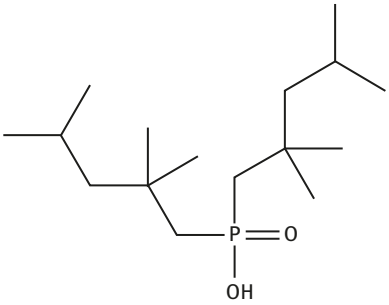

(a)

bis(2,2,4-trimethylpentyl) monothiophosphinic acid

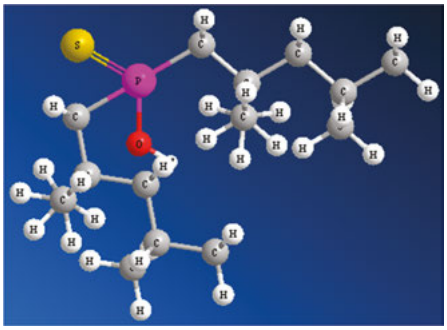

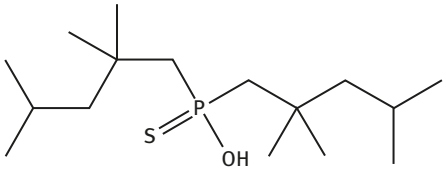

(b)

bis(2,2,4-trimethylpentyl) dithiophosphinic acid

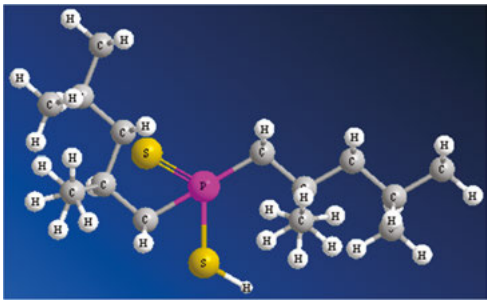

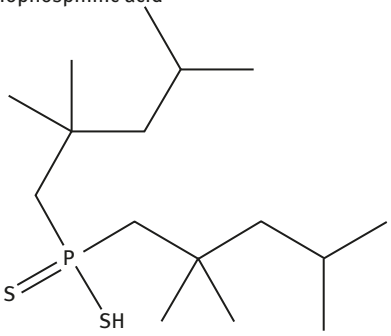

(c)

Figure 1.7: Structures of (a) bis(2,2,4-trimethylpentyl) phosphinic acid – HPOO, (b) bis(2,2,4-trimethylpentyl) monothiophosphinic acid – HPSO, and (c) bis(2,2,4-trimethylpentyl) dithiophosphinic acid – HPSS. Figures done by the authors using CHem3D by Perkin Elmer.

approximately the same cohesive energy with water, but shorter tail alcohols have less cohesive energy with the organic phase than long chain alcohols so more molecules of shorter tail alcohols are required for the formation of reverse micelles.

Addition of cosurfactant above the MCC value increases the concentration of alcohol at the interface of the water pools causing a decrease in the dielectric constant of the water in the pools which, in turn, shifts the equilibria of the surfactant from its dissociated (active) form to the undissociated form. The undissociated form of the surfactant then migrates to the cosurfactant-rich organic phase, decreasing the number of surfactant molecules available for the formation of reverse micelles. In this case, the cosurfactant becomes a cosolvent for the undissociated form of the surfactant.

These effects are better seen in graphical form. Figures 1.8 and 1.9 show the results for the NaPOO anionic surfactant that it was the most promising one to form reverse micelles.

Note after the facts: In the preparation of work for manuscript [18], published 4 years after manuscript [17], it was noted that Paatero and Sjoblom [19]

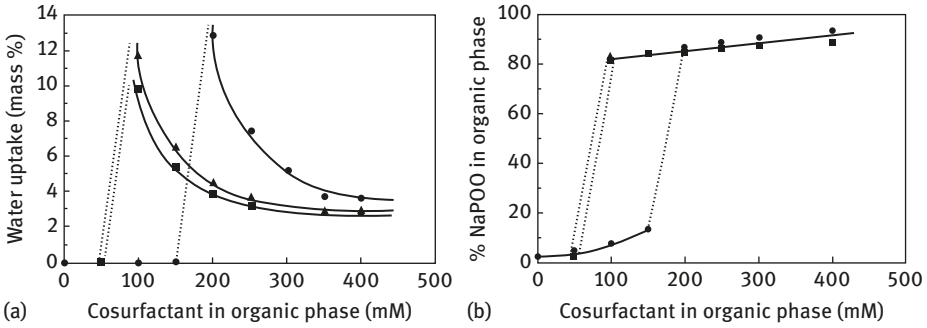

Figure 1.8: Effect of alcohol chain length and concentration on (a) water uptake and (b) surfactant distribution for (■) decanol, (▲) octanol, and (●) pentanol at 100 mM NaPOO and 100 mM NaCl. Reprinted from [17]. Copyright (2017), with permission from Elsevier.

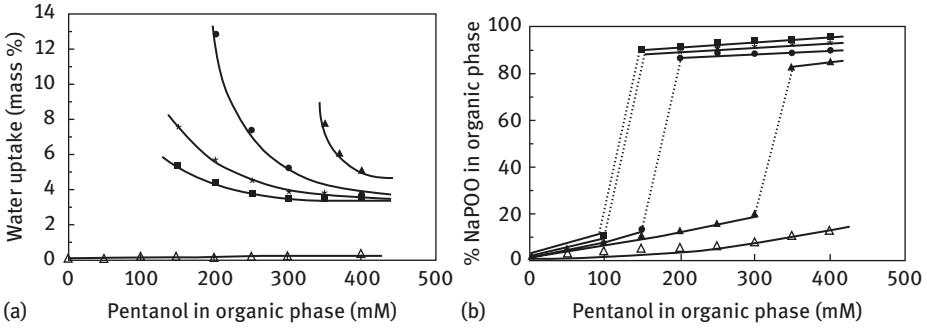

Figure 1.9: Effect of salt concentration on (a) water uptake and (b) surfactant distribution for (Δ) 0, (▲) 50, (●) 100, (*) 200, and (■) 300 mM NaCl at 100 mM NaPOO in the isooctane/pentanol system. Reprinted from [17]. Copyright (2017), with permission from Elsevier.

had reported the formation of reverse micelles with sodium di(2,2,4-trimethylpentyl) phosphinate in hexane using free di(2,2,4-trimethylpentyl) phosphinic acid as cosurfactant. This information was not known at the time of publishing manuscript [17].

1.5 Reverse Micelle Formation Using a Sodium Di(*n*-Octyl) Phosphinate Surfactant

In the search for new surfactants, able to form reverse micelles that could be used for the extraction of biomolecules and heavy metals, di(*n*-octyl) phosphinic acid was synthesized and neutralized with NaOH to obtain sodium di(*n*-octyl) phosphinate. The presence of two long straight hydrocarbon chains (see Figure 1.10), instead of two short branched chains of the 2,2,4-trimethylpentylphosphinates, was thought to give more stable reverse micelles and make the surfactant less likely to migrate to the aqueous phase. Isooctane was used as the nonpolar organic phase; sodium chloride was added to the aqueous phase and the two cosurfactants tested were n-decanol and di(*n*-octyl) phosphinic acid.

The results of this study were quite surprising. As shown in Figures 1.11–1.13, in all cases there was a limited range of cosurfactant-to-surfactant mole ratio in which there was water uptake into the organic phase. As has also been observed for other

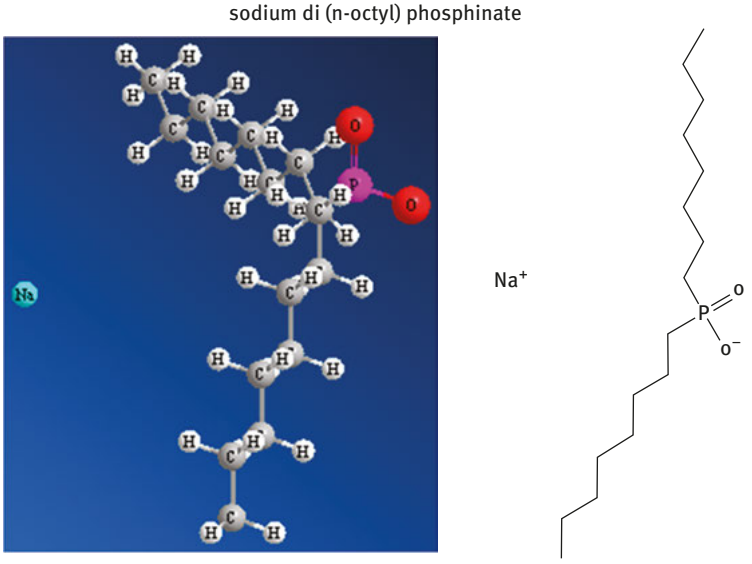

Figure 1.10: Structure of a sodium di(*n*-octyl) phosphinate. Figure done by the authors using CHem3D by Perkin Elmer.

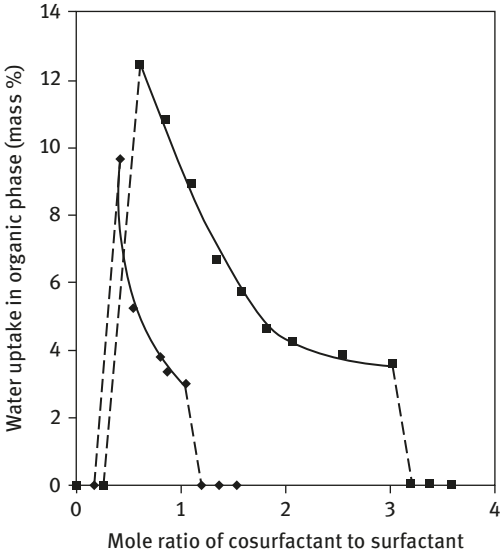

Figure 1.11: Effect of the cosurfactant-to-surfactant ratio on the water uptake in the isooctane phase at a concentration of 0.15 molal sodium di(*n*-octyl) phosphinate and 0.1 M NaCl: (■) *n*-decanol and (♦) di(*n*-octyl) phosphinic acid. Reprinted from [18]. Copyright (2017), with permission from Elsevier.

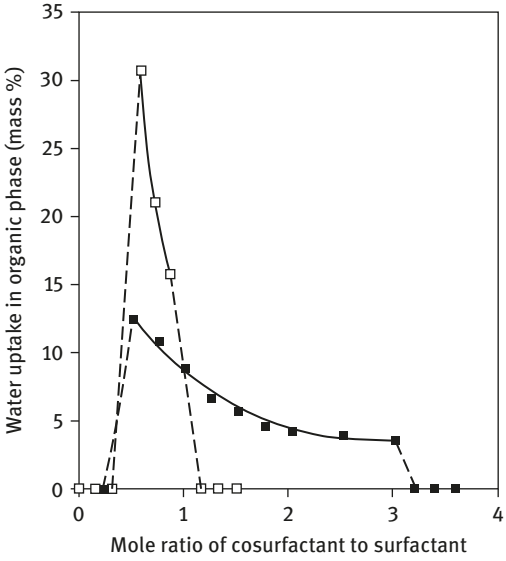

Figure 1.12: Effect of the cosurfactant-to-surfactant ratio on the water uptake in the isooctane phase at two *n*-decanol concentrations and 0.1 molal NaCl: (■) 0.15 molal *n*-decanol and (□) 0.30 molal *n*-decanol. Reprinted from [18]. Copyright (2017), with permission from Elsevier.

surfactants, below a certain concentration of cosurfactant in the organic phase, the surfactant molecules remained in the aqueous phase and there was no water uptake in the organic phase. Above that concentration, the surfactant molecules migrated to the organic phase giving a maximum in the water uptake. Any addition of cosurfactant would decrease the water uptake. All of this was expected. The abnormal behavior was the presence of an upper limit in the cosurfactant-to-surfactant ratio,

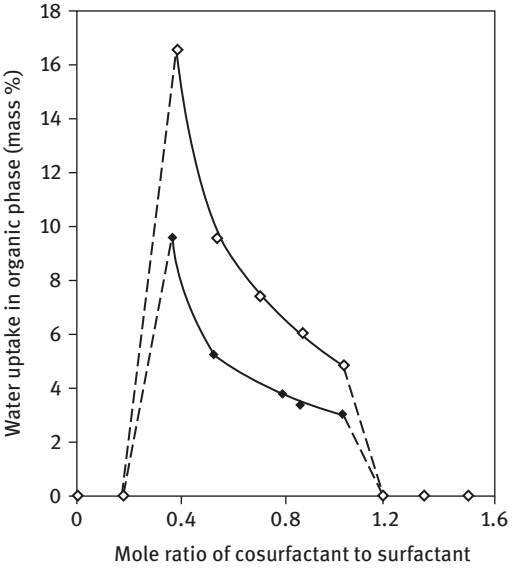

Figure 1.13: Effect of the cosurfactant-to-surfactant ratio on the water uptake in the isooctane phase at different di(*n*-octyl) phosphinic acid concentrations and 0.1 molal NaCl: (♦) 0.15 molal di(*n*-octyl) phosphinic acid and (◊) 0.30 molal di(*n*-octyl) phosphinic acid. Reprinted from [18]. Copyright (2017), with permission from Elsevier.

above which the water uptake decreases to zero with both the decanol and the di(*n*-octyl) phosphinic acid cosurfactants. These two cosurfactants are very different in chemical nature. Decanol is a nonionic amphiphilic compound with low solubility in water and its performance as cosurfactant at low concentrations changing to cosolvent at higher concentrations is similar to that of other aliphatic alcohols. Still, its abrupt pass from cosurfactant to cosolvent was surprising. On the other hand, di(*n*-octyl) phosphinic acid and its sodium salt are insoluble in aliphatic hydrocarbons and their solubility in isooctane at certain ratios has been explained by the mechanism of formation of acid soaps [20, 21]. Thus, it is possible that the mechanism of forming microemulsion is different for both surfactants, and the similitude in the behavior of both with respect to the water uptake is still to be explained. As with the study of formation of microemulsions by the contact method and the titration method, it was felt that there was much room to explore further the field, but such studies were beyond our area of competence and interest.

1.6 Reverse Micelle Formation Using DODAC

Reverse micelles formed by cationic surfactants generally solubilize less water in the organic phase than reverse micelles formed by anionic surfactants and usually they require the use of a cosurfactant. Reverse micelles formed with trioctylmethyl ammonium chloride (TOMAC), also known as Aliquat 336, had been used to extract proteins and it was thought that their low water uptake would prevent the use of this

surfactant for the extraction of large negatively charged proteins [22–24]. At that time the idea that the size of the micellar water pool was determinant in the capacity of a surfactant to extract solutes from aqueous solutions was prevalent. A surfactant with two long tails and two short tails was visualized as easier to pack around a water pool than a surfactant with three long tails and one short tail. Therefore, it was decided to purify dioctyldimethyl ammonium chloride (DODAC, CAS No. 5538-94-3, see Figure 1.1(b)) from the commercial surfactant Bardac LF-80 sold by Lonza Inc., which contains 80% by weight of DODAC in a water ethanol solution. It is important to mention here that this compound has other synonymous names. According to MeSH (medical subject heading) entry terms, it is called DODMA-Cl or DODMAC cpd [25]. Other authors [26] used the name DODMAC for dioctadecyl dimethyl ammonium chloride (CAS No. 107-64-2); it is a different surfactant with 18 carbon atoms per chain (not 8 as in our case).

Dioctyldimethyl ammonium chloride (CAS No. 5538-94-3), in the original publications by our group called DODMAC and here called DODAC, is corrosive to skin and harmful to eyes, respiratory system, and gastrointestinal track.

Finding the conditions to form reverse micelles with this previously untested surfactant was not easy. The concentration of alcohol cosurfactant required in the organic phase was much larger than the concentration required with TOMAC, but once the minimum alcohol concentration was attained, the water uptake in the organic phase was much larger than that with TOMAC. Figure 1.14 shows the comparison of behavior of both surfactants with decanol as cosurfactant. Once it was determined that a high concentration of cosurfactant was required to form microemulsions with DODAC, the results started following into place. Figure 1.15 shows the effect of the hydrocarbon chain length of the alcohol on the water uptake of the DODAC reverse micelles. At low concentration of alcohol, the longer the hydrocarbon chain, the larger the water uptake. However, this is reversed at high alcohol

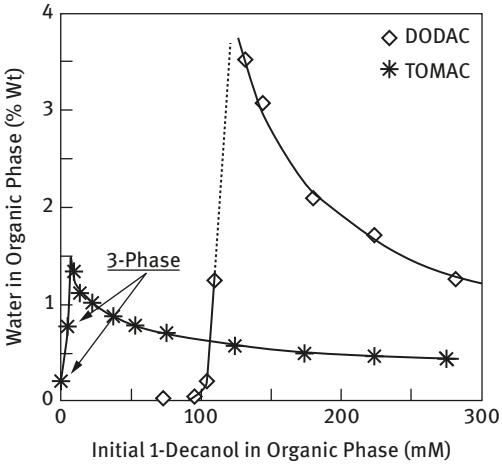

Figure 1.14: Effect of surfactant structure on water uptake with 1-decanol as cosurfactant. Initial organic: 50 mM surfactant; initial aqueous: 68 mM NaOH and 44 mM H_3PO_4 at pH 6.8. Reprinted from [9]. Copyright (2017), with permission from Elsevier.

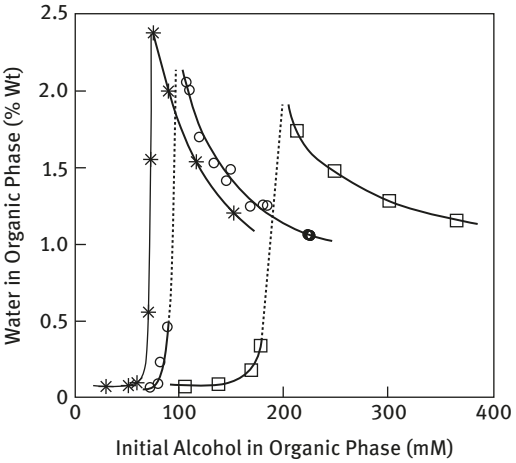

Figure 1.15: Effect of hydrocarbon chain length of normal alcohol on water uptake. Initial organic: 50.1 mM DODAC; initial aqueous: 300 mM NaOH at pH 6.8. (*) 1-decanol, (○) 1-heptanol, (□) 1-pentanol. Reprinted from [9]. Copyright (2017), with permission from Elsevier.

concentration. Finally, Figure 1.16 shows the effect of salt concentration in the initial aqueous phase. The distribution of surfactant is shown on the right-hand-side vertical axis and the water uptake is shown on the left-hand-side vertical axis. Without salt, the DODAC is at the interface forming micelles in the aqueous phase. When salt is added and the alcohol concentration in the organic phase is high enough, it migrates to the organic phase giving a maximum the water uptake. Excess of salt increases the dielectric constant of the water in the water pools of the reverse micelles and decreases the water uptake.

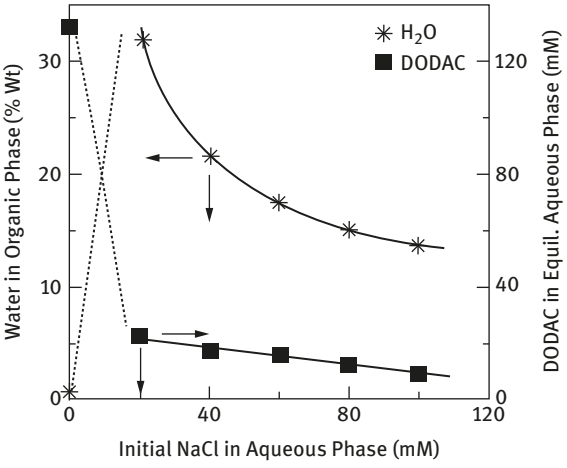

Figure 1.16: Effect of NaCl on water uptake in organic phase and on DODAC in the equilibrium aqueous phase. Initial organic: 200 mM DODAC and 200 mM 1-decanol; initial aqueous: NaCl at pH 6.8. Reprinted from [9]. Copyright (2017), with permission from Elsevier.

1.7 Studies on the Behavior of DODAC and DODAB Reverse Micellar Systems

Following the success in forming reverse micelles with the ionic surfactant DODAC (called DODMAC in our previous publications), the commercial surfactant $(CH_3)_2N(C_8H_{17})_2Br$, obtained from Pfaltz and Bauer (Waterbury, CT), containing 80% dioctyldimethyl ammonium bromide in an aqueous solution, was used and the bromide form of the ionic surfactant, here called DODAB and in our publications called DODMAB, was purified. Reverse micelles were formed in isooctane-decanol-surfactant/water-salt systems. Sodium salts with different anions and chloride salts with different cations were used in the aqueous phase. Experiments carried out with both the commercial products and the purified surfactants showed that the water uptake and the anion distribution between an aqueous phase and a reverse micellar phase were unaffected by the presence of water in Bardac LF-80 and the presence of water and ethanol in the case of the commercial DODAB. Figures 1.17 and 1.18 show the effect of sodium salts with different monovalent anions and with different bivalent anions, respectively, on the DODAC reverse micellar system. In Figure 1.18, the water uptake in the case of NaCl salt is included for comparison.

Figures 1.19 and 1.20 show interesting comparisons of the behavior of DODAC and DODAB reverse micellar systems in the presence of different salts. In Figure 1.19, both DODAC and DODAB are in micellar systems containing either NaCl or NaBr in the aqueous phase. In the case of DODAC with NaCl or DODAB with NaBr, the increase in the concentration of salt in the aqueous phase above the minimum required to form reverse micelles causes a decrease in the water uptake from the maximum water uptake obtained at the minimum electrolyte

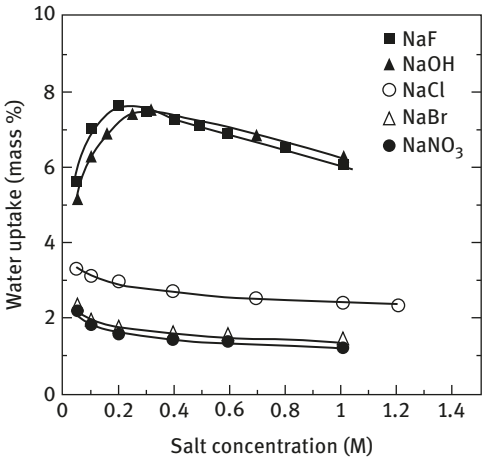

Figure 1.17: Water uptake as a function of salt concentration for sodium salts with different monovalent ions in organic phase and for DODAC in the equilibrium aqueous phase. Initial organic: 0.1 M DODAC and 0.25 M 1-decanol; initial aqueous: salt no pH adjustment. Reprinted from [27]. Copyright (2017), with permission from Elsevier.

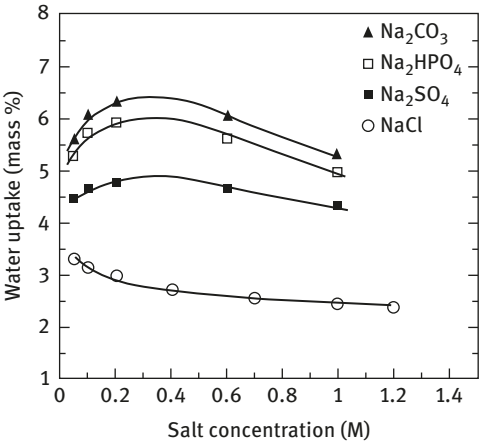

Figure 1.18: Water uptake as a function of salt concentration for sodium salts with different divalent ions in organic phase and for DODAC in the equilibrium aqueous phase. Initial organic: 0.1 M DODAC and 0.25 M 1-decanol; initial aqueous: salt no pH adjustment. The data for NaCl are shown for comparison. Reprinted from [27]. Copyright (2017), with permission from Elsevier.

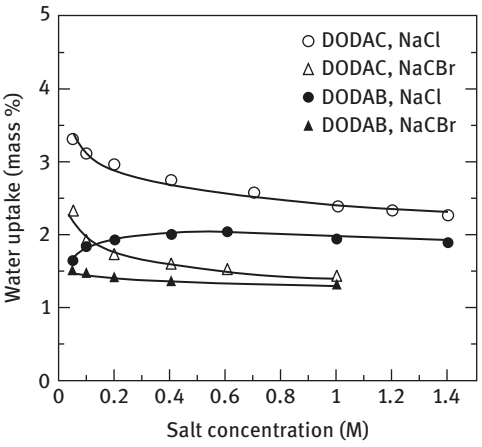

Figure 1.19: Water uptake as a function of salt concentration for surfactants with different counterions. Initial organic: 0.1 M DODAC or DODAB and 0.25 M 1-decanol; initial aqueous: salt no pH adjustment. Reprinted from [27]. Copyright (2017), with permission from Elsevier.

concentration. DODAC reverse micellar systems with NaCl aqueous phase give higher water uptake than DODAB reverse micellar systems with NaBr in the aqueous phase. The interesting case is the comparison of the DODAC reverse micellar systems with NaBr in the aqueous phase and the DODAB reverse micellar systems with NaCl in the aqueous phase. While the addition of NaBr in the DODAC systems decreases the water uptake, the addition of NaCl in the DODAB reverse micellar systems increases the water uptake. The increase in the water uptake of a reverse micellar system with the addition of salt, seen in Figures 1.18 and 1.19, needs some explanation. For this it is interesting to observe that, as shown in Figure 1.19, at high concentration of salt in the aqueous phase, the water uptake of the DODAC–NaBr system approaches from above the water uptake of the DODAB–NaCl system. On the other hand, at high concentration of NaCl the DODAB–NaCl system approaches

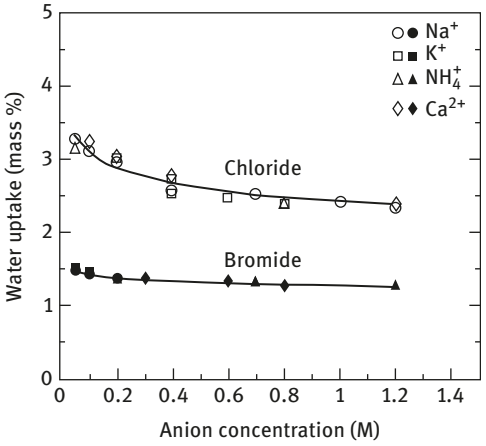

Figure 1.20: Water uptake as a function of anion concentration for chloride and bromide salts with different cations. Initial organic: 0.1 M DODAC or DODAB and 0.25 M 1-decanol; initial aqueous: salt no pH adjustment. Open symbols refer to chloride salts and DODAC; closed symbols refer to bromide salts and DODAB. Reprinted from [27]. Copyright (2017), with permission from Elsevier.

from below the water uptake of the DODAC–NaCl system. Thus, it is clear that the chloride form of the surfactant has a higher water uptake than the bromide form and the ion exchange in the head of the surfactant is the cause of this effect. The same explanation holds for the maximum water uptakes shown in Figures 1.17 and 1.18. The exchange of the anion of the surfactant with the anion in the aqueous phase produces surfactant forms that have higher water uptakes but in the concentration of salt increase in the aqueous phase beyond the upper limit of the ion exchange the water uptake decreases as expected. Figure 1.17 shows that the presence of different cations in the aqueous phase does not affect the water uptake capacity of the reverse micellar systems formed by DODAC or DODAB.

Two additional interesting studies presented in [27] are the effect on the water uptake of the pH and of surfactant and salt concentrations in the aqueous phase for DODAC in isooctane with decanol cosurfactant. These results are presented in Figures 1.21 and 1.22. Figure 1.21 shows the effect of pH, adjusted with HCl or NaOH, for the different values of the concentration of NaCl in the aqueous phase. For pH below 8 adjusted with HCl, the system contained only one anion and as the cation has no effect the water uptake was not affected. At pH above 8, the pH was adjusted with NaOH, so the system contained two anions and two forms of the surfactant coexisted. At pH below 11, the water uptake was not affected by the concentration of NaCl; it increased in the range of pH from 11 to 13.5 and then decreased. The effect of pH was higher at low salt concentration and it was negligible at concentrations larger than 0.2 M. At pH above 12, reverse micelles were formed without adding NaCl to the aqueous phase. The NaOH added to fix the pH exchanged the anion with the surfactant and acted as salt that, when in excess, decreased the water uptake. Figure 1.22 shows the effect of the surfactant concentration, at different salt concentrations at pH 13.5, on the water uptake. The salt-free results again correspond to the formation of reverse micelles in the presence of NaOH. The water uptake increases linearly with the

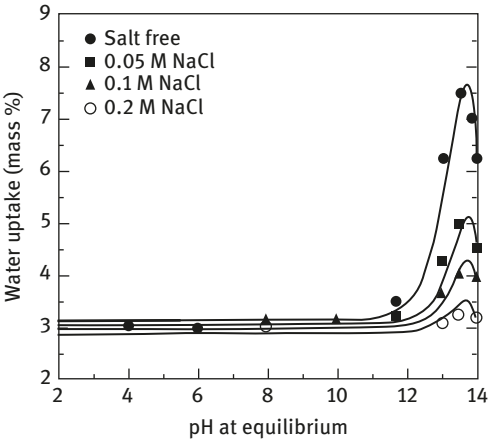

Figure 1.21: Water uptake as a function of equilibrium pH for various initial salt concentrations. Initial organic: 0.1 M DODAC and 0.25 M 1-decanol; initial aqueous: NaCl and NaOH. Reprinted from [27]. Copyright (2017), with permission from Elsevier.

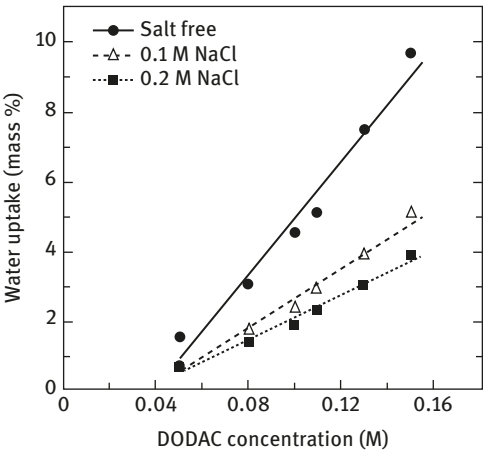

Figure 1.22: Water uptake as a function of surfactant concentration for various initial salt concentrations. Initial organic: DODAC and 0.25 M 1-decanol; initial aqueous: NaCl at pH 13.5, adjusted with NaOH. Reprinted from [27]. Copyright (2017), with permission from Elsevier.

surfactant concentration and the slope of the increase is larger for lower salt concentrations. There is no water uptake for salt concentrations below 0.025 M, independent of the surfactant concentration.

The interesting experimental results obtained in this study of DODAC and DODAB in water decanol isooctane reverse micellar systems were modeled differently of what was done for dinonylnaphtalenesulfonic acid (HD) in Section 1.3. In the case of dinonylnaphtalenesulfonic acid (HD), the reverse micelles had a rather small water uptake, so they were visualized as the heads of the surfactant covered by counterions with a small central water pool. In the case of DODAC and DODAB, on the other hand, the water pool was large enough to consider the ions in aqueous solutions.

As convincingly shown in Figure 1.20, it was considered that there were no cations in the water pool. At this stage, the model was restricted to the case of

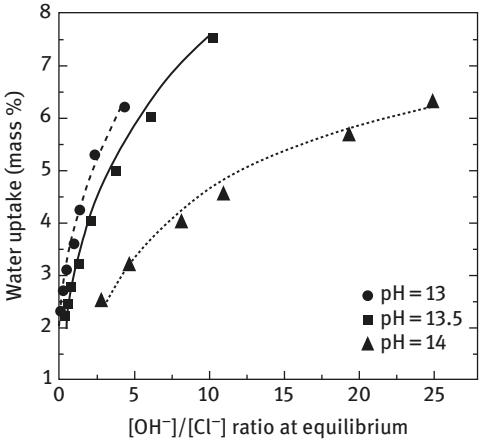

Figure 1.23: Water uptake as a function of $[OH^-]/[Cl^-]$ ratio at equilibrium for various pH. Initial organic: 0.1 M DODAC and 0.25 M 1-decanol; initial aqueous: NaCl and NaOH. Reprinted from [27]. Copyright (2017), with permission from Elsevier.

monovalent anions and considered that the concentration of free anions in the water pool was the same as that in the aqueous phase, so any exchange of anions between the water phase and the water pools did not change the ionic strength of any of the two. This fact was confirmed experimentally. Based on the results shown in Figure 1.22, the water uptake was considered to be a linear function of the concentration of the surfactant in the organic phase. Finally, 1:1 electrolytes are at concentrations below 1.2 M; as in the equilibrium constants the activity coefficients of chloride and the other univalent anion appear always as a ratio, activities were replaced by the molar concentrations of the ions. The detailed algebra is given elsewhere [27] and it will be discussed in Chapter 2. At this point, we only show two results of the model performance. Figure 1.23 compares the predicted (solid lines) and experimental values (points) of the water uptake of DODAC as a function of the equilibrium values of the ratio $[OH^-/Cl^-]$ at different values of pH, while Figure 1.24 compares the prediction of the model (solid lines) with experimental values (points) of the water uptake of DODAC as a function of the equilibrium values of the ratio $[OH^-/Cl^-]$ at different values of surfactant concentrations.

1.8 Effect Volume Ratio and Composition of the Phases on the DODAC Reverse Micellar System Ion Distribution

After obtaining the experimental results for DODAC reverse micellar systems presented above, it was reasonable to ask what would be the effect of changes on the ion distribution in some of the variables that had been kept constant in

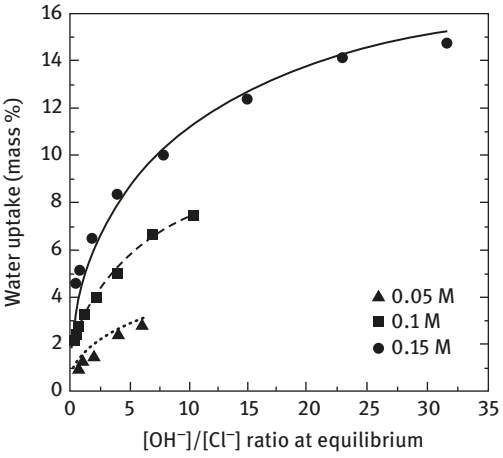

Figure 1.24: Water uptake as a function of $[OH^-]/[Cl^-]$ ratio at equilibrium for various surfactant concentrations. Initial organic: DODAC and 0.25 M 1-decanol; initial aqueous: NaCl at pH 13.5, adjusted with NaOH. Reprinted from [27]. Copyright (2017), with permission from Elsevier.

the previous experiments. These variables were the volume ratio of the two phases, the concentrations of surfactant and alcohol in the organic phase and the concentration of electrolyte in the aqueous phase. Hydroxide and chloride ions were chosen to study the ion distribution. In different experiments either NaCl, NaOH, KOH, or $Ca(OH)_2$ was added to the aqueous phase. The concentrations of the ionic species Cl^-, OH^-, H^+, and either Na^+, K^+, or Ca^{2+}, present in the final aqueous phase were measured. It was found that the concentration of decanol, ranging from 200 mM to 350 mM, had no effect on the ion distribution. Both the results of water uptake and surfactant distribution were insensitive to the nature of the cation present and were function only of the concentration of the OH^- ion in a solution. As expected, the chloride concentration in the aqueous phase and the bound concentration of OH^- in the organic phase increased with the addition of NaOH and tended to a plateau that corresponds to the saturation of the surfactant. As shown in Figure 1.25, these two concentrations fell on a single curve at the conditions of the experiments. The effect of volume ratio and surfactant concentration was better studied as a function of $r[S]^0$, defined as the product of initial volume of the organic phase over the initial volume of the aqueous phase, r, times the initial concentration of surfactant in the organic phase, $[S]^0$. This parameter is more representative of the effective presence of surfactant with respect to the aqueous phase and it was changed either by fixing the initial volume ratio to unity and changing the initial surfactant concentration or by keeping the surfactant concentration at 100 mM and changing the volume ratio. The experimental results in the case of 100 mM NaOH in the initial aqueous phase with and without addition of NaCl are shown in Fig 1.26. The solid lines in Figures 1.25 and 1.26 represent the predictions obtained from a model discussed in Chapter 2.

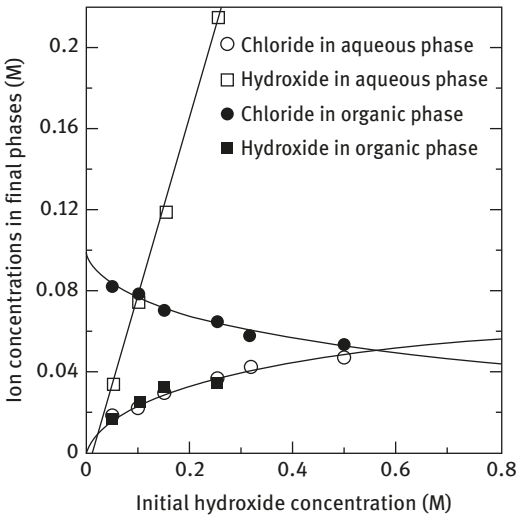

Figure 1.25: Distribution of ions as a function of initial hydroxide concentration. Initial organic phase: 100 mM DODAC and 250 mM decanol; initial aqueous phase: NaOH; initial volume ratio: unity. Solid lines represent the predictions of the model. Reproduced with the permission from [28]. Copyright American Chemical Society 2017.

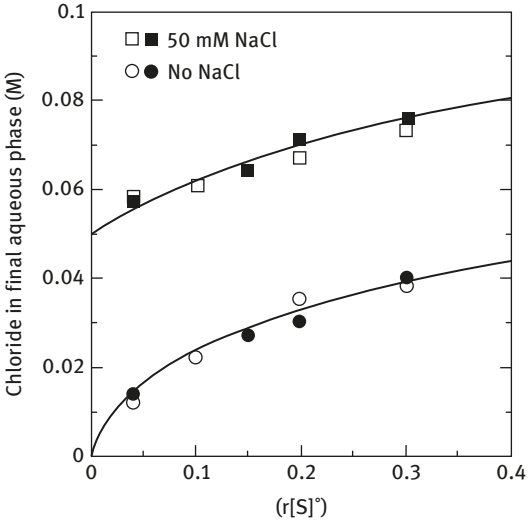

Figure 1.26: Final chloride concentration in the aqueous phase as a function of the ($r[S]^0$) term for different initial NaCl concentrations: initial organic phase: DODAC and 250 mM decanol; initial aqueous phase: NaCl and 100 mM NaOH. The open symbols refer to the variation in surfactant concentration, while the closed symbols refer to the variation in volume ratio. Solid lines represent the predictions of the model. Reproduced with the permission from [28]. Copyright American Chemical Society 2017.

1.9 DODAC Reverse Micellar Systems in Long Linear Alkane Phase with Linear Alcohol Cosurfactants

At the time this work was done [29], it was known that the most used anionic surfactant, sodium bis(2-hexylethyl) sulfosuccinate (AOT), did not form reverse micelles if the organic phase was an unbranched alkane with more than 12 carbon atoms in the hydrocarbon chain [30, 31]. Considering that the branching in the

hydrocarbon chain of alkanes increases their solubility in water while the increase in length of the hydrocarbon chain in unbranched alkanes and alcohols decreases their solubility in water, it was decided to study the formation of reverse micelles of DODAC in an organic phase formed by long-linear-chain alkanes with long-linear-chain alcohols as cosurfactants. Solvents from octane to hexadecane with 1-decanol or 1-dodecanol cosurfactants were used as organic phase. Sodium chloride was used as the electrolyte in the aqueous phase. DODAC formed reverse micelles with all the solvents as organic phase. Figure 1.27 shows the water uptake of DODAC reverse micelles as a function of the carbon chain length of the solvent with decanol cosurfactant and the salt content in the aqueous phase as parameter. Surprisingly, the water uptake increased with solvent chain length. The increase was larger at lower salt concentrations but was still present at high salt concentration. Reverse micelles also formed in all solvents using NAOH instead of NaCl in the aqueous phase and gave higher water uptake than those formed using NaCl. This is clearly an effect of exchange of the anion of the surfactant in the reverse micelles. With all solvents, a slow addition of alcohol to the organic phase in contact with the aqueous phase containing NaCl produced a clear transition from a Winsor I system to a Winsor III system and then to a Winsor II system. This is an experiment that can be performed as demonstration to students using Bardac LF-80, the commercial product containing DODAC in an aqueous solution, as the purity of the surfactant was not a factor in the formation of reverse micelles. The only warning is that although diluted in the commercial product, DODAC is a harmful chemical as noted in the first paragraph of Section 1.6. The effect of the initial concentration of alcohol on the water uptake in

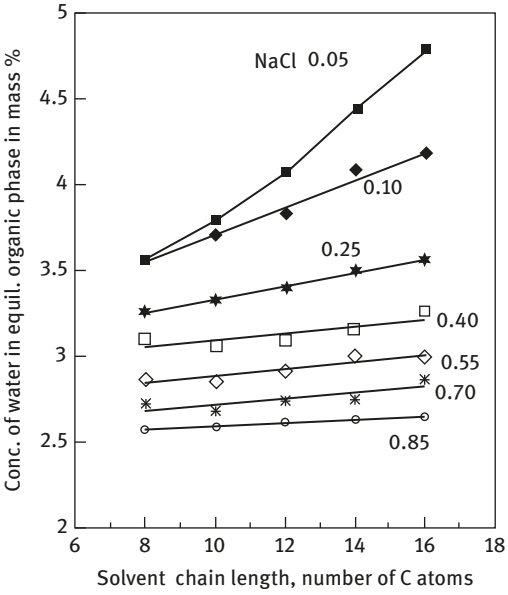

Figure 1.27: Effect of solvent chain length on the equilibrium concentration of water in the organic phase, for different values of the initial aqueous phase concentration of NaCl, in mol·dm^{-3}, at 296.1 K. Initial organic phase: 0.10 mol·dm^{-3} DODAC and 0.25 mol·dm^{-3} 1-decanol; initial aqueous phase: 20 mL of NaCl solution; initial organic phase volume: 20 mL. Reproduced with the permission from [29]. Copyright American Chemical Society 2017.

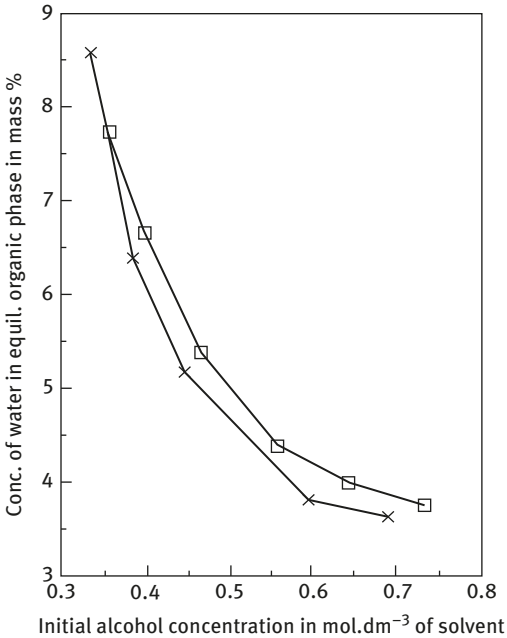

Figure 1.28: Effect of the initial concentration of alcohol on the equilibrium concentration of water in the organic phase at 296.1 K, for two different alcohols: (□) 1-dodecanol and (X) 1-decanol. Solvent: tetradecane; formulation: 20 mL of an aqueous solution of 0.2 in mol·dm^{-3} DODAC and 0.1 in mol·dm^{-3} NaCl plus 20 mL of tetradecane and a variable weight of alcohol. Reproduced with the permission from [29]. Copyright American Chemical Society 2017.

a tetradecane organic phase is shown in Figure 1.28 for two alcohols. There is no water uptake below a minimum concentration of alcohol, at which the water uptake jumps to a high value that decreases at larger concentrations of alcohol. The behavior of reverse micellar systems of DODAC in organic phases of the other long chain normal alkanes was similar. Decane as a solvent produced the larger water uptake with 1-decanol as cosurfactant.

1.10 A Closing Remark Regarding the Review of Preliminary Studies of Reverse Micellar Systems

The experimental studies reexamined in this chapter are now 25 years old. All these results were published in peer-reviewed international journals and the references are given below. Looking in retrospect, it was felt that the knowledge accumulated was dispersed in bits and pieces and it was time to give in a cohesive structure showing the steps of the rational thinking that inspired the pass from one study to the next. The next chapters show the results accumulated since these preliminary studies were performed. An attempt has been made by the different authors to detect literature of more recent years following their steps in each field.

References

[1] By Brenton (talk) – Own work, Public Domain, https://commons.wikimedia.org/w/index.php?curid=61878049
[2] http://www.chemicalbook.com/CASEN_5538-94-3.htm
[3] Winsor PA. Solvent Properties of Amphiphilic Compounds, Butterworth, London, 1954.
[4] Leodidis EB, Hatton TA. J Phys Chem 1991, 95, 5957.
[5] Eike HF. J Colloid Interface Sci 1970, 68, 440.
[6] Ashrafizadeh SN, Demopoulos GP. J Colloid Interface Sci 1995, 173,448.
[7] Leung R, Shah DO. J Colloid Interface Sci 1987, 120, 330.
[8] Rabie HR, Helou D, Weber ME, Vera JH. J Colloid Interface Sci 1997, 189, 208.
[9] Wang W, Weber ME, Vera JH. J Colloid Interface Sci 1994,168, 422.
[10] Kunin R. Ion Exchange and Solvent Extraction, Marcel Dekker, New York, 1973.
[11] Ashrafizadeh SN, Weber ME, Vera JH. Ind Eng Chem Res 1993, 32,125.
[12] Haghtalab A, Vera JH. Can J Chem Eng 1992, 70, 574.
[13] Bromley LA. AIChE J 1973, 19, 313.
[14] Wilson GM. J Am Chem Soc 1964, 86, 127.
[15] Wilczek-Vera G, Vera JH. J Chem Thermodyn 2016, 99, 65.
[16] Wilczek-Vera G, Vera JH. Classical Thermodynamics of Fluid Systems, CRC, Taylor & Francis, Boca Raton, FL, London, NY, 2017.
[17] Khoshkbarchi MK, Vera JH. J Colloid Interface Sci 1995, 170, 562.
[18] Esalah JO, Weber ME, Vera JH. J Colloid Interface Sci 1999, 218, 344.
[19] Paatero E, Sjoblom J. Hydrometallurgy 1990, 25, 231.
[20] Eckwall, P. Colloid Polym Sci 1988, 266, 279.
[21] Laughlin R. The Aqueous Phase Behavior of Surfactants, Academic Press Inc., San Diego, CA, 1994.
[22] Jolivalt C, Minier M, Renon H. J Colloid Interface Sci 1990, 135, 85.
[23] Kreig GA, Hustedt H. Chem Eng Sci 1992, 47, 99.
[24] Brandani G, Giacomo GD. J. Colloid Interface Sci 1993, 28, 411.
[25] https://pubchem.ncbi.nlm.nih.gov/compound/Dimethyldioctylammonium_chloride#section=Synonyms
[26] Laughlin RG, Munyon RL, Burns JL, Coffindafer TW, Talmon Y. J Phys Chem 1990, 96, 374.
[27] Rabie HR, Weber ME, Vera JH. J Colloid Interface Sci 1995, 174, 1.
[28] Rabie RH, Vera JH. Langmuir 1996, 12, 3580.
[29] Zabaloy MS, Vera JH. J Chem Eng Data 1996, 41, 1499.
[30] Ladanowski, C. M Eng Thesis, McGill University, 1991.
[31] Miletti, G. M Eng Thesis, McGill University, 1989.

Hamid R. Rabie

2 Reverse Micellar Studies

2.1 Introduction

Reverse micellar systems are complex ionic surfactant structures with water pools in an organic phase. Compounds present in the original organic and aqueous phases distribute between the two phases in the presence of reverse micelles. The final distribution of the charged molecules or ions and the water uptake into the organic phase have been a focus of widespread research. The first part of this chapter discusses the ion distribution and water uptake of reverse micellar systems and formulates a universal theory of ion distribution for reverse micelles. In the remainder of this chapter, we extend the analysis to the extraction of amino acids and proteins from aqueous solutions into reverse micelles.

Reverse micelles have a major potential of technological and biological importance for a wide range of applications such as oil recovery, lubrication, detergency, catalysis, metal, and biomolecular extraction, or use for probes in immunological processes and drug delivery [1]. However, theoretical models describing such complex systems, based on a better understating of their behavior, are required before we can fully utilize them for industrial applications. Experimental work is important to shed light and orient the formulation of models representing the facts we experience. Thus, we have collected necessary data and developed a comprehensive model to accurately predict the ion distribution and water uptake in reverse micellar systems.

The real breakthrough came when we saw that the anion of a salt does not have any effect on the water uptake of the aerosol OT (AOT) reverse micellar system (an anionic surfactant), as long as all the salts have the same cation (Figure 2.1) [2].

Similar results were found for dioctyldimethyl ammonium chloride (DODAC; a cationic surfactant) for the effect of cations in aqueous solutions. In this case, the cation of a salt does not have any effect on the water uptake of the DODAC reverse micellar system as long as all the salts have the same anion [3] (Figure 2.2).

These results indicated that only the ions that are exchangeable with the surfactant counterion alter the water uptake. This led to the universal theory of ion distribution equilibria for reverse micellar systems [2]. Several binary and ternary systems were studied with different surfactants and salts at different compositions to validate this theory.

https://doi.org/10.1515/9783110564808-002

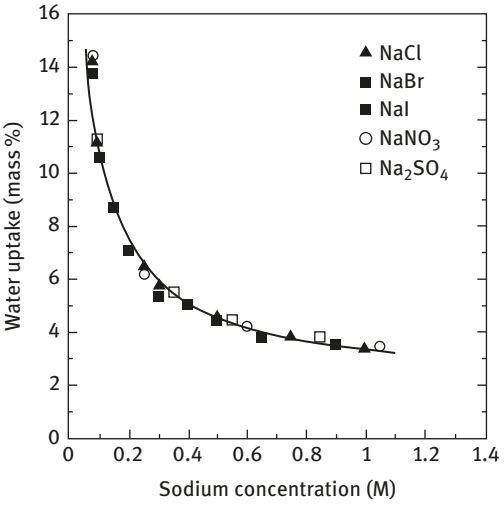

Figure 2.1: Water uptake as a function of initial sodium concentration for salts with different anions; initial organic: 0.1 M AOT; initial aqueous: salt. Reprinted with permission from (Langmuir, 1995, 11, 1162). Copyright (2017) American Chemical Society.

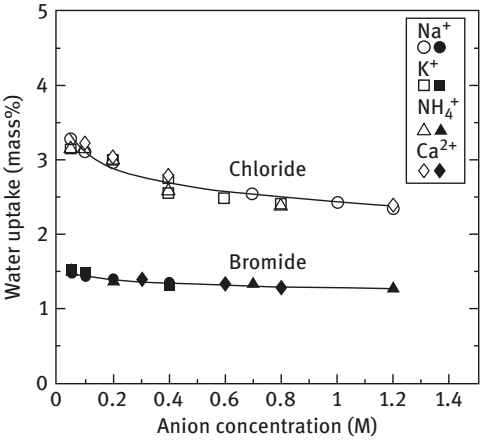

Figure 2.2: Water uptake as a function of initial anion concentration for chloride or bromide salts with different cations; initial organic phase: 0.1 M DODAC or DODAB, 0.25 M decanol; initial aqueous phase: salt; Reprinted with permission from (Journal of Colloid and Interface Science, 1995, 174, 1). Copyright (2017) Elsevier.

2.2 Universal Theory of Ion Distribution in Reverse Micellar Systems

In this work, the extraction of ions from an aqueous phase to the water pools of reverse micelles is modeled using a thermodynamic approach similar to the one used for ion exchange with resins. The detailed treatment can be found in the work by Rabie and Vera [2]. The ions in the excess aqueous phase are extracted into the reverse micellar water pools by solvent extraction. Then, these ions

undergo an ion exchange reaction from the water pools onto the surfactant surface of the reverse micelles. For each counterion, the partitioning of counterions (e.g., cation in the anionic AOT surfactant system) is denoted by a partition coefficient, Λ_i,

$$\Lambda_i = \bar{C}_{i,\mathrm{f}} / \; C_i \tag{2.1}$$

where C_i is the molar concentration of counterion i in the aqueous phase, and $\bar{C}_{i,\mathrm{f}}$ is the molar concentration of the counterion i free in the water pools. The free counterions in the water pools undergo a reaction of ion exchange with the counterions bound to the surfactant head groups. Most of the equations discussed later are provided as an illustration for the case of an anionic surfactant with sodium as counterion. However, similar equations can be applied for any other system. Following Shallcross et al. [4] and Bajpai et al. [5], the ion exchange reaction is given by a reversible reaction:

$$z_i \; S\mathrm{Na} + M_{i,\mathrm{f}}^{z_i^+} \; \rightleftharpoons \; S_{z_i} M_{\mathrm{i}} + z_i \mathrm{Na}_{\mathrm{f}}^{+} \tag{2.2}$$

where the free ion $M_{i,\mathrm{f}}$ in the water pool exchanges the surfactant bound counterion Na^+ in the reverse micelles. In eq. (2.2), z_i is the charge number of ion M_i and subscript "f" refers to the free ions present inside the water pool. The equilibrium constant for this reaction, $K_{\mathrm{Na}}^{\mathrm{i}}$, can be represented in terms of molar concentrations of cation i and sodium denoted as $\bar{C}_{i,\mathrm{b}}$ and $\bar{C}_{\mathrm{Na,b}}$, respectively, bound to the surfactant. The concentrations of free cation i and sodium in the water pool are denoted as $\bar{C}_{i,\mathrm{f}}$ and $\bar{C}_{\mathrm{Na,f}}$, respectively:

$$K_{\mathrm{Na}}^{i} = \left(\frac{\bar{C}_{i,\mathrm{b}}}{\bar{C}_{i,\mathrm{f}}}\right)\left(\frac{\bar{C}_{\mathrm{Na,f}}}{\bar{C}_{\mathrm{Na,b}}}\right)^{z_i} \tag{2.3}$$

Equations (2.2) and (2.3) are written for an anionic surfactant. However, they can be directly used for cationic surfactants as well. In a ternary surfactant counterion system, the three equilibrium constants must satisfy the so-called triangular relation [5] of the form

$$(K_j^i)^{z_{\mathrm{r}}} (K_{\mathrm{r}}^j)^{z_i} (K_i^{\mathrm{r}})^{z_j} = 1 \tag{2.4}$$

Combining eqs. (2.1) and (2.3) results in

$$K_{\mathrm{sNa}}^{\mathrm{i}} = \left(\frac{\bar{C}_{i,\mathrm{b}}}{C_i}\right)\left(\frac{C_{\mathrm{Na}}}{\bar{C}_{\mathrm{Na,b}}}\right)^{z_i} \tag{2.5}$$

Equation (2.6) describes an ion exchange reaction between the cations in the excess aqueous phase and sodium of the surfactant in the organic phase with equilibrium constant K^{i}_{sNa}, denoted by

$$K^{i}_{sNa} = K^{i}_{Na} \frac{\Lambda_i}{\Lambda^{z_i}_{Na}} \tag{2.6}$$

We use the basic assumptions of electroneutrality [7] and monodispersity [7] of the reverse micelles. For the mass balances on the anionic surfactant and cations, the experimental conditions are defined as follows. In the initial state, an aqueous phase of volume V^0 containing H_2O, n different cations with concentrations C^0_i, including Na^+, and chloride anion with concentration $C^0_{Cl^-}$ is contacted with an organic phase of volume $\bar{V}^0$ containing isooctane and surfactant with concentration $\bar{C}^0_S$.

In the final state (at equilibrium), the aqueous phase will have volume V containing surfactant, cations, and chloride anion at concentrations of C_s, C_i, and C_{Cl^-}, respectively. The organic phase has volume $\bar{V}$ containing isooctane, surfactant ($\bar{C}_s$), free cations ($\bar{C}_{i,f}$), bound cations ($\bar{C}_{i,b}$), chloride anion ($\bar{C}_{Cl^-}$), and H_2O in reverse micelles.

The concentrations of free ions in the organic phase are defined as moles of counterion per unit volume of water pool, while the concentrations of surfactant and bound counterions in the organic phase are defined as moles of surfactant or bound ions per unit volume of organic phase. We need to make a clear distinction here about the definitions of concentrations of bound counterions and surfactant in the organic phase. In our earlier work [2], we used the total organic phase volume as the basis for these concentrations. The work done by Rabie and Vera [2] uses this definition, which is the main topic of this section. However, as we gathered more results, we recognized that this definition of concentrations in organic phase at higher water uptake reduces the accuracy of the universal theory of ion distribution. As such, we reported this finding in the work by Rabie and Vera [3] and provided updated equations to account for it. In the updated version, we used the water-free organic phase volume for the concentrations of surfactant and bound counterions.

The basic equations remain the same with the same calculation method, except for some minor changes detailed later. Thus, here we provide the second versions of such equations based on the water-free organic phase volume where it applies. The mass balances for sodium is then represented as

$$VC_{Na} + \bar{V}\bar{C}_{Na,b} + w\bar{V}\bar{C}_{Na,f} = V^0 C^0_{Na} + \bar{V}^0 \bar{C}^0_S \tag{2.7a}$$

where w is the volume ratio of water in the organic phase at equilibrium and it is only a function of the ion concentrations at equilibrium. The same equation based on the bound counterion concentration in the water-free organic phase volume is

$$VC_{\mathrm{Na}} + \bar{V}^0\bar{C}_{\mathrm{Na,b}} + w\bar{V}\bar{C}_{\mathrm{Na,f}} = V^0C^0_{\mathrm{Na}} + \bar{V}^0\bar{C}^0_{\mathrm{S}} \tag{2.7b}$$

For each of the other cations present in the initial aqueous phase, we can write

$$VC_i + \bar{V}\bar{C}_{i,\mathrm{b}} + w\bar{V}\bar{C}_{i,\mathrm{f}} = V^0C^0_i \tag{2.8a}$$

and similarly, the same equation based on the bound counterion concentration in the water-free organic phase volume is

$$VC_i + \bar{V}^0\bar{C}_{i,\mathrm{b}} + w\bar{V}\bar{C}_{i,\mathrm{f}} = V^0C^0_i \tag{2.8b}$$

Note that in eq. (2.5), it is assumed that the surfactant solubilized in the aqueous phase is completely dissociated. Assuming that in reverse micelles all the surfactant sites are filled with either sodium or other cations, we can write

$$\bar{V}\bar{C}_{\mathrm{Na,b}} + \bar{V}\sum\nolimits_{i=1}^{(n-1)}(z_i\bar{C}_{i,\mathrm{b}}) + \ VC_{\mathrm{s}} = \bar{V}^0\bar{C}^0_{\mathrm{S}} \tag{2.9a}$$

The same equation based on the bound counterion concentration in the water-free organic phase volume is then formulated as

$$\bar{V}^0\bar{C}_{\mathrm{Na,b}} + \bar{V}^0\sum\nolimits_{i=1}^{(n-1)}(z_i\bar{C}_{i,\mathrm{b}}) + VC_{\mathrm{s}} = \bar{V}^0\bar{C}^0_{\mathrm{S}} \tag{2.9b}$$

Equations (2.9a) and (2.9b) assume that all the surfactant in the oil phase is found in the reverse micellar interface. Based on the results of Aveyard et al. [6] and Rabie and Vera [2], this is a reasonable assumption for the AOT surfactant at the salt concentrations studied in this work.

The partition coefficient of AOT between the oil and the water phases was measured with a surfactant electrode as described by Rabie and Vera [2]. In all cases, the fraction of AOT in the bulk water was less than 1%. Similar results have been found by other workers [7, 8]. Therefore, we can assume that the concentration of AOT surfactant in the aqueous phase at equilibrium is zero ($C_{\mathrm{s}} = 0$). This will then simplify the mass balances on surfactant (eqs. 2.9a and 2.9b). In case of water-free organic phase volume basis for bound counterions, the equation is reduced to

$$\sum\nolimits_{i=1}^{n}(z_i\bar{C}_{i,\mathrm{b}}) = \ \bar{C}^0_{\mathrm{S}} \tag{2.9c}$$

Since the organic solvents are insoluble in the aqueous phase, the only source volume change in the organic or aqueous phase is the solubilized water in the reverse micelles. Thus, the relationship between the initial and final volumes of each phase can be written as

$$V^0 - V = \bar{V} - \bar{V}^0 = w\bar{V} \tag{2.10}$$

where w is the volume fraction of water in organic phase at equilibrium. Combining eqs. (2.7)–(2.10) results in a useful relation between the initial and equilibrium concentrations of ions in the aqueous solution:

$$\sum_{i=1}^{n}(\Lambda_i' z_i C_i) = \sum_{i=1}^{n}(z_i C_i^0) \tag{2.11}$$

The term Λ_i' in eq. (2.11) is defined by the following equation:

$$\Lambda_i' = 1 + \frac{wr}{1-w}(\Lambda_i - 1) \tag{2.12}$$

with "r" is defined as the initial volume ratio of the organic to the aqueous phase

$$r = \bar{V}^0 / V^0 \tag{2.13}$$

The value of Λ_i' is unity either when water uptake is close to zero or when the value of Λ_i is unity. Following Leodidis and Hatton [7], we can apply the following ratios of equivalents to describe the final and initial conditions in the system:

$$R_i = C_{\mathrm{Na}} / z_i C_i \tag{2.14a}$$

$$R_i^0 = C_{\mathrm{Na}}^0 / z_i C_i^0 \tag{2.14b}$$

$$\delta = \frac{\bar{V}^0 \bar{C}_{\mathrm{S}}^0}{V^0 \sum_{i=1}^{(n-1)}(z_i C_i^0)} \tag{2.15}$$

It is important to note that when no NaCl is added to the initial aqueous phase; R_i^0 and $(1/\delta)$ are equal to zero. However, the value of R_i will not be zero as sodium is the original counterion of the surfactant and it can exchange with other cations present in the initial aqueous phase.

When the values of R_i for all cations are known, the following equations, obtained by combining eq. (2.11) and the mass balance of a particular ion, are be used to calculate its concentration in the aqueous and organic phases at equilibrium:

$$z_i C_i = \frac{\sum_{j=1}^{n}(z_i C_i^0)}{\sum_{j=1}^{n}(\Lambda_j' \frac{R_i}{R_j})} \tag{2.16}$$

Equation (2.16) stands for any cation including sodium. For all cations, excluding sodium, the concentration of bound cations in the organic phase can be calculated from the following equation:

$$\bar{C}_{i,\mathrm{b}} = \frac{C_i^0 - \Lambda_i' C_i}{r/(1-w)} \tag{2.17}$$

The concentration of bound sodium in organic phase is determined from the following equation:

$$\bar{C}_{\mathrm{Na,b}} = \frac{C_{\mathrm{Na}}^0 - \Lambda_{\mathrm{Na}}' C_{\mathrm{Na}} + r\bar{C}_{\mathrm{S}}^0}{r/(1-w)} \tag{2.18}$$

The concentrations of free cations in the organic phase are found from eqs. (2.1) and (2.16).

Leodidis and Hatton [7] experimentally found that in a system of AOT and $M\mathrm{Cl}_z$, the ratio δ was the most suitable parameter to determine the behavior of the cation liquid–liquid extraction. In their system, no NaCl was initially present in the aqueous phase, and as such, the R^0 parameter was zero. When they plotted R_i, the ratio of sodium to cation concentration in the final aqueous solution against the parameter δ, the data of three different experimental results collapsed onto a single plot.

They did not provide any explanation for this interesting behavior. As discussed later, the solution of eqs. (2.1), (2.5), and (2.7)–(2.10) provides a simple correlation between the initial and the equilibrium conditions of the system, which explains the findings of Leodidis and Hatton [7]. For the cases of a binary counterion system, for example, NaCl and one other electrolyte $M\mathrm{Cl}_{z1}$ for AOT, and a ternary counterion system, for example, NaCl and two other electrolytes $M\mathrm{Cl}_{z1}$ and $M\mathrm{Cl}_{z2}$, for AOT, an analytical solution can be obtained from the above equations.

The final expressions are given below. It is important to note that these expressions are written for AOT reverse micellar system. However, the same equations can be used for all other anionic or cationic surfactants if the sodium, other cations added to the aqueous phase, and the anion are replaced by the original surfactant counterion, by the other surfactant counterions added to the aqueous phase, and by the surfactant coion, respectively.

2.2.1 Binary Counterion Systems

For a binary counterion system, the analytical solution is written as

$$K_{\mathrm{s}}^i = \left(\frac{r}{\Lambda_{\mathrm{Na}}'(1-w)}\right)^{(z_i-1)} \frac{\left(R_i - \frac{\Lambda_i'}{\Lambda_{\mathrm{Na}}'} R_i^0\right)\left(1 + R_i^0\right)^{(z_i-1)} R_i^{z_i}}{\left(\delta\left(\frac{\Lambda_i'}{\Lambda_{\mathrm{Na}}'} + R_i\right) - R_i + \frac{\Lambda_i'}{\Lambda_{\mathrm{Na}}'} R_i^0\right)^{z_i}} \tag{2.19}$$

where K^i_{sNa} has been replaced by K^i_s for simplicity. The relationship between R_i and δ for two limits of δ, infinity and zero, can be written as

$$\delta \to \infty \quad R_i = K^i_s \left(\frac{r(1 + R^0_i)}{\Lambda'_{Na}(1-w)} \right)^{(1-z_i)} \delta^{z_i} \tag{2.20a}$$

and

$$\delta \to 0 \quad R_i = \frac{\Lambda'_i}{\Lambda'_{Na}} R^0_i \tag{2.20b}$$

Equation (2.19) combined with an equation for the water uptake as a function of equilibrium concentrations of the ions can be used to calculate the distribution of ions and the water uptake. However, in most cases, the water uptake is small enough, so the change in the volumes of the organic and the aqueous phases, from the initial and the equilibrium states, can be ignored. Therefore, the volumes of aqueous and organic phases are assumed to be constant and denoted by V and $\bar{V}$, respectively.

Since the volume of organic phase is considered to be constant, the concentration of surfactant in the organic phase stays at its initial value, denoted by $\bar{C}^0_S$. As described in eq. (2.12), the assumption of small w gives Λ_i' close to unity. For monovalent cations under these assumptions, eq. (2.19) can be solved for R_i to give

$$2R_i = R^0_i + K^i_s(\delta - 1) + \sqrt{\left(R^0_i + K^i_s(\delta - 1)\right)^2 + 4K^i_s\left(R^0_i + \delta\right)} \tag{2.21}$$

We note that for monovalent salts eq. (2.21) is valid for any value of water uptake if the values of Λ_i for sodium and for the other cation are the same. Equation (2.21) shows that the ratio of equilibrium equivalents of sodium to another cation in the final aqueous phase is only a function of the R^0_i and δ parameters. As long as the R^0_i and δ parameters are fixed, no matter how the experiments are carried out by, for example, changing the initial concentration of salts in the aqueous solution, changing the surfactant concentration in the organic phase, or changing the volume ratio of the two phases in contact, the value of R_i ratio remains the same.

It is important to note that for these systems, the effect of four independent variables (initial concentrations of surfactant, NaCl and $M\mathrm{Cl}_{zi}$, and volume ratio of the two phases) can be determined by only two dimensionless groups and one constant. When the initial concentration of NaCl is zero, the number of parameters is reduced to one, δ. This was the case studied by Leodidis and Hatton [7].

The above analysis also shows that a single data point can be used to determine the value of the equilibrium constant. For a binary system containing $M\mathrm{Cl}_{zi}$ and having zero initial concentration of NaCl, that is, $R^0_i = 0$, when the values of δ and

volume ratio r are unity, the equilibrium constant of cation M^{z_i+} with sodium is written as

$$K_s^i = (R_i)^{(z_i+1)} \quad \text{at} \quad \delta = 1; \quad r = 1; \quad R_i^0 = 0 \tag{2.22}$$

Thus, the experimental measurement of R_i for one point determines with the values of K_s^i valid for all other conditions.

2.2.2 Ternary Counterion Systems

In a ternary system, having three cations when no NaCl is initially added, to the aqueous phase, two equations are simultaneously solved to find the distribution of ions in the final aqueous solution. These two equations relate the R ratios of the two cations:

$$K_s^1 = \left(\frac{r}{(1-w)}\right)^{(z_1-1)} \frac{\left(\frac{R_1\Lambda_2' + R_2\Lambda_1' + R_1R_2\Lambda_{Na}'}{R_1(1+f)} - \Lambda_1'\right)}{\left(\frac{\delta\left(R_1\Lambda_2' + R_2\Lambda_1' + R_1R_2\Lambda_{Na}'\right)}{R_1R_2} - \Lambda_{Na}'\right)^{z_1}} \tag{2.23}$$

$$K_s^2 = \left(\frac{r}{(1-w)}\right)^{(z_2-1)} \frac{\left(\frac{f\left(R_1\Lambda_2' + R_2\Lambda_1' + R_1R_2\Lambda_{Na}'\right)}{R_1(1+f)} - \Lambda_2'\right)}{\left(\frac{\delta\left(R_1\Lambda_2' + R_2\Lambda_1' + R_1R_2\Lambda_{Na}'\right)}{R_1R_2} - \Lambda_{Na}'\right)^{z_2}} \tag{2.24}$$

In these equations, the subscripts or superscripts 1 and 2 refer to the cations 1 and 2, respectively, and f is defined by the following equation:

$$f = z_2\ C_2^0 /\ z_1\ C_1^0 \tag{2.25}$$

Both R_2 and R_1 are zero when δ is zero, but their ratio, $R_2/R_1 = C_1/C_2$ is equal to $1/f$. At large values of δ, this ratio is written as

$$\frac{R_2}{R_1} = \frac{K_2}{K_1 f}\left(\frac{r\delta}{\Lambda_{Na}'(1-w)}\right)^{(z_1-z_2)} \tag{2.26}$$

It is important to note that, when both cations have the same charge number, this ratio is independent of δ, r, and water uptake. When water uptake is negligible, the values of Λ' are almost unity. The values of the equilibrium constants can be determined from the data for binary counterion systems as shown by eq. (21) and then the same values are used to predict the ion distributions for different conditions of a ternary system.

2.2.3 Results and Discussion for Universal Theory of Ion Distribution in Reverse Micellar Systems

The work published by Rabie and Vera [2] contains extensive experimental results for binary and ternary systems under various conditions that are compared with the predictions of the model. This section shows some of those results and highlighting the key findings and conclusions. The universal ion distribution theory accurately represents the experimental results and explains different experimental findings.

1. The model uses one single parameter for each counterion. This parameter, which depends only on the nature of the counterion (charge, hydrated size, and electrostatic free energy of hydration), is the equilibrium constant of the ion exchange between the counterion in aqueous phase and the original counterion that is bound to the surfactant head group.
2. This parameter is determined from a single data point in a binary system of the original surfactant counterion and the other counterion added to the system.
3. The equilibrium constant found from a single data point in a binary counterion system is used for the prediction of multicomponent systems.
4. This mathematical model is in excellent agreement with experimental results and provides better correlation and predictions than other phenomenological models.
5. Dimensionless groups are defined to regroup several independent variables. These dimensionless form of the mode, with few dimensionless groups rather than many independent variables, has definite advantages for treatment of such complex systems.
6. This model is based on the mathematical assumption that all surfactant head groups are bound to cations present in the water pool or, in another words, the surfactant is not dissociated. In reality, a part of the surfactant is dissociated, and its dissociation fraction can be calculated as discussed in Section 2.3. However, as shown in the same section, surfactant dissociation has no impact on the overall ion distribution. This means that the universal ion Distribution theory can predict the ion distribution accurately with or without considerations for surfactant dissociation.

In these experiments, the value of δ is changed in the following ways: (i) by changing the initial concentration of salt while the initial AOT and NaCl concentrations was kept constant with the volume ratio r, set at unit; (ii) by changing the initial AOT concentration in the organic phase, while the initial salt concentration in the aqueous phase was kept constant with the volume ratio set at unity; and (iii) by changing the volume ratio, while keeping the initial AOT concentration in the organic phase and the initial salt concentration in the aqueous phase constant.

Figure 2.3 shows that when the initial NaCl concentration in the aqueous phase is zero, the ratio of sodium to potassium concentration in the final aqueous phase is plotted against the parameter δ; the data of three different experimental results

collapse onto a single line. The solid line shows predictions of the model (eq. 2.20) with K_s equal to 1.96. The equilibrium constant was obtained from a single data point using eq. (2.22). Such a plot is called a universal curve [7], and Rabie and Vera [2] showed for the first time the reason for existence of such universal curve. The universal curve for potassium asymptotically approaches the "uniform distribution" or "no selectivity" curve at low values of δ.

Similar results have been obtained for various initial NaCl to KCl concentration, R^0, in aqueous phase. The universal distribution curve for calcium, a divalent cation, is shown in Figure 2.4, with zero initial NaCl concentration in the aqueous phase, $R_i^0 = 0$, and the volume ratio, r, equal to unity. The solid line shows the predictions of the model

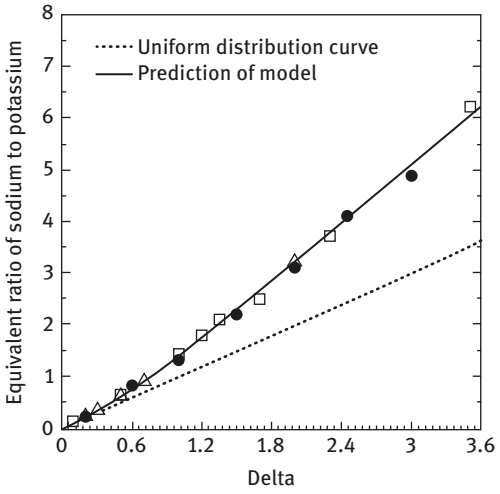

Figure 2.3: Universal curve for potassium. Equivalent ratio of sodium to potassium at equilibrium in the aqueous phase vs δ parameter with variation of KCl concentration (▯), of surfactant concentration (●), and with the phase volume ratio (Δ). Reprinted with permission from (Langmuir, 1995, 11, 1162). Copyright (2017) American Chemical Society.

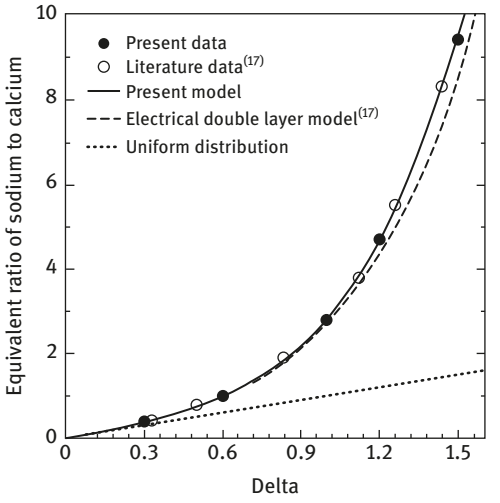

Figure 2.4: Universal curve for calcium (equivalent ratio of sodium to calcium at equilibrium in the aqueous phase vs δ parameter) for initial volume ratio set at unity. Comparison of the predictions of the present model and the predictions of the electrical double layer. Reprinted with permission from (Langmuir, 1995, 11, 1162). Copyright (2017) American Chemical Society.

(eq. 2.19), and the dotted line shows the predictions obtained by the electrical double layer model [7]. The model proposed here shows a better agreement with the experimental results even at higher values of δ. As shown by eq. (2.19), for cations with a charge number unity, R is also a function of the initial volume ratio.

Rabie and Vera [2] also reported the universal curves for calcium at various initial volume ratios and zero initial NaCl concentration in aqueous phase. As accurately predicted by the model, we see that the effect of volume ratio tends to become insignificant at lower values of δ. Leodidis and Hatton [7] did not observe this effect since they changed the volume ratio working with low values of δ where the effect is less noticeable.

Similar results have been obtained for different salts. The equilibrium constants for some monovalent and divalent cations are listed in Table 2.1. For more discussion, this table also gives the values for τ_i (size parameter of ion i) and A_i (ionic parameter). The equations for calculations of these two parameters are provided elsewhere [7]. The values of the electrostatic free energy change upon moving an ion from vacuum to a solvent of dielectric ε, and the hydrated radius of ion (which were used for calculation of A_i and τ_i, respectively) were calculated from the same sources [9, 10] used by Leodidis and Hatton [7].

For all cations studied here, the agreement between the experimental results and the predictions of the model based on a single value of the equilibrium constant was within 0.5–2.0%. Cations with larger equilibrium constants are preferentially extracted into the water pools. Divalent cations have larger values of the equilibrium constant when compared to monovalent cations as a result of the stronger electrostatic interactions.

On the other hand, monovalent cations with the same hydrated size (K^+, Rb^+, and Cs^+) have almost the same equilibrium constant, while the divalent cations with the same hydrated size (Ca^{2+}, Sr^{2+}, and Ba^{2+}) have significantly different equilibrium constants. This is because of the difference in the hydration free

Table 2.1: Values of equilibrium constants for eq. (5) and of the size and ionic parameters [2].

	K_s^i	τ_i	A_i (kcal/mol)
Na^+	1.00	4.0	99.6
K^+	1.96	3.2	81.6
Rb^+	2.08	3.1	76.5
Cs^+	2.13	3.1	68.7
Ca^{2+}	21.9	6.0	384.4
Sr^{2+}	32.6	6.0	344.1
Ba^{2+}	62.3	5.8	318.1
Zn^{2+}	8.76	6.8	489.6
Cu^{2+}	0.15	6.5	502.7

energy [7]. As shown in Table 2.1, it is important to note that within the cations with the same charge number, decreasing the τ_i or A_i increases the equilibrium constant.

The ternary counterion system of sodium–calcium–zinc was studied to check the predictive capabilities of the theory. The experimental results were obtained for zero initial NaCl concentration in the aqueous phase and a volume ratio set at unity, $r = 1$. Figure 2.5 shows the R_{Ca}, equivalent ratio of sodium to calcium, as a function of δ for various initial salt equivalent ratios, f. Similar results were obtained for zinc. The values of equilibrium constants, found from a single binary data point, were used to predict the behavior of the ternary system as shown by the solid lines in Figures 2.5 and 2.6. The agreement between the experimental data and the results of the theory is excellent. The experiments were performed by changing: (i) the initial surfactant concentration; (ii) the initial $CaCl_2$ concentration; and (iii) the initial $ZnCl_2$ concentration.

The equivalent ratio of calcium to zinc (R_{Zn}/R_{Ca}) data at equilibrium are plotted against δ for various values of f in Figure 2.6. As shown, this ratio decreases from its initial value, $1/f$, and then stays constant at higher values of δ for any values of f. As explained in eq. (2.26), since calcium and zinc have the same charge numbers, the upper limit of this ratio is equal to K_{Zn}/fK_{Ca}. The experimental results show the same limiting values for large values of δ.

Figure 2.7 illustrates a comparison between the predictions of the present model and the Gibbs excess model [10, 11]. In this figure, the data of molar excess ratio of calcium to zinc in the organic phase, are shown as a function of the equilibrium mole fraction of zinc in the aqueous phase. The predictions of the model are in good agreement with the experimental results while the Gibbs excess model underpredicts the data.

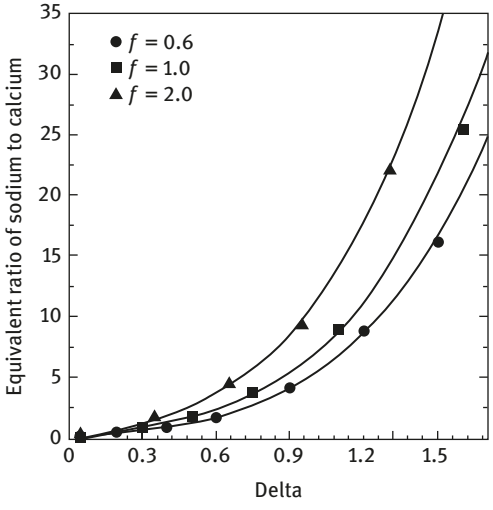

Figure 2.5: Equivalent ratio of sodium to calcium at equilibrium in the aqueous phase vs δ parameter for different ratio of zinc to calcium in the aqueous phase. Reprinted with permission from (Langmuir, 1995, 11, 1162). Copyright (2017) American Chemical Society.

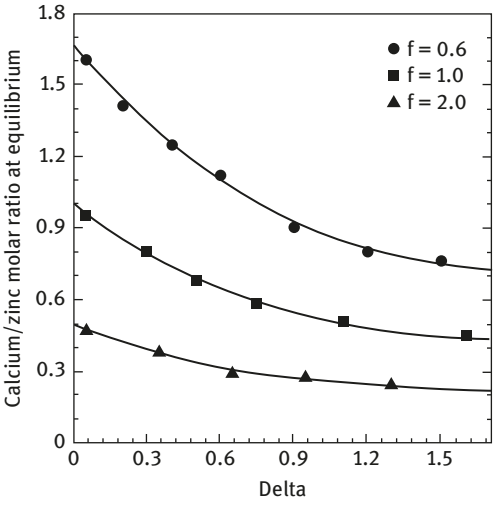

Figure 2.6: Equivalent ratio of calcium to zinc at equilibrium in the aqueous phase vs δ parameter for different initial equivalent ratio of zinc to calcium in the aqueous phase. Reprinted with permission from (Langmuir, 1995, 11, 1162). Copyright (2017) American Chemical Society.

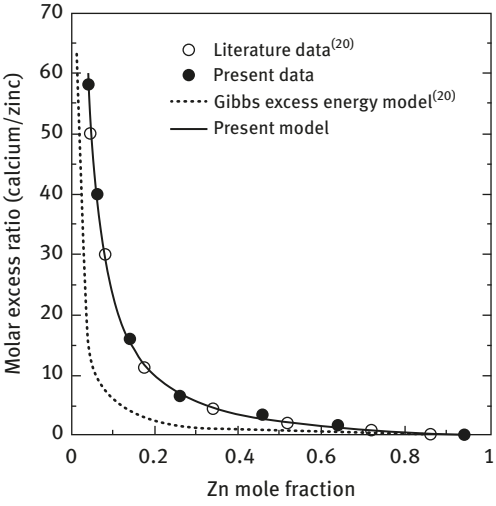

Figure 2.7: Equivalent ratio of calcium to zinc at equilibrium in the organic phase vs the mole fraction of zinc at the equilibrium in the aqueous phase. Comparison of the predictions of the present model and the Gibbs excess energy model. Reprinted with permission from (Langmuir, 1995, 11, 1162). Copyright (2017) American Chemical Society.

2.3 Dissociation Fraction of Surfactant and Counterion Binding

In the previous section, we showed the mechanism of ion distribution and identified the main driving forces for extraction. We found that ion exchange reactions between the surfactant counterion and the other counterion present in the system, through the

addition of salts, are the most important aspect to the explanation of the solubilization of ions. This ion exchange reaction changes the nature of the surfactant counterion. The accuracy of the results obtained with dimensionless form of the model shows that the model is physically meaningful. It has also been observed that changing the nature of surfactant counterion has a significant effect on water uptake [3, 7, 12, 13].

Surfactant molecules are able to dissociate at the reverse micellar interface producing a surface charge density at the inner core of the reverse micelles. The experimental results of Wong et al. [14] for the system of AOT–heptane–water–NaCl have shown that as much as 28% of sodium was dissociated from the AOT head groups in the largest water pool of their study corresponding to 6 wt% of water in the organic phase. The calculated values for the fraction of surfactant dissociated change between 20% and 35% [7, 15–17]. However, it is important to note that the dissociation fraction is greatly influenced by the counterion of the surfactant [7].

In this section, we present a mathematical model to predict surfactant dissociation fraction in the reverse micelles for different conditions of surfactant concentration, and salt type and concentration, in mixed salt systems. We will also show that surfactant dissociation fraction has no impact on the overall ion distribution between the two phases. In addition, the ion distribution calculations can be done, as given by the universal ion distribution theory discussed in Section 2.2, assuming that all surfactant molecules at the reverse micellar interface are bound to either the original surfactant counterion or other counterions.

In the next section, we present how the degree of dissociation can affect the water uptake, and a mathematical model is shown to predict the water uptake. The details for experimental procedures and materials can be found elsewhere [2, 18].

2.3.1 Modeling Based on Active Interface Theory

There are basically four distinct regions in the reverse micellar systems where a solute can be solubilized. These are (i) the organic phase continuum, (ii) the interface of the surfactant hydrophilic groups and the water pool in the reverse micelles, (iii) the water pool inside the reverse micelles, and (iv) the excess aqueous phase. These regions are shown in Figure 2.8.

In the following equations, a notation with a bar represents the organic phase even though the solute may be localized in any of the first three regions, while a notation without bar represents the excess aqueous phase. The notations are basically similar to those given in Section 2.2 and are not repeated here. Salts and many other solutes such as amino acids are basically insoluble in the organic phase. Therefore, we only consider the last three regions. Here we make the assumption that all the surfactant molecules are aggregated. The conditions where this assumption is valid are discussed elsewhere [19]. The partitioning of any species is

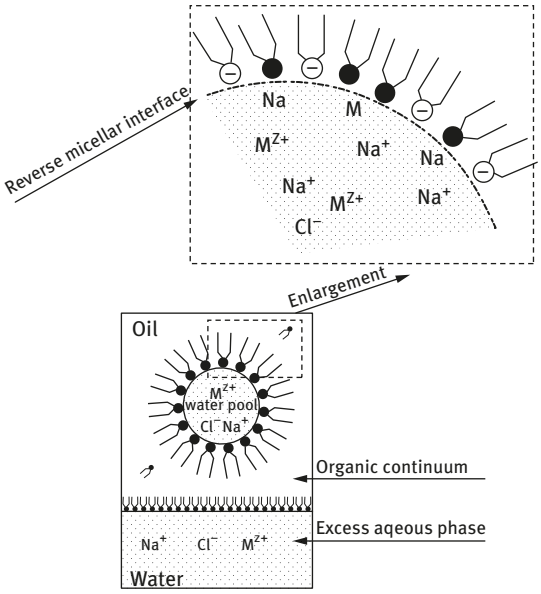

Figure 2.8: Solubilization sites according to the active interface model (the Na group is the sodium salt of the AOT surfactant). Reprinted with permission from (J. Phys. Chem. B, 1997, 101, 10295). Copyright (2017) American Chemical Society.

considered to happen from excess aqueous phase to the water pool and from water pool to the reverse micellar interface.

For the water pool of the reverse micelle, the partitioning of any solute from an excess aqueous phase to the water pool of the reverse micelles is shown by a partition coefficient Λ:

$$\Lambda = \bar{C}_f / C \tag{2.27}$$

where C is molar concentration of a solute, such as salt, in the aqueous phase and $\bar{C}_f$ is the molar concentration of the same solute in the water pool. Equation (2.27), which results from phase equilibrium consideration, assumes that the ratio of the activity coefficients i is insensitive to changes in the equilibrium conditions, and it can be used in the partition coefficient. It has been shown before that the partition coefficient of solute can be assumed to be unity, even for very low water uptake [2, 20].

To test the model for binding of counterions and surfactant dissociation fraction, we used the sodium (or potassium) bis(2-ethylhexyl) sulfosuccinate (AOT)–water-in-oil microemulsion system in contact with an aqueous phase containing (n–1) chloride salts in addition to NaCl. As the coion of a surfactant has no significant impact on the ion distribution [2] of a surfactant and on the water uptake [2, 12, 17], we use chloride salts of all surfactant counterions. The initial and final conditions of the system are the same as described in Section 2.2.

In the case of an anionic surfactant, the anions cannot interact with the reverse micellar interface because of the strong repulsive forces, and they are mainly in the

water pools of the reverse micelles in equilibrium with the excess aqueous phase (Winsor II system). Therefore, the assumption that Λ is unity for any solute results in

$$\bar{C}_{\mathrm{Cl,f}} = C_{\mathrm{Cl}} \tag{2.28}$$

The other implication of this assumption is that the extraction of solutes into a freshly formed water pool does not have any impact on the final concentrations of solutes in the excess aqueous phase, and as such, it does not affect the overall ion distribution. In this model, the concentrations of the surfactant and the bound ions in the organic phase are defined as moles of surfactant or bound ion per unit volume of water-free organic phase. This volume is the same as the initial organic phase volume, due to the fact that the solubility of organic solvent in water is very small. It has been observed that the fraction of AOT in the bulk water, at equilibrium, is always less than 1% [2, 6], and as such the concentration of surfactant in the organic phase at equilibrium can be assumed to be the same as its initial value, $\bar{C}_{\mathrm{S}} = \bar{C}^{0}_{\mathrm{S}}$.

This definition of concentrations in organic phase are different from that given in Section 2.2 and is used for simplicity. This has no impact on the final results. There are several equations that are similar to those from Section 2.2 and we make reference to them when needed. When our new definition of concentration in organic phase results in a change of any equation, we show the new version here. The relation between initial and the final volumes of each phase can be obtained from eq. (2.10).

2.3.2 Dissociation Fraction in a Single-Counterion System

First, we analyze a simple system that contains only one counterion: AOT–heptane–water–NaCl. The counterion of such system is sodium. The dissociation reaction of surfactant can be shown as

$$S\mathrm{Na} \rightleftharpoons S^{-} + \mathrm{Na}^{+} \tag{2.29}$$

with the equilibrium constant in terms of concentrations:

$$K_{\mathrm{d}}^{\mathrm{Na}} = \frac{\bar{C}_{\mathrm{ds}}\ \bar{C}_{\mathrm{Na,f}}}{\bar{C}_{\mathrm{Na,b}}} \tag{2.30}$$

$K_{\mathrm{d}}^{\mathrm{Na}}$ is not a thermodynamic equilibrium constant, since it is defined in terms of concentrations instead of activities. The activity coefficients of the species involved in this reaction are included in $K_{\mathrm{d}}^{\mathrm{Na}}$. The same consideration is used for other equilibrium constants. The mass balance of sodium is shown in eq. (2.7), but it needs to be changed slightly here due to our definition of concentration of bound counterions in this section being based on water-free organic phase volume:

$$VC_{\mathrm{Na}} + \bar{V}^0\bar{C}_{\mathrm{Na,b}} + w\bar{V}\bar{C}_{\mathrm{Na,f}} = V^0C^0_{\mathrm{Na}} + \bar{V}^0\bar{C}^0_{\mathrm{S}} \tag{2.7b}$$

The mass balance of surfactant is

$$\bar{C}_{\mathrm{Na,b}} + \bar{C}_{\mathrm{ds}} = \bar{C}^0_{\mathrm{S}} \tag{2.31}$$

Combining eqs. (2.7b), (2.10), (2.28), (2.30), and (2.31) and the equations of electroneutrality in the water pool and excess aqueous phase results in

$$K^{\mathrm{Na}}_{\mathrm{d}} = \frac{f\left(C^0_{\mathrm{Na}} + 55.5f/w_0\right)}{(1-f)} \tag{2.32}$$

where "f" is the fraction of surfactant dissociated and it defined by

$$f = \bar{C}_{\mathrm{ds}}/\ \bar{C}^0_{\mathrm{S}} \tag{2.33}$$

In eq. (2.32), w_0 is the moles of water per mole of surfactant in the organic phase at equilibrium and this is related to w, water uptake in volume fraction, through the following equation:

$$w_0 = \frac{55.5w}{\bar{C}^0_{\mathrm{S}}(1-w)} \tag{2.34}$$

Equation (2.32) can be used to determine the value of equilibrium constant of dissociation. Wong et al. [14] reported 0.28 fraction of surfactant dissociation and 49.3 mole water per mole of surfactant in heptane for an initial concentration of 67 mM of NaCl in aqueous solution used as titrant for the formation of the reverse micelles with titration method.

As shown by Rabie et al. [21], at equal electrolyte and surfactant concentrations, the water uptake obtained by titration method is lower than that obtained by contact method. This is because of the lower effective ionic strength inside water pools of reverse micelles formed by contact method when compared with those formed by titration method [21]. Therefore, for contact method used in this work, NaCl concentration used in eq. (2.32) should be slightly higher than 67 mM.

Since the extra effective concentration inside water pool is not known, we assume the equilibrium corresponding to 67 mM of NaCl. This is not a bad assumption as a 10% change in NaCl concentration, at 67 mM level, results in less than 1.7% change in the value of the equilibrium constant. Besides, as stated by Wong et al. [14], the 28% dissociation is an estimation. Therefore, using these results and eq. (2.32), the value of $K^{\mathrm{Na}}_{\mathrm{d}}$ is found to be 0.1486 M.

This value for $K^{\mathrm{Na}}_{\mathrm{d}}$ is used throughout this work to obtain the fraction of surfactant dissociated for different surfactant and salt concentrations (or ionic strength) in

mixed salt systems. This value is also for different solvents. Although a solvent has definite effect on the water uptake and size of reverse micelles, when the reverse micelles are formed, it does not have any significant impact on the reactions that happen inside the reverse micelles between the different solutes and the surfactant head groups, except for very penetrating solvents [2, 19]. Therefore, the value of equilibrium constant found for one solvent can be used for other Winsor II systems having different solvents.

Another important correlation, which can be obtained combining eqs. (2.7b), (2.10), (2.28), and (2.31), and the equations of electroneutrality in the water pool and excess aqueous phase, is given as

$$C_{\mathrm{Na}} = C^{0}_{\mathrm{Na}} \tag{2.35}$$

This equality shows that dissociation of surfactant has no effect on equilibrium concentrations of ions in the aqueous phase. The extra ions released to the water pool, from the dissociation reaction, are not able to enter the excess aqueous phase because of the need for maintaining the electroneutrality in the reverse micelles. Therefore, the overall ion distribution can be obtained independently from the dissociation fraction, assuming all surfactant molecules are bound to either sodium or other cations. In this case, calculations are recued to the universal theory of ion distribution [2] as discussed in Section 2.2.

2.3.3 Dissociation Fraction in a Multicounterion System

In a multicounterion system, the free counterions in the water pool of reverse micelles undergo an ion exchange reaction with the original surfactant counterion bound to the surfactant head group at the reverse micellar interface. For AOT, since the surfactant S is anionic, any $M^{z_i^+}_{i,\mathrm{f}}$ cation can exchange with the original surfactant counterion, Na^+, in the water pool. This ion exchange is shown by eq. (2.2) along with its equilibrium constant in terms of concentrations shown in eq. (2.3). For simplicity, K^i_{s} is used as the equilibrium constant instead of K^i_{Na}. The values for equilibrium constants for different cations have been reported elsewhere [2] and are also presented in Table 2.1.

The values of equilibrium constants were measured by ion distribution experiments and are used in this work as well. Therefore, there is no adjustable parameter to fit in this work for calculation of the counterion binding. This new form of surfactant, $S_{z_i}M_i$, can also undergo the dissociation reaction in the water pool. However, this reaction is not independent from reactions (2.2) and (2.29). The dissociation reaction of $S_{z_i}M_i$ in the water pool is presented as

$$S_{z_i}M_i \rightleftharpoons z_i S^- + M^{z_i^+}_{i,f} \tag{2.36}$$

Table 2.2: Values of equilibrium constants for eq. (5) and of the size and ionic parameters [18].

	K_s^i	K_d^i	τ_i	A_i(kcal/mol)	$C_{i,m}$	$w_0^{\bullet,i}$
Na^+	1.00	0.1486	4.0	99.6	0.080	6.5
K^+	1.96	0.0758	3.2	81.6	0.060	4.7
Rb^+	2.08	0.0714	3.1	76.5	0.060	5.1
Cs^+	2.13	0.0698	3.1	68.7	0.055	6.8
Sr^{2+}	32.6	0.0007	6.0	344.1	0.035	4.8
Ba^{2+}	62.3	0.0004	5.8	318.1	0.035	2.3

with the equilibrium constant of

$$K_d^i = \frac{\bar{C}_{ds}\bar{C}_{i,f}}{\bar{C}_{i,b}} = \frac{K_d^{Na}}{\left(K_d^i\right)^{z_i}} \tag{2.37}$$

Table 2.2 lists the equilibrium constants of ion exchange reactions and of the dissociation reactions, for some monovalent and divalent cations together with the minimum amount of salt needed for the formation of reverse micelles and the water uptake constant. This table also contains the values of the size parameter of ion i, τ_i, which is a dimensionless ionic radius, and of the ionic parameter A_i, which is calculated from the free energy of hydration. The values of the ion exchange equilibrium constant, the size parameter of the ion, and the ionic parameter are obtained from literature [2]. The significance of the size parameter of ion, the ionic parameter, the minimum amount of salt for the formation of reverse micelles, and the water uptake constant are discussed in more detail in the next section regarding water uptake of reverse micellar systems.

For a multicounterion system, the mass balance of sodium is the same as in eq. (2.7b). The mass balance of surfactant is written as

$$\bar{C}_{Na,b} + \sum_{i=1}^{(n-1)} (z_i \bar{C}_{i,b}) + \bar{C}_{ds} = \bar{C}_S^0 \tag{2.38}$$

where this summation runs over all the counterions except sodium. For each of the other cations present in the initial aqueous phase, the mass balance is similar to eq. (2.8). For simplicity as explained earlier, the concentration of bound ions in the organic phase are based on the water-free organic volume. Therefore, the mass balance for any other cations present in the initial aqueous phase is updated and shown as

$$VC_i + \bar{V}^0 \bar{C}_{i,b} + w\bar{V}\bar{C}_{i,f} = V^0 C_i^0 \tag{2.8b}$$

Combining equations of electroneutrality in the organic phase and in the aqueous phase with eqs. (2.7b), (2.8b), (2.28), and (2.38) results in

$$\sum_{i=1}^{n}(z_i C_i) = \sum_{i=1}^{n}(z_i C_i^0) \tag{2.39}$$

where these summations run over all the counterions. Equation (2.39) is a useful relation between the initial and equilibrium (Winsor II system) concentrations of ions in the aqueous phase. This equation shows that the total equivalent of counterions in the aqueous phase remains at its initial value.

If no surfactant molecule is dissociated at the reverse micellar interface, the concentration of dissociated from of surfactant is zero and all surfactant sites will be filled with either sodium or another counterion. Therefore, there is no additional cation released in the water pool as a result of surfactant dissociation. In this case, assuming that the value of Λ is unity for each of the solutes, the concentration of any free counterion in the water pool is the same as that in the excess aqueous phase. Therefore, eq. (2.3) can be written based on concentrations of ions in the excess aqueous phase instead of those in the water pool as presented in eq. (2.5). The calculations are performed in two steps for a system containing n different counterions including sodium.

Step 1: As discussed before, the dissociation of surfactant has no effect on the concentrations of ions in the excess aqueous phase. Therefore, these concentrations are obtained assuming that all surfactant sites are filled. This is the same as the universal theory of ion distribution discussed in Section 2.2. Therefore, there are n equations of the type of eq. (2.27), n –1 equations of the type of eq. (2.8b), n –1 equations of the type of eq. (2.3), and eqs. (2.10), (2.7b), and (2.39), while value of Λ for any solute is set at 1. It is important to note that the water uptake, w, does not appear while solving these equations.

Step 2: The concentrations of different species in different regions of the organic phase are calculated using the results of step 1, for ion concentrations in the excess aqueous phase, and the following equations: n – 1 equations of the type of eq. (2.8b), and n – 1 equations of the type of eq. (2.3) and eqs. (2.10), (2.30), (2.7b), and (2.38). Then the dissociation fraction is calculated from eq. (2.33). In this step, the water uptake is used in the model as a known value. However, as explained in the next section, the model is extended to provide an equation that relates the water uptake to the dissociation fraction. While the above equations are written for sodium salt of an anionic surfactant, such as AOT, they are general for any other anionic or cationic surfactant.

2.3.4 Results and Discussion for Active Interface Model and Dissociation Fraction

An interesting finding is the distribution of chloride, the coion in this study, in single and multicounterion systems for different concentrations of surfactant and salts for a

wide range of water uptakes. Our experimental data showed that the final concentrations of chloride in the excess aqueous phase was almost the same as its initial value. A slight decrease was observed, but it was insignificant. Similar results have been observed for cationic surfactant systems [22]. This justifies the assumption of unity for the value of Λ for any solute. If chloride concentration in water pool was different from that in aqueous phase at equilibrium, a difference would be detected between its initial and final concentrations in the aqueous phase at moderate water uptakes.

The numerical results of the dissociation fraction of AOT at the reverse micellar interface in the presence of chloride salts of different monovalent cations (Na^+,K^+, Cs^+) are presented in Figure 2.9. These results were obtained using experimental water uptake data [3]. In the case of sodium in Figure 2.7, the system has only one counterion, while in the other cases, there are two counterions present.

Figure 2.9 shows that for any cation, the dissociation fraction decreased with the initial salt concentrations. More surfactant molecules were dissociated in the presence of sodium than other monovalent cations for the same salt concentration, whereas the dissociation fraction followed a similar curve for potassium and cesium with a slightly higher dissociation for the latter.

Figure 2.10 shows similar results for divalent cation (Ca^{2+}, Sr^{2+}, Ba^{2+}) in chloride salts. Similar to monovalent cations, the dissociation fraction decreased with the addition of salt and stayed almost constant at higher salt concentrations. Significantly lower dissociation fractions were observed for divalent cations than for monovalent cations. This is because of the stronger electrostatic interactions of divalent cations with the surfactant head groups. The most interesting aspect of this model is that there is no adjustable parameter and that no geometrical consideration is needed to account for binding. The only required information is the water content in the organic phase at equilibrium.

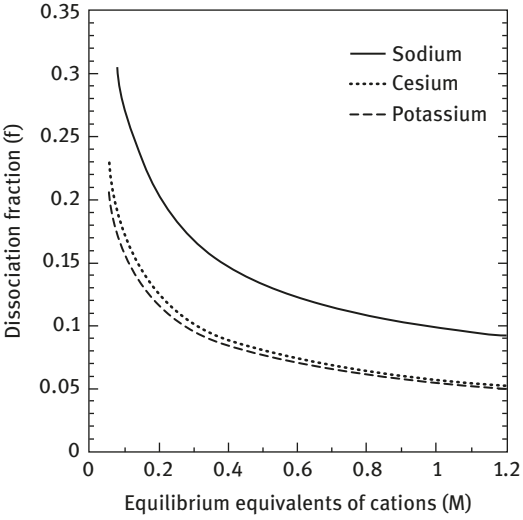

Figure 2.9: Dissociation fraction as a function of equilibrium equivalents of cations in the aqueous phase for different monovalent cations: initial organic phase, 0.1 M AOT; initial aqueous phase, chloride salt. The lines are the predictions of the present model. Reprinted with permission from (J. Phys. Chem. B, 1997, 101, 10295). Copyright (2017) American Chemical Society.

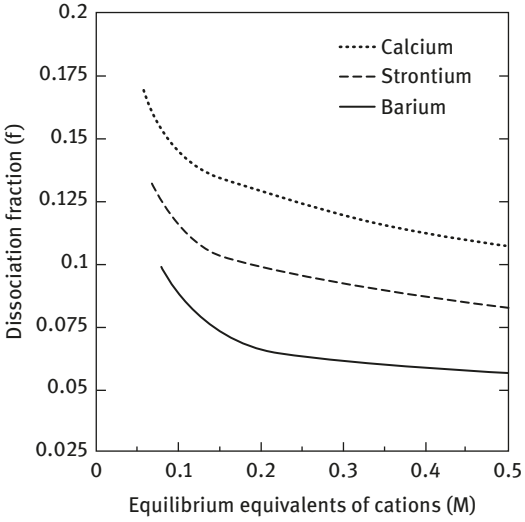

Figure 2.10: Dissociation fraction as a function of equilibrium equivalents of cations in the aqueous phase for different divalent cations: initial organic phase, 0.1 M AOT; initial aqueous phase, chloride salt. The lines are the predictions of the present model. Reprinted with permission from (J. Phys. Chem. B, 1997, 101, 10295). Copyright (2017) American Chemical Society.

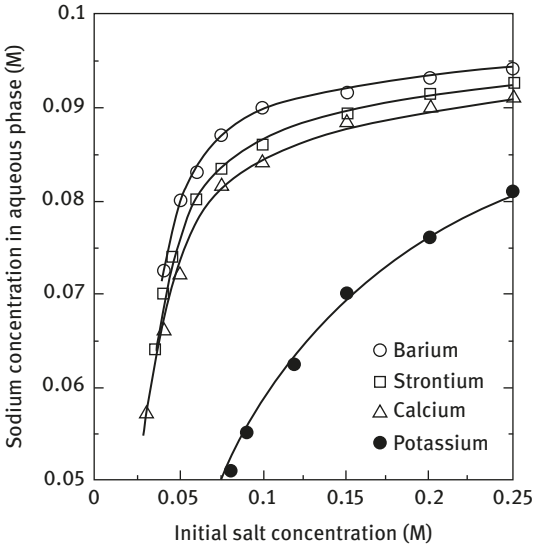

Figure 2.11: Equilibrium concentration of sodium in the excess aqueous phase as a function of initial salt concentration for different cations: initial organic phase, 0.1 M AOT; initial aqueous phase, chloride salt. The lines are the predictions of the present model. The experimental data are from present work. Reprinted with permission from (J. Phys. Chem. B, 1997, 101, 10295). Copyright (2017) American Chemical Society.

For the sake of completeness, the experimental data and calculated results for ion distribution of different cations (K^+, Ca^{2+}, Sr^{2+}, Ba^{2+}) in chloride salts are presented in Figure 2.11. The experimental conditions are similar to those used in Figures 2.9 and 2.10. In this figure, the equilibrium concentration of sodium in the excess aqueous phase is plotted against the initial salt concentration. In this case, no sodium was added initially to the aqueous phase. The presence of sodium in the aqueous phase at equilibrium is because of the exchange of surfactant counterion with the added cation.

Barium released more sodium into aqueous phase than other cations. The results for cesium, not shown in Figure 2.11, were close to those of potassium but slightly higher [18]. The solid lines are predications of the model. As explained before, the numerical results were obtained independent of the water uptake and of the dissociation fraction. Additional results on ion distribution equilibria and also on dimensionless representation of the ion distribution are presented in Section 2.2.

As shown in Table 2.2 and in Figures 2.9–2.11, cations with larger ion exchange equilibrium constants are preferentially drawn into the reverse micellar interface; however, they dissociate less. Divalent cations have larger values of ion exchange constants and lower dissociation fraction when compared to the monovalent cations due to stronger electrostatic interactions. Monovalent cations with the same hydrated size (K^+, Rb^+, Cs^+) have almost the same ion exchange and dissociation equilibrium constants, while divalent cations with the same hydrated size (Ca^{2+}, Sr^{2+}, Ba^{2+}) have significantly different ion exchange and dissociation equilibrium constants. This is because of the difference in the hydration free energy [2]. As listed in Table 2.2, within the cations with the same charge number, decreasing the τ_i or A_i favors the increase of ion exchange equilibrium constant and decrease of dissociation equilibrium constant.

As shown before [7] for the contact method, a minimum amount of salt is needed to pass from a Winsor type III to a Winsor type II, or reverse micellar system. This minimum amount of salt changes with nature of the counterion introduced into the system through addition of salt. In Table 2.2, the minimum amount of salt needed to form reverse micelles is listed for different cations. As shown in this table, this minimum amount of salt is greater for cations with greater dissociation constant or smaller ion exchange equilibrium constant. Our experimental data have shown that reverse micelles were not formed with chlorides of Li^+, Be^{2+}, and Mg^{2+}. Similar observations were made by Leodidis and Hatton [17].

According to the conclusions of Table 2.2, we can expect to obtain significantly greater dissociation with these cations in comparison to that obtained with sodium. Therefore, the system cannot pass from Winsor III to Winsor II type system. In the next section, we will discuss the water uptake of reverse micellar systems and present different models to predict the water uptake. One of the models are based on the dissociation fraction and will be expanded in detail in the next section.

2.4 Water Uptake of Reverse Micellar Systems and Predictive Models

In Chapter 1, some of the water uptake results obtained with DODAC and DODAB, two cationic surfactants, were presented. We saw that DODAC reverse micellar systems with NaCl aqueous phase give higher water uptake than DODAB reverse micellar systems with NaBr in the aqueous phase. It is interesting to note that while

the addition of NaBr in the DODAC systems decreases the water uptake, the addition of NaCl in the DODAB reverse micellar systems increases the water uptake. At high concentration of salt in the aqueous phase, the water uptake of the DODAC–NaBr system approaches from above the water uptake of the DODAB–NaCl system. On the other hand, at high concentration of NaCl, the DODAB–NaCl system approaches from below the water uptake of the DODAC–NaCl system.

It is clear that the chloride form of surfactant has a higher water uptake than the bromide form and the ion exchange in the head of the surfactant is the cause of this effect. The exchange of the anion of the surfactant with the other anion in the aqueous phase produces surfactant forms that have higher water uptakes but as the concentration of salt increases in the aqueous phase beyond the upper limit of the ion exchange the water uptake decreases as expected. These experimental results led us to believe that ion exchange reactions and the redistribution of ions are the first critical step in understanding the reverse micellar systems and as such the water uptake. As discussed in the previous section, the ion distribution is not impacted by water uptake and surfactant dissociation and can be accurately calculated using the universal theory of ion distribution with the single ion exchange constant, obtained from a single data point, for each counterion. After calculating the distribution of ions, we can then calculate the water uptake based on predictive models.

We have taken two approaches to modeling of the water uptake of reverse micellar systems:

1. Generalized water uptake model
2. Active interface model

The generalized water uptake model is inspired by the experimental results obtained for different cationic and anionic surfactants at different conditions, suggesting that the water uptake is a function of different forms of surfactant (after counterion bindings) in the organic phase and the ionic strength of the water pool. After ion distribution at equilibrium, there are different counterions bound to the surfactant having different water uptake characteristics. In addition, the ionic strength of the water pool has an impact on the water uptake independent of the counterions. The water uptake, in molar water per water-free organic phase, contributed by each form of surfactant is represented by a general equation as follows:

$$W_i = F(I_c)\bar{C}_{i,b} \tag{2.40}$$

This approach assumes that all surfactant head groups are bound to the counterions resulting in different forms of surfactant. The total water uptake is the sum of all the water uptakes contributed by different forms of surfactant.

$$W = \sum_{i=1}^{n}(W_i) \tag{2.41}$$

The water uptake, w, is expressed as molar water uptake per water-free organic phase. The water uptake as moles of water per moles of surfactant, w_0, is related to molar water uptake as follows:

$$w_0^i = W_i / \bar{C}_s^0 \tag{2.42}$$

The active interface model is based on the surfactant dissociation fraction. The dissociation of surfactant produces a surface charge density at the reverse micellar interface, causing a repulsive force between the surfactant head groups. For a single counterion system, the water uptake is assumed to be a function of the dissociation fraction only. In case of multicounterion system, a mixing rule is used to obtain the total water uptake contributed by different forms of surfactant. In this treatment, the water uptake is expressed as moles of water per moles of surfactant, w_0, and eq. (2.42) can be used to convert it to molar water uptake, W.

2.4.1 Generalized Water Uptake Model – Linear Form

For the $F(I_c)$ function, we have used two different forms: a linear form and a power form. In our earlier studies of a simpler system containing DODAC and salts at different pH, a linear form was sufficient to describe the water uptake. However, as we experimented with more systems and different conditions, we recognized that a power form is more suitable to describe the water uptake of different anionic and cationic surfactants in a multicounterion system at different salt concentrations. Therefore, this form was called the generalized water uptake model. To cover the full treatment, we will discuss both approaches starting with the linear version.

The molar water uptake for any form of surfactant is expressed as a function of ionic strength of the aqueous phase, I_c, and the concentration of surfactant in that given form:

$$W_i = (K_1 - K_2 I_c)\bar{C}_{i,b} \tag{2.43}$$

where K_1 and K_2 are dimensional parameters. It is further assumed that these constants change between different forms of surfactants by simply a multiplier

$$\frac{W_1}{\bar{C}_{1,b}} = \alpha \frac{W_2}{\bar{C}_{2,b}} \tag{2.44}$$

where α is a dimensionless parameter. We applied this model only to a simpler binary system of DODAC at different pH. The hydroxide group acts as a counterion exchanging the original surfactant counterion, chloride with an ion exchange equilibrium constant. The different forms of surfactant are denoted as SCl (form 1) and SOH (form

2) for the original DODAC and the hydroxide form of surfactant, respectively. The ionic strength of the solution is defined as

$$I_c = \frac{1}{2} \sum_{i=1}^{n} (z_i^2 \, C_i) \tag{2.45a}$$

Because of electroneutrality and the simple monovalent system for this study

$$I_c = C_{Cl} + C_{OH} \tag{2.45b}$$

In the work of Chou and Shah [23], the additive behavior described by eq. (2.41) was observed for the effect of NaCl and $CaCl_2$. In addition, α in their system was unity for the second form of surfactant. Thus, the water uptake measured as a function of ionic strength was the same for any ratio of the concentrations of the two salts in their mixed aqueous solution.

Assuming that concentrations of free ions in the water pool are the same as the concentrations of ions in the excess aqueous phase, the ion exchange of hydroxide with chloride does not change the ionic strength of the aqueous solution meaning that for this simpler system. Therefore, the ionic strength of the aqueous solution at equilibrium is the same as the initial ionic strength. Figure 2.12 shows the relation between the initial and the measured equilibrium ionic strength for different surfactant, NaCl and NaOH concentrations, confirming this assumption.

Similar results were found by Bruno et al. [8] for AOT reverse micelles with chloride as the surfactant coion. For this system, the sum of concentrations of chloride form of surfactant and hydroxide form of surfactant will be equal to the total surfactant concentration in the organic phase. These concentrations are based on the water-free organic volume, and as before, the amount of organic solvent

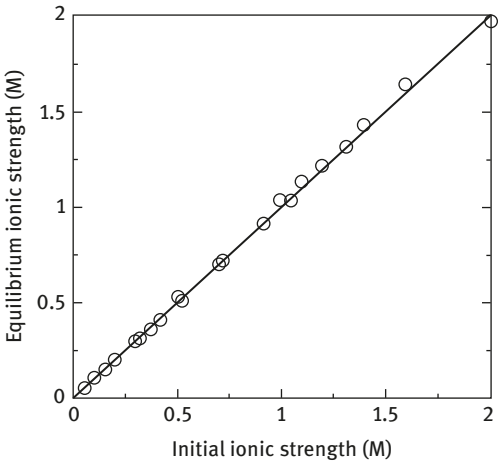

Figure 2.12: Equilibrium ionic strength as a function of initial ionic strength. Reprinted with permission from (J. of Colloid and Interface Science, 1995, 174, 1). Copyright (2017) Elsevier.

present in aqueous phase is assumed to be insignificant. With this consideration and combining eqs. (2.41), (2.43), (2.44) and the ion exchange reaction constant, K_s:

$$W = (K_1 - K_2\ I_c)\ \bar{C}_s^0\ \frac{1 + \alpha K_s\ C_{OH}/C_{Cl}}{1 + K_s\ C_{OH}/C_{Cl}} \tag{2.46}$$

The relationship between the water uptake in mass fraction W', and in molarity, W, is

$$W' = \frac{18.016\ W}{18.016\ W + d} \tag{2.47}$$

where d is the density of the water-free organic phase in gram/liter. Figure 2.13 shows the variation of water uptake of DODAC reverse micelles as a function of the ratio of hydroxide concentration to chloride concentration at equilibrium. The experiments were carried out by varying the NaCl concentration for each pH at a fixed DODAC concentration of 0.1 M. The parameters in eqs. (2.43) and (2.44) were found by a least-squares fit of eqs. (2.46) and (2.47) to the data in Figure 2.13. The values of parameters are K_1 = 17.9 mole H_2O/mol surfactant, K_2 = 8.1 mol H_2O/(mol surfactant x M ions in aqueous phase), α = 5.06, and K_s = 0.096. The curves in Figure 2.13 are the least-squares fits with these parameters.

Figure 2.14 shows the water uptake as a function of ratio of hydroxide concentration to chloride concentration at equilibrium for three surfactant concentrations. The curves are the predictions of eqs. (2.46) and (2.47) using the parameters given above; no additional fitting was done.

The values of K_s and α for three additional anions, F^-, Br^-, and NO_3^-, are given in Table 2.3. The values for OH^- are included for comparison. For Cl^-, both K_s and α are unity. The values of K_1 and K_2 are the same for all anions.

The curves in Figure 2.15 also show the water uptake predicted by the model without any additional fitting. The model describes the maximum obtained in the

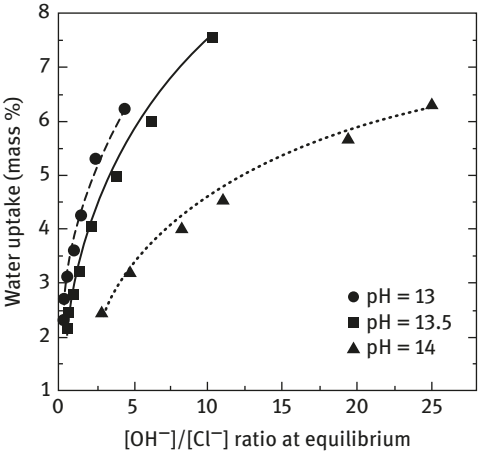

Figure 2.13: Water uptake as a function of C_{OH}/C_{Cl} ratio at equilibrium for various pH; initial organic phase: 0.1 M DODAC, 0.25 M decanol; initial aqueous phase: NaCl, NaOH. Reprinted with permission from (J. of Colloid and Interface Science, 1995, 174, 1). Copyright (2017) Elsevier.

Table 2.3: <TBLCAP>Values of K_s and α for different anions with K_1 = 17.9 mol H_2O/mol surfactant and K_2 = 8.1 mol H_2O/(mol surfactant x *M* ions in aqueous phase) [12].

	K_s	α
OH^-	0.096	5.06
F^-	0.103	5.15
Br^-	2.04	0.64
NO_3^-	2.00	0.58

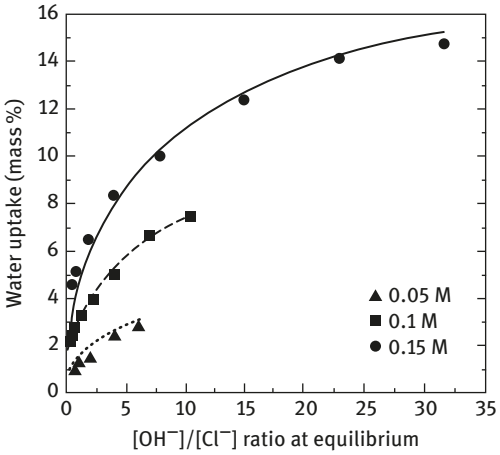

Figure 2.14: Water uptake as a function of C_{OH}/C_{Cl} ratio at equilibrium for various surfactant concentrations; initial organic phase: DODAC, 0.25 M decanol; initial aqueous phase: NaCl, pH 13.5. Reprinted with permission from (J. of Colloid and Interface Science, 1995, 174, 1). Copyright (2017) Elsevier.

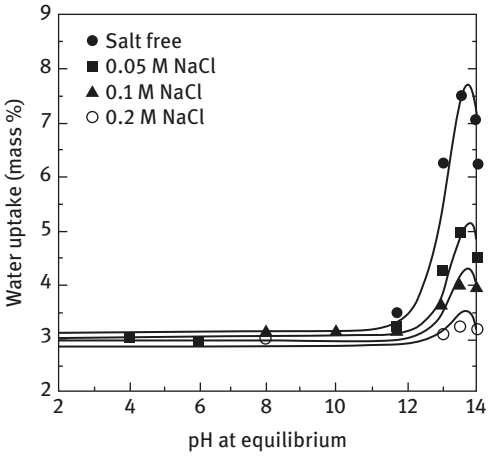

Figure 2.15: Water uptake as a function of equilibrium pH for various initial salt concentrations; initial organic phase: 0.1 M DODAC, 0.25 M decanol; initial aqueous phase: NaCl and NaOH. Reprinted with permission from (J. of Colloid and Interface Science, 1995, 174, 1). Copyright (2017) Elsevier.

experiments at high pH and the absence of any effect at low PH. The predictions of the model are in good agreement with the experimental results.

For a mixed monovalent salts system, the water uptake can be found form the following equation applying the same method as described earlier but with the summation over all the counterions:

$$W = (K_1 - K_2\, I_c)\, \bar{C}_s^0\, \frac{1 + \sum(\alpha_i K_{si}\, C_i/C_{Cl})}{1 + \sum(K_{si}\, C_i/C_{Cl})} \tag{2.48}$$

2.4.2 Generalized Water Uptake Model – Power Form

In this version of the model, a power form is used, which is applicable to more reverse micellar system. At equilibrium, the molar water uptake of $S_{z_i}M_i$ form the surfactant, with its concentration in the organic phase equal to $z_i\bar{C}_{i,b}$ can be written as

$$W_i = \alpha_i\, I_C^{\beta_i}\, z_i\bar{C}_{i,b} \tag{2.49}$$

where α_i and β_i are dimensionless parameters. From here on, parameters α_i and β_i are referred to as water uptake constants. In eq. (2.49), I_c is the ionic strength of the excess aqueous phase at equilibrium as shown in eq. (2.45), with summation over all the ions. Using the equation of electroneutrality in aqueous phase, the ionic strength of the aqueous phase can be written only as a function of the concentrations of counterions. For example, the ionic strength of monovalent electrolytes is

$$I_c = \sum_{i=1}^{n} C_i \tag{2.50}$$

where the summation is only over the counterions. We use an anionic surfactant like AOT for the rest of the discussions. But the same method can be applied to other types of surfactants. Assuming that all the counterion sites of an anionic surfactant in the reverse micelles are filled with either sodium or other cations, the mass balance of the surfactant is then formulated as

$$\sum_{i=1}^{n} z_i\bar{C}_{i,b} = \bar{C}_S^0 \tag{2.51}$$

Equation (2.51) assumes that all surfactant in the organic phase is found in the reverse micellar interface. In the light of the results of Aveyard et al. [6], this is a reasonable assumption for the AOT surfactant at the salt concentrations used in this work. We use the same definition of molar ratio of water to surfactant in the organic phase at equilibrium as defined in eq. (2.42) for water uptake contributed by each form of the surfactant or the same can be used for total water uptake.

Combining eqs. (2.41), (2.42), (2.49), and (2.51) yields the following equation for a system of n different counterions, including the original counterion of the surfactant:

$$w_0 = \frac{\sum_{i=1}^{n} \alpha_i \, I_C^{\beta_i} \, z_i \bar{C}_{i,b}}{\sum_{i=1}^{n} z_i \bar{C}_{i,b}} \tag{2.52}$$

where w_0 is the total water uptake as molar ratio of water to surfactant. The relation between water uptake in molar ratio, volume fraction, and molar concentration per water-free organic phase has been provided in previous sections. In eq. (2.52), water uptake is a function of concentrations of ions in the aqueous phase at equilibrium. The ion distribution can be found using the universal ion distribution theory discussed in Section 2.2. The water uptake model can be solved together with the ion distribution calculations to provide both the ion distributions at equilibrium and the water uptake.

To solve these equations, a first guess can be made for the water uptake value in the volume fraction (w). The first guess is found by solving eqs. (2.42), (2.45), (2.47), and (2.52) and the equation of electroneutrality, assuming uniform distribution for all counterions. This set of equations is called here the first set. Furthermore, this value of the water uptake is used to solve the remaining equations, or the second set, to find the ion distribution. Then, the values of ion distributions are substituted into the first set of equations to obtain a new value for water uptake. The iterations between these two sets of equations can be considered to have converged when the difference in the water uptake between two consecutives iterations is less than 1%.

2.4.3 Dimensionless Form of Generalized Water Uptake Model – Power Form

In this section, the equilibrium and initial conditions are expressed in terms of dimensionless groups. These dimensionless groups are as follows: R_i, R_i^0, the equilibrium and the initial equivalent ratios, respectively, of the original surfactant counterion, for example, sodium for AOT, to the ith counterion in the aqueous phase; δ, the initial equivalent ratio of surfactant in the organic phase to the equivalents of all counterions, excluding original surfactant counterion, in the aqueous phase; r, the initial volume ratio of the organic to the aqueous phase; and w, the volume fraction of water in the organic phase at equilibrium. The mathematical relations for these dimensionless groups are given here again for clarity:

$$R_i = \frac{C_{Na}}{z_i C_i} \tag{2.53a}$$

$$R_i^0 = \frac{C_{Na}^0}{z_i C_i^0} \tag{2.53b}$$

$$\delta = \frac{\bar{V}^0 \bar{C}_S^0}{V^0 \sum_{i=1}^{n-1} (z_i C_i^0)} \tag{2.53c}$$

$$r = \frac{\bar{V}^0}{V^0} \tag{2.13}$$

$$\Lambda_i' = 1 + \frac{wr}{1-w}(\Lambda_i - 1) \tag{2.12}$$

Using the dimensionless groups and after some algebra, the following dimensionless form of the generalized water uptake model is obtained:

$$w_0 = \frac{\alpha_{Na} I_C^{\beta_{Na}} \delta \sum_{i=1}^{n-1} \left(\frac{1}{R_i^0}\right) + \sum_{i=1}^{n} \left(\frac{\alpha_i I_C^{\beta_i} \theta_i}{R_i^0}\right)}{\delta \sum_{i=1}^{n-1} \left(\frac{1}{R_i^0}\right) + \sum_{i=1}^{n} \left(\frac{\theta_i}{R_i^0}\right)} \tag{2.54}$$

where the summations from 1 to *(n - 1)* are over all counterions, excluding the original surfactant counterion. In eq. (2.54), θ_i is defined as

$$\theta_i = 1 - \frac{\Lambda_i' R_i^0}{R_i} \frac{\sum_{j=1}^{n} \left(\frac{1}{R_j^0}\right)}{\sum_{j=1}^{n} \left(\frac{\Lambda_j'}{R_j}\right)} \tag{2.55}$$

where R_i is a function of R_i^0, δ, r, and w only [2]. The term Λ_i' is defined in eq. (2.12). Equation (2.54) shows that water uptake can described as a function of the dimensionless groups R_i^0, δ, r, and I_c, which depend only on the initial conditions of the system.

For mixed monovalent counterion systems, using the equilibrium constant K_s^i, eq. (2.54) can be written as

$$w_0 = \frac{\sum_{i=1}^{n} \left(\frac{\alpha_i I_C^{\beta_i} K_s^i}{R_i}\right)}{\sum_{i=1}^{n} \left(\frac{K_s^i}{R_i}\right)} \tag{2.56}$$

The solution of the dimensionless form of the generalized water uptake model is simpler than the solution of the individual equations specially when there is an analytical solution for the second set of equations. This solution, which gives the ion distribution, can also be expressed in dimensionless form as discussed earlier.

The following experimental results were obtained in Winsor II systems. The data are reported as equilibrium water uptake; molar water uptake (W_t), water uptake in wt% (W'), or the molar ration of water to surfactant (w_0) in the organic phase. For

most experiments, the initial volume ratio of the organic to aqueous phase was unity. Except where noted, the pH was not adjusted, and the equilibrium phases had pH values between 7 and 8. The model predictions are compared with the water uptake results of the AOT reverse micellar system for different concentrations of salts and surfactant and for different volume rations of the two phases. As described below, the water uptake constants were obtained from eqs. (2.49) and (2.52). The predictions of the model have been obtained assuming that the value of Λ_i is unity for all counterions.

In Figure 2.16, the equilibrium molar ratio of water to surfactant in the organic phase, w_0, is plotted against the initial concentration of sodium in the aqueous phase for three salts: NaCl, NaSCN, and Na_2CO_3. For the sake of comparison, data obtained by other authors [8] are also shown. These salts have the same cation, sodium, but different anions. All salts had the same water uptake for the same initial sodium concentration. This figure shows that only the ions that are exchangeable with the surfactant counterion alter the water uptake.

Figure 2.17 shows molar water uptake data in the presence of chloride salts having different monovalent and divalent cations. These salts are CsCl, KCl, $SRCl_2$, and $BaCl_2$. The NaCl data from Figure 2.16 are included for comparison. The water uptake significantly decreases as the salt concentration increases. This is due to the increase in ionic strength of the aqueous phase, which produces a higher charge density inside the reverse micelles. The repulsive interactions between surfactant heads are reduced; they come closer and the size of the reverse micelles decreases, thus reducing the water uptake [7].

Furthermore, different cations (even cations with the same charge and approximately the same hydrated size) produce significant differences in the water uptake [7]. These salts alter the water uptake since they have cations different from sodium.

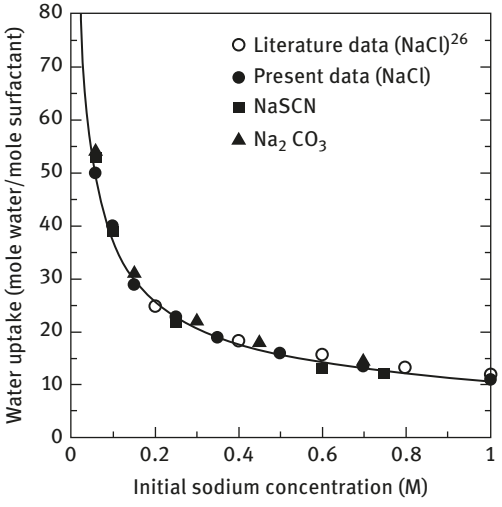

Figure 2.16: Water uptake as a function of initial sodium concentration of salts with different anions; initial organic phase: 0.1 M AOT in isooctane; initial aqueous phase: salt. Reprinted with permission from (Fluid Phase Equilibria, 1996, 122, 169). Copyright (2017) Elsevier.

This effect and the ionic strength effect are considered through the values of α_i and β_i parameters in the model.

These values were evaluated by a least-square fit with eq. (2.49) to the NaCl water uptake results in Figure 2.16. The values of the water uptake constants for other cations were found by least-square fit with eqs. (2.42) and (2.52) to the water uptake data for each cation shown in Figure 2.17. These values are listed in Table 2.4 together with the equilibrium constants listed earlier for different cations. The same values are used throughout this section for the prediction of the water uptake under different conditions of salt concentrations, for single or mixed salt systems and different surfactant concentrations and volume ratios of the two phases. The solid lines are the comparison between predictions of the model based on these values and the points representing the experimental data.

Figure 2.18 shows the effect of initial surfactant concentration on the molar water uptake for various initial NaCl concentrations. For each NaCl concentration, the water uptake increased linearly with the surfactant concentration starting from zero, when no surfactant was added to the organic phase. This means that the molar ratio of water to surfactant, w_0, was a constant at each level of NaCl concentration. The solid lines

Table 2.4: Water uptake constants and equilibrium constants for various cations [2, 3].

	α_i	β_i	K_s^i
Na^+	10.5	−0.54	1.00
K^+	5.77	−0.11	1.96
Cs^+	7.42	−0.25	2.13
Ba^+	3.50	−0.09	62.3

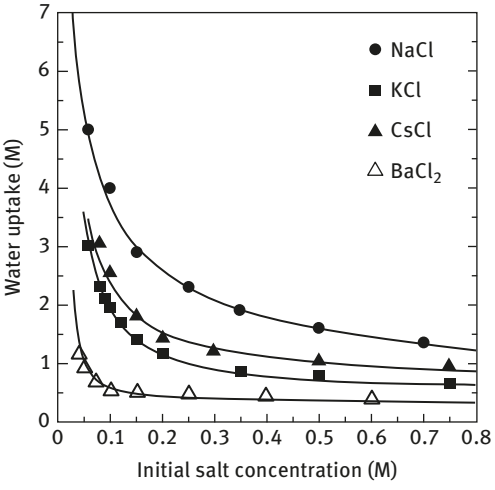

Figure 2.17: Water uptake as a function of initial salt concentration for salts with different cations; initial organic phase: 0.1 M AOT in isooctane; initial aqueous phase: salt. Lines are calculated with the model. Reprinted with permission from (Fluid Phase Equilibria, 1996, 122, 169). Copyright (2017) Elsevier.

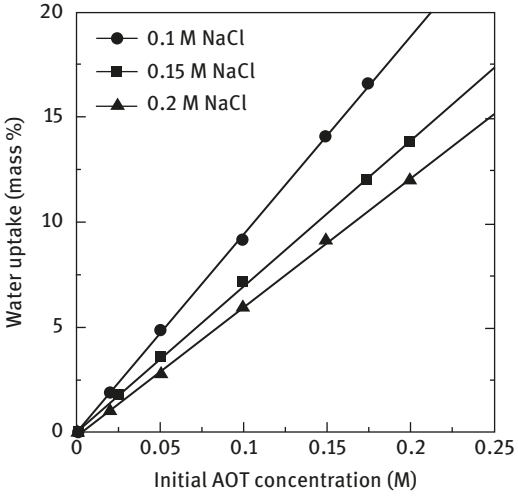

Figure 2.18: Water uptake as a function of surfactant concentration for various NaCl concentrations; initial organic phase: AOT in isooctane; initial aqueous phase: NaCl. Lines are calculated with the model. Reprinted with permission from (Fluid Phase Equilibria, 1996, 122, 169). Copyright (2017) Elsevier.

show the prediction of the model. The slope of the line is larger for lower NaCl concentrations. All lines pass through the (0,0) point.

The results in Figure 2.18 are in total agreement with the findings of Fletcher [24] who also used sodium chloride in his phase equilibrium experiments. Using a salt with a cation different from the original surfactant counterion, for example, sodium for AOT, makes a mixed counterion system. In this case, eq. (2.49) cannot describe the total water uptake and eq. (2.52) should be used instead. In a single counterion system, changing the surfactant concentration alters the numbers of reverse micelles in the organic phase but has no effect on the size of the reverse micelles and so it does not affect the w_0, the molar ratio of water to surfactant [24].

Figure 2.19 shows the effect of surfactant concentration on the molar ratio of water to AOT for different initial KCl concentrations in the aqueous phase when no NaCl was added. Data obtained by other authors [17] for this system are also included for comparison. The solid lines in this figure show the prediction of the model. It is important to note that this system is a mixed counterion system of sodium and potassium since sodium is the original counterion of the surfactant. As shown in Figure 2.19, w_0 is not constant and increases with the surfactant concentration. This, as discussed earlier, is due to the ion exchange of potassium with the sodium of the surfactant and consequently to the redistribution of the cations between the two phases. As shown before, when no NaCl was initially added to the aqueous phase, the R_k ratio is only a function of δ. Changing the AOT concentration results in changing the value of δ that alters the value of R_k and through that the concentrations of cations in the two phases. Finally, this change on AOT concentration results in a variation of w_0 as predicted through eq. (2.54).

Figure 2.20 depicts the data for the variation of water uptake in weight percent as a function of the initial KCl concentration in the aqueous phase for three different

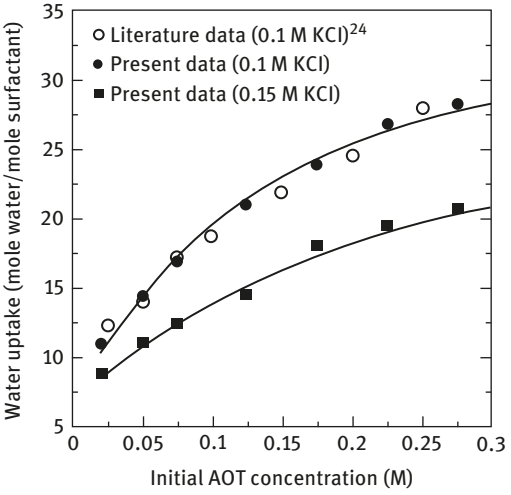

Figure 2.19: Water uptake as a function of surfactant concentration for various initial KCl concentrations; initial organic phase: AOT in isooctane; initial aqueous phase: KCl. Lines are calculated with the model. Reprinted with permission from (Fluid Phase Equilibria, 1996, 122, 169). Copyright (2017) Elsevier.

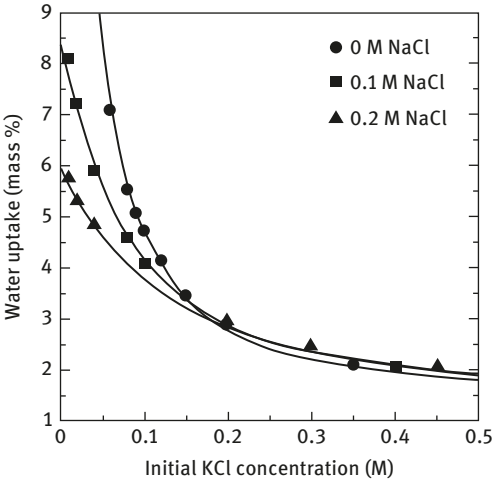

Figure 2.20: Water uptake as a function of initial KCl concentration for various initial NaCl concentrations; initial organic phase: 0.1 M AOT in isooctane; initial aqueous phase: KCl and NaCl. Lines are calculated with the model. Reprinted with permission from (Fluid Phase Equilibria, 1996, 122, 169). Copyright (2017) Elsevier.

initial NaCl concentrations. The initial AOT concentration in the organic phase was 0.1 M in all cases. The solid lines in this figure and the following figures are the predictions of the model. The water uptake decreases with an increase in the KCl concentration for any initial value of the NaCl content. The higher the NaCl content, the lower the water uptake at low KCl concentrations. However, at higher concentrations of KCl, the water uptake is higher for higher NaCl content. This complex experimental behavior is accurately predicted by the model.

The water uptake experimental results in molarity are plotted against the initial concentration of KCl in Figure 2.21, for three different initial AOT concentrations. The

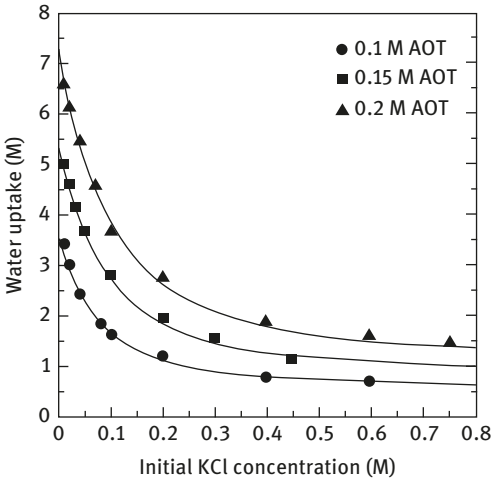

Figure 2.21: Water uptake as a function of initial KCl concentration for various initial AOT concentrations; initial organic phase: AOT in isooctane; initial aqueous phase: KCl and 0.1 M NaCl. Lines are calculated with the model. Reprinted with permission from (Fluid Phase Equilibria, 1996, 122, 169). Copyright (2017) Elsevier.

initial concentration of NaCl in the aqueous phase was 0.1 M in all cases. The water uptake decreases with the initial KCl concentration for all initial AOT concentrations in the organic phase.

Figure 2.22 presents the equilibrium ratio of water to surfactant in the organic phase as a function of initial KCl concentration for different initial volume ratios of the organic phase to the aqueous phase. The initial AOT concentration in the organic phase was 0.1 M, with no NaCl added to the initial aqueous phase. The water uptake results for two different AOT concentrations, with the initial volume ratio set at unity, are also included in this figure. These data, with conditions of $r = 1$ and 0.05 M or 0.2 M AOT, collapse over the data of 0.1 M AOT and different initial volume ratios with $r = 0.5$ or 2, respectively. It is interesting to observe that the corresponding conditions have the same δ value for any initial KCl concentration. This confirms that the concentrations of the species are not suitable variables to describe the distribution of species between the two phases of a reverse micellar system. Instead, the equivalent ratios should be used as prescribed by the present model and the ion distribution model.

Figure 2.23 displays the equilibrium molar ratio of water to surfactant in the organic phase, w_0, versus the initial NaCl concentration in the aqueous phase for different initial KCl concentrations. The initial AOT concentration in the organic phase was 0.1 M and the initial volume ratio was fixed at 0.01. At such a low volume ratio, very small organic phase volume compared to that of aqueous phase, the addition of sufficient amount of KCl to the aqueous phase results in the exchange of almost all the sodium as the surfactant counterion. Thus, almost all of the surfactant molecules are in the form of potassium salt rather than in the original form of sodium salt. Under these conditions, as can be seen comparing the results at very low NaCl concentrations in Figure 2.23, the water uptake drops to smaller values

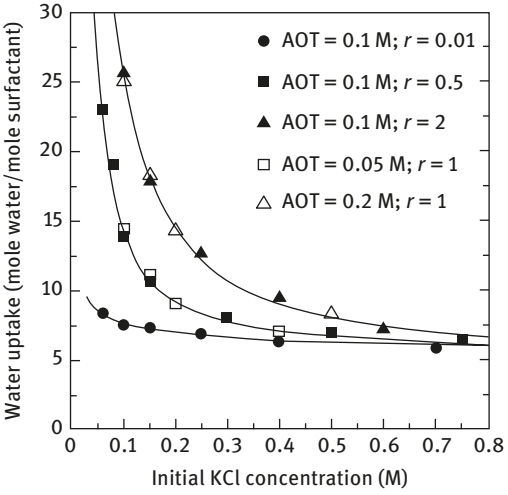

Figure 2.22: Water uptake as a function of initial KCl concentration for various initial volume ratio of organic to aqueous phase (with 0.1 M initial AOT concentration) and for various initial AOT concentrations (with the initial volume ratio of organic to aqueous phase of unity); initial organic phase: AOT in isooctane; initial aqueous phase: KCl. Lines are calculated with the model. Reprinted with permission from (Fluid Phase Equilibria, 1996, 122, 169). Copyright (2017) Elsevier.

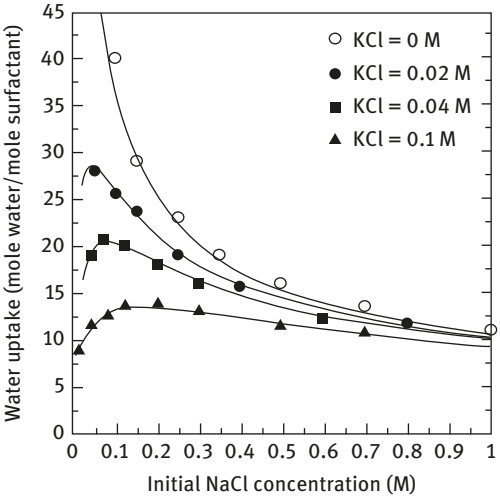

Figure 2.23: Water uptake as a function of initial NaCl concentration for various initial KCl concentrations at 0.01 initial volume ratio of organic to aqueous phase; initial organic phase: 0.1 M AOT in isooctane; initial aqueous phase: NaCl and KCl. Lines are calculated with the model. Reprinted with permission from (Fluid Phase Equilibria, 1996, 122, 169). Copyright (2017) Elsevier.

since water uptake of the potassium salt of the surfactant is lower than that of the sodium salt. Further addition of NaCl to the aqueous phase can re-exchange potassium from surfactant molecules and regain the higher water of the sodium salt of the surfactant. This can be seen by comparing the results for intermediate NaCl concentrations. However, at higher NaCl content, the water uptake decreases due to the dominant effect of ionic strength. The maximum in the water uptake reflects these opposing trends. For higher KCl concentrations, the maximum occurs at higher NaCl concentrations. This is obvious since more sodium is needed to re-exchange more potassium from the surfactant molecules.

More results have been reported by Rabie and Vera [3], showing the presence of the maximum in water uptake and the accurate predication capability of the model for different conditions and for other systems such as DODAC.

2.4.4 Active Interface Model

In Section 2.3, we discussed the dissociation fraction of surfactant. Surfactant molecules are able to dissociate at the reverse micellar interface and produce a surface charge density at the inner core of the reverse micelles. A mathematical model was presented for the prediction of the dissociation fraction of surfactant in the reverse micelles for different conditions of surfactant concentration, and salt type and concentration, in mixed salt systems. We showed that the dissociation fraction of surfactant has no effect on the overall ion distribution between the two phases. In addition, the ion distribution calculations can be done using the universal ion distribution theory discussed in Section 2.2, assuming that all surfactant molecules at the reverse micellar interface are bound to either the original surfactant counterion or other counterions.

In this section, we discuss the impact of the degree of dissociation on water uptake and a mathematical model is presented to predict the water uptake. This is called the active interface model. The active interface model is based on surfactant dissociation fraction. The dissociation of surfactant produces a surface charge density at the reverse micellar interface, which in turn results in a repulsive force between the surfactant head groups. For a single counterion system, the water uptake is only a function of dissociation fraction. In the case of multicounterion systems, a mixing rule is used to obtain the total water uptake contributed by different forms of surfactant. In this case, the water uptake is expressed as moles of water per moles of surfactant, w_0, and eq. (2.42) can be used to convert it to molar water uptake, W.

For a single counterion system, the water uptake is assumed to be only a function of dissociation fraction with the following expression as suggested by the experimental results:

$$w_0 = w_0^{\bullet} \exp(\alpha f) \tag{2.57}$$

where $w_0^{\bullet}$ is the water uptake when the dissociation fraction is zero and it corresponds to the water uptake of a system when the aqueous phase is a highly concentrated salt solution. In eq. (2.57), α is a dimensionless water uptake constant and is assumed to be the same for all counterions. In the case of mixed counterions, the following mixing expression is applied to calculate the value of $w_0^{\bullet}$ for the mixture of counterions from the single-counterion values:

$$w_0^{\bullet} = \sum_{i=1}^{n} Y_i \; w_0^{\bullet,i} \tag{2.58}$$

where ionic strength fraction is defined as

$$Y_i = \frac{z_i^2 \; C_i}{\sum_{k=1}^{n} (z_k^2 \; C_k)} \tag{2.59}$$

The other possible mixing rule is similar to eq. (2.58) using the charge fraction instead of the ionic strength fraction. The equivalent fraction is defined similar to eq. (2.59) using the term z instead of z^2. Our calculations for divalent cations show that there is less agreement between the predictions of the present model and experimental results when an equivalent fraction is used in eq. (2.58). The present model provides the results for the dissociation fraction at the reverse micellar interface, the ion distribution between aqueous and organic phases, and the water uptake.

Having the water uptake, the size of the reverse micelles and aggregation number are calculated from different geometrical models from the simplest [25] to the more sophisticated one [7]. Any of these models can use the experimental water uptake data for the calculation of size of reverse micelles. Little differences are observed between the results obtained from different models. Therefore, the key point is the knowledge of water uptake.

The following geometrical correlations have been proposed [7, 25] for the radius of the water pool, R_{wp}, and the aggregation number of surfactant, n_s:

$$R_{wp} = \frac{3V_w w_0}{A_s} \tag{2.60}$$

$$n_s = \frac{36\pi \; V_w^2 w_0^2}{A_s^3} \tag{2.61}$$

where the volume of a water molecule, V_w, is 30 Å^3 cube and A_s is the area occupied by the head group of a surfactant molecule at the reverse micellar interface. For AOT reverse micelles, Karpe and Ruckenstein [25] assumed A_s to be fixed at 55 Å^2, and Leodidis and Hatton [7] proposed expressing A_s as a function of w_0 from experimentally determined dependence of A_s on w_0 that have been measured by Eicke and Rehak [26]:

$$A_s = 57 - 11 \exp(-0.09163 \; (w_0 - 10)) \tag{2.62}$$

Equation (2.62) shows that A_s is a week function of water uptake. Eastoe et al. [27] studied the effect of surfactant counterion on structure and properties of reverse micelles formed by metal bis(2-ethylhexyl) sulfosuccinate. They saw that even for very low water uptake ($w_0 < 5$), spherical surfactant aggregates are present for the

following counterions: Na^+, K^+, Rb^+, Cs^+, and Ca^{2+}. Increasing w_0 promotes the spherical shape over the cylindrical shape aggregates obtained for transitional metals at low values of w_0. They used Small-Angle Neutron Scattering (SANS) data to calculate the area occupied by head group of a surfactant molecule (A_s).

They observed that this area did not depend on the nature of the counterion for the series of Na^+, K^+, Rb^+, Cs^+, and Ca^{2+} and is equal to 64 ± 6 $Å^2$. Considering that the results of Eastoe et al. [27] were obtained in a different solvent and at very low water uptakes ($w_0 < 5$), this area is very close to the 55 $Å^2$ used by Karpe and Ruckenstein [25]. Therefore, as a simplifying assumption, we consider that A_s stays constant at 55 $Å^2$ for all counterions used in this work. However, this assumption is not crucial for the model presented here.

The procedure for evaluation of parameters used in eq. (2.57) is discussed below. As in Figure 2.9, the dissociation fraction of the AOT–NaCl system is calculated using experimental water uptake results. When these results are plotted as a function of logarithm of water uptake results, as presented in Figure 2.24 for Na(AOT)–NaCl, a linear relation is obtained. This figure also contains the results of K(AOT)–KCl, which are discussed below.

The slope of the line is $1/\alpha$ and the intercept of this line with x axis provides the value of $w_0^{\bullet,i}$ for sodium. These parameters are $\alpha = 7.53$ and $w_0^{\bullet,Na} = 6.5$ moles of water per mole of surfactant. As discussed earlier, the value of α is assumed to be the same for any counterion and the value of $w_0^{\bullet,i}$ corresponds to water uptake of an organic phase, in contact with a highly concentrated salt solution with dissociation fraction approaching zero. However, making such an electrolyte solution may not be possible for many salts because of the solubility limit in water.

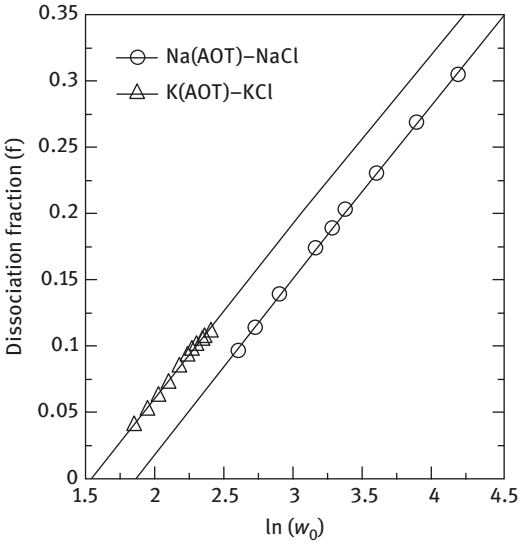

Figure 2.24: Dissociation fraction as a function of logarithm of water uptake; initial organic phase: 0.1 M Na(AOT) or K(AOT); initial aqueous phase: NaCl or KCl. Reprinted with permission from (J. Phys. Chem. B, 1997, 101, 10295). Copyright (2017) American Chemical Society.

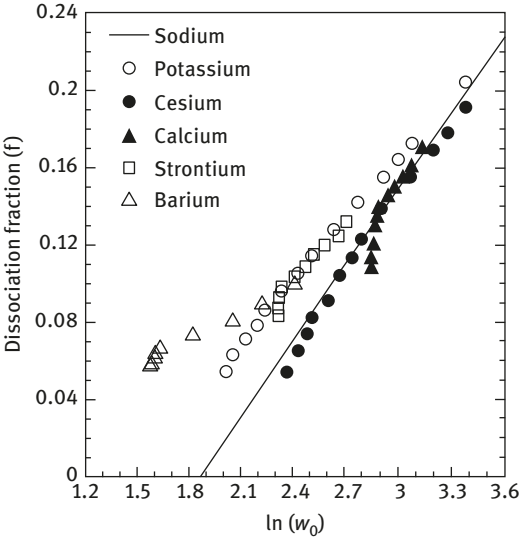

Figure 2.25: Dissociation fraction as a function of logarithm of water uptake; initial organic phase: 0.1 M AOT; initial aqueous phase: chloride salt. Reprinted with permission from (J. Phys. Chem. B, 1997, 101, 10295). Copyright (2017) American Chemical Society.

Figure 2.25 presents the dissociation fraction values for Na(AOT) for a system in which different cations are added. This figure also contains the data for sodium shown as a solid line. The dissociation fraction for different monovalent and divalent cations approaches that of sodium at higher water uptakes corresponding to lower slat concentrations. Under these conditions, the system has smaller amount of added counterion and most of the surfactant head groups are engaged with sodium, the original surfactant counterion, either in bound or dissociated forms. As such, the system behavior approaches that of the Na(AOT)–NaCl system. The values of $w_0^{\bullet,i}$ listed in Table 2.2 for different cations are obtained with a least-squares fit of eqs. (2.57) and (2.58) to the results of Figure 2.25 and the ion distribution data.

In principle, the value of $w_0^{\bullet,i}$ for any cation can be obtained using a method similar to that of Figure 2.24, with the surfactant form of that cation instead of sodium. We did experiments with potassium form of surfactant to verify the assumption of having the same α for any counterion. As shown in Figure 2.24, the dissociation fraction results for K(AOT)–NaCl as a function of logarithm of water uptake also follows a linear relation with a slope very close to that for Na(AOT)–NaCl, validating our assumption. The values of the parameters α and $w_0^{\bullet,\mathrm{K}}$ then were obtained as 7.67 and 4.63 from the results of the K(AOT)–KCl system. Interestingly, the value of $w_0^{\bullet,\mathrm{K}}$ = 4.63 is also very close to the value 4.7 (in Table 2.2) obtained from the results of the Na(AOT)–KCl system.

At this stage knowing the water uptake parameters, the complete set of equations can be used to calculate the dissociation fraction and the water uptake. Therefore, there is no need for experimental water uptake data for the prediction of the

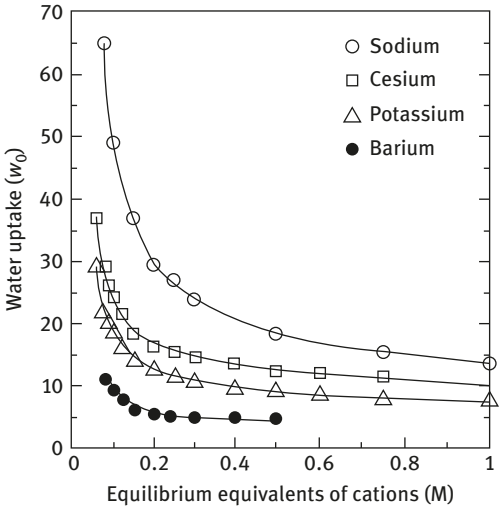

Figure 2.26: Water uptake as a function of equilibrium equivalents of cations in the aqueous phase for different cations; initial organic phase: 0.1 M AOT; initial aqueous phase: chloride salt. Reprinted with permission from (J. Phys. Chem. B, 1997, 101, 10295). Copyright (2017) American Chemical Society.

dissociation fraction. The calculated and experimental water uptake results are shown in Figure 2.26 for some monovalent and divalent cations. The calculated values shown as solid lines reproduce the experimental results within 0.5–2%.

As the water uptake is well predicted by the model, our dissociation fraction results, using the complete set of equations, followed closely the results of Figures 2.9 and 2.10 for different cations. The results of Figure 2.9 and 2.10 were obtained using experimental water uptake data. Interestingly, the poorest predictions shown in Figure 2.26 are for Ba, which, in turn, has the lowest water uptake. In fact, the assumption of a head group area A_s of 55 Å^2 for AOT is probably questionable at such a low water uptake.

The current model predictions are compared with water uptake results for the system of AOT–isooctane–NaCl–KCl–water for different conditions of the initial surfactant, NaCl, and KCl concentrations and of the initial volume ratio of the phases. An excellent agreement is obtained. For comparison, two sets of results are shown in Figure 2.27. This figure shows the water uptake as a function of surfactant concentration for different KCl concentrations. No NaCl was added initially, and the initial volume ratio was set at unity.

The model predictions shown as solid lines are in a very good agreement with experimental results. As discussed earlier and shown before [3, 24], the water uptake in moles of water per mole of surfactant does not change with AOT concentration in the presence of sodium salt. However, as shown in Figure 2.27, the water uptake is not constant and increases with surfactant concentration for any initial KCl concentration. This system is a mixed counterion system of sodium and potassium. Therefore, some of the surfactant molecules at the reverse micellar interface are in potassium form and some in sodium form. As

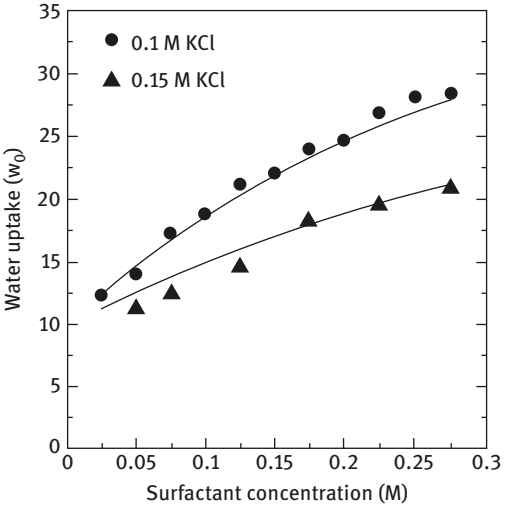

Figure 2.27: Water uptake as a function of surfactant concentration for different initial KCl concentration; initial organic phase: AOT; initial aqueous phase: KCl. Reprinted with permission from (J. Phys. Chem. B, 1997, 101, 10295). Copyright (2017) American Chemical Society.

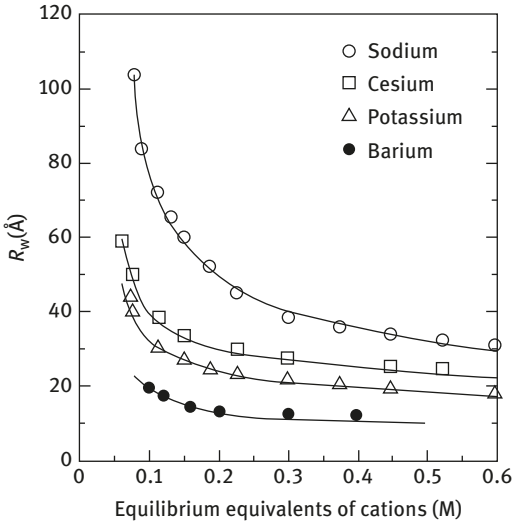

Figure 2.28: Radius of the water pool as a function of equilibrium equivalents of cations in the aqueous phase for different cations; initial organic phase: 0.1 M AOT; initial aqueous phase: chloride salt. Reprinted with permission from (J. Phys. Chem. B, 1997, 101, 10295). Copyright (2017) American Chemical Society.

such, surfactant nature is changed, and this determines both the dissociation fraction and water uptake.

The reverse micellar sizes are calculated from eq. (2.60) with water uptake numerical results shown in Figure 2.26 are presented in Figure 2.28. The calculated results presented in Figure 2.26 are in close agreement with the calculated results of Leodidis and Hatton [7] depicted as solid circles in Figure 2.28.

2.5 Counterion Effect of Amino Acids in Reverse Micelles

This section discusses the effect of amino acids at zwitterionic condition on water uptake of AOT reverse micellar system. The details can be found in the work from Rabie and Vera [28]. This section shows that amino acids can act similar to a counterion affecting the reverse micelles. The amino acid at zwitterionic condition ($A_{f\pm}$) in the water pool can react with the sodium salt of an anionic surfactant, SNa, at the reverse micellar interface:

$$\mathrm{SNa} + A_{f\pm} \rightleftharpoons \mathrm{SANa} \tag{2.63}$$

where, as in the previous sections, subscript "f" refers to the free species inside the water pool and serves to distinguish them from those bound at the reverse micellar interface. SANa stands for the complex of surfactant and amino acid with sodium (Na) as counterion.

The SANa complex can dissociate to release Na into the water pool and leave a surfactant–amino acid anion, SA^-, with one negative charge [19]:

$$\mathrm{SANa} \rightleftharpoons \mathrm{SA}^- + \mathrm{Na}_f^+ \tag{2.64}$$

These reactions, along with the mass balances of different species in the system, have provided excellent predictions for the extraction of different amino acids under various conditions of mixed salt aqueous system [19]. These results are discussed in detail in Chapter 6. The resulting expression for partitioning of amino acid is not repeated here. This expression uses the equilibrium constants of eq. (2.63) and (2.64) (K_c and K_d, respectively) and the initial conditions of the system to calculate the concentrations of different species at equilibrium. The values of these equilibrium constants for different amino acids are provided in Chapter 6.

The equilibrium constant of eq. (2.54) was found to be very small [19]. Therefore, the change in the concentration of Na in the aqueous phase is negligible [19]. Considering this fact, and that for a zwitterionic amino acid dipolar molecule there is no net charge, the ionic strength of the aqueous phase can be assumed to remain unchanged in the presence of a zwitterionic amino acid. In addition, it can safely be assumed that most of the amino acid molecules at the reverse micellar interface are in the form of the complex SANa [19]. Therefore, we use here the total concentration of amino acid, at the reverse micellar interface, as the concentration of the surfactant–amino acid complex. This concentration, $\bar{C}_{A,b}$ is

$$\bar{C}_{A,b} = \frac{C_A^0 - C_A}{r} \tag{2.65}$$

The concentration of the surfactant in the form of SNA can be from the following relation:

$$\bar{C}_{\mathrm{Na,b}} = \bar{C}_{\mathrm{S}}^{0} - \frac{C_{\mathrm{A}}^{0} - C_{\mathrm{A}}}{r} \tag{2.66}$$

In this section, we model the water uptake of the system in the presence of the different forms of surfactant with the linear model presented in Section 2.4.1:

$$\frac{W_{\mathrm{SNA}}}{\bar{C}_{\mathrm{Na,b}}} = \frac{\alpha_{\mathrm{NA}}}{\alpha_{\mathrm{A}}} \frac{W_{\mathrm{SANa}}}{\bar{C}_{\mathrm{A,b}}} \tag{2.67}$$

Equation (2.67) is similar to eq. (2.44) except the parameter α in eq. (2.44) is replaced with the ratio shown in eq. (2.67). The water uptakes of different forms are considered at the same ionic strength of the aqueous phase. The dimensionless parameters α_{NA} and α_{A} are characteristics values for each forms of the surfactant. These values for AOT system and different cations have been reported earlier [3].

We use the same assumption as in Section 2.4.1 that all the counterion sites of the surfactant are filled at the reverse micellar interface. Combining the equations yields the following relation for the water uptake:

$$w_0 = w_0^{\star}\left(1 + \frac{\left(\frac{\alpha_{\mathrm{A}} - \alpha_{\mathrm{Na}}}{\alpha_{\mathrm{Na}}}\right)\bar{C}_{\mathrm{A,b}}}{\bar{C}_{\mathrm{S}}^{0}}\right) \tag{2.68}$$

The term $w_0^{\star}$ is simply the water uptake in terms of moles of water per mole of the surfactant when no amino acid is present in the system. As stated earlier, eq. (2.68) applies to the case of an amino acid or zwitterionic condition, so it can be assumed that its presence does not change the ionic strength. In fact, the calculations are simpler when the equilibrium ionic strength is the same as the initial ionic strength. This is consequent of the fact that the water pool has the same composition as the excess aqueous phase.

The concentration of amino acid complex SANa can be found as prescribed in Chapter 6 using the same counterion binding approach as discussed through this chapter. By knowing the α parameters, we can then calculate the water uptake for a wide range of initial system conditions. The water uptake results and model predictions are presented below. For amino acids that are not extracted at the reverse micellar interface at their zwitterionic condition, the value of their concentration at reverse micellar interface as complex SANA is zero. Therefore, the water uptake does not change in the presence of these amino acids.

In the following results, equal volumes of the two phases were used for all experiments. The data are reported as equilibrium water uptake, molar ratio of

water to surfactant in organic phase (w_0), or fractional transfer of water to organic phase (t_w), which is proportional to w_0:

$$t_w = \frac{r\,\bar{C}_S^0}{55.5}\,w_0 \tag{2.69}$$

the value of α_A can be evaluated from fitting limited experimental data. Knowing this parameter, and suing the values reported for α_{Na} and w_0^*, it is possible to predict the water uptake for other conditions. However, the main purpose of this work was to show that departure of water uptake from w_0^*, in the presence of amino acids, is due to the counterion effect of the amino acid. Therefore, using the experimental results for w_0^* and the equilibrium water uptake, the parameter in eq. (2.68) has been determined. The evaluation of this parameter is explained below.

Equation (2.68) shows that the water uptake varies linearly with the final amino acid concentration in the organic phase. It was previously found that a linear relation exists between the final amino acid concentration in the organic phase and its initial concentration in the aqueous phase [19, 20]. This fact is well predicted by this model. Figure 2.29 shows the water uptake, in moles of water per mole of surfactant, as a function of the initial amino acid concentration for phenylalanine, leucine, and glycine. The initial concentration of AOT in the organic phase was 200 mM with 130 mM Na. The data of phenylalanine were duplicated in this work. As shown in this figure, the water uptake increased linearly for each of the amino acids. However, in glycine, the presence of amino acid has no effect on the water uptake. This is to be expected since glycine is not extracted into the reverse micellar interface at its zwitterionic condition [19, 20]. The value of the coefficient in eq. (2.68) was evaluated by a least-squares fit of eq. (2.68) to the data of water uptake in Figure 2.29. The value of this parameter is 7.0 for phenylalanine. Similar calculation for leucine gave the value of 9.8.

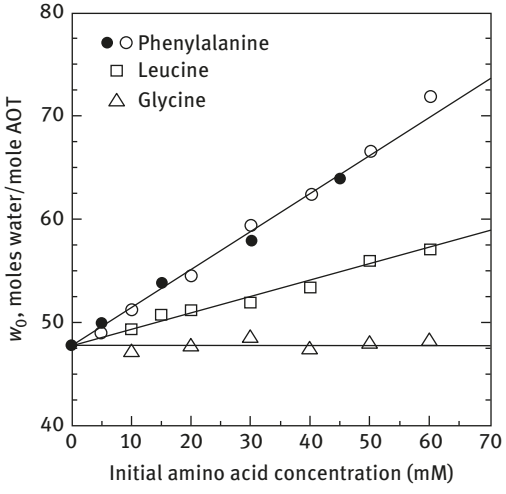

Figure 2.29: Water uptake as a function of initial amino acid concentration for different amino acids; initial organic phase: 200 mM AOT in isooctane; initial aqueous phase: 130 mM sodium and amino acid. Reprinted with permission from (Fluid Phase Equilibria, 1997, 135, 269). Copyright (2017) Elsevier.

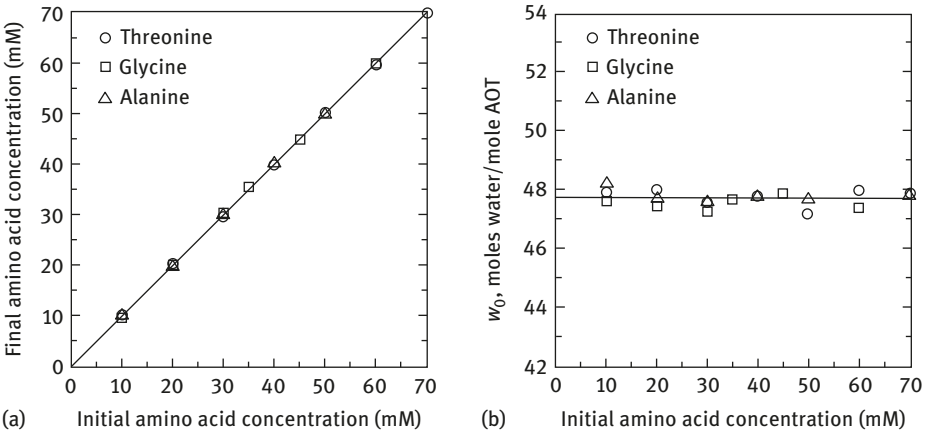

Figure 2.30: (a) Effect of initial amino acid concentration on the residual amino acid concentration in the excess aqueous phase for different amino acids; (b) Effect of amino acid concentration on the water uptake for different amino acids; initial organic phase: 250 mM AOT in isooctane; initial aqueous phase: 100 mM sodium and amino acid. Reprinted with permission from (Fluid Phase Equilibria, 1996, 122, 169). Copyright (2017) Elsevier.

In Figure 2.30(a), the results of the final amino acid concentration in the excess aqueous phase are plotted as a function of the initial amino acid concentration for threonine, glycine, and alanine. The initial concentration of AOT was 250 mM with 100 mM NA. As shown, the data fell on the 45° line. It means that although these amino acids were extracted to the water pools, no amino acid was extracted at the reverse micellar interface. As discussed elsewhere [19], depending on the nature of the amino acids, some of them can interact with the reverse micellar interface and some cannot. Phenylalanine and leucine are two amino acids that are interfacially active at their zwitterionic state.

Figure 2.30(b) shows the water uptake data in moles of water per mole of surfactant for the results of Figure 2.30(a). As expected, w_0 remains constant and did not vary with the initial amino acid concentration for any of the amino acids. Similar results were obtained for different initial AOT and salt concentrations. These experimental findings confirm that only the amino acids that are present at the reverse micellar interface can alter the water uptake, and this is consistent with the basic concepts of the present model. In the next two figures, the predictions of the model are compared with the experimental results for one of the interfacially active amino acid.

Figure 2.31 shows the water uptake, w_0, as a function of the initial phenylalanine concentration in mM for various initial Na concentrations. The initial surfactant concentration was 200 mM in isooctane. The solid line for the case of 130 mM Na shows the correlation capability of the model and the other solid lines are the predictions of the model. In Figure 2.31, the water uptake increases linearly for any initial Na concentrations from the corresponding water uptake of a system without an

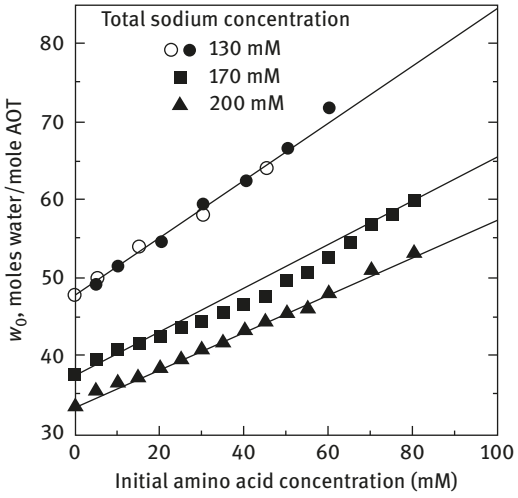

Figure 2.31: Water uptake as a function of initial phenylalanine concentration for different sodium concentrations; initial organic phase: 200 mM AOT in isooctane; initial aqueous phase: sodium and phenylalanine. Reprinted with permission from (Fluid Phase Equilibria, 1996, 122, 169). Copyright (2017) Elsevier.

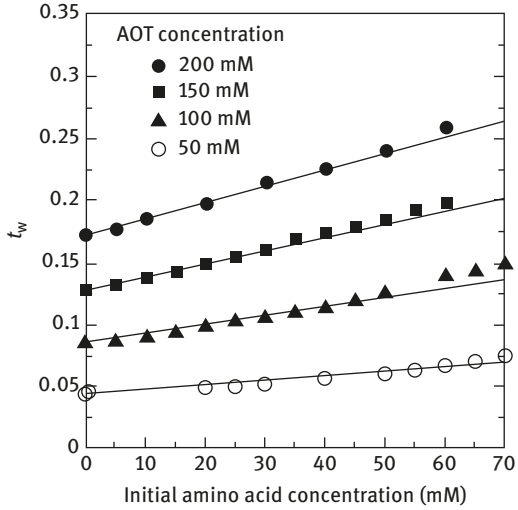

Figure 2.32: Water uptake as a function of initial phenylalanine concentration for different AOT concentrations; initial organic phase: AOT in isooctane; initial aqueous phase: 130 mM sodium and phenylalanine. Reprinted with permission from (Fluid Phase Equilibria, 1996, 122, 169). Copyright (2017) Elsevier.

amino acid that agrees well with the predictions of the model. The water uptake was higher for lower salt concentrations.

Figure 2.32 presents the water uptake data as t_w as a function of the initial phenylalanine concentration for various initial surfactant concentrations. The initial Na concentration was fixed at 130 mM with an initial volume ratio of one. Similar to the results of Figure 2.31, the water uptake increased linearly with the initial amino acid concentration for any initial AOT concentration. For a fixed initial amino acid concentration, the water uptake increased with the surfactant concentration. The predictions of the model, shown as solid lines, are in good agreement with the experimental data.

2.6 A Simple Model for Reverse Micellar Extraction of Proteins

This last section is focused on extending the principles of ion distribution theory to the extraction of proteins into the reverse micellar phase. The details can be found in the work by Rabie and Vera [29]. As before, the experiments are done using the contact method and the model uses the equilibrium constant for the ion exchange of the protein and the surfactant counterion and the equilibrium constant of protein in the aqueous phase to express the extraction of proteins for the effects of salt type and concentration, pH, surfactant concentration, and volume ratio of the two phases.

As discussed in this section, the negatively charged proteins are extracted from the aqueous phase by exchanging chloride counterion of DODAC (a cationic surfactant) at the reverse micellar interface. The introduction of other counterions different from chloride in the system through addition of salts has a significant impact on extraction. The added counterions can exchange the chloride of surfactant and changing its nature and, therefore, altering the extraction of the negatively charged proteins. Although the model presented here is focused on a cationic surfactant system, it is fully applicable to other surfactants including anionic ones.

This model for extraction of proteins with reverse micelles in a Winsor II system is based on the following assumptions:

1. At equilibrium, the concentration of any solute in the water pool is assumed to be the same as that in the excess aqueous phase.
2. At equilibrium, all the surfactant is in the organic phase participating at the reverse micellar interface.
3. The equilibrium constant of ion exchange reactions are expressed in terms of concentrations.
4. The solubility of solutes in the organic solvent is negligible.
5. The presence of protein has no significant effect on distribution of other ions.
6. Even though a protein molecule can have different charge numbers, for simplicity it is assumed that only two forms of protein exist. These are a protein at its isoelectric point with no net charge and a protein carrying z negative charges (in the case of cationic surfactant studies here; but the same can be applied for other systems and anionic surfactants).

Assumptions 1–4 have already been discussed in the previous sections. Assumption 5 is valid under the experimental conditions of this study since the concentration of protein used here is extremely small. A concentration of 1 g/L of α-chymotrypsin is equivalent to 40 μM. Assumption 6 is used as due to steric effects (considering the geometry of reverse micelles and the conformation of protein), a protein molecule with several charges cannot bind all of the charges to the surfactant head groups.

Therefore, there should be a maximum number of binding sites for a specific protein, despite the fact that this number cannot be measured experimentally.

The positively charged proteins do not have any major role in the extraction of proteins with DODAC; therefore, there is no need to consider them in this study. The value of z was determined by trial and error. Different values were assumed to obtain the best fit of the model presented below and the experimental data of protein extraction shown in Figure 2.33 (discussed later in this section). When increasing the value of z did not enhance the correlation of experimental results, the lowest value was selected. As such, the value of z was obtained as 2. The present model is structured for a cationic surfactant like DODAC in the presence of one protein and hydroxide and chloride anions. However, the model can be applied to other cationic and anionic surfactants with ad hoc modifications, and it can be extended to systems containing more than one protein and two anions.

Proteins in the aqueous phase at their isoelectric points have no net charge. However, in the presence of acids or bases proteins undergo a series of reactions, which result in a net charge. Proteins can gain one or several charges, positive or negative, depending on pH. For example, α-chymotrypsin can gain charges from −16 to +14 in a pH range varying from 12 to 3 [30]. The reaction of a protein molecule at its isoelectric point (P^i) with hydroxide to produce a protein with z negative changes (P^{z-}) can be given as

$$P^i + z\mathrm{OH}^- \rightleftharpoons P^{z-} \tag{2.70}$$

The equilibrium constant of reaction (2.70) in terms of concentrations is

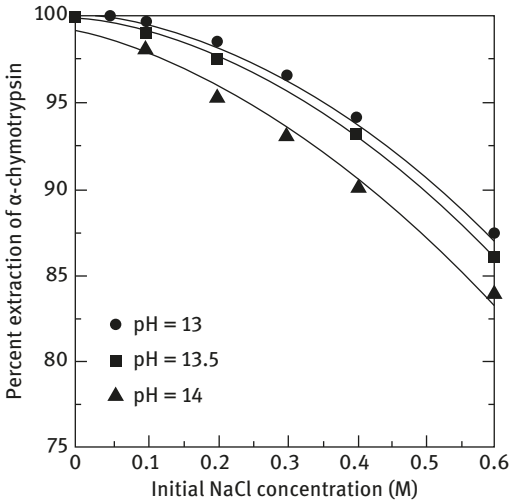

Figure 2.33: Extraction of α-chymotrypsin as a function of NaCl concentration for different pHs; initial organic phase: 100 mM DODAC, 250 mM decanol in isooctane; initial aqueous phase: 0.5 g/L protein. Reprinted with permission from (Separation Science and Technology, 1998, 33(8), 1181). Copyright (2017) Taylor & Francis.

$$K_{Pz} = \frac{C_{Pz-}}{C_{Pi}\ (C_{OH})^z} \tag{2.71}$$

The negatively charged protein in the water pool undergoes an ion exchange reaction with surfactant counterion similar to what was discussed in Section 2.2 with equilibrium constant denoted as K_S^{Pz} for simplicity. The equations of mass balance on protein are also used along with similar definitions as in Section 2.2. As previously shown [22], hydroxide can also undergo an ion exchange reaction with the chloride of the surfactant with equilibrium constant denoted as K_S^{OH}. This equilibrium constant for DODAC system has been reported as 0.096 [12, 22]. The SOH form of surfactant can also extract the protein. However, the corresponding reactions are not independent from the other reactions presented above.

The data presented as the overall percent extraction of protein to the organic phase are calculated from

$$\xi_P = 100 \times \left(C_P^0 - C_P\right)/C_P^0 \tag{2.72}$$

Combining the equilibrium constant equations (for K_{Pz} , K_S^{Pz}, and K_S^{OH}), the mass balance on protein with $z = 2$ results in the following equation. The full treatment is provided in reference [29]:

$$\xi_P = \frac{100 \times r}{\frac{1}{K_S^{Pz}\,K_{Pz}}\left(\frac{C_{Cl}}{C_{Cl,b}\,C_{OH}}\right)^z + \frac{1}{K_S^{Pz}}\left(\frac{C_{Cl}}{C_{Cl,b}}\right)^z + r} \tag{2.73}$$

In eq. (2.73), the concentrations of chloride and hydroxide in the excess aqueous phase and the concentration of bound chloride at the reverse micellar interface are calculated using the ion distribution theory in Section 2.2. In eq. (2.73), there are two parameters (K_{Pz} and K_S^{Pz}). The evaluation of these parameters is discussed below.

Using the value of $z = 2$, the two parameters were obtained by a least-squares fit of eq. (2.73) to the data in Figure 2.33. These values are $K_{Pz} = 3.2 \times 10^{24}$ and $K_S^{Pz} = 250$. The curves in Figure 2.33 are the least-squares fits with these parameters. As shown in Figure 2.33, the extraction decreased with the addition of NaCl or NaOH (used for pH adjustment) providing chloride or hydroxide, respectively. These ions compete with the protein molecules for extraction with the surfactant head groups.

Figure 2.34 presents the effect of surfactant concentration on extraction of α-chymotrypsin for different initial NaCl concentrations. The curves are the model predictions using the parameters given above; no additional fitting was performed. The surfactant concentration effect on extraction does not appear directly in eq. (2.73). However, it affects the extraction through changes in the distribution of hydroxide and chloride as shown previously [22].

As shown in Figure 2.34, the extraction increases with the addition of surfactant reaching a plateau at higher surfactant concentrations. The minimum amount of

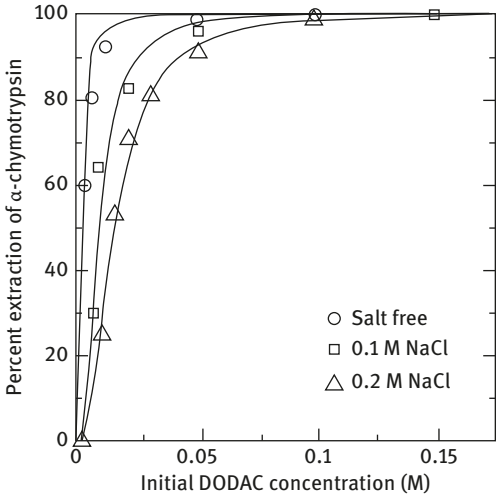

Figure 2.34: Extraction of α-chymotrypsin as a function of DODAC concentration for different initial NaCl concentrations; initial organic phase: 250 mM decanol in isooctane; initial aqueous phase: 0.5 g/L protein, pH 13.5. Reprinted with permission from (Separation Science and Technology, 1998, 33(8), 1181). Copyright (2017) Taylor & Francis.

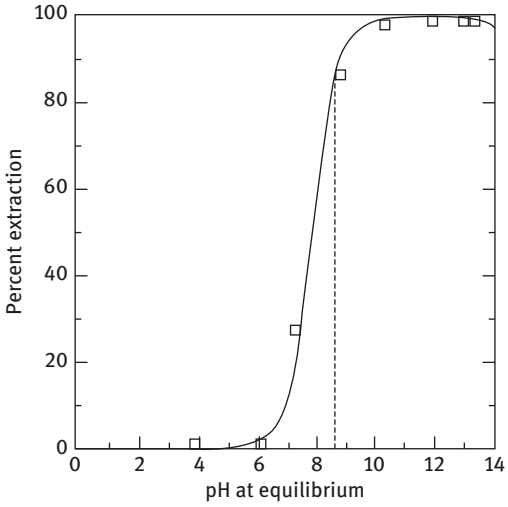

Figure 2.35: Effect of pH on the extraction of a-chymotrypsin; initial organic phase: 100 mM DODAC, 250 mM decanoal in isooctane; initial aqueous phase: 0.5 g/L protein, 100 mM NaCl. Reprinted with permission from (Separation Science and Technology, 1998, 33(8), 1181). Copyright (2017) Taylor & Francis.

surfactant required to extract α-chymotrypsin quantitatively from the aqueous phase (for example 90% extraction) increases with initial salt concentration. Similar results have been obtained by Fletcher and Parrot [31] for extraction of α-chymotrypsin with AOT in heptane and by Ichikawa et al. [32] for extraction of cytochrome c with AOT in isooctane.

Figure 2.35 shows the extraction of α-chymotrypsin as a function of pH. The curve in this figure presents the predictions of the model without any additional fitting. The model predictions are in good agreement with the experimental results. The dashed line in Figure 2.35 indicates the approximate isoelectric point of the protein. Over a

wide range of pH above the isoelectric point, while protein molecules are negatively changed, almost 100% extraction was obtained.

Previous results for TOMAC and AOT showed [33] that the maximum extraction of different proteins was 40–70% for TOMAC and about 80–100% for AOT, both in a narrow pH range. This significant drop in extraction of proteins at favorable pH values, which is a characteristic of AOT and TOMAC, was not observed with DODAC. This significant drop was found [32, 33] to be because of the formation of a surfactant–protein complex usually precipitating at the interface between aqueous phase and organic phase. No precipitate was observed for the results with DODAC.

This chapter concludes by mentioning another work done by Wang and Vera [34]. In that work, a thermodynamic model for the partition of all ionic species in reverse micellar extraction of amino acids with a cationic surfactant was presented. The model is rather complex and in its initial form it included at least 15 binary interaction parameters for a flash calculation of the water uptake and the concentrations of five ionic species in the two phases. After rational simplifications, N parameters were required to represent data for N ionic species. These parameters could be evaluated from data for as few as five experimental points. Good results were shown for the extraction of aspartic acid, glutamic acid, and threonine from aqueous solutions with reverse micelles formed by a cationic surfactant in isooctane with 1-decanol cosurfactant.

2.7 Citations

The works presented in this chapter have been cited by several other researchers over the years [35–85].The ion distribution theory and counterion binding phenomena have been cited and the basic of the theory has been applied [35, 37–42, 48, 51, 52, 57, 60, 62, 63, 65, 68, 69, 73, 76]. The partitioning of several different solutes between aqueous phase and reverse micellar organic phase has been studied. In the work by Wille and Prusiner [41], they observed a novel crystallization of proteins grown from reverse micelles that can shed light into understanding of the underling events for prion diseases. In another work by El Seoud and Pires [68], they used hydrogen nuclear magnetic resonance and Fourier-transform infrared to study the reverse micelles using a cationic surfactant with different counterions. Interestingly, they observed that water does not seem to exist as structurally different layers but rather one pseudophase. Different counterions had different dissociation constants but they did not affect the finding about water state. This finding confirms some of the basic assumptions for the ion distribution theory. Reverse micelles have received great attention for the formation of nanoparticles [60, 65]. The presence of different ions and water uptake have significant impact on size and structure of these nanoparticles. In another example, the work of Goncalves et al. [52] uses the ion exchange concept for counterion exchange selectivity of copper into AOT reverse micelles.

The water uptake of reverse micelles has a great influence on the extraction, enzymatic activities, formation and structures of nanoparticles, and many other processes involving reverse micelles. The water uptake, the water state, and water properties in the reverse micellar phase have been studied over the years. In the work of Simorellis et al. [64], they used NMR spectroscopy to monitor the quantity and structure of encapsulated water at temperatures as low as −30 °C, indicating the presence of transient water populations. Nassar and Hussain [66, 67] showed that the mathematical model based on correlations for water uptake by Winsor type II microemulsions can account for the effect of system variables on the iron hydroxide nanoparticle uptake by AOT reverse micelles.

The extraction of different proteins and amino acids has been studied over a wide range of conditions and using different reverse micellar systems. The basics of couterion exchange model for the prediction of extraction have been used and expanded to other systems. For example, Haghtalab and Osfouri [58, 59] used such approach for CTAB (cetyltrimethylammonium bromide) and NaDEHP (sodium bis(2-ethylhexyl)phosphate) systems. In addition, the precipitation of proteins with surfactant has been reported widely. Proteins may undergo different modifications in the reverse micellar systems. For example, Zaho et al. [80] used far-ultraviolet circular dichroism spectroscopy to study the conformations of protein from soybean flour.

References

[1] Luzar A, Bratko D. J Chem Phys 1990, 92, 642.
[2] Rabie HR, Vera JH. Langmuir 1995, 11, 1162.
[3] Rabie HR, Vera JH. Fluid Phase Equilibr 1996, 122, 169.
[4] Shallcross DC, Hermann CC, McCoy BJ. Chem Eng Sci 1988, 43, 279.
[5] Bajpai RK, Gupta AK, Rao MG. J Phys Chem 1973, 77, 1288.
[6] Aveyard R, Binks BP, Clark S, Mead J. J Chem Soc Faraday Trans 1, 1986, 82, 125.
[7] Leodidis EB, Hatton TA. Langmuir 1989, 5, 741.
[8] Bruno P, Caselli M, Luisi PL, Maesgtro M, Traini A. J Phys Chem 94, 1990, 5908.
[9] Conway BE. Ionic Hydration in Chemistry and Biophysics, Elsevier, Amsterdam, 1981.
[10] Noyes RM. J Am Chem Soc 1962, 84, 513.
[11] Vijayalakshmi CS, Gulari E. Sep Sci Technol 1991, 26, 291.
[12] Rabie HR, Weber ME, Vera JH. J Colloid Interface Sci 1995, 174, 1.
[13] Abuin EB, Rubio MA, Lissi EA. J Colloid Interface Sci 1993, 158, 129.
[14] Wong M, Thomas JK, Nowak T. J Am Chem Soc 1977, 99, 4730.
[15] Beunen JA, Ruckenstein E. J Colloid Interface Sci 1983, 96, 469.
[16] Evans DF, Mitchell DJ, Ninham BW. J Phys Chem 1984, 88, 6344.
[17] Leodidis EB, Hatton TA. In Structure and Reactivity in Reverse Micelles, Pileni, MP, Ed., Elsevier, New York, 1989.
[18] Rabie HR, Vera JH. J Phys Chem B 1997, 101, 10295.
[19] Rabie HR, Vera JH. Ind Eng Chem Res 1996, 35, 3665.

[20] Leodidis EB, Hatton TA. J Phys Chem 1990, 94, 6400.
[21] Rabie HR, Helou D, Weber ME, Vera JH. J Colloid Interface Sci 1997, 189, 208.
[22] Rabie HR, Vera JH, Langmuir 1996, 12, 3580.
[23] Chou S, Shah DO. J Colloid Interface Sci 1981, 80, 311.
[24] Fletcher PDI. J Chem Soc Faraday Trans 1, 1986, 82, 2651.
[25] Karpe P, Ruckenstein E. J Colloid Interface Sci 1990, 137, 408.
[26] Eicke HF, Rehak J. Helv Chim Acta 1976, 59, 2883.
[27] Eastoe J, Fragneto G, Robinson BH, Williams J, Heenan RK. J Phys Chem 1993, 97, 1459.
[28] Rabie HR, Vera JH. Fluid Phase Equilibr 1997, 135, 269.
[29] Rabie HR, Vera JH. Sep Sci Technol 1998, 33(8),1181.
[30] Haynes CA, Tamura K, Korfer HR, Blanch HW, Prausnitz JM. Sep Sci Technol 1992, 96, 905.
[31] Fletcher PDI, Parrot D. J Chem Soc Farady Trans 1, 1988, 84, 1131.
[32] Ichikawa S, Imai M, Shimizu M. Biotechnol Bioeng 1992, 39, 20.
[33] Dekker M, Leser ME. Highly Selective Separations in Biotechnology (G. Street Ed.), Chapman & Hall, London, 1994.
[34] Wang W, Vera JH. Sep Sci Technol 1997, 32, 1189.
[35] Choi K, Tedder DW. Ind Eng Chem Res 1996, 35(6), 2048.
[36] Zabaloy MS, Vera JH, J Chem Eng Data 1996, 41, 1499.
[37] Choi K, Tedder DW. AICHE J 1997, 43, 196.
[38] Moulik SP, Paul BK. Adv Colloid Interface Sci 1998, 78, 99.
[39] Garcia-Rio L, Mejuto JC, Ciri R, Blagoeva IB, Leis JR, Ruasse M-F. J Phys Chem 1999, 103, 4997.
[40] Silber JJ, Biasutti A, Abuin E, Lissi E. Adv Colloid Interface Sci 1999, 82, 189.
[41] Wille H, Prusiner SB, Biophys J 1999, 76, 1048.
[42] Fang X, Yang C. J Colloid Interface Sci 1999, 212, 242.
[43] Rodrigues EMG, Milagres AMF, Pessoa Jr. A. Process Biochem 1999, 34, 121.
[44] Kilikian BV, Bastazin MR, Minami NM, Goncalves EMR, Junior AP. Braz J Chem Eng 2000, 17, 1678.
[45] Soni K, Madamwar D, Process Biochem 2000, 36, 311.
[46] Poppenborg LH, Brillis AA, Stuckey DC. Sep Sci Technol 2000, 35, 843.
[47] Singh R, Dutta PK. Langmuir 2000, 16, 4148.
[48] Rosoff M. Nano-Surface Chemistry, Marcel Dekker, Inc., 2001
[49] Hebbar HU, Hemavathi AB, Sumana B, Raghavarao KSMS. Sep Sci Technol 2001, 46, 1656.
[50] Shin YO, Vera JH. Biotech Bioeng 2002, 80, 537.
[51] Lida M, Asayama K, Ohkawa S. Bull Chem Soc Jpn 2002, 75, 521.
[52] Goncalves SAP, De Pauli SH, Tedesco AC, Quina FH, Okano LT, Bonilha BS. J Colloid Interface Sci 2003, 267, 494.
[53] Rho S, Kang CH, Korean Journal of Chemical Engineering, 2003, 20, 517.
[54] Shin YO, Weber ME, Vera JH. Fluid Phase Equilibr 2003, 207, 155.
[55] Rohloff CM, Shimek JW, Dungan SR. J Colloid Interface Sci 2003, 261, 514.
[56] Kim SJ, Cho YH, Park W, Han D, Chai C-H, Imm JY. J Agric Food Chem 2003, 51, 7805.
[57] Ganguli D, Ganguli M: Inorganic Particle Synthesis via Macro-and Microemulsions, Springer Science + Business Media, LLC, 2003.
[58] Haghtalab A, Osfouri S. Sep Sci Technol 2003, 38, 553.
[59] Haghtalab A, Osfouri S. Iran J Biotechnol 2004, 2, 106.
[60] Kitchens CL, McLeod MC, Roberts CB. Langmuir 2005, 21, 5166.
[61] Uskokovic V, Drofenik M. Surf Rev Lett 2005, 12, 239.
[62] Romero L, Keunchkarian S, Reta M. Anal Chim Acta 2006, 565, 136.
[63] Reta M, Waymas O, Silber JJ. J Phys Org Chem 2006, 19, 219.
[64] Simorellis AK, Van Horn WD, Flynn PF. J Am Chem Soc 2006, 128, 5082.
[65] Cheng H, Sabatini DA. Sep Sci Technol 2007,42, 453.

[66] Nassar NN, Husain MN. J Colloid Interface Sci 2007, 316, 442.
[67] Nassar NN, Husain MN. Langmuir 2007, 23, 13093.
[68] El Seoud OA, Pires PAR. Prog Colloid Polym Sci 2008, 134, 110.
[69] Fanun M. Microemulsions: Properties and Applications, CRC Press, 2008.
[70] Mazzola PG, Lopes AM, Hasmann FA, Jozala AF, Penna TCV Magalhaes PO, Rangel-Yagui CO, Pessoa Jr A. J Chem Technol Biotechnol 2008, 83, 143.
[71] Khvostichenkov DS, Anderson SI. Energy Fuels 2008, 22, 3096.
[72] Tonova K, Lazarova Z, Biotechnol Adv 2008, 26, 516.
[73] Zakharova LY, Syakaev VV, Voronin MA, Valeeva FV, Ibragimova AR, Ablakova YR, Kazakova EK, Latypov SK, Konovalov AI. J Phys Chem 2009, 113, 6182.
[74] Mohd-Setapar SH, Wakeman RJ, Tarleton ES. Chem Eng Res Des 2009, 87, 833.
[75] Dong L, Wu J, Zhou X, Kang Q. J Chem Eng Jpn 2009, 42, 9.
[76] Romero L, Grisales JO, Reta M. Talanta 2010, 81, 1431.
[77] Nassar NN. J Dispersion Science Technol 2010, 31, 1714.
[78] Leclercq L, Nardello-Rataj V, Turmine M, Azarousal N, Aubry JM. Langmuir 2010, 26, 1716.
[79] Li X, He G, Liu D, Wang M, Xiao G. J Dispersion Sci 2011, 32, 415.
[80] Zhao X, Ao Q, Du F, Zhu Q. Food Anal Methods 2011, 4, 268.
[81] Dimitrova P, Bart HJ. Open Process Chem J 2011, 4, 1.
[82] Dhaneshwar AD, Chaurasiya RS, Hebber HU. Biotechnol Prog 2014, 30, 845.
[83] Mudzhikova GV, Brodskaya EN. Colloid J 2015, 77, 306.
[84] Ding X, Cai J, Guo X. Sep Purif Technol 2016, 158, 367.
[85] Osfouri S, Tayebi T, Azin R. Phys Chem Res 2018, 6, 105.

Ana Soto and Mohammad K. Khoshkbarchi

3 Solubilities of Amino Acids in Aqueous Electrolyte Solutions

3.1 Amino Acids

Amino acids are simple organic compounds that contain both a basic amino group and an acidic carboxyl group. Twenty-two of them are building blocks of peptides and proteins. They are called proteinogenic or natural amino acids and are characterized by an amino group and a side chain, both attached in the alpha position to the carboxyl functional group. These naturally occurring amino acids are in the L-enantiomeric form, that is in the L-α-form, except glycine (aminoacetic acid), the simplest of them which is achiral. D-Isomers are uncommon in living organisms. Nonproteinogenic amino acids are found in some living metabolites such as antibiotics and other microbial products, in bacterial cell walls and cell pools of some plants, and so on, but never in proteins. Figure 3.1 shows some common amino acids of proteins and Figure 3.2 shows some natural nonproteinogenic amino acids.

Amino acids are extremely important products in various branches of industry, especially in food, pharmaceutical, cosmetic, and agricultural industries. Moreover, they are also attractive feedstocks for chemical production due to their physicochemical properties and low toxicity which means they are considered environmental friendly. The methods of production of amino acids can be classified into extraction from proteins; chemical synthesis that generally produces racemic mixtures, although asymmetric synthesis from prochiral precursors can be used to obtain L-amino acids; fermentation of natural products (sugars and molasses), and enzymatic catalysis [1]. Industrial interest is focused on L-amino acids due to their nutritive properties. For many amino acids, isolation from natural raw materials is the most competitive production process. However, economical and full life cycle assessments are required to select the best process for each amino acid.

Regardless of the production method, the presence of impurities is inevitable and these can be removed by a variety of separation and purification techniques. Crystallization and precipitation are two commonly used processes. The knowledge of how these impurities (electrolytes in many cases) affect the solubility of the biomolecule is needed. In other applications, several additives (salts, acids, bases, etc.) are intentionally added in solution crystallization as a way to control size and polymorphism of the crystalline products. The knowledge of the solubilities of amino acids in the presence of different electrolytes is useful for the rational design of these processes.

https://doi.org/10.1515/9783110564808-003

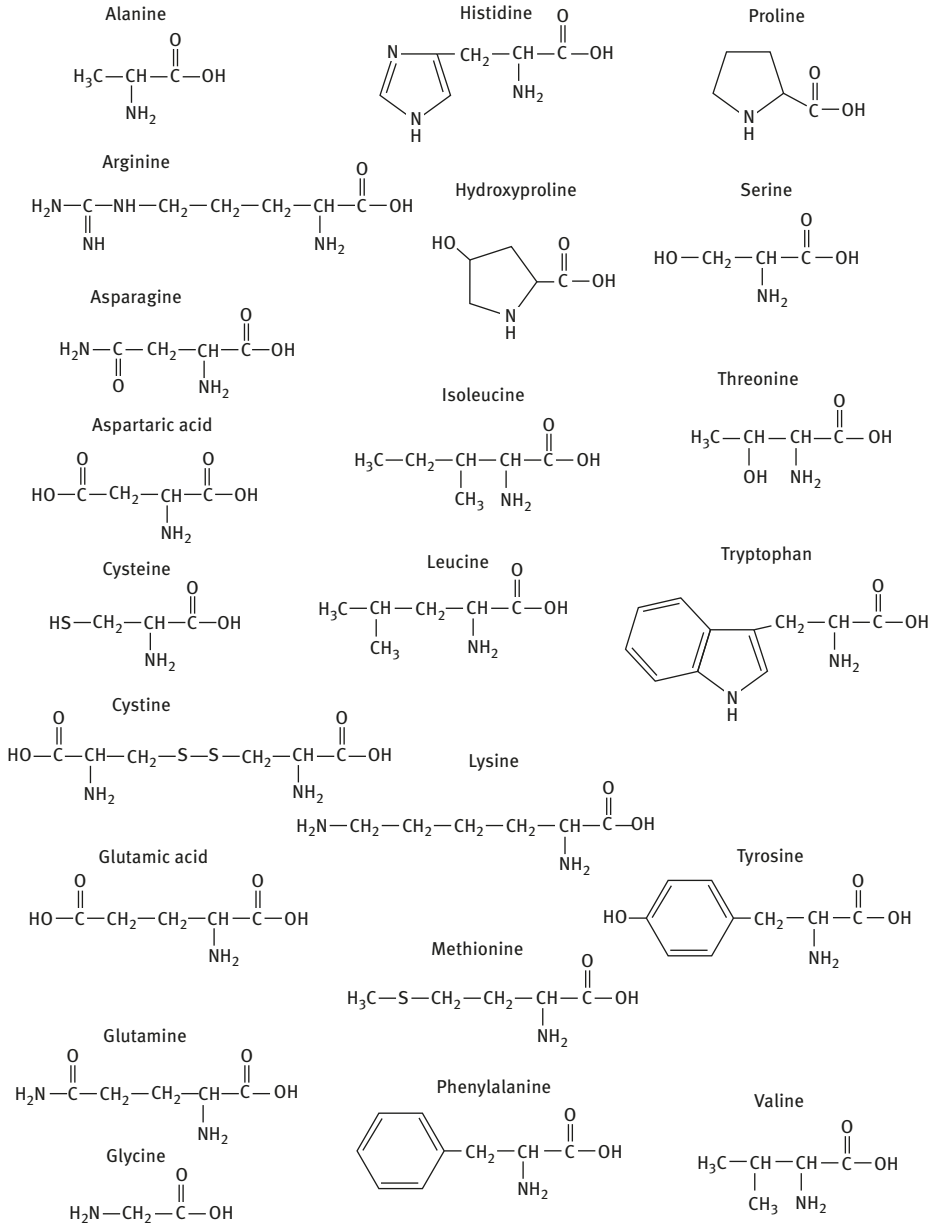

Figure 3.1: Common proteinogenic amino acids [1].

In an aqueous solution, amino acids undergo a pH-dependent dissociation. From low to high pH, the amino acid passes from its cationic to anionic form via the natural zwitterionic form. Thus, in the neutral pH range the amino acid exists as the ampholyte (zwitterion):

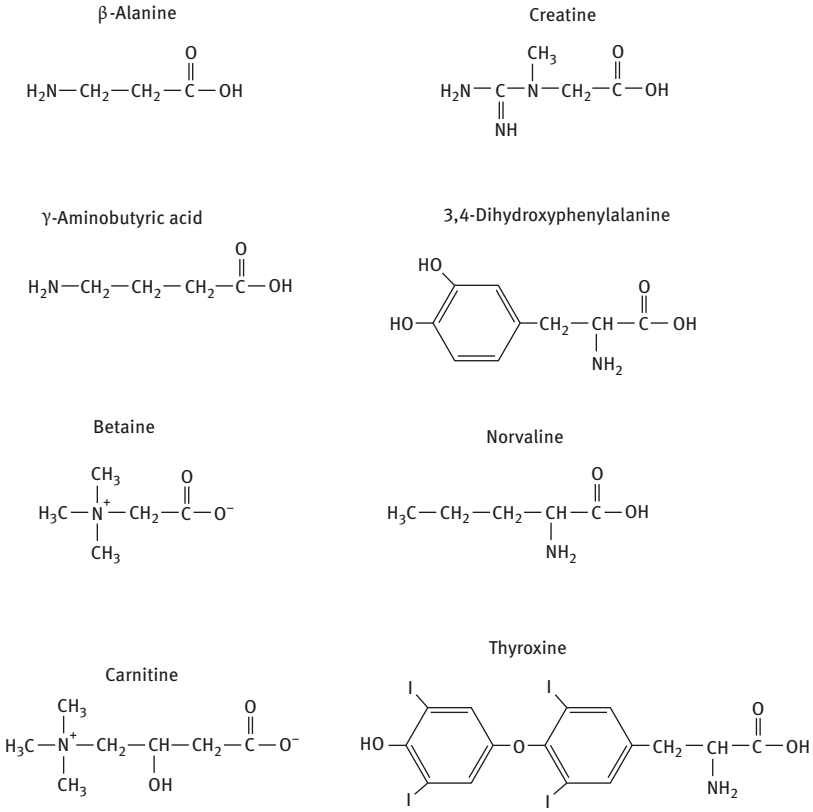

Figure 3.2: Several nonproteinogenic amino acids [1].

$$NH_2RCOOH \leftrightarrow NH_3^+ RCOO^- \qquad K_D = \frac{[NH_3^+ RCOO^-]}{[NH_2RCOOH]} \tag{3.1}$$

In the presence of an acid, the following reaction occurs from right to left:

$$NH_3^+ RCOOH \leftrightarrow H^+ + NH_3^+ RCOO^- \qquad K_1 = \frac{[H^+][NH_3^+ RCOO^-]}{[NH_3^+ RCOOH]} \tag{3.2}$$

and in the presence of a base, the following reaction occurs from left to right:

$$NH_3^+ RCOO^- \leftrightarrow H^+ + NH_2RCOO^- \qquad K_2 = \frac{[H^+][NH_2RCOO^-]}{[NH_3^+ RCOO^-]} \tag{3.3}$$

The isoelectric point is defined as the pH at which the net electric charge of a dissolved amino acid is zero and is calculated as

$$pI = \frac{pK_1 + pK_2}{2} = \frac{-\log K_1 - \log K_2}{2} \tag{3.4}$$

3.2 Solubility of Amino Acids in Aqueous Electrolyte Solutions: Experimental Protocol

The measurement of the solubility of amino acids in aqueous or electrolyte solutions at constant temperature and atmospheric pressure does not require expensive or complicated experimental procedures (Figure 3.3). The commonly used methods are synthetic-optical and analytical.

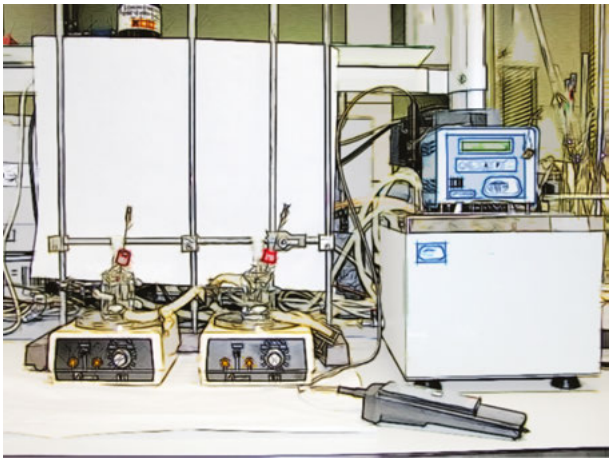

Figure 3.3: Equipment commonly used in the measurement of solubilities of amino acids at atmospheric pressure: thermostated cells with agitation device.

In synthetic-optical methods, the solubility of the amino acid in an aqueous or an aqueous electrolyte solutions at a fixed temperature and atmospheric pressure is determined by direct addition and dissolution of controlled amounts of the biomolecule to the corresponding liquid solvent thermostated at the desired temperature. The system is continuously stirred and the dissolution of the added amino acid is visually observed. The procedure is repeated by adding the solute until reaching the solubility limit, manifested by undissolved solute at the bottom of the flask. Another possibility consists of the preparation of a supersaturated solution and the addition of pure solvent until total solubilization. Laser monitoring or dynamic light scattering systems can be used to better detect precipitation and solubilization.

In analytical methods, the solvent is placed in a thermostated flask provided with a stirrer. The amino acid is added in excess of the amount required for saturation. The solution is agitated, the mixing stopped, and the solutions are allowed to settle down. The periods for each step have to be previously defined to ensure equilibrium. Samples of the supernatant liquid phase are withdrawn, filtered, and analyzed. Simple gravimetric analyses (by water evaporation) or analytical techniques, such

as liquid chromatography or the formol titrimetry method, can be used to determine the composition and thus the solubility of the amino acid in the aqueous or electrolyte solution. Another possibility for analysis is to carry out a quantitative dilution of the phase and use the measurement of a physical property like density or refractive index. A previous calibration curve (composition-physical property) is required.

Although less common in the case of amino acids, measurements of solubility can also be taken by calorimetric techniques. Castronuovo et al. [2] showed that the simultaneous determination of all thermodynamic parameters characterizing the dissolution of a substance in a given solvent (solubility, dissolution enthalpy, and dilution enthalpy) is possible using a commercial calorimeter. The basis of the method is the determination of the heat upon the addition of solvent to a saturated solution, until a homogeneous solution is formed.

3.3 Effect of NaCl and KCl on the Solubility of Amino Acids in Aqueous Solutions at 298.2 K: Measurements and Modeling

Despite the need for data of solubility of amino acids in aqueous electrolyte solutions for the correct understanding and design of amino acid production and purification processes, when Khoshkbarchi and Vera published solubilities of glycine, DL-alanine, DL-valine, and DL-serine in aqueous solutions of NaCl and KCl in 1997 [3], literature data on this topic were scarce. However, Cohn and Edsall [4] had shown that different electrolytes may have very different effects on biomolecules. The presence of an electrolyte may increase the solubility of an amino acid in water (salting-in) or decrease it (salting-out).

Solubilities were measured by preparing solutions with different molalities of salt and adding the amino acid at constant temperature (298.2 K), until a supersaturated solution was obtained. When equilibrium was reached, the supernatant phase was filtered and the composition was determined by gravimetric analysis.

At low electrolyte concentrations, NaCl and KCl have a salting-out effect on glycine solubility, but on increasing electrolyte concentration a salting-in effect is observed (Figure 3.4(a)). This behavior was explained by Khoshkbarchi and Vera to be due to the long-range interactions between glycine molecules and charged ions that predominate at low electrolyte concentrations, and the formation of ion-pair complexes at higher salt concentrations. The ion pairs would suppress the long-range electrostatic forces and screen the hydrophobic interactions of the hydrocarbon backbone of the amino acid. Also, the (experimentally observed) formation of different crystalline forms of glycine in the solid phase at different electrolyte concentrations could be involved in this behavior. Solubilities of glycine in the presence of KCl

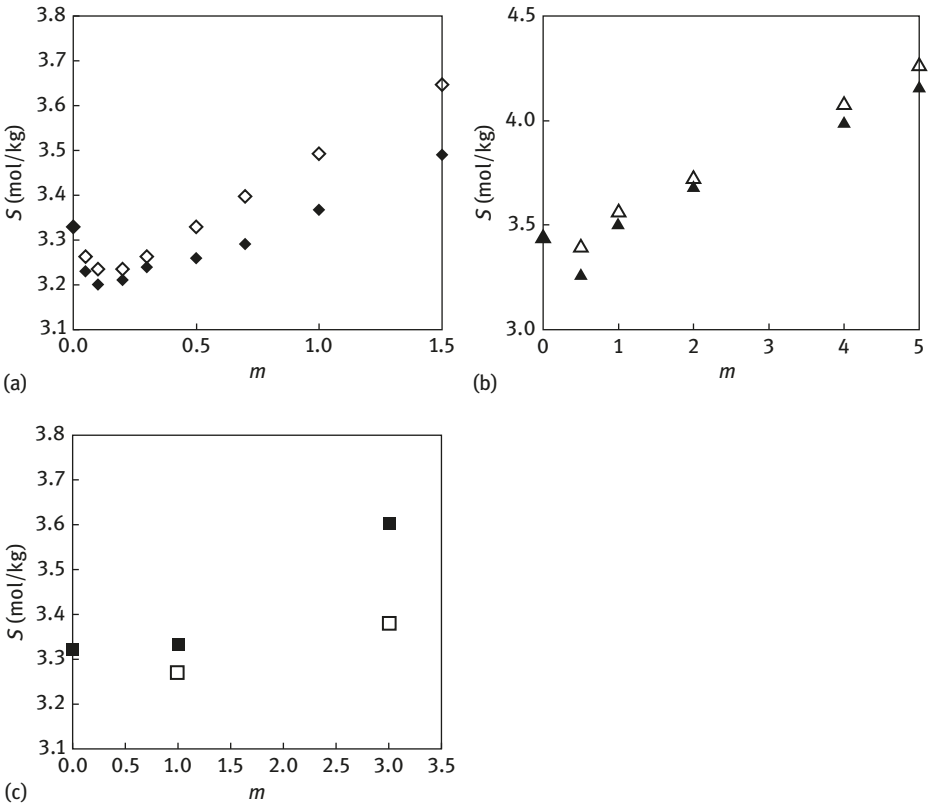

Figure 3.4: Solubilities of glycine in aqueous solution at 298.2 K and atmospheric pressure as a function of salt molality. Data grouped by authors. a) ◆ NaCl [3]; ◇ KCl [3]; b) ▲ NaCl [5]; Δ KCl [5]; c) ■ NaCl [6]; □ KCl [6].

were found to be higher than with NaCl over the whole range of electrolyte concentration. These effects can be attributed to the differences between the physicochemical properties of the ion-pair complexes formed between the amino acid and the sodium or the potassium ions. The later would screen more the hydrophobic and electrostatic interactions.

Figures 3.5(a) and 3.6 present data obtained by Khoshkbarchi and Vera [3] for solubilities of DL-alanine and DL-valine, respectively, in aqueous solutions of NaCl and KCl. They show a salting-out effect of NaCl and a salting-in effect of KCl, again attributable to the nature of the ion-pair complexes formed, and to a more pronounced effect of hydrophobic interactions than in the case of glycine (larger hydrocarbon backbones). In contrast, the hydroxyl group of DL-serine increases the polarity of the molecule and increases its tendency to dissolve in ionic solutions, which is why both NaCl and KCl have a salting-in effect on this amino acid solubility (Figure 3.7).

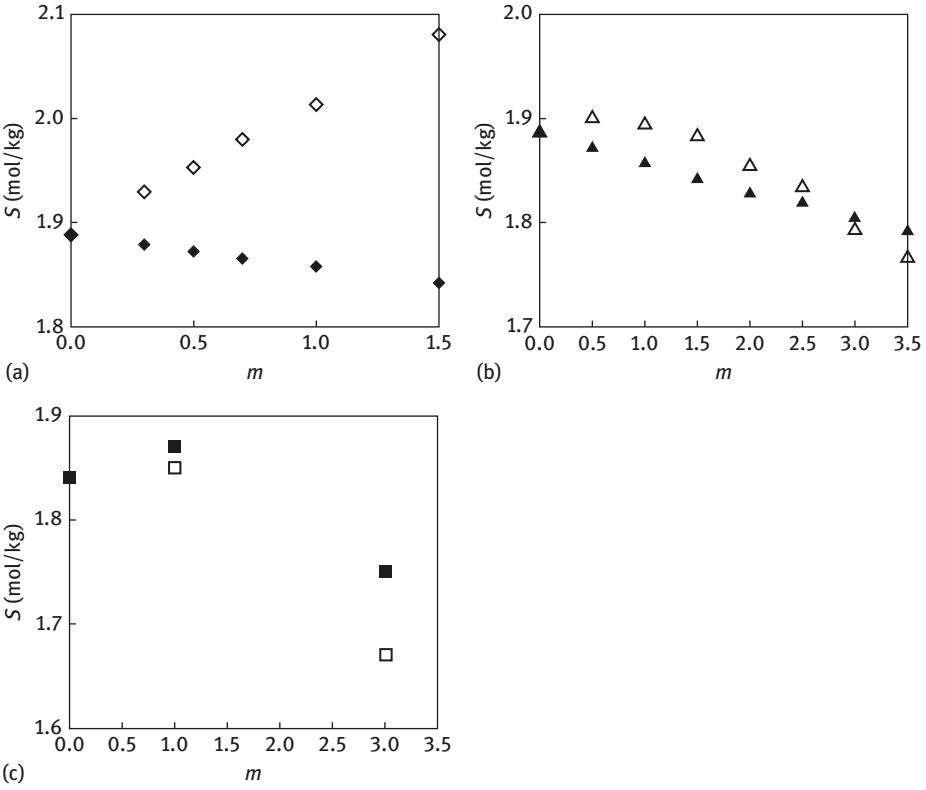

Figure 3.5: Solubilities of alanine in aqueous solution at 298.2 K and atmospheric pressure as a function of salt molality. Data grouped by authors. a) ◆ NaCl [3]; ◇ KCl [3]; b) ▲ NaCl [9]; Δ KCl [9]; c) ■ NaCl [6]; □ KCl [6].

The solubilities of these amino acids were later determined by other authors [5–10] and the significant differences observed between the data reported are noteworthy. Roy et al. [5] found a similar behavior (Figure 3.4(b)) to that observed by Khoshkbarchi and Vera for glycine: a salting-out effect at low concentrations of salt (NaCl or KCl) that changes to a salting-in effect with increasing electrolyte concentration, always with higher solubilities in the case of KCl. As Held et al. [6] do not determine solubilities at low concentrations (Figure 3.4(c)), the v-shaped behavior cannot be observed; however, a notable discrepancy appears with their data as solubilities are found to be higher in the case of NaCl.

The apparent agreement among data of Khoshkbarchi and Vera [3] and Roy et al. [5] is not quantitative, as shown in Figure 3.8. Figure 3.8(a) shows data obtained for solubilities of glycine in NaCl aqueous solutions by Khoshkbarchi and Vera [3], Roy et al. [5], Held et al. [6], and Han and Tan [7]. These last authors are the only group that identify the polymorph form of glycine used (γ-glycine). Differences among all

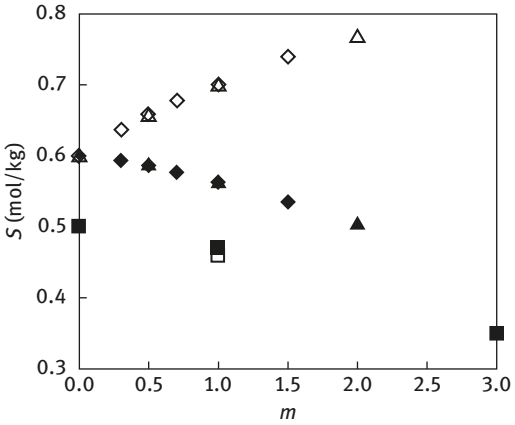

Figure 3.6: Solubilities of valine/norvaline in aqueous solution at 298.2 K and atmospheric pressure as a function of salt molality. ◆ Valine + NaCl [3]; ◇ valine + KCl [3]; ▲ norvaline + NaCl [10]; Δ norvaline + KCl [10]; ■ valine + NaCl [6]; □ valine + KCl [6].

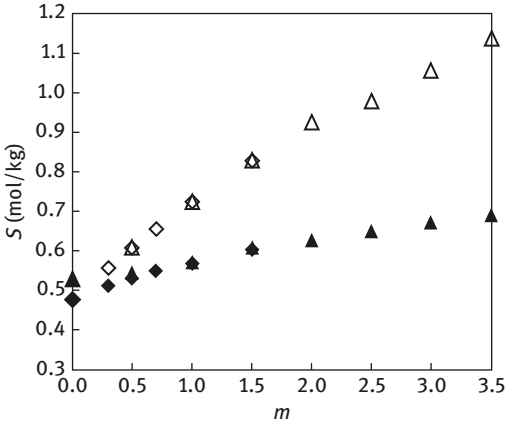

Figure 3.7: Solubilities of serine in aqueous solution at 298.2 K and atmospheric pressure as a function of salt molality. ◆ NaCl [3]; ◇ KCl [3]; ▲ NaCl [9]; Δ KCl [9].

the authors, except Roy et al. [5] who obtain slightly higher solubilities in all the range, are more noticeable at lower concentrations where the long-range interactions between glycine molecules and charged ions predominate. After a certain low concentration, all the authors agree in the salting-in effect of NaCl on glycine solubility. A comparison was also done for KCl in Figure 3.8(b). This system was also measured by

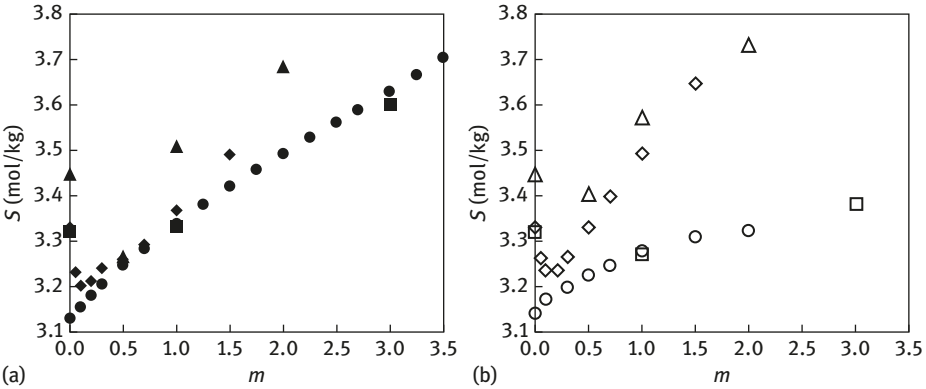

Figure 3.8: Solubilities of glycine in aqueous solution at 298.2 K and atmospheric pressure as a function of salt molality. Data grouped by cation. a) ◆ NaCl [3]; ▲ NaCl [5]; ■ NaCl [6]; ● NaCl [7]; b) ◇ KCl [3]; Δ KCl [5]; □ KCl [6]; ○ KCl [8].

Ferreira et al. [8]. Discrepancies are significant at lower electrolyte concentrations. Increasing the KCl concentration, data of Khoshkbarchi and Vera [3] are in relatively good agreement with data of Roy et al. [5], showing both a considerable increase of solubility when increasing salt concentration. On the other hand, Held et al. [6] and Ferreira et al. [8] data are also in good agreement but the increase of solubility with salt concentration is clearly lower. Even when discrepancies are in the first decimal place, the development of optimal process designs requires accurate experimental data and thermodynamic models to avoid undesirable results and costs.

Figure 3.5 shows the solubilities of DL-alanine in NaCl and KCl aqueous solutions according to the data measured by Khoshkbarchi and Vera [3], Roy et al. [9], and Held et al. [6]. It should be mentioned that the two first authors are measuring solubilities of DL-alanine and the latter of L-alanine. All the authors found a salting-out effect for NaCl. For KCl at high salt concentration, both Roy et al. [9] and Held et al. [6] found a salting-out effect while at low salt concentrations, Khoshkbarchi and Vera [3] found a salting-in effect. This salting-in effect seems to be confirmed by the scarce data of Roy [9] in this region. This behavior with alanine could be due to the different isomers used but it would not be a justification in the case of glycine. Data shown in Figure 3.9 (a) exhibit a relative agreement in the case of solubilities in NaCl aqueous solutions. Data of Han and Tan [7] are also included in the figure and are in very good agreement with the data determined by Held et al. [6]. However, the first authors worked with the racemic mixture and Held et al. [6] with the L-enantiomer. Figure 3.9(b) shows a relatively good match among Held et al. [6] and Ferreira et al. [8] (again only Held et al. [6] worked with a pure enantiomer) but the solubilities presented by Roy et al. [9] are higher and Khoshkbarchi and Vera [3] are the only group that found a salting-in effect in the presence of KCl.

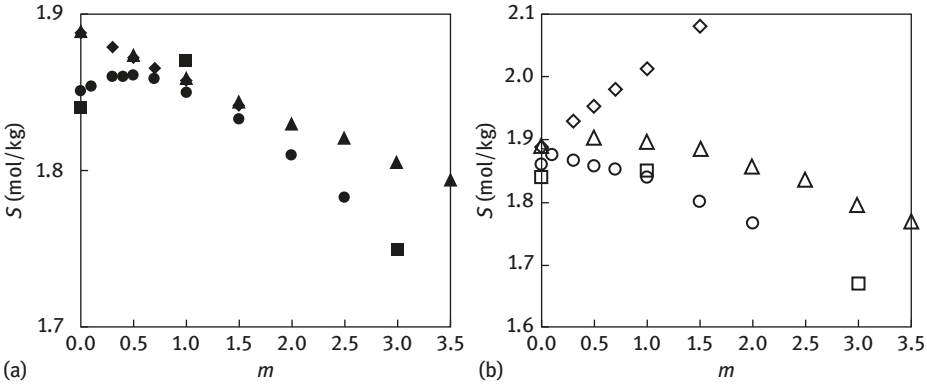

Figure 3.9: Solubilities of alanine in aqueous solution at 298.2 K and atmospheric pressure as a function of salt molality. Data grouped by cation. a) ◆ NaCl [3]; ▲ NaCl [9]; ■ NaCl [6]; ● NaCl [7]; b) ◇ KCl [3]; Δ KCl [9]; □ KCl [6]; ○ KCl [8].

A good agreement can be seen in Figures 3.6 and 3.7 for solubilities measured by Khoshkbarchi and Vera [3] and Roy et al. [9, 10]. The agreement in Figure 3.7 for serine is expected. However, the agreement in Figure 3.6 is surprising since Khoshkbarchi and Vera [3] worked with DL-valine (2-amino-3-methylbutyric acid) and Roy et al. [10] worked with DL-norvaline (amino-n-valeric acid), an amino acid $C_5H_{11}NO_2$ isomeric with valine and usually made synthetically (see Figures 3.1 and 3.2). Solubilities measured by Held et al. [6] for L-valine are lower, showing a decrease when the concentration of the electrolyte increases, with little influence of the cation of the salt.

For all the amino acids except glycine (the simplest amino acid and the only one that has no enantiomers because it has two hydrogen atoms attached to the central carbon atom), if both enantiomers are present in a solid sample, the solubility of the solid mixture is generally found to be different than that of a pure enantiomers because the solid-state interactions of the two enantiomers are different. This can be seen, for instance, in the work of Polenske and Lorenz [11], where different solubilities are found for DL-methionine and L-methionine in water. In fact, these authors claim that characterization of the ternary phase diagram formed by the two isomers and water is critical for enantioseparation by crystallization procedures. Thus, differing results could be expected in the case of alanine, valine, and serine in experiments conducted by Held et al. [6] due to the fact that they are the only authors that use the L-enantiomeric form, in contrast to other authors who instead use the racemic mixture. However, data obtained for the system L-alanine + water + KCl by Held et al. [6] and for DL-alanine + water + KCl by Ferreira et al. [8] are in good agreement. An attempt could be made to justify different solubilities obtained for DL-amino acids based on the possibly different proportions of each isomer in the mixture.

Table 3.1: Solubility of glycine in water at several pH [12].

M	*S* (mol/kg)
5.38	2.812
6.04	2.758
6.89	2.885
7.63	3.096

Differences among solubilities obtained by different authors for the same systems could be explained, besides experimental errors, by their being based on different compositions when mixtures of the two isomers are used. Another critical parameter could be pH. The solubilities at 298.2 K of glycine in water were measured at pH ranging from 2.48 to 10.21 by Lu et al. [12] and values, as it is expected, differ significantly. Table 3.1 shows values at pH close to 7.

Furthermore, most amino acids exhibit polymorphism in the solid state and polymorphs differ in their physicochemical properties, including solubility. Yang et al. [13] have shown that the solubilities of two polymorphs of glycine (α-form and γ-form) in water are different and that, even when the α-form is generally available commercially, the polymorphic transformation of the α-form to the γ-form in aqueous solutions is possible [14]. At 20 °C and a stirring rate of 350 rpm, the complete transformation of α-form into the γ-form required ca. 55 h. With the addition of NaCl, the transformation was accelerated significantly. In an 80 g/L NaCl solution, complete transformation occurred within 16 h. Moreover, the transformation rate also increased with temperature, the stirring rate, and the decrease of the seed size. According to these results, besides the electrolyte, stirring and settling down times can affect the amino acid polymorph forms obtained and thus solubility. In the case of DL-alanine, it is confirmed that the presence of different inorganic salts in aqueous solutions of the amino acid reveal an unusual growth behavior of DL-alanine *c*-axis but do not induce different polymorphs [15]. No evidence has been found in the literature about the existence of different polymorphs in aqueous solutions of valine or serine at room temperature.

To facilitate comparison, Table 3.2 shows the main parameters of the experimental protocol used by different authors in the measurement of glycine solubility in the presence of NaCl and KCl. The authors have tried to explain the deviations obtained in experimental data [6–8] but the discrepancies are still not fully understood. Authors working with similar experimental protocol, for example, Khoshkbarchi and Vera [3] and Ferreira et al. [8], present in fact very different results. In many cases, information given is not sufficient to reproduce the experimental protocol. Moreover, besides the polymorph form of the amino acid, the characterization of the racemic mixture (in the case of amino acids different from glycine), the pH

Table 3.2: A comparison among experimental methods used to measure the solubility of glycine in aqueous solution of NaCl and KCl.

	Pradhan and Vera [3]	Roy et al. [5]	Held et al. [6]	Han and Tan [7]	Ferreira et al. [8]
Polymorph*	No details	No details	No details	γ-Glycine	No details
Stirring time	48 h	No details	72 h	No details	48 h
Settling time	7 h	No details	Centrifugation +5 h	No details	7 h
Analysis method	Gravimetric	Formol titrimetry	Gravimetric	Density measurement[1]	Gravimetric

*α-Glycine is the commercial form generally available
[1]Crystal dissolution and solution desupersaturation

of solution, and so on, other aspects should also be considered, for instance, the preparation procedure (the order of addition of components), oven temperatures that could degrade the amino acid or retain water, and errors associated with salt precipitation.

Khoshkbarchi and Vera developed a model [3] to correlate the solubilities of amino acids in aqueous electrolyte solutions employing a perturbed hard-sphere model previously proposed by the same authors [16] to represent the activity coefficient of the amino acid.

The solubility of an amino acid in an aqueous electrolyte solution can be expressed as

$$m_{AA} = \frac{m_{AA}{}^{o}\gamma_{AA}{}^{o}}{\gamma_{AA}} \frac{f_{AA}{}^{S}}{f_{AA}{}^{oS}} \tag{3.5}$$

where m is the saturation molality; γ the molality scale, unsymmetrically normalized, activity coefficient; f the fugacity; the subscript AA is amino acid, and the superscripts o and S indicate the absence of electrolyte and solid state. The standard-state fugacity is chosen by considering the amino acid at infinite dilution in pure water as the reference state. At constant temperature, if solid phases with and without electrolyte are pure and have the same crystalline form, then $f_{AA}{}^{S}/f_{AA}{}^{oS}$ is equal to unity and the equation can be simplified. However, Khoshkbarchi and Vera found that, even when no adsorption of salt in the amino acid solid phase was experimentally observed, the effect of salt in the crystallographic form of the solid phase of the amino acid was clearly visualized. Thus, they proposed a simple algebraic empirical form for the ratio of fugacities:

$$\frac{f_{AA}{}^{S}}{f_{AA}{}^{oS}} = \frac{1}{1 + am_{S}{}^{b}} \tag{3.6}$$

where a and b are adjustable parameters whose values can be determined by curve fitting of the solubility experimental data at various electrolyte concentrations.

The activity coefficients can be calculated from a model based on the perturbation theory [16]:

$$\ln \gamma_{AA}(\rho_{AA}) = \ln {\gamma_{AA}}^{HS} - \frac{4\pi}{kT}\left\{\frac{8}{9}\rho_{AA}{\sigma_{AA}}^3 \in_{AA} + \frac{8}{9}\rho_S{\sigma_{AA,S}}^3\sqrt{\in_{AA} \in_S}(1+2n\rho_{AA}) + \frac{\rho_S\bar{\alpha}_S{\bar{D}_{AA}}^2}{3(4\pi \in_0 \in_r)^2 kT{\sigma_{AA,S}}^3} + \frac{\rho_{AA}{\bar{D}_{AA}}^4}{9(4\pi \in_0 \in_r)^2 kT{\sigma_{AA}}^3} + \frac{\rho_S{z_S}^2e^2{\bar{D}_{AA}}^2}{6(4\pi \in_0 \in_r)^2 kT\sigma_{AA,S}}\right\} \tag{3.7}$$

$$\ln {\gamma_{AA}}^{o}({\rho_{AA}}^{o}) = \lim_{\rho_S \to 0} \ln \gamma_{AA}(\rho_{AA}) \tag{3.8}$$

where ρ is the number density, $\in_0$ is the permittivity of vacuum, $\in_r$ is the relative dielectric constant of the medium, $\in$ is the depth of the potential well, σ is the size parameter, $\bar{D}$ is the dipole moment, $\bar{\alpha}$ is the polarizability, z is the charge number, e is the basic electric charge, k is the Boltzmann constant, and T is the absolute temperature. The binary interaction parameters l and n are characteristic of each water – electrolyte–amino acid system and can be evaluated from independent measurements of the activity coefficients of amino acids in aqueous electrolyte solutions. The contribution of the hard sphere to the activity coefficient is calculated by the model proposed by Mansoori et al. [17]:

$$\ln {\gamma_{AA}}^{HS} = -\ln(1-\xi_3) + \frac{\pi P^{HS}{\sigma_i}^3}{6kT} + E + 3F \tag{3.9}$$

$$\xi_n = \frac{\pi}{6}\sum_{k\approx 1}^{n}\rho_k{\rho_k}^n (n = 0,\ 1,\ 2,\ 3) \tag{3.10}$$

$$E = \frac{3\xi_2\sigma_i + 3\xi_1{\sigma_i}^2}{1-\xi_3} + \frac{9{\xi_2}^2{\sigma_i}^2}{2(1-\xi_3)^2} - \frac{{\xi_2}^3{\sigma_i}^3}{{\xi_3}^3}\left[2\ln(1-\xi_3) + \frac{\xi_3(2-\xi_3)}{1-\xi_3}\right] \tag{3.11}$$

$$F = \frac{{\xi_2}^2{\sigma_i}^2}{{\xi_3}^2}\left[2\ln(1-\xi_3) + \frac{\xi_3}{1-\xi_3} - \frac{{\xi_3}^2}{2(1-\xi_3)^2}\right] \tag{3.12}$$

$$P^{HS} = \frac{6kT}{\pi}\left[\frac{\xi_0}{1-\xi_3} + \frac{3\xi_1\xi_2}{(1-\xi_3)^2} + \frac{{\xi_2}^3(3-\xi_3)}{(1-\xi_3)^3}\right] \tag{3.13}$$

where σ is the size parameter of the hard spheres and ρ is the number density of the components.

This model was able to adequately correlate experimental solubilities of glycine, DL-alanine, DL-valine, and DL-serine in aqueous solutions with various NaCl and KCl concentrations [3]. For all the amino acids except glycine only one correlation parameter (a) was required (b was set to 1). Later, these solubilities were also adequately fitted by other subsequently developed models [5, 18, 21, 23, 25].

A model was developed by Sadeghi [18] to represent the liquid–solid equilibrium behavior of amino acids and small peptides in aqueous solutions as a function of temperature, ionic strength, and amino acid compositions. The polymer–electrolyte Wilson model [19] was modified to that aim. The combinatorial contribution term defined to account for the entropy of mixing molecules of different sizes was omitted and polymer molecules were replaced by small amino acid molecules. The model had predictive power not only for the solubilities of pure amino acids in water or electrolyte solutions but also for mixtures of amino acids, and results were comparable with those obtained with Chen's version of the Non-Random Two-Liquid (NRTL) model [20]. These models were later modified by Sadeghi [21] by considering cells with random composition for the reference Gibbs energies or enthalpies of local composition cells with a central amino acid molecule and a central ion. The models correlated data, published by Khoshkbarchi and Vera and other authors, with comparable deviations to those obtained with the original modeling.

An approach based on the Statistical Associating Fluid Theory (SAFT) [22] to predict the solubility of amino acids (single compounds or mixtures) in aqueous and aqueous electrolyte solutions was presented by Seyfi et al. [23] in 2009. In the case of electrolyte solutions, ion contribution was considered as a restrictive primitive mean spherical approximation model [24]. Authors used experimental data of activity coefficients of amino acids in water to obtain the parameters of the amino acids for the model, and predicted the solubility of several amino acids in aqueous solutions with low deviations from experimental data. The same authors later modeled these data [25] taking advantage of a version of the SAFT approach for chain molecules formed from spherical segments with attractive potentials of Variable Range (SAFT-VR). [26] coupled with the Yukawa potential, which can reflect the Coulombic interactions found in electrolyte solutions. In this case, the parameters of the model for individual ions were obtained by correlation of the mean ionic activity coefficients of salts. The model proved to be a reliable approach in studying the phase behavior of amino acid containing solutions.

Held et al. [5] used the electrolyte Perturbed-Chain Statistical Association Fluid Theory (ePC-SAFT) by Cameretti et al. [27] for modeling properties of aqueous electrolyte solutions of amino acids, specifically solubilities and osmotic coefficients. The model was used in a predictive mode only requiring pure-component parameters, for the ions and for the amino acids, obtained through the fitting of binary salt/water and amino acid/water systems. The results of the predictions were quantitative in the case of the osmotic coefficients and with relative low deviations in the case of solubilities. In the case of DL-alanine in KCl aqueous solutions, the model predicts a salting-out

effect obtaining solubilities closer to experimental data obtained by themselves and Ferreira et al. [8].

3.4 Effect of the Cation and the Anion of an Electrolyte on the Solubility of DL-Aminobutyric Acid in Aqueous Solutions: Measurement and Modeling

Continuing with the study of solubility of amino acids in water in the presence of electrolytes, Soto et al. [28] determined the solubility of DL-aminobutyric acid in aqueous solutions of NaCl, KCl, $NaNO_3$, and KNO_3 at 298.2 K and atmospheric pressure, allowing in this way the analysis of the influence of cation and anion on the equilibrium. Results can be seen in Figure 3.10 together with data published posteriorly by Mondal et al. [29] for the solubility of this amino acid in the presence of KCl.

The solubility of DL-aminobutyric acid in aqueous electrolyte solutions depends on the nature of both the cation and the anion of the electrolyte. Figure 3.10 shows that the nitrate ion produces a salting-in effect whereas the chloride ion produces a salting-out effect. The effect of the cation is smaller. In the case of nitrates, solubilities are higher with sodium than with potassium, but with the chloride anion the influence of the cation is minimal. The solubilities of the amino acid are more affected at higher electrolyte concentrations because the formation of ion-pair complexes is favored. Again, significant discrepancies were found in the case of KCl electrolyte among data published by Soto et al. [28] and Mondal et al. [29] even though both

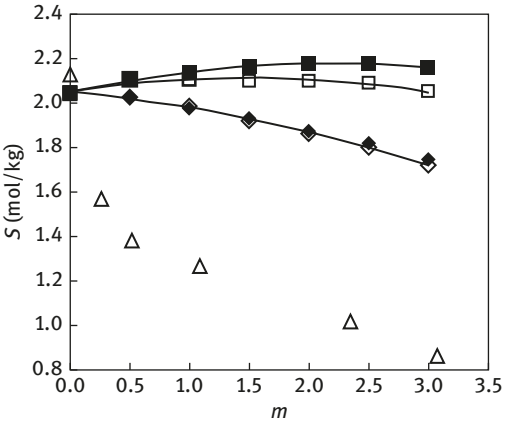

Figure 3.10: Solubilities of aminobutyric acid in aqueous solution at 298.2 K and atmospheric pressure as a function of salt molality. ◆ NaCl [28]; ◇ KCl [28]; ■ $NaNO_3$ [28]; □ KNO_3 [28]; Δ KCl [29].

authors found a salting-out effect. The fact that the amino acid samples used could widely differ in the proportion of optical isomers, the different analytical techniques (as explained above), pH, and different stirring and settling down times could partly account for the differences.

To model these new solubility data, eq. (3.5) was used. However, on this occasion, due to the lack of data, it was assumed that ${f_{AA}}^{S}/{f_{AA}}^{oS}$ was equal to unity:

$$m_{AA} = \frac{{m_{AA}}^{o}{\gamma_{AA}}^{o}}{\gamma_{AA}} \tag{3.14}$$

The activity coefficients were calculated by a model proposed by Khoshkbarchi and Vera [30], which considers the contributions of long- and short-range interactions to the excess Gibbs free energy as follows:

$$G^{E} = G^{E}_{LR}(x_W, x_S, x_{AA} = 0) + G^{E}_{SR}(x_W, x_S, x_{AA}) - G^{E}_{SR}(x_W, x_S, x_{AA} = 0) \tag{3.15}$$

where the subscript LR stands for the long-range interactions term (water-electrolyte) and SR stands for the short-range interactions term (water–amino acid, amino acid–electrolyte, and the change in the interaction between the electrolyte and water due to the presence of the amino acid). x_W, x_S, x_{AA} are the mole fractions of water, electrolyte, and amino acid, respectively.

Assuming that at neutral pH the amino acid molecules are in their zwitterionic form, the biomolecule is not considered to contribute to the ionic strength of the system. As the long-range interaction term of the model is considered only as a function of ionic strength, there is no contribution from this term to the activity coefficient of the amino acid. The short-range term is calculated with the original form (mole fraction scale) of the NRTL model [31]:

$$\ln \gamma_i^{NRTL} = \frac{\sum_{j=1}\tau_{ji}x_j e^{-\alpha\tau_{ji}}}{\sum_{j=1}x_j e^{-\alpha\tau_{ji}}} + \sum_{j=1}\frac{x_j e^{-\alpha\tau_{ij}}}{\sum_{k=1}x_k e^{-\alpha\tau_{kj}}}\left(\tau_{ij} - \frac{\sum_{k=1}x_k\tau_{kj}e^{-\alpha\tau_{kj}}}{\sum_{k=1}x_k e^{-\alpha\tau_{kj}}}\right) \tag{3.16}$$

However, as solubilities are presented in molality, the activity coefficient requires a suitable conversion [30]. Thus, the unsymmetrically normalized, molal-based, NRTL model is used:

$$\ln\gamma_{AA} = \ln\gamma_{AA}^{NRTL} - \lim_{x_{AA}\to 0,\ x_S\to 0}\ln\gamma_{AA}^{NRTL} - \ln[1 + 0.001M_W(m_{AA} + m_S)] \tag{3.17}$$

The model with two adjustable parameters ($\tau_{AA\text{-}S} = \tau_{S\text{-}AA}$ and $\tau_{W\text{-}S} = \tau_{S\text{-}W}$) accurately correlated with the solubilities of DL-aminobutyric in aqueous electrolyte solutions (Figure 3.10).

3.5 Effect of Acids and Bases on the Solubility of Amino Acids

The influence of pH on the solubility of amino acids is of great importance not only because acids and bases are generally used in the methods of synthesis and purification of those biomolecules, but also because amino acid solubility is tunable by pH. When an acid or a base is added, the zwitterionic form is converted to the cationic or anionic form of the amino acid, respectively. Moreover, the counterion of the acid or the base interacts with the charged amino acid molecules forming ion complexes that change the solubility of the biomolecule.

To investigate the application of this idea, Pradhan and Vera [32] determined the solubility of glycine, DL-alanine, DL-valine, and DL-serine in aqueous solutions with different acids (HCl or HNO_3) and bases (NaOH or KOH) at 298.2 K using gravimetric analyses.

The first question to answer was whether the use of different acids or bases could affect the solubility of the amino acid at a fixed pH. Figure 3.11 shows solubilities of DL-alanine in aqueous solutions at different pH prepared by the addition of NaOH/HCl or KOH/HNO_3. The same test was carried out by Tseng et al. [33] using the first two chemicals. Several interesting conclusions can be established from Figure 3.11. The lowest solubility appears for the zwitterionic form which prevails at pH close to the isoelectric point p*I* and increases at high or low pH due to displacement toward anionic or cationic species of the amino acid. The method of obtaining the desired pH has no effect on the results. It was shown that the influence of the counterion of the acid or base used is negligible, indeed the concentration of the counterion is low in

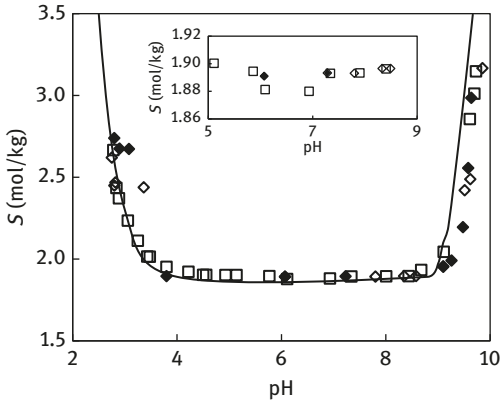

Figure 3.11: Solubility variation of alanine in aqueous solution at 298.2 K and atmospheric pressure as a function of the pH. ◆ Regulated with NaOH/HCl [32]; ◇ regulated with KOH/HNO_3 [32]; □ regulated with NaOH/HCl [33].

the whole range of the pH measurements. Moreover, Tseng et al. [33] showed the agreement of their data with solubilities obtained by Pradhan and Vera [32] (Figure 3.11). The pH may then be a very significant parameter in the comparison of data of solubilities of amino acids.

The solubility in Figure 3.11 can be calculated using eq. (3.14):

$$m_A = \frac{m_A{}^o \gamma_A{}^o}{\gamma_A} \tag{3.18}$$

Pradhan and Vera [32] proposed the calculation of the activity coefficient of the amino acid using the following equation:

$$x_A \gamma^x_{A\pm} = \left[1 + \frac{[H^+]}{K_1}\left(\frac{\gamma^x_{A\pm}}{\gamma^x_{A+}}\right) + \frac{K_2}{[H^+]}\left(\frac{\gamma^x_{A\pm}}{\gamma^x_{A-}}\right)\right] \exp\left(\frac{\Delta s}{R} - \frac{\Delta h}{RT}\right) \tag{3.19}$$

where A refers to the amino acid in all the possible forms: zwitterionic (A±), cationic (A+) and anionic (A–). γ^x is the rational activity coefficient, K_1 and K_2 are defined by eqs. (3.2) and (3.3), and Δs and Δh are the changes in the molar entropy and enthalpy of the amino acid between the standard state and the solid state.

Equation (3.19) simplifies in the isoelectric region where the cationic and anionic forms of the amino acid are at infinite dilution:

$$x_{A\pm} \gamma^x_{A\pm} = \left[1 + \frac{[H^+]}{K_1}\gamma^x_{A\pm} + \frac{K_2}{[H^+]}\gamma^x_{A\pm}\right] \exp\left(\frac{\Delta s}{R} - \frac{\Delta h}{RT}\right) \tag{3.20}$$

At low and high pH, the activity coefficients of the charged species were determined by simplifying eq. (3.19) as follows:

$$\gamma^x_{A+} = \frac{[H^+]\exp\left(\frac{\Delta s}{R} - \frac{\Delta h}{RT}\right)}{K_1\left\{x_A - \left(1 + \frac{K_2}{[H^+]}\right)\exp\left(\frac{\Delta s}{R} - \frac{\Delta h}{RT}\right)\right\}} \tag{3.21}$$

$$\gamma^x_{A-} = \frac{K_2\exp\left(\frac{\Delta s}{R} - \frac{\Delta h}{RT}\right)}{[H^+]\left\{x_A - \left(1 + \frac{[H^+]}{K_1}\right)\exp\left(\frac{\Delta s}{R} - \frac{\Delta h}{RT}\right)\right\}} \tag{3.22}$$

Equations (3.21) and (3.22) are not applicable at very high concentrations of acids or bases.

And, as explained above, the molality-based activity coefficient, γ^m_A, is converted to the rational activity coefficient as follows:

$$\gamma^x_A = \gamma^m_A[1 + 0.0018(m_s + m_A)] \tag{3.23}$$

where m_s is the molality of the acid or base.

Data in Figure 3.11 have been successfully represented by other models proposed in literature [34,35]. Fuchs et al. [34] used the PC-SAFT equation of state. Pure-component parameters for amino acids were fitted to vapor pressures and densities of their aqueous solutions. Only one temperature-independent binary parameter was required to model solubilities in water. The influence of pH on the solubility was described using the information of the pK_a values of the amino acids. Mercier Franco et al. [35] also modeled several amino acid solubilities as a function of pH, considering simultaneous calculation of phase and chemical equilibria to describe the solid–liquid equilibrium. The liquid-phase nonideality was considered using an extended Pitzer model for polyelectrolyte solutions. A statistical thermodynamic interpretation of Pitzer's binary interaction parameters was also presented in their work.

Figures 3.12 and 3.13 show the effect of bases (NaOH and KOH) on the solubility of glycine and DL-serine, and DL-alanine and DL-valine, respectively. Accordingly with Figure 3.11, the presence of the bases generates a salting-in, increasing the solubility of the amino acids with the increase of the concentration of the base. At the same concentration of the base, potassium produces a higher salting-in effect than sodium in all the amino acids likely due to the different complexes formed by each cation with the anionic amino acid. Figures 3.14 and 3.15 show the effect of acids (HCl and HNO_3) on the solubility of the amino acids. In this case, a complex is formed with the anions of the acids and the cationic form of the amino acid. At a fixed concentration of the acid, HNO_3 increases the solubility of all the amino acids more than HCl.

New insights into glycine polymorphism have been presented by Han et al. [36]. These authors measured the solubilities of α-glycine and γ-glycine in aqueous solutions of inorganic bases (NaOH and KOH) and acids (HCl, HNO_3, and H_2SO_4). Unlike Pradhan

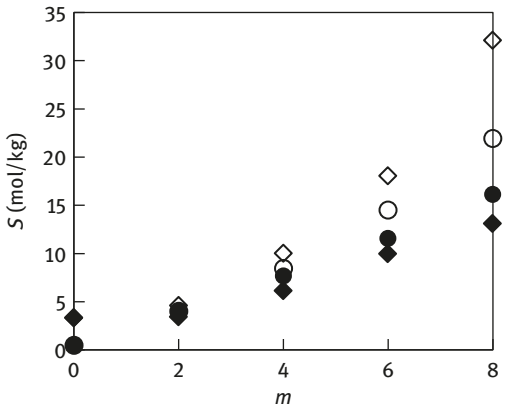

Figure 3.12: Effect of bases (NaOH and KOH) in the solubility of glycine and serine in aqueous solution [32]. ◆ Glycine + NaOH; ◇ glycine + KOH; ● serine + NaOH; ○ serine + KOH.

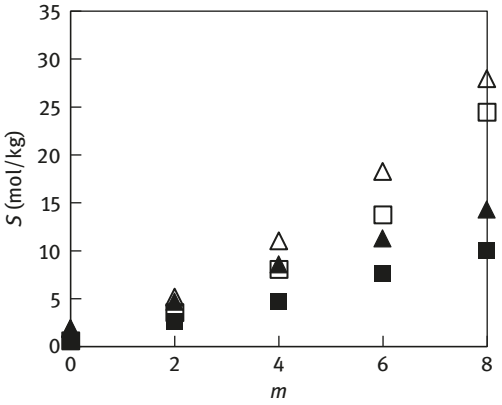

Figure 3.13: Effect of bases (NaOH and KOH) in the solubility of alanine and valine in aqueous solution [32]. ▲ Alanine + NaOH; alanine Δ + KOH; ■ valine + NaOH; □ valine + KOH.

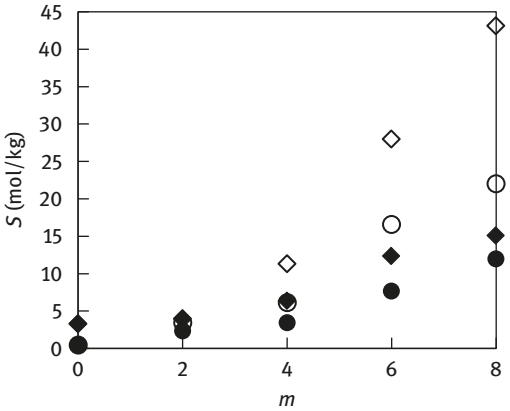

Figure 3.14: Effect of acids (HCl and HNO_3) in the solubility of glycine and serine in aqueous solution [32]. ◆ Glycine + HCl; ◇ glycine + ● HNO_3; serine + HCl; ○ serine + HNO_3.

and Vera [32] they only worked up to molalities equal to unity, making comparison of the data difficult. As in the case of solubilities in water, a prolonged equilibration led to the total transformation of α-glycine to γ-glycine affecting solubility results. The authors found that inorganic acid and bases can promote the growth of the metastable α-glycine. It was found that in basic solutions, γ-glycine growth remains dominated by α-glycine growth, yet γ-glycine is crystallized preferentially. The relative nucleation rates, rather than the relative growth kinetics, of the two glycine polymorphs play a dominant role in determining the polymorphic outcome of the process.

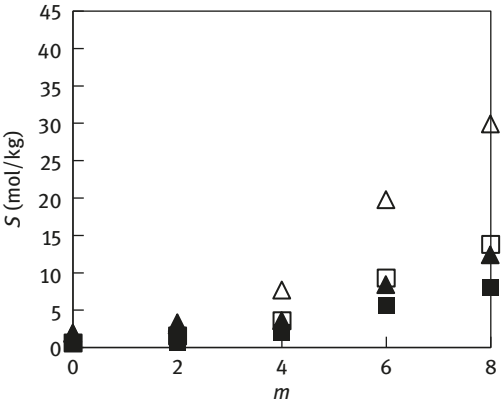

Figure 3.15: Effect of acids (HCl and HNO_3) in the solubility of alanine and valine in aqueous solution [32]. ▲ Alanine + HCL; Δ alanine + HNO_3; ■ valine + HCl; □ valine + HNO_3.

3.6 Measurements and Modeling of the Solubility of a Mixture of Two Amino Acids in Aqueous Solutions

The solubility of amino acids in water is affected not only by the presence of electrolytes but also by other amino acids. The fractionation of mixtures of amino acids is an usual stage in processes of extraction, separation, and concentration of these biomolecules, and solubility data are required for the design of the operation.

Soto et al. [37] measured the solubility in water of mixtures of glycine and DL-aspartic acid or DL-phenylalanine at 298.2 K and atmospheric pressure using gravimetric analyses. Results can be seen in Figure 3.16. For the systems studied in this work, the presence of one amino acid increases the solubility of another.

In aqueous solutions, amino acids are found in their zwitterionic form. Physical bonds are formed between the charged amino and carboxyl groups. For two unlike amino acids, this may result in the formation of amino acid complexes in addition to the dimers formed among molecules of the same amino acid. These interactions affect the solubility of an amino acid in the presence of another amino acid.

For a mixture of two amino acids, the solubility of an amino acid in the presence of another can be calculated using eq. (3.14). The superscript 0 in this case refers to the property in an aqueous solution of a single amino acid. In this work, the activity coefficients were determined by NRTL [31] and a Simplified Perturbed Hard-Sphere (SPHS) [38] models.

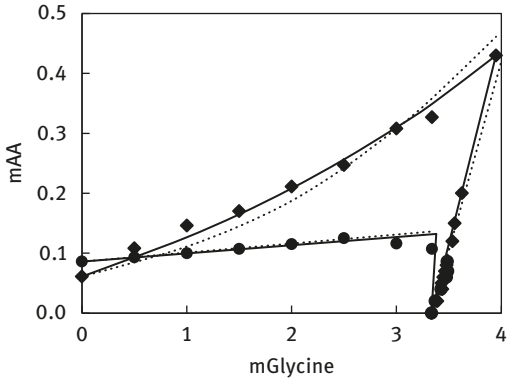

Figure 3.16: Solubilities for ◆ water + glycine + aspartic acid and ● water + glycine + phenylalanine at 298.2 K and atmospheric pressure.

The NRTL unsymmetrically normalized, similarly to eq. (3.17), is written as

$$\ln \gamma_i = \ln\ \gamma_i^{\mathrm{NRTL}} - \ln\ \gamma_i^{\mathrm{NRTL},\infty} + \ln\left(1 + 0.001 M_{\mathrm{W}} \sum m_i\right) \tag{3.24}$$

where M is the molecular weight of solvent which in this case is water and ∞ denotes the infinite dilution activity coefficient.

The nonrandomness factor α and the binary interaction parameters (τ) for water–amino acid pairs were obtained from a previous study [30]. Due to the lack of data, binary interaction parameters for DL-aspartic acid and DL-phenylalanine with water were set to zero. Two adjustable parameters, binary interaction parameters between amino acids, are required to correlate solubility data.

The SPHS model [38] is

$$\ln \gamma_i = \ln \gamma_i^{\mathrm{hs}} - \sum_{j=1}^{N} \frac{4\pi\rho_j}{kT} \left\{ \frac{8}{9} \in_{ij} \sigma_{ij}{}^3 + \frac{D_i{}^2 D_j{}^2}{9(4\pi \in_0 \in_{\mathrm{r}}) kT \sigma_{ij}{}^3} \right\} \tag{3.25}$$

where ρ is the number density, σ is the size parameter, $\in$ is the depth of potential well, D is the dipole moment, k is the Boltzmann constant, T is the absolute temperature, and $\in_0$ and $\in_r$ are the permittivity of the vacuum and relative dielectric constant, respectively. The contribution of the hard-sphere system to the activity coefficient is calculated by the model proposed by Mansoori et al. [17] (eqs. (3.9)–(3.13)).

The following mixing rules were used for the size parameter and the depth of the potential well:

$$\sigma_{ij} = \frac{\left(\sigma_i + \sigma_j\right)}{2} \tag{3.26}$$

$$\in_{ij} = \sqrt{\in_i \in_j} \tag{3.27}$$

The values of the depths of potential well and size parameters of amino acids for water–amino acid systems were obtained from a previous study [38]. For the amino acids for which the values of the size parameter and depth of potential well were not available, they were treated as two adjustable parameters.

As shown in Figure 3.16, the NRTL model can extrapolate the activity coefficients of amino acids to concentrations higher than their saturation concentration in pure water, better than the SPHS model.

Grosse Daldrup et al. [39] modeled the behavior of aqueous solutions of two amino acid solubilities with similar p*I*s using the PC-SAFT equation of state. Pure-component parameters for amino acids were fitted to different experimental data, such as solubilities, binary mixture densities, and amino acid activity coefficients. The ternary solubility behavior was described with only one temperature-independent parameter between the two solutes that was adjusted to the ternary solubility data. Mixtures containing more than three components can also be modeled. This work was later extended [40] to model mixtures of amino acids with different p*I*s. Accounting for the association/dissociation equilibria of the amino acids in aqueous solution and using PC-SAFT simultaneous modeling of pH and solubility of mixtures of two amino acids were possible. Data obtained by Soto et al. [37] for the solubility in water of mixtures of glycine and DL-aspartic acid were successfully modeled with just one binary interaction parameter.

3.7 Effect of Anions on the Solubility of Zwitterionic Amino Acids

Focusing the effort on the analysis of the effect of anions on the solubility of amino acids, and as a continuation of previous works, Pradhan and Vera [41] determined the solubility of glycine, DL-alanine, DL-valine, and DL-serine in the presence of $NaNO_3$ and KNO_3 at 298.2 K and atmospheric pressure. This allows a comparison with data previously determined for NaCl and KCl [3].

As in the case of NaCl and KCl [3], at low electrolyte concentrations $NaNO_3$ and KNO_3 have a salting-out effect on glycine solubility, but on increasing electrolyte concentration a salting-in effect is observed (Figure 3.17(a)). Similarly to chloride salts, this may be due to the long-range interactions that predominate at low electrolyte concentrations, and the formation of ion-pair complexes at higher salt concentrations. Combined with the anion nitrate, the influence of the cation in the solubility of

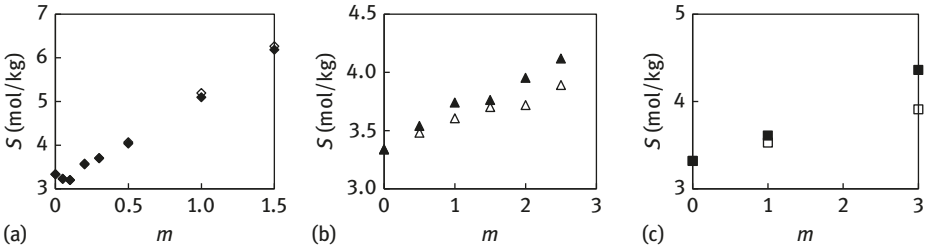

Figure 3.17: Solubilities of glycine in aqueous solution at 298.2K and atmospheric pressure as a function of salt molality. Data grouped by authors. (a) ◆ $NaNO_3$ [41]; ◇ KNO_3 [41]; b) ▲ $NaNO_3$ [43]; Δ KNO_3 [43]; c) ■ $NaNO_3$ [6]; □ KNO_3 [6].

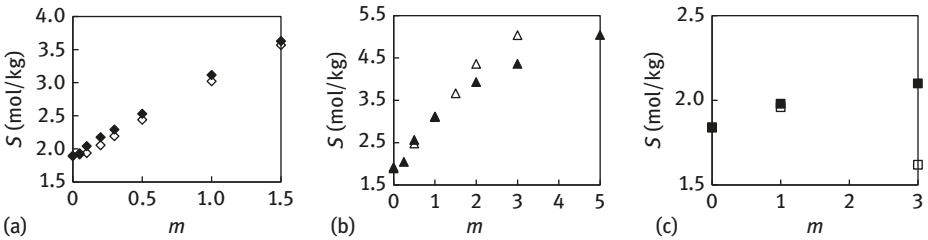

Figure 3.18: Solubilities of alanine in aqueous solution at 298.2K and atmospheric pressure as a function of salt molality. Data grouped by authors. (a) ◆ $NaNO_3$ [41]; ◇ KNO_3 [41]; b) ▲ $NaNO_3$ [44]; Δ KNO_3 [45]; c) ■ $NaNO_3$ [6]; □ KNO_3 [6].

glycine is not very significant, leading to solubilities slightly higher at high concentration of salt with potassium (as with the chloride anion). Figures 3.18(a), 3.19, and 3.20 also show a salting-in effect of nitrates on the solubility of DL-alanine, DL-valine, and DL-serine. Only in the case of DL-alanine, higher solubilities are found with the sodium anion. However, this inverse behavior was also found for DL-aminobutyric acid in aqueous solutions of $NaNO_3$ and KNO_3 [28]. In any case, the influence of the cation of the salt on the solubility of the amino acids is limited. However, by comparing Figures 3.4–3.7 with Figures 3.17–3.20, it can be concluded that there is a strong effect of the anion on the solubility of these biomolecules. The nitrate anion increases the solubility of the amino acids more than the chloride anion. These results are in good agreement with conclusions obtained by Tomé et al. [42] using molecular simulation. These authors found that the chloride anion has a negligible effect on the amino acid's aqueous solubility, or at most a slight salting-out effect since it avoids interacting with the apolar parts of the amino acids. The nitrate however interacts with the hydrophobic moieties of the solute and thus increases its solubility. Results obtained in that work support the idea that the salting in/out effects are controlled by the presence or absence of interactions with the nonpolar moieties of the amino acids.

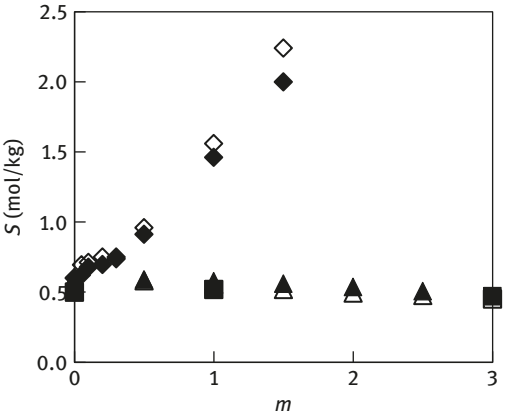

Figure 3.19: Solubilities of valine/norvaline in aqueous solution at 298.2K and atmospheric pressure as a function of salt molality. ◆ Valine + $NaNO_3$ [41]; ◇ Valine + KNO_3 [41]; ▲ Norvaline + $NaNO_3$ [43]; Δ Norvaline + KNO_3 [43]; ■ Valine + $NaNO_3$ [6]; □ Valine + KNO_3 [6].

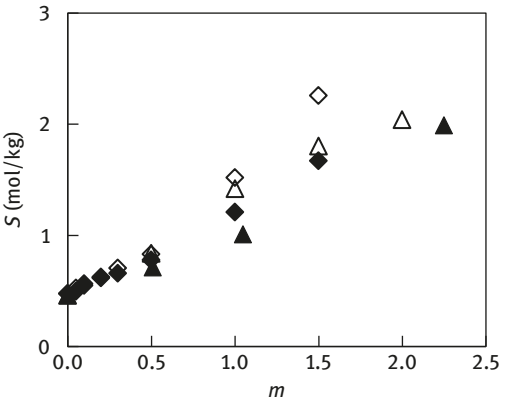

Figure 3.20: Solubilities of serine in aqueous solution at 298.2K and atmospheric pressure as a function of salt molality. ◆ $NaNO_3$ [41]; ◇ KNO_3 [41]; ▲ $NaNO_3$ [46]; Δ KNO_3 [45].

The solubilities of glycine, DL-alanine, DL-valine, and DL-serine in the presence of nitrate salts were later determined by other authors [43–46] and, as in the case of chloride salts, the significant differences observed are noteworthy. Roy et al. [43] (Figure 3.17(b)) and Held et al. [6] (Figure 3.17(c)) confirmed the salting-in effect of nitrate salts on the solubility of glycine. However, in contrast to Pradhan and Vera [41] both authors found higher solubilities with sodium cation.

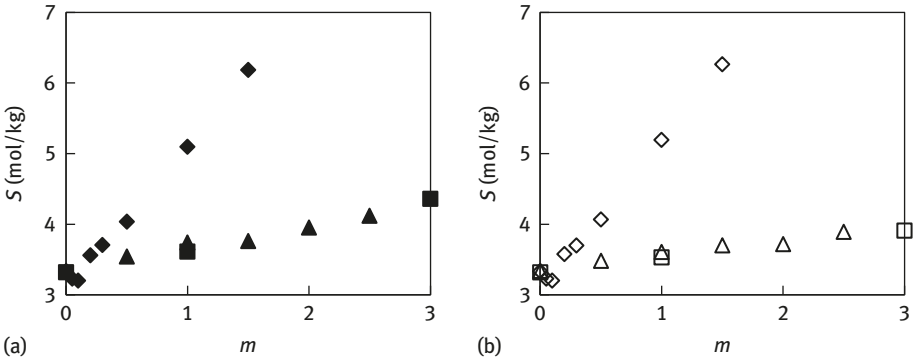

Figure 3.21: Solubilities of glycine in aqueous solution at 298.2K and atmospheric pressure as a function of salt molality. Data grouped by cation. a) ◆ $NaNO_3$ [41]; ▲ $NaNO_3$ [43]; ■ $NaNO_3$ [6]; b) ◇ KNO_3 [41]; Δ KNO_3 [43]; □ KNO_3 [6].

Figure 3.21 shows a very significant discrepancy among data obtained by Roy et al. [43] and Held et al. [6] (that are in good agreement) with those obtained by Pradhan and Vera [41], which show a much greater increase in the solubility of glycine with salt concentration than the other authors.

Figure 3.22 shows the solubilities of DL-alanine in $NaNO_3$ and KNO_3 aqueous solutions according to data measured by Pradhan and Vera [41], Roy et al. [44, 45], and Held et al. [6]. The two first authors are measuring solubilities of DL-alanine and the latter of L-alanine. All the authors found a salting-out effect of both salts but in this case Khoshkbarchi and Vera [3] and Held et al. [6] obtained higher solubilities with sodium than with potassium and Roy et al. [44, 45] found the opposite behavior. In contrast to the results with glycine, Figure 3.22 shows that in this case data of Pradhan and Vera [41] and Roy et al. [44, 45] are in good agreement, and the increase of solubility with salt concentration obtained by Held et al. [6] is much smaller. However, the system with $NaNO_3$ was also measured by Han and Tan [7] for DL-alanine and the data perfectly match with those obtained by Held et al. [6] for L-alanine.

Figure 3.19 shows that the increase in solubility of DL-valine with salt concentration determined by Pradhan and Vera [41] is much more pronounced than the increase in solubility of L-valine determined by Held et al. [6]. Interestingly, data obtained by Roy et al. [43] for norvaline (an isomer of valine) are in good agreement with those obtained by Held et al. [6] for L-valine. Data obtained by Pradhan and Vera [41] and Roy et al. [45, 46] for solubility of DL-serine show the same tendency (Figure 3.20) with higher solubilities obtained by the first authors.

A consideration of all the data reported for the effect of chloride and nitrate anions on the solubility of aminoacids does not allow to go beyond saying that the amino acid structure and the presence of salt affect the solubility of these biomolecules in water. In the case of the anion, the influence is much greater (higher

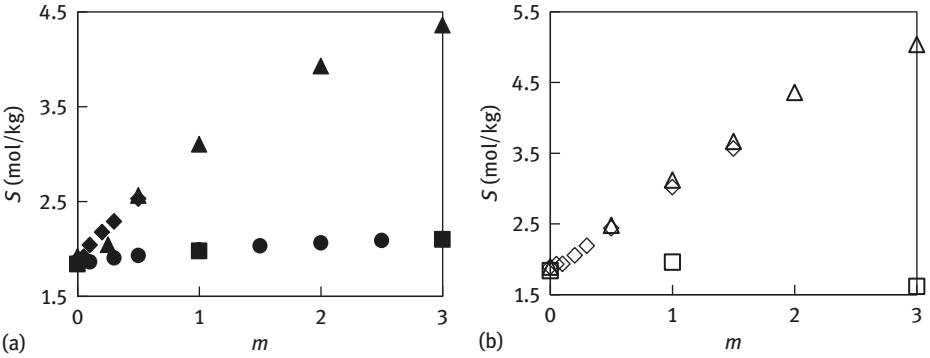

Figure 3.22: Solubilities of alanine in aqueous solution at 298.2K and atmospheric pressure as a function of salt molality. Data grouped by cation. a) ◆ $NaNO_3$ [41]; ▲ $NaNO_3$ [44]; ■ $NaNO_3$ [6]; ● NaNO3 [7]; b) ◇ KNO_3 [41]; Δ KNO_3 [45]; □ KNO_3.

solubilities are obtained with nitrate anion) than the influence of the cation, which is why there is such a high discrepancy among authors about the influence of sodium and potassium on solubilities.

3.8 Closing Remarks

Although a wide variety of studies about the solubilities of amino acids in aqueous electrolyte solutions have been presented [47], there are significant discrepancies among published results. New measurements are required to shed light on the reasons for the map of behaviors currently found. To avoid new discrepancies, a clear description of the experimental protocol followed, including detailed method of preparation of samples, time and temperatures employed in the process of reaching equilibrium, a detailed characterization of the chemicals (the proportion of isomers in the amino acid, quantity and type of impurities, etc.), and pH of the water used, as well as the characterization of the solid phase (crystals) found at the equilibrium conditions is necessary. A rigorous study of the uncertainties and their influence on the solubility data is also required.

References

[1] Wiley-VCH Ullmann's Encyclopedia of Industrial Chemistry, 7th ed., Wiley-VCH Verlag GmbH, Weinheim, Germany, 2011.
[2] Castronuovo G, Elia V, Niccoli M, Velleca F. Thermochim Acta 1998, 320, 13.
[3] Khoshkbarchi MK, Vera JH. Ind Eng Chem Res 1997, 36, 2445.

[4] Cohn EJ, Edsall JT. Proteins, Amino Acids and Peptides as Ions and Dipolar Ions, Hafner Publisher Company, New York, USA, 1965.
[5] Roy S, Hossain A, Mahali K, Dolui BK. Russ J Phys Chem A 2015, 89, 2111.
[6] Held C, Reschke T, Müller R, Kunz W, Sadowski G. J Chem Thermodyn 2014, 68, 1.
[7] Han G, Tan RBH. Chem Eng Sci 2009, 64, 3983.
[8] Ferreira LA, Macedo EA, Pinho SP. Ind Eng Chem Res 2005, 44, 8892.
[9] Roy S, Hossain A, Dolui BK. J Chem Eng Data 2016, 61, 132.
[10] Roy S, Guin PS, Dolui BK. J Mol Liq 2015, 211, 294.
[11] Polenske D, Lorenz H. J Chem Eng Data 2009, 54, 2277.
[12] Lu J, Wang XJ, Yang X, Ching CB. J Chem Eng Data 2006, 51, 1593.
[13] Yang X, Wang X, Ching CB. J Chem Eng Data 2008, 53, 1133.
[14] Yang X, Lu J, Wang XJ, Ching CB. J Raman Spectrosc 2008, 39, 1433.
[15] Han G, Chow PS, Tan RBH. Cryst Growth Des 2012, 12, 5555.
[16] Khoshkbarchi MK, Vera JH. Ind Eng Chem Res 1996, 35, 4755.
[17] Mansoori GA, Carnahan NF, Starling KE, Leland TW. J Chem Phys 1971, 54, 1523.
[18] Sadeghi R. Fluid Phase Equilibr 2007, 260, 266.
[19] Sadeghi R. J Chem Thermodyn 2005, 37, 323.
[20] Chen CC, Zhu Y, Evans LB. Biotechnol Prog 1989, 5, 111.
[21] R Sadeghi. Can J Chem 2008, 86, 1126.
[22] Chapman WG, Gubbins KE, Jackson G, Radosz M. Ind Eng Chem Res 1990, 29, 1709.
[23] Seyfi S, Pazuki G, Aghamiri SF, Beheshti M. Fluid Phase Equilibr 2009, 287, 15.
[24] Papaiconomou N. PhD Dissertation, Regensburg University, Regensburg, 2003.
[25] Anvari MH, Pazuki G, Seyfi-Kakhki S, Bonakdarpour B. J Mol Liq 2013, 184, 24.
[26] Gil-Villegas A, Galindo A, Whitehead PJ, Mills SJ, Jackson G, Burgess AN. J Chem Phys 1997, 106, 4168.
[27] Cameretti LF, Sadowski G, Mollerup JM. Ind Eng Chem Res 2005, 44, 3355 ibid 8944.
[28] Soto A, Arce A, Khoshkbarchi MK, Vera JH. Biophys Chem 1998, 73, 77.
[29] Mondal S, Ghosh S, Hossain A, Mahali K, Roy S, Dolui BK. Russ J Phys Chem A 2016, 90, 1798.
[30] Khoshkbarchi MK, Vera JH. AIChE J 1996, 42, 2354.
[31] Renon H, Prausnitz JM. AIChE J 1968, 14, 135.
[32] Pradhan AA, Vera JH. Fluid Phase Equilibr 1998, 152, 121.
[33] Tseng HC, Lee CY, Weng WL, Shiah IM. Fluid Phase Equilibr 2009, 285, 90.
[34] Fuchs D, Fischer J, Tumakaka F, Sadowski G. Ind Eng Chem Res 2006, 45, 6578.
[35] Mercier-Franco LF, Mattedi S, Pessôa-Filho PA. Fluid Phase Equilibr 2013, 354, 38.
[36] Han G, Chow PS, Tan RBH. Cryst Growth Des 2012, 12, 2213.
[37] Soto A, Arce A, Khoshkbarchi MK, Vera JH. Fluid Phase Equilibr 1999, 158–160, 893.
[38] Khoshkbarchi MK, Vera JH. Ind Eng Chem Res 1996, 35, 4319.
[39] Daldrup JBG, Held C, Ruether F, Schembecker G, Sadowski G. Ind Eng Chem Res 2010, 49, 1395.
[40] Daldrup JBG, Held C, Sadowski G, Schembecker G. Ind Eng Chem Res 2011, 50, 3503.
[41] Pradhan AA, Vera JH. J Chem Eng Data 2000, 45, 140.
[42] Tomé LIN, Gomes MJJRB, Coutinho, JAP. J Phys Chem B 2010, 114, 16450.
[43] Roy S, Guina PS, Mondal S, Ghosh S, Dolui BK. J Mol Liq 2016, 222, 313.
[44] Roy S, Mahali K, Mondal S, Mondal RP, Dolui BK. Russ J Gen Chem 2015, 85, 162.
[45] Hossain S, Roy S. J Mol Liq 2018, 249, 1133.
[46] Mondal S, Roy S, Ghosh S, Mahali K, Dolui BK. J Sol Chem 2016, 45, 1755.
[47] Hossain A, Roy S, Dolui BK. J Mol Liq 2017, 232, 332.

Mohammad K. Khoshkbarchi and Ana Soto

4 Activity Coefficients of Amino Acids in Aqueous Electrolyte Solutions

4.1 Introduction

The cost of separation and purification of biomolecules used in drugs and food products accounts for a considerable portion of their total production cost. The growing demand for a number of complex biochemical products requires the development and design of efficient and cost-effective separation processes. These processes are designed based on the physical behavior of biomolecules in solutions and application of the principles of phase equilibria and ways to manipulate them to achieve the desired behavior. For example, biochemical crystallization process in the presence of electrolytes takes advantage of the salting-in or salting-out phenomenon to achieve controlled precipitation of a target biomolecule in a system with solid and liquid phases in equilibrium, or evaporation process in the presence of electrolytes that takes advantage of vapor pressure alteration due to the interactions between water, ions, and biomolecules, in a multiphase system with vapor, liquid, and solid in equilibrium. As such, accurate design, modeling, simulation, and operation of these processes highly depend on the understanding of the interactions and accurate prediction of phase behavior and thermodynamic properties of biomolecules in solutions.

Amino acids are the most basic biomolecules and are the building blocks of more complex biomolecules such as proteins. Amino acids have broad range of applications in the food industry. Amino acids possess unique properties due to their chemical structure that consists of an amino and a carboxyl group on a hydrocarbon backbone. The amino and carboxyl groups of amino acids can dissociate in aqueous solutions and become positively and negatively charged, respectively. In the presence of a proton donor agent, the amino acid carboxyl group gains a proton and the amino acid molecule becomes positively charged, whereas in the presence of a proton acceptor agent, the amino group of the amino acid loses a proton and the amino acid molecule becomes negatively charged. As a result, an amino acid can be classified as an ampholyte as it can react with both a base and an acid.

Glycine is the simplest amino acid with no isomer. However, other amino acids have at least two optical isomers with identical grouping of atoms in their molecules and only differ in their effects on the plane-polarized light. One of these isomers is called the L-form that rotates the plane-polarized light to the left (Latin: laevus – on the left) and the other one is called the D-form that rotates the plane-polarized light to the right (Latin: dexter – on the right). In the presence of equal amounts of

https://doi.org/10.1515/9783110564808-004

these isomers in a mixture, their optical effects will be neutralized, and the mixture is called the racemate form or the DL-form of the amino acid. There are other isomeric forms of an amino acid based on the location of the amino group on its hydrocarbon backbone. If both carboxyl and amino groups are attached to the α carbon, the amino acid is called α-amino acid, and if the amino group is attached to the carbon next to the α carbon, the amino acid is called β-amino acid.

Amino acids when dissolved in aqueous solutions form several ionic species due to the ionization of their carboxyl and amino groups. After dissolving in water, the carboxyl group of the amino acid loses a proton and becomes negatively charged, whereas the amino group gains a proton and becomes positively charged. Therefore, an amino acid could carry both a negative and a positive charge, and in this state, they are referred to as zwitterions. It is this property of amino acids that makes them more favorable to dissolve in polar solvents such as water. While, at moderate pH values, amino acids are zwitterions, their charged state can change with the pH of the solution and they can turn into anions or cations. The pH value at which the numbers of positive and negative charges on the amino acid molecule are equal is referred to as the isoelectric point. The formation of different ionic forms of the amino acids is given by the following reactions:

$$\mathrm{NH_2RCOOH} \rightleftharpoons \mathrm{NH_3^+ RCOO^-}$$

$$\mathrm{NH_3^+ RCOOH} \rightleftharpoons \mathrm{H^+ + NH_3^+ RCOO^-}$$

$$\mathrm{H^+ + NH_2RCOO^-} \rightleftharpoons \mathrm{NH_3^+ RCOO^-}$$

Although there are various thermodynamic properties such as the chemical potential or Gibbs free energy that represent the interactions among components of a system and can be used to predict the phase equilibrium, the activity coefficient is most commonly used to represent the deviation of a system from ideal behavior and to develop models for phase equilibrium calculations. The deviation from the ideal solution behavior is a result of the interactions among the constituent components of the system.

A necessary condition for equilibrium in any multiphase system at a given temperature T, pressure P, and composition x is defined by the principles of thermodynamics that at equilibrium fugacities of every component in all phases of the system, $f_i^{\text{phase } N}$, should be equal.

$$f_i^{\text{phase I}}\left(T,\ P,\ x^{\text{phase I}}\right) = f_i^{\text{phase II}}\left(T,\ P,\ x^{\text{phase II}}\right) = f_i^{\text{phase III}}\left(T,\ P,\ x^{\text{phase III}}\right) = \cdots \tag{4.1}$$

For a nonelectrolytic component i, the fugacity is, in turn, related to the activity coefficient, $\gamma_i(T,\ P,\ x)$, as

$$x_i\gamma_i(T,\ P,\ x)f_i^{\circ}(T,\ P) = f_i(T,\ P,\ x) \tag{4.2}$$

where $f_i^{\circ}(T,\ P)$ is the fugacity of component i at the standard state. This standard state based on the Lewis–Randall (symmetric) convention, suitable for solvents such as water, is defined as

$$\gamma_i \to 1 \text{ as } x_i \to 1 \tag{4.3}$$

The standard state convention commonly used for solutes, such as amino acids or electrolytes that in their pure form usually exist in the solid state, is based on the Henry convention (unsymmetric). In this convention, the limit of the activity coefficient, represented by *, is defined as the component at its infinite dilution as

$$\gamma_i^{\star} \to 1 \text{ as } x_i \to 0 \tag{4.4}$$

For electrolytes in aqueous solutions that dissociate and form ionic species, it is customary and convenient to define the activity coefficient as the mean ionic activity coefficient, $\gamma_{\pm}$, which is related to the activity coefficient of its constituent ionic species as

$$\gamma_{\pm} = \left(\gamma_{+}^{\nu_+}\gamma_{-}^{\nu_-}\right)^{1/\nu} \tag{4.5}$$

where ν_+ and ν_- represent the numbers of positively and negatively charged ions dissociated from an electrolyte, respectively, and $\nu = \nu_+ + \nu_-$.

Therefore, accurate measurement and knowledge of the activity coefficients of amino acids in aqueous electrolyte solutions provide an important insight into their interactions and behavior in solutions and are important for accurate determination and prediction of phase behavior and the distribution of the components among all phases present in the system.

4.2 Measurement Methods

Although activity coefficient cannot be directly measured, there are a number of methods for measuring other thermodynamic properties that can be related to the activity coefficient. Some of these methods include vapor pressure measurement, freezing point depression, boiling point elevation, and isopiestic and electrode potential measurements. The isopiestic and ion-selective electrodes (ISE) are the

most commonly used methods for measuring the activity coefficients of amino acids in electrolyte solutions and are briefly discussed in the following section.

4.2.1 Ion-Selective Electrodes

Ion-selective electrodes (ISE) are electrochemical half cells that in a mixture of ions respond selectively to a particular ion using a potential difference created across a semipermeable membrane in the electrode/electrolyte interface. The magnitude of this potential difference depends on the activity of the ion toward which they are selective. The potential of the ISE should be measured against another half cell, called as the reference electrode, which can maintain a constant potential relative to the sample solution under investigation. The difference between the potentials of the ISE and the reference electrode is determined by the activity of the electrolyte present in the solution and a combination of the reference electrode, junction, and asymmetry potentials.

Consider the following cells, marked as type (1), containing an electrolyte at molality m_E,

Cation ISE | electrolyte (m_E) | reference electrode
Anion ISE | electrolyte (m_E) | reference electrode

The Nernst equation for the potentials, E, of a cation and an anion ISE can be related to the activity coefficients of the cation, γ_+, and the anion of the electrolyte, γ_-, as,

$$E_+ = E_+^\circ + \frac{RT}{z_+F}\ln(m_+\gamma_+) + \mathrm{E_j} \tag{4.6}$$

$$E_- = E_-^\circ + \frac{RT}{z_-F}\ln(m_-\gamma_-) + \mathrm{E_j} \tag{4.7}$$

where R is the universal gas constant, F represents the Faraday number, z is the charge number, and the plus and minus subscripts represent the cation and the anion, respectively. The terms E_+° and E_-° represent the standard potentials of every cell, which are a combination of the reference electrode, and asymmetry potentials. $\mathrm{E_j}$ is the junction potential.

When the same reference electrode is used in both cells against the anion and the cation ISE, the difference between the potentials of the two cells of type (1), ΔE_1, can be related to the molality of the electrolyte and the mean ionic activity coefficient of the electrolyte, $\gamma_\pm^{(1)}$, as,

$$\Delta E_1 = E_+ - E_- = E_+^\circ - E_-^\circ + \frac{RT(z_+ + z_-)}{z_+z_-F}\ln\left((\nu_+^{\nu_+}\nu_-^{\nu_-})^{(\nu_+ + \nu_-)}m_E\gamma_\pm^{(1)}\right) \tag{4.8}$$

The aforementioned equation can be simplified as

$$\Delta E_1 = \Delta E^{\circ} + S\ln\left(\left(\nu_+{}^{\nu_+}\nu_-{}^{\nu_-}\right)^{(\nu_+ + \nu_-)} m_E \gamma_{\pm}^{(1)}\right) \tag{4.9}$$

where ΔE° represents the difference between the standard potentials of the cells and S is the slope of the cells.

The junction potential that arises at the interface of the reference electrode is a sensitive function of the solution composition. As in this method, the reference electrode is measured against two ISEs and the obtained potentials are subtracted; the effect of the junction potential is eliminated, leading to more accurate measurements. In addition, by employing two ISEs and measuring them simultaneously against a reference electrode, the changes in the potentials of the reference electrode in the course of the experiments are also cancelled out.

The potential of an electrochemical cell changes in the presence of other solutes due to the interactions between the solute, electrolyte, and water. This is reflected in the change of the mean ionic activity coefficient of the electrolyte in the presence of a solute. Consider the following cells, marked as type (2), which contain the same electrolyte at the same concentration as that of the type (1) cells and also contain an amino acid at molality, m_A,

Cation ISE | electrolyte (m_E) + amino acid (m_A) | reference electrode
Anion ISE | electrolyte (m_E) + amino acid (m_A) | reference electrode

The presence of the amino acid, due to its interactions with the electrolyte, changes the values of the difference between the potentials of the new cell, ΔE_2, and therefore the mean ionic activity coefficient of the electrolyte in the cells, $\gamma_{\pm}^{(2)}$. Similar to eq. (4.9), the difference between the potentials of the cell can be related to the mean ionic activity coefficient of the electrolyte as

$$\Delta E_2 = \Delta E^{\circ} + S\ln\left(\left(\nu_+{}^{\nu_+}\nu_-{}^{\nu_-}\right)^{(\nu_+ + \nu_-)} m_E \gamma_{\pm}^{(2)}\right) \tag{4.10}$$

Combining eqs. (4.9) and (4.10) results in the following equation that relates the mean ionic activity coefficients of the electrolyte in the cells in the presence and absence of an amino acid to the measured differences in potentials in cells of type (1) and type (2) as

$$\ln\left(\frac{\gamma_{\pm}^{(2)}}{\gamma_{\pm}^{(1)}}\right) = \frac{\Delta E_2 - \Delta E_1}{S} \tag{4.11}$$

The measured ratios of the mean ionic activity coefficients of the electrolyte in the presence and absence of an amino acid are usually fitted to a virial expansion correlation as

$$\nu ln \frac{\gamma_{\pm}^{(amino\ acid)}}{\gamma_{\pm}^{(no-amino\ acid)}} = C_1 m_A + C_2 m_E m_A + C_3 m_A^2 + C_4 m_E m_A^2 + C_5 m_A^3 + C_6 m_E m_A^2 \quad (4.12)$$

where m_A represents molality of the amino acid and m_E represents molality of the electrolyte. This correlation considers all the components of the system as undissociated and molecular and ignores the presence of any ionic or zwitterion species in the solution. The coefficients, C_i, are the virial expansion coefficients with unique values for every amino acid–electrolyte pair. The ratio of the activity coefficient of the amino acid in the presence of the electrolyte, $\gamma_A^{(elec)}$, to that in the absence of the electrolyte, $\gamma_A^{(no\text{-}elec)}$, can be obtained by combining the following equation with eq. (4.12):

$$\nu \left(\frac{\partial \ln \gamma_{\pm}}{\partial m_A} \right)_{T,P,m_E} = \left(\frac{\partial \ln \gamma_A}{\partial m_E} \right)_{T,P,m_A} \quad (4.13)$$

Resulting in the following correlation,

$$\ln \frac{\gamma_A^{(elec)}}{\gamma_A^{(no\text{-}elec)}} = C_1 m_E + \frac{1}{2} C_2 m_E^2 + 2C_3 m_E m_A + \frac{1}{3} C_4 m_E^3 + 3C_5 m_E m_A^2 + C_6 m_A m_E^2 \quad (4.14)$$

The first coefficient of eqs. (4.12) and (4.14) represents the pairwise interactions between amino acid and electrolyte molecules. A negative value for C_1 indicates attractive interactions between the amino acid and electrolyte, whereas a positive value indicates a repulsive interaction.

It is important to mention that there are studies that have employed only one ISE (usually a cation ISE) versus a reference electrode to measure the mean ionic activity coefficient of the electrolyte in the presence of an amino acid [1, 2]. The main drawback of identifying the mean ionic activity coefficient of the electrolyte with the potential of a single ISE is evident in eq. (4.10), which indicates that to relate the potential of electrodes to mean ionic activity coefficient, two ISEs are required. Another deficiency of this method is the uncompensated effect of the junction potential that happens at the interface of the reference electrode junction. The junction potential is a sensitive function of the solution composition and varies with the change in the solution composition. The application of two ISEs at the same time also reduces the effect of variations in the reference electrode potentials with time.

4.2.2 Isopiestic Method

The isopiestic method is a relative measurement method in which a reference sample with known activity is brought to equilibrium with the sample under

investigation. The two samples must contain the same volatile component (in this case water). In this method, the samples are placed in a sealed chamber and in contact with each other. The solvent is evaporated and transferred from one sample to other until thermodynamic equilibrium is reached. Once the equilibrium is reached, the samples will have identical solvent activities and therefore equal vapor pressures. After measuring the concentration of the sample under investigation, the osmotic coefficient, ϕ, can be calculated as

$$\phi = \frac{\ln(\gamma_w x_w)}{\ln x_w} \tag{4.15}$$

A simplified version of this equation is commonly used as

$$\phi = \frac{-\ln(\gamma_w x_w)}{M_w \sum_i \nu_i m_i} \tag{4.16}$$

where M_w is the molecular weight of water and ν_i and m_i are the stoichiometric coefficient and molality of the solutes, respectively. The mean ionic activity coefficient of the electrolyte can be calculated from the following equation:

$$\ln\gamma_{\pm} = (\phi - 1) + \int_0^{m_E} (\phi - 1) d\ln(m_E) \tag{4.17}$$

The activity coefficient of the amino acid can be calculated by combining eqs. (4.17) and (4.13) as

$$\nu \left(\frac{\partial \ln\gamma_{\pm}}{\partial m_A}\right)_{T,P,m_E} = \left(\frac{\partial \ln\gamma_A}{\partial m_E}\right)_{T,P,m_A} = \frac{\nu m_E \phi - \nu m_E \phi_E^0 - m_A \phi_A^0}{m_A m_E} \tag{4.18}$$

where ϕ_E^0 is the osmotic coefficient of binary water+electrolyte at m_E molality and ϕ_A^0 is the osmotic coefficient of binary water+amino acid at m_A molality.

Although both isopiestic method and electrode potential measurement using ISE are considered to be accurate methods for measuring activity coefficient of amino acids in electrolyte solutions, there are some variations reported using different techniques. For ISE cells, the largest uncertainty is introduced by the effect of the junction potentials that are considered to be equal in the derivation of eq. (4.8), and for the isopiestic method, the uncertainty in the measurement of the concentration of the target solution after equilibrium is reached. To show the effects of these uncertainties in the measurements, the experimental data obtained for NaCl–glycine system reported in four different investigations are shown in Figure 4.1. Figure 4.1 compares the ratios of the mean ionic activity coefficients of NaCl in the presence and absence of glycine as a function of

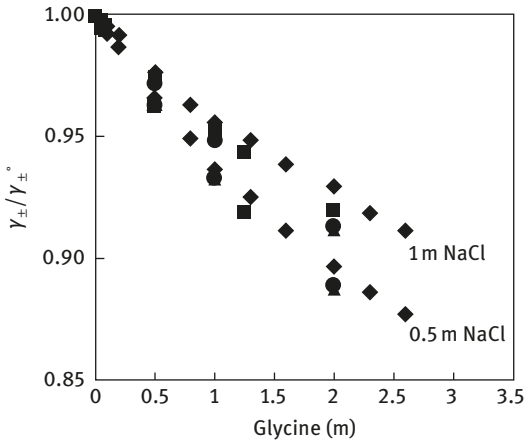

Figure 4.1: The ratio of the mean ionic activity coefficients of NaCl in the presence and absence of glycine as a function of glycine molality: ◆ ISE [3], ▲ ISE [1], ■ ISE [4], ● isopiestic [5].

amino acid molality at two different levels of NaCl concentrations [1, 3–5]. As shown in this figure, the measured data using different methodologies are in acceptable agreement. The variations are less at lower glycine concentrations and increase with an increase in both NaCl and glycine concentrations.

4.3 Activity Coefficient of Amino Acids in Aqueous Electrolyte Solutions

The measurement of activity coefficients of amino acids in electrolyte solutions has been the subject of several studies. Table 4.1 summarizes the results of these studies for various amino acid–electrolyte pairs in aqueous solutions at 298.15 K and presents them in the form of the coefficients of eqs. (4.12) and (4.14). The chemical structures of these amino acids are shown in Chapter 3.

Table 4.1 shows a wide variation in the coefficients for different amino acid–electrolyte pairs. This indicates that the interactions between amino acids and ions are strongly influenced by both the chemical structure of the amino acid and the natures of the cations and anions of the electrolyte. Amino acids in their zwitterionic form interact with water and other simple ions in the solutions through both complex long-range electrostatic and short-range forces. This is mainly due to the coexistence of both oppositely charged amino and carboxyl group and a hydrocarbon backbone in their chemical structure. This provides amino acids with a considerable dipole moment, which gives rise to the importance of dipole–dipole and ion–dipole interactions between amino acid molecules, water, and simple ions. Although amino acids at moderate pH values carry equal number of positive and negative charges and the entire molecule can be considered neutral, their individual charged groups interact through electrostatic forces with each other as well as other simple ions

Table 4.1: Coefficients of eqs. (4.12) and (4.14) for amino acids in aqueous electrolyte solutions at 298.15 K.

Amino acid	Electrolyte	C_1	C_2	C_3	C_4	C_5	C_6	Ref.
Glycine	NaCl	−0.232720	0.178438	0.037054	−0.050052	−0.002981	−0.016483	[3]
	KCl	−0.236801	0.275358	0.019314	−0.132479	0.000267	−0.007068	[6]
	$NaNO_3$	−0.104930	0.11990	−0.11307	−0.06431	0.02559	0.01391	[7]
	KNO_3	−0.457793	0.622482	0.053941	−0.320274	−0.002268	−0.043574	[8]
	NaBr	−0.327	0.097	0.110	−0.049	−0.024	0.012	[9]
DL-Alanine	NaCl	−0.165701	0.298762	0.038005	−0.159047	−0.002202	−0.024528	[3]
	KCl	−0.14171	0.33313	0.01955	−0.09034	0.01164	−0.05671	[10]
	$NaNO_3$	−0.17588	0.30107	−0.06667	−0.13952	0.03244	−0.01697	[10]
DL-Valine	NaCl	0.057467	−0.012617	0.066026	0.10374	0.076180	−0.051883	[11]
	KCl	0.02606	0.16650	−0.01748	0.08020	0.14888	−0.04222	[12, 13]
	$NaNO_3$	−0.084055	0.278430	−0.159087	−0.083077	−0.162547	−0.038425	[8]
L-Valine	NaBr	−0.230	0.128	0.872	−0.189	−1.134	0.409	[9]
DL-Serine	NaCl	−0.21004	0.31734	−0.14858	−0.14726	0.24504	−0.04878	[14]
	KCl	−0.28658	0.32205	0.06190	−0.10156	0.03492	−0.07793	[14]
	$NaNO_3$	−0.461178	0.475671	0.186180	−0.183626	−0.054472	−0.194646	[8]
	KNO_3	−0.490994	0.941036	−0.019429	−0.550696	0.142561	−0.088478	[8]
DL-Threonine	NaCl	−0.11861	0.27538	0.00100	−0.12747	0.01246	−0.02775	[15]
	$NaNO_3$	−0.14585	0. 30745	−0.12561	−0.15699	0.06189	−0.01435	[15]
DL-Methionine	NaCl	0.15883	0.24817	−1.83288	−0.08235	4.92509	0.00309	[7]

present in the solution. The existence of simple ions in the solutions is the result of the dissociation of the electrolyte. The hydrocarbon groups in amino acids also interact with other molecules, mainly through short-range forces. At higher concentrations, the charged groups of amino acids can form physically bonded ion pairs between charged groups of amino acids and oppositely charged simple ions, reducing the dipole–dipole and ion–dipole interactions. In addition, oppositely charged groups of amino acid molecules can form physical bonds promoting association in the solution. The formation of these complexes, due to the neutralization of the amino acid charged groups, reduces the electrostatic interactions and therefore the effect of the long-range interactions. This gives rise to the importance of the short-range interactions as a result of the interactions between the hydrocarbon backbone of the amino acid with other molecules and ions. This effect is similar to the ion condensation phenomena in polyelectrolytes. It is noteworthy that the activity coefficients of some of simple peptides and antibiotics in aqueous electrolyte solutions have also been the subject of some studies [16, 17]. However, in this chapter, we focus our attention on the amino acids as their simpler structures may allow for a clearer comparison with more conclusive observations.

Before looking at the behavior of amino acids in aqueous electrolyte solutions, it is important to study the activity coefficient of amino acids in aqueous solutions. Figure 4.2 shows the effect of concentration of several amino acids amino acids on their activity coefficients in aqueous solutions [18]. The comparison shows the importance of the nature and structure of the hydrocarbon backbone of amino acids on their interactions in aqueous solutions and their activity coefficients. It can be seen that as

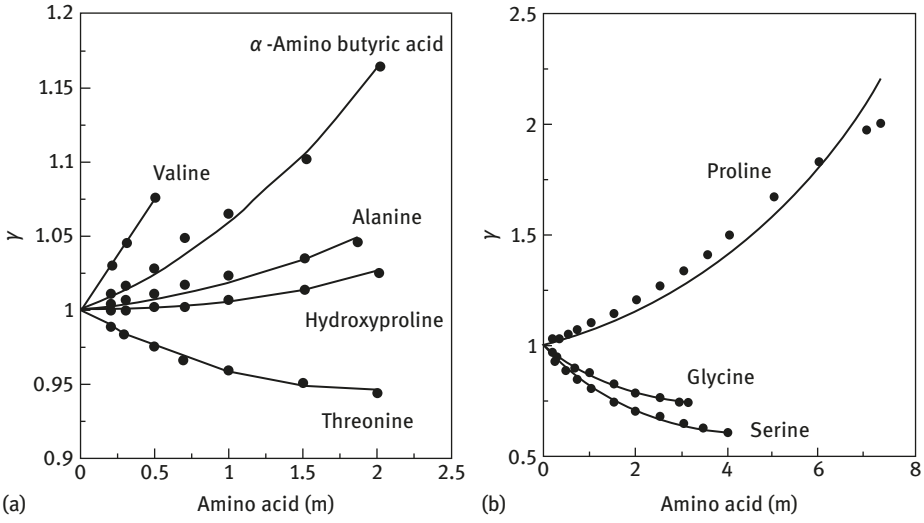

Figure 4.2: Activity coefficients of amino acids in aqueous solution. Solid circles represent the experimental data [18] and the lines are for visual aide only.

the hydrocarbon backbone of the amino acid grows its activity coefficient increases, which can be attributed to the effect of the strong hydrophobic–hydrophilic interactions. As shown for a fixed amino acid concentration, the activity coefficient increases in the order of glycine, DL-alanine, and DL-valine, which are next to each other in the homologous series and are different by one $-CH_2$ group. Although the hydrocarbon backbone of serine is larger than glycine, due to the presence of an –OH group in its hydrocarbon backbone is more hydrophilic and therefore its activity coefficient is less then the activity coefficient of glycine.

The comparative study of the experimental data of the activity coefficient of amino acids in aqueous electrolyte solutions helps to better understand the nature of the interactions in aqueous solutions of amino acids and electrolytes. Glycine is the simplest amino acid with only one $-CH_2$ group in its hydrocarbon backbone. Figures 4.3–4.6 show the effect of concentration of glycine and different electrolytes on the ratio of the

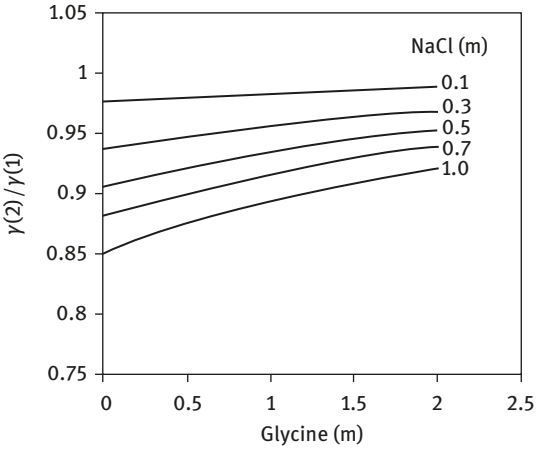

Figure 4.3: Effect of concentration of glycine and NaCl on the activity coefficient ratio of glycine.

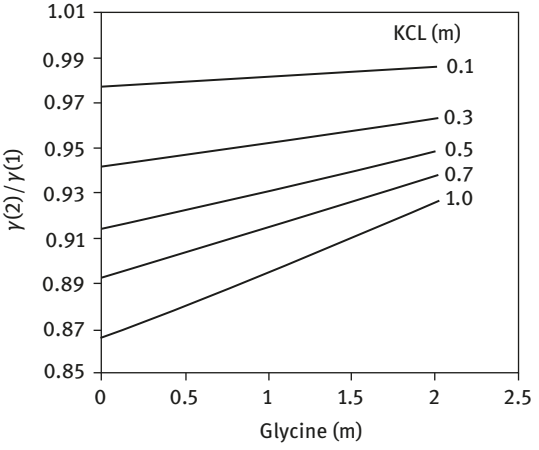

Figure 4.4: Effect of concentration of glycine and KCl on the activity coefficient ratio of glycine.

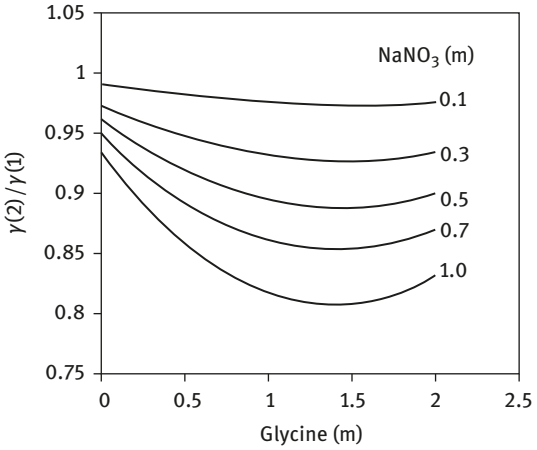

Figure 4.5: Effect of concentration of glycine and $NaNO_3$ on the activity coefficient ratio of glycine.

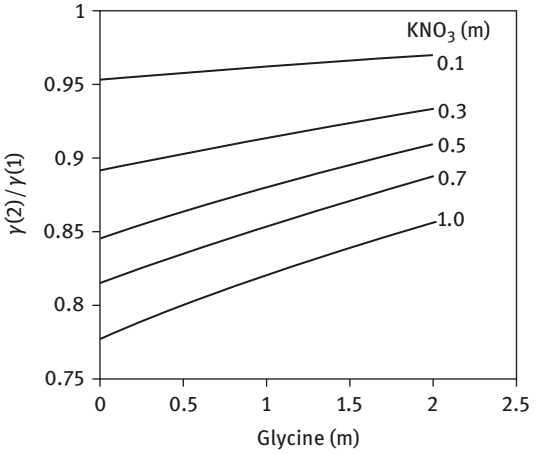

Figure 4.6: Effect of concentration of glycine and KNO_3 on the activity coefficient ratio of glycine.

activity coefficient of glycine in the presence and absence of an electrolyte [3, 6–8]. The electrolytes studied are NaCl, KCl, $NaNO_3$, and KNO_3, respectively.

As can be seen from these figures, the presence of an electrolyte significantly influences the activity coefficient ratio of glycine. For all electrolytes studied, the interactions between the electrolyte and glycine are more pronounced at higher concentrations of the electrolyte. It is interesting to note that although NaCl and KNO_3 do not share a common ion, both of them show similar qualitative trend, and for all electrolyte concentration levels studied, an increase in the glycine concentration diminishes the effect of the electrolyte concentration on the activity coefficient ratio of glycine. However, despite $NaNO_3$ shares a sodium cation with NaCl and a nitrate anion with KNO_3, they do not show a common qualitative effect on the activity coefficient ratio of

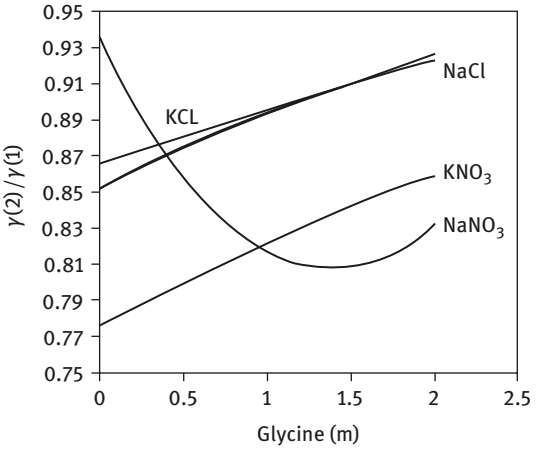

Figure 4.7: Effect of concentration of glycine on its activity coefficient ratio in the presence of 1.0 m NaCl, KCl, $NaNO_3$, and $NaNO_3$.

glycine. This is clearly shown in Figure 4.7, where the effect of the four electrolytes at 1.0 m on the activity coefficient ratio of glycine is depicted.

As shown in Figure 4.7 for glycine in a 1.0 m $NaNO_3$ solution, the activity coefficient ratio of glycine substantially decreases as the concentration of glycine increases; it passes through a minimum at 1.5 m concentration of glycine and decreases thereafter. Similar effect can be observed for DL-alanine [3, 10] in the presence of NaCl, KCl, and $NaNO_3$ as shown in Figure 4.8. It should be noted that DL-alanine differs from glycine by one $-CH_3$ group.

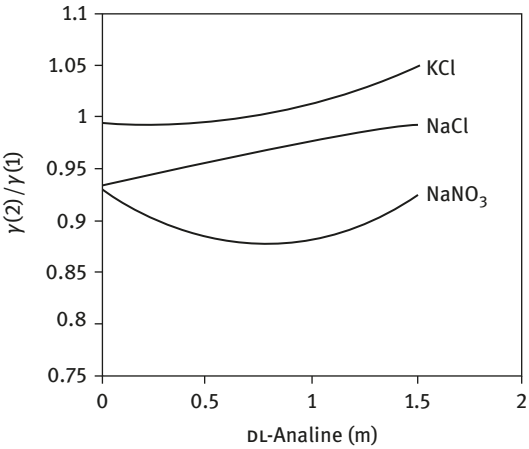

Figure 4.8: Effect of concentration of DL-alanine on its activity coefficient ratio in the presence of 1.0 m NaCl, KCl, and $NaNO_3$.

As it is evident from Figure 4.8, the qualitative trend for the effect of the DL-alanine concentration on its activity coefficient ratio is similar in the presence of KCl and NaCl but different in the presence of $NaNO_3$. The experimental data show that although the activity coefficient ratio of DL-alanine in the presence of $NaNO_3$ passes through a

minimum, the same phenomenon does not happen for the other electrolytes studied. Similar phenomenon was observed for systems contacting glycine and electrolytes.

After glycine and DL-alanine, DL-valine is next in the homologous series of amino acids with an additional $-CH_2$ group in its hydrocarbon structure. Figure 4.9 compares the activity coefficient of DL-valine in the presence of 1.0 m NaCl, KCl, and $NaNO_3$ [8, 11–13]. The comparison shows that similar to the systems containing glycine and DL-alanine, the activity coefficient ratio of the DL-valine increases in the presence of the NaCl and KCl, but decreases in the presence of $NaNO_3$ over the entire range of DL-valine concentration studied. As the solubility of DL-valine is lower than that of glycine and DL-alanine, the curve showing the effect of $NaNO_3$ does not pass through a minimum value.

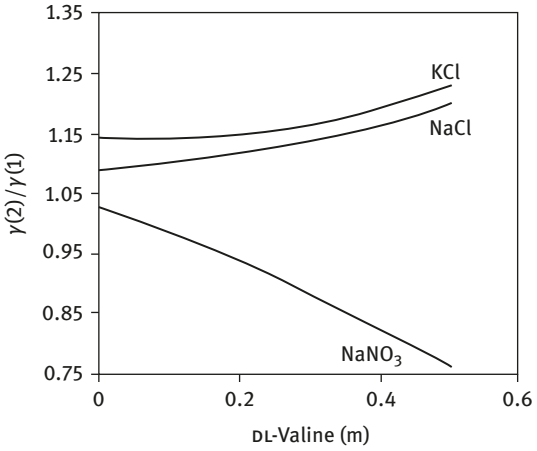

Figure 4.9: Effect of concentration of DL-valine on its activity coefficient ratio in the presence of 1.0 m NaCl, KCl, and $NaNO_3$.

Figure 4.10 depicts the effect of the concentration of NaCl on the trace activity coefficient of six amino acids [3, 7, 11, 14, 15]. The trace activity coefficient of an amino acid in

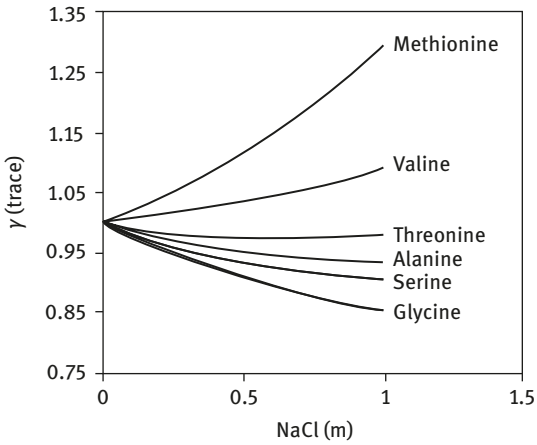

Figure 4.10: Effect of the concentration of NaCl on the trace activity coefficient of six amino acids.

the aqueous solution of an electrolyte is the value of its activity coefficient when its molality approaches zero. To calculate the trace activity coefficient, all amino acid molalities in eq. (4.14) have been set to zero. Although, at infinite dilution, the effect of short-range interactions is minimized, the wide difference between effect of the NaCl concentration on the trace activity coefficient of amino acids further shows the importance of the ion–dipole and dipole–dipole interactions compared to the steric effects and long-range electrostatic interactions. From this figure it can also be seen that, at a certain NaCl molality, the trace activity coefficient of an amino acid increases as the hydrocarbon backbone of the amino acid becomes larger. This effect remains the same over the entire range of NaCl molality studied. The trace activity coefficient curves of DL-alanine and DL-serine, whose hydrocarbon backbones differ with each other by an –OH group, are close to each other. The trace activity coefficient curve of DL-serine lays between the trace activity coefficient of glycine and DL-alanine and is farther than DL-alanine to the trace activity coefficient curve of DL-valine over the entire range of NaCl molality studied. This could be attributed to the presence of an –OH group in the hydrocarbon backbone of DL-serine, which renders it more hydrophilic than DL-alanine and therefore renders its behavior more similar to the behavior of glycine than to the behavior of DL-valine.

The experimental data for the effect of temperature on the activity coefficient of amino acids in aqueous and aqueous electrolyte solutions are scarce.

Figure 4.11 shows the effect of temperature on the activity coefficient of glycine and DL-alanine at three different temperatures [18]. As can be seen from this figure, the activity coefficients of both amino acids increase as the temperature increases. The effect of temperature on the activity coefficient of both amino acids studied is less at higher temperatures. While glycine activity decreases with concentration and increases with temperature, for DL-alanine, at lower temperature, the activity coefficient decreases with concentration until it

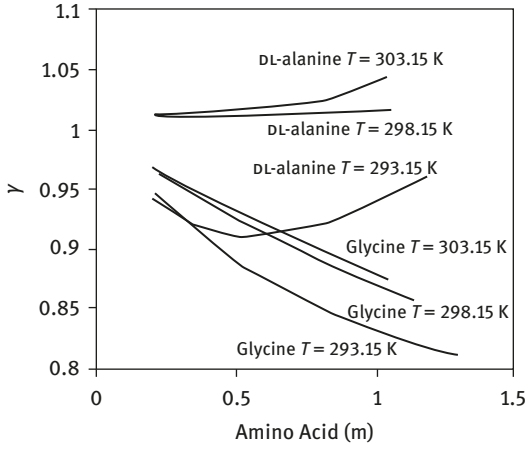

Figure 4.11: Effect of temperature on the activity coefficient of glycine and DL-alanine at three different temperatures.

goes through a minimum and then increases as the concentration of DL-alanine increases. At higher temperatures, however, the activity coefficient of DL-alanine increases with an increase in the amino acid concentration. Similar effect was reported for the effect of temperature and concentration on the activity coefficient of DL-α-aminobutyric acid in aqueous solutions [19, 20]. The nature of the amino acid–water interaction is of hydrophobic–hydrophilic type, which in this case indicates that the pairwise interactions are less negative with an increase in the size of the hydrocarbon backbone of the amino acid. As temperature increases, the forces become more repulsive and the hydrophobic interactions become more stable.

Table 4.2 summarizes the results of two studies for glycine+NaCl and L-valine +NaCl at 308.15 K and presents them in the form of the coefficients of eqs. (4.12) and (4.14).

Table 4.2: Coefficients of eqs. (4.12) and (4.14) for amino acids in aqueous electrolyte solutions at 308.15 K.

Amino acid	Electrolyte	C_1	C_2	C_3	C_4	C_5	C_6	Ref.
Glycine	NaCl	−0.119013	0.430755	−0.041625	−0.347782	0.012940	−0.004695	[6]
L-Valine	NaCl	−0.646165	1.039549	2.329650	−0.696925	−3.227851	−0.175362	[13]

Figure 4.12 compares the activity coefficient of glycine in the presence of NaCl at two different temperatures of 298.15 and 308.15 K [3, 6]. The data show that temperature strongly influences the activity coefficient of glycine in the presence of NaCl. An increase in temperature appears to diminish the interactions in the system, leading to a more ideal behavior. The effect of temperature on the activity coefficient of glycine is more pronounced at higher electrolyte concentrations and lower glycine concentrations.

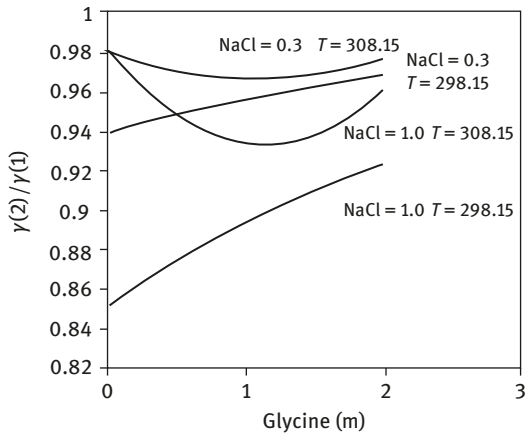

Figure 4.12: Effect of the temperature on the ratio of activity coefficient of glycine.

Figure 4.13 compares the effect of concentrations of two isomeric forms of DL-alanine on the ratio of the mean ionic activity coefficients of NaCl in the presence and absence of the amino acid. The comparison is at two concentrations of NaCl, 0.1 and 0.5 m. The amino acids compared are DL-α-alanine [3] and DL-β-alanine [21], which are isomers and differ in the position of the amino groups on their hydrocarbon backbones. As is shown in this figure, over the entire range of amino acid and NaCl concentrations studied, β-alanine shows a greater interaction with NaCl than α-alanine. This can be attributed to the differences in the distance between charged groups of these amino acids. As the charges on β-alanine are farther apart from each other than in the case of α-alanine, it exhibits a higher dipole moment and thus in larger interactions with both water molecules and charged ions. This is supported by the calculated values of the dipole moments of these amino acids using a quantum mechanical approach, which shows that the dipole moment of DL-β-alanine is considerably larger than the dipole moment of DL-α-alanine. This also further indicates that the highly dipolar character of amino acids plays a more dominant role in their interactions with other molecules in solution than their ionic property.

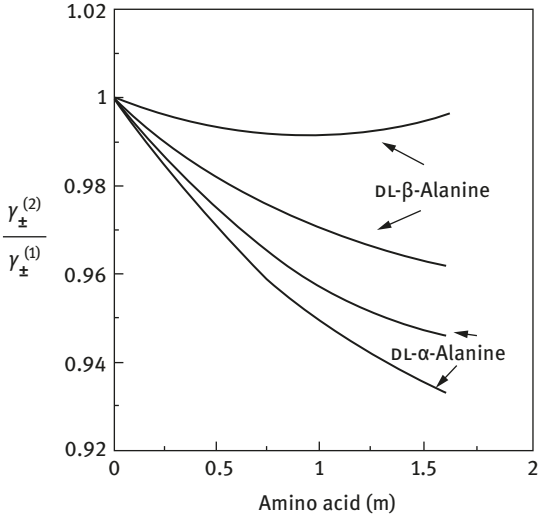

Figure 4.13: Effect of the NaCl and amino acid concentrations on the ratio of mean ionic activity coefficient of NaCl for two isomers of DL-alanine.

Robinson et al. [22] using the isopiestic method showed that the vapor pressure of aqueous solutions of D-alanine, L-alanine, and DL-alanine are identical, within the accuracy of the measurements. This, in turn, indicates that the different optical isomers of the alanine have identical activity coefficients. The comparison between the activity coefficient of DL-alanine and L-alanine in aqueous NaCl solutions also confirms that that the activity coefficients of the optical isomers of alanine in aqueous NaCl solutions are also identical within the precision of the measurements.

4.4 Solubility and Activity Coefficients of Amino Acids in Aqueous Electrolyte Solutions

In Chapter 3, we showed that the measured solubilities of amino acids in electrolyte solutions reported in the literature present significant discrepancies. Although these variations could be partly attributed to uncertainties of the experimental measurement techniques used, other physical factors could also play a role. For DL-amino acids, one possible factor has been attributed to the different proportions of optical isomers that form a DL-amino acid. As mentioned before, a DL-amino acid is a mixture of two optical isomers of L-amino acid and D-amino acid. Khoshkbarchi et al. [14] showed that the activity coefficients of optical isomers of an amino acid in aqueous electrolyte solutions are equal.

In the case of glycine, discrepancies in solubilities could be due to the possible polymorphic transformation of the form of the amino acid used during the experiments. Figure 4.14 shows a comparison of the ratio of the activity coefficient of glycine in the presence or absence of NaCl according to data reported in different studies [1, 3–5]. As can be seen from this figure, the experimental data are in relatively good agreement, although some discrepancies are observed. Yang et al. [23] observed the polymorphic transformation of glycine in water and NaCl solutions. As discussed in Chapter 3, this transformation takes place in water over a long duration and is significantly accelerated with the addition of NaCl. The data shown in Figure 4.14 do not show larger deviations at higher glycine concentrations or higher NaCl concentrations and are likely a result of using different experimental techniques.

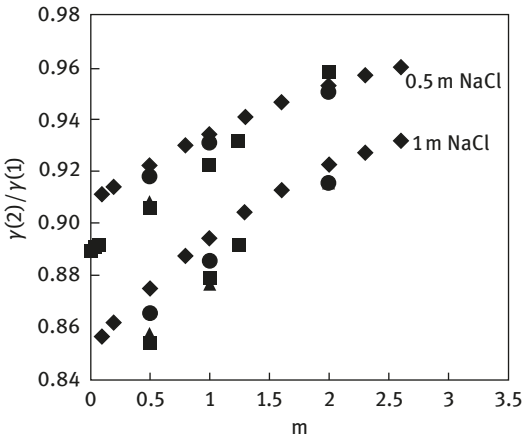

Figure 4.14: Ratio of activity coefficients of glycine in the presence and absence of NaCl as a function of glycine molality: ◆ ISE [1], ▲ ISE [2], ■ ISE [4], ● Isopiestic [5].

Therefore, the presence of different optical isomers or polymorphs does not affect activity coefficients of amino acids in aqueous electrolyte solutions. The solubility depends on the fugacity of the solid phase that depends on the type of crystals formed

with different isomers or polymorphs in the solid state. The formation of different crystalline forms of amino acids at different electrolyte concentrations was observed by Khoshkbarchi and Vera [24] suggesting that the determining factor on the solubility is the activity of the solid phase. Consequently, different proportions of isomers in the sample or polymorphic transformations could be a justification for the discrepancies in the observed solubilities.

4.5 Concluding Remarks

The presence of electrolytes greatly influences the behavior of amino acids in aqueous solution. This is mainly due to the unique structure of amino acids that in the same molecule possess both charge groups as well as hydrocarbon groups, giving rise to different types of interactions between amino acid molecules and electrolytes. The nature of these interactions is both long-range, resulting from electrostatic interactions between the charged groups of amino acids and the ions dissociated from the electrolyte in aqueous solutions, and short-range, taking place between hydrocarbon backbone of amino acids, water, and ions. Measurement of the activity coefficient of amino acids in aqueous electrolyte solutions is an effective way to study these interactions. Knowledge of the activity coefficient can be directly used to predict the phase behavior of amino acids in aqueous electrolyte solutions, which is necessary for the design and development of separation processes. Experimental data show that the interactions in the aqueous solution of electrolytes and amino acids are strongly influenced by both the structure of the hydrocarbon backbone of the amino acid and the nature of the electrolyte. Comparison of the experimental data for α- and β-isomers of DL-alanine suggested the importance of the dipole–dipole and ion–dipole interactions. While the effect of structural isomers of amino acids shows to have a drastic impact on their behavior in aqueous solutions, the optical isomers, L and D, have minimal-to-no impact on the behavior of amino acids in solutions. The experimental data also suggest the possibility of the formation of amino acid–ion pairs as well as association between oppositely charged amino and carboxyl groups of the amino acid. The temperature strongly influences the activity coefficient of amino acids with more pronounced effect at higher electrolyte concentrations. At higher temperatures, the system exhibits a behavior closer to ideal behavior.

References

[1] Phang S, Steel BJ. J Chem Thermodyn 1974, 6, 537.
[2] Rodriduez-Raposo R, Fernandez-Mérida L, Esteso MA. J Chem Thermodyn 1994, 26, 1121.

[3] Khoshkbarchi MK, Vera JH. Ind Eng Chem Res 1996, 35, 2735.
[4] Sîrbu F, Iulian O. J Chem Eng Data 2010, 55, 3853.
[5] Schrier EE, Robinson RA. J Biol Chem 1971, 9, 2870.
[6] Kamail-Ardakani H, Modarress H, Taghikhani V, Khoshkbarchi MK. J Chem Thermodyn 2001, 33, 821.
[7] Soto-Campos AM, Khoshkbarchi MK, Vera JH. Biophys Chem 1997, 67, 97.
[8] Gao C, Vera JH, Can. J Chem Eng 2001, 79, 392.
[9] Khavaninzadeh A, Modarress H, Taghikhani V, Khoshkbarchi MK. J Chem Thermodyn 2003, 35, 1553.
[10] Soto-Campos AM, Khoshkbarchi MK, Vera JH. Fluid Phase Equilibr 1998, 142, 193.
[11] Khoshkbarchi MK, Vera JH. AIChE J 1996, 42, 2354.
[12] Khoshkbarchi MK, Vera JH. J Sol Chem 1996, 25, 865.
[13] Khavaninzadeh A, Modarress H, Taghikhani V, Khoshkbarchi MK. J Chem Thermodyn 2002, 34, 1297.
[14] Khoshkbarchi MK, Soto-Campos AM, Vera JH. J Sol Chem 1997, 26, 941.
[15] Soto-Campos AM, Khoshkbarchi MK, Vera JH. J Chem Thermodyn 1997, 29, 609.
[16] Chung YM, Vera JH, Biophys Chem 2001, 92, 77.
[17] Hamelinka JM, Rudolphb ESJ, van der Wielen LAM, Vera JH. Biophys Chem 2002, 95, 97.
[18] Cohn EK, Edsall JT, including chapters by Kirkwood JG, Mueller H, Oncley JL and Scatchard G. Proteins, amino acids and peptides as ions and dipolar ions. Reinhold Publishing Corporation, New York, 1943.
[19] Chung YM, Vera JH, Fluid Phase Equilibr 2002, 203, 99.
[20] Romero CM, Gonzalez ME, Fluid Phase Equilibr 2006, 250, 99.
[21] Raposo RR, Garcia-Garcia GE, Fernandez-Merida L, Esteso MA. J Electroanal Chem 1998, 454, 59.
[22] Robinson RA, Smith PK, Smith ERB. Trum Faraday Soc 1942, 36, 63.
[23] Yang X, Lu J, Wang XJ, Ching CB. J Raman Spectrosc 2008, 39, 1433.
[24] Khoshkbarchi MK, Vera JH. Ind Eng Chem Res 1997, 36, 2445.

Mohammad K. Khoshkbarchi

5 Modeling of Activity Coefficient of Amino Acids and Simple Peptides in Aqueous Electrolyte Solutions

5.1 Introduction

The continuously increasing production of various types of biochemical products has rendered the design of high-efficiency, large-scale, and cost-effective bioseparation processes exceedingly important. The accurate design, modeling, simulation, and operation of these processes require accurate prediction and modeling of phase behavior and thermodynamic properties of biomolecules in solutions. Many biochemical separation processes, such as salt-induced precipitation of biomolecules, deal directly with the interactions between biomolecules and electrolytes in aqueous solutions.

Activity coefficient is an important thermodynamic property that represents the departure of a system from ideality as a result of interactions among its constituent components. Activity coefficient is directly related to other important thermodynamic properties such as chemical potential and fugacity, which are in turn essential for accurate modeling of phase behavior in a system. Therefore, developing accurate models for activity coefficient is the first step towards accurate prediction of the phase behavior of mixtures and the determination of the distribution of the components in a mixture among all phases present in the system.

5.2 General Thermodynamic Definitions

Activity coefficient is best described in the context of chemical potential, which is an important fundamental thermodynamic property for phase equilibrium calculations. Chemical potential is at the heart of one of the main conditions of phase formation which would indicate that for a system at equilibrium at a given temperature T and pressure P the chemical potentials of every component in all phases of the system, $\mu_i^{\text{phase } N}$, are equal:

$$\mu_i^{\text{phase I}}\left(T,\ P,\ x^{\text{phase I}}\right) = \mu_i^{\text{phase II}}\left(T,\ P,\ x^{\text{phase II}}\right) = \mu_i^{\text{phase III}}\left(T,\ P,\ x^{\text{phase III}}\right) = \cdots \tag{5.1}$$

For an ideal solution, the chemical potential of component i is related to its composition, x_i, through,

$$\mu_i\,(\text{ideal solution}, T,\ P,\ x) = \mu_i^{\circ}(T,\ P) + RT\ \ln x_i \tag{5.2}$$

https://doi.org/10.1515/9783110564808-005

where μ_i, μ_i° are, respectively, the chemical potentials of the component i in the mixture and at a conveniently selected standard state. To account for the departure of a real solution from ideal solution behavior, a correction factor known as activity coefficient, γ_i, is introduced as

$$\mu_i\ (\text{real solution},\ T,\ P,\ x) = \mu_i^\circ(T,\ P) + RT\ \ln\left(\gamma_i\,(T,\ P,\ x)x_i\right) \tag{5.3}$$

The activity coefficient is also related to other thermodynamic properties such as the partial molar excess Gibbs energy, $\bar{G}_i^{\mathrm{E}}$, or the fugacity, f_i, of the component i in a mixture as follows:

$$\begin{aligned}\bar{G}_i^{\mathrm{E}} &= \mu_i\,(\text{real solution},\ T,\ P,\ x) - \mu_i\,(\text{ideal solution},\ T,\ P,\ x)\\ &= RT\ \ln\left(\gamma_i(T,\ P,\ x)\right) = RT\ \ln\frac{f_i\,(T,\ P,\ x)}{x_i f_i^\circ\,(T,\ P)}\end{aligned} \tag{5.4}$$

where $f_i^\circ(T,\ P)$ is the fugacity of pure compound i at the same pressure and temperature of the system. To complete the definition of the activity coefficient, it is important to discuss the two conventions known as symmetric and unsymmetric which are also, respectively, referred to in the literature as the Lewis–Randall and Henry standard-state conventions. In the symmetric convention used above, the standard state is defined as the component in the pure state which defines the limit of the activity coefficient as

$$\gamma_i \to 1\ \text{ as }\ x_i \to 1 \tag{5.5}$$

This convention is more suitable for solvents such as water, which in the pure form can exist in the same state as the state of the solution. Whereas in unsymmetric convention, indicated by superscript *, a reference state is taken as the component at the infinite dilution, and a standard state as a hypothetically ideal infinitely dilute solution extrapolated to mole fraction or molality equal to unity, depending on the units of concentration used. In this convention, the limit of the activity coefficient in the mole fraction scale of concentration is

$$\gamma_i^\star \to 1\ \text{ as }\ x_i \to 0 \tag{5.6}$$

This convention is more suitable for solutes such as amino acids or electrolytes as in the pure form they are usually solid and do not exist in the same state as the state of the solution. To convert the excess Gibbs energy from symmetric convention to unsymmetric convention, the following normalizing relation can be used:

$$G^{\star\mathrm{E}} = G^{\mathrm{E}} - RT\sum_i x_i\ \ln\gamma_i^\infty \tag{5.7}$$

where γ_i^{∞} represents the value of the activity coefficient at infinite dilution.

The above equations are derived with the view that the molecules in the system are nondissociable. Electrolytes, on the other hand, dissociate in aqueous solutions and form ionic species. Although activity coefficient can be defined for each ionic species in the solution, it is customary and convenient to define the activity coefficient of an electrolyte as the mean ionic activity coefficient, $\gamma_{\pm}$, which can be related to the activity coefficients of its constituent ionic species as follows:

$$\gamma_{\pm} = \left(\gamma_{+}^{\nu_{+}} \gamma_{-}^{\nu_{-}}\right)^{1/\nu} \tag{5.8}$$

where ν_{+} and ν_{-} represent the numbers of positively and negatively charged ions dissociated per mole of electrolyte, respectively, and $\nu = \nu_{+} + \nu_{-}$. Activity coefficients can also be given in either mole fraction, x, or molality, m, basis. The following equation shows the conversion from one convention to another:

$$\ln \gamma_i^{(x)} = \ln \gamma_i^{(m)} + (1 + 0.001 M_E m_E) \tag{5.9}$$

where M_E is the molecular weight of the electrolyte and m_E represents the molality of the electrolyte in the solution. By convention, the product $M_E \cdot m_E$ is dimensionless.

5.3 Modeling Activity Coefficient of Amino Acids in Aqueous Electrolyte Solutions

The unique structure of simple amino acids and peptides, which have dissociable carboxyl and amino functional groups on a hydrocarbon backbone, has rendered the interactions between amino acids and electrolytes in aqueous solution complex and modeling their activity coefficients a challenging task. In aqueous solutions, the carboxyl and amino groups of amino acids become negatively and positively charged, respectively, transforming the monoacid molecules into simple polyelectrolytes. At moderate pH values, both amino and carboxyl groups dissociate, becoming ionic, and the entire amino acid molecule carries no net charge. Amino acids in this state are referred to as zwitterions and the pH at which this occurs is designated as their isoelectric point, PI. As a result, the interactions between amino acid–amino acid, water–amino acid, and ion–amino acid are governed by various types of long-range and short-range forces.

Amino acids, due to the presence of the charged carboxyl and amino groups on their hydrocarbon backbones, exhibit a considerable dipole moment, which gives rise to dipole–dipole interactions between amino acid molecules and water, and also to charge–dipole interactions between amino acid molecules and simple ions. While at moderate pH values amino acids could be considered neutral (carrying equal

positive and negative charges), their individual charged groups can interact with each other as well as with other simple ions dissociated from electrolytes present through both long-range and short-range electrostatic interactions. The hydrocarbon groups in amino acids also interact with other molecules, mainly through short-range forces. The consideration of different combinations of these forces has provided the framework for developing models for activity coefficients of amino acids in aqueous electrolyte solutions.

The most notable early development in the modeling of the activity coefficient of amino acids was presented by Kirkwood [1], where the amino acid molecules were described using various shape factors and positions of charges on them. This model is suitable for qualitative representation of activity coefficient of amino acids in electrolyte solutions at low concentrations. Since the pioneering work of Kirkwood there have been several studies attempting to develop models for the activity coefficient of amino acids in aqueous solutions, both in the presence and in the absence of simple electrolytes. Relying on the principles of superposition theory, the proposed models combine the contributions of the long-range and short-range interactions to the excess free energy. Thus, the excess Gibbs free energy, G^{E}, of the system can be written as the contribution of the long-range (LR) interactions and short-range (SR) interactions as follows:

$$G^{\mathrm{E}} = G^{\mathrm{E,LR}} + G^{\mathrm{E,SR}} \tag{5.10}$$

Or equivalently, the above equation can be described in terms of the activity coefficient as follows:

$$\ln \gamma_i^{\star} = \ln \gamma_i^{\star,\mathrm{LR}} + \ln \gamma_i^{\star,\mathrm{SR}} \tag{5.11}$$

5.4 Modeling Contribution of Long-Range Interactions

Most models for the long-range interactions are derived using various approximations to the solution of the Poisson–Boltzmann equation. The most common models used for amino acids are discussed bellow.

Debye–Hückel model

The Debye–Hückel model is one of the earliest theoretical models for the activity coefficient of ions in solutions:

$$\ln \gamma_{\pm} = \frac{-A|z_+ z_-|\sqrt{I}}{1 + B\sqrt{I}} \tag{5.12}$$

where A is the Debye–Hückel parameter, B is an adjustable parameter, and I is the molality-based ionic strength calculated from the sum of the molality of each ion in the solution, m_i, and its charge number, z_i, as follows:

$$I = \frac{1}{2}\sum m_i z_i^2 \tag{5.13}$$

By convention, both the numerator and the denominator of eq. (5.12) are dimensionless. The parameter A can be calculated as a function of temperature as follows:

$$A\left(\mathrm{kg}^{1/2}\,\mathrm{mol}^{-1/2}\right) = 1.131 + 1.335\times10^{-3}T(C) + 1.164\times10^{-5}T(C)^2 \tag{5.14}$$

Equation (5.12) is in fact a simplified version of the Debye–Hückel model that does not consider the contribution of the ions to volume of the solution and considers ions as point charges. Therefore, this model is only suitable for ionic systems at low concentrations, with only ion–ion electrostatic interactions and does not account for zwitterion–ion interactions or any other short-range interactions.

The models used to represent the long-range interactions in aqueous solutions of amino acids and electrolytes are usually represented by one of the extensions of the Debye–Hückel model. Some of the notable extensions of the Debye–Hückel model used to model the long-range interactions in aqueous solutions containing amino acids include:

Bromley model

$$\ln\gamma_{\pm} = \frac{-A|z_+z_-|\sqrt{I}}{1+\sqrt{I}} + \frac{(0.138+0.6B)|z_+z_-|I}{(1+[1.5I/|z_+z_-|])^2} \tag{5.15}$$

where B is an adjustable parameter.

Khoshkbarchi–Vera model

$$\ln\gamma_{\pm} = \frac{-A|z_+z_-|\sqrt{I_x}}{1+\rho\sqrt{I_x}} + B_x\frac{I_x^{3/2}}{1+\rho\sqrt{I_x}} + C_x\ln\left(1+I_x^{2/3}\right) \tag{5.16}$$

where A is the Debye–Hückel constant in mole fraction basis and B and C are two adjustable parameters that depend on the nature of the electrolyte, with $\rho = 9$ and I_x is the mole fraction-based ionic strength defined as

$$I_x = \frac{1}{2}\sum x_i z_i^2 \tag{5.17}$$

Pitzer–Debye–Hückel model

$$\ln \gamma_i = -\left(\frac{1000}{M_s}\right)^{1/2} A_\phi \left[\left(\frac{2z_i^2}{b}\right)\right] \ln\left(1 + b\sqrt{I_x}\right) + \frac{z_i^2\sqrt{I_x} - 2{I_x}^{3/2}}{1 + b\sqrt{I_x}} \tag{5.18}$$

where A_ϕ is the Debye–Hückel osmotic coefficient parameter which is related to the Debye–Hückel parameter A defined in eq. (5.14) [4] and b is the distance of closest approach.

Briel and Mollerup model

An important extension of the Debye–Hückel model which considers the zwitterion–ion interactions as well as ion–ion interactions was presented in the pioneering work of Kirkwood and later simplified and presented by Briel and Mollerup [5], where the excess Helmholtz energy of the system is presented as

$$\begin{aligned}\frac{A^E}{RT} = {} & \frac{N_A}{RT\varepsilon_0 D}\sum\nolimits_{i\in\text{ions}} \frac{x_i z_i^2 e^2}{(\kappa\alpha_i)^3}\kappa\left[\frac{3}{2} + \ln(1+\kappa\alpha_i) - 2(1+\kappa\alpha_i) + \frac{1}{2}(1+\kappa\alpha_i)^2\right] \\ & - \frac{3}{8}\frac{N_A}{RT\varepsilon_0 D}\sum\nolimits_{i\in\text{ions}} \frac{x_i z \mu_i^2}{\alpha_i(\kappa\tau_i)^2}\left[\kappa^2\tau_i - \ln\left(1+\kappa^2\tau_i\right)\right]\end{aligned} \tag{5.19}$$

With

$$\tau = b^3/6\alpha \tag{5.20}$$

$$\kappa^2 = \frac{e^2 N}{kTV\varepsilon_0 D}\sum\nolimits_{i\in\text{ions}} x_i z_i^2 \tag{5.21}$$

where b is the diameter of a complex ion, α is the distance of the closest approach which can be approximated by the hydrated ion diameter of the ion. Although this model is of great theoretical importance, it is limited to very low concentrations of solutes and for modeling more concentrated solutions requires modifications and extensions to be incorporated in the effect of the short-range interactions.

Mean spherical approximation (MSA) model

The MSA model of electrolyte for primitive systems was first applied to model the activity of ions in electrolyte solutions by Blum [6, 7]. This model considers ions as electrically charged hard spheres and its primitive nature indicates that the solvent is a dielectric continuum. The model divides the ionic activity coefficient to the contributions of two terms, one representing a reference system usually represented by a hard sphere model and the other representing the electrostatic interactions in the

system. The models for hard sphere systems are discussed in the next section. The contribution of the electrostatic term to the ionic activity coefficient is given by

$$\ln \gamma_i = \frac{z_i e^2}{\epsilon_0 \epsilon_r kT}\left(\frac{2\Gamma a_i}{\alpha^2 \sigma_i} - \frac{z_i}{\sigma_i}\right) + \frac{P_n \sigma_i}{4\Delta}\left(\Gamma a_i + \frac{\pi}{12\Delta}\alpha^2 P_n \sigma_i^2\right) \tag{5.22}$$

$$\Delta = 1 - \frac{\pi}{6}\sum_i \rho_i \sigma_i^3 \tag{5.23}$$

$$\alpha^2 = \frac{4\pi e^2}{\epsilon_0 \epsilon_r kT} \tag{5.24}$$

$$P_n = \frac{1}{\Omega}\sum\nolimits_k \frac{\rho_k z_k \sigma_k}{1 + \Gamma\sigma_k} \tag{5.25}$$

$$\Omega = 1 + \frac{\pi}{2\Delta}\sum\nolimits_k \frac{\rho_k \sigma_k^3}{1 + \Gamma\sigma_k} \tag{5.26}$$

$$a_i = \frac{\alpha^2\left[z_i - \frac{\pi}{2\Delta}P_n\sigma_i^2\right]}{2\Gamma(1 + \Gamma\sigma_i)} \tag{5.27}$$

$$\Gamma = \frac{\alpha}{2}\left\{\sum_i \rho_i\left[\frac{z_i - \frac{\pi}{2\Delta}P_n\alpha_i^2}{1 + \Gamma\sigma_i}\right]^2\right\}^{0.5} \tag{5.28}$$

where $\in_0$ is the permittivity of vacuum, $\in_r$ is the relative dielectric constant of the medium, and k is the Boltzmann constant. In the limit of small ion diameters, eq. (5.28) simplifies to the Debye–Hückel model. To calculate the ionic activity coefficient, eqs. (5.22)–(5.28) should be solved simultaneously.

5.5 Modeling Contribution of Short-Range Interactions

The simplest assumption made to develop models for the activity coefficients of amino acids in aqueous electrolyte solutions considers all the components of the system as undissociated and molecular and ignores the presence of any ionic or zwitterion species in the solution. A model developed based on this point of view uses the virial expansion, proposed by Scatchard and Pentiss [8], where the activity coefficient of amino acid in the presence of the electrolyte, $\gamma_A^{(elec)}$, is related to the

activity coefficient of amino acid in the absence of the electrolyte, $\gamma_A^{(\text{no-elec})}$, molality of the amino acid, m_A, and molality of the electrolyte, m_E, as,

$$\ln \frac{\gamma_A^{(\text{elec})}}{\gamma_A^{(\text{no-elec})}} = C_1 m_E + \frac{1}{2} C_2 m_E^2 + 2C_3 m_E m_A + \frac{1}{3} C_4 m_E^3 + 3C_5 m_E m_A^2 + C_6 m_A m_E^2 \tag{5.29}$$

The coefficients, C_i, are the virial expansion coefficients with unique values for every amino acid–electrolyte pair. The mean ionic activity coefficient of the electrolyte in the presence of the amino acid, $\gamma_{\pm}^{(\text{amino acid})}$, is related to the mean ionic activity coefficient of the electrolyte in the absence of the amino acid, $\gamma_{\pm}^{(\text{no-amino acid})}$, by combining the following equation with eq. (5.29):

$$\nu \left(\frac{\partial \ln \gamma_{\pm}}{\partial m_A} \right)_{T,P,m_E} = \left(\frac{\partial \ln \gamma_A}{\partial m_E} \right)_{T,P,m_A} \tag{5.30}$$

Resulting in the following correlation:

$$\nu \ln \frac{\gamma_{\pm}^{(amino\ acid)}}{\gamma_{\pm}^{(no\text{-}amino\ acid)}} = C_1 m_A + C_2 m_E m_A + C_3 m_A^2 + C_4 m_E m_A^2 + C_5 m_A^3 + C_6 m_E m_A^2 \tag{5.31}$$

As in this simple model, the amino acid, water, and electrolyte are considered to be molecular and undissociated, the effect of the short-range interactions is in fact lumped into the virial expansion terms, rather than representing them separately using a short-range interaction term. Considering the large number of parameters in this model, it lacks any predictability capability and it does not accurately represent amino acid, water, and electrolyte systems at their infinite dilution limit. However, this model has been successfully employed as a good correlation to fit the experimental data [9].

To account for the electrostatic interactions and to be able to represent the mean ionic activity coefficient of the electrolyte at low concentrations, Fernandez-Mérida et al. [10] used the modified Pitzer model [11] for aqueous solutions of an electrolyte and a nonelectrolyte to model the activity coefficients of amino acids in electrolyte solutions. The Pitzer model employs a combination of an electrostatic term and a virial series expansion to account for all the interactions and is based on the framework presented in eq. (5.10). In this model, for an electrolyte solution containing W_w (kg) of water, the unsymmetric excess Gibbs free energy is given as

$$\frac{G^E}{W_w RT} = f(I) + \sum_i \sum_j m_i m_j \lambda_{ij}(I) + \sum_i \sum_j \sum_k m_i m_j m_k \Lambda_{ijk} + \cdots \tag{5.32}$$

where m is the molality of species, $f(I)$ is the contribution of the short-range interactions as a function of ionic strength, I. The parameters λ_{ij} and Λ_{ijk} are two-body and three-body interactions terms.

Using the framework presented in eq. (5.10), the electrolyte versions of the local composition models such as Non Random Two Liquid (NRTL) [12] and Wilson model [13] have been employed to model the activity coefficients of amino acids in electrolyte solutions. In these models, the short-range forces are assumed to be due to the nonelectrostatic interactions between water, amino acid, and ions (only nonelectrostatic interactions). In the local composition model, four different types of cells are considered with a solvent, amino acid, anion, or cation at the center of each cell. The like-ion interactions are considered to be so strong that cells with central cations contain no other cations and cells with central anions contain no other anions. Because of this assumption, only the cells with water or an amino acid molecule at the center are electrically neutral and the cells with a cation or an anion at the center contain only amino acid, water, and counterions and therefore they are not electrically neutral. To reduce the number of parameters, the energy parameters of the local composition models were assumed to be symmetrical.

Khoshkbarchi and Vera [9] developed a framework for modeling activity coefficients of amino acids in aqueous electrolyte solutions assuming that the long-range interaction term accounts for all the interactions in a binary water–electrolyte system, whereas the short-range interaction term takes into account all the interactions between water–amino acid, amino acid–electrolyte, and the change in the interactions between water–electrolyte due to the presence of the amino acid. As such, the new framework considers the dissociation of electrolytes in water but assumes that amino acid zwitterions remain electrically neutral, exhibiting only short-range interactions with other molecules in the system. To incorporate this assumption in the model, eq. (5.10) was modified as

$$G^{E} = G^{E,\,LR} + G^{E,\,SR} - \lim_{x_A \to 0} G^{E,\,SR} \tag{5.33}$$

Following Cheluget et al. [14], the mean ionic activity coefficient of the electrolyte, $\gamma_{\pm}$, and the activity coefficient of the amino acid, γ_A, were calculated from

$$\ln \gamma_{\pm} = \frac{1}{\nu}\left(\frac{\partial G^{E}/RT}{\partial n_E}\right)_{T,P,n_A,n_W} + 1 - \frac{1}{\nu}(x_A + x_W) \tag{5.34}$$

$$\ln \gamma_A = \left(\frac{\partial G^{E}/RT}{\partial n_A}\right)_{T,P,n_E,n_W} + 1 - (x_E + x_W) \tag{5.35}$$

As in this model, the short-range term considers all the species in the system as undissociated, a variety of molecular-based models can be used to represent the short-range interactions. Khoshkabrchi and Vera [9] showed that both the NRTL and

Wilson models can represent these interactions with good accuracy. It is important to note that both models are derived on a mole fraction basis, whereas most long-range interaction models, described before, are developed on the molality basis. Thus, to consistently combine the two models together they need to be converted into the same basis. Therefore, the following conversion factors should be used in this framework:

$$G^{\mathrm{E,\ LR,}\ (x)} = G^{\mathrm{E,\ LR,}\ (m)} + n_{\mathrm{E}} RT \ln\left([\nu_+{}^{\nu_+} \nu_-{}^{\nu_-}] m_{\mathrm{E}}^{\nu-1} \left(1 + 0.001 M_{\mathrm{W}} \sum\nolimits_i m_i\right)\right) \tag{5.36}$$

$$G^{\mathrm{E,\ SR,}\ (x)} = G^{\mathrm{E,\ SR,}\ (m)} + n_{\mathrm{A}} RT \ln\left(1 + 0.001 M_{\mathrm{W}} \sum\nolimits_i m_i\right) \tag{5.37}$$

where M_{W} is the molecular weight of water and m_i is the molality of the component i. Applying eq. (5.7) to eq. (5.37) will convert the $G^{\mathrm{E,\ LR,}\ (x)}$ to unsymmetric normalization, $G^{*\mathrm{E,\ LR,}\ (x)}$. The expression for the mean ionic activity coefficient of the electrolyte and activity coefficient of amino acids can be derived by combining eqs. (5.35) and (5.36) as follows:

$$\begin{aligned} \ln \gamma_{\pm}^{(m)} = \ln \gamma_{\pm}^{(m),\ \mathrm{LR}} + \frac{1}{\nu} \Bigg\{ & \ln \gamma_{\mathrm{E}}^{(x),\ \mathrm{SR}} - \lim_{x_{\mathrm{A}} \to 0} \left(\ln \gamma_{\mathrm{E}}^{(x),\ \mathrm{SR}} \right) \\ & + \ln\left(\frac{1 + 0.001 M_{\mathrm{W}} m_{\mathrm{E}}}{1 + 0.001 M_{\mathrm{W}} (m_{\mathrm{E}} + m_{\mathrm{A}})} \right) \Bigg\} \end{aligned} \tag{5.38}$$

$$\ln \gamma_{\mathrm{A}}^{(m)} = \ln \gamma_{\mathrm{A}}^{(x),\ \mathrm{SR}} - \lim_{x_{\mathrm{A}} \to 0,\, x_{\mathrm{E}} \to 0} \left(\ln \gamma_{\mathrm{A}}^{(x),\ \mathrm{SR}} \right) - \ln(1 + 0.001 M_{\mathrm{W}} (m_{\mathrm{E}} + m_{\mathrm{A}})) \tag{5.39}$$

From the above two equations it is clear that as the amino acid concentration in the mixture approaches zero, the mean ionic activity coefficient of the electrolyte represented by eq. (5.38) reduces to the contribution of the long-range interactions to a binary electrolyte–water system. Similarly, in eq. (5.39) as the concentration of the electrolyte approaches zero, the equation simplifies to the contribution of short-range interactions in a binary amino acid–water system.

Pazuki et al. [15] used this framework to develop a model for the activity coefficient of amino acids in electrolyte solutions. The main difference between this model and the one proposed by Khoshkbarchi and Vera [9] is that for the short-range interactions, instead of the NRTL model, the NRTL-NRF model was used. The NRTL-NRF (Non Random Factor) model was originally developed by Haghtalab and Vera [16] for nonelectrolytic systems and later extended by Haghtalab and Sarkisian [17] to model the electrolyte systems. In the NRTL-NRF model, the molecular activity coefficient of the components (including the electrolyte) is given by

$$\ln \gamma_i = \sum\nolimits_j x_j \left[\left(\Gamma_{ji} - 1\right) \lambda_{ji} + \left(\Gamma_{ij} - 1\right) \lambda_{ij} + \sum\nolimits_k x_k \left(1 - \Gamma_{ij} \Gamma_{kj}\right) \lambda_{ij} \right] \tag{5.40}$$

where λ_{ji} is an adjustable binary interaction parameter and with coordination number Z usually set to 10 the term Γ_{ij} is given by

$$\Gamma_{ij} = \frac{\exp\left(-\frac{\lambda_{ij}}{Z}\right)}{x_i + \sum_k x_k \exp\left(-\frac{\lambda_{ki}}{Z}\right)} \tag{5.41}$$

The short-range interactions have also been modeled using a group contribution method such as UNIFAC (UNIQUAC Functional-group Activity Coefficients, UNIQUAC is short for UNIversal QUAsiChemical) [18–20], where the short-range interaction contribution to the activity coefficient is divided into the contribution of a combinatorial term and a residual term. The model can be converted to an unsymmetric convention by subtracting their values at infinite dilution as follows:

$$\ln \gamma_i^{\star,\,\mathrm{SR}} = \left(\ln \gamma_i^{\mathrm{Residual}} + \ln \gamma_i^{\mathrm{Combinatorial}}\right) - \left(\ln \gamma_i^{\mathrm{Residual},\,\infty} + \ln \gamma_i^{\mathrm{Combinatorial},\,\infty}\right) \tag{5.42}$$

The UNIFAC parameters can be assumed to be the same as the standard UNIFAC parameters proposed by Larsen et al. [21], or fitted to new sets of parameters for more accuracy and to account for the particular form of every amino acid. For example, Kuramochi et al. [19] proposed new sets of parameters for the residual term for the asymmetric carbons in the structure of the amino acids and distinguished between primary and secondary amine groups in the amino acid structure. The parameters R and Q of the combinatorial terms were calculated from the Bondi's method and it was assumed that these parameters for the charged amino and carboxyl group remain the same. This model only considers the interactions between ions and water, amino and carboxyl groups, and the interactions between ions and other functional groups are ignored. The main advantage of models based on group contribution method is that they are predictive and, particularly in the absence of the experimental data, can easily be extended to amino acids with more complex structures and may be even to proteins. It should be noted that as the complexity of the molecules increases, the accuracy of the prediction of this model decreases. Although UNIFAC has been extended to electrolytic systems, as the number of interactions between ions and other groups is too large compared to small body of data available, to the best of our knowledge no successful UNIFAC model for aqueous solutions of amino acids in the presence of electrolytes has been reported.

Equations of state based on the perturbation theory have also been employed to model the activity coefficients of amino acids in aqueous and aqueous electrolyte solutions. Khoshkbarchi and Vera [22, 23] presented a model for the activity coefficients of amino acids in aqueous solutions based on a first-order perturbation theory in a primitive framework. The permittivity

of the model implied that the solvent (water) was treated as a dielectric continuum and not a component of the system. In this framework, the residual Helmholtz free energy of the system, A^{r}, is expressed as the contributions of a reference term, A^{ref}, and a perturbation term, A^{per}, as follows:

$$A^{r} = A^{ref} + A^{per} \tag{5.43}$$

The activity coefficient is related to the residual Helmholtz free energy by

$$\ln \gamma_{A} = \rho \left(\frac{\partial A^{r}/RT}{\partial n_{A}} \right)_{T,P,n_{E},n_{W}} \tag{5.44}$$

The equation for activity coefficient of amino acid can be obtained by combining eqs. (5.43) and (5.44) as follows:

$$\ln \gamma_{A} = \ln \gamma_{A}^{hs} + \ln \gamma_{A}^{per} \tag{5.45}$$

In this model, the reference system was chosen to be a hard sphere mixture. Although there are several expressions proposed to model the activity coefficient of hard spheres, the model proposed by Mansoori et al. [24] has received a great deal of attention and is used in most studies. In this model the activity coefficient of a component with hard diameter, σ, is given by

$$\ln \gamma_{A}{}^{HS} = -\ln(1-\xi_{3}) + \frac{\pi P^{HS} \sigma_{i}{}^{3}}{6kT} + E + 3F \tag{5.46}$$

$$E = \frac{3\xi_{2}\sigma_{i} + 3\xi_{1}\sigma_{i}{}^{2}}{1-\xi_{3}} + \frac{9\xi_{2}{}^{2}\sigma_{i}{}^{2}}{2(1-\xi_{3})^{2}} - \frac{\xi_{2}{}^{3}\sigma_{i}{}^{3}}{\xi_{3}{}^{3}} \left[2\ln(1-\xi_{3}) + \frac{\xi_{3}(2-\xi_{3})}{1-\xi_{3}} \right] \tag{5.47}$$

$$F = \frac{\xi_{2}{}^{2}\sigma_{i}{}^{2}}{\xi_{3}{}^{2}} \left[\ln(1-\xi_{3}) + \frac{\xi_{3}}{1-\xi_{3}} - \frac{\xi_{3}{}^{2}}{2(1-\xi_{3})^{2}} \right] \tag{5.48}$$

$$P^{HS} = \frac{6kT}{\pi} \left[\frac{\xi_{0}}{1-\xi_{3}} + \frac{3\xi_{1}\xi_{2}}{(1-\xi_{3})^{2}} + \frac{\xi_{2}{}^{3}(3-\xi_{3})}{(1-\xi_{3})^{3}} \right] \tag{5.49}$$

$$\xi_{n} = \frac{\pi}{6} \sum\nolimits_{k} \rho_{k} \sigma_{k}{}^{n} \qquad (n = 0,\ 1,\ 2,\ 3) \tag{5.50}$$

where k is the Boltzmann constant and ρ represents the number density.

The perturbation term was expressed by the first-order Barker–Henderson [25] perturbation theory as follows:

$$\ln \gamma_A{}^{\text{per}} = 2\pi \frac{\partial}{\partial \rho_A} \left[\sum_j \sum_l \rho_j \rho_l \int_{\sigma_{ji}}^{\infty} u_{jl}(r) g_{jl}^{\text{hs}}(r) r^2 dr \right] \tag{5.51}$$

where the sums run over all components in the system, $u(r)$ is the interaction energy as a function of the intermolecular distance, r, and $g_{jl}^{\text{hs}}(r)$ represents the radial distribution function of the hard sphere system. To arrive to a model with analytical solution, the radial distribution function of the hard sphere system is approximated by the following simple expression:

$$g_{jl}^{\text{hs}}(r) = \begin{cases} 0 & r < \sigma_{jl} \\ 1 & r \geq \sigma_{jl} \end{cases} \tag{5.52}$$

The perturbation interaction energies can include the effect of various forces, such as dispersion, dipole, quadrupole, and interaction forces. Due to the primitive nature of this model and very large dipole moment of amino acids, the Lennard–Jones, $u^{\text{L-J}}(r)$, and dipole–dipole, $u^{\text{D-D}}(r)$, interactions were only included, and other energies of interactions have been ignored as

$$u(r) = u^{\text{L-J}}(r) + u^{\text{D-D}}(r) \tag{5.53}$$

This indicates that the perturbation term is a combination of the contributions of the Lennard–Jones residual Helmholtz free energy, $A^{\text{L-J}}$, and dipole–dipole residual Helmholtz free energy, $A^{\text{D-D}}$, as follows:

$$A^{\text{r}} = A^{\text{ref}} + A^{\text{D-D}} + A^{\text{L-J}} \tag{5.54}$$

The Lennard–Jones (6–12) dispersion forces and the averaged Keesom dipole–dipole interactions were represented using models proposed by Maitland et al. [26] as follows:

$$u_{ij}^{\text{L-J}}(r) = 4\epsilon_{ij} \left(\frac{\sigma_{ij}^{12}}{r^{12}} - \frac{\sigma_{ij}^{6}}{r^{6}} \right) \tag{5.55}$$

$$u_{ij}^{\text{D-D}}(r) = \frac{D_i^2 D_j^2}{3(4\pi\epsilon_0\epsilon_r)^2 kTr^6} \tag{5.56}$$

where ϵ_0 is the permittivity of vacuum, ϵ_r is the relative dielectric constant of the medium, ϵ is the depth of the potential well. Combining eqs. (5.45)–(5.56) would

result in the following equation for the activity coefficient of amino acids in aqueous solutions as follows:

$$\ln \gamma_{\mathrm{A}} = \ln \gamma_{\mathrm{A}}^{\mathrm{hs}} + \sum_i \frac{4\pi\rho_j}{kT}\left\{\frac{8}{9}\epsilon_{\mathrm{Aj}}\sigma_{\mathrm{Aj}}^3 + \frac{D_A^2 D_j^2}{9(4\pi\epsilon_0\epsilon_{\mathrm{r}})^2 kT\sigma_{\mathrm{Aj}}^3}\right\} \tag{5.57}$$

Using similar concept, Liu et al. [38] developed a model based on perturbation theory for amino acids in aqueous solutions. In this model, water was considered to be a component and not a dielectric continuum and as such it was a nonprimitive model. Amino acid molecules were assumed to be multisegment chains of hard spheres. In this framework, the residual Helmholtz free energy, A^{r}, is expressed as the contributions of a reference system, assumed to be hard spheres, A^{hs}, and a perturbation term which is a combination of the Lennard–Jones residual Helmholtz free energy, $A^{\mathrm{L\text{-}J}}$, dipole–dipole residual Helmholtz free energy, $A^{\mathrm{D\text{-}D}}$, and chain residual Helmholtz free energy, A^{chain}, as follows:

$$A^{\mathrm{r}} = A^{\mathrm{hs}} + A^{\mathrm{D\text{-}D}} + A^{\mathrm{L\text{-}J}} + A^{\mathrm{chain}} \tag{5.58}$$

The addition of the contribution of the chain residual Helmholtz free energy indicates that the model assumes that amino acids are chain-like molecules composed of segments. As the reference system for this model is a hard sphere system for segment mixtures, the chain residual Helmholtz free energy accounts for the change of energy due to the formation of hard chains from hard spheres. The expression for the hard sphere system for segment mixtures is given as [24]

$$\frac{A^{\mathrm{hs}}}{NkT} = \frac{6}{\pi\rho}\left[\frac{3\zeta_1\zeta_2 - \zeta_2^3/\zeta_3^2}{1-\zeta_3} + \frac{\zeta_2^3/\zeta_3^2}{1-\zeta_3} + \frac{\zeta_2^3}{\zeta_3^2}\right] - \sum_i x_i m_i \ln(1-\zeta_3) \tag{5.59}$$

where ζ_2 is the packing factor which is related to the segment hard sphere diameter, d_{ii}, as

$$\zeta_l = \frac{\pi\rho}{6}\sum_i x_i m_i d_{ii}^l \tag{5.60}$$

The contribution of the chain residual Helmholtz free energy for a system comprising amino acids, each with different number of segments, m_i, with hard sphere diameter, d_{ii}, can be represented by an equation proposed by Chapman et al. [28] as follows:

$$\frac{A^{\mathrm{chain}}}{NkT} = \sum_i x_i(1-m_i)\ln g_{ii}^{\mathrm{hs}}(d_{ii}) \tag{5.61}$$

where $g_{ii}^{\mathrm{hs}}(d_{ii})$ is the radial distribution function of the hard sphere model used as the reference system. The contribution of the Lennard–Jones residual Helmholtz free

energy, $A^{\text{L-J}}$, can be obtained from the Barker–Henderson perturbation theory using an expression developed by Cotterman et al. [29] as follows:

$$\frac{A^{\text{L-J}}}{NkT} = \sum_i \frac{1}{T_r} x_i m_i \left(A_1^{\text{L-J}} + \frac{A_2^{\text{L-J}}}{T_r} \right) \tag{5.62}$$

$$A_1^{\text{L-J}} = \rho_r \left(-8.595 - 4.5424\rho_r - 2.1268\rho_r^2 + 10.285\rho_r^3 \right) \tag{5.63}$$

$$A_2^{\text{L-J}} = \rho_r \left(-1.905 + 9.9724\rho_r - 22.216\rho_r^2 + 15.904\rho_r^3 \right) \tag{5.64}$$

$$\rho_r = \frac{6}{\sqrt{2}\pi}\zeta_3 \quad \text{and} \quad T_r = \frac{kT}{\varepsilon} \tag{5.65}$$

For the contribution of the dipole–dipole residual Helmholtz free energy, $A^{\text{D-D}}$, Henderson et al. [27] have proposed a second and third perturbation terms using the Padé approximation as follows:

$$A^{\text{D-D}} = \frac{A_2^{\text{D-D}}}{1 - A_3^{\text{D-D}}/A_2^{\text{D-D}}} \tag{5.66}$$

$$\frac{A_2^{\text{D-D}}}{NkT} = \sum_i x_i \frac{-27y^2}{24\pi\rho d^3} \left(\frac{1 + 0.18158\rho d^3 - 0.11467\rho^2 d^6}{1 - 0.49303\rho d^3 + 0.06293\rho^2 d^6} \right) \tag{5.67}$$

$$\frac{A_3^{\text{D-D}}}{NkT} = \sum_i x_i \frac{135y^3}{384\pi\rho d^3} \left(\frac{1 + 1.12754\rho d^3 + 0.56192\rho^2 d^6}{1 - 0.05495\rho d^3 + 0.13332\rho^2 d^6} \right) \tag{5.68}$$

$$d = \left(\sum_i x_i m_i d_{ii}^3 \right)^{1/3} \tag{5.69}$$

$$y = \frac{4\pi\beta\rho \sum_i x_i \mu_i^3}{36\pi\epsilon_0} \tag{5.70}$$

As the dipole moment is a property of the entire molecule and not every segment, for the contribution of the dipole–dipole interactions the amino acid is not divided into segments.

Extended Khoshkbarchi-Vera Model

Khoshkbarchi and Vera [30], using the framework they developed [9], extended their model [22, 23] based on the perturbation theory, presented in eq. (5.71), to aqueous solutions of amino acids and electrolytes. For the short-range interactions, the model uses the MSA model of electrolytes, eq. (5.22). This model assumes

that ions are electrically charged spheres, which leads to the assumption that the long-range interaction term accounts for all the interactions in a binary water–electrolyte system and can be represented by the MSA. Whereas the short-range interaction term takes into account all the interactions between water and amino acid, amino acid and electrolyte, and the change in the interactions between water and electrolyte due to the presence of the amino acid. The model employs perturbation theory with interaction terms represented by the dipole–dipole and Lennard–Jones interactions, similar to the model discussed in eqs. (5.43)–(5.56). In this framework, the residual Helmholtz free energy, A^{r}, of the system is described as follows:

$$A^{\mathrm{r}}(T,\ V,\ x) = A^{\mathrm{LR}}(\rho_{\mathrm{E}}) + A^{\mathrm{SR}}(\rho_{\mathrm{E}},\ \rho_{\mathrm{A}}) - A^{\mathrm{SR}}(\rho_{\mathrm{E}} = 0,\ \rho_{\mathrm{A}}) \tag{5.71}$$

The contribution of the short-range residual Helmholtz free energy, A^{SR}, is expressed as a combination of the contributions of a hard sphere reference system, A^{hs}, and a perturbation term, A^{per}, as follows:

$$A^{\mathrm{r}} = A^{\mathrm{hs}} + A^{\mathrm{per}} \tag{5.72}$$

The contribution of hard sphere term is taken from eqs. (5.46)–(5.50), and the perturbation model and energy of interactions presented in eqs. (5.55)–(5.56) have been used to derive an expression for the contribution of the perturbation term. In addition to the interactions in eq. (5.53), the effect of angle-averaged charge–dipole, $u_{ij}^{\text{C-D}}$, and dipole-induced dipole, $u_{ij}^{\text{D-ID}}$, interactions were also considered [26]:

$$u_{ij}^{\text{D-ID}}(r) = \frac{-\alpha_j D_i^2 - \alpha_i D_j^2}{(4\pi\epsilon_0\epsilon_{\mathrm{r}})^2 r^6} \tag{5.73}$$

$$u_{ij}^{\text{C-D}}(r) = \frac{-e^2 z_i^2 D_j^2}{6(4\pi\epsilon_0\epsilon_{\mathrm{r}})^2 kTr^4} \tag{5.74}$$

where α_j is the polarizability. The short-range contribution to the activity coefficient is derived as

$$\begin{aligned}\ln\gamma_i = \ln\gamma_i^{HS} - \frac{4\pi}{kT}\sum\nolimits_j \rho_j \Bigg\{ &\frac{4}{9}\sigma_{ij}{}^3\left[(\epsilon_{ij}+\epsilon_{ji}) + \rho_i \frac{\partial(\epsilon_{ij}+\epsilon_{ji})}{\partial\rho_i}\right] \\ &+ \frac{\alpha_j D_i^2 + \alpha_i D_j^2}{3(4\pi\epsilon_0\epsilon_{\mathrm{r}})^2 kT\sigma_{ij}{}^3} + \frac{D_i^2 D_j^2}{9(4\pi\epsilon_0\epsilon_{\mathrm{r}})^2 kT\sigma_{ij}{}^3} + \frac{z_i{}^2 e^2 \bar{D}_j{}^2}{6(4\pi\epsilon_0\epsilon_{\mathrm{r}})^2 kT\sigma_{ij}}\Bigg\}\end{aligned} \tag{5.75}$$

SAFT Approach

A more advanced and complex form of the above methodology proposed to model the activity coefficient of amino acids in aqueous electrolyte solutions is based on the statistical associating fluid theory (SAFT) equation of state [31]. In the structure of the SAFT model the residual Helmholtz free energy, A^{r}, is divided into the contributions of a reference hard sphere system, A^{hs}, to consider the repulsive forces due to the size exclusion, dispersion forces to account for attractive forces between hard spheres, A^{disp}, formation of hard sphere chains, A^{chain}, association energy between molecules, A^{assoc}, and long-range interactions between charged particles, A^{ionic}, as follows:

$$A^{\mathrm{r}}(T,\ V,\ x) = A^{\mathrm{hs}} + A^{\mathrm{disp}} + A^{\mathrm{chain}} + A^{\mathrm{assoc}} + A^{\mathrm{ionic}} \tag{5.76}$$

Although there are numerous studies and models in the literature to formulate each of these terms the most notable ones are the association and the ionic contribution terms.

The association term can be represented using a formulation proposed by Chapman et al. [32] interpreted from the Wertheim's association theory as follows:

$$A^{\mathrm{assoc}} = \sum\nolimits_i x_i \left[\sum_{A_i} \left[\ln X^{A_i} - \frac{X^{A_i}}{2} \right] + \frac{M_i}{2} \right] \tag{5.77}$$

where X^{A_i} represents the fraction of site A on molecule i that does not form a bond and M_i is the total number of the association sites on the molecule i. The values of X^{A_i} can be calculated iteratively from a set of equations as follows:

$$X^{A_i} = \frac{1}{1 + \rho \sum_j x_j \sum_{B_j} X^{B_j} \Delta^{A_i B_j}} \tag{5.78}$$

with

$$\Delta^{A_i B_j} = g\left(d_{ij}\right) \left[e^{\frac{\varepsilon^{A_i B_j}}{kT}} - 1 \right] d_{ij}^3 b_{ij} \beta^{A_i B_j} \tag{5.79}$$

The following mixing rules could be used for the size parameters, d_{ij}, and the energy parameters, $\beta^{A_i B_j}$ and $\varepsilon^{A_i B_j}$:

$$d_{ij} = \frac{d_i + d_j}{2} \tag{5.80}$$

$$\beta^{A_i B_j} = \frac{\beta^{A_j} + \beta^{B_j}}{2} \quad \text{or} \quad \beta^{A_i B_j} = \sqrt{\beta^{A_j} + \beta^{B_j}} \tag{5.81}$$

$$\varepsilon^{A_iB_j} = \frac{\varepsilon^{A_j} + \varepsilon^{B_j}}{2} \quad \text{or} \quad \varepsilon^{A_iB_j} = \sqrt{\varepsilon^{A_j} + \varepsilon^{B_j}} \tag{5.82}$$

To reduce the number of parameters, it can be assumed that water and amino acid molecules can both self-associate and cross-associate. Although different types of association sites could be envisioned for an amino acid molecule, one possible set could be the two association sites (one of type A and one of type B) for every amino, carboxyl, and hydroxyl groups on the amino acid molecules and four association sites (two of type A and two of type B) on the water molecules. The other set of association sites proposed by Held et al. [33] assumes that only the amino and the carboxyl groups participate in association and are considered to be the association sites. To further simplify the model, for the contribution of the ionic term to the Helmholtz free energy, the models developed based on the MSA are the most widely used. In this model, the MSA for electrolytes has been simplified to reduce the calculation complexity and the number of parameters by assuming that all ions have the same effective average diameters, σ, as

$$A^{\text{ionic}} = -\frac{2\Gamma^3 V}{3\pi}\left(1 + \frac{3}{2}\sigma\Gamma\right), \quad \Gamma = \frac{1}{2\sigma}\left(\sqrt{1 + 2\sigma\kappa} - 1\right), \quad \kappa^2 = \frac{e^2 N}{kTV\varepsilon_0\epsilon}\sum_{i\in\text{ions}} x_i z_i^2 \tag{5.83}$$

where V is the total volume, ε_0 is the vacuum permeability, and ϵ is dielectric constant of the solvent.

5.6 Application of the Model to Fit Experimental Data

A comparison of the results obtained from the Extended Khoshkbarchi-Vera model eq. (5.75) with experimental data is presented in Figures 5.1 and 5.2 for several amino acids and in Figure 5.3 for peptides [23].

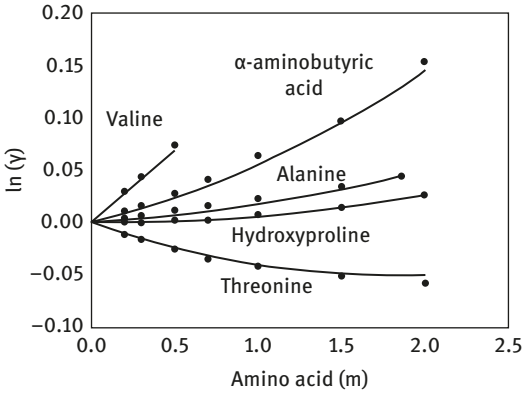

Figure 5.1: Activity coefficients of five amino acids at various molalities. Key: (•) experimental data [34], (–) result of the modeling. Reprinted with permission from [23]. Copyright (2018) American Chemical Society.

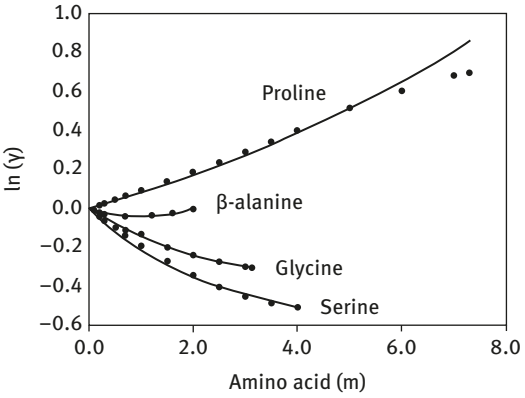

Figure 5.2: Activity coefficients of four amino acids at various molalities. Key: (•) experimental data [34], (–) result of the modeling. Reprinted with permission from [23]. Copyright (2018) American Chemical Society.

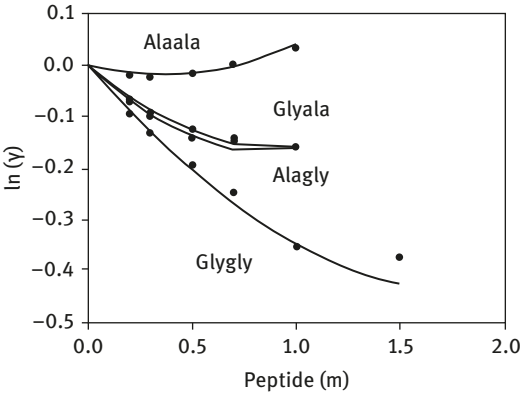

Figure 5.3: Activity coefficients of four peptides at various molalities. Key: (•) experimental data [34], (–) result of the modeling. Reprinted with permission from [23]. Copyright (2018) American Chemical Society.

Notably, similar if not better results are obtained using a model with a less sophisticated expression for the radial distribution function [22]. However, although the increased complexity of the refined model presented here makes the numerical work more difficult, its stronger theoretical basis gives more physically meaningful values of the size parameters and of the depth of the potential wells. Values of the parameters regressed from fitting the experimental data have been reported elsewhere [23].

5.7 Concluding Remarks

In aqueous electrolyte solutions, the presence of the charged amino and carboxyl groups on the hydrocarbon backbone of amino acids gives rise to the importance of both short-range and long-range interactions. The nature of these interactions is

more complex than the conventional electrolyte solutions, as an amino acid molecule at moderate pH values may carry no net change, despite possessing charged amino and carboxyl groups. This behavior of amino acids has inspired researchers to develop their models for the activity coefficient of amino acids in aqueous electrolyte solutions by combining theoretical models that each represents these interactions separately. The models proposed to represent the short-range interactions are mostly based on the extensions of the Debye–Hückel model. Whereas for the short-range interaction variety of models have been proposed based on the local composition, group contribution, electrolyte–local composition, perturbation theory, and statistical thermodynamic models such as the MSA [35–37]. Some of these models are simple and lump various effects together, and some, using the superposition theory, divide them into the contribution of various effects such as association, electrostatic, and hard sphere. While none of these models fully harness all the complexities of the interactions in these systems and some of the assumptions made in the development of their theory can be disputed, all of them represent the activity coefficient of amino acids in aqueous electrolyte solutions with acceptable accuracy. Unfortunately, none of these models are predictive or universal, and they all rely on variety of adjustable parameters that are not experimentally measureable and need to be fitted to the experimental data of particular water–amino acid–electrolyte systems.

Acknowledgements: The author is grateful to Professor Ana Soto from the Department of Chemical Engineering, Universidade de Santiago de Compostela, Spain, for helpful discussions.

References

[1] Kirkwood JG. Chem Rev 1939, 24, 233.
[2] Bromley LA. AIChE J 1973, 19, 313.
[3] Khoshkbarchi MK, Vera JH. AIChE J 1996, 42(1),249.
[4] Pitzer KS. J Phys Chem 1973, 77, 268.
[5] Mollerup JM, Briel MP. Fluid Phase Equilib 2006, 242, 129.
[6] Blum LJ. Chem Phys 1974, 61, 212.
[7] Blum LJ, Hoye JS. Phys Chem 1977, 81, 1311.
[8] Scatchard G, Pentiss S. J Am Chem Soc 1934, 56, 2314.
[9] Khoshkbarchi MK, Vera JH. AIChE J 1996, 42, 2354.
[10] Fernandez-Mérida LR, Rodriduez-Raposo GE, Garcia-Garcia, Esteso MA. J Electroanal Chem 1994, 379, 63.
[11] Pitzer KS, Activity Coefficients in Electrolyte Solutions, Pitkowicz MR, CRC Press, Boca Raton, FL, 1991.
[12] Chen CC, Zhu Y, Evans LB. Biotechnol Prog 1989, 5, 111.
[13] Sadeghi R. Fluid Phase Equilib 2007, 260, 266.
[14] Cheluget EL, Wilczek-Vera G, Vera JH. Can J Chem Eng 1992, 70, 313.
[15] Pazuki G, Rohani AA, Dashtizadeh A. Fluid Phase Equilib 2005, 231, 171.

[16] Haghtalab A, Vera JH. AIChE J 1988, 34, 803.
[17] Haghtalab A, Sarkisian E. Sci Iran 1998, 5, 67.
[18] Gupta RB, Heidemann RA. AIChE J 1990, 36, 333.
[19] Kuramochi H, Noritomi H, Hoshino D, Nagahama K. Biotechnol Prog 1996, 12, 371.
[20] Pinho SP, Silva CM, Macedo EA. Ind Eng Chem Res 1994, 33, 1341.
[21] Larsen BL, Rasmussen P, Fredenslund A. 1987, 26, 2274.
[22] Khoshkbarchi MK, Vera JH. Ind Eng Chem Res 1996, 35, 4319.
[23] Khoshkbarchi MK, Vera JH. Ind Eng Chem Res 1998, 37, 3052.
[24] Mansoori GA, Carnahan NF, Starling KE, Leland TW. J Chem Phys 1971, 54, 1523.
[25] Barker JA, Henderson D. J Chem Phys 1967, 47, 4714.
[26] Maitland GC, Rigby M, Smith EB, Wakeham WA, Intermolecular Forces, Clarendon Press: Oxford, 1981.
[27] Henderson D, Blum L, Tani A. ACS Symp Ser 300 1986, 300, 281.
[28] Chapman WG, Gubbins G, Jackson G, Radosz M. Ind Eng Chem Res 1990, 29, 1709.
[29] Cotterman RL, Schwarz BJ, Prausnitz JM. AIChE J 1986, 32, 1787.
[30] Khoshkbarchi MK, Vera JH. Ind Eng Chem Res 1996, 35, 4755.
[31] Chapman WG, Jackson G, Gubbins KE. Mol Phys 1988, 65, 1057.
[32] Jackson G, Chapman WG, Gubbins KE. Mol Phys 1988, 65, 1.
[33] Held C, Reschke T, Müller R, Kunz W, Sadowski G. Thermodyn 2014, 68, 1.
[34] Fasman G. D. Handbook of Biochemistry and Molecular Biology, 3rd ed.; Physical and Chemical Data; CRC: Cleveland, 1976, Vol. 1.
[35] Taghikhani V, Modarress H, Khoshkbarchi MK, Vera JH. Fluid Phase Equilib 2000, 167(2),161.
[36] Taghikhani V, Vera JH. Ind Eng Chem Res 2000, 39(3), 759.
[37] Ghotbi C, Azimi G, Taghikhani V, Vera JH. Ind Eng Chem Res 2003, 42(6), 1279.
[38] Liu JC, Lu JF, Li YG. Fluid Phase Equilib 1998, 142, 67.

Younok Dumortier Shin

6 Extraction of Biomolecules from Aqueous Solutions by Reverse Micelles

6.1 Introduction

Biomolecules such as amino acids and proteins have important industrial uses. Traditional methods to purify the biomolecules include crystallization, chromatography separation, and filtration. Luisi et al. first investigated the use of the quaternary ammonium salt trioctylmethylammonium chloride (TOMAC) in cyclohexane to solubilize various proteins including α-chymotrypsin and pepsin [1]. Since then, many researchers conducted studies to further understand the solubilization and the stability of biomolecules extracted into a reverse micellar phase. Di-(2-ethylhexyl) sulfosuccinate surfactant (AOT) has been widely used for the purification of biomolecules by reverse micellar extraction [2–7]. The electrostatic interaction between the biomolecules and the ionic surfactants was considered to be the main driving force to extract the biomolecules out of the initial aqueous phase and solubilized into an organic phase containing reverse micelles. Although many studies reported the advantages of the reverse micellar systems for purification of biomolecules, the use of this technology for actual commercial use was limited. As such, the efforts to further develop the reverse micellar extraction method continued to make this technology more suitable for practical use.

New cationic and anionic reverse micellar systems were proposed to expand our understanding of the reverse micellar extraction behavior for biomolecule separation. A reverse micellar system using dioctyl dimethyl ammonium chloride (DODAC) was studied by Wang et al. [8]. That work showed the effect of cosurfactants, such as decanol, on the water uptake in the organic phase. An excess or defect of cosurfactant in the organic phase resulted in Winsor type I or type III systems (refer to Chapter 1 for more explanation on the Winsor types). The formation of new anionic reverse micellar systems, as an alternative to AOT, was performed using the anionic surfactants di-(2,4,4-trimethylpentyl) sodium phosphinate, referred to as R_2POONa, di-(2,4,4-trimethylpentyl) sodium monothiophosphinate, referred to as R_2PSONa and di-(2,4,4-trimethylpentyl) sodium dithiophosphinate, referred to as R_2PSSNa [9]. Chapter 1 of this book summarized the behavior of DODAC and the three dialkyl sodium phosphinate surfactants to form new reverse micellar solutions. The different electrolytes in the aqueous phase, and the concentration of surfactant and cosurfactant in the organic phase showed a strong influence in the water uptake in the organic phase, a similar behavior as previously reported using AOT and TOMAC reverse micellar systems [1–7].

https://doi.org/10.1515/9783110564808-006

Our research work for the reverse extraction of biomolecules started with knowledge of the formation of reverse micelles with the above surfactants and focused on the use of these new reverse micellar systems for the extraction of biomolecules, specifically amino acids and proteins. Amino acids are the building blocks of large biological molecules such as proteins. Their molecular structure consists of one-carboxyl group and one-amino group attached to a hydrocarbon chain. Both carboxyl and amino groups undergo ion exchange in an aqueous solution. At a low pH, the amino group is positively charged and at high pH the carboxyl group is negatively charged. The pH at which the amino and carboxyl groups change their charge is often referred to as disassociation constant or p*K*. The change in the charge group in different amino acids is the basic mechanism of the surface charge of proteins, which varies depending on the pH of the aqueous solution. The isoelectric point of a given protein, p*I*, refers to the pH of the solution at which the number of negatively charged carboxyl groups is the same as the number of positively charged amino acid groups to yield a net neutral surface charge in the protein molecule.

In this chapter, we summarize the results of our studies on the extraction behavior of various amino acids and proteins into the newly developed reverse micellar systems, DODAC, and three different diallyl sodium phosphinates described earlier. In addition, the observation of a white precipitate formed at the aqueous and organic interface during the extraction into and out of organic phase shed a light on the protein–surfactant interaction mechanism in the aqueous phase during protein extraction. This topic is also discussed in this chapter.

6.2 Reverse Micellar Extraction of Amino Acids Using DODAC

This section summarizes our research work to use DODAC to extract amino acids [10, 11]. The study of reverse micellar extraction of amino acids using TOMAC and AOT showed that the pH of the aqueous solution, the type, and the concentration of electrolytes have an important role in the extraction efficiency, demonstrating the main driving force for the extraction of biomolecules is the electrostatic interaction between the charged biomolecule and the charges of the surfactant headgroups as well as the property of the water pool in the reverse micellar phase [1, 12–14].

A new cationic surfactant, DODAC, was purified in our laboratory. The reverse micellar behaviors using this new cationic surfactant were studied in terms of the concentration and the type of salts, the pH, and the concentration and the types of cosurfactants used [8]. To continue with our research, the DODAC reverse micellar system was tested for the extraction of three amino acids: DL-glutamic acid (Glu), DL-aspartic acid (Asp), and DL-threonine (Thr).

6.2.1 Experimental Conditions

The initial aqueous solutions and DODAC reverse micellar solutions were prepared at a target amino acid and DODAC concentrations. As a cosurfactant, 1-decanol was used to form the reverse micelles in the organic phase. The water uptake in the organic phase was measured by the Karl Fischer titration method. The ion concentration in the aqueous phase was measured using atomic absorption and ion chromatography methods. The DODAC concentration in the aqueous phase was measured using gas chromatography. The concentration of amino acids was measured using the o-phthaldialdehyde (OPA)-labeling method [15, 16].

The OPA-labeling experiment showed that the glutamine concentration measurement at a high pH was a strong function of time between the initial solution preparation and the reverse micellar extraction. When the amino acid solution was freshly made, the ultraviolet (UV) reading was high and rapidly decreased to reach a steady state within 1 week. This reading remained steady for up to 4 weeks. The UV concentration readings for the other three amino acids, aspartic acid, glutamic acid, and threonine, were stable regardless of the age of the solution. In order to ensure stable UV reading for the concentration measurement, the extraction experiments were conducted allowing 1 week settling time for glutamine solutions.

The concentration of ions and amino acid in the reverse micellar phase was calculated using the difference in the concentration measurement in the aqueous phase before and after the contact with the reverse micellar solution.

6.2.2 Effect of DODAC and Decanol Concentration on Water Uptake

Figure 6.1 shows the water uptake in the reverse micellar phase as a function of DODAC concentration when the decanol concentration was fixed at 250 mM (Figure 6.1(a)), and as a function of decanol concentration when the DODAC concentration was fixed at 200 mM (Figure 6.1(b)). As shown in Figure 6.1(a), the water uptake increased exponentially with an increased DODAC concentration and then suddenly dropped to zero at the DODAC molality of 0.43. At this molality, a third phase, rich in DODAC, appeared between the aqueous and the organic phases. Above this molality, the DODAC migrated into the aqueous phase, and no reverse micelles were formed. As such there was no water uptake measured in the organic phase. On the other hand, Figure 6.1(b) shows that the decanol concentration has a narrow window at which the maximum water uptake can be obtained in the reverse micellar phase. At the molality below 0.3, no reverse micellar phase was formed and as such the water uptake was zero. When the decanol concentration was at 0.3, the maximum water uptake was observed, however, decreased rapidly with a further increase in decanol concentration in the organic phase. Wang et al. [8] suggested that

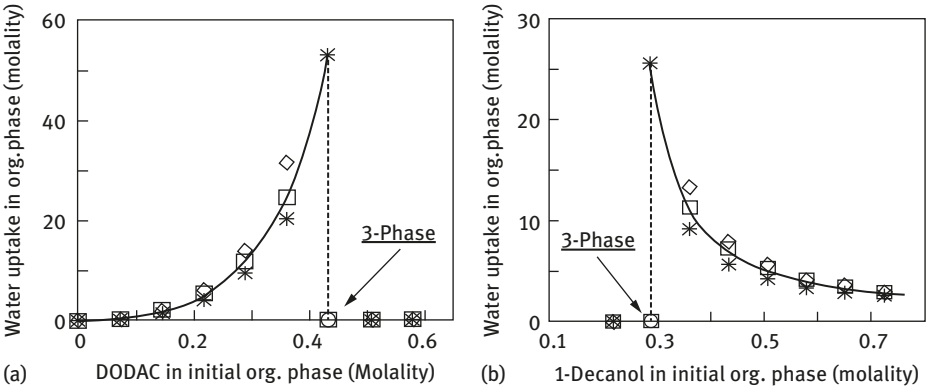

Figure 6.1: Effect of DODAC (a) and 1-decanol (b) in the initial organic phase on the water uptake. Initial organic: (a) 250 mM 1-decanol, (b) 200 mM DODAC. Initial aqueous: no NaCl, (□) 5 mM Asp at pH 12.6, (✳) 5 mM Glu at pH 12.5, (◇) 5 mM Thr at pH 12.6.

cosurfactants such as decanol participate in the interfacial region of the reverse micelles to screen the repulsive forces between the positively charged headgroups of DODAC, and consequently, the size of the reverse micelles and the water uptake decreases. They also suggested that with an increased concentration of decanol, the organic phase becomes more polar and as a result some surfactants dissolved in the bulk organic phase, thus reducing the number of reverse micelles formed. The presence of different amino acids in the aqueous phase showed negligible impact to the water uptake as shown in Figure 6.1(a) and (b). The water uptake profile in the reverse micellar phase after being contacted with different aqueous solutions containing different types of amino acids followed the same trend, indicating that the water uptake is independent of the nature of the amino acid being extracted.

Figure 6.2 shows the effect of DODAC concentration on the water uptake when the molar ratio between decanol and DODAC was kept constant at 2.5. There were no reverse micelles formed at concentrations of DODAC below 0.05 molality. Above 0.05 molality, the water uptake increases linearly with the concentration of DODAC. It was our assumption that the increased water uptake in the reverse micellar phase was due to the increased number of reverse micelles as there were more DODAC and decanol available to form the reverse micelles rather than to assume that more DODAC and decanol created much bigger water pool in the reverse micellar phase. This was based on the knowledge that the molar ratio of 1-decanol to DODAC at the interface of the reverse micelles determined the curvature of the interface and thus the size of the reverse micelles [8]. Similar to Figure 6.1, the different types of amino acids in the aqueous phase did not have any influence in the amount of water uptake. As shown in Figure 6.2, the water uptake in the reverse micellar phase was a strong function of the surfactant concentration regardless of different types of amino acids present.

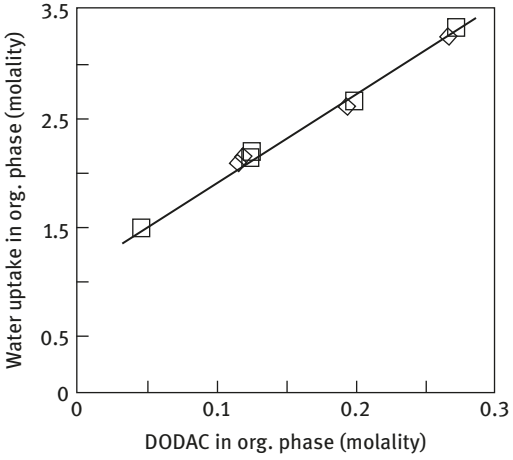

Figure 6.2: Effect of DODAC and 1-decanol at constant initial molar ratio on the water uptake. Initial organic: molar ratio of 1-decanol to DODAC = 2.5. Initial aqueous: no NaCl, pH 12.6, (□) 5 mM Asp, (◇) 5 mM Thr.

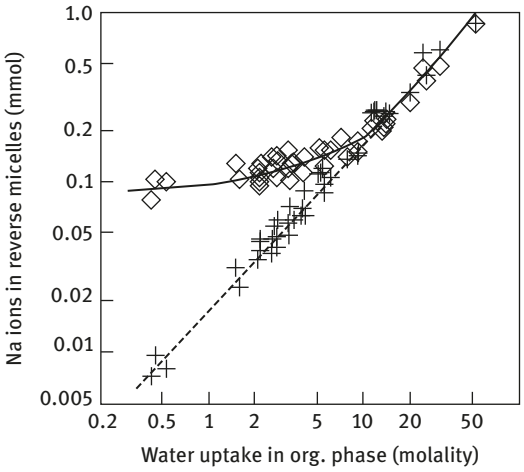

Figure 6.3: Effect of the water uptake on the total number of moles of Na^+ ions inside the reverse micelles. Initial aqueous: 5 mM Asp, Glu, and Thr; pH 12.5–12.6; no NaCl. (◇) $N_{Na+,Ref}$, (+) $N_{Na+,Ref}$/Ref.

Theoretical calculations suggest that, due to the microscopic size of reverse micelles and the charged interface formed by the headgroups of ionic surfactants, the dielectric constant of the water pool is lower than that of the bulk aqueous phase [17, 18]. A lower dielectric constant should favor the undissociated forms of ionic species. To examine this hypothesis, we used the Na^+ ions as an indicator. In the aqueous phase, the Na^+ ions were considered to be completely dissociated, and the free sodium ions should not go into the cationic reverse micelles. Figure 6.3 shows the total number of moles of Na^+ ions inside the reverse micelles as a function of the water uptake at different concentrations of DODAC and 1-decanol for different amino acids. The diamonds show the concentration of Na^+ ions in the reverse micellar phase, calculated using the difference in the concentration

measurement in the aqueous phase before and after the contact with the reverse micellar solution with an assumption that the Na^+ ions extracted from the aqueous phase are fully solubilized in the reverse micellar phase. The crosses show a reference number of moles of Na^+ ions inside the reverse micelles, calculated by assuming that the concentration of Na^+ ions inside the reverse micelles is the same as the measured equilibrium concentration in the aqueous phase. For water uptake above about 10 molality, the total number of moles of Na^+ ions inside the reverse micelles was identical to the reference value indicating that the concentration of Na^+ ions inside the reverse micelles was equal to that in the bulk aqueous phase. On the other hand, for water uptake below 10 molality, the measured concentration of Na^+ ions inside the reverse micelles was almost constant and higher than that in the bulk aqueous phase. This indicates that, as the size of the reverse micelles becomes smaller, the nature of the water inside the reverse micelles is different from that of the bulk water and the Na^+ ions tend to associate with the anions in the reverse micelles. Based on the data shown in Figure 6.3, we have concluded that the salt concentration in the water pool can be much higher than that of aqueous phase, especially at a low water uptake, resulting in different physicochemical properties inside the reverse micelles containing different types of amino acids.

6.2.3 Partition Coefficient of Amino Acid as a Function of Surfactant and Cosurfactant Concentrations

The partition coefficient, K_A, is defined as the ratio between the concentration of amino acid in the reverse micellar phase and the concentration of amino acid in the equilibrium aqueous phase. Figure 6.4 shows the partition coefficients of the three amino acids measured as a function of DODAC concentration when decanol concentration was fixed at 250 mM (Figure 6.4(a)), and as a function of decanol concentration when the DODAC concentration was fixed at 200 mM (Figure 6.4(b)). Different types of amino acids were used to prepare aqueous solutions at 5 mM concentration.

As shown in Figure 6.4(a), the aspartic and glutamic acids, which have two negative charges, have partition coefficients almost ten times larger than the singly charged threonine. For all amino acids, the partition coefficient decreased with an increased DODAC concentration in the reverse micellar phase. When the DODAC concentration was fixed at 200 mM, the partition coefficient of different amino acids increased with an increased decanol concentration (Figure 6.4(b)). The partition coefficient was higher for glutamic than aspartic acid in this case. The partition coefficient for threonine was lower than for glutamic and aspartic acids, similar to the trend shown in Figure 6.4(a). The partition coefficient trends shown in Figure 6.4(a) and (b) are opposite to the water uptake profile shown in Figure 6.1 (a) and (b). The water uptake increased with an increased DODAC concentration.

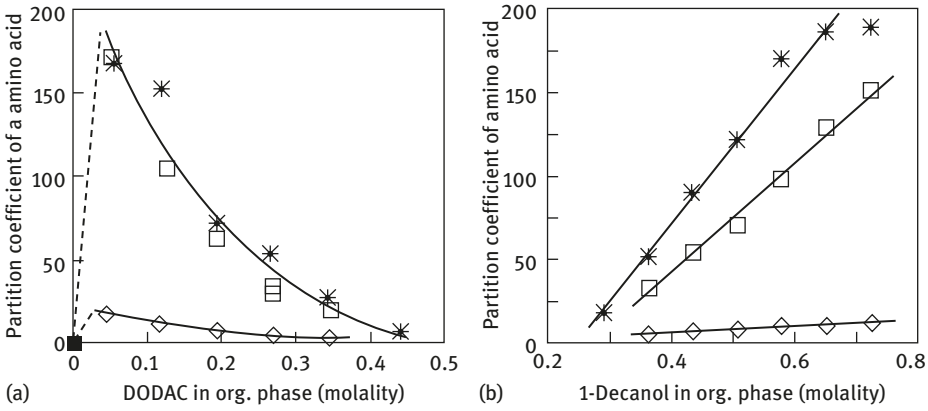

Figure 6.4: Effect of DODAC (a) and 1-decanol (b) in the equilibrium organic phase on the partition coefficient of amino acids. Initial organic: (a) 250 mM 1-decanol and (b) 200 mM DODAC. Initial aqueous: no NaCl, (□) 5 mM Asp, pH 12.6; (✳) 5 mM Glu, pH 12.5; (◇) 5 mM Thr, pH 12.6.

Despite the increased water uptake, the partition coefficient for the amino acids decreased. Similarly, the water uptake decreased with an increased decanol concentration. However, the partition coefficient of the amino acids increased with an increase in decanol concentration. These results indicate that the change in the partition coefficient was not due to the different amount of amino acids being extracted into the reverse micellar phase, but rather due to the different amount of water pool in the reverse micellar phase. For example, as shown in Figures 6.1(b) and 6.4(b), an increase in the molality of 1-decanol from 0.4 to 0.8 decreased the water uptake by a factor of around 2.7 and increased the partition coefficients of the amino acids by almost the same proportion. As the partition coefficient was calculated based on the concentration of the amino acids in the water pool versus that in the aqueous phase, the small amount of water pool gives a higher concentration of the amino acids within the reverse micellar phase and this results in a large partition coefficient.

As the partition coefficient is strongly affected by the water uptake, we considered the molar distributions of the ions in the organic and aqueous phases. For a species i, the molar distribution ratio, D_i, is defined as the ratio of the number of moles of species i in the equilibrium organic phase to the number of moles of species i in the equilibrium aqueous phase. Figure 6.5 shows the molar distribution ratios for the different ionic species during the extraction of aspartic acid. Also plotted on the right-hand side of this figure is the volume ration between aqueous and organic phases at equilibrium. Initially, the two phases had the same volume; however, at equilibrium, the ratio decreased to less than 1.0 depending on the water uptake from the aqueous phase into the reverse micellar phase. Figure 6.5(a) shows an increase in the molar distribution

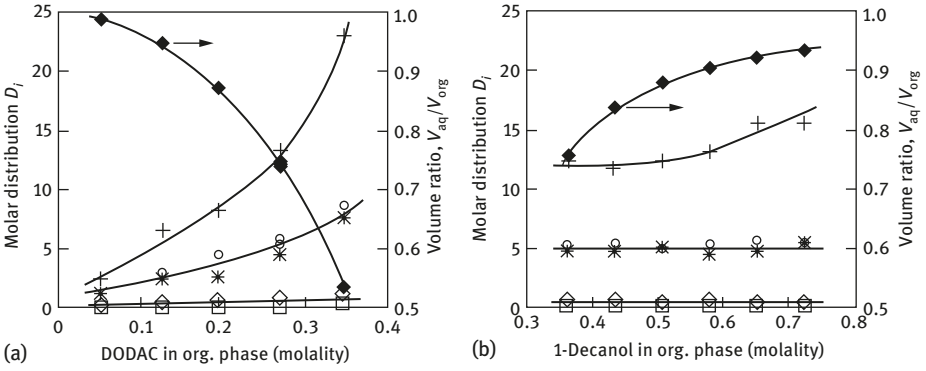

Figure 6.5: Effect of DODAC and decanol in the equilibrium organic phase on the molar distribution ratio of all the ionic species for the extraction of aspartic acid. Initial organic: (a) 250 mM 1-decanol and (b) 200 mM DODAC. Initial aqueous: 5 mM Asp, pH 12.6, no NaCl; (○) Asp; (✳) Cl; (◇) OH; (□) Na; (+) DODAC; (◆) V_{aq}/V_o.

ratio as a function of DODAC concentration. The molar distribution ratio of Cl^- ions was very close to that of aspartic acid while the molar distribution ratio of OH^- ions was much lower than that of Cl^- ions and aspartic acid. The molar distribution ratio of Na^+ ions was quite small. These results indicate that the positively charged surfactant head binds better with Cl^- as with aspartic acid compared to the OH^- ions and extracted into the reverse micellar phase. The positively charged Na^+ remained in the aqueous phase, due to the electrostatic repulsion between the surfactant head and the Na^+ ions. Figure 6.5(b) shows that, when the DODAC concentration was constant, an increase in the concentration of 1-decanol affects the volume ratio of the aqueous to organic phases, but with an exception of DODAC, it does not affect the molar distribution ratios of the ionic species. Based on this finding, it was concluded that while the concentration of alcohol can affect the dissociation equilibrium of the ionic species, it does not change the total number of moles of the bound and free ions in the reverse micelles.

6.2.4 Partition Coefficient of Amino Acid as a Function of Ionic Strengths and the pH

Many studies in the literature have shown the effect of ionic strengths and pH on the extraction behavior of various biomolecules [1–7]. To examine whether the similar behavior was observed using the DODAC reverse micellar system, the partition efficiency of the three amino acids was studied as a function of different pH and ionic strength while keeping the DODAC and decanol

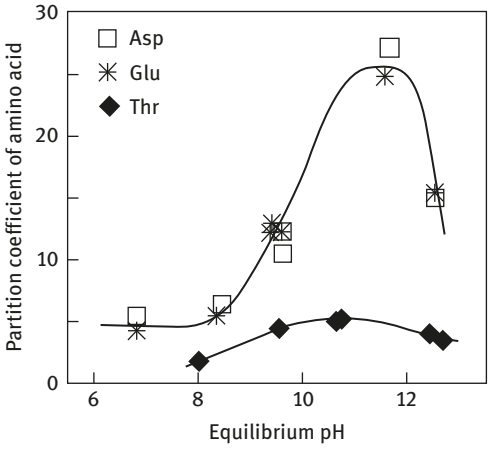

Figure 6.6: Effect of equilibrium pH on the partition coefficients of aspartic acid, glutamic acid and threonine: initial organic, 200 mM DODAC, 250 mM 1-decanol; initial aqueous, 5 mM amino acid, 51.2 mM NaCl.

concentration constant at 200 and 250 mM, respectively. Figure 6.6 shows the partition coefficients of the amino acids as a function of pH of the equilibrium aqueous phase. For aspartic acid and glutamic acid, the partition coefficients were about 5 in the pH range between 6 and 8 and increased significantly as the pH further increased to 11. After that, the partition coefficient decreased significantly again at pH 12. This trend was the same for both aspartic and glutamic acids. Both of aspartic and glutamic acids have net charge of −2 in this pH range and thus have a strong potential to replace the Cl^- counterions of DODAC in the reverse micelles. At pH higher than 12, the decrease in the partition coefficients of aspartic acid and glutamic acid can be explained by an increased amount of OH^- ions that compete with the amino acid ions as the counterions for DODAC. The partition coefficient of threonine, at pH values between 8 and 10.7, increased slightly due to the change in charge of threonine from 0 to −1, and decreases at pH larger than 11 due to the strong competition from OH^- ions. The partition coefficients of all three amino acids are almost the same at the same charged state of −1, which occurs at pH 7 for aspartic and glutamic-acids and at pH 10.7 for threonine. These results demonstrate that the electrostatic force is the main driving force for the extraction of amino acids by DODAC reverse micelles, which is consistent with the conclusions reached using AOT and TOMAC reverse micellar systems in the literature. Using small-angle neutron scattering for the study of protein extraction, Sheu et al. [19] also found that the driving force for protein extraction was reduced with the decrease of the attractive electrostatic force between the protein and the charged wall of the reverse micelles. Based on the assumption that the pK values of amino acids inside the reverse micelles are same as those in the bulk water [20–22], the partition coefficients of the amino acids shown in Figure 6.6 indicate that the pH inside the reverse micelles is close to the pH in the bulk aqueous phase.

6.2.5 Conclusions

Reverse micellar extraction of amino acids using DODAC reverse micellar systems showed that the electrostatic interaction between the opposite charge of amino acid and the ionic surfactant headgroup plays an important role. Similar to the previous studies using TOMAC and AOT systems, the amino acid extraction efficiency depended strongly on the pH and the ionic strength of the initial aqueous solution as well as the surfactant concentration. The selectivity of amino acids relative to chloride, and the water uptake in the reverse micellar phase were independent on the types of amino acids used. The water uptake did not show any direct impact on the extraction efficiency of the amino acids, indicating that the driving force for the amino acids to be solubilized into the reverse micellar phase was due to the electrostatic interaction, rather than the formation of the water pool as the main driving force for the amino acids to be solubilized inside of the reverse micelles in the organic phase.

6.3 Reverse Micellar Extraction and Back-Extraction of L-Lysine with Three Dialkyl Sodium Phosphinates in Pentanol/Isooctane Mixtures

The most widely studied anionic surfactant is AOT, the bis(2-ethylhexyl) sulfosuccinate sodium salt [23]. Besides AOT, few anionic surfactants were studied in the literature for the reverse micellar extraction of amino acids. Our research found that three dialkyl sodium phosphinate surfactants could form reverse micellar phase in isooctane/alcohol mixture [9]. The chemical structures of these new anionic surfactants are provided in Figure 6.7. Based on this information, the extraction behavior of L-lysine into different reverse micellar systems was studied as a function of pH and the salt concentration [24]. Since all these surfactants have the same two hydrocarbon tails and differ only in their headgroups, their comparative study gave insights on the effect of the structure of the surfactant headgroup on the reverse micellar extraction of L-lysine. L-lysine was chosen as a model biomolecule for our study.

In addition to the extraction into the reverse micellar phase, another important aspect in the reverse micellar extraction process is the recovery of the amino acids from the reverse micellar phase. Typically, a new aqueous phase containing a high salt concentration is used to induce the amino acids to be extracted back into the fresh aqueous phase. This process is often referred to as *back-extraction*. Thus, our research was carried out to examine the

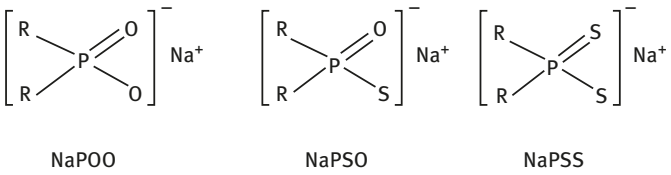

NaPOO NaPSO NaPSS

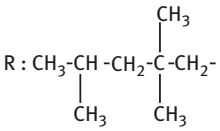

Figure 6.7: Structure of bis(2,4,4-trimethylpentyl) sodium phosphinate (NaPOO), bis(2,4,4-trimethylpentyl) sodium monothiophosphinate (NaPSO), bis(2,4,4-trimethylpentyl) sodium dithiophosphinate (NaPSS).

extraction of L-lysine into the reverse micellar phase and back-extracted into a fresh aqueous phase.

6.3.1 Experimental Conditions

The preparation of two anionic surfactants for reverse micellar formation required a purification step to first remove impurities in the purchased acidic form of the three dialkyl sodium phosphinate surfactants. The surfactant purification was carried out by using a copper salt precipitation method [25]. After the purification, the acidic forms of the surfactant, R_2POOH and R_2PSSH, were converted to the sodium forms, R_2POONa and R_2PSSNa, using 0.5 N NaOH. The sodium forms of the surfactants, R_2POONa and R_2PSSN, are water soluble. In contrast, the acidic forms of these surfactants, R_2POOH, R_2PSOH, and R_2PSSH, are water insoluble. The initial R_2POONa and R_2PSSNa reverse micellar solutions were prepared using a surfactant containing aqueous solution at a known surfactant concentration contacted with an isooctane solution containing known amount of decanol (cosurfactant). Upon phase separation, all the surfactants in the initial aqueous phase were solubilized into the organic phase. For back-extraction, an equal volume of 1 N HCl solution was used. The surfactant concentrations reported in our research correspond to the concentration of surfactant in the initial reverse micellar phase. Similar to the work done with DODAC reverse micellar system described in Section 6.5.2, the OPA method was used to measure the amino acid concentration in the aqueous solutions. The

amino acid concentration in the reverse micellar phase was obtained using a mass balance between the amino acid concentration in the initial phase and after being in contact with the reverse micellar phase.

6.3.2 Effect of pH on the Extraction of L-Lysine and on the Water Uptake

As a starting point, we examined the effect of pH on the extraction efficiency using NaPOO, NaPOS, and NaPSS reverse micellar systems. The surfactant and the cosurfactant concentration were kept constant at 100 and 400 mM, respectively. As shown in Figure 6.8, the partitioning of L-lysine into the reverse micellar system depended strongly on the pH of the aqueous solution, and on the different headgroups of the surfactants. The amino acid, L-lysine, has three pK values, pK_1 = 2.18, pK_2 = 8.95, and pK_3 = 10.53, associated with the dissociation constant of carboxyl group, amino group, and the aliphatic amino acid group attached to the molecule [26]. At a pH value higher than pK_2 = 8.95, L-lysine has no charge and therefore has no tendency to exchange with the counterion of the surfactant molecules. At pH values between pK_1 and pK_2, the L-lysine has one net positive charge (two positive and one negative charges), and it exchanges with the counterions of the surfactant molecules. At pH values between 2.18 and 8.95, the extraction presents a plateau where pH does not have a major effect on the extraction of L-lysine. At a pH value lower than 2.18, where the L-lysine has two positive charges, it exchanges favorably with the counterion of the surfactant. On the other hand, at a very low pH, the concentration of H^+ ions is high resulting in the ion exchange between H^+ and Na^+ ions rather than between L-lysine and Na^+. Therefore, at pH lower than pK_1, there is first an increase and then a dramatic decrease in the extraction efficiency. The

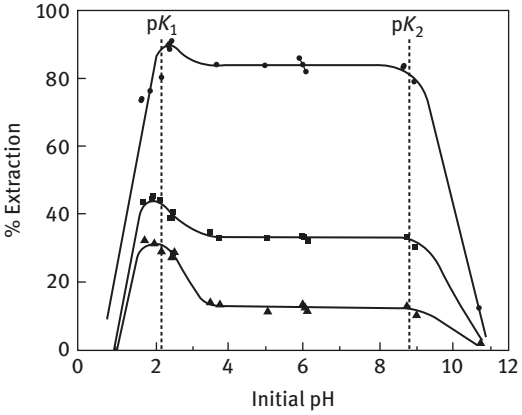

Figure 6.8: Effect of surfactant structure and pH on the extraction of L-lysine for (▲) NaPOO, (■), NaPSO, and (●) NaPSS at 400 mM pentanol, 100 mM surfactant, 40 mM NaCl and 5 mM L-lysine.

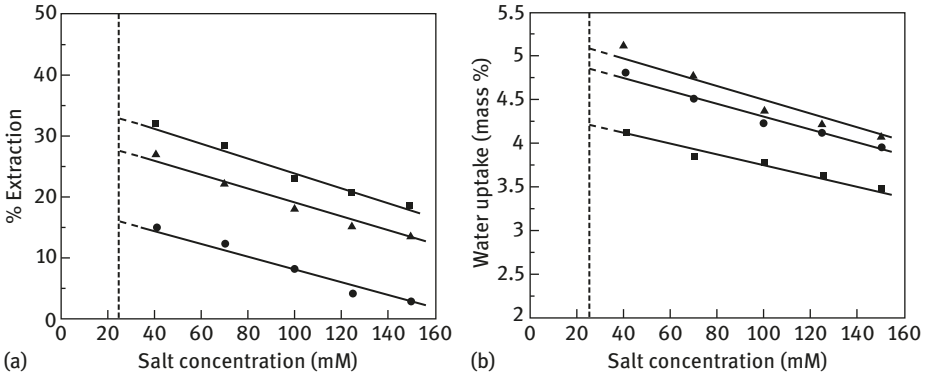

Figure 6.9: Effect of NaCl concentration on (a) extraction of L-lysine and (b) water uptake for (■) pH 1.74, (▲), pH 2.27 and (●) pH 3.75 at 400 mM pentanol, 100 mM NaPOO, and 5 mM L-lysine.

water uptake measurement in the earlier study showed that the water uptake decreased sharply at a low pH due to the exchange of the surfactant counterion with H^+ ions which resulted in an acidic form of the surfactant which was water insoluble and thus limited ability to contain water pool in the organic phase [9]. The results shown in Figure 6.9 confirmed that the reverse micelles are formed only at a pH higher than 1. In all extraction experiments, the final concentration of surfactant in the aqueous phase was 6.3 mM. Based on this information, it was assumed that most surfactants initially introduced in the experiment were solubilized in the organic phase forming reverse micelles.

6.3.3 Effect of Salt Concentration on the Extraction of L-Lysine and on the Water Uptake

The effect of ionic strength in the aqueous phase was studied in terms of extraction efficiency and the water uptake. As expected, the salt concentration was an important factor which influenced the L-lysine partitioning into the reverse micellar phase. Figure 6.9 shows that the extraction efficiency and the water uptake decreased with an increased ionic strength in the aqueous phase. The dashed line in Figure 6.9 at NaCl concentration of 25 mM indicates the salt concentration at which the surfactants become more water soluble and as such do not form reverse micelles in the organic phase. An increased salt concentration in the aqueous phase increased the salt concentration inside the reverse micelles and therefore the amino acid is kept out of the reverse micelles (salting-out effect).

In terms of water uptake in the different reverse micellar systems (not shown in the figure), the water uptake was the highest for NaPOO (up to 5.5 mass %) in

the pH range between 4 and 11. In comparison, the water uptake was slightly less than 5.4% for NaPSO, and less than 3% for NaPSS. While the water uptake was the highest for NaPOO reverse micellar system, the maximum extraction efficiency was only 30% for this reverse micellar system as shown in Figure 6.9. On the other hand, the maximum extraction efficiency was about 40% for the NaPSO reverse micellar system, while maximum extraction efficiency reached up to 80% for the NaPSS reverse micellar system (not shown in the figure). This result indicates that the partitioning of amino acid is not only a function of electrostatic interaction and ionic strength of the aqueous solution but also the functional groups in the surfactant that creates different degrees of interaction between the surfactant and the amino acid. When the electronegativity of the S atom in the organophosphorus compounds is higher than that of the O atom [27], the sulfur substitution in the surfactant head group enhances the extraction.

6.3.4 Back-Extraction of L-Lysine

Experiments were conducted to investigate the back-extraction of the L-lysine from the organic phase reverse micellar solution. Reverse micellar extraction of L-lysine was performed under different conditions of pH and salt concentration. The use of a new fresh aqueous phase containing 1 N HCl provided about 90–96% of the initial L-lysine being extracted back into the receiving aqueous solution. The reason for the successful back-extraction was because the sodium form of the surfactant goes through an ion exchange, at a low pH, to form an acidic form of the surfactant which does not form reverse micelles. Since the acidic form of these surfactants is water insoluble, the concentration of the surfactant in the receiving aqueous phase was below the detection limit of the assay.

6.3.5 Conclusions

It was successfully demonstrated that the new anionic reverse micellar systems using three different dialkyl sodium phosphinates can be used for the purification of L-lysine. Similar to the other reverse micellar systems studied in the literature, the main driving force for the extraction of amino acid was the electrostatic interaction between oppositely charged biomolecule and the surfactant head group. In addition to the electrostatic interaction as the main driving force for the extraction of biomolecule into a reverse micellar phase, our study also found that the different surfactant head group had an impact to the extraction efficiency and the water uptake.

6.4 Reverse Micellar Extraction of Proteins Using DODAC

This section summarizes the use of DODAC for the protein extraction [28, 29]. For the extraction of proteins using cationic surfactants, such as DODAC, the pH of the aqueous solution should be set above the p*I* of the proteins, as they need to be negatively charged for their extraction into cationic reverse micelles. Most reverse micellar extraction work for proteins found in the literature, including the previous sections in this chapter, highlighted the importance of the electrostatic interaction between the proteins and the charged head group of the surfactants and the size exclusion as the key driving force for the protein solubilization into, and out of, both anionic and cationic reverse micellar systems [2, 30–36]. While most researchers believed that the proteins are entrapped in the water pool inside of the reverse micellar phase, some authors reported that the direct interaction between oppositely charged protein molecule and the surfactant head group had a greater effect on the protein extraction. Carlson and Nagarajan [37] speculated that the first step in extraction of a protein into the organic phase is the formation of a transferable complex between protein and surfactant molecules. Adachi and Harada [38] suggested that extraction of cytochrome c involved complexation between AOT and cytochrome c when the aqueous phase containing protein became direct contact with an organic phase containing reverse micelles.

As described in Section 6.2, DODAC was used successfully to extract amino acids from the aqueous solution. As a continuation of this work, the reverse micellar extraction mechanism of the new cationic surfactant DODAC was studied for protein extraction as a function of different pH and ionic strengths in the protein containing aqueous solution, as well as the effect of the surfactant and cosurfactant concentration in the organic phase.

6.4.1 Experimental Conditions

The formation of DODAC reverse micelles followed the same experimental steps as described in Section 6.2.1. The protein solutions were prepared using a single protein solubilized in the aqueous solution at a target pH and salt concentration. Three different proteins were used to generate three different single-protein containing solutions: albumin, α-chymotrypsin, and lysozyme. Once the protein containing aqueous phase was contacted with the reverse micelle containing organic phase, the mixture was set aside to allow for phase separation. Once the two phases separated and formed clear solutions, the samples were taken for analysis for the pH, ions, and water uptake, following similar procedures to those described in Section 6.2.1. For the protein extraction efficiency, two different calculation methods were utilized. The protein concentration in the aqueous phase was measured before

and after being contacted with the reverse micellar phase, and the extraction efficiency was calculated based on the percentage of the proteins removed from the initial aqueous phase. As a second method, instead of assuming that all proteins extracted from the aqueous phase was fully solubilized into the reverse micellar phase as in eq. (6.1) which was the calculation used in the previous sections of this chapter, the protein concentration in the organic phase was measured directly using an UV spectrophotometer at 280 nm which was then subtracted by the UV reading at 310 nm to eliminate the absorbance signal produced by the reverse micellar solution from the signal produced by the proteins entrapped within.

In this chapter, the extraction efficiency of various proteins into organic solutions containing DODAC reverse micelles was reviewed using these two different calculations.

6.4.2 Effect of pH on Protein Extraction and Water Uptake

Figure 6.10 shows the extraction of albumin, α-chymotrypsin, and lysozyme as a function of equilibrium pH. The dashed lines indicate the approximate isoelectric points of these proteins. The extraction efficiency shown in this figure was calculated using the protein concentration measurement before and after being in contact with the DODAC reverse micellar solution assuming all proteins extracted from the aqueous phase were fully solubilized into the reverse micellar phase. As shown in this figure, the protein extraction increased significantly as the pH of the solution was above the isoelectric point of each protein. For both α-chymotrypsin and lysozyme, 100% extraction of the protein was obtained at pH 9 and 11, respectively, whereas the maximum extraction efficiency for albumin was about 90%. The lower extraction of

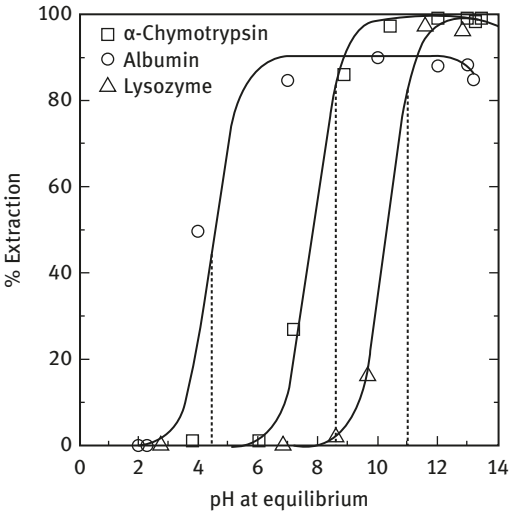

Figure 6.10: Effect of pH on the extraction of proteins: initial organic phase, 100 mM DODAC, 250 mM decanol in isooctane; initial aqueous phase, 0.5 g/L protein, 100 mM NaCl.

albumin can be attributed to the size exclusion effect. Above the isoelectric point, where the protein is negatively charged, a reaction between the protein molecules and positively charged surfactant head groups occurs.

Previous work conducted using TOMAC and AOT showed that the maximum extraction of different proteins for TOMAC was 40–70% and about 80–100% for AOT [39]. Also, some researchers reported the formation of white precipitate at the aqueous and organic phase interface, which reduced the extraction efficiency of the proteins into the reverse micellar systems [3, 40, 41]. In order to further examine the reverse micellar extraction of protein into a DODAC reverse micellar phase, the extraction efficiency of proteins into the DODAC reverse micellar solution was plotted in terms of the actual amount of protein measured in the organic phase. For this experiment, an initial aqueous solution containing lysozyme was utilized, and the pH of the initial aqueous solution was set at 12, which was above the isoelectric point of lysozyme. Figure 6.11 shows the mass of lysozyme solubilized in the reverse micellar phase as a function of the initial mass of lysozyme introduced to the aqueous phase (closed symbols in the figure). Four to six replicates were used for each point, and the reproducibility is indicated in the figure with the error bars showing the 95% confidence interval. Note that most error bars are too small to be noticeable in this figure, indicating an excellent reproducibility of data. In this experiment, the DODAC and the decanol concentrations were fixed at 100 and 250 mM, respectively. The mass of

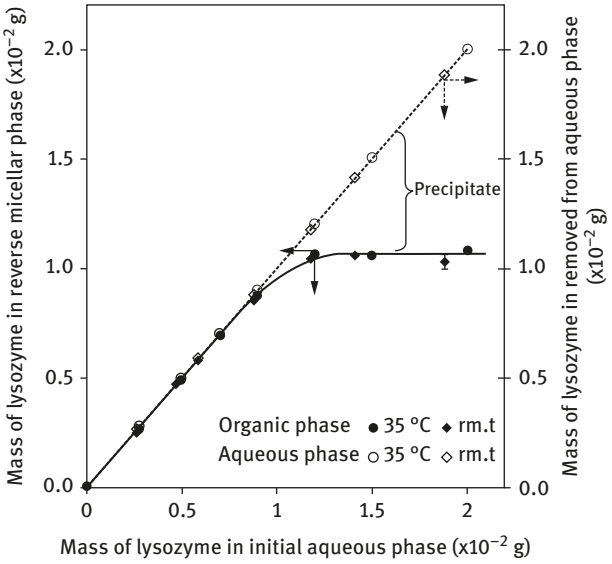

Figure 6.11: Equilibrium mass of lysozyme solubilized in organic phase (closed symbols) and mass of lysozyme removed from aqueous phase (open symbols) at 35 °C and at room temperature (rm.t); $V_a = V_o = 10$ mL; initial reverse micellar phase, 100 mM DODAC, 250 mM decanol; initial aqueous phase, 0.1 M NaCl, pH = 12.0 adjusted with NaOH.

lysozyme removed from the aqueous solution is also shown in this figure on the right-hand side ordinate (open symbols in the figure).

Two different temperatures were used in the experiment to examine whether the protein extraction and the temperature had any correlation. As shown in Figure 6.11, at room temperature, when the initial mass of lysozyme in the aqueous phase was less than 0.8×10^{-2} g, and the mass of lysozyme solubilized into the reverse micellar phase matched the mass of lysozyme removed from the aqueous phase (i.e., 100% extraction efficiency). As the mass of lysozyme in the initial aqueous solution further increased above 0.8×10^{-2} g, the mass of lysozyme in the reverse micelles reached a plateau, indicating that there is a solubility limit of lysozyme in the DODAC reverse micellar phase. On the other hand, the mass of lysozyme remaining in the aqueous phase, after being in contact with the organic phase, continued to be below the detection limit indicating full extraction of lysozyme out of the aqueous phase after being contacted with the DODAC reverse micellar solution. The difference in the mass of lysozyme removed from the aqueous phase and that solubilized into the DODAC reverse micellar phase is due to the formation of white insoluble moiety at the aqueous–organic interface. The amount of white moiety became more visible when the initial lysozyme concentration increased to 1.2 g/L or higher. The white moiety is believed to be a lysozyme–surfactant complex [6, 38, 42], which was also confirmed in our research that the formation of this white precipitate was observed only in the presence of lysozyme in the aqueous phase and in the presence of surfactant in the organic phase, indicating that the moiety is indeed lysozyme–DODAC complex. The change in the temperature from the room temperature to 35 °C did not have any impact to the protein solubilization into the reverse micellar phase.

The water uptake in the DODAC reverse micellar phase is presented in Figure 6.12, as a function of the initial mass of lysozyme in the aqueous phase. Although the increase in the temperature from room temperature to 35 °C had little effect on the solubilization limit of lysozyme in the DODAC reverse micellar phase, as shown in Figure 6.11, the temperature has a noticeable effect on the water uptake as shown in Figure 6.12.

The water uptake in a DODAC reverse micellar phase was described in terms of the dissociation of the surfactant [43]. Thus, the change in water uptake due to the change in temperature, shown in Figure 6.12, is believed to be due to the change in the degree of dissociation of DODAC. In the literature, the solubilization of biomolecules has been explained by a size exclusion mechanism, which indicates that a decrease in the water uptake results from a decrease in the size of reverse micelles, and large molecules such as proteins are excluded from the reverse micellar phase. However, from Figures 6.11 and 6.12, the water uptake and the solubilization of lysozyme show independent behavior in the DODAC reverse micellar phase. The fact that a larger water uptake at 35 °C does not get reflected in a larger solubility of lysozyme in the reverse micellar phase, although all lysozyme was removed from the aqueous phase, confirms that the extraction of the protein is due to the

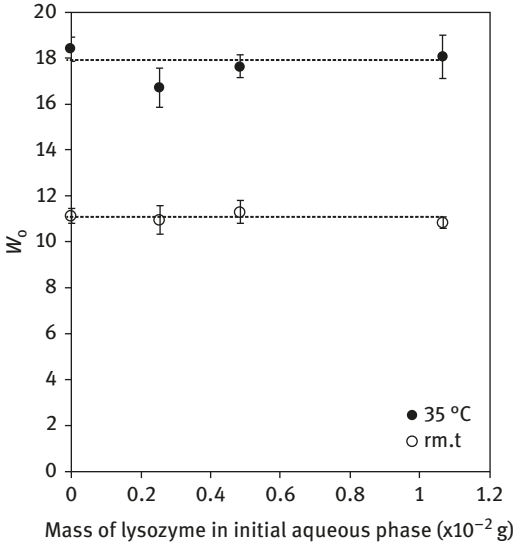

Figure 6.12: Effect of temperature of the water uptake in DODAC reverse micellar phase at 35 °C (closed symbols) and at room temperature (open symbols); $V_a = V_o = 10$ mL; initial organic phase, 100 mM DODAC, 250 mM decanol; initial aqueous phase, 0.1 M NaCl; pH = 12.0 adjusted with NaOH.

electrostatic interaction between oppositely charged protein and the surfactant head group, rather than the protein being solubilized into the water pool inside of the reverse micelles in the organic phase.

The water uptake in a DODAC reverse micellar phase was described in terms of the dissociation of ions, which has a specific hydration size [43]. The change in water uptake due to the change in temperature, shown in Figure 6.12, is believed to be due to the change in the dissociation of ions due to the change in temperature. Although the size of the reverse micelles was believed to influence the protein solubilization the reverse micellar phase in the literature, our findings suggest that the water uptake and the solubilization of lysozyme show independent behavior in the DODAC reverse micellar phase. The excess lysozyme extracted out of the aqueous phase but not being solubilized into the reverse micellar phase precipitated at the aqueous–organic interface, confirming the formation of a water-insoluble lysozyme–DODAC complex as previously reported in the literature [37–38]. Once formed, since it is water insoluble, the complex does not dissolve into the water pool of the reverse micelles or into the bulk aqueous phase.

The water uptake in the DODAC reverse micellar system was studied as a function of different types of proteins used. Similar to the findings with amino acids as described in Section 6.2, the water uptake in the reverse micellar phase was independent on the types of proteins used. Figure 6.13 shows the water uptake as a function of pH of the protein solution. Interestingly, the water uptake increased sharply at pH values greater than 12 and decreased rapidly at pH 13.5. As the concentration of DODAC and decanol was fixed in this experiment, it was assumed that a larger water uptake is due to larger reverse

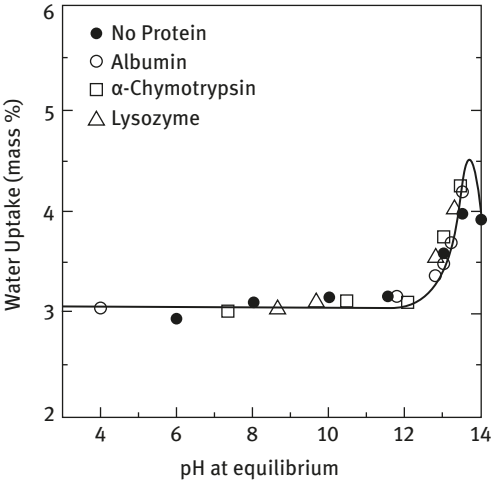

Figure 6.13: Effect of pH on the water uptake with and without the presence of proteins: initial organic phase, 100 mM DODAC, 250 mM decanol in isooctane; initial aqueous phase, 0.5 g/L protein, 100 mM NaCl.

micelles. The presence of different proteins such as albumin, α-chymotrypsin, and lysozyme showed no effect on the water uptake. If the solubilization for albumin in the reverse micellar phase was limited due to the size of the water pool, it would be expected to have a higher extraction of albumin at pH values greater than 12. However, no increase in the extraction of albumin was observed at pH values higher than 11 as shown in Figure 6.10.

The results shown in Figures 6.10 and 6.13 also confirm that the size of the water pool had minimum impact to the extraction behavior of proteins tested for our research.

6.4.3 Effect of Type and Concentration of Salts on Protein Extraction

While many research studies in the literature were conducted in terms of the ionic strength of the protein containing solution, there was limited information available that examined the effect of different counterions and co-ions on the protein extraction efficiency by reverse micellar systems. As such, we have conducted series of experiments using different types of salts in the aqueous phase and measured the protein extraction efficiency by DODAC reverse micellar system. Since the surfactant studied here was a cationic surfactant, anions are counterions and cations are the co-ions of the surfactant. Table 6.1 summarizes the extraction efficiency as a function of different co-ions. In this table, the extraction results for albumin and α-chymotrypsin using the chloride salts of sodium, potassium, and cesium are presented. As shown in this table, the protein extraction efficiency was independent on the different types of chloride

Table 6.1: Effect of co-ion on the percent extraction of albumin and α-chymotrypsin: initial organic phase, 125 mM DODAC, 250 mM decanol; initial aqueous phase, 0.5 g/L protein, pH 13.

Salt (mM)	Albumin			α-Chymotrypsin		
	NaCl	KCl	CsCl	NaCl	KCl	CsCl
100	88.5	88.0	89.0	99.5	100	99.0
300	86.0	85.3	86.5	97.0	98.0	98.0
400	85.0	84.0	84.0	95.3	94.5	95.0
500	82.0	81.9	81.5	93.0	93.0	91.8
600	79.0	78.8	80.0	91.0	90.0	89.5

salts. The protein extraction efficiency showed a decreasing trend with an increased amount of salt, which indicates salting-out effect. This indicates that the binding between the charged protein and the DODAC surfactant head was much stronger than the different co-ions present in the solution such as Na^+, K^+, and Cs^+. This was in an agreement with the ion-exchange hypotheses that the surfactant DODAC still goes through the same dissociation from its counterion, which is Cl^- for DODAC, regardless of different co-ions present, Na^+, K^+, Cs^+, and binds to the opposite change proteins in the aqueous phase. Similar phenomenon was noted in the reverse micellar studies in the literature [43–45].

The effect of different counterions on the solubilization of lysozyme was studied using an initial lysozyme solution containing 0.1 M KCl. The initial reverse micellar phase was prepared using KCl, prior to the actual extraction experiment. The pH of the initial lysozyme aqueous solution was adjusted to 12.0 ± 0.1 using either NaOH or KOH. Thus, when the pH was adjusted with KOH, the total potassium concentration in the lysozyme solution was 0.11 M. When the pH was adjusted with NaOH, the total potassium concentration in the lysozyme solution was 0.10 M. In each of these two experiments, the concentration of sodium ion in the aqueous phase was 0 and 0.01 M, respectively. Figure 6.14 shows the effect of hydroxide ion on the extraction of lysozyme in the DODAC reverse micellar phase. The solid line represents the mass of lysozyme solubilized in organic phase when the ionic strength and the pH of the aqueous phase were adjusted with NaCl and NaOH, as already presented in Figure 6.11.

As shown in Figure 6.14, when the pH was adjusted with KOH, the maximum mass of lysozyme solubilized in reverse micelles was around 0.5×10^{-2} g. However, when the pH was adjusted with NaOH, the mass of lysozyme solubilized in reverse micelles increased to about 1.08×10^{-2} g, corresponding to the results obtained with NaCl (the solid line). Even though the total amount of sodium added to the aqueous phase from the pH adjustment differs by 0.01 M, while the potassium concentration was almost constant at 0.1 M, the solubility

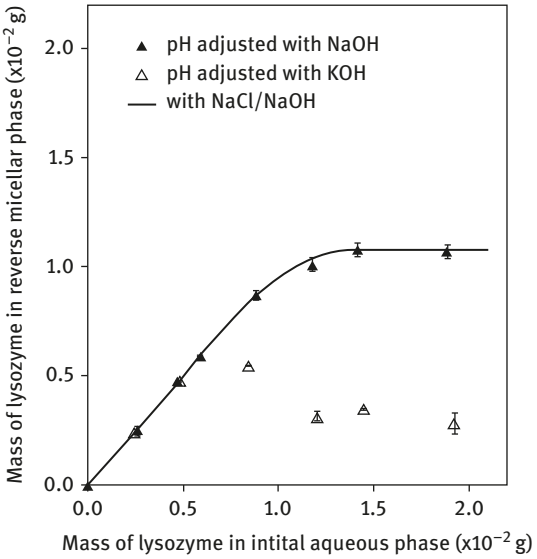

Figure 6.14: Effect of sodium and potassium ions on solubilization of lysozyme at room temperature; $V_a = V_o = 10$ mL; initial reverse micellar phase, 100 mM DODAC, 250 mM decanol; initial aqueous phase, 0.1 M KCl, pH = 12.0 adjusted with NaOH (closed symbols) or KOH (open symbols). The solid line represents the mass of lysozyme solubilized in organic phase with NaCl and NaOH shown in Figure 6.11.

limit of lysozyme increased almost twice when the pH adjustment was made with NaOH instead of KOH. From these results, one can conclude that the presence of different mixture of counterions and co-ions has a significant effect on the solubilization of lysozyme into a DODAC reverse micellar phase. In our study, the physical situation is additionally complicated by the presence of a surfactant cation and of two different aqueous phases: the bulk water and the water pool in the reverse micellar phase. As shown in Figure 6.11, the DODAC surfactant formed an insoluble moiety with lysozyme. Other cations, such as Na^+ or K^+, can replace the surfactant ion and bind with lysozyme to solubilize it into the water pool of the reverse micelles. Our experimental results show that the order in which the cations displace the surfactant from the protein moiety is $Na^+ > K^+$. This order corresponds to the Hofmeister ion series, which states that Na^+ binds more strongly with proteins than K^+ [46, 47].

The effect of sodium and calcium ions on the solubility limit of lysozyme was then studied using $CaCl_2$ and $Ca(OH)_2$ to adjust the ionic strength and the pH of the initial aqueous solution. The initial reverse micellar solution was prepared prior to the actual extraction experiments using $CaCl_2$. The initial lysozyme solution was prepared using 0.05 and 0.1 M $CaCl_2$. However, the pH adjustment using $Ca(OH)_2$ was limited by the solubility of calcium hydroxide in aqueous solution. The maximum pH that can be obtained using $Ca(OH)_2$ was about 11.0 ± 0.2. The solubilization limit of lysozyme into DODAC reverse micellar phase when the pH was adjusted with $Ca(OH)_2$ was found to be less than 0.2 g/L lysozyme in the organic phase. This result can be explained by the fact that pH was not high enough to induce a negative net surface charge on

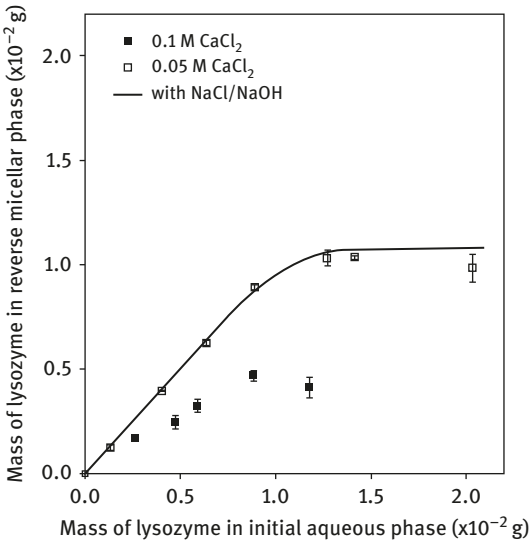

Figure 6.15: Effect of sodium and calcium ions on solubilization of lysozyme at room temperature; $V_a = V_o = 10$ mL; initial reverse micellar phase, 100 mM DODAC, 250 mM decanol; initial aqueous phase, 0.1 M $CaCl_2$ (closed symbols) and 0.05 M $CaCl_2$ (open symbols), pH = 12.0 adjusted with NaOH. The solid line represents the mass of lysozyme solubilized in organic phase with NaCl and NaOH shown in Figure 6.11.

the lysozyme. In addition, $CaCl_2$ is a strong denaturant of proteins [46], and forms insoluble calcium carboxylate salts involving the carboxylate groups of proteins [47]. In order to increase the pH to 12, an additional 0.009 M of hydroxide ion would have been required in the initial lysozyme solution. Figure 6.15 shows the equilibrium mass of lysozyme solubilized in the reverse micellar phase when the ionic strength was adjusted to 0.1 M $CaCl_2$ and the pH was adjusted initially with $Ca(OH)_2$ and then with NaOH to pH 12.0 ± 0.1. Four replicates were used to obtain these results, and the error bars indicate the 95% confidence interval. As shown in this figure, when 0.05 M $CaCl_2$ was added to the aqueous phase, the mass of lysozyme solubilized in the DODAC reverse micellar phase followed the same trend as the results observed with sodium chloride (drawn in solid line), shown in Figure 6.11.

The effect of sodium ions, introduced from the pH adjustment, on the solubility of lysozyme is again confirmed from this figure.

6.4.4 Effect of Decanol and Surfactant Concentrations on Protein Extraction

Table 6.2 shows the effect of decanol concentration on protein extraction from the initial aqueous phase in eq. (6.4) using different proteins and different NaCl concentrations. We have examined the effect of different ratio of DODAC and decanol concentration in the extraction of amino acids in Section 6.2. The conclusion from that study was that the partition coefficient of the amino

Table 6.2: Effect of decanol concentration on the percent extraction of albumin and α-chymotrypsin: initial organic phase, 100 mM DODAC; initial aqueous phase, 0.5 g/L protein, pH 13.

Decanol (mM)	Albumin	α-Chymotrypsin		
	100 mM NaCl	100 mM NaCl	400 mM NaCl	700 mM NaCl
200	86	98	91	81
250	88	99	94	78
300	86	100	95	80
350	89	100	91	78

acids depended more on the size of the water pool which increased with an increased DODAC concentration and decreased with an increased decanol concentration. In other words, the actual amount of amino acids extracted into the reverse micellar phase was constant (100% extraction) within the range of DODAC and decanol concentration tested in the study.

As shown in Table 6.2, a similar trend was observed for the extraction of proteins in that the increase in the decanol concentration did not have any effect on the protein extraction out of the initial aqueous phase. The decrease in extraction efficiency was observed when the salt concentration increased from 100 to 700 mM as shown in Table 6.2.

With the knowledge that the surfactant and cosurfactant concentration had no effect on the actual protein extraction efficiency, the effect of different solvents to form reverse micellar phase was examined. Table 6.3 presents the experimental data of the percent extraction of albumin and α-chymotrypsin along with the water uptake data for four different solvents. Neither the alcohol concentration nor the nature of the solvent had any significant effect on the extraction of the proteins studied. The different solvent did have effect on the water uptake in the organic phase. A change from isooctane to decane resulted in an increase in water uptake for both albumin and α-chymotrypsin. The results presented in this table indicates the similar finding in Section 6.2 in that the protein solubilization and the water uptake in the reverse micellar phase are independent phenomenon rather than the formation of water pool in the reverse micelles allows the proteins to be solubilized within. The actual amount or the size of the water pool seems to have less significance when compared to the pH and the type and the concentration of the salts used in the aqueous phase which showed significant effect in the protein solubilization.

The extraction efficiency summarized in Tables 6.2 and 6.3 is based on the percent protein removed from the initial protein solution after being contacted with the reverse micellar phase. Table 6.4 shows how much of the protein extracted out of the aqueous solution was in fact solubilized into the reverse

Table 6.3: Effect of different solvents on the percent extraction of albumin and α-chymotrypsin: initial organic phase, 100 mM DODAC, 250 mM decanol; initial aqueous phase, 0.5 g/L protein, 100 mM NaCl, pH 13.

Solvent type	Albumin		α-Chymotrypsin	
	Percent extraction (%)	Water uptake (mass %)	Percent extraction (%)	Water uptake (mass %)
Isooctane	88.0	3.76	97.5	3.80
Octane	89.0	3.95	99.5	3.91
Nonane	88.5	4.02	96.5	3.99
Decane	86.5	4.11	99.5	4.16

Table 6.4: Maximum mass of lysozyme solubilized in 10 mL reverse micellar phase, as a function of δ at room temperature: initial aqueous phase, 1.5 g/L lysozyme, 0.1 M NaCl, pH = 12.0 adjusted by NaOH; V_a = 10 mL.

	Mass of lysozyme solubilized in the reverse micellar phase ($\times 10^2$ g)			
δ	50 mM DODAC	80 mM DODAC	100 mM DODAC	200 mM DODAC
1	–	–	0.0	0.0
1.25	0.14	0. 14	0.58	1.08
2.5	0.15	0.63	1.08	1.08
3	0.25	0.64	1.08	1.08
4	0.07	0.08	0.15	0.10

Note: δ is the molar ratio between decanol and the DODAC.

micellar phase. The molar ratio between decanol and the DODAC was noted as δ in this table. Table 6.4 shows the equilibrium mass of lysozyme obtained in the reverse micellar phase as a function of δ. The formation of reverse micelles required the δ value of a minimum 1.25. A molar ratio of 1 between decanol and DODAC was found to be insufficient to extract lysozyme into the organic phase. In fact, for 50 and 80 mM DODAC, no water uptake was detected in the organic phase ($w_o < 0.1$). For 100 and 200 mM DODAC, even though the reverse micelles were present in the organic phase ($w_o \approx 12$), no extraction of lysozyme was observed. Wang et al. [8] reported that there is a narrow range of δ required to form DODAC reverse micelles in the organic phase. However, from Table 6.4, it is seen that the range of δ for the lysozyme extraction is even narrower than that for the formation of reverse micelles.

When δ was set at 1.25, the solubilization of lysozyme took place in the reverse micellar phase. However, a further increase in δ above the value of 3 resulted in a decrease in the lysozyme solubilization in the reverse micellar phase. When δ was set

at 4, the mass of lysozyme in the organic phase decreased dramatically to the order of about 0.1×10^{-2} g, for all surfactant concentrations. On the other hand, the lysozyme concentration in the aqueous phase was below the detection limit of the high-performance liquid chromatography (HPLC) in all cases. Depending on the amount of lysozyme actually solubilized in the reverse micellar phase, a noticeable amount of white substance was observed at the aqueous–organic interface. The phenomenon observed from the results presented in Table 6.4 is that the extraction of lysozyme in the organic phase increased with the surfactant concentration up to a limit. Once that limit is reached, a further increase in the surfactant concentration had little effect on the lysozyme extraction into the reverse micellar phase. In addition, there exists a lower and an upper limit in the decanol concentration that should be used in the organic phase to extract lysozyme.

The mass of lysozyme in the organic phase at various surfactant concentrations is depicted in Figure 6.16. As shown in this figure, no solubilization of lysozyme in the organic phase was observed at 0 mM DODAC as the change in the aqueous phase lysozyme concentration was below the HPLC detection limit. As DODAC was added to form reverse micelles, lysozyme was extracted into the organic phase. At 50 and 80 mM DODAC, the maximum values of 0.18 and 0.65×10^{-2} g lysozyme were obtained in 10 mL organic phase, respectively. A noticeable increase in the white insoluble moiety was observed at the aqueous–organic interface when the initial mass of lysozyme in the aqueous phase was increased above the saturation limit. The mass transfer of lysozyme from the aqueous phase into the organic phase was blocked by the white moiety as it forms at the aqueous-organic interface, resulting in a sudden decrease in the mass of lysozyme obtained in the organic phase. At 100 mM DODAC, a

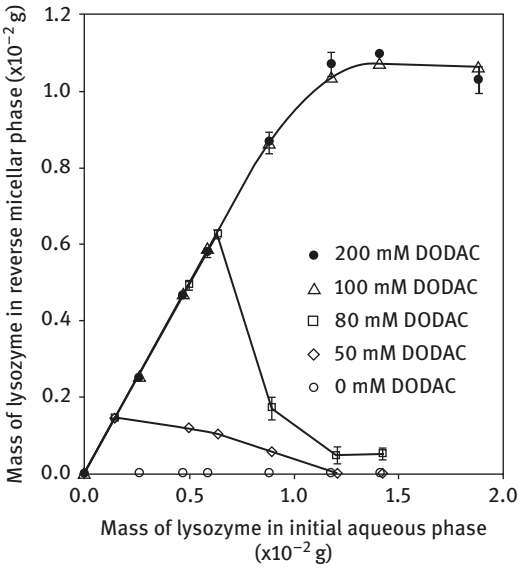

Figure 6.16: Equilibrium mass of lysozyme in DODAC reverse micellar phase at room temperature; $V_a = V_o = 10$ mL: initial reverse micellar phase, $\delta = 2.5$ in isooctane; initial aqueous phase, 0.1 M NaCl, pH = 12.0 adjusted with NaOH.

solubilization limit of 1.08×10^{-2} g lysozyme was obtained in the organic phase. However, a further increase in the surfactant concentration to 200 mM DODAC resulted in no significant change in the solubility limit. Although the water uptake in the reverse micellar phase is larger at 200 mM DODAC than at 100 mM DODAC [28, 43–45], the solubilization limit of lysozyme at these two DODAC concentrations was nearly the same. Despite the surfactant concentration, lysozyme was completely removed from the aqueous phase upon contact with DODAC. These results confirm that once the surfactant–lysozyme complex is formed, its extraction into the reverse micellar phase is independent of the water uptake. The extraction of lysozyme into a DODAC reverse micellar phase is constrained by the saturation limit of the protein, not by the water uptake, in the reverse micellar phase. This finding corresponds well to the findings reported in the literature [37–38] that the first step in extraction of a protein into the organic phase is the formation of a transferable complex between protein and surfactant molecules, which takes place with a direct contact with the protein and the surfactant during reverse micellar extraction process.

6.4.5 Conclusions

Solubilization of proteins into reverse micellar phase was a function of the pH and the type and concentration of the salt in the aqueous phase. The size exclusion theory did not describe the solubilization behavior of lysozyme into the DODAC reverse micellar phase as the water uptake did not show any correlation with the extraction efficiency of the proteins into the reverse micellar system. The interaction between the counterions of the surfactant, the types of anions present in the aqueous phase, and the overall surface charge of the protein at a given pH had the biggest impact on the protein extraction out of and into the reverse micellar system. It was found that the extraction of proteins into organic phase containing DODAC reverse micelles has a saturation limit. Depending on the type or the concentration of cations, the amount of lysozyme extracted into the organic phase varies and so does the amount of the white-insoluble complex formed at the aqueous–organic interface. While the extraction of lysozyme out of the aqueous phase showed 100%, the solubilization of lysozyme had a maximum solubility limit in the DODAC reverse micellar phase. The mass of lysozyme not solubilized into the reverse micellar phase precipitated at the aqueous–organic interface.

6.5 Reverse Micellar Extraction of Proteins Using Two Dialkyl Phosphinate

This section summarizes the use of two dialkyl phosphinate surfactants for the purification of proteins [48]. The new anionic surfactants were successfully used to extract

L-lysine as described in Section 6.3. A subsequent study by Ashrafizadeh and Khoshkbarchi showed that the extraction of the amino acid took place in a pH range wider than that observed for an AOT reverse micellar system [49]. In that study, the recovery of lysine from the R_2POONa and R_2PSSNa reverse micellar phases was performed using HCl solution in contact with the biomolecule containing reverse micellar phase. The sodium form of the surfactant undergoes an ion-exchange process in an acidic solution to form water-insoluble organic compounds, R_2POOH and R_2PSSH.

With this knowledge, a study was performed to further examine the extraction of proteins into the R_2POONa and R_2PSSNa reverse micellar phases. In this study, lysozyme was used as a model protein. The use of acetone for the lysozyme recovery from the R_2POONa and R_2PSSNa reverse micellar phases was examined. The reason for the use of acetone for lysozyme recovery, rather than using a fresh aqueous solution, was based on more recent finding that the use of polar organic solvent improved the recovery of biomolecules from the reverse micellar systems [50]. The use of strong acids such as 2 N HCl, which was used in the research of Ashrafizadeh and Khoshkbarchi, was not desirable due to the fact that such strong acid often results in a protein denaturation. In this section, the comparison of results obtained from these reverse micellar systems provides insight on the effect of different surfactant head groups on the solubilization behavior and the recovery of lysozyme.

6.5.1 Experimental Conditions

The preparation of R_2POONa and R_2PSSNa reverse micellar phases followed the same procedures described in Section 6.3.1. Once the reverse micellar solution was prepared, an aqueous solution containing target lysozyme and salt concentrations was in contact with known concentration of reverse micellar solutions. For back-extraction, an equal volume of acetone was added directly to the reverse micellar solution containing protein. The surfactant-free lysozyme was then recovered and solubilized into a fresh aqueous phase. The enzymatic activity of lysozyme in the initial and the final aqueous phases was measured using the procedure described by Davies et al. [51].

6.5.2 Effect of pH and Temperature on Lysozyme Extraction

Figure 6.17 shows the percent extraction of lysozyme defined as the percentage of lysozyme protein solubilized into the reverse micellar phase compared to the amount in the initial aqueous phase. For simplicity, R_2POONa and R_2PSSNa are referred to as POO and PSS in the figures. For R_2POONa reverse micellar phase, the lysozyme initially added to the aqueous phase was all extracted into the reverse micellar phase with pH ranging from 6 to 10. The extraction efficiency decreased at pH above 11 (the p*I* of lysozyme). At pH 12, only 20% of the initial lysozyme was extracted

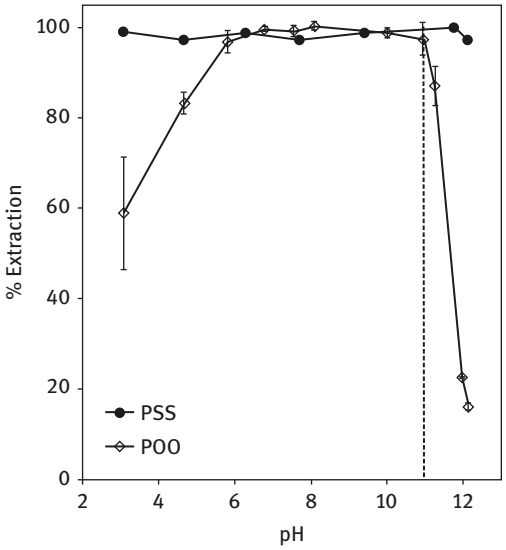

Figure 6.17: Effect of pH on extraction of lysozyme into R_2PSSNa (closed symbols) and R_2POONa (open symbols) reverse micellar phases; $V_a = V_o = 10$ mL; initial reverse micellar phase, 100 mM surfactant, 150 mM decanol; initial aqueous phase, 0.5 g/L lysozyme, 0.1 M NaCl, pH adjusted with NaOH. The dotted line represents the p*I* of lysozyme.

into the reverse micellar phase. This is due to the change in the surface charge of lysozyme. In addition, the extraction efficiency decreased when the pH decreased below 5. This phenomenon is due to the change in the counterions of the surfactant. Increasing hydrogen ions in the aqueous phase results in the ion exchange between Na^+ (counterion of the surfactant) and H^+. The acidic form of surfactant, R_2POOH, does not form reverse micelles. As a result, the percent extraction of lysozyme decreased as the number of surfactant molecules available to form reverse micelles decreased.

Compared to the R_2POONa reverse micellar system, the extraction of lysozyme into an R_2PSSNa reverse micellar phase was independent of the pH of the aqueous phase. Almost 100% mass of initial lysozyme was solubilized into reverse micellar phase even at pH 12. The electrostatic interaction theory cannot explain this phenomenon. Another noticeable result shown in this figure is that a 100% extraction of lysozyme was obtained with the dithiophosphinate surfactant at pH lower than 3. Even though the R_2PSSNa surfactant undergoes ion exchange to form an acidic form at this pH, the percent extraction remained at 100%. The different pH effect on the extraction behavior of lysozyme, observed between R_2POONa and R_2PSSNa reverse micellar phases, is explained by the presence of the two different surfactant head groups. The extraction of amino acids into the R_2PSSNa was much higher than the R_2POONa reverse micellar solutions as previously discussed in Section 6.3. The electronegativity of the S atom in the organophosphorus compounds which is higher than that of the O atom [27] could be a reason for such high extraction efficiency observed using the R_2PSSNa reverse micellar system. Another reason for such high extraction efficiency could be the sulfur interaction with lysozyme, which contains

four disulfide bonds [52]. In peptides, a covalent bond occurs when a disulfide linkage, R-S-S-R, is formed between two cysteine residues. The disulfide bonds in two different peptide chains link the otherwise separate chains together [53]. Thus, the presence of sulfur head group in the surfactant could influence the disulfide bond in the lysozyme that led to a strong affinity between the surfactant and the protein.

Figure 6.18 shows the mass of lysozyme solubilized in a 100 mM R_2POONa reverse micellar phase as a function of the initial mass of lysozyme in the aqueous phase at room temperature (21–23 °C), and a constant temperature of 35 °C. As shown in this figure, the mass of lysozyme solubilized in the reverse micellar phase increased with an increase in the initial mass of lysozyme in the aqueous phase until it reached a solubilization limit in the reverse micellar phase. At 35 °C, a limit of 0.92×10^{-2} g lysozyme was observed in a 10 mL reverse micellar solution. The mass of the solubilized lysozyme in the reverse micellar phase remained at this limit, even though the initial mass of lysozyme in the aqueous phase was higher than this value. On the other hand, the mass of lysozyme removed from the aqueous phase, on the right-hand side in the figure, showed a complete removal of proteins from the aqueous phase after being in contact with the surfactant. The difference between the mass removed from the aqueous phase and mass solubilized into the reverse micellar phase is the mass of lysozyme precipitated at the aqueous–organic interface. Formation of a white

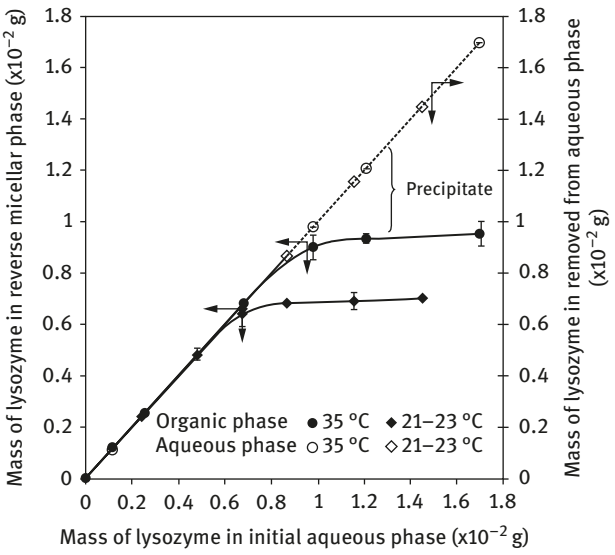

Figure 6.18: Equilibrium mass of lysozyme extracted in R_2POONa reverse micellar phase (closed symbols) and mass of lysozyme removed from aqueous phase (open symbols) at 35 °C and at room temperature (21–23 °C); $V_a = V_o = 10$ mL; initial reverse micellar phase, 100 mM R_2POONa, 150 mM decanol; initial aqueous phase, 0.1 M NaCl, pH = 6.0 ± 0.5 adjusted with NaOH.

precipitate became more noticeable when the initial lysozyme mass in the aqueous phase was higher than the solubilization limit found in the reverse micellar phase.

The change in temperature between 35 °C and room temperature showed an increase in the solubilization limit of lysozyme in the 100 mM R_2POONa reverse micellar phase. At room temperature, the solubilization limit of lysozyme in 10 mL reverse micellar solution was 0.68×10^{-2} g, compared to the limit of 0.92×10^{-2} g obtained at 35 °C. The white precipitate became more noticeable when the initial mass of lysozyme in the aqueous phase was higher than the indicated saturation limit. In comparison, as shown in Figure 6.14, the study of the solubilization behavior of lysozyme into a cationic reverse micellar system, using DODAC, showed that the temperature change from room temperature to 35 °C did not have any effect on the solubilization limit.

For both R_2POONa and DODAC reverse micellar systems, a complete removal of lysozyme was obtained when the pH of the aqueous solution was set below the p*I* of the anionic surfactant and higher than the p*I* of the cationic surfactant. A formation of a white precipitate at the aqueous–organic interface was observed in both reverse micellar systems when the initial lysozyme concentration was higher than the previously established solubilization limit in the reverse micellar phase. This phenomenon indicates that the extraction of lysozyme from the aqueous phase is due to the electrostatic interactions between the oppositely charged lysozyme and the surfactant head group. The solubilization behavior of lysozyme into a reverse micellar system, and the formation of white precipitate at the interface, however, cannot be explained using the electrostatic mechanism alone.

6.5.3 Effect of Cosurfactant and Surfactant Concentration on Lysozyme Extraction into R_2POONa Reverse Micellar Phase

Figure 6.19 shows the effect of surfactant concentrations on the solubilization limit of lysozyme in the organic phase containing 50–200 mM R_2POONa. For simplicity, R_2POONa was denoted as POO in the figure. The molar ratio of decanol to surfactant, denoted as δ, was set at 1.5. As shown in this figure, the solubilization limit of lysozyme was observed in each reverse micellar phase. At 50 mM R_2POONa, the largest value of the solubilized lysozyme was about 0.25×10^{-2} g in a 10 mL reverse micellar solution. Upon contact with the surfactant, all lysozyme was extracted out of the aqueous phase, which is indicated as the 100% extraction line in the figure. Thus, a difference in mass was found between the mass removal from the aqueous phase and the mass solubilization into the reverse micellar phase. At 50 mM R_2POONa, the mass of lysozyme solubilized into the reverse micellar phase was less than the 100% extraction line, and all samples showed that a solid phase was formed between the aqueous phase and the organic phase.

As also shown in Figure 6.19, an increase in the surfactant concentration increased the solubilization limit of lysozyme in the R_2POONa reverse micellar system. At 80 mM

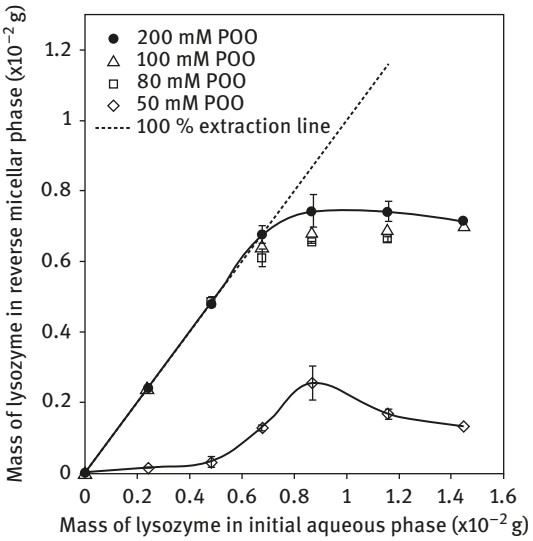

Figure 6.19: Equilibrium concentration of lysozyme in various R_2POONa reverse micellar phases at room temperature; $V_a = V_o = 10$ mL; initial reverse micellar phase, $\delta = 1.5$; initial aqueous phase, 0.1 M NaCl, pH = 6.0 ± 0.5 adjusted with NaOH.

R_2POONa, the mass of lysozyme solubilized in the reverse micellar phase reached up to 0.60×10^{-2} g in a 10 mL reverse micellar solution. The lysozyme precipitate was observed at the interface when the initial lysozyme concentration exceeded this value. However, a further increase in the surfactant concentration from 80 to 100 mM resulted only in a marginal increase in the lysozyme solubilization in the reverse micellar phase. At 200 mM R_2POONa, a limit of 0.75×10^{-2} g lysozyme was obtained in 10 mL reverse micellar solution. A similar behavior was observed for the extraction of lysozyme in a DODAC reverse micellar phase (Table 6.4). The solubilization limit of lysozyme increased with an increase in the surfactant concentration up to a limit, and a further increase from this limit in the surfactant concentration did not increase the solubilization limit of lysozyme into an R_2POONa reverse micellar phase.

The water uptake values in a 100 and 200 mM R_2POONa reverse micellar phase were both around 37 ± 5 mol of water per mole of surfactant. In other words, the increase in the surfactant concentration increases the water concentration in the organic phase. Similar to the DODAC reverse micellar system reviewed in Section 6.3, the water content did not have any effect on the lysozyme solubilization into the R_2POONa reverse micellar phase. Instead, lysozyme precipitated at the aqueous–organic interface when the saturation limit of protein was reached in the reverse micellar phase.

6.5.4 Solubilization of Lysozyme into an R_2PSSNa Reverse Micellar Phase

Figure 6.20 shows the effect of surfactant concentration and different ionic strength on the lysozyme extraction into the R_2PSSNa reverse micellar phase. The mass of lysozyme

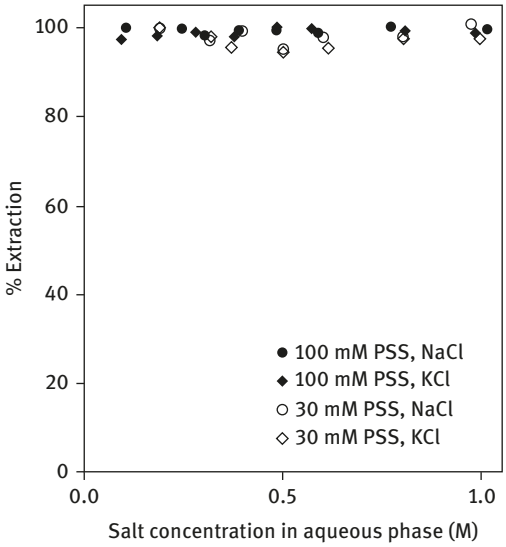

Figure 6.20: Effect of ionic strength of aqueous phase on extraction of lysozyme into 100 mM (closed symbols) and 30 mM (open symbols) R_2PSSNa reverse micelles at room temperature: $V_a/V_o = 1$; initial reverse micellar phase, $\delta = 1.5$; initial aqueous phase, 0.5 g/L lysozyme, pH = 6.0 ± 0.5 adjusted with either NaOH or KOH.

solubilized in the organic phase increased linearly with the increase in the initial mass of lysozyme in the aqueous phase, that is, up to 15×10^{-2} g. Thus, the reverse micellar solution containing 30 mM R_2PSSNa can extract up to 15 g/L lysozyme. This is about 21 times higher than the amount extracted into an R_2POONa reverse micellar system. Similarly, a complete extraction of lysozyme into the 80 and 100 mM R_2PSSNa reverse micellar phases was obtained, that is, up to 15 g/L. The change in temperature from room temperature to 35 °C had no effect, that is, 100% extraction in the organic phase containing 30 mM or more R_2PSSNa reverse micelles up to the initial lysozyme concentration of 15 g/L. These results, together with the phenomenon shown in Figure 6.8, clearly indicate that the biomolecules such as amino acid and lysozyme have a strong affinity to the sulfur containing surfactant. Further studies could be carried out to test the effect of the sulfur interaction between the surfactant and lysozyme by conducting independent experiments using glutathione or cysteine to block the sulfur head group of R_2PSSNa. These studies, however, were beyond the scope of this work.

6.5.5 Effect of Volume Ratio for the Lysozyme Extraction

Table 6.5 summarizes the equilibrium concentrations of lysozyme obtained in the reverse micellar phase at various volume ratios between the aqueous and organic phases (V_a/V_o). Using 0.1 M NaCl, the concentration of lysozyme in the reverse micellar phase reached up to 0.2 g/L using the 100 mM R_2POONa reverse micellar phase at a volume ratio of 2. However, a further increase in the volume ratio resulted in a noticeable decrease in the lysozyme concentration in the organic phase. At $V_a/V_o = 6$, zero solubilization of lysozyme was obtained in the reverse micellar phase. On the other

Table 6.5: Concentration of lysozyme obtained in an R_2POONa reverse micellar phase as a function of volume ratio between aqueous and organic phases; initial reverse micellar phase: $\delta = 1.5$; initial aqueous phase, 0.1 g/L lysozyme, 0.1 M NaCl or KCl, no pH adjustment in the aqueous phase.

V_a/V_o	Lysozyme concentration in reverse micellar phase (g/L)			
	100 mM R_2POONa		200 mM R_2POONa	
	NaCl	KCl	NaCl	KCl
1	0.10	0.10	0.10	0.10
2	0.20	0.20	–	–
3	0.21	0.30	0.29	0.30
4	0.08*	0.39	0.40	0.39
5	0.02*	0.50	0.48	0.47
6	0*	0.19*	0.37*	0.60
7	0*	0*	0.35*	0.67

* No lysozyme was detected in the aqueous phase after extraction, and a white precipitate was observed at the aqueous-organic interface.

hand, the concentration of lysozyme in the aqueous phase was below the HPLC detection limit, indicating a 100% removal of the protein from the aqueous phase. Thus, the loss of protein resulted in the formation of a white precipitate at the aqueous–organic interface. In contrast, from Figure 6.18, the solubilization limit of lysozyme into a 100 mM R_2POONa reverse micellar phase was around 0.67 g/L at room temperature.

Also shown in Table 6.5, the lysozyme concentration in the reverse micellar phase showed a higher value when 0.1 M KCl was used in the initial lysozyme solution, instead of 0.1 M NaCl. Using KCl, the lysozyme concentration in the 100 mM R_2POONa reverse micellar phase reached up to 0.5 g/L at $V_a/V_o = 5$. At the same volume ratio, using 0.1 M NaCl, the lysozyme concentration in the organic phase was only 0.02 g/L. The difference in the solubilization behavior of lysozyme due to the presence of different cations is believed to be due to the ion exchange of the counterions of the anionic surfactant, R_2POONa. The $R_2POO^-K^+$ reverse micellar phase extracted more lysozyme than the $R_2POO^-Na^+$ reverse micellar phase. As depicted in Table 6.5, an increase in the surfactant concentration to 200 mM R_2POONa caused an increase in the lysozyme concentration in the reverse micellar phase. At a volume ratio of 4, using 0.1 M KCl lysozyme solution, the lysozyme concentration in the organic phase reached 0.67 g/L, which is close to the solubilization limit shown in Figure 6.19. The results shown in Table 6.5 suggest that the important factor for the lysozyme solubilization into R_2POONa reverse micellar phase is not the concentration, but the amount of salt in contact with the surfactant. By having a $V_a/V_o = 4$, for an aqueous solution containing 0.1 g/L lysozyme and 0.1 M NaCl, the amount of sodium ions in contact with R_2POONa was four times as much as the case of a solution containing 0.4 g/L lysozyme and 0.1 M NaCl in contact with an equal volume

of organic phase. This interesting phenomenon suggests that the protein extraction depends on the establishment of a chemical equilibrium that affects the phase equilibrium. The finding that the volume ratio has an effect on the reverse micellar extraction of protein has not been previously recorded in the literature.

In order to test the hypothesis of the salt effect in the volume ratio experiments, the extraction efficiency of lysozyme into a 100 mM R_2POONa reverse micellar phase was examined as a function of the salt concentration with an aqueous phase in contact with an equal volume of the organic phase. The initial lysozyme concentration was set at 0.1 g/L, and the decanol concentration in the reverse micellar phase was set at 150 mM. As expected, the extraction efficiency of lysozyme into the 100 mM R_2POONa reverse micellar phase was close to 100% at a range between 0.1 M KCl and 0.6 M KCl. As the KCl concentration further increased to 0.8 M, the percent extraction into the reverse micellar phase decreased. However, when NaCl was used in the aqueous phase, instead of KCl, more noticeable decrease in the extraction efficiency was obtained with the increase in the salt concentration. At 0.5 M NaCl, the extraction efficiency of the lysozyme solution was only about 65%. Further increase in the NaCl concentration to 0.6 M resulted in an extraction efficiency of about 40% compared with the 100% efficiency obtained with 0.6 M KCl. The results showed that the extraction efficiency did not decrease as much with 200 mM surfactant at a higher salt concentration compared to the same condition tested using 100 mM surfactant. Even though an increase in the surfactant concentration did not have any significant effect on the saturation limit of lysozyme, as shown in Figure 6.19, the increase in the surfactant concentration in the organic phase allowed a better tolerance to an increase in the salt concentration and produced higher extraction efficiency.

Table 6.6 summarizes the effect of volume ratio on the extraction of lysozyme into an R_2PSSNa reverse micellar phase. The extraction of lysozyme into an R_2PSSNa reverse micellar phase was independent of the volume ratio between the aqueous and the organic phase. Closed to 100% extraction of lysozyme was obtained at all volume ratios tested. Figure 6 shows the effect of

Table 6.6: Concentration of lysozyme obtained in R_2PSSNa reverse micellar phase as a function of volume ratio between aqueous and organic phases; initial reverse micellar phase: $\delta = 1.5$; initial aqueous phase, 0.1 g/L lysozyme, 0.1 M NaCl or KCl, no pH adjustment in aqueous phase.

V_a/V_o	Lysozyme concentration in reverse micellar phase (g/L)			
	30 mM R_2PSSNa		100 mM R_2PSSNa	
	NaCl	KCl	NaCl	KCl
1	0.10	0.10	0.10	0.09
3	0.30	0.28	0.29	0.30
5	0.48	0.50	0.47	0.50
7	0.70	0.70	0.67	0.70

the type and the concentration of salts on the extraction efficiency of lysozyme into an R_2PSSNa reverse micellar phase. Within the experimental error, 100% extraction efficiency was obtained in the salt concentration range between 0.1 and 1.0 M. The use of sodium and potassium cations had negligible effect on the extraction efficiency, indicating a strong affinity of the lysozyme to the R_2PSSNa reverse micelles.

6.5.6 Lysozyme Recovery from Reverse Micellar Systems

The lysozyme-containing reverse micellar samples were contacted with an equal volume of the acetone. Table 6.7 shows the percent recovery of lysozyme from the R_2POONa and R_2PSSNa reverse micellar samples. The percent recovery of lysozyme from a 100 mM R_2POONa reverse micellar phase was about 60% when the volume ratio varied within 1–3. In comparison, the percent recovery of lysozyme from the R_2PSSNa reverse micellar phase was only 13% at V_a/V_o=1 and decreased dramatically to almost zero percent at V_a/V_o = 3. The enzymatic activity of the recovered lysozyme from an R_2POONa reverse micellar phase showed about 45,000 ± 5,000 units/mg protein. The activity of the lysozyme in the initial aqueous solution before contact with the organic phase was 48,000 ± 5,000 units/mg protein. In comparison, the lysozyme recovered from R_2PSSNa reverse micellar phase showed an activity of less than 10,000 units/mg protein. From these results, it is concluded that the solubilization of lysozyme into an R_2PSSNa reverse micellar phase was due to the sulfur interactions between surfactant and the protein, and such strong affinity of lysozyme to the R_2PSSNa surfactant resulted in a significant decrease in the lysozyme recovery. Although it might be of interest to perform experiments contacting directly R_2PSSNa with lysozyme to measure the change in the enzyme activity, these studies were considered to be beyond the scope of this work. For chemical engineering purposes, it was concluded that R_2PSSNa is not a useful surfactant to purify lysozyme.

Table 6.7: Recovery of lysozyme as a function of the volume ratio between aqueous and organic phases: 0.1 g/L lysozyme, 0.1 M NaCl or KCl.

		% Recovered	
V_a/V_o	$C_{Lys,\ o,eq\ (g/L)}$	100 mM R_2POONa	30 mM R_2PSSNa
1	0.1	60 ± 10	13 ± 1
2	0.2	65 ± 10	8 ± 1
3	0.3	58 ± 10	<1

6.5.7 Conclusion

A solubilization limit of lysozyme was observed in the R_2POONa reverse micellar phase. The use of acetone to recover lysozyme from the R_2POONa reverse micellar gave an efficiency of about 60%. The presence of sulfur group in the R_2PSSNa surfactant resulted in a strong affinity of lysozyme to the surfactant, and the small amount of recovered lysozyme from the R_2PSSNa reverse micellar phase showed a significant decrease in the enzymatic activity. The effect of volume ratio shown in the R_2POONa reverse micellar extraction suggests that the solubilization of lysozyme into a reverse micellar phase is in fact determined by a chemical equilibrium that affects the phase equilibrium. A further study on the formation of a white precipitate at the aqueous–organic interface is in progress to relate the solubilization limit of protein in a reverse micellar phase to the formation of an insoluble lysozyme–surfactant complex.

6.6 Mechanism of Lysozyme Solubilization into Reverse Micellar Phase Using AOT

This section summarizes the research work to further examine the precipitation behavior of proteins using AOT reverse micellar system [54]. In literature, electrostatic interaction, interfacial kinetics [2–7], the size of water pool in the reverse micelles [30–36], and type of mixing [38] are found to have a significant effect on the precipitating behavior of proteins at the aqueous–organic interface. Some researchers reported that the formation of white precipitate at the aqueous and organic phase interface reduced the extraction efficiency of the proteins into the reverse micellar systems [3, 40–41]. As discussed in Sections 6.4 and 6.5, the protein solubilization using lysozyme as a model protein also found to have a maximum level. Once that solubilization limit is reached, the lysozyme extracted from the aqueous phase precipitates at the aqueous–organic interface, which we believed to be due to the formation of the protein–surfactant water-insoluble complex. The protein–surfactant complex which precipitated at the interface was viewed as an undesirable product, since the protein was thought to be denatured [55]. Attempts were made to avoid the formation of a protein–surfactant complex by using new surfactants to form the reverse micellar phases [38, 56].

Even though the technology was first suggested many years ago, reverse micellar extraction still suffered from poor recovery efficiency and protein loss at the aqueous–organic interface. As such, our research focused on better understanding of the white precipitate formed at the aqueous–organic interface along with the solubilization of the proteins in the reverse micellar phase. To do this work, we selected lysozyme as a model protein and AOT for reverse micellar system. The reason for this selection was to avoid any denaturing of protein due to a high pH which is required for lysozyme to be extracted into the DODAC reverse micellar system. The protein denaturing caused by

the high pH could also be a cause for such protein precipitation, which we wanted to avoid. Assuming that the white precipitate at the interface is protein–AOT complex which is insoluble either in the aqueous phase and in the reverse micellar phase, series of experiments were performed to extract the lysozyme from the aqueous phase using either reverse micellar phase or by direct addition of the AOT containing aqueous solution without an organic phase to form reverse micelles. The solubilization of the white precipitate in AOT containing reverse micellar phase was also studied in this research. A comparison of solubilization of the lysozyme–surfactant complex in reverse micelles with the direct extraction of lysozyme into a reverse micellar phase suggested a mechanism to explain the latter process.

6.6.1 Experimental Conditions

An organic phase containing a calculated amount of AOT and an aqueous phase containing a measured amount of lysozyme were prepared for the reverse micellar extraction experiments. For the direct precipitation method, an aqueous solution containing AOT was added directly to the lysozyme containing aqueous phase. No pH adjustment was made to the initial AOT or lysozyme containing aqueous solutions. The solubility of AOT in water was reported to be 15 g/L or 33.8 mM in the temperature range from 20 to 70 °C [57]. The critical micelle concentration of AOT in water is in the range from 2.5 to 4.1 mM at 25 °C [58]. The initial concentration of AOT in the lysozyme solution was fixed between 0.02 and 1.5 mM, in order to avoid the formation of micelles. As soon as the AOT solution was added, the insoluble lysozyme–AOT complex was formed. The lysozyme–ligand complex was recovered through centrifugation.

For the measurement of the solubility product of the lysozyme–AOT complex, the lysozyme–AOT complex formed by direct addition of AOT obtained by centrifugation was dispersed in fresh distilled water. The mixture was stirred for 24 h at room temperature. An excess solid phase was visible in the bottom of the test tube. The concentrations of lysozyme and AOT in the aqueous phase were measured after filtering the solution through a 0.45 μm filter.

The analytical methods for the lysozyme concentrations in the aqueous phase and in the reverse micellar phase as well as the enzymatic activity in the aqueous phase before and after being in contact with or direct addition to the reverse micellar phase were measured following the same procedures described in Section 6.4.1.

6.6.2 Reverse Micellar Extraction of Lysozyme as a Function of AOT Concentration

Figure 6.21 shows the concentration of lysozyme in the reverse micellar phase as a function of the initial lysozyme concentration in the aqueous phase. As the

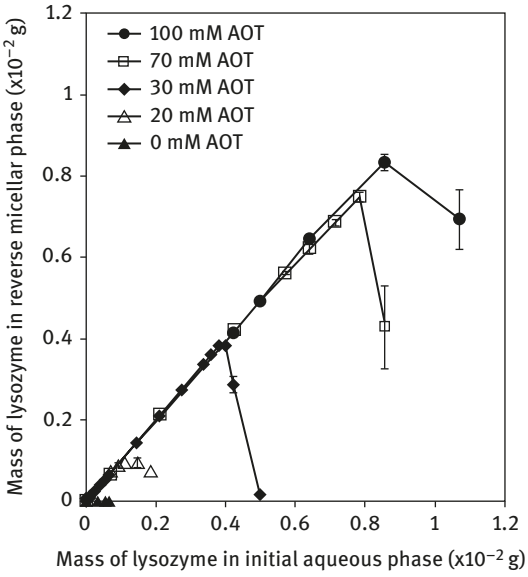

Figure 6.21: Solubilization of lysozyme into AOT reverse micellar phases; initial aqueous phase, 0.1 M NaCl, pH = 6.0 ± 0.5 adjusted with NaOH; initial volumes of aqueous and organic phases = 10 mL.

surfactant concentration in the organic phase increased, the amount of lysozyme solubilized into the reverse micellar phase increased. For the case of 0 mM AOT reverse micellar phase, no lysozyme was solubilized in the organic phase, confirming that lysozyme was insoluble in isooctane. At 20 mM AOT, the maximum concentration of lysozyme in the reverse micellar phase was 0.09 mM. The samples prepared with an aqueous phase containing 0.1–0.15 mM lysozyme showed a lysozyme concentration of 0.09 mM in the organic phase, indicating that this is the saturation limit of lysozyme in the 20 mM AOT reverse micellar phase. With an initial lysozyme concentration of 0.18 mM, the reverse micellar phase contained about 0.07 mM lysozyme. On the other hand, the equilibrium lysozyme concentration in the aqueous phase after contact with the reverse micellar phase was below the detection limit of HPLC for all samples, indicating essentially the complete removal of lysozyme from the aqueous phase. The lysozyme removed from the aqueous phase but not solubilized into the reverse micellar phase formed a white precipitate at the aqueous–organic interface.

An increase in AOT concentration in the organic phase further increased the solubility limit of lysozyme in the AOT reverse micellar phase. At 30 mM AOT, the extraction of lysozyme into the reverse micellar phase was complete up to an initial lysozyme concentration of 0.38 mM. The samples prepared with an aqueous phase containing 0.5 mM lysozyme resulted in a sudden decrease in the lysozyme concentration in the 30 mM AOT reverse micellar phase. Similarly, a solubilization limit of lysozyme in the 70 and 100 mM AOT reverse micellar phase was 0.75 and 0.83 mM, respectively. When the initial lysozyme concentration in the aqueous phase was greater than the saturation limit value, a noticeable decrease in the lysozyme

concentration in the reverse micellar phase was obtained, and a white precipitate at the aqueous–organic interface was observed. A similar phenomenon was observed in a previous study using an AOT [36].

6.6.3 Solubilization Mechanism of Lysozyme into a Reverse Micellar Phase

Based on the results in Figure 6.21, and based on the previous findings in the literature [37–38], we proposed a mechanism of lysozyme extraction into a reverse micellar phase as follows:

i. Upon contact, lysozyme forms a complex with the ligand due to electrostatic interactions.
ii. The lysozyme–AOT complex has a low solubility in water and isooctane, since no solubilization of lysozyme was observed in the pure isooctane phase as shown in Figure 6.21.
iii. The complex solubilizes in a reverse micellar phase if present; otherwise, the complex remains as solid.
iv. The solubilization of the lysozyme–AOT complex takes place until the saturation limit of lysozyme in the reverse micellar phase is reached. The excess lysozyme–AOT complex remains at the aqueous–organic interface.

In order to verify this hypothesis, two-step experiments were performed. First, the lysozyme was directly precipitated from the aqueous phase using AOT as a precipitation ligand. This precipitate was then solubilized into reverse micellar phases containing different concentrations of AOT.

First, the precipitation of lysozyme was performed using an initial lysozyme aqueous solution containing 0.15–5 g/L (0–0.36 mM) lysozyme. No pH and salt concentration adjustment was made to the lysozyme solution. Figure 6.22 shows the pH of the initial lysozyme aqueous solution. The pH of the lysozyme solution, containing buffer with the commercial lysozyme, decreased from 5.8 to 4.2 as the lysozyme concentration increased from 0.01 to 0.36 mM. Two sets of experiments were performed, and the difference in the pH between the replicates was about ±0.1.

An aqueous phase containing AOT was then pipetted into the initial lysozyme aqueous solution to form a lysozyme–AOT precipitate. Figure 6.23 shows the percent removal of lysozyme from the aqueous solution as a function of the molar ratio, R, between AOT and lysozyme initially added to the solution. Increasing the molar ratio increased the percent removal until a mole ratio of about 10, at which 100% removal of lysozyme was obtained. When R was greater 10, the excess AOT remained in the aqueous phase. When R was less than 10, the concentration of AOT remaining in the solution was below the detection limit of HPLC, indicating that all of the ligand added

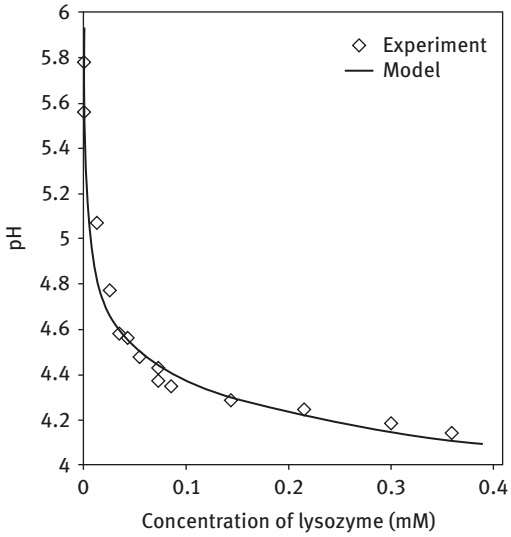

Figure 6.22: Initial pH of the aqueous solution as a function of lysozyme concentration at room temperature.

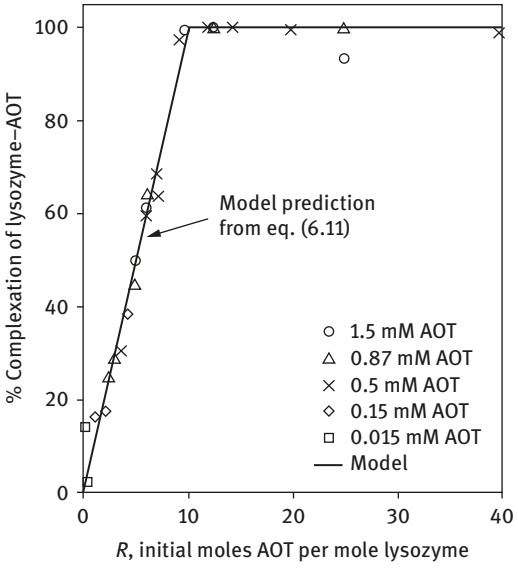

Figure 6.23: Percent of lysozyme precipitated with AOT: no salt added and no pH adjustment.

to the solution formed lysozyme–ligand complex and precipitated. The linear trend line in Figure 6.23 indicates that the complete removal of lysozyme is obtained at a molar ratio of 10. In other words, 1 mol of precipitated lysozyme was complexed with 10 mol of AOT.

Figure 6.24 shows the equilibrium pH after the lysozyme–ligand complex was formed. The pH of the solution increased as more lysozyme was removed from the

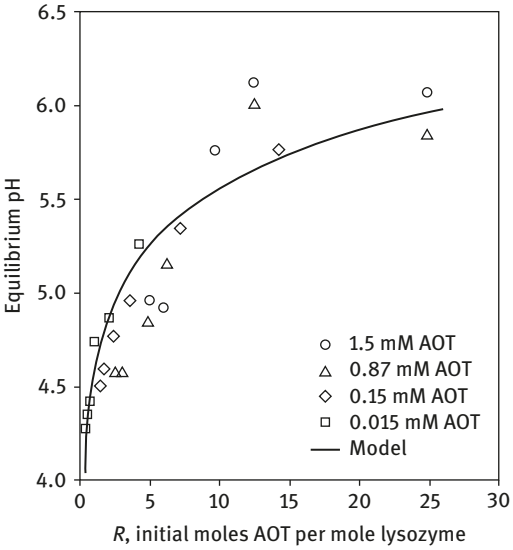

Figure 6.24: Equilibrium pH of the aqueous phase upon removal of lysozyme as an insoluble lysozyme–AOT complex: no salt added and no pH adjustment.

aqueous phase. When lysozyme was removed completely ($R \geq 10$), the excess ligand remained in the solution, and the pH was approximately 6.

Once the dried lysozyme–ligand complex was obtained, it was added to an aqueous phase containing 0.1 M NaCl and contacted with an equal volume of an isooctane phase containing 5–100 mM AOT. The mixture was stirred vigorously for 72 h to ensure the complete solubilization of lysozyme–AOT complex. After a phase separation of 12 h, the organic and aqueous phase samples were collected for lysozyme analysis. Figure 6.25 shows the concentration of lysozyme achieved in an AOT reverse micellar phase using lysozyme–ligand complex, compared with the reverse micellar extraction result from Figure 6.21. The error bars indicate 95% confidence interval.

As shown in Figure 6.25, for both experiments, the concentration of lysozyme increased in the reverse micellar phase as the concentration of AOT increased. For the reverse micellar extraction, duplicate results showed less than 1% standard deviation, and the error bars are not visible in the figure indicating the excellent reproducibility of data. For the solubilization of the lysozyme–AOT complex into the reverse micellar phase, the 95% confidence interval was more noticeable. This is believed to be due to the vigorous stirring and the time taken to solubilize the dry lysozyme–ligand complex into a reverse micellar phase, which could cause physical changes to the lysozyme. Nevertheless, the concentration of lysozyme in the reverse micellar phase obtained by solubilizing the lysozyme–AOT complex showed the same trend as the reverse micellar extraction experiment. On the other hand, the lysozyme concentration in the aqueous phase was below the detection limit of the HPLC, confirming the insolubility of lysozyme–AOT complex in the aqueous phase. Based on this

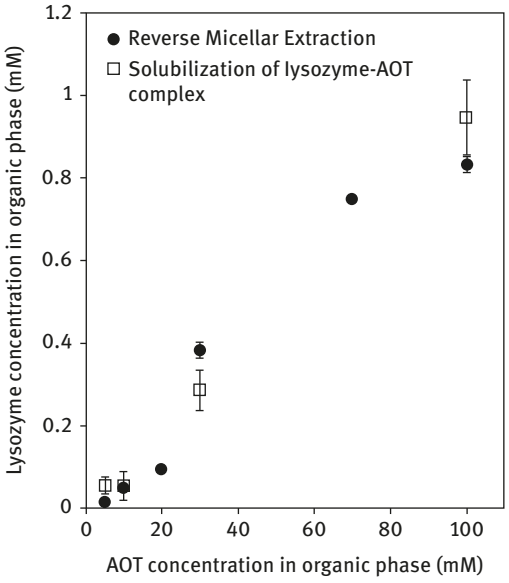

Figure 6.25: Concentration of lysozyme in AOT reverse micellar phase initially introduced as insoluble lysozyme–AOT complex and extracted from an aqueous phase using a reverse micellar phase.

result, we believe that the mechanism for the reverse micellar extraction of lysozyme consists of two steps: first, the formation of the water-insoluble lysozyme–AOT complex that precipitates out of the aqueous phase and then the solubilization of this lysozyme–AOT complex in the reverse micellar phase. Once the reverse micellar phase reaches the saturation limit, as shown in Figure 6.21, the lysozyme –AOT complex remains as a precipitate at the interface.

6.6.4 Modeling of Lysozyme–AOT Complex Formation

For modeling, the term *ligand* is used here for AOT because it was used as a ligand to form insoluble compound rather than as a surface-active agent. The term, *crystallized lysozyme*, indicates the bulk lysozyme as obtained from the lysozyme vendor. The *lysozyme–ligand complex* indicates the white-insoluble complex formed upon the addition of AOT to the initial lysozyme aqueous solution, and *ligand-free lysozyme* indicates the AOT-free solid lysozyme precipitated with acetone.

The model proposed here is based on the following assumptions:

1. The commercially available crystallized lysozyme contains hydrochloric acid (chlorohydrate compounds). Thus, the positively charged lysozyme has chloride ions as counterions in an aqueous phase.
2. Lysozyme forms an insoluble complex when associated with a well-defined number, Z, of anionic ligand residues. Lysozyme complexed with less than Z number of ligands is soluble in the aqueous phase.

3. No inorganic salts are removed from the aqueous phase with the insoluble lysozyme–ligand complex.
4. With hydrogen ion rather than sodium as its counterion, AOT is insoluble in water.
5. Sodium acetate and sodium chloride are fully ionized in lysozyme solution.

Assumption (1) above is based on a study of the variation of pH of the solution as lysozyme is dissolved in water as shown in Figure 6.22. The nature of the crystallized lysozyme depends on the type of acid solution used in the crystallization process [59]. It was assumed that hydrochloric acid was used to precipitate with the commercial lysozyme. Assumption (2) is based on the results shown in Figure 6.21. When the lysozyme was in excess, all added AOT formed an insoluble complex with the lysozyme, and the concentration of surfactant in the aqueous phase was negligible. When AOT was in excess, all lysozyme was removed from the aqueous phase. Thus, the insoluble complex forms only when a mole of lysozyme binds with Z moles of ligand. Assumption (3) is based on the results of the sodium and chloride ion balances before and after the formation of the insoluble complex. When measured with atomic absorption spectroscopy and ion chromatography, the change in the sodium and chloride ion concentrations, before and after the formation of lysozyme–ligand insoluble complex, was undetectable within experimental error. Assumption (4) is suggested by the pH change in the aqueous phase upon the addition of AOT solution, as shown in Figure 6.24.

The second step in the modeling was to estimate the surface charge of the protein. For lysozyme, the protein molecule contains 14 acidic (aspartic, tyrosine, and glutamic) amino acid residues and 19 basic (arginine, histidine, and lysine) amino acid residues [60]. Barlow and Thornton [61] reported the ionic groups of lysozyme as 11 acidic groups excluding tyrosine, and 18 basic groups excluding histidine. The dissociation constants of most of these ionizable groups are reported in the literature [60, 62, 63]. Kuramitsu and Hamaguchi indicated that one carboxylic group is in the interior of the protein molecule and it does not ionize in solution, and that we can use the following equation for the net surface charge, Z, of chicken egg white lysozyme [62]:

$$Z = 19 - \sum_{i=1}^{32} \frac{K_i \cdot \alpha}{H^+ + K_i \cdot \alpha} \tag{6.1}$$

where K_i is the dissociation constant of hydrogen from group i, and α is a parameter describing the electrostatic interactions between a protein molecule containing a net surface charge of Z and a proton [62, 64]. The equation considers 32 ionic groups out of the 33 groups reported by Sakakibara and Hamaguchi [60],

leaving one interior carboxylic group [62]. The *net surface charge* of a protein is an average over a large number of individual forms of molecule constantly giving up and taking on protons, and its actual net charge at any moment can be greater or less than the average value of Z [64].

The net surface charge of lysozyme calculated from eq. (6.1) was between +9 and +11 in the pH range between 5.8 and 4.2. For simplicity, the net surface charge of lysozyme was considered to be constant at +10 in the model. The *crystallized lysozyme* obtained from the manufacturer contained about 5–10 wt% sodium acetate and sodium chloride (as per the manufacturer's certificate of analysis). The initial lysozyme was assumed to contain 5% NaCl and 5% C_3H_2ONa. The equilibrium pH of an aqueous solution containing an initial concentration of lysozyme, $C_{\mathrm{Lys,\ O}}$, was calculated from a charge balance:

$$C_{\mathrm{Lys,\,O}} \cdot Z + C_{\mathrm{H}^+} + C_{\mathrm{Na}^+} = C_{\mathrm{OH}^-} + C_{\mathrm{Cl}^-} + C_{\mathrm{C_2H_3O_2}^-} \tag{6.2}$$

where $C_{\mathrm{C_2H_3O_2}^-}$ indicates the acetate ion concentration. The value of C_{OH^-} is obtained using the ion product for water, K_{w}, taken as 10^{-14} [65], and the dissociation constant of acetic acid, K_{a}, taken as 1.8×10^{-5} [66]:

$$K_{\mathrm{w}} = C_{\mathrm{H}^+} \cdot C_{\mathrm{OH}^-} \tag{6.3}$$

$$K_{\mathrm{a}} = \frac{C_{\mathrm{H}^+} \cdot C_{\mathrm{C_2H_3O_2}^-}}{C_{\mathrm{HC_2H_3O_2}}} \tag{6.4}$$

Equations (6.3) and (6.4) were solved for C_{H^+} at different concentrations of lysozyme, and these values were used to calculate the pH values. These results are shown in Figure 6.23. If the presence of HCl in lysozyme is ignored, the equations fail to reproduce the variation pH shown in the figure.

The modeling of the lysozyme–surfactant complex formation was carried out by first estimating the dissociation constant. At a pH less than its pI, lysozyme has an overall positive surface charge ($Z > 0$). Assuming Cl^- as counterion, the dissociation constant of lysozyme can be written as

$$K_{\mathrm{LysCl}_{10}} = \frac{C_{\mathrm{Lys}^{+10}} \cdot (C_{\mathrm{Cl}^-})^{10}}{C_{\mathrm{LysCl}_{10}}} \tag{6.5}$$

By the common ion effect, the solubility of AOT is limited in an acidic solution or in a salt solution, which is written as

$$K_{\mathrm{LH}} = C_{\mathrm{H}^+} \cdot C_{\mathrm{L}^-} \tag{6.6}$$

$$K_{\mathrm{LNa}} = C_{\mathrm{Na}^+} \cdot C_{\mathrm{L}^-} \tag{6.7}$$

where L^- is the negatively charged group of AOT or ligand. The dissociated lysozyme reacts with L^- forming an insoluble lysozyme–ligand complex. The solubility product of this complex, $K_{\mathrm{LysL}_{10}}$, is

$$K_{\mathrm{LysL}_{10}} = (C_{\mathrm{Lys}^{+10}}) \cdot (C_{\mathrm{L}^-})^{10} \tag{6.8}$$

The solubility product of AOT, $K_{\mathrm{LNa}} = 1.1 \times 10^{-3}$ (M^2) was obtained from the data reported by Caryl [57]. The solubility product of the lysozyme–ligand complex, $K_{\mathrm{LysL}_{10}}$, was determined experimentally to be 4×10^{-55} (M^{11}). The values of $K_{\mathrm{LysCl}_{10}}$ and K_{LH} were adjusted to fit the data. Values of $K_{\mathrm{LysCl}_{10}} = 2.5 \times 10^{-23}$ (M^{10}), and $K_{\mathrm{LH}} = 9.2 \times 10^{-9}$ (M^2) gave a good fit to the data depicted in the figures.

The values of $K_{\mathrm{LysCl}_{10}}$ and $K_{\mathrm{LysL}_{10}}$ are very small because the concentration of one of the ions is raised due to the power 10 in eqs. (6.5) and (6.8). These values indicate that the lysozyme is associated with chloride in solution unless the ligand, AOT, is present. The solubility product of lysozyme–AOT is in the order of 10^{-55} indicating that the complex is virtually insoluble in water and precipitates upon formation.

The moles of lysozyme–ligand complex formed in the aqueous phase, n_{LysL_Z}, can then be calculated using the mole balances on the lysozyme and the ligand as follows:

$$C^0_{\mathrm{Lys}} = C_{\mathrm{Lys}^{+10}} + C_{\mathrm{LysCl}_{10}} + \frac{n_{\mathrm{LysL}_{10}}}{V} \tag{6.9}$$

$$C^0_L = C_{L^-} + 10 \cdot \frac{n_{LysL_{10}}}{V} \tag{6.10}$$

where $n_{\mathrm{LysL}_{10}}$ refers to the moles of the insoluble lysozyme–ligand complex formed in the solution, V refers to the total volume of the mixture, and $C_{\mathrm{LysCl}_{10}}$ indicates the concentration of lysozyme that is associated with the chloride ions and not available to react with the ligand. Finally, the percent removal of lysozyme as precipitated complex is calculated as

$$\frac{\%\ \mathrm{Removal} = n_{PL_{10}}}{C_{P0} \cdot V \times 100} \tag{6.11}$$

The results predicted using eq. (6.11) are plotted in Figure 6.23 shows the percent removal of lysozyme as the insoluble complex with AOT for different mole ratios of AOT to lysozyme. Assuming $Z = 10$ and using the experimentally measured $K_{\mathrm{LysL}_{10}}$ value, the model calculation of the percent mass removal agrees well with the experimental results. Figure 6.24 compares the model results with measure values of the equilibrium pH of the aqueous solution after the precipitation of the lysozyme–ligand complex. The value of K_{LH} was adjusted to fit these data. Figure 6.26 shows the effect of sodium chloride concentration on the formation of the lysozyme–ligand

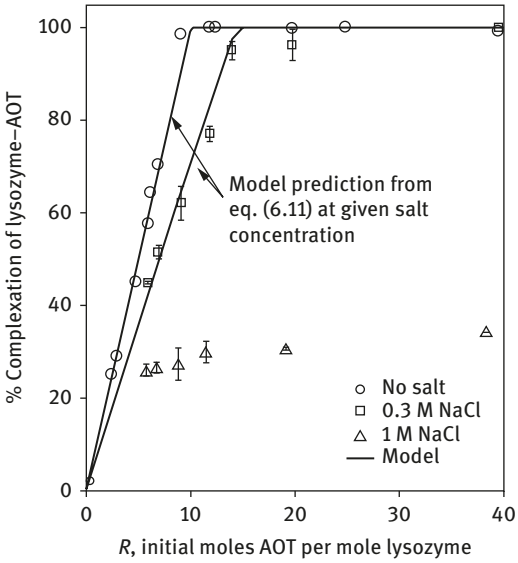

Figure 6.26: Effect of salt on the percent removal of lysozyme forming an insoluble complex with AOT.

complex using the adjusted value of $K_{\mathrm{LysCl}_{10}}$. The model agrees well with the experimental results at salt concentrations up to 0.3 M. For 1 M NaCl, the model predicts zero percent removal because essentially all of the lysozyme and the ligand remain associated with their counterions. The experimental results show about 30–35% removal of lysozyme, which is almost independent of the molar ratio, R. This phenomenon is believed to be due to the salt precipitation of lysozyme [67, 68].

6.6.5 Conclusions

A new method for lysozyme purification is proposed. The method uses the commercially available anionic surfactant, AOT, to precipitate lysozyme from an aqueous solution. In Chapter 7, we demonstrate that the white precipitate formed by direct contact with AOT surfactant can be recovered with its initial enzymatic activities by using polar organic solvents. In other words, there is no longer a need for an organic phase to form a reverse micellar phase. As shown in our work, the direct precipitation method requires significantly less AOT than the reverse micellar extraction method to extract lysozyme from an aqueous phase. This precipitation method has advantages over the fractional sedimentation method, which requires long processing time (many hours) and the gradient gels operating under protein denaturing conditions [69]. Results presented in this work also suggest that the solubilization of lysozyme into an AOT reverse micellar phase consists of two steps: formation of lysozyme–AOT complex to precipitate from the aqueous phase and the solubilization of lysozyme–AOT complex into the reverse micellar phase.

6.7 Summary

Our research discovered new ionic surfactants for extraction of biomolecules from aqueous phase. The extraction behavior of the different biomolecules using the new reverse micellar systems showed similar finding that electrostatic interaction between the charged biomolecule and the ionic surfactant heads is key factor in both forward and backward extractions. The types and concentration of the salts and cosurfactants have significant effect on the extraction behavior of the biomolecules into the reverse micellar phase. The biomolecules extracted from the aqueous phase did not necessarily solubilized into the reverse micellar phase fully and this resulted in a formation of white precipitate at the aqueous–organic interface.

The reverse micellar systems continue to draw attention to many researchers, because of its potential to be an effective new way to purify proteins that are important for industrial and therapeutic use. Successful use of reverse micellar systems has been reported for the purification of antibiotics [70] and soybean proteins [71, 72]. Imm et al. successfully extracted polyphenol oxidase from apple skin [73] to further demonstrate the possibility of using reverse micellar technology for wide range of application. The use of a novel nonionic surfactant sorbitan trioleate (Span 85) modified with Cibacron Blue F-3GA (CB) or mixed surfactants to form reverse micellar phase, either to reduce the denaturing effect caused from ionic surfactant head or to further improve the ecological friendlessness by biodegradable surfactants, is also being continuously investigated in literature [74]. In order to further improve the back-extraction efficiency, different researchers have successfully employed different back-extraction techniques such as the use of isopropanol and mechanical agitation with glass beads to recover Stem Bromelain from AOT reverse micellar system [75], the use of chaotropes such as urea and guanidine hydrochloride to extract and recover kallikrein and lipase from cetyltrimethylammonium bromide (CTAB) reverse micellar phase [76, 77], and trypsin from AOT reverse micellar system [78].

The practical application of the reverse micellar system for protein purification was further demonstrated by Nandini and Rastogi, who successfully purified lipase from *Aspergillus niger* fermentation broth using CTAB [79]. Many researchers have developed other innovated ways for utilizing reverse micellar system to further improve the purification efficiency [80–82].

References

[1] Luisi PL, Bonner FJ, Pellegrini A, Wiget P, Wolf R. Helv Chim Acta 1979, 62, 740.
[2] Dungan SR, Bausch T, Hatton TA, Plucinski P, Nitsch W. J Colloid Interface Sci 1991, 45, 33.
[3] Göklen KE, Hatton TA. Sep Sci Technol 1987, 22, 831.
[4] Jarudilokkul J, Poppenborg LH, Stuckey DC. Biotechnol Bioeng 1999, 62, 593.
[5] Naoe K, Kai T, Kawagoe M, Imai M. Biochem Eng J 1999, 3, 79.

[6] Paradkar VM, Dordick JS. Biotechnol Prog 1993, 9, 199.
[7] Wolbert RBG, Hilhorst R, Voskuilen G, Nachtegaal H, Dekker M, Van't Riet K, Bijsterbosch BH. Eur J Biochem 1989, 184, 627.
[8] Wang W, Weber ME, Vera JH. J Colloid Interface Sci 1994, 168, 422.
[9] Khoshkbarchi MK, Vera JH. J Colloid Interface Sci 1995, 170, 562.
[10] Wang W, Weber ME, Vera JH. Biotechnol Bioeng 1995, 46, 343.
[11] Wang W, Weber ME, Vera JH. Ind Eng Chem Research 1995, 34, 599.
[12] Thien MP, Hatton TA, Wang DIC. Biotechnol Bioeng 1988, 32, 604.
[13] Furusaki S, Kishi K. J Chern Eng Jpn 1990,23, 91.
[14] Leodidis EB, Hatton TA. Academic Publishers, Dordrecht, Netherlands, 1990.
[15] Roth M. Anal Chem 1971, 43, 880.
[16] Church FC, Swaisgood HE, Porter DH, Catignani GL. J Dairy Sci 1983, 66, 1219.
[17] Karpe P, Ruckenstein E. J Colloid lnterf Sci 1991, 141, 534.
[18] Leodidis EB, Hatton TA. Langmuir 1989, 5, 741.
[19] Sheu E, Goklen KE, Hatton TA, Chen SH. Biotechnol Prog 1986, 2, 175.
[20] Smith RE, Luisi PL. Helv Chim Acta 1980, 63, 2302.
[21] El Seoud, OA, Chinelatto AM. J Colloid Interface Sci 1983, 95, 163.
[22] Karpe P, Ruckenstein E. J Colloid Interface Sci 1990, 137, 408.
[23] Eicke HF, Kvita P. Plenum Press, New York, 1984.
[24] Khoshkbarchi MK, Vera JH. Sep Sci Technol 1995, 30, 2301.
[25] Partridge JA, Jensen RC. J Inorg Nucl Chem 1969, 31, 2587.
[26] Lehninger AL. Biochemistry, Worth Publishers, New York, 1975.
[27] Sole KC, Hiskey JB. Hydrometallurgy 1992, 30, 345.
[28] Rabie HR, Suyyagh T, Vera JH. Sep Sci Technol 1998, 33, 241.
[29] Shin YO, Vera JH. Biotechnol Bioeng 2002, 80, 538.
[30] Aires-Barros MR, Cabral JMS. Biotechnol Bioeng 1991, 38, 1302.
[31] Kelley BD, Wang DIC, Hatton TA, Ibid 1993, 42, 1199.
[32] Giovenco S, Verheggen F, Laane C. Enzyme Microbiol Technol 1987, 9, 470.
[33] Rahaman RS, Chee JY, Cabral JMS, Hatton TA. Biotechnol Prog 1988, 4, 218.
[34] Abbott NL, Hatton TA. Chem Eng Prog 1988, 84, 31.
[35] Sun Y, Ichikawa S, Sugiura S, Furusaki S. Biotechnol Bioeng 1998, 58, 58.
[36] Lye GJ, Asenjo JA, Pyle DL. Biotechnol Bioeng 1995, 47, 509.
[37] Carlson A, Nagarajan R. Biotechnol. Prog 1992, 8, 85.
[38] Adachi M, Harada M. J Phys Chem 1993, 97, 3631.
[39] Dekker M, ME Leser ME. Chapman & Hall, London, 1994.
[40] Göklen KE, Hatton TA. Sep Sci Technol 1987, 22, 831.
[41] Ichikawa S, Imai M, Shimizu M. Biotechnol Bioeng 1992, 39, 20.
[42] Imai M, Natsume T, Naoe K, Shimizu M, Ichikawa S, Furusaki S. Bioseparation 1997, 6, 325.
[43] Rabie HR, Vera JH. Ind Eng Chem Research 1996, 35, 3665.
[44] Rabie HR, Vera JH. Langmuir 1995, 11, 1162.
[45] Rabie HR, Vera JH. Ibid 1996, 12, 3580.
[46] Baldwin, RL. Biophys J 1996, 71, 2056.
[47] Collins KD. Biophys J 1997, 72: 65.
[48] Shin YO, Vera JH. Can J Chem Eng 2004, 82, 349.
[49] Ashrafizadeh SN, Khoshkbarchi MK. Sep Sci Technol 1998, 33, 2579.
[50] Goto M, Hashimoto Y, Fujita T, Ono T, Furusaki S. Biotechnol Prog 2000, 16, 1079.
[51] Davies RC, Neuberger A, Wilson BM. Biochim Biophys Acta 1964, 178, 294.
[52] Brown JR. Biochem J 1964, 92, 13.
[53] McMurry J. Brooks/Cole Publishing, CA, USA, 1992.

[54] Shin YO, Weber ME, Vera JH. Biotechnol Prog 2003, 19, 928.
[55] Jauregi P, Varley J. Biotechnol Bioeng 1998, 59, 471.
[56] Ono T, Goto M, Nakashio F, Hatton TA. Biotechnol Prog 1996, 12, 793.
[57] Caryl CR. Ind Eng Chem 1941, 33, 731.
[58] Linfield WM. Marcel Dekker, NY, USA, 1976.
[59] Alderton G, Ward WH, Fevold HL. J Biol Chem 1945, 157, 43.
[60] Sakakibara R, Hamaguchi K. J Biochem 1968, 64, 613.
[61] Barlow DJ, Thornton JM. Biopolymers 1986, 25, 1717.
[62] Kuramitsu S, Hamaguchi K. J Biochem 1980, 87, 1215.
[63] Tanford C, Roxby R. Biochemistry 1972, 11, 2192.
[64] Edsall JT, Wyman J. Academic Press, NY, USA, 1958.
[65] Smith RM, Martell AE. Plenum Press, NY, USA, 1976.
[66] Noggle JH. HarperCollins College Publishers, NY, USA, 1996.
[67] Curtis RA, Prausnitz JM, Blanch HW. Biotechnol Bioeng 1998, 57, 11.
[68] Kuehner DE, Blanch HW, Prausnitz JM. Fluid Phase Equilib 1996, 116, 140.
[69] Arvanitis DN, Yang W, Boggs JM. J Neurosci Res 2002, 70, 8.
[70] Chuo SC, Ahmad A, Mohd-Setapar SH, Ripin A. Pharma Chemica 2014, 6, 37.
[71] Zhao X, Li Y, He X, Zhong N, Xu Z, Yang L. Mol Biol Rep 2010, 37, 669
[72] Bu G, Yang Y, Chen F, Liao Z, Gao Y, Yang H, Li R, Liu K, Zhao J. Int J Food Sci Technol 2014, 49, 1079.
[73] Imm JY, Kim SC. Food Chem 2009, 113, 302.
[74] Liu Y, Dong X, Sun Y. Chin J Chem Eng 2008, 16, 949.
[75] Dhaneshwar AD, Chaurasiya RS, Hebbar HU. Biotechnol Prog 2014, 30, 845.
[76] Zhou B, Wan J, Wang J, Cao X. Process Biochem 2012, 47, 229.
[77] Yu T, Cao X. Appl Biochem Biotechnol 2014, 172, 3287.
[78] Wan J, Li Q, Zhou F, Liu J, Cao X. Sep Purif Technol 2013, 116, 307.
[79] Nandini KE, Rastogi NK. Process Biochem 2009, 44, 1172.
[80] Shi Z, Peterson RW, Wand AJ. Langmuir 2005, 21, 10632.
[81] Cao XL, Li T, Ito Y. J Liq Chromatogr Relat Technol 2007, 30, 2593
[82] Noh KH, Imm JY. Food Chem 2005, 93, 95.

Remy Dumortier and Eva Rodil

7 Removal of Metals from Aqueous Solutions by Complexation using Surfactants

7.1 Introduction

Metals in water streams and groundwater present considerable health and environmental hazards, and thus a proper disposal of industrial waste water-containing metals is important. Different techniques for the removal or recovery of the metals in aqueous solution such as precipitation, extraction, biosorption, and ion exchange are used. Their advantages and disadvantages have been discussed by Fu and Wang [1], Peters et al. [2], and Patterson [3].

Precipitation processes widely used to remove metal ions from aqueous solutions include the formation of hydroxides, carbonates [4], or sulfides [5]. The disadvantages of most precipitation processes are the large consumption of precipitating agent and the difficulties found in the filtration of the sludge. Organic reactants used to precipitate metals in solution [6] have been limited by poor regeneration and the high cost of the organic precipitating agent.

The affinities of metal ions for ligands containing negatively charged oxygen donor atoms are strongly related to their affinity for the hydroxide ion. The stability constant of hydroxide complexes for a particular metal ion is, therefore, useful for describing its complexing behavior with ligands containing negative oxygen donors. The size and the charge of a metal ion are also important in determining the affinity of hydroxide for a metal ion and the associated stability constant. The greater the charge on the ions and the smaller the ions, the greater would be the affinity. From this point of view, small ions of the same charge are favored, and the stability of complexes should increase with the charge on the metal ions. For the following reaction,

$$M^{m+} + OH^- \longleftrightarrow M(OH)^{m-1} \tag{R7.1}$$

where M is a metal and m is the charge number of the metal ion. The associated stability constant is

$$K_{1,M} = \frac{C_{M^{m+}} C_{OH^-}}{C_{MOH^{m-1}}} \tag{7.1}$$

The stability of hydroxide complexes of Li^+, Zn^{2+}, Al^{3+}, and Th^{4+} are $K_{1,Li} = 10^{-0.36}$, $K_{1,Zn} = 10^{-5.0}$, $K_{1,Al} = 10^{-9.01}$, and $K_{1,Th} = 10^{-10.8}$, respectively [7]. The stability of the hydroxide complexes increases with the charge of the metal ion. While an effect of the charge on the stability constant is obvious in this case, there is not a simple dependence between the metal ion radius and stability constant for ions of the same charge.

https://doi.org/10.1515/9783110564808-007

For Al^{3+}, Ga^{3+}, Fe^{3+}, In^{3+}, and Ti^{3+}, the ionic radius of the metals increases with the ionic radius of $Al^{3+} < Ga^{3+} < Fe^{3+} < In^{3+} < Ti^{3+}$. In this case, the stability constant of indium hydroxide complex $K_{1,In}$ does not follow the expected metal ion radius trend of the other metal ions [7].

Another approach for estimating the preference of individual metal ions for ligands depends on the charge density of the metal and the ligand. Different classifications are proposed in the literature. In early studies, metal ions were classified under A and B type depending on their relative affinity for ligands in aqueous solutions [8]. These two types, A and B, were later renamed as hard and soft, respectively, as Pearson developed the hard and soft acids and bases principle (HSAB) [9, 10]. The HSAB concept is a simple and useful method to estimate relative stabilities of complex ions. According to this principle, H^+ is a very small ion and it has a very high charge density. Thus, species that react strongly with it are called strong bases. Metals that are like H^+ should behave in a similar manner. These metals are called class A metals or hard metals. Following this classification, metal ions referred as soft or B type (e.g., Cd^{2+}, Hg^{2+}) prefer to form complex with soft bases such as phosphorus, which are less electronegative donor atoms. The hard metal ions, such as Ga^{3+} and Al^{3+}, form complexes with hard bases such as oxygen, which are more electronegative donor atoms.

Metal ions at the borderline show no preferences and can complex with hard or soft bases. Most stable complexes are formed when the metal and ligand have similar charge densities, that is, hard with hard and soft with soft. In a similar way, metals with low charge densities (soft or class B) prefer large, polarizable ligands, for they too have low charge density. The classifications of some Lewis acids and bases are listed in Table 7.1.

Table 7.1: Classifications of Lewis acids and bases.

Hard	Borderline	Soft
Classification of some Lewis acids [9]		
H^+, Li^+, Na^+, K^+, Be^{2+}, Mg^{2+}, Ca^{2+}, Sr^{2+}, Al^{3+}, Ga^{3+}, In^{3+}, Fe^{3+}, Co^{3+}, As^{3+}, Si^{4+}, Ti^{4+}, Zr^{2+}	Fe^{2+}, Co^{2+}, Ni^{2+} Cu^{2+}, Zn^{2+}, Pb^{2+}	Cu^+, Ag^+, Au^+, Hg^+, Pd^{2+}, Cd^{2+}, Pt^{2+}, Hg^{2+}, CH_3Hg^+, $Co(CN)_5{}^{2-}$, Pt^{4+}, BH_3, $GaCl_3$, I_2, Br_2, ICN
Classification of some Lewis bases [11]		
H_2O, OH^-, F^-, $CH_3CO_2{}^-$, $PO_4{}^{3-}$, $SO_4{}^{2-}$, $CO_3{}^{2-}$, $ClO_4{}^-$, $NO_3{}^-$, ROH, RO^-, R_2O, NH_3, RNH_2, N_2H_4	$C_6H_5NH_2$, C_5H_5N, $N_3{}^-$ $NO_2{}^-$, $SO_3{}^{2-}$	R_2S, RSH, RS^-, I^-, SCN^-, $S_2O_3{}^{2-}$, R_3P, R_3As, CN^-, CO, $(RO)_3P$, C_2H_4, H^-, R^-

Where R is an alkyl chain.

Adapted with permission from Pearson R G. Hard and Soft Acids and Bases. Journal of the American Chemical Society USA 1963, 85 (22), 3533–39. Copyright (1963) American Chemical society.

Adapted with permission from Pearson R G, Songstad J. Applications of the Principle of Hard and Soft Acids and Bases to Organic Chemistry. Journal of the American Chemical Society USA 1967, 89 (8), 1827–36. Copyright (1967) American Chemical society.

Finally, the consideration of the electronic interactions of metals and ligands is also useful in interpreting their affinity. For example, the presence of the $3d^{10}$ electron core in zinc makes the cation much more strongly polarizing than the corresponding ion of Group 2, Ca^{2+}. Thus, zinc tends to have many of the properties associated with tripositive Group 13 ions such as Al^{3+} and Ga^{3+} [12].

This chapter focuses on the use of sodium carboxylate groups [13, 14] and the use of organophosphorus compounds [15–19] as precipitating reagent to extract metals from aqueous solutions. The formation of the insoluble solid complexes in the aqueous solution in the presence of sodium carboxylate groups and organophosphorus compounds as well as the metal–ligand affinity and interaction mechanism are discussed.

7.2 Removal of Lead Using Sodium Caprate

Different soluble reagents, sodium carboxylate group, sodium propionate (CH_3CH_2COONa) [13], sodium caprate [$CH3(CH2)_8COONa$] [14], and sodium oleate [$CH_3(CH_2)_7CH{:}CH(CH_2)_7COONa$] [13], were evaluated for the removal of lead from aqueous solutions. Preliminary experiments showed that sodium propionate did not form a precipitate with lead, while sodium oleate formed a suspension that was very difficult to filter. Since sodium caprate formed an easily filterable precipitate, the removal of lead with this reagent was studied [13, 14]. The effect of the pH, concentrations of lead, and type of salts on the removal process was determined and is reported in this section. A procedure to regenerate the sodium caprate reagent is also provided [14].

7.2.1 Experimental Conditions

Sodium caprate was added to a feed solution containing fixed concentrations of lead, calcium, nitrate, and chloride ions. All chemicals were reagent grade and were used without purification. The samples were mixed and allowed to equilibrate for 24 h at 24 ± 1 °C. The precipitate was filtered using a fast flow filter paper or with a 0.45 μm filter. The precipitate was then dried and used for the regeneration of the caprate reagent. The filtrate pH and its concentrations of lead, calcium, and caprate were measured. Lead and calcium were measured using atomic absorption spectroscopy, while the concentration of caprate was measured using a total organic carbon analyzer [13]. Three replicates were run for each experiment.

The regeneration of sodium caprate was performed in two steps. First, the lead caprate precipitate was acidified with HNO_3 to precipitate capric acid. The capric acid precipitate was then filtered out of the aqueous solution. In the second step, a NaOH

solution was used to treat the capric acid and to regenerate it in its sodium form. The same number of moles of NaOH than capric acid was added to the solution. The sodium caprate solution obtained was diluted with distilled water to the concentration needed to repeat the lead removal process.

The solubility products of lead caprate and capric acid were experimentally determined as described by Husein et al. [14]. The lead caprate and capric acid precipitates were dissolved in distilled water. The equilibrium pH and the equilibrium concentrations of lead and caprate were then measured. The values of the solubility products for lead caprate and capric acid were calculated using reactions (R7.3) and (R7.10).

7.2.2 Calculation Procedure

Sodium caprate was used to remove lead by forming an easily filterable precipitate with the metal.

The removal of lead or calcium was noted as

$$R_{(\mathrm{M})} = \left(1 - \frac{C_{(\mathrm{M})}}{C^0_{(\mathrm{M})}}\right) \times 100 \tag{7.2}$$

where $C_{(\mathrm{M})}$ is the total metal concentration remaining in the treated solution and $C^0_{(\mathrm{M})}$ is the total initial metal concentration added to a volume equal to the sum of the feed and added reagent volumes.

The percent loss of caprate to the treated solution was calculated as follows:

$$L_{(\mathrm{R})} = \left(\frac{C_{(\mathrm{R})}}{C^0_{(\mathrm{R})}}\right) \times 100 \tag{7.3}$$

where $C_{(\mathrm{R})}$ is the total caprate concentration in the treated solution and $C^0_{(\mathrm{R})}$ is the total initial caprate concentration added to a volume equal to the sum of the feed and added reagent volumes.

7.2.3 Effect of the Caprate-to-Lead Mole Ratio

A feed solution containing a fixed 7 mM (1,450 mg/L) lead added as $Pb(NO_3)_2$ was prepared. The pH of the solution was pH° 4.4. The hydrolysis of Pb^{2+} shown in R7.2 explains the low initial pH:

$$Pb^{2+} + H_2O \longleftrightarrow PbOH^+ + H^+ \tag{R7.2}$$

The sodium caprate in the reagent solution was adjusted to increase the mole ratio of caprate to lead.

Figure 7.1 shows that the removal of lead increased linearly with an increase of the mole ratio of caprate to lead up to a mole ratio of 2. At this ratio, the percentage removal of lead was 99.5 ± 0.2% and the percentage loss of caprate was 0.8 ± 0.3%. At higher mole ratios, the percentage removal increased slightly, while the percentage loss of caprate increased linearly. As less lead remained in solution to be hydrolyzed, the pH increased from 4.4 to reach a value of about 7.0.

On the basis of these observations, the following reaction was proposed to describe the precipitation process:

$$PbR_{2(s)} \longleftrightarrow Pb^{2+} + 2R^{-} \qquad (R7.3)$$

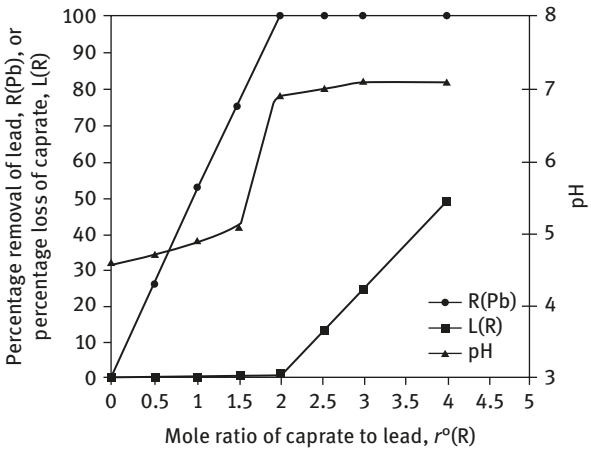

Figure 7.1: Effect of caprate-to-lead ratio on the removal of lead, loss of caprate reagent, and equilibrium pH. $C^{0}_{(Pb)}$ = 7.0 mM, pH° = 4.4 [14]. Reproduced with permission from Husein M, Vera J H, Weber M E. Removal of Lead from Aqueous Solutions with Sodium Caprate. Separation Science and Technology USA 1998, 33(12), 1889. Copyright (1998) Taylor & Francis (http://www.informaworld.com).

7.2.4 Effect of Lead Feed Concentration

The concentration of lead in the feed was varied from 0.35 to 7.0 mM (72.5–1,450 mg/L) while keeping a mole ratio of caprate to lead of 2.0. Figure 7.2 shows that the equilibrium concentrations of lead and caprate were independent of the feed concentration of lead. As the feed concentration of lead increased, the removal

of lead by the caprate increased, resulting in a decrease of the caprate loss. On the basis of this observation, the solubility product equation for the lead caprate can be written as

$$K_{\text{sp, PbR}_2} = C_{\left(\text{Pb}^{2+}\right)} \times \left[C_{(\text{R}^-)}\right]^2 \tag{7.4}$$

assuming that at equilibrium all lead exists as Pb^{2+} and all caprate exists as R^-.

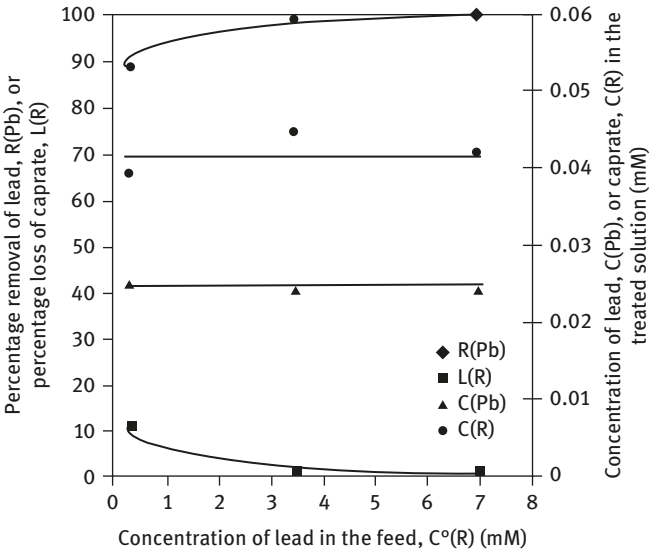

Figure 7.2: Effect of feed concentration of lead on the removal of lead, the percentage loss of caprate, and the equilibrium concentrations of lead (C_{Pb}) and caprate (C_R). pH° = 4.4, ratio of caprate to lead = 2.0 [14]. Reproduced with permission from Husein M, Vera J H, Weber M E. Removal of Lead from Aqueous Solutions with Sodium Caprate. Separation Science and Technology USA 1998, 33(12), 1889. Copyright (1998) Taylor & Francis (http://www.informaworld.com).

7.2.5 Effect of Feed pH

The pH° of a feed containing 7 mM $Pb(NO_3)_2$ was decreased from 4.4 to 1.7 by adding HNO_3. The mole ratio of nitrate to lead, $r°_{(NO3)}$, increased from 2 at pH° 4.4 to 6 at pH° 1.7. The mole ratio of caprate to lead was fixed at 2.0. Figure 7.3 shows that the lead removal decreased with decreasing pH°, while the caprate loss was constant at 2.8 ± 0.4% for pH° values of 3.5 or less. At equilibrium, the pH of the solution was always higher than the pH of the feed. Reactions (R7.3)–(R7.5) explain

the decrease in lead removal, the minimum loss of caprate, and the difference between pH° and pH:

$$RH_{(aq)} \longleftrightarrow H^+ + R^- \quad \text{(R7.4)}$$

$$RH_{(S)} \longleftrightarrow RH_{(aq)} \quad \text{(R7.5)}$$

Capric acid is a weak acid. It is present in an unionized form in solution or can precipitate, thanks to its relatively long carbon chain. The removal of lead decreased and the equilibrium pH increased due to the competition between hydrogen and lead ions. From eq. (R7.5), the soluble capric acid and the caprate precipitate are in equilibrium in the solution, resulting in a constant equilibrium concentration of caprate in the solution and thus a constant percentage loss. Without acid addition, the initial pH of the 7 mM $Pb(NO_3)_2$ solution was 4.4. This low pH resulted from the hydrolysis of Pb^{2+} described in reaction (R7.2). At this pH, hydrogen ion could not compete with lead and little capric acid formed, giving a lower percentage loss of caprate. When almost all the lead was removed with caprate, the pH of the solution returned to a value about 7 as described in the following reactions:

$$Pb(OH)^+ + 2R^- \longleftrightarrow PbR_{2(s)} + OH^- \quad \text{(R7.6)}$$

$$OH^- + H^+ \longleftrightarrow H_2O \quad \text{(R7.7)}$$

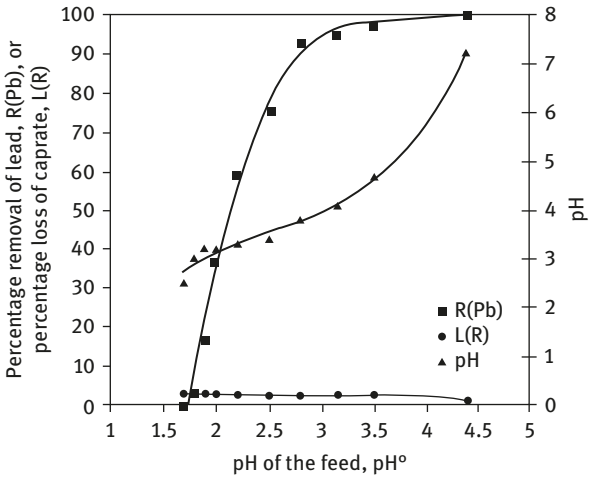

Figure 7.3: Effect of feed pH on the removal of lead, the percentage loss of caprate, and the equilibrium pH. $C^0_{(Pb)}$ = 7.0 mM, ratio caprate to lead = 2.0 [14]. Reproduced with permission from Husein M, Vera J H, Weber M E. Removal of Lead from Aqueous Solutions with Sodium Caprate. Separation Science and Technology USA 1998, 33(12), 1889. Copyright (1998) Taylor & Francis (http://www.informaworld.com).

7.2.6 Effect of Caprate-to-Lead Ratio at Low pH°

For a feed at pH° 1.8 containing a fixed 7 mM $Pb(NO_3)_2$, the mole ratio of caprate to lead was increased from 2 to 4. Figure 7.4 shows that by increasing the ratio from 2.0 to 4.0, the lead removal increased linearly and the loss of caprate decreased slightly. The caprate concentration at equilibrium was constant at 40 ± 4 mg/L. The caprate precipitated results in an increase of the equilibrium pH. These results can be explained by reactions (R7.3)–(R7.5).

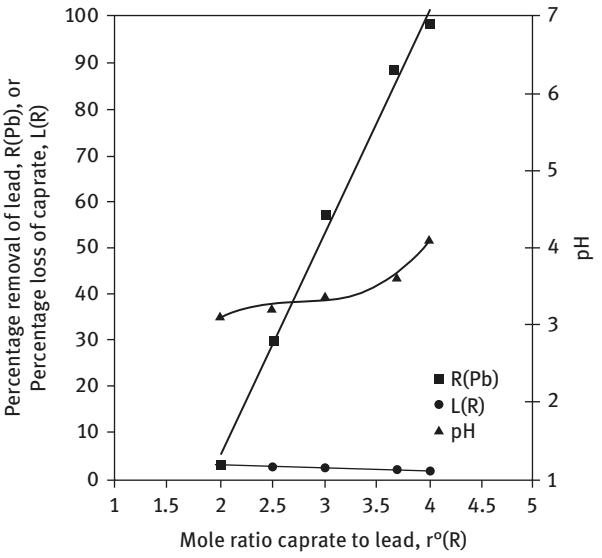

Figure 7.4: Effect of mole ratio of caprate to lead on the removal of lead, the loss of the caprate, and the equilibrium pH. $C^0_{(Pb)}$ = 7.0 mM, pH° = 1.8 [14]. Reproduced with permission from Husein M, Vera J H, Weber M E. Removal of Lead from Aqueous Solutions with Sodium Caprate. Separation Science and Technology USA 1998, 33(12), 1889. Copyright (1998) Taylor & Francis (http://www.informaworld.com).

7.2.7 Effect of Calcium in the Feed

The removal of calcium by sodium caprate containing 3.5 and 7 mM of $Ca(NO_3)_2$ was performed at a mole ratio of caprate to calcium of 2.0. The results showed that the removal of calcium increased from 44% to 75% as the concentration of calcium increased.

Based on the affinity of the caprate for calcium, the selectivity of sodium caprate for lead against calcium was determined by adding $Ca(NO_3)_2$ to the feed. For a feed

concentration of 7 mM $Pb(NO_3)_2$ and a ratio caprate to lead of 2.0, the mole ratio of calcium to lead in the feed, r^o(Ca), was varied from 0.5 to 4.0.

Table 7.2 lists that the percentage removal of lead and the percentage loss of caprate were independent of the mole ratio of calcium to lead. No calcium was removed for any value of r^o(Ca). The caprate reagent precipitated lead selectively; however, when added to a solution containing only $Ca(NO_3)_2$, caprate formed a precipitate with calcium.

Table 7.2: Effect of calcium on the removal of lead using sodium caprate [13].

r^o(Ca)	$r^o(NO_3)$	Percentage removal of lead	Percentage removal of calcium	Percentage loss of caprate
0.0	2.0	99.5 ± 0.2	0	0.8 ± 0.3
0.5	3.0	99.4 ± 0.4	0	1.1 ± 0.5
1.0	4.0	99.6 ± 0.4	0	1.1 ± 0.4
2.0	6.0	99.4 ± 0.4	0	1.1 ± 0.5
3.0	8.0	99.3 ± 0.6	0	0.8 ± 0.4
4.0	10.0	99.4 ± 0.5	0	1.2 ± 0.5

7.2.8 Effects of Chloride and Nitrate in the Feed

Chloride, which is present in most water streams, increases the solubility of heavy metals by forming soluble complexes. In the case of lead, these complexes are $PbCl^+$, $PbCl_2(aq)$, $PbCl_3^-$, and $PbCl_4^-$ [20]. The effect of chloride concentration on the removal of lead was investigated by adding NaCl to the feed solution. The mole ratio of chloride to lead, r^o(Cl), was increased from 2 to 200 by adding NaCl to a feed with a concentration of 7.4 mM $PbCl_2$ and a ratio caprate to lead of 1.9. Since nitrate is considered an inert ion, experiments were also performed in a nitrate media to evaluate the effect of the ionic strength. Lead nitrate was used in these experiments. The concentration of NO_3^- was adjusted using $NaNO_3$ to achieve similar values of $r^o(NO_3)$. Figure 7.5 shows that the removal of lead was essentially independent of $r^o(NO_3)$ or r^o(Cl), and thus of the ionic strength of the solution. By increasing the concentrations of chloride or nitrate in solution, the equilibrium pH of the solution increased due to the effect of the ionic strength of the solution on the activity coefficient of hydrogen [21, 22]. An increase in the ionic strength decreases the activity coefficient of hydrogen ion.

The equilibrium pH increase in the chloride media can be explained by the following reaction:

$$PbOH^+ + Cl^- \longleftrightarrow PbCl^+ + OH^- \qquad (R7.8)$$

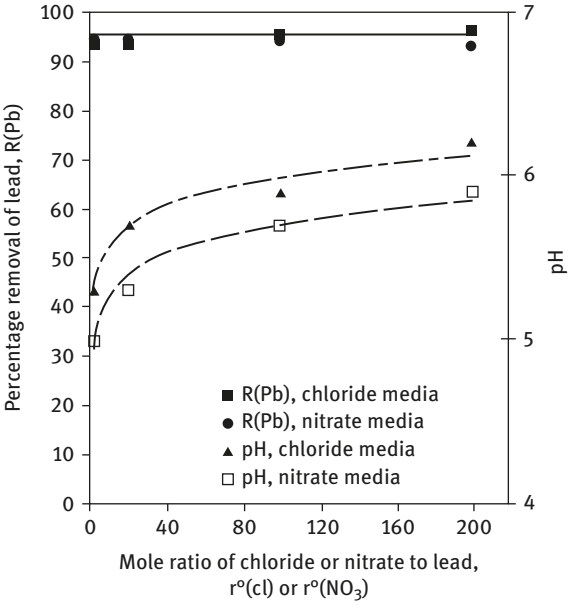

Figure 7.5: Effect of chloride and nitrate on the removal of lead and the equilibrium pH. $C°(Pb)$ = 7.4 mM, $r°(Ca)$ = 0, $r°(R)$ = 1.9 [14]. Reproduced with permission from Husein M, Vera J H, Weber M E. Removal of Lead from Aqueous Solutions with Sodium Caprate. Separation Science and Technology USA 1998, 33(12), 1889. Copyright (1998) Taylor & Francis (http://www.informaworld.com).

7.2.9 Regeneration of Sodium Caprate

Following the two-step regeneration process of the sodium caprate presented in the above section, a regeneration of 98.9 ± 0.3% was achieved. The lead was concentrated to 50 mM at the end of the process, seven times its feed concentration.

7.2.10 Modeling of Lead Removal

A chemical equilibrium model was developed to predict the experimental results for the effect of different lead concentrations in the feed and the effect of pH on the removal step using sodium caprate. The major assumptions for the model were that the activity coefficients of all species were 1, the nitrate and sodium ions were inert in solution, and that the feed and reagent solution volumes were additive. The formation of lead hydroxyl complex and solubility of the capric acid were given as follows:

$$PbOH^+ \longleftrightarrow Pb^{2+} + OH^- \quad \text{(R7.9)}$$

$$RH(s) \longleftrightarrow H^+ + R^- \quad \text{(R7.10)}$$

where $K_{sp,\ RH} = C_{H+} \times C_{R-}$.

$K_{sp,\ PbR_2}$ and $K_{sp,\ RH}$ were calculated to be 1.1×10^{-13} and 2.6×10^{-9}, respectively [14]. The values of $K_{1,Pb}$ from R7.9 and K_w from R7.7 were taken from the literature [23, 24]. The material balance and the charge balance were written as reported by Husein et al. [14].

For a caprate-to-lead ratio of 2.0, Figure 7.6 shows a good agreement between the lead removal and the caprate loss models and the experimental results obtained at different pH°. The predicted equilibrium pH was generally within 0.2 pH unit of the experimental equilibrium pH data.

Figure 7.7 also shows a good agreement between the model predictions for the effect of the mole ratio of caprate to lead, $r°(R)$, at pH° 1.8 and the experimental results.

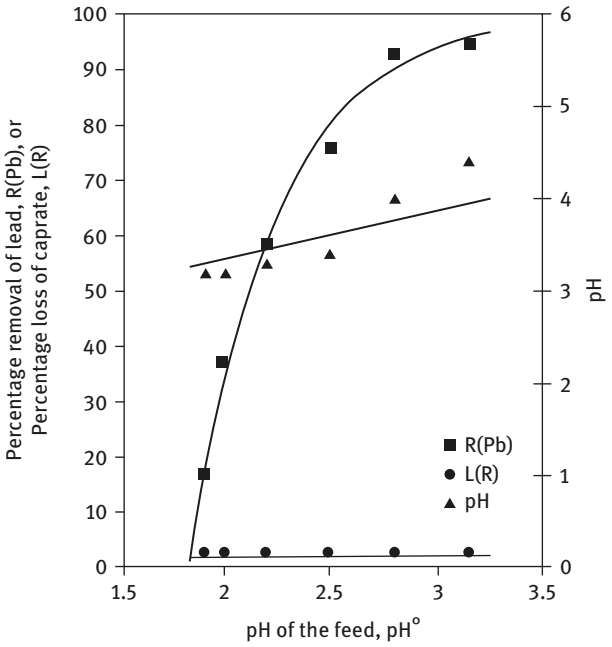

Figure 7.6: Effect of pH° on the removal of lead, the loss of the caprate, and the equilibrium pH. $C°(Pb)$ = 7.0 mM, caprate-to-lead ratio = 2.0. Points: experiments. Lines: model [14]. Reproduced with permission from Husein M, Vera J H, Weber M E. Removal of Lead from Aqueous Solutions with Sodium Caprate. Separation Science and Technology USA 1998, 33(12), 1889. Copyright (1998) Taylor & Francis (http://www.informaworld.com).

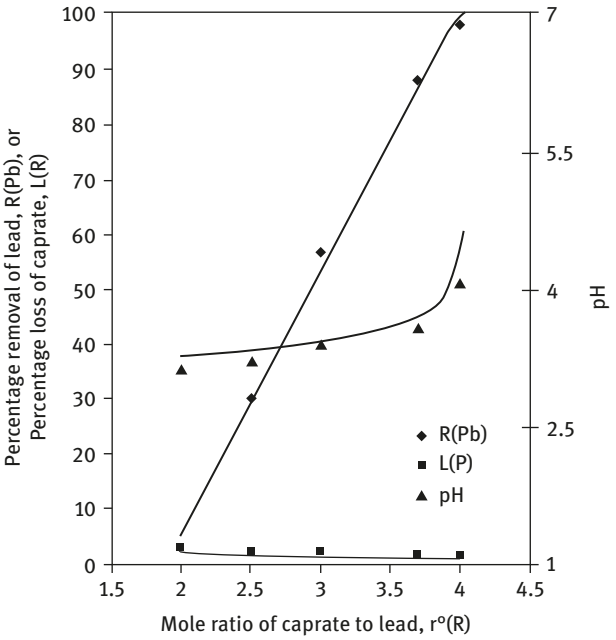

Figure 7.7: Effect of the mole ratio of caprate to lead on the removal of lead, the loss of caprate, and the equilibrium pH. $C°(Pb) = 7.0$ mM, $pH° = 1.8$, $r°(NO_3) = 4.0$. Points: experiments. Lines: model [14]. Reproduced with permission from Husein M, Vera J H, Weber M E. Removal of Lead from Aqueous Solutions with Sodium Caprate. Separation Science and Technology USA 1998, 33(12), 1889. Copyright (1998) Taylor & Francis (http://www.informaworld.com).

7.2.11 Conclusion

A high removal of lead was obtained in an easily filterable precipitate by mixing a solution of lead ions with sodium caprate. The lead removal by complexation with the caprate was achieved for solutions with an initial lead concentration between 0.35 mM (72 mg/L) and 7 mM (1,450 mg/L). For a feed of 7 mM lead and a mole ratio of caprate to lead of 2.0, a 99.5 ± 0.2% lead removal was achieved with a minimum loss of caprate of 0.8 ± 0.3%. For a fixed mole ratio of caprate to lead of 2.0, the feed concentration of lead did not impact the equilibrium concentrations of lead and caprate in the supernatant, which were 5 ± 2 and 7 ± 1 mg/L, respectively. The removal of the lead decreased with a decrease of the pH feed. The equilibrium concentration of caprate remained constant in this case due to the equilibrium reaction between the solid and soluble forms of capric acid. It was also observed that by adding more caprate at a low pH of the feed the removal of lead increased without changing the caprate equilibrium concentration in solution. The removal of lead was not affected by the presence of calcium, chloride, or nitrate in the feed solution. The experimental results were predicted with good accuracy without fitted

parameters using a model based on the chemical reaction equilibria between different solutes and the assumption that all activity coefficients are unity.

7.3 Removal of Metals using Sodium Di-(*n*-octyl) and Sodium Di-(*n*-dodecyl) Phosphinates

The extraction of metal ions from an aqueous phase into an organic solution using organophosphorus acids is well established [25]. Organophosphorus acids are generally viscous liquids, slightly soluble in water but highly soluble in many organic solvents [26]. Thus, different media and different solvents are used to enhance the extraction of metal ions with organophosphorus ligands.

The structure of the organophosphorus extractant group is also important as some extractants can have a better affinity for a metal than others and thus increase the extraction efficiency. Peppard et al. [27] and Preston [28] reported that the direct C–P bond enhances the liquid–liquid extraction properties of the extractant and thus the extraction efficiency follows the order [28]: Di-alkyl phosphinic > Di-alkyl phosphonic > Di-alkyl phosphoric.

However, the use of organophosphorus compounds in the extraction processes can be limited by the following:

- the oxidation of the organophosphorus compounds, which produces new but generally less efficient organophosphorus compounds [29];
- the formation of a dimer in the organic phase, described by Danesi et al. [30], which inhibits the removal of the metal;
- the formation of a crud at the solvent/aqueous phase interface, which inhibits the extraction and represents a loss of the extractant and of metal [31].

To overcome the disadvantages associated with the extraction process and other different recovery processes [32, 33], such as the formation of soluble metal sulfide species at excess dosage of sulfide, the long equilibrium time for the precipitation of metals as hydroxides, the sensitivity of the membrane material to acid or salt solutions for the membrane process, and the interference of other metal ions in ion exchange resins, our research focused on the complexation of organophosphorus sodium salts with metal ions that had not been studied before. Using the affinity of organophosphorus extractants [28, 34] for metals, the sodium di-(*n*-alkyl) phosphinate, referred to as R_2POONa, and two other organophosphorus ligands, *O*,*O*-di-(alkyl) dithiophosphoric acid, referred to as $(RO)_2PSSH$, and sodium monoalkyl ester phosphinate, referred to as (RO)POOHNa, were investigated. All of these ligands had straight alkyl chains. While the octyl and a dodecyl carbon chains of R_2POONa were used to see the effect of the straight alkyl chain length on the removal of the metal, only the octyl forms of $(RO)_2PSSH$ and (RO)POOHNa were studied [35].

Preliminary results by Esalah et al. [16] and Dumortier [35] showed that R_2POONa was an effective ligand for the removal of metals from an aqueous solution compared to the other organophosphorus ligands tested. The metal–ligand complexes formed had the advantages of being highly insoluble in water and allowing a good regeneration of the ligand at the end of the cycle. The following section summarizes our findings for the R_2POONa ligand.

7.3.1 Experimental Conditions

The R_2POONa ligand was synthesized with either an octyl or a dodecyl carbon chain by peroxide-catalyzed reactions between the appropriate 1-alkene (octene or dodecene) and hypophosphorus acid following the procedure described by Williams and Hamilton [36] and modified by Peppard et al. [37]. The ligands produced, di-(*n*-octyl) and di-(*n*-dodecyl) phosphinic acids, were then purified and converted to their sodium salts as described by Esalah [38].

A ligand stock solution was prepared for all the ligands except for the sodium di-(*n*-dodecyl) phosphinate. Because of the low solubility of the sodium di-(*n*-dodecyl) phosphinate, the solid powder form of the ligand was added directly to the metal-containing solution. The concentration of phosphorus in the stock solution, and thus of organophosphorus ligand, was measured by inductively coupled plasma atomic emission spectroscopy (ICP-AES).

The metal stock solutions were prepared using either a metal salt (nitrate, chloride, and sulfate) dissolved in water or a solution of metal nitrate. The metal stock solutions were acidified to avoid the formation of metal–hydroxide complexes and titrated. The appropriate acid (HNO_3, HCl, or H_2SO_4) was used depending on the counter ion desired for our experiments.

The metal solutions were prepared by mixing the metal stock solution with distilled water, a salt (when required), and an acid or a base, depending on the pH desired. The amount of acid or base necessary to adjust the pH of the metal solution was based on the titration of the metal stock solution.

The ligand was added either initially diluted in an aqueous solution (sodium di-(*n*-octyl) phosphinate) or directly in its powder form (sodium di-(*n*-dodecyl) phosphinate). The amount of ligand stock solution added was a function of the desired ligand to metal(s) molar ratio. After the addition of the ligand as a solution or as a powder, the solution was mixed slowly, and a minimum reaction time of 30 s was allowed. For longer experiments, the solution was mixed continuously. At the end of the experiments, the pH of the solutions was measured, and the solutions were filtered with 0.2 μm filters before analysis. The concentration of phosphorus and of the different metals remaining in the aqueous solution were determined by ICP-AES. The solid complexes formed were analyzed by X-ray diffraction and by Fourier transform infrared spectrophotometer.

The regeneration of the sodium di-(*n*-octyl) phosphinate ligand and the recovery of the metal from the solid complexes were performed by mixing the solid complex obtained at the end of the experiment in an aqueous solution with 3 M NaOH and a solvent (ethyl ether or chloroform). After agitation and subsequent phase disengagement, two phases were obtained. The lower aqueous phase containing the concentrated metal solution was analyzed with an ICP-AES to determine the final concentration of metal and phosphorus. The upper solvent phase containing the ligand agent was evaporated. The ligand was regenerated at the end of the process in its sodium form.

7.3.2 Effect of pH on Metal Ions and Sodium Di-(*n*-Octyl) Phosphinate Ligand

To understand the behavior of the metal ions in the presence of ligand, the effect of pH in a solution containing the metals nitrate and no ligand and in a solution containing the ligand and no metals was studied.

The percentage removal of the metal, R_M, and recovery of the ligand, R_L, from the aqueous solution is defined as

$$R_i = \frac{n_i^0 - n_i}{n_i^0} \times 100 \tag{7.5}$$

where subscript i stands for the metal or ligand. The initial number of moles in the aqueous solution is $n_i°$ and the number of moles remaining in the treated solution at equilibrium is n_i.

The percentage loss of the ligand, L_L, is defined as

$$L_L = \frac{n_L}{n_L^0} \times 100 \tag{7.6}$$

where n_L is the number of moles of phosphorus ligand in the aqueous solution at equilibrium, and n_L^0 is the number of moles of phosphorous ligand in the initial aqueous solution. In the figures, the data are shown as symbols and lines.

Figure 7.8 shows the percent removal of gallium in its insoluble hydroxyl complexes, $Ga(OH)_{3(s)}$, as a function of the final pH. The initial pH° of the gallium nitrate aqueous solution was adjusted with HNO_3 and NaOH. The initial concentration of gallium was $C_{Ga}^{\circ}$of 0.36 mM (25 mg/L). No ligand was present in the solution. As observed, gallium precipitated between a pH of 3 and 7.5, with a maximum at pH 6.4 after 1 day. In this pH range, gallium forms the insoluble hydroxyl complexes $Ga(OH)_{3(s)}$. Depending on the pH and the concentration of gallium, hydroxyl complexes are formed with gallium:

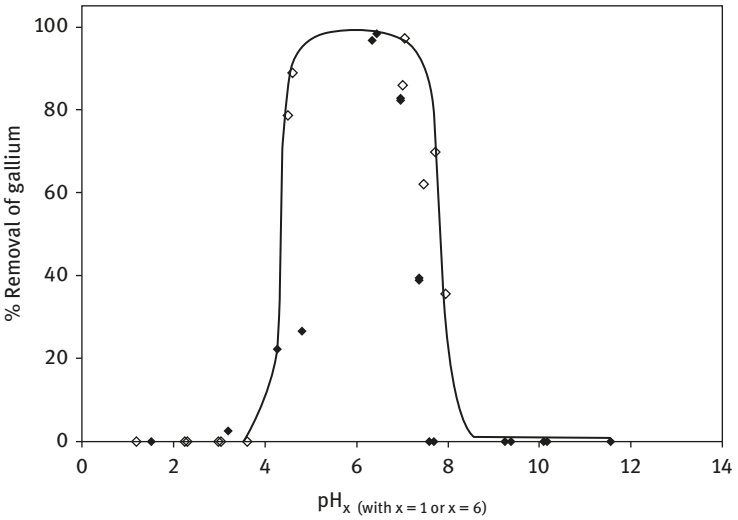

Figure 7.8: Precipitation of gallium in aqueous solution as a function of pH and time: after 1 day (◆) and after 6 days (◇) [C^{o}_{Ga}= 0.36 mM] [35].

$$Ga^{3+} + nOH^{-} \longleftrightarrow Ga(OH)_{n}^{3-n} \quad \text{(R7.11)}$$

where n = 1, 2, 3, and 4 at the low equilibrium concentrations of gallium studied. At pH below 3, gallium is in the form of Ga^{3+}, followed by the formation of the soluble complexes $Ga(OH)^{2+}$ and $Ga(OH)_2^+$ at higher pH values. For a pH above 7.5, the soluble complex $Ga(OH)_4^-$ becomes predominant and the removal of gallium decreases. Because of reaction (7.7), the pH decreases as water is ionized and free protons H^+ are produced. After 6 days, more gallium was removed from the solution over a wider pH range than after 1 day. This slow precipitation of gallium hydroxide was also reported by Uchida and Okuwaki [39] with up to 2 or 3 months needed to reach equilibrium.

The effect of the pH on other metal ions such as aluminum, indium, iron, and calcium was also studied at concentration of 0.925 mM (25 mg/L), 0.22 mM (25 mg/L), 0.36 mM(20 mg/L), and 1.13 mM (45 mg/L), respectively. For aluminum, the insoluble aluminum trihydroxide, $Al(OH)_{3(s)}$, precipitated between pH 4 and 9, with a maximum removal at a pH of about 7. At pH about 9, the soluble $Al(OH)_4^-$ is formed, and the consumption of OH^- lowered the pH of the aluminum solutions. For indium, the precipitation of $In(OH)_{3(s)}$ started at pH 3 and was essentially complete above pH 4. For iron, the precipitation of iron hydroxide began at pH 2 and was essentially complete at pH 4. Both indium and iron were removed from the aqueous solution up to pH 12.

In the case of calcium, insoluble hydroxide complexes do not form up to pH above 12 [40]. The effect of pH on the removal of the sodium di-(*n*-octyl)

phosphinate ligand from an aqueous solution was performed at two initial concentrations of ligand, 1 mM (310 mg/L) and 2 mM (650 mg/L). The pH of the solutions was adjusted with HNO_3 and NaOH. The natural pH of the ligand in aqueous solution was about 8. By decreasing the pH of the solution below this pH, the ligand was removed from the aqueous solution in the form of the water insoluble di-(*n*-octyl) phosphinic acid, $HL_{(s)}$:

$$H^+ + L^- \longleftrightarrow HL_{(S)} \tag{R7.12}$$

More than 90% of the ligand was removed at pH < 6. The ligand was also removed from a solution at pH 13. The addition of sodium hydroxide increased the pH and the concentration of Na^+, the counter ion of the ligand. At large Na^+ concentration, the amount of ligand solubilized in the aqueous solution decreased due to the reaction:

$$NaL_{(S)} \longleftrightarrow Na^+ + L^- \tag{R7.13}$$

The effect of the concentration of sodium on the removal of the ligand was confirmed by adding $NaNO_3$ to a solution with a ligand concentration of 0.86 mM (270 mg/L) to give a mole ratio of sodium to ligand of 1,260. For an equilibrium pH 6.9 = 0.1, the removal of the ligand from the aqueous solution was 85% compared to around 30% when no sodium was added, as shown in Figure 7.9.

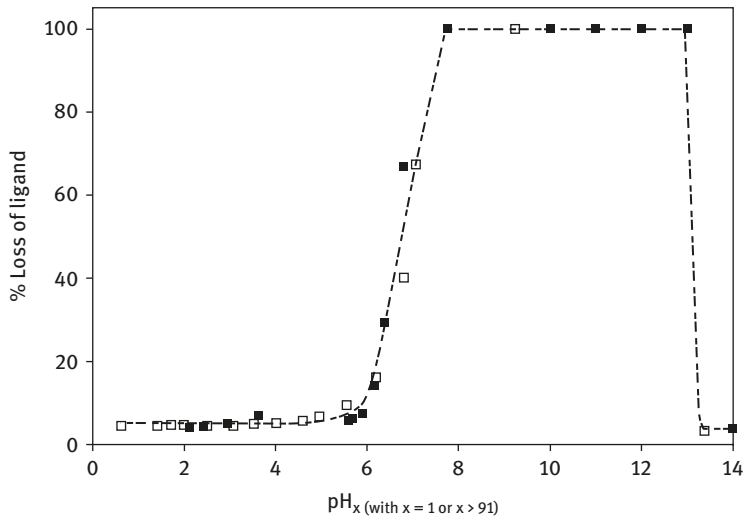

Figure 7.9: Percent loss of sodium di-(*n*-octyl) phosphinate in the aqueous solution as a function of pH_x [C_L°: 1 mM (■), 2 mM (□)]. For values of pH lower than 10, $pH_X = pH_1$; for values of pH higher than 10, $pH_X > pH_{91}$ (pH measured after 13 weeks) [35].

7.3.3 Effect of the Chain Length on the Removal of Single Metal Ions

The effect of the chain length of the sodium di-(*n*-alkyl) phosphinate was studied by treating a feed solution of either lead or gallium with octyl and dodecyl alkyl chains. For lead, the aqueous solution contained 4.97 mM (1,030 mg/L) lead at pH° = 4.1 and the mole ratio of ligand to lead was increased from 0 to 2.87. Figure 7.10 shows that there was little difference in the percentage removal or in the equilibrium pH between the two systems. Similarly, the stoichiometry of the overall precipitation reaction using sodium di-(*n*-alkyl) phosphinate is suggested to be

$$Pb^{2+} + 2L^{-} \longleftrightarrow Pb(L)_{2(s)} \qquad (R7.14)$$

The difference between the two systems was found in the residual concentrations of lead and ligand at a mole ratio ligand to metal of 2.0. The increase in the chain length of the ligand increased the stability of the precipitate (complex), and hence the solubility (dissociation) of the precipitate in water was decreased. For the same hydrophilic group, increasing the number of carbon atoms in the hydrophobic group increases the intermolecular forces between the chains, and decreases the solubility of the compound in water.

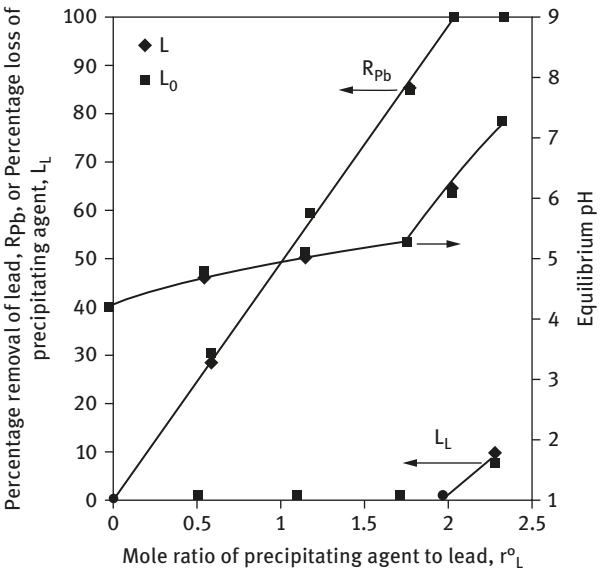

Figure 7.10: The effect of mole ratio of sodium di-(*n*-alkyl) phosphinate to lead on the removal of lead and the equilibrium pH ($C°_{Pb}$ = 4.97 mM, pH°=4.1) [15]. Reproduced with permission from Esalah J O, Weber M E, Vera J H. Removal of lead from aqueous solutions by precipitation with sodium di-(n-octyl) phosphinate. Sep. Pur. Technol. USA 2000, 18, 25–36. Copyright (2000) Elsevier.

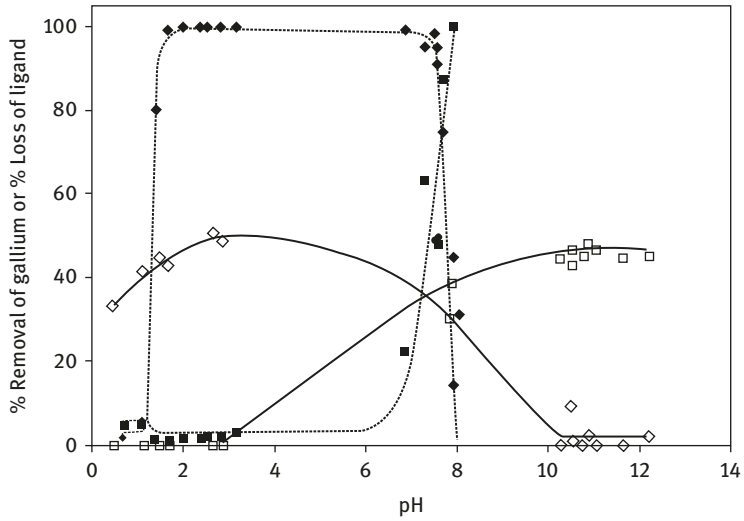

Figure 7.11: Effect of pH on the percent removal of gallium (◆,◇); percent loss of sodium di-(*n*-octyl) phosphinate (■); and percent loss of sodium di-(*n*-dodecyl) phosphinate (□) [C°_{Ga}= 0.36 mM; $r^{\circ}_{L/Ga}$= 3] [35].

For gallium, the removal of the metal by the two sodium di-(*n*-alkyl) phosphinate ligand was tested using different pH, with the optimum ratio $r^{\circ}_{L/Ga}$= 3 and C°_{Ga}= 0.36 mM. Figure 7.11 shows that a better removal of gallium using the sodium di-(*n*-octyl) phosphinate ligand compared to the dodecyl form was obtained. The higher solubility of the sodium di-(*n*-octyl) phosphinate in water compared to the dodecyl form allowed a better removal of the gallium in this case.

The sodium di-(*n*-dodecyl) phosphinate remaining in solution after the complexation with gallium was below the detection limit, indicating that the ligand was removed either by complexation with the gallium or in its acidic form. At a pH higher than 8, as the ligand became more water soluble, and about 50% of the sodium di-(*n*-dodecyl) phosphinate ligand remained in the solution. The gallium also remained in the aqueous phase due to the formation of the soluble $Ga(OH)_4^-$.

7.3.4 Removal of Metal Ions with Sodium Di-(*n*-Octyl) Phosphinate

Different parameters affect the complexation of metal ions with sodium di-(*n*-octyl) phosphinate. The optimum conditions for parameters such as time, pH, mole ratio of ligand to metal, temperature, and the presence of other ions are defined in this section for different metal ions, that is, lead, cadmium, gallium, aluminum, indium, iron, calcium, and zinc. The selective removal of the metals with sodium di-(*n*-octyl)

phosphinate is then discussed for lead, cadmium, and zinc solution as well as gallium in solution with aluminum, indium, iron, calcium, or zinc. These metals are found in lead-contaminated industrial waste water and in mining and electronic effluents for gallium.

Following the removal of the metals from the aqueous solution by the ligand, the metals were recovered from the insoluble metal ligand complex formed. The metals were concentrated in an aqueous phase, while the ligand was extracted in an organic phase. The ligand was subsequently regenerated in its sodium form. The recovery process steps and the regeneration of the ligand are explained is this section. Finally, a mathematical model is presented to describe the removal behavior of the metals with the sodium di-(*n*-octyl) phosphinate ligand.

7.3.4.1 Effect of Mole Ratio, pH, and Temperature

The effect of the mole ratio and pH was performed on different metals. The example of the removal of gallium by complexation with the ligand is shown in Figure 7.12. In this case, the initial pH° was fixed at 2.64 before the addition of the ligand. The initial concentration of gallium nitrate was constant at 0.48 mM (33 mg/L), while the amount of ligand was increased for a total volume of 15 mL. At this pH and

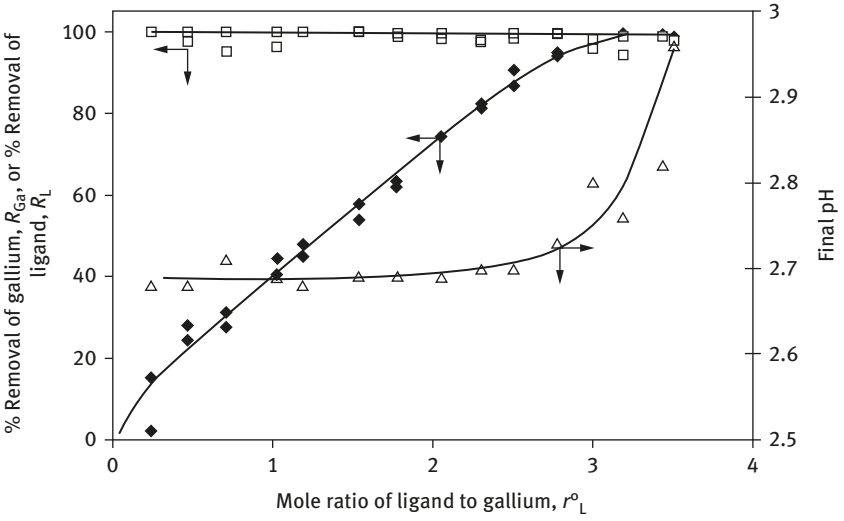

Figure 7.12: Effect of mole ratio of sodium di-(*n*-octyl) phosphinate to gallium on the percent removal of gallium (♦); percent removal of sodium di-(*n*-octyl) phosphinate (□); and the final pH (Δ) [$C^\circ_{Ga} = 0.48$ mM (33 mg/L), $pH^\circ_{Ga} = 2.64$, $pH^\circ_L = 8$][19]. Reproduced with permission from Dumortier R, Weber M E, Vera J H. Removal and recovery of gallium from aqueous solutions by complexation with sodium di-(n-octyl) phosphinate. Hydrometallurgy USA 2005, 76, 207–15. Copyright (2005) Elsevier.

concentration of gallium, no hydroxyl complexes form. Nearly complete removal of gallium was obtained by complexation at a mole ratio ligand to gallium of around 3. The equilibrium concentrations of gallium and ligand remaining dissolved in the aqueous solution were 0.58 ± 0.1 and 1.3 ± 0.5 mg/L, respectively. At a mole ratio of 3.2, the addition of more ligand decreased the level of soluble gallium below the detection limit of the ICP. Further addition of ligand increased the equilibrium pH due to the formation of the acidic form of the ligand (reaction (7.12)).

The effect of the pH on the removal of gallium was investigated at a mole ratio of ligand to gallium of 3 and an initial concentration of gallium of 0.36 mM (25 mg/L). The pH° of the initial solution containing the gallium was adjusted with HNO_3 and NaOH. As observed in Figure 7.13, the highest removal was obtained at an equilibrium pH between 2 and 7. In this pH range, the concentration of gallium remaining in the aqueous solution was below the ICP detection limit. For the equilibrium pH between 2 and 3, the gallium is removed by complexation with the ligand as the gallium did not precipitated in this pH range by complexation with the hydroxyl ions (Figure 7.8). The abrupt change of the equilibrium pH between pH 3 and 7 was due to the competition between ligand and OH^- ions for the gallium. As explained earlier, gallium can react with the ligand and thus release its OH^- or the ligand can form an acidic insoluble precipitate with the H^+ ions. This results in an increase of the equilibrium pH. For an acidic solution below a pH of 2, while the gallium remained

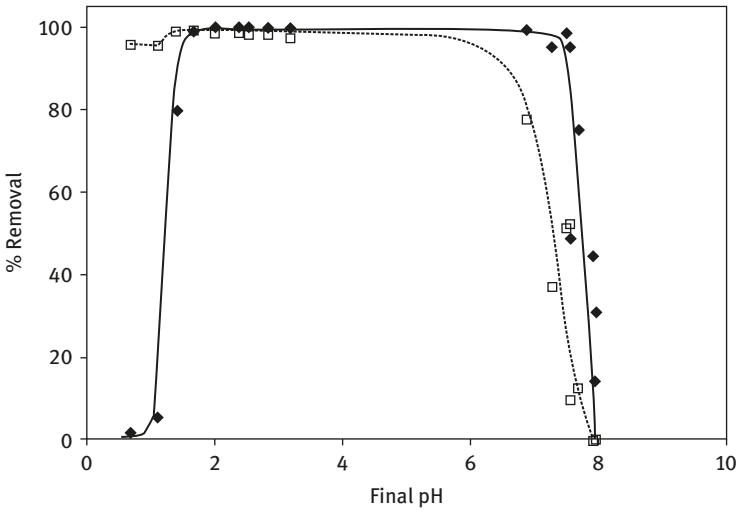

Figure 7.13: Effect of pH on the percent removal of gallium (◆); percent removal of sodium di-(*n*-octyl) phosphinate (□); [C°_{Ga} = 0.36 mM (25 mg/L), r°_{L}= 3] [19]. Reproduced with permission from Dumortier R, Weber M E, Vera J H. Removal and recovery of gallium from aqueous solutions by complexation with sodium di-(n-octyl) phosphinate. Hydrometallurgy USA 2005, 76, 207–15. Copyright (2005) Elsevier.

in the aqueous solution, the ligand was removed in its acidic insoluble form and the equilibrium pH increased. However, because of the strong acidity and the small amount of ligand added, the difference between the initial and equilibrium pH was minimal in this area. For a basic solution with pH close to 8, the natural pH of the ligand, gallium, was mainly removed, as shown in Figure 7.8, by forming the stable insoluble complex $Ga(OH)_{3(s)}$. As less ligand reacts with gallium and as less H^+ ions are available, the ligand stays solubilized in the aqueous solution.

The same effect of the mole ratio and pH was observed for lead, cadmium, zinc, aluminum, indium, iron, and calcium. On the basis of these observations, the removal of a cationic metal, M^{m+}, with the anionic ligand, L^-, is written as

$$M^{m+} + mL^- \longleftrightarrow M\,L_{m(s)} \qquad \text{(R7.15)}$$

In the case of gallium, aluminum, indium, and iron where $m = 3$, the total removal of the metal by the ligand was obtained for a ratio $r^\circ = 3$. For calcium, lead, zinc, and cadmium, where $m = 2$, the total removal of the metal by the ligand was obtained for a ratio $r^\circ = 2$. For this ratio, the effect of pH on the removal of the metals is shown in Figure 7.14.

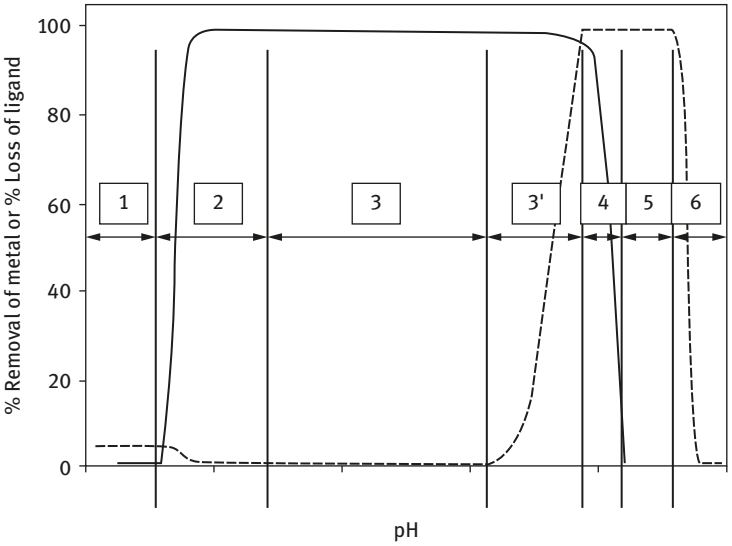

Figure 7.14: Effect of the pH on the percent removal of a metal, and percent loss of sodium di-(*n*-octyl) phosphinate at the optimum r° (— Ligand, — metal, region X; see text) [35].

The removal of the metal and ligand can be divided into six regions:

1. Removal of the ligand in its acidic form (reaction (7.12)): In this region, hydrogen ions compete with the metal ion for the ligand. Because of the high concentration

of H^+, the ligand forms HL. Owing to its low solubility in water, most of the HL complex precipitates as $HL_{(s)}$, but some ligand remains in the solution as a weak acid, HL. In this region, the metal remains in solution. For gallium and aluminum solutions, region 1 was below pH_1 1.1.

2. Formation of the ligand–metal complex (reaction (7.15)): As the pH increases, the concentration of H^+ decreases, and the ligand reacts with the metal to form the insoluble ligand–metal complex. Unreacted ligand is still removed in its acidic form. For gallium solutions, pH_1 was between 1.1 and 3; for aluminum solutions, pH_1 was between 1.1 and 4.
3. 3 and 3′. Removal of the metal with the ligand or in its insoluble hydroxide form (reactions (7.15) and (7.11) for gallium): In this region, the ligand and the hydroxide ions compete for the metal. In the 3′ region, the metal is removed mainly in its hydroxide form; hence, more ligand remains in solution. For gallium solutions, pH_2 was between 3 and 8.
4. Metal is removed in its hydroxide form (reaction (7.11) for gallium): The soluble metal hydroxide complex (e.g., $Ga(OH)_4^-$) begins to form. The ligand remains in solution as it does not react with the hydroxide complex. For gallium solutions, pH_2 was about 8.
5. Both metal and ligand remain in the solution: The metal forms a soluble hydroxy complex, for example, $Ga(OH)_4^-$. The ligand does not form an insoluble salt due to the low concentration of the cation from the base added to increase pH (reaction (7.13)). For gallium solutions, pH_2 was above 8.
6. Removal of the ligand in its salt form (reaction (7.13)) caused by the high concentration of the cation from the base: The metal remains in solution as a soluble hydroxide complex. Generally, the pH was above 12 as shown in Figure 7.9.

The effect of temperature on the concentration of metal and ligand remaining in solution was also investigated. Figure 7.15 shows the case of a gallium solution with a fixed concentration of 0.36 mM (25 mg/L) and a mole ratio of ligand to gallium of 3. The concentration of ligand is expressed in milligram per liter in the graph and the concentration of gallium is the concentration remaining in the filtrate. As the temperature increased, the concentration of gallium in the aqueous solution decreased to an undetectable level above 40 °C. The concentration of ligand in the solution was about 1.5 mg/L at 20 °C, and at 60 °C the concentration increased to about 12 mg/L, which is less than 5 % of the added ligand. The ratio of ligand removed to gallium removed was about 2.9 at 60 °C. For an initial acidic pH, two different types of insoluble complexes are present: the acidic form of the ligand and a complex formed between the ligand and gallium. At low temperature, the ligand is removed in its acidic form, leaving some gallium dissolved in the aqueous solution. As the temperature is increased, the acid form of the ligand is more soluble, allowing a better removal of gallium.

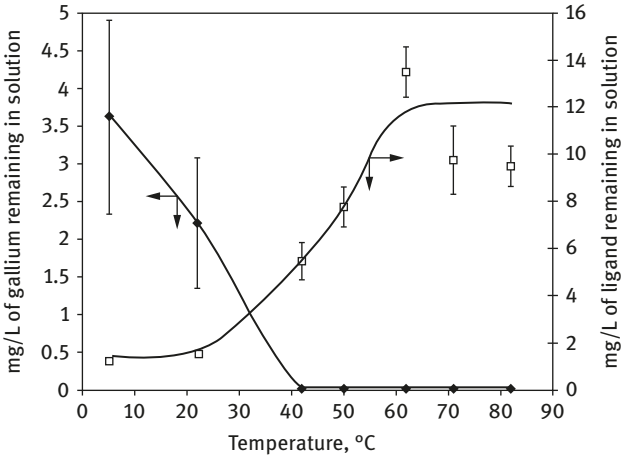

Figure 7.15: Effect of temperature on the residual concentration of gallium (◆) and sodium di-(*n*-octyl) phosphinate (□) [pH°_{Ga} = 2.2, final pH = 2.22 ± 0.2, C°_{Ga}= 0.36 mM (25 mg/L), r°_{L} = 3].[19]. Reproduced with permission from Dumortier R, Weber M E, Vera J H. Removal and recovery of gallium from aqueous solutions by complexation with sodium di-(n-octyl) phosphinate. Hydrometallurgy USA 2005, 76, 207–15. Copyright (2005) Elsevier.

7.3.4.2 Effect of Chloride, Sulfate, and Sodium Ions

Chloride, sulfate, and sodium are present in most water streams. While chloride and sulfate ions form complexes with metals, sodium can react with the ligand (reaction (7.13)).

In the case of gallium, the following complexes are formed with the chloride and sulfate:

$$Ga^{3+} + nCl^{-} \longleftrightarrow GaCl_n^{3-n}, \tag{R7.16}$$

$$Ga^{3+} + nSO_4^{2-} \longleftrightarrow Ga(SO_4)_n^{3-2n}, \tag{R7.17}$$

where n = 1, 2, 3, and 4.

Table 7.3 reports the effect of the ions Na^+, Cl^-, and SO_4^{2-} on the percent removal of gallium for an initial concentration of gallium of C°_{Ga}= 0.36 mM (25 mg/L) and a total volume of 20 mL. The mole ratio of ligand to gallium was between 2.25 and 3. In all cases, the concentration of ligand in the final filtrate was below the detection limit of the ICP, representing a complete removal of the ligand from the solution. For $NaNO_3$, the mole ratio was fixed at 3 in order to observe the competition between gallium and sodium for the ligand. At an equilibrium pH of 2.3, the removal of gallium decreased by 8% for mole ratios of sodium to gallium between 0 and 300. For a mole ratio of 1,500, representing 37 g/L of $NaNO_3$ dissolved in the aqueous

solution, the decrease was only 2% more. The removal of ligand through reaction (7.13) requires appreciable Na^+.

The anions Cl^- and SO_4^{2-} inhibit the removal of gallium much more than Na^+ because they form complexes with gallium. For the anions, a lower mole ratio of ligand to gallium was used to observe complexation of the anion with gallium. The gallium salt solution was prepared 24 h before the addition of the ligand. The removal efficiency decreased 30% for chloride at a mole ratio of 130; for sulfate the decrease was 40% at a mole ratio of 150. It should be noted that Na^+ had a small effect on the removal of gallium for the mole ratio 150 and 300. However, the effect on the removal of gallium in the presence of NaCl at a mole ratio of 130 and Na_2SO_4 at a mole ratio of 300 is mostly due to the anions Cl^- and SO_4^{2-}. Finally, no increase in the efficiency was noticed at lower or higher concentration of NaCl and Na_2SO_4, indicating that all the complex form of the anions Cl^- and SO_4^{2-} with gallium inhibit its complexation with the ligand. This was also confirmed by the sharp decrease in the removal of gallium with the increase in concentration of chloride ions up to a mole ratio of chloride to gallium of 30, where the efficiency reached 67% [35]. For a mole ratio of 650, representing 0.27 g/L of NaCl dissolved in the aqueous solution, the decrease was only 4% more. In the case of SO_4^{2-} ions, the removal efficiency reached a plateau of about 45% above a mole ratio of sulfate to gallium of 100. The removal efficiency did not change up to a mole ratio of 1,000.

Table 7.3: Effect of the cation Na^+ and the anionsCl^-, SO_4^{2-} on the removal efficiency of gallium [C°_{Ga}= 0.36 mM (25 mg/L)] [35].

Salt	Mole ratio ligand/Ga	% Removal R_{Ga} no salt	Final pH no salt	Ions	Mole ratio ion/Ga	% Removal R_{Ga} with salt	Final pH with salt
$NaNO_3$	3	94.7 ± 3.0	2.3	Na^+	150	89.4 ± 1.4	2.28
					300	87 ± 1.5	2.28
					1,500	84.7 ± 2.7	2.23
NaCl	2.5	90.1 ± 0.5	1.88	Cl^-	30	67.2 ± 0.7	1.91
					130	63.8 ± 1.4	1.93
					650	63.2 ± 3.2	1.93
Na_2SO_4	2.25	71.3 ± 1.6	2.04	SO_4^{2-}	100	45.6 ± 0.9	2.06
					150	43.7 ± 0.3	2.06
					1,000	44.9 ± 0.8	2.07

In the case of aluminum, the effect of chloride concentration on their removal was performed by adding sodium chloride to the feed solution. The initial solution contained 0.925 mM (25 mg/L) aluminum at pH° = 2.75 and a ligand metal ratio of 2.5. The mole ratio of chloride to aluminum (r_{Cl}°) was increased from 10 to 400 by the addition of sodium chloride. The chloride system was compared with a nitrate system where aluminum nitrate was the source of aluminum and the nitrate concentration was increased by the addition of $NaNO_3$.

Figure 7.16 shows, by increasing the value of $r_{Cl}°$ or $r_{NO3}°$, the percentage removal of aluminum decreased while the equilibrium pH remained constant. The increase in the sodium concentration due to the addition of sodium salts displaced reaction (7.13) to the left, resulting in a decrease in the availability of ligand to react with aluminum.

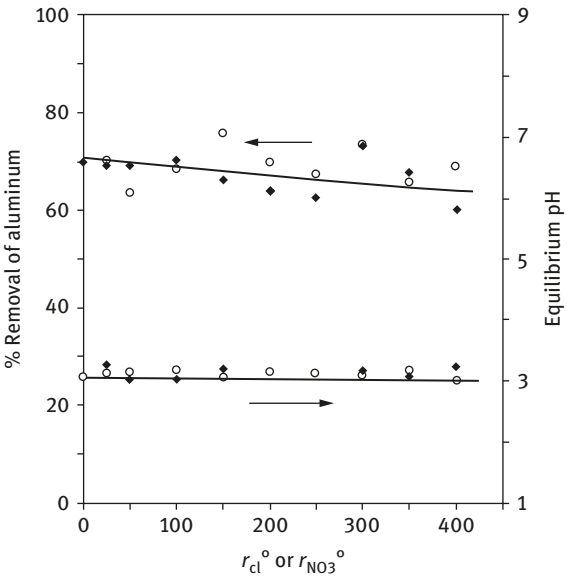

Figure 7.16: Effect of chloride (using NaCl) and nitrate (using $NaNO_3$) concentration on the removal of aluminum and equilibrium pH using sodium di-(*n*-octyl) phosphinate. $C^o_{Al} = 0.925$ mM, $r^o_L = 2.5$, pH° = 2.75. Chloride (◆), nitrate (○) [18]. Reproduced with permission from Rodil E, Dumortier R, Vera J H. Removal of aluminum from aqueous solutions using sodium di-(n-octyl) phosphinate. Chemical Engineering Journal USA 2004, 97, 225–32. Copyright (2004) Elsevier.

For a weak electrolyte (such as Al $L_{3(S)}$), an increase in the ionic strength of the system, by the addition of another electrolyte without a common ion (Al^{+3} or L^-), decreases its mean ionic activity coefficient and thus it increases its degree of dissociation, that is, its solubility [18].

7.3.4.3 Metal Selectivity by Sodium-(n-Octyl) Phosphinate

The selectivity of the ligand for metals was studied for different systems. In the case of calcium, a 2+ charge metal ion, and gallium, a 3+ charge metal ion, an initial solution containing 1.13 mM (45 mg/L) of calcium nitrate and 0.36 mM (25 mg/L) of gallium nitrate, which represents a mole ratio of calcium to gallium of 3.15, was studied. In the initial aqueous solution, the mole ratio of ligand to

calcium, $r^{\circ}_{L/Ca}$, was 2, and the mole ratio of gallium to the ligand, $r^{\circ}_{L/Ga}$, was 6.2. As shown in Figure 7.17, in the pH range from 2 to 5, gallium was removed from the aqueous phase through the formation of an insoluble complex with the ligand. Although the ligand was well in excess of the amount needed to completely remove gallium, no calcium was removed. As the pH increased from 5 to 8, excess ligand reacted with calcium to form an insoluble complex, resulting in removal of calcium. At a pH 9 or higher, less than 3% of the gallium was removed, whereas more than 90% of the calcium and ligand were removed due to the formation of a calcium–ligand complex, through reaction (7.18).

$$Ca^{2+} + 2L^{-} \longleftrightarrow CaL_{2(s)} \qquad \text{(R7.18)}$$

Thus, by using the di-(*n*-octyl) phosphinate ligand, gallium is selectively removed from aqueous phase in a pH range between 2 and 5 in the presence of calcium. A good selectivity of the sodium di-(*n*-octyl) phosphinate for gallium was also obtained in aqueous solutions over metals such as Al and Zn [17].

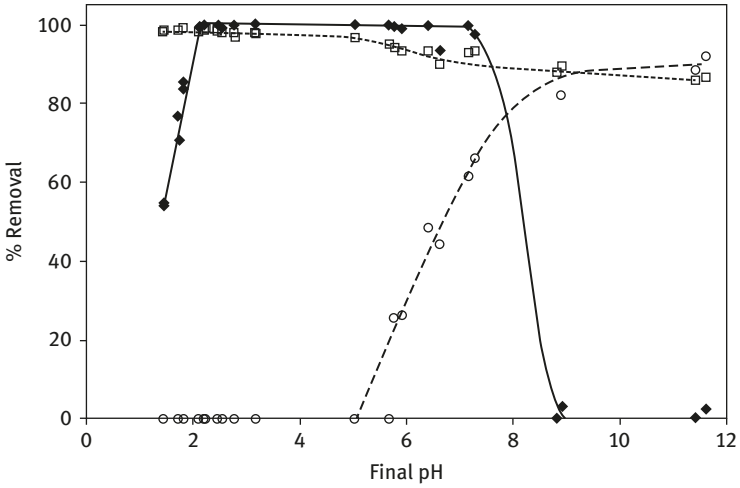

Figure 7.17: Effect of pH on the percent removal of gallium (◆); percent removal of calcium (○); and percent removal of sodium di-(*n*-octyl) phosphinate (□) [C°_{Ga} = 0.36 mM (25 mg/L), C°_{Ca} = 1.13 mM (45 mg/L), $r^{\circ}_{L/Ca}$ = 2] [19]. Reproduced with permission from Dumortier R, Weber M E, Vera J H. Removal and recovery of gallium from aqueous solutions by complexation with sodium di-(n-octyl) phosphinate. Hydrometallurgy USA 2005, 76, 207–15. Copyright (2005) Elsevier.

The different affinities of the sodium di-(*n*-octyl) phosphinate for metals are listed in Table 7.4. As observed, the ligand has more affinity for the hard acid metals. On the basis of HSAB theory developed by Pearson [9], Ca^{2+}, Fe^{3+}, Ga^{3+}, and In^{3+} are hard acids, Cd^{2+} is a soft acid, and Zn^{2+}, Pb^{2+}, and Cu^{2+} are part of the borderline. The sodium di-(*n*-octyl) phosphinate ligand is also a hard base due to its oxygen groups.

Table 7.4: Selectivity of sodium di-(*n*-octyl) phosphinate for metals.

Selectivity	Reference
$Pb^{2+} > Ca^{2+}$	Esalah [38]
$Zn^{2+} > Pb^{2+} > Cd^{2+}$	
$Ga^{3+} > Al^{3+}$	Dumortier [35]
$Ga^{3+} > Zn^{2+}$	
$Ga^{3+} > Ca^{2+}$	
$In^{3+} > Ga^{3+}$	
$Fe^{3+} > Ga^{3+}$	

In the HSAB theory, hard acids prefer to bind to hard bases and soft acids prefer to bind to soft bases. However, metals ions bind strongly to ligands that are basic to protons irrespective of the metal ions are hard or soft [9]. Thus, Cd^{2+}, a soft acid, was also removed by complexation with the ligand [38]. In the case of metal of different charges, such as Ga^{3+} and Zn^{2+} or Ga^{3+} and Ca^{2+}, the affinity of the ligand increases with the increase of the charge of the metal ion. The same results were observed for the extractability of metals using organophosphorus acids [41].

For ions of same charge, Esalah [38] reported the importance of the ionic radius in the case of Zn^{2+}, Pb^{2+}, and Cd^{2+}. The ionic radius of Pb^{2+} is bigger than Cd^{2+} and can explain the affinity of the ligand for Pb^{2+} [9]. The effect of the ionic radii and of the charge on the selectivity of the ligand can also be explained by a covalent character. The general rules of Fajans for covalent character according to Miessler and Tarr [42] are as follows:

1. For a given cation, covalent character increases with an increase in the size of the anion.
2. For a given anion, covalent character increases with a decrease in the size of the cation.
3. Covalent character increases with increasing charge on either ion.
4. Covalent character is greater for cations with a nonnoble gas electronic configuration.

However, the ligand has a higher affinity for Zn^{2+}, which has the same charge as Pb^{2+} and Cd^{2+} but a smaller radius [38]. Hard metal ions, such as gallium and aluminum, prefer ligands with hard donor atoms, such as the O contained in the sodium di-(*n*-octyl) phosphinate. Generally, the affinities of metal ions for ligands containing negatively charged oxygen donor atoms are related to their affinity for the hydroxide ion. The value of log $K_{(OH-)}$ for a particular metal ion is, therefore, a good indicator of the complexing behavior of the metal with a ligand containing negative oxygen donors [7]. For Al^{3+} and Ga^{3+}, log $K_{(OH-)}$ is −9.09 and −11.4, respectively [40]. Thus, the ligand should have a stronger affinity for Ga^{3+}. The Ga^{3+} cation is also more strongly polarized than Al^{3+} due to

the presence of the $3d^{10}$ electron core resulting in a high effective nuclear charge on the Ga^{3+} ion. The electronegativities of Al^{3+} and Ga^{3+} are 1.61 and 1.81, respectively [42]. Since the sodium di-(*n*-octyl) phosphinate ligand is an electron donor, the ligand again should have a stronger affinity for Ga^{3+}.

To explain the affinity of the ligand for metals of same charge, the use of the absorption bands of the metal–ligand complexes was also investigated. Different stretching modes occurred in the metal–ligand insoluble complex. The P–O and the P–C stretching vibrations are considered to be the most informative regions [44–46]. The P–O has a strong absorption bands in the 1,000–1,200 cm^{-1} region, while P–C has a lower absorption in the 700–800 range. Table 7.5 lists the frequencies assigned to the ν_{sym} and ν_{asym} stretching modes as well as the frequency difference associated $\Delta\nu$ for different metal–di-(*n*-octyl) phosphinate complexes. The higher stretching band was associated with ν_{asym} and the lower one with ν_{sym}.

In the case of the P–C bands, ν_{sym}[PC] was virtually the same for all the complexes except for Cd^{2+} and Pb^{2+}, while ν_{asym}[PC*] varied between 802 and 817. Haynes et al. [45] reported two different structural forms α and β of the $Cu[(n\text{-}C_8H_{17})_2PO_2^*]_2$. The P–O bands of the two forms were close for this compound. However, a significant difference was observed for the ν_{asym}[PC*], where the stretch band of α was in the 770–775 cm^{-1} range and β was shifted to about 805 cm^{-1}.

Thus, the removal of the metal using the soluble sodium di-(*n*-octyl) phosphinate mainly produced β for the metals charge (II). In the case of the (III) metals, a difference between the ν_{asym}[PC*] of iron and the other metals can certainly be attributed to this polymorphism.

Also observed in Table 7.5, $\nu_{sym}(POO^-)$ increased when the charge of the metal ion varied from (II) to (III) except for Fe^{3+}. For the charge (II), larger energy variations were observed for Ca^{2+} and Zn^{2+}, while Al^{3+} and Fe^{3+} differed from the close bands of Ga^{3+} and In^{3+}. Overall, the $\nu_{asym}(POO^-)$ stretching mode of the

Table 7.5: Absorption bands of the (POO^-) and (PC) stretching modes for different metal–di-(*n*-octyl) phosphinate complexes measured with Fourier transform infrared spectrophotometer [35].

Element	$\nu_{asym}[POO^{-}*]$ (±1 cm^{-1})	$\nu_{sym}[POO^{-}*]$ (±1 cm^{-1})	$\Delta\nu$ (±2 cm^{-1})	ν_{asym}[PC*] (±1 cm^{-1})	ν_{sym}[PC*] (±1 cm^{-1})	$\Delta\nu$ (±2 cm^{-1})
Na^+	1,148	1,041	107	815	720	95
Pb^{2+}	1,089	1,020	69	815	714	101
Cd^{2+}	1,098	1,022	76	813	714	99
Ca^{2+}	1,137	1,026	111	806	720	86
Zn^{2+}	1,136	1,049	87	808	720	88
Ga^{3+}	1,126	1,050	76	816	720	96
Al^{3+}	1,149	1,080	69	817	720	97
In^{3+}	1,130	1,052	78	815	720	95
Fe^{3+}	1,102	1,040	62	802	720	82

sodium and aluminum di-(*n*-octyl) phosphinate appeared at the highest energy. Ferraro et al. [46] reported that for the sodium form of the P,P′-di-(2-ethylhexyl) methanediphosphinic acid, the highest energy indicated a weak interaction and a highly ionic Na–O bond. The bonds become more covalent as the value of the $\Delta\nu$ decrease. However, in this study, aluminum had a higher affinity for the ligand than the sodium. While the $\nu_{asym}(POO^{-})$ stretching mode associated with aluminum was at the highest energy, the metal complex had a lower $\Delta\nu$ compare to gallium and indium. Ferraro et al. [46] reported spectral complications due to structural differences between the metal complexes of interest. To verify if the sodium di-(*n*-octyl) phosphinate and the aluminum di-(*n*-octyl) phosphinate complexes have the same structure, an x-ray diffraction was carried out. As observed in Figures 7.18 and 7.19, the sodium form of the ligand had sharp narrow diffraction peaks compared to the aluminum–ligand complex, which had broader peaks (halo). These spectra showed a more amorphous behavior of the aluminum–ligand complex than the sodium–ligand complex. As sodium complexes differently than aluminum with the ligand, their bond with the ligand is certainly different and cannot be compared.

Ferraro et al. [46] also reported a good correlation between the ionic potential Φ and $\Delta\nu$. Using the same notation, Figure 7.20 shows Φ versus $\Delta\nu$. While the affinity of the ligand for the highest charges and biggest ionic radius is represented in the ionic potential, the metal (II) and the metal (III) had two different behaviors with the ligand. For the metal (II), the small linear slope is generally indicative of a similar bonding across the series. In the case of the metal (III), a more disperse behavior was observed. No correlation could be obtained between the two parameters, Φ and Δν. This can be explained again using the X-ray diffraction of the aluminum and gallium

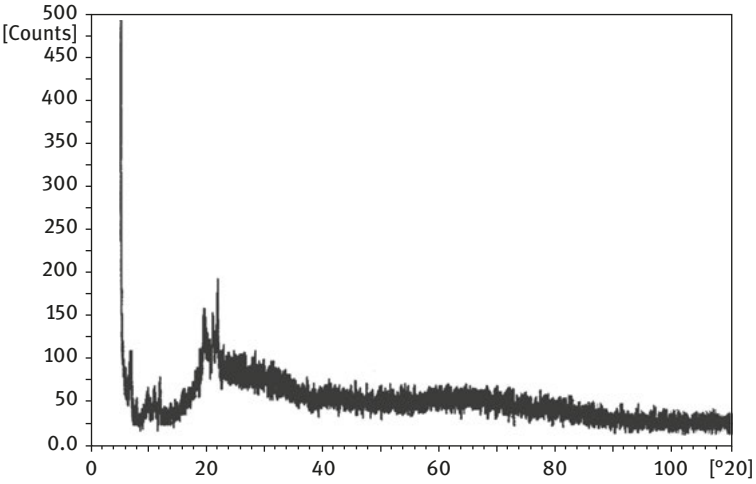

Figure 7.18: X-ray diffraction of the insoluble complex formed between aluminum and the sodium di-(*n*-octyl) phosphinate ligand at a mole ratio of 3 [35].

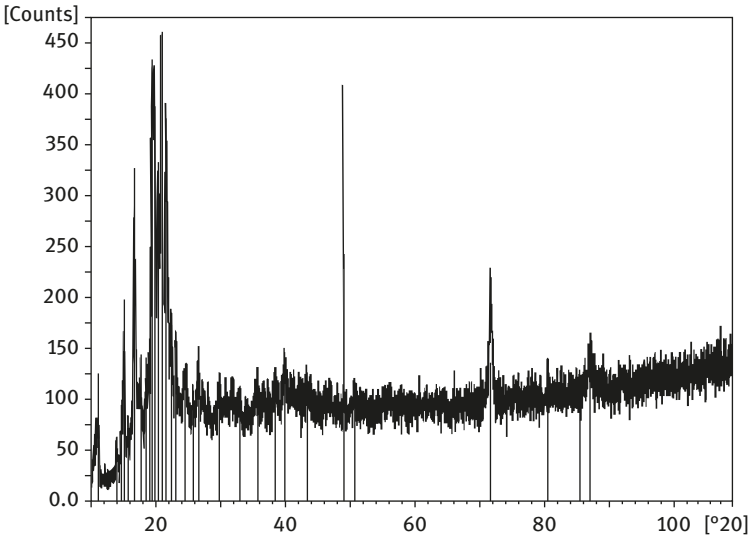

Figure 7.19: X-ray diffraction of the sodium di-(*n*-octyl) phosphinate [35].

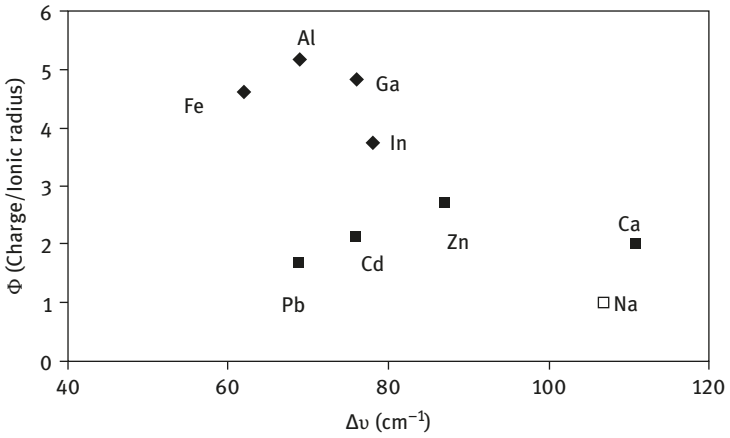

Figure 7.20: Ionic potential (Φ) of the metal ion versus Δ*v* for various insoluble di-(*n*-octyl) phosphinate/metal complexes formed at $r^{\circ} = 3$ (◆ : Elements charged 3 +; ■ : Elements charged 2+; □ : Element charged 1+) [35].

complexes. Figure 7.21 shows a crystalline structure with its sharp narrow diffraction peaks for the gallium complex as obtained for the sodium form of the ligand. The different amorphous structure of the aluminum complex makes the correlation more difficult [46]. In this case, the affinity of the ligand for the gallium over the aluminum is more related to the structure of the metal–ligand complex. The same explanation

can be given for the affinity of the ligand for the Fe (III) over the Ga (III) considering the large difference, $\Delta\nu$, of the respective P–O and P–C bands of the metal–ligand complexes. This effect of the structure on the selectivity was also observed for the extraction of Co (II) and Ni (II) using the same ligand, di-(*n*-octyl) phosphinic acid, in toluene solutions [30].

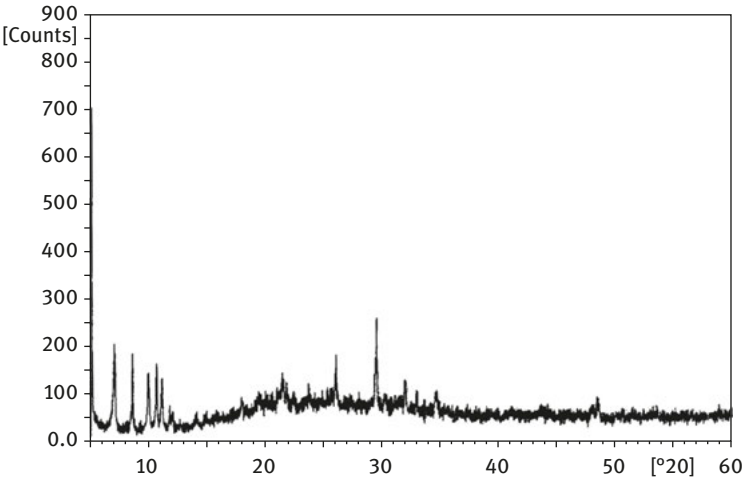

Figure 7.21: X-ray diffraction of the insoluble complex formed between gallium and the sodium di-(*n*-octyl) phosphinate ligand at a mole ratio of 3 [35].

In summary, of the many factors determining the affinity of the sodium di-(*n*-octyl) phosphinate for metal ions, the following factors are significant:

- the hard and soft theory (the hard ligand reacts with the hard metals)
- the charge of the metal (higher charges have more affinity)
- the ionic radius (larger is the radius, better the affinity)
- the structure of the complex
- the electronegativity of the metals (including the influence of the orbital).

7.3.4.4 Recovery of Metal Ions and Regeneration of the Precipitating Agent

Two phases, one organic and the other aqueous, are used to dissolve the metal–ligand complex and separate the metal from the ligand. The metal is concentrated in the aqueous phase and the ligand is extracted into the organic phase. For gallium, the initial insoluble $GaL_{3(s)}$ complex was formed by adding the ligand to an aqueous solution containing 0.36 mM of gallium at a mole ratio of ligand to gallium of 3. The equilibrium pH was 2. The solid complex was separated from the initial aqueous solution, and one of the two recovery approaches was performed:

a. Recover gallium in an acid aqueous phase. In this case, the ligand is extracted in the organic phase in its acidic form and further treatment is needed to convert it back to its sodium form.
b. Recover gallium in a basic aqueous solution. The ligand is extracted in its sodium form.

Figure 7.22 shows the recovery of gallium in an acidic aqueous solution using either diethyl ether or chloroform. At an equilibrium pH below 0.5 for diethyl ether and 1.5 for chloroform, gallium concentrated over 80% in the aqueous solution. The amount of ligand dissolved in the aqueous solution was below the detection limit of the ICP. The ligand was extracted in its acidic form in the solvents. No gallium was detected in the ligand regenerated after evaporation of the organic phase. As the pH increased, the concentration of gallium in the aqueous solution decreased and a mixture of gallium and ligand precipitated at the water/solvent interphase. While at acidic pH, the H^+ ions compete with gallium for the ligand, the GaL_3 complexes are more stable close to the optimum pH of 2 obtained for the removal of gallium with the ligand. Furthermore, a decrease in pH between the initial and equilibrium pH was observed in this area, indicating the formation of hydroxyl complexes with gallium.

The ligand was extracted by both the chloroform and the diethyl ether solvents. The advantages of the chloroform over the diethyl ether are as follows:

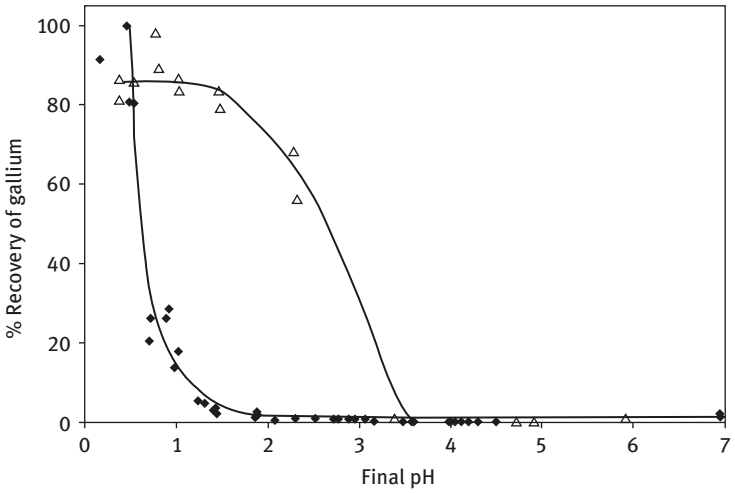

Figure 7.22: Effect of pH on the percent recovery of gallium in the aqueous phase using diethyl ether (◆) or chloroform (Δ) [19]. Reproduced with permission from Dumortier R, Weber M E, Vera J H. Removal and recovery of gallium from aqueous solutions by complexation with sodium di-(n-octyl) phosphinate. Hydrometallurgy USA 2005, 76, 207–15. Copyright (2005) Elsevier.

- Its lower solubility in water. When lower amounts of diethyl ether were added to dissolve the complex implicating a higher concentration of ligand in the diethyl ether phase, the solubility of the solvent inhibited the complete extraction of the ligand. Some ligand remained solubilized with the solvent in the aqueous solution.
- Higher pH than the diethyl ether to recover the gallium from the complex gallium ligand in an acidic aqueous solution.

However, because of the need to evaporate the solvent to regenerate the ligand, the higher boiling point of chloroform is a disadvantage.

In the second approach, gallium was recovered, and the ligand was regenerated at the same time in its sodium form using a basic aqueous solution. The complex was dissolved in a 3 N NaOH solution and diethyl ether. In this strong basic condition, the hydroxyl ions compete with the ligand for the gallium and the sodium ions compete with gallium for the ligand. More than 98% of gallium was concentrated in the aqueous solution, while all the ligand was extracted into the diethyl ether phase. The ligand was then regenerated by evaporating the ether phase. No gallium was detected in the regenerated ligand. Thus, the recovery of gallium using concentrated NaOH solution presents an advantage over the recovery in acidic solution as the ligand is regenerated in its sodium form and the amount of gallium recovered is higher.

7.3.4.5 Model of the Complexation and Precipitation of the Metals

The affinity of the different metals and their complexation with sodium di-(*n*-octyl) phosphinate ligand are discussed in the previous sections. Here is the summary of the phenomena observed and the conclusions:

- The sodium di-(*n*-octyl) phosphinate was removed from aqueous solutions in its acidic or sodium form or by complexation with a metal ion.
- Complete removal of metal was obtained when the metal ion and the ligand were oppositely charged. The formation of metal complexes with counter ions, such as chloride and sulfate, inhibited the removal of metals.
- Better removal of the metals with the ligand was generally obtained in acidic conditions. In basic solutions, metal hydroxide precipitates formed. Under these conditions, the addition of the ligand helped increasing the size of the precipitated particles, hence allowing better separation between the aqueous phase and the solid phase.

Based on these observations, a model on the complexation of the metals ions with the sodium di-(*n*-octyl) phosphinate ligand was developed for different pH.

The model takes into account the presence of competing ions such as the hydroxide counter ions and the possible formation of carbonate complexes from CO_2 in the air.

The following assumptions were made in order to obtain a workable model:

a. The phases are in equilibrium.
b. The total volume of the reaction mixture is constant throughout the reaction time.
c. The temperature is constant at 25 °C; thus, the stability constants at this temperature are considered.
d. The concentration of CO_2 in air and the atmospheric pressure are constant at 370 mg CO_2/L of air [47] and 1 atm, respectively.
e. The liquid phase is a dilute solution, and the activity coefficients of the different solutes are equal to 1.
f. The gas is ideal and the density of water is 1 g/mL.
g. Sodium di-(*n*-octyl) phosphinate and the metal nitrates are strong electrolytes, that is, dissociate completely into their positive and negative ions.

7.3.4.5.1 Complexes and Their Stability Constants

The successive equilibrium from the reaction of a cation M^{m+} reacting with an anion A^- is represented by

$$M^{m+} + nA^- \longleftrightarrow M(A)_n^{m-n} \tag{R7.19}$$

with n = 1, 2, and 3 for m = 2 and n = 1, 2, 3, and 4 for m = 3.

Based on this reaction, the stability constant, $K_{n,M}$, was defined as

$$K_{n,M} = \frac{C_{M^{m+}} C_{A^n}{}^{m-n}}{C_{MA_n}{}^{m-n}} \tag{7.7}$$

where C is molar concentration (moles per liter of solution) of given species. The solubility product was defined as

$$K_{sp,MA_n} = C_{M^{m+}} C_{A^-}{}^n \tag{7.8}$$

The number of moles of M, n_M, is given by

$$n_M = VC_M \tag{7.9}$$

where V is the total volume in liter of the solution.

7.3.4.5.2 CO_2 from the Air

CO_2 dissolves in aqueous solutions to an extent determined by its partial pressure and its interaction with other solutes in water. Reaction (7.20) is an equilibrium reaction between the gaseous and the aqueous forms of CO_2:

$$CO_{2(g)} \overset{K_{1,CO_2}}{\longleftrightarrow} CO_{2(aq)} \tag{R7.20}$$

This equilibrium can be described by Henry's law. The concentration of CO_2 in the aqueous solution, $C_{CO_{2(aq)}}$, is proportional to the partial pressure of gaseous CO_2:

$$C_{CO_{2(aq)}} = K_{1,CO_2} P_{CO_2} \tag{7.10}$$

where K_{1,CO_2} was selected for an ionic strength equal to 0 and at ambient temperature [48] with P_{CO_2} in atm.

In acidic solutions (pH < 5), the main species present in aqueous solutions at equilibrium is $CO_{2(aq)}$. At higher pH, bicarbonate and carbonate ions form according to reactions (R7.21) and (R7.22):

$$CO_{2(aq)} + 2H_2O \overset{K_{2,CO_2}}{\longleftrightarrow} HCO_3^- + H_3O^+_{(aq)} \tag{R7.21}$$

and

$$HCO_3^- + H_2O \overset{K_{2,CO_2}}{\longleftrightarrow} CO_3^{2-} + H_3O^+_{(aq)} \tag{R7.22}$$

where $K_{2,CO_2} = \frac{C_{HCO_3^-} C_{H^+}}{C_{CO_{2(aq)}}}$ and $K_{3,CO_2} = \frac{C_{CO_3^{2-}} C_{H^+}}{C_{HCO_3^-}}$ are obtained from literature [48].

7.3.4.5.3 Hydrolysis of Metal

The formation of the metal hydroxide complexes is mainly pH and concentration of metal dependent. In gallium solutions with more than 100 mg/L Ga (1.4 mM), one or more polynuclear species, such as $Ga_{26}(OH)_{65}^{13-}$, can exist at pH above 3. However, for solutions where Ga is below 10 mg/L (0.14 mM), the following four mononuclear complexes can form based on reaction (7.11) [40, 49]:

$$Ga(OH)^{2+} \longleftrightarrow Ga^{3+} + OH^- \tag{R7.23}$$

$$Ga(OH)_2^+ \longleftrightarrow Ga^{3+} + 2OH^- \tag{R7.24}$$

$$Ga(OH)_3 \longleftrightarrow Ga^{3+} + 3OH^- \tag{R7.25}$$

$$Ga(OH)_4^- \longleftrightarrow Ga^{3+} + 4OH^- \tag{R7.26}$$

where $K_{1,Ga} = \frac{C_{Ga^{3+}} C_{OH^-}}{C_{Ga(OH)^{2+}}}$, $K_{2,Ga} = \frac{C_{Ga^{3+}} C^2_{OH^-}}{C_{Ga(OH)_2^+}}$, $K_{3,Ga} = \frac{C_{Ga^{3+}} C^3_{OH^-}}{C_{Ga(OH)_3}}$ and $K_{4,Ga} = \frac{C_{Ga^{3+}} C^4_{OH^-}}{C_{Ga(OH)_4^-}}$ are obtained from literature [40].

If $Ga(OH)_3$ precipitates, an additional relationship must be satisfied:

$$Ga(OH)_{3(S)} \longleftrightarrow Ga^{3+} + 3OH^- \quad \text{(R7.27)}$$

where $K_{sp,Ga} = C_{Ga^{3+}} C^3_{OH^-}$ is obtained from literature [40] .

The precipitation of $Ga(OH)_{3(s)}$ occurs when the concentration of soluble gallium in saturated solution, $C_{Ga_{soluble}}$, is superior to the initial concentration of gallium (i.e., $C_{Ga_{soluble}} = \frac{K_{sp,Ga}}{C^3_{OH}} > C^\circ_{Ga}$). The gallium hydroxide precipitate was assumed to be the amorphous form $Ga(OH)_{3(s)}$ (R7.27) and not the oxyhydroxide GaO(OH) form (R7.28 and R7.29):

$$GaO(OH)_{(S)} \longleftrightarrow Ga^{3+} + 3OH^- \quad \text{(R7.28)}$$

where $K_{sp_2,Ga} = C_{Ga^{3+}} C^3_{OH^-}$ is obtained from literature [40].

While GaO(OH) is a more stable complex than $Ga(OH)_{3(s)}$, it forms by aging $Ga(OH)_{3(s)}$. The oxyhydroxide form solubilizes in water according to

$$GaO(OH)_{(S)} \longleftrightarrow Ga(OH)_3(aq) \quad \text{(R7.29)}$$

where $K_{sp_3,Ga} = C_{Ga(OH)_3(aq)}$ is obtained from literature [40].

The same applies to dilute aluminum solutions where four mononuclear complexes can be formed depending on the pH of the solution: $Al(OH)^{2+}$,$Al(OH)_2^+$, $Al(OH)_3$, and $Al(OH)_4^-$. The solubility constant of Gibbsite, which is the stable form of aluminum hydroxide at room temperature, was considered [40]. The equilibrium, as described in reaction (7.30), was reached after 1–3 months:

$$Al(OH)_{3(S)} \longleftrightarrow Al^{3+} + 3OH^- \quad \text{(R7.30)}$$

where $K_{sp,Al} = C_{Al^{3+}} C^3_{OH^-}$ is obtained from literature [40].

For gallium, a total of 14 different species listed in Table 7.6 were considered when the pH of the aqueous solution is adjusted by the addition of NaOH or HNO_3.

A mass balance and a charge balance of the system were performed. The speciation of gallium as a function of pH is shown in Figure 7.23. The calculation was made for a total concentration of gallium of 0.36 mM (25 mg/L). Themodel showed that $Ga(OH)_{3(s)}$ precipitates at a pH between 3 and 8 while a small amount of $Ga(OH)_3$ remained in the solution in its soluble form. Experimental data were compared with the computed values as shown in Figure 7.24. As more time was

Table 7.6: Possible species in an aqueous solution of gallium nitrate at different pH values adjusted by HNO_3 or NaOH [35].

Liquid	Total	Solid	Total	Gas	Total
Ga^{3+}, $GaOH^{2+}$,$Ga(OH)_2^+$, $Ga(OH)_3$, $Ga(OH)_4^-$, H^+, OH^-, CO_2, HCO_3^-, CO_3^{2-}, NO_3^-, Na^+	12	$Ga(OH)_{3(s)}$	1	CO_2	1

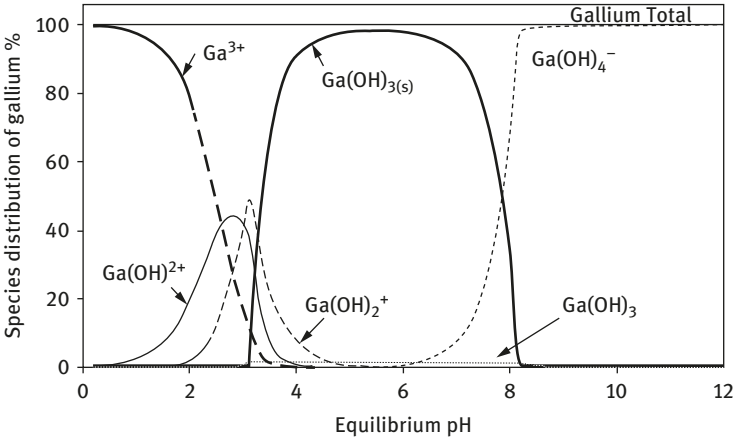

Figure 7.23: Distribution of gallium species in aqueous solutions at different pH [C°_{Ga}] = 0.36 mM, values calculated with parameters from Baes and Mesmer [35, 40].

given to the phase to reach equilibrium, the experimental data approached the computed values. Because of the small amount of gallium used in these experiments and the fact that the solution was not seeded with $Ga(OH)_{3(s)}$ to favor the precipitation, a smaller amount of precipitate formed after 1 day. The difference between the experimental and computed values is expected because the values of the stability constants and the solubility products reported by Baes and Mesmer [40] were obtained using seeded solutions and a longer contact time.

7.3.4.5.4 Model of the Sodium Di-(*n*-octyl) Phosphinate Ligand Removal

As mentioned previously, the sodium di-(*n*-octyl) phosphinate ligand can be removed from aqueous solutions containing no metals either in its acidic form or in its sodium form. A stability constant of the ligand in its acidic form was used in this case as it was observed during the experiments that a small amount

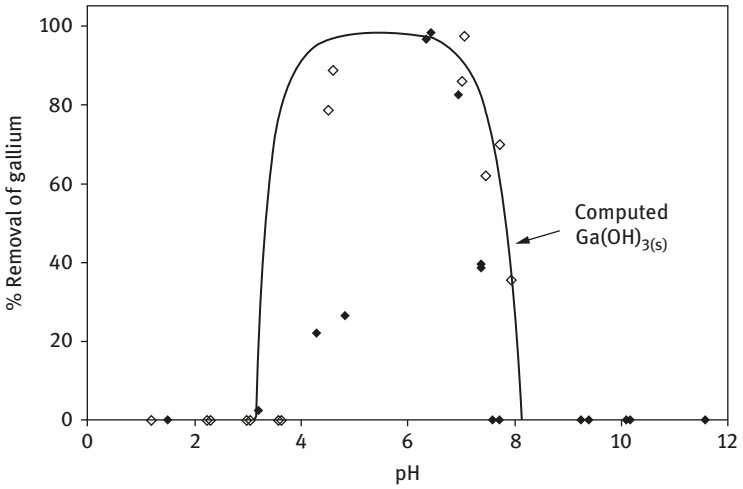

Figure 7.24: Precipitation of gallium in aqueous solution at different pH values. [C°_{Ga}= 0.36 mM; experimental removal of $Ga(OH)_{3(s)}$ obtained after: 1 day (◆), 6 days (◇); line: computed $Ga(OH)_{3(s)}$] [35].

of ligand remained in solution. The following reactions were considered to model the solubility of the organophosphorus ligand in aqueous solutions at different pH values:

$$HL \longleftrightarrow H^+ + L^- \qquad \text{(R7.31)}$$

From reaction (7.12): $HL_{(S)} \longleftrightarrow H^+ + L^-$ $K_{sp,HL}= 10^{-10}$
From reaction (7.13): $NaL_{(S)} \longleftrightarrow Na^+ + L^-$ $K_{sp,NaL}= 10^{-4.7}$

All values of the stability constants were parameters fitted [35].

Figure 7.25 shows the computed and the experimental values of the percent loss of sodium di-(*n*-octyl) phosphinate for two concentrations of the ligand. At low pH, the ligand is mainly removed in its insoluble acidic form. The small loss of ligand was due to the formation of its soluble acidic form as described in reaction 7.31. At higher pH, the ligand remained in solution at its natural pH. The ligand is removed in its sodium form at pH above 12 due to the excess of sodium from the sodium hydroxide. The model also showed a slight shift as the ligand concentration increased from 1 to 2 mM. The experimental values agreed with the computed values, indicating the differences in the percent loss of ligand as the concentration increased from 1 to 2 mM was only marginal. A pH 13, the difference between the computed and experimental value is due to the slow formation of the sodium form of the ligand. Longer time would be required to reach equilibrium.

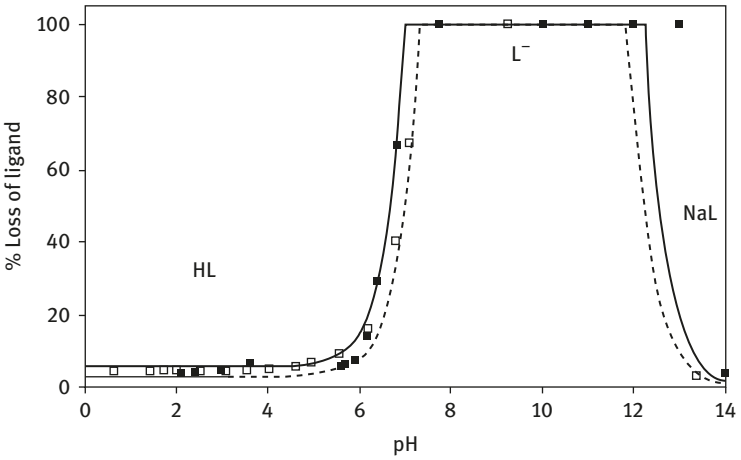

Figure 7.25: Comparison between the computed and the experimental values of the percent loss of sodium di-(*n*-octyl) phosphinate for two concentrations of the ligand [C_L°= 1 mM (■) and 2 mM (□); model: line C_L°= 1 mM, dashed line C_L°= 2 mM] [35].

7.3.4.6 Model of the Metal Removal by the Sodium Di-(n-octyl) Phosphinate Ligand

The equilibrium constants of the metal–ligand complexes were adjusted parameters [35]. For gallium, the formation of soluble GaL_3 was neglected; thus, the value of K_{GaL_3} was not reported in reaction (7.32). The following equilibrium constants were used for the model:

$$GaL_3 \longleftrightarrow Ga^{3+} + 3L^- \quad K_{Ga}L_3\text{negligible} \qquad \text{(R7.32)[35]}$$

$$GaL_{3\,(S)} \longleftrightarrow Ga^{3+} + 3L^- \quad K_{sp,\,GaL_3} = 2.5 \times 10^{-30} \qquad \text{(R7.33)[35]}$$

$$AlL_3 \longleftrightarrow Al^{3+} + 3L^- \quad K_{AlL_3} = 5 \times 10^{-22} \qquad \text{(R7.34)[35]}$$

$$AlL_{3\,(S)} \longleftrightarrow Al^{3+} + 3L^- \quad K_{sp,\,AlL_3} = 2 \times 10^{-27} \qquad \text{(R7.35)[35]}$$

$$InL_3 \longleftrightarrow In^{3+} + 3L^- \quad K_{InL_3} = 5 \times 10^{-29} \qquad \text{(R7.36)[35]}$$

$$InL_{3\,(S)} \longleftrightarrow In^{3+} + 3L^- \quad K_{sp,\,InL_3} = 3.7 \times 10^{-35} \qquad \text{(R7.37)[35]}$$

$$FeL_3 \longleftrightarrow Fe^{3+} + 3L^- \quad K_{FeL_3} = 6 \times 10^{-30} \qquad \text{(R7.38)[35]}$$

$$FeL_{3\,(S)} \longleftrightarrow Fe^{3+} + 3L^- \quad K_{sp,\,FeL_3} = 9 \times 10^{-36} \qquad \text{(R7.39)[35]}$$

$$ZnL_{2(S)} \longleftrightarrow Zn^{2+} + 2L^- \quad K_{sp,\,ZnL_2} = 2.7 \times 10^{-17} \qquad \text{(R7.40)[38]}$$

$$CdL_{2(S)} \longleftrightarrow Zn^{2+} + 2L^- \quad K_{sp,\,CdL_2} = 9.52 \times 10^{-16} \qquad \text{(R7.41)[38]}$$

$$PbL_{2(S)} \longleftrightarrow Pb^{2+} + 2L^- \quad K_{sp,\,PbL_2} = 9.18 \times 10^{-17} \qquad \text{(R7.42)[38]}$$

All the different forms of metals, including the complexes with hydroxide and the ligand, were accounted for in the mass balance except for the soluble ZnL_2, CdL_2, PbL_2, and GaL_3.

The following case is for a solution containing gallium nitrate and the ligand. The algorithm to find the gallium removed, and the equilibrium pH as well as the concentrations of the other species is based on the following:

7.3.4.6.1 Mass Balance of Ga(III)

$$n^{\circ}_{Ga} = n_{Ga^{3+}} + n_{GaOH^{2+}} + n_{Ga(OH)_2^+} + n_{Ga(OH)_3} + n_{Ga(OH)_{3(s)}} + n_{Ga(OH)_4^-} + n_{GaL_{3(s)}} \tag{7.11}$$

7.3.4.6.2 Mass Balance of Nitrate

The nitrate in solution came from the nitric acid used to adjust the initial pH and/or from the metal nitrate.

$$n^{\circ}_{NO_3} = 3n^{\circ}_{Ga} + n^{\circ}_{HNO_3} = n_{NO_3^-} \tag{7.12}$$

7.3.4.6.3 Mass Balance of Sodium

The sodium was added to the solution either in the form of NaOH to adjust the initial pH or in the form of sodium di-(*n*-octyl) phosphinate.

$$n^{\circ}_{Na} = n_{Na^+} + n_{NaL_{(S)}} \tag{7.13}$$

7.3.4.6.4 Mass Balance of Ligand

$$n^{\circ}_{L} = n_{L^-} + n_{NaL_{(s)}} + n_{HL_{(s)}} + n_{HL} + 3n_{GaL_{3(s)}} \tag{7.14}$$

7.3.4.6.5 Charge Balance Equation Expressing Electroneutrality of the Solution

$$\begin{aligned} &3n_{Ga^{3+}} + 2n_{GaOH^{2+}} + n_{Ga(OH)_2^+} + n_{Na^+} + n_{H^+} = \\ &n_{Ga(OH)_4^-} + n_{L^-} + n_{NO_3^-} + n_{OH^-} + n_{HCO_3^-} + 2n_{CO_3^{2-}} \end{aligned} \tag{7.15}$$

Figure 7.26 shows the comparison between the experimental data and the model. The experimental data and the computed values were in good agreement in the pH range considered. The ligand was initially removed in its acidic form below a pH of 1. When

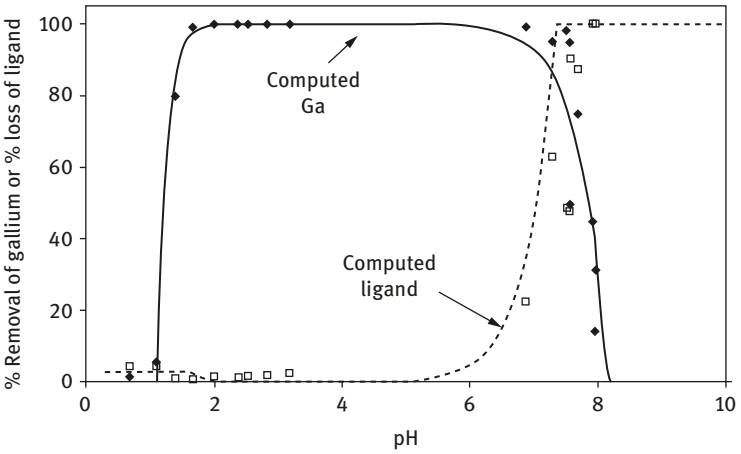

Figure 7.26: Comparison between the computed and the experimental values for the effect of the pH on the percent removal of gallium (◆); and percent loss of sodium di-(*n*-octyl) phosphinate (□) [C°_{Ga}= 0.36 mM, $r^{\circ}_{L/Ga}$= 3; experimental values after 2 days] [35].

gallium formed a complex with the ligand, the removal of the ligand from the solution increased as the soluble ligand was removed either with gallium or in its acidic form. Between pH about 7 and 8, the model showed that gallium is mostly removed in its hydroxide form, while the ligand remains in the solution. The close agreement between the calculated and the measured values can be considered as an indication that the assumptions in the model are reasonable and that the values of the solubility products and the mass-stability constants are correct.

The model based on the solubility products of the precipitates measured in this work and the available literature data for stability constants of the other reactions was also tested for

- 3+ charge metals ions: Al^{3+}, In^{3+}, and Fe^{3+} [35];
- 2+ charge metal ions: Zn^{2+}, Cd^{2+}, and Pb^{2+} [38].

A close agreement between the calculated and the measured values was also obtained for these other metals [35, 38].

In conclusion, the model based on the solubility products of the precipitates measured in this work and the available literature data for stability constants of the other reactions gives results that are in good agreement with the experimental data.

7.4 Summary

Sodium caprate was successfully used to remove lead in aqueous solutions by precipitation. A high removal above 99% was achieved at a mole ratio of caprate

to lead of 2 in a feed concentration of 7 mM (1,450 mg/L) lead. The presence of calcium, chloride, or nitrate in the feed did not affect the removal of lead by the sodium caprate. After separation of the precipitate from the aqueous solution, the sodium caprate was regenerated by adding HNO_3 to the lead caprate precipitate. The lead was recovered in a concentrated aqueous solution, while the capric acid generated was converted to the sodium caprate by adding sodium hydroxide. About 99% of the sodium caprate was recovered at the end of the process.

A new precipitation process was reported for the removal and recovery of metal ions from aqueous solutions using sodium di-(*n*-octyl) phosphinate and sodium di-(*n*-dodecyl) phosphinate. Because of the higher solubility of the sodium di-(*n*-octyl) phosphinate when water compared to the dodecyl form, a better metal removal was obtained for sodium di-(*n*-octyl) phosphinate. The metal–ligand complexes formed had low solubility in water and the ligand was easily regenerated. The metal ions were recovered from the insoluble ligand–metal complexes using diethyl ether or chloroform in contact with an aqueous solution. While the metal was solubilized in the aqueous phase, the ligand was extracted in the organic phase and recovered by evaporating the organic phase. The ligand was then regenerated to its sodium form by the addition of a concentrated NaOH solution.

Of the many factors determining the affinity of the sodium di-(*n*-octyl) phosphinate for metal ions, the following factors are significant:

- the hard and soft theory (the hard ligand reacts with the hard metals),
- the charge of the metal (higher charges have more affinity),
- the ionic radius (larger is the radius, better the affinity),
- the structure of the complex,
- the electronegativity of the metals (including the influence of the orbital).

While chemical precipitation is commonly used methods for removing heavy metal ions, recent researches focused on low cost, high efficiency, and ease of use methods for waste water treatment [50–55]. However, additional research later performed by Esalah and Husein [56] on the removal of heavy metals from aqueous solutions by precipitation using organophosphorus ligand showed that the sodium form of the mono- and di-(*n*-hexa-decyl) phosphinate offered more advantages over the previously studied sodium dioctyl and dodecyl phosphinates. The organophosphorus ligands removed different heavy metals and had a much lower solubility in water, which contributed lower loss of the reagent. The optimum process conditions resulted in a residual concentration of the heavy metals tested below the acceptable levels for most regions. The selectivity of the ligand was in the order of Pb > Cd > Co and Ni > Hg. At the end of the process, 99.99% of the ligand was regenerated and the metals was recovered and concentrated more than 100 times in an aqueous solution.

References

[1] Fu F, Wang Q. J Environ Manage 2011, 407.
[2] Peters R, Ku Y, Bhattacharyya D. AIChE Symp Series 1985, 165.
[3] Patterson J. Butterworth, Pub., 2nd Ed., Butterworth, Pub., Boston, MA, 1985.
[4] Patterson J, Allen H Scala J. J Water Pol Control Fed. USA 1977, 49, 2397.
[5] Bhattacharyya D, Jumawan A, Grieves R. Sep Sci Technol USA 1979, 14(5),441.
[6] Brooks C. J of Metals USA 1986, 38, 50.
[7] Martell AE, Hancock RD. Plenum Press, New York, NY, 1996.
[8] Schwarzenbach G. Adv Inorg Radiochem USA 1961, 3(257), 265.
[9] Pearson RG. J Am Chem Soc USA 1963, 85(22),3533.
[10] Pearson RG. J Chem Ed USA 1987, 64(7), 561.
[11] Pearson RG, Songstad J. J Am Chem Soc USA 1967, 89(8),1827.
[12] Massey AG. Inorg Chem, 2nd ed, J. Wiley & Sons, New York, NY, 2000, 208.
[13] Husein M. Eng. Thesis, McGill Univ, Montreal, Canada, 1996.
[14] Husein M, Vera JH, Weber ME. Sep Sci Technol USA 1998, 33(12),1889.
[15] Esalah JO, Weber ME, Vera JH. Sep Pur Technol USA 2000, 18, 25.
[16] Esalah JO, Weber ME, Vera JH. Can J Chem Eng Canada 2000, 78, 948.
[17] Dumortier R, Rodil E, Weber ME, Vera JH. Water Res USA 2004, 38, 1745.
[18] Rodil E, Dumortier R, Vera JH. Chem Eng J USA 2004, 97, 225.
[19] Dumortier R, Weber ME, Vera JH. Hydrometal USA 2005, 76, 207.
[20] Hahne H, Kroontje W. J Environ Qual USA 1973, 2, 444.
[21] Meissner HP. Newman SA, Barner HE, Klein M, Sandler SI. Washington DC, Am Chem Soc, 1980, 495.
[22] Demopoulos G, Papangelakis V. AIChE J USA 1995, 41, 171.
[23] Schock M. J Am Water Works Assoc USA 1980, 72, 695.
[24] Solomons TWG. John Wiley & Sons Inc, New York, NY, 1996.
[25] Manuel V, Pinto JJ, Mendiguchia C, Moreno C. Cent Eur J of Chem Germany 2014, 12, 348.
[26] De AK, Khopkar SM, Chalmers RA. Van Nostrand Reinhold Co., New York, NY, 1970.
[27] Peppard DF, Ferraro JR, Mason GW. J Inorg Nucl Chem USA 1959, 12, 60.
[28] Preston JS. Hydrometal USA 1982, 9, 115.
[29] Rickelton WA, Mihaylov IO, Love BJ, Louie PK, Krause E. US patent 5,759,512, 1998.
[30] Danesi PR, Reichley-Yinger L, Mason G, Kaplan L, Horwitz EP, Diamond H. Sol Ext Ion Exc USA 1985, 3, 435.
[31] Sole KC. Aguilar M, Cortina JL. 1st Ed., CRC Press, Boca Raton, FL, 2008, 141.
[32] Volesky B, Volesky B. Ed., CRC Press, Boca Raton, FL, 1990.
[33] Env Prot Agen. 625/R-97/004. 1997.
[34] Wang Q, Tsunoda K, Akaiwa H, Sugiya M, Watanabe T. Anal Sci USA 1996, 12, 931.
[35] Dumortier R. PhD Thesis, McGill Univ, Montreal, Canada, 2005.
[36] Williams R, Hamilton L. J Am Chem Soc USA 1952, 74, 5418.
[37] Peppard D, Mason G, Lewy S. J Inorg Nucl Chem USA 1965, 27, 2065.
[38] Esalah JO. PHD Thesis, McGill Univ, Montreal, Canada, 1997.
[39] Uchida M, Okuwaki A. J Sol Chem USA 1997, 26(7),699.
[40] Baes CF, Mesmer RE. Krieger Pub Comp, Malabar, FL, 1986.
[41] Ritcey GM, Ashbrook AW. Elsevier, New York, NY, 1984.
[42] Miessler GL, Tarr DA. 2nd Ed., Prentice-Hall Canada Inc., Toronto, Canada, 1998, 153.
[43] Huheey JE. 3rd Ed., Harper & Row, New York, NY, 1983, Append 1.
[44] Pitts JJ, Robinson MA, Trotz SI. J Inorg Nucl Chem USA 1969, 31, 3685.
[45] Haynes JS, Oliver KW, Thompson RC. Can J Chem Canada 1985, 63, 1111.

[46] Ferraro J, Herlinger AW, Chiarizia R. Solvent Ext Ion Exch USA 1998, 16(3), 775.
[47] Keeling CD, Whorf TP. Compend Data on Glob Chang. Carbon Dioxide Inform Anal Cent, Oak Ridge Nat Lab, US Dep Energ, Oak Ridge, TN, 2003.
[48] Butler JN. 1st Ed., John Wiley & Sons, New York, 1998.
[49] Martell AE, Motekaitis RJ. VCH, New York, NY, 1988.
[50] Guo J, Han Y, Mao Y, Wickramaratne MN. Colloids Surf A USA 2017, 529, 801.
[51] Wang X, Wang L, Wang Y, Tan R, Ke X, Zhou X, Geng J, Hou H, Min Z. Cryst USA 2017, 7, 270, 1.
[52] Mehduzadeh S, Sadjadi S, Ahmadi SJ, Outokesh M. J Env Health Sci Eng USA 2014, 12(7), 1.
[53] Moosa AA, Ridha AM, Hussien NA. Am J Mat Sci USA 2016, 6(4), 105.
[54] Aziz HA, Adlan MN, Ariffin KS. Bioresour Technol USA 2008, 99(6),1578.
[55] Dravanjooghi Karimi MH, Davoodi M, Dursun AY, Ehsani MR, Karimpour I, Ameri E. Adsorpt Sci Technol USA 2018, 0(0),1.
[56] Esalah J, Husein MM. Sep Sci Technol USA 2008, 43(13), 3461.

Younok Dumortier Shin and Eva Rodil

8 Extraction of Proteins from Aqueous Solutions by Complexation Using Surfactants

8.1 Introduction

In Chapter 6, we have reviewed the extraction of different biomolecules into the newly developed cationic and anionic reverse micellar systems. As mentioned in Chapter 6, biomolecules such as proteins, which are produced using bacterial cells, mammalian cells, or plant extracts, have significant industrial and therapeutic values. Traditional methods to purify proteins include crystallization, column chromatography, or electrophoresis [1], the use of polymers coupled with an affinity ligand [2–6], and liquid–liquid extraction using reverse micellar solutions [7]. Although the ionic surfactants were traditionally considered as a protein denaturant [8, 9], successful extraction of proteins using the different cation and anion surfactants [10–21] showed a potential advantage of this technique as a cost-efficient way to purify proteins.

Further study of the reverse micellar extraction revealed that the proteins form a complex with the oppositely charged surfactant head which is water insoluble. This phenomenon was described in more detail in Chapter 6.6. Depending on the concentration of surfactant and cosurfactant in the organic phase, and the type and concentration of the salts in the aqueous phase, the protein–surfactant complex precipitated out of the aqueous phase is solubilized into the reverse micellar phase up to a saturation limit. Once this limit is reached, the precipitated protein–surfactant complex remains at the aqueous–organic phase interface as a white precipitate.

With this knowledge, we have continued with our research to recover the proteins from the reverse micellar phase into a new aqueous phase. During the back-extraction experiments, the similar type of white precipitate noted during the forward extraction (i.e., extraction of proteins from the initial aqueous phase into a reverse micellar phase) was also observed at the interface of the fresh aqueous phase and the reverse micellar phase. This chapter summarizes the findings from our attempt to recover the proteins from the reverse micellar phase which eventually led to the idea of using the ionic surfactant as a direct precipitation reagent for protein purification, rather than having to involve organic phase containing cosurfactants to form reverse micellar phase.

https://doi.org/10.1515/9783110564808-008

8.2 Comparison of Two Methods to Recover Proteins from Reverse Micellar Phases

The aim of this research was to compare two methods of protein recovery from a reverse micellar phase: back extraction and solvent precipitation [22]. Two reverse micellar systems were used: one formed with the anionic surfactant sodium di(2-ethylhexyl) sulfosuccinate (AOT) and the other formed with the cationic surfactant dioctyl dimethyl ammonium chloride (DODAC). Lysozyme was chosen as a model protein to prepare a protein-loaded reverse micellar solution. To increase the recovery efficiency in the back-extraction step, we attempted to break the reverse micellar structure either by controlling the salt concentration or by adding decanol, ethanol, or ethyl acetate as cosolvents.

Instead of using a fresh aqueous phase to recover the protein from the reverse micellar phase, an alternate method using a polar organic solvent was attempted during our study. This method is referred to as "polar solvent precipitation method" in this chapter.

8.2.1 Experimental Conditions

The lysozyme solutions were prepared at different pH and salt concentrations to maximize the solubilization of lysozyme into either AOT reverse micellar phase or DODAC reverse micellar phase. For an AOT reverse micellar solution, the initial lysozyme-containing protein solution was adjusted to pH below its pI = 11. In contrast, for a DODAC containing reverse micellar solution, the pH of the lysozyme-containing solution needed to have the pH adjusted higher than 12 in order to create the electrostatic interaction for the protein to be solubilized into the reverse micellar phase. The reverse micellar phase containing either AOT or DODAC was prepared by dissolving the target amount of surfactant in the organic phase. For DODAC, decanol was used as a cosurfactant. The reverse micellar solution containing lysozyme was prepared by contacting the equal volume of the initial protein solution and the reverse micellar solution. This reverse micellar phase containing lysozyme was then contacted either with a fresh aqueous solution as a direct back-extraction method or with different polar organic solvents as a polar solvent precipitation method to improve the recovery efficiency. For the direct back-extraction method, the reverse micellar phase containing known amount of lysozyme was contacted with a fresh aqueous phase set at different pH and ionic strengths. During this back-extraction step, different types of cosolvents, such as ethanol and ethyl acetate, were also added as an attempt to improve the recovery efficiency.

Instead of the direct back-extraction method, a solvent precipitation method was used by contacting the lysozyme-containing reverse micellar solution with known

amount of polar organic solvents such as acetone. Upon contact with the polar organic solvent, the reverse micellar solution and the polar organic solvents formed a single-phase clear solution. The lysozyme was separated from the ionic surfactant and precipitated as surfactant-free white particles. The organic solvent, surfactant, and cosurfactant remained as a single-phase clear solution. The surfactant-free protein was then recovered from the mixture by centrifugation. The recovered protein was then solubilized into a fresh aqueous phase. In this study, the amount of protein recovered in the final aqueous phase was of interest.

The concentrations of lysozyme and surfactant in the aqueous phase were measured using high-performance liquid chromatograph (HPLC) technology. The concentration of lysozyme in the organic phase was measured using UV spectrophotometer at 280 nm subtracted by the UV reading at 310 nm to eliminate the absorbance signal produced by the reverse micellar solution from the signal produced by the proteins entrapped within. The enzymatic activities of lysozyme in the initial and final aqueous phases were measured using the procedures described by Davis et al. [23]. All experiments were carried out using two to six replicates. The results presented here are the average values and the sample standard deviations.

8.2.2 Back Extraction of Lysozyme from the Reverse Micellar Phases

Figure 8.1 presents the percent of lysozyme remaining in the reverse micellar phases after being contacted with a fresh aqueous solution on the left-hand-side axis, and

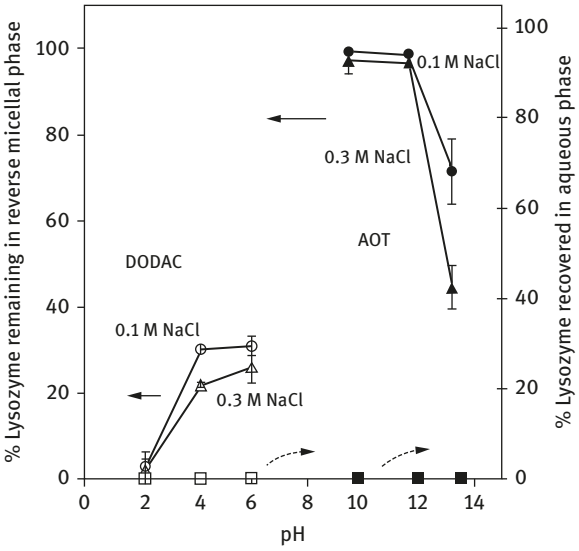

Figure 8.1: Percent of lysozyme in the reverse micellar phase and in the receiving aqueous phase after back extraction at room temperature. Initial reverse micellar phase: 100 mM DODAC (open symbols) or 30 mM AOT (filled symbols) containing 1 g/L lysozyme.

the percent of lysozyme extracted into the receiving aqueous solution on the right-hand-side axis. When the pH of the receiving aqueous solution was 9.8, about 1.2 units lower than the p*I* of lysozyme, over 90% of the lysozyme remained in the reverse micellar phase at both 0.1 and 0.3 M NaCl. An increase in the pH to 12.0 showed little change in the percentage of lysozyme remaining in the reverse micellar phase. When the pH was 13.6, the percent of lysozyme remaining in the reverse micellar phase decreased to 71% at 0.1 M NaCl and 44% at 0.3 M NaCl. These results confirm the electrostatic repulsion between the negatively charged lysozyme and the AOT surfactant head group [24, 25], and also the salting-out effect [13, 26]. The increase in the salt concentration results in a "dewatering effect" [27] of the reverse micellar phase; thus, the proteins are removed from the reverse micelles due to size exclusion [16, 28, 29].

However, the concentration of lysozyme in the receiving aqueous phase in all cases was below the detection limit indicating that no lysozyme was solubilized into the receiving aqueous phase; instead, the lysozyme formed a white precipitate at the aqueous–organic interface. As the pH and the salt concentration increased, an increasing amount of lysozyme was removed from the reverse micellar phase. This lysozyme was not solubilized into the receiving aqueous phase, but it precipitated at the aqueous–organic interface. This phenomenon suggests that the lysozyme removed from the reverse micellar phase formed an insoluble complex with the surfactant. The pH and the ionic strength adjustments were not sufficient to separate the AOT from the lysozyme.

Similarly, there was no recovery of lysozyme from a DODAC reverse micellar phase into a fresh aqueous phase. When the pH of the aqueous solution was 2.2, at 0.1 or 0.3 M NaCl, only 2% of the lysozyme remained in the reverse micellar phase. At this pH, lysozyme has an overall positive surface charge resulting in an electrostatic repulsion between lysozyme and the positively charged DODAC surfactant head group. At a pH of 4.2, more lysozyme remained in the reverse micellar phase. When the pH was 6.0, the lysozyme remaining in the reverse micellar phase at 0.1 M and 0.3 M NaCl was about 30% and 26%, respectively. This result supports with the electrostatic repulsion mechanism and the dewatering effect. However, the concentration of lysozyme in the receiving aqueous phase was below the detection limit. As more lysozyme was removed from the reverse micellar phase, an increasing amount of white precipitate was observed at the aqueous–organic interface. Ethanol or ethyl acetate was added to the DODAC reverse micellar phase in order to increase the percent recovery. However, similar to the AOT reverse micellar system, although the percent of lysozyme remaining in the reverse micellar phase decreased upon the addition of ethanol, lysozyme was not solubilized in the fresh aqueous phase.

To increase the recovery of lysozyme into the receiving aqueous phase, ethanol or ethyl acetate was added to into the reverse micellar phase. Having 400 mM ethanol in the 30 mM AOT reverse micellar phase, while the receiving aqueous phase was set at pH 12.0 and 0.1 M NaCl, only 3.2 ± 0.2% of the lysozyme remained in the reverse micellar

phase. However, the concentration of lysozyme in the aqueous phase was below the HPLC detection limit. Although the percent of lysozyme remaining in the reverse micellar phase decreased from 99% to 3.2% with the addition of ethanol, no lysozyme was recovered in the aqueous phase. The behavior was similar for ethyl acetate.

An attempt was also made to break the reverse micelles by reducing the salt concentration below 0.05 M NaCl in the receiving aqueous phase. At this salt concentration, no reverse micelles are formed in the organic phase [30]. The pH of the receiving aqueous solution was 13.6. Upon contact, both lysozyme and AOT were solubilized in the aqueous phase, which became milky. The salt concentration of the aqueous phase was then increased to induce the formation of reverse micelles. If the electrostatic repulsion theory were correct, the lysozyme should remain in the aqueous phase while AOT should migrate into the organic phase forming reverse micelles. When the salt concentration was increased to 0.3 M NaCl, the aqueous and organic phases became clear, but a white precipitate formed at the aqueous–organic interface, and the lysozyme concentration in both the aqueous and organic phases was below the detection limit. The use of an aqueous receiving phase with a pH and salt concentration adjustment was not sufficient to dissociate lysozyme from the AOT.

For both the AOT and the DODAC reverse micellar systems, the manipulation of pH and the salt concentration in the receiving aqueous phase or the addition of alcohols to the reverse micellar phase did not produce solubilization of lysozyme into a fresh aqueous phase. The fact that the lysozyme became water insoluble upon contact with a cationic or an anionic surfactant suggests the formation of a lysozyme–surfactant complex.

8.2.3 Solvent Precipitation from the Reverse Micellar Phases

Instead of using a fresh aqueous phase to recover the lysozyme from the reverse micellar phase, different types of polar organic solvent were used to first separate the lysozyme from the surfactant. The surfactant-free lysozyme precipitated, while the reverse micellar solution formed a single-phase clear solution with the polar organic solvent. The precipitated lysozyme, free of the ionic surfactant, was then solubilized into a fresh aqueous phase. The percent recovery of the protein was calculated using the following equation:

$$\%\ \text{recovery} = \left(\frac{C_f \cdot V_f}{C_o \cdot V_o}\right) \times 100 \tag{8.1}$$

where C_o and C_f are the lysozyme concentrations in the reverse micellar solution and in the final aqueous phase after recovery, respectively. The volumes of the initial reverse micellar solution and the final aqueous solution are denoted as V_o and V_f, respectively.

Table 8.1 summarizes the effect of different polar solvents used to obtain the surfactant free lysozyme. In this experiment, the polar organic solvents listed in the table were contacted with an equal volume of reverse micellar phase. The concentration of lysozyme in the reverse micellar phase was confirmed to be 1 g/L measured by UV method. All solvents, except for pentanol, provided complete removal of lysozyme from the reverse micellar phase. The reverse micellar phase formed one clear phase with acetone, methyl acetate, and methyl ethyl ketone, and the lysozyme precipitated at the bottom of the test tube. The precipitated lysozyme in the polar organic solvent was recovered by centrifugation and then solubilized in a fresh aqueous phase, which was distilled water in this case. The use of formaldehyde and acetonitrile gave two clear liquid phases, and a white precipitate formed at the solvent–organic interface. For the alcohols, methanol gave two clear liquid phases and a white precipitate formed at the solvent–organic interface, while isopropanol formed homogeneous clear solutions, and the lysozyme precipitated at the bottom of the test tubes. No precipitation was found when pentanol was used, and the concentration of lysozyme in the final aqueous phase was below the detection limit. The largest recovery was 72% using acetone as the polar solvent and distilled water as the final aqueous phase. An increase in the hydrophobicity of the solvent from acetone to methyl acetate and methyl ethyl acetate significantly reduced the recovery of lysozyme. The lysozyme recovered using formaldehyde and acetonitrile was insoluble in the final aqueous solution at any pH from 1 to 14, as well as in isooctane. For the alcohols, the precipitate obtained from methanol was water insoluble. The use of isopropanol gave a lysozyme recovery of 18%.

Table 8.1: Effect of polar solvents on the percent of lysozyme precipitated and subsequently recovered: initial reverse micellar phase, 30 mM AOT with 1 g/L lysozyme; final aqueous phase, distilled water.

Polar solvents	% mass of lysozyme removal from reverse micellar phase	% recovery in the final aqueous phase (Equation 8.1)
Acetone	100	72 ± 2
Methyl acetate	100	3 ± 1
Isopropanol	100	18 ± 1
Methyl ethyl ketone	100	0
Formaldehyde	*100	0
Acetonitrile	*100	0
Methanol	*100	0
Pentanol	0	0

*the lysozyme precipitated at the solvent-reverse micellar phase interface.

In order to ensure that the recovered protein still maintained its enzymatic activity, the percent recovery was measured using the enzymatic activity assay described by Davis et al. [23]. Table 8.2 summarizes the lysozyme activity before and after being contacted with the surfactant-containing solution. Before it was solubilized into the AOT reverse micellar phase, the lysozyme activity was 48,000 ± 3,000 units/mg protein. As shown in this table, the lysozyme precipitated by acetone retained its original activity.

Table 8.2: Percent lysozyme activity recovered from the reverse micellar extraction: initial reverse micellar phase, 30 mM AOT with 1 g/L lysozyme; final aqueous phase, distilled water.

Polar solvents	Lysozyme activity in the initial protein solution in 10^3 U/mg protein	Lysozyme activity in the final aqueous phase recovered in 10^3 U/mg protein	% denaturation
Acetone	48 ± 3	48 ± 3	0
Methyl acetate	48 ± 3	18 ± 3	63%
Isopropanol	48 ± 3	35 ± 5	27%

According to Luisi et al. [31], lysozyme denatures in AOT reverse micelles. However, when recovered from the reverse micelles by solvent precipitation with acetone and solubilized into a fresh aqueous phase, lysozyme recovered its original activity. When precipitated by methyl acetate, only 37% of the original activity was recovered. The use of isopropanol resulted in 73% of its original value. The AOT concentration in the aqueous phase was below the detection limit of the HPLC method for all cases. Since the lysozyme recovered using acetone showed the same activity as the initial lysozyme sample, it was concluded that the recovered lysozyme either maintained or recovered its original protein folding structure.

The decreased activity of the lysozyme recovered by methyl acetate or isopropanol was believed to be due to either some degree of protein denaturing that was not fully recovered during the back-extraction process or the protein still containing some amount of AOT attached to it. To test the hypothesis, the precipitate obtained with each of these solvents was washed in acetone several times, dried, and then solubilized in distilled water. Table 8.3 gives the percent of lysozyme recovered after being washed with acetone and the values obtained without acetone washing. The lysozyme activity measurement was used to calculate the recovery efficiency using the following equation:

$$\% \text{ activity recovered} = \frac{a_f \cdot C_f \cdot V_f}{a_i \cdot C_i \cdot V_i} \times 100 \tag{8.2}$$

where a_i and a_f are the activity measurements of lysozyme in the initial protein solution and the final aqueous solution. The concentrations of the lysozyme in the

initial and final aqueous solutions were denoted as C_i and C_f, and the volumes of the initial and final aqueous solutions were denoted as V_i and V_f.

As shown in Table 8.3, the percent recovery increased significantly after washing with acetone. These results suggest that either acetone removes more than the other polar solvents the AOT attached to the solid lysozyme in the back-extraction step or acetone helps refolding denatured lysozyme which then recovers its original activity in the final aqueous solution. The lysozyme recovered after the acetone wash showed the initial enzymatic activity; however, there was a decrease in the amount of lysozyme recovered in the final aqueous phase (data not shown). Similar to the results shown in Tables 8.1 and 8.2, the percent recovery of the protein in the final aqueous phase was due to the amount of protein recovered, rather than protein denaturation.

Table 8.3: Comparison of the effect of washing with acetone on the percent recovery of lysozyme dissolved in distilled water. The percent recovery was calculated using eq. (8.2).

Polar solvents	Without acetone wash (%)	With acetone wash (%)
Methyl acetate	3 ± 1	55 ± 5
Methyl ethyl ketone	0	24 ± 5
Isopropanol	18 ± 1	65 ± 5

Further study was conducted to evaluate the effect of different aqueous solutions on the lysozyme recovery. Three different aqueous solutions were tested: a 25 mM phosphate buffer solution, an aqueous NaOH solution at pH = 11 (the p*I* of lysozyme), and distilled water. The effect of different volume ratios of acetone to the fresh aqueous phase was also studied. In this study, the percent mass recovery was used to evaluate the recovery efficiency. The highest recovery of 70% was obtained with distilled water at a volume ratio of unity. At most, 50% of the lysozyme was recovered in a 25 mM phosphate buffer solution, while an aqueous phase at a pH of 11 recovered only 20% of the lysozyme.

While the recovery of lysozyme from the AOT reverse micellar solution was successful using acetone as the polar organic solvent and distilled water as the final aqueous phase, from a DODAC reverse micellar system there was no recovery of lysozyme in the final aqueous phase. When equal volumes of acetone and a DODAC reverse micellar phase containing lysozyme were contacted, a clear liquid phase resulted, and the lysozyme precipitated as a white solid. Unlike the lysozyme recovered with acetone from an AOT reverse micellar system, the lysozyme recovered from a DODAC reverse micellar phase was not soluble in distilled water, i.e., the concentration of lysozyme in the final aqueous phase was below the HPLC detection limit. One hypothesis for the zero recovery of lysozyme in the fresh aqueous phase could be that this was due to the extreme pH (pH = 12) required to extract the lysozyme into the cationic surfactant reverse micellar solution.

To investigate this further, a lysozyme-containing solution at a pH of 12 was contacted with an equal volume of acetone. No DODAC, decanol or isooctane, was present in this experiment. The lysozyme, which precipitated from the aqueous phase upon contact with the acetone solution, was not soluble in a fresh aqueous solution. In contrast, when the initial lysozyme solution was left at a pH ≅ 5, the natural pH of the lysozyme-containing aqueous solution without any pH adjustment, the recovery of lysozyme into a fresh aqueous phase after precipitation with acetone was 75 ± 10%. The conclusion of this study indicates that the lysozyme goes through denaturing process at a pH higher than its p*I* and it cannot be recovered when dissolved into a fresh aqueous solution.

8.2.4 Recovery of Lysozyme from the Direct Precipitation Method

Sections 6.3 and 6.6 of Chapter 6 described in detail the formation of white precipitate at the aqueous–organic interface during the reverse micellar extraction step [32]. The amount of white precipitate formed at the interface depended on the protein concentration reached its saturation limit in the reverse micellar phase, and the saturation limit depended on the types of salts used in the initial aqueous phase and the surfactant and cosurfactant concentration in the organic phase. Similarly, a white precipitate was observed during the back-extraction step as described in Section 8.2.2. With the knowledge that a polar organic solvent such as acetone can dissociate the protein from surfactant to improve the protein recovery from the reverse micellar phase as shown in Table 8.3, we then tested whether acetone can also help in recovering the protein from the white precipitate formed during the forward- and back-extraction steps.

First, we tested the purity and the activity of lysozyme recovered from the white precipitate formed at the aqueous–organic interface during the reverse micellar extraction process. The white precipitate was collected after centrifugation. Upon the addition of acetone, the white lysozyme–AOT precipitate was dissolved within 1–2 min. The surfactant-free lysozyme was then slowly precipitated as white flakes from this solution, while the AOT remained in the acetone phase.

As an alternative, we first added an aqueous solution containing known amount of AOT. The advantage of AOT was that this surfactant had good solubility in water so that the AOT-containing aqueous solution could be added directly to the initial aqueous solution containing known amount of protein. When the AOT solution was added, white precipitate was formed which floated on the top. This precipitate, which believed to be AOT–lysozyme complex, was recovered using centrifugation and contacted with acetone solution. Similar to the experiments performed using the white precipitate obtained during the reverse micellar extraction, the precipitate obtained by direct addition of AOT solution also solubilized immediately upon

contact with acetone. The surfactant-free lysozyme was recovered as white flakes which were then solubilized into a fresh aqueous phase.

The percent recovery of lysozyme, either from the white precipitate obtained during reverse micellar extraction or by direct contact with AOT, was similar. Using eq. (8.1), the percent mass recovery of lysozyme was 70 ± 18% for both cases. Some loss of solid precipitate occurred during washing and handling during centrifugation. The activity of lysozyme solubilized in the final aqueous phase was between 45,000 and 51,000 units/mg protein, while the activity of lysozyme in the initial aqueous solution before the contact with AOT was 48,000 ± 3,000 units/mg protein. These results confirmed that the direct contact with AOT to form a white precipitate did not cause any permanent denaturing of the protein and that the recovered lysozyme showed the same activity as the initial lysozyme. The recovery of lysozyme from the AOT reverse micellar phase using acetone was 75% (Table 8.1). This again suggests that the mechanisms of reverse micellar extraction and direct precipitation of lysozyme are similar. As such, we concluded that the reverse micellar extraction of lysozyme using AOT surfactant can be simplified by using a direct precipitation method. This direct method eliminates the use of an isooctane organic phase to form reverse micellar phase.

8.2.5 Conclusions

The recovery of lysozyme from the reverse micellar phases formed with an anionic surfactant (AOT) and formed with a cationic surfactant (DODAC) was studied using back-extraction and polar solvent precipitation methods. Back extraction using a fresh aqueous phase with pH and salt concentration adjustment reduced the lysozyme concentration in the reverse micellar phase, but no lysozyme was recovered into the aqueous phase from either the AOT or the DODAC reverse micellar phases. Polar solvent precipitation with acetone recovered lysozyme from the AOT reverse micellar phase with its original activity. Active lysozyme could not be recovered from the DODAC reverse micellar phase regardless of the different conditions of aqueous solution or the polar solvents used. It is believed that the high pH needed to extract lysozyme into the reverse micellar phase denatured the protein.

The results obtained from this study provided new information toward improving the current protein recovery method by using the surfactants as a direct precipitation agent instead of the reverse micellar extraction process. As a practical application, the use of AOT as a precipitating ligand was studied to test the selectivity of the method. The following sections summarize the results obtained using the surfactant as a direct precipitation agent, without forming a reverse micellar phase, and the use of a polar organic solvent to recover the precipitated protein into a fresh aqueous phase.

8.3 Precipitation and Recovery of Cytochrome C and Hemoglobin Using AOT and Acetone

The purpose of this research was to test the use of ionic surfactant to form protein-surfactant complex [33]. The investigation on the white precipitate during the reverse micellar extraction and the back extraction provided an interesting finding that the AOT surfactant can be used as a direct precipitation reagent that eliminates the use of a reverse micellar phase, as described in Section 8.2. Since that study was conducted using only one model protein, lysozyme, our research continued to try the same technique for other proteins of interest. In this section, two new model proteins, cytochrome c and hemoglobin, were selected to test the feasibility of using the AOT as a direct precipitation agent to effectively purify these two proteins.

Reverse micellar extraction for two transport proteins, cytochrome c and hemoglobin, was reported to follow the principle of electrostatic interaction between the protein and the surfactant as a key factor for protein solubilization in the reverse micellar phase [34–36]. Adachi and Harada reported that the cytochrome c first forms an ion-pair complex with the surfactant at a characteristic surfactant-to-protein ratio [37]. However, this ion-pair does not have sufficient hydrophobicity to be solubilized into an organic phase, and it precipitates at the aqueous–organic interface. Their study concluded that, in order for cytochrome to be solubilized into a reverse micellar phase, additional surfactant is required to provide with a hydrophobic surface around the protein. The extraction of hemoglobin with common commercial surfactants, such as AOT or trioctylmethylammonium chloride (TOMAC), was found to be unsatisfactory due to the precipitation of hemoglobin at the aqueous–organic interface. Thus, a new surfactant, dioleyl phosphoric acid, DOLPA, was used to form a reverse micellar phase, and the extraction and recovery of hemoglobin was attempted [38].

The objective of the work discussed below was to examine whether the direct precipitation method using a surfactant could be used to recover two transport proteins, cytochrome c and hemoglobin, and compare the overall purification efficiency with other methods published in the literature.

8.3.1 Experimental Conditions

The initial protein solutions containing either cytochrome c or hemoglobin were prepared at various pH and salt concentrations. As the surfactant-containing solution was to be added directly to the protein-containing solution without needing a reverse micellar phase, an aqueous solution containing AOT (up to 5 g/L) was prepared without requiring any cosolvents or any pH or salt concentration adjustment. In order to avoid the formation of micelles in the aqueous phase, the experiments were conducted ensuring that the concentration of AOT in the mixture was always less

than its critical micellar concentration, which was known to be between 2.5 mM and 4.1 mM at 25 °C [39].

The precipitated protein–surfactant complex was dissolved in acetone as a polar organic solvent and distilled water as a fresh aqueous solution. The surfactant-free protein in the polar organic solvent precipitated as white flakes which were recovered using centrifugation and then solubilized into a fresh aqueous solution. In order to ensure that we only measured the proteins fully solubilized in the fresh aqueous solution, the samples were filtered through 0.2 μm filters prior to being injected to the HPLC for protein concentration analysis. The percent precipitation and the recovery of proteins reported in this section were calculated based on the protein mass according to eqs. (8.1) and (8.2).

One point noted in this experiment was that no proteins were recovered when a pure acetone solution was used to separate protein from the protein–AOT complex formed in an initial aqueous phase that had no pH or salt concentration adjustment. As we will see in the following sections, the initial aqueous solution containing cytochrome c did not require any pH adjustment to obtain 100% precipitation. For those samples, the cytochrome c protein remained in the acetone phase, and no surfactant-free protein was obtained. In order to initiate the surfactant-free protein precipitation process, a small amount of NaCl solution (less than 10 μL of 0.1 M NaCl) was added to the acetone phase to neutralize the charges of the dissociated protein and the surfactant. The surfactant-free cytochrome c then slowly precipitated out from the acetone phase. This solid protein recovered was washed with acetone to further remove any residual surfactant. The qualitative and quantitative analyses of the final product were then carried out by dissolving the recovered-solid protein into a fresh aqueous phase.

8.3.2 Precipitation of Cytochrome C and Hemoglobin

The extraction of proteins using ionic surfactants depends on the electrostatic interaction between the oppositely charged protein and the ionic surfactant head. As such, the first step in our research was to find the pH range at which the protein precipitation by AOT surfactant was optimum. Figure 8.2 shows the percent precipitation of proteins as a function of the initial pH of the protein solution. A complete precipitation of cytochrome c was obtained at pH range between 4.5 and 6.8. An increase in pH from 7 to 8 resulted in a dramatic decrease in the formation of cytochrome c–AOT complex, and the precipitation was near 0%. In comparison, the precipitation of hemoglobin was about 90% or higher in the pH range between 3 and 5. At pH of 6.4, about 13% precipitation of hemoglobin was obtained. At pH higher than 7, the precipitation was 0%.

The results observed in Figure 8.2 agree well with the electrostatic interaction theory established from the reverse micellar extraction work, which considered that the driving force for the removal of proteins from an aqueous phase

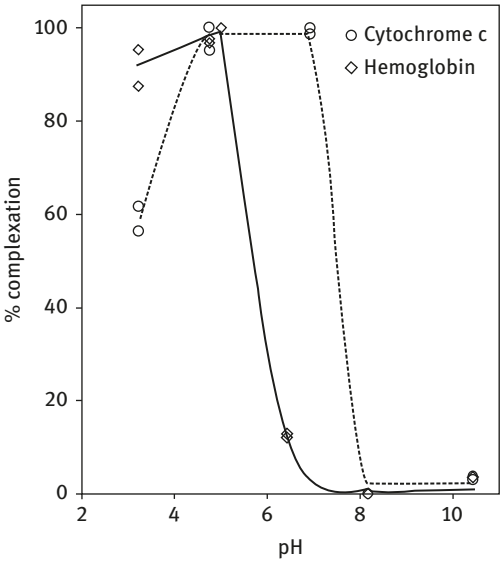

Figure 8.2: Effect of pH on the precipitation of cytochrome c (O) and hemoglobin (◊): initial aqueous phase, 0.3 g/L either cytochrome c or hemoglobin, pH adjusted using HCl or NaOH, 0.33 mM AOT

is the interaction of protein with oppositely charged surfactant head group [7, 12, 40–42]. This finding confirmed that the extraction mechanism by AOT does not depend on whether the AOT was introduced directly or by organic phase to form reverse micellar phase. Since cytochrome c showed 100% complexation at neutral pH (i.e., pH 6–8), subsequent studies did not include any pH adjustment in the initial aqueous phase to form the protein–AOT complex. In contrast, since the hemoglobin had a narrow range of pH at which the protein precipitation was optimum, subsequent precipitation studies for this protein involved the pH adjustment to 5.0 in the initial protein solution by using a sodium phosphate buffer.

Figure 8.3 shows the percent precipitation of cytochrome c as a function of the molar ratio of AOT to the protein, denoted as *R*. As more AOT was added, the percent mass of cytochrome c precipitated increased, and a 100% precipitation was obtained when the molar ratio between AOT and cytochrome c was 11. Below this molar ratio, the concentration of AOT in the remaining aqueous solution was below the detection limit of the HPLC, indicating that all the AOT was precipitated with the protein. The molar ratio at which 100% complexation was obtained in Figure 8.3 is 11 indicating that the precipitation of cytochrome c occurs when 11 moles of AOT associate with a mole of protein. Protein molecules combining with less than 11 molecules of AOT do not precipitate. Cytochrome c has an overall surface charge of about +11 at the pH range of the solution used [43], indicating that the number of AOT required to form a water-insoluble cytochrome c–AOT complex is exactly the number of moles required to neutralize the surface charge of the cytochrome c. In comparison, a previous study of the reverse micellar extraction of cytochrome c into an AOT reverse micellar phase

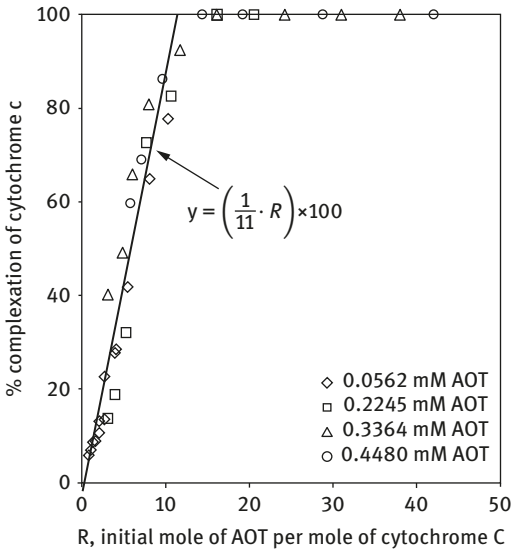

Figure 8.3: Percent precipitation of cytochrome c as a function of R, molar ratio between AOT and cytochrome c: initial aqueous phase, 0.1 to 1.0 g/L cytochrome c, 0.33 mM AOT.

showed that the minimum of 260 moles of AOT was required to purify one mole of cytochrome c [36]. In the present study, 11 moles of AOT were sufficient to purify one mole of cytochrome c.

Figure 8.4 shows the effect of the salt concentration on the precipitation of cytochrome c measured at pH 6. As the salt concentration increases, the percent precipitation of cytochrome c decreased. At 0.1 M NaCl, 100% precipitation was obtained at a molar ratio of 20 between AOT and cytochrome c. An increase in the salt concentration further decreased the precipitation efficiency, and at 0.6 M NaCl, about 60% precipitation of cytochrome c was obtained at a molar ratio of 50 between AOT and the protein. The increase in the salt concentration results in the competition of chloride ion with the negative-charged head group of AOT to bind with the cytochrome c, resulting in the decrease in the formation of cytochrome c–AOT complex.

The initial experiment for the precipitation of hemoglobin using an initial aqueous solution without any pH or salt concentration adjustment gave only 13% complexation. The natural pH of the hemoglobin solution ranged between 6.0 and 6.33, and at this pH, as shown in Figure 8.2, the precipitation of hemoglobin decreased dramatically. Thus, the pH of the hemoglobin solution was adjusted to pH 5.0 in order to further improve the precipitation of hemoglobin. The complexation of hemoglobin as a function of molar ratio is shown in Figure 8.5.

As the molar ratio between AOT and hemoglobin increased, the percent precipitation of the protein increased. At $R = 30$ or higher, a precipitation efficiency of 100% was obtained. When R was lower than this value, the formation of hemoglobin–AOT

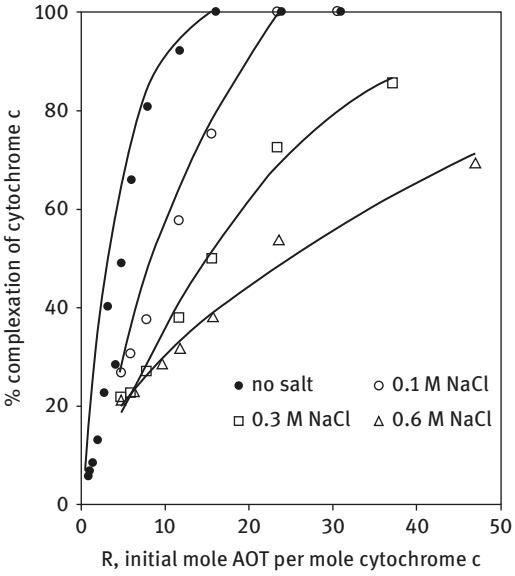

Figure 8.4: Effect of salt on the precipitation of cytochrome c: initial aqueous phase, 0.1 to 1.0 g/L cytochrome c, 0.33 mM AOT.

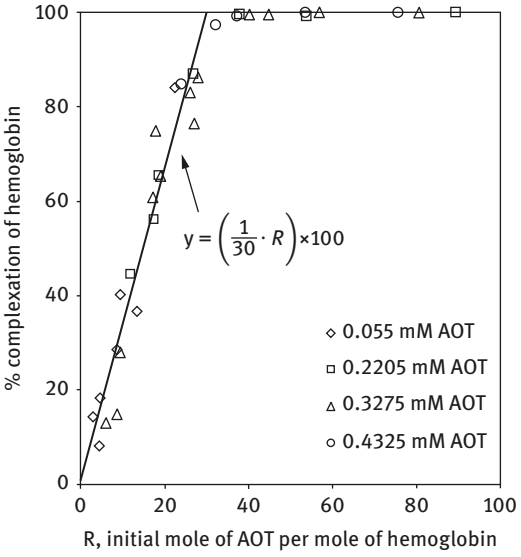

Figure 8.5: Percent precipitation of hemoglobin as a function of R, molar ratio between AOT and hemoglobin: initial aqueous phase, 0.1 to 1.0 g/L hemoglobin, no salt added.

complex decreased, and the concentration of AOT in the aqueous solution was below the detection limit of the HPLC indicating that all AOT precipitated with hemoglobin at a molar ratio of 30 between AOT and the protein. In comparison, the extraction of hemoglobin into a reverse micellar system using a newly developed surfactant dioleyl phosphoric acid, DOLPA, required 13,000 moles of DOLPA per one mole of hemoglobin [38]. Furthermore, the reverse micellar extraction method for

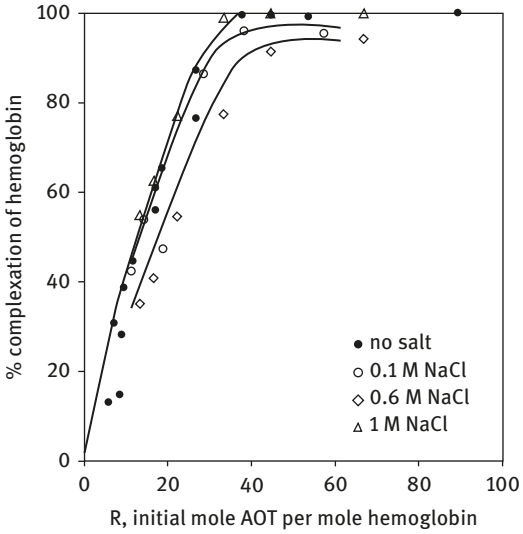

Figure 8.6: Effect of salt on the precipitation of hemoglobin: initial aqueous phase, 0.1 to 1.0 g/L hemoglobin, 0.22 mM AOT.

hemoglobin using DOLPA reverse micellar system required long processing times, about 60 h for the extraction and recovery steps. In our work, 30 moles of AOT were sufficient to purify one mole of hemoglobin and the precipitation occurred within minutes of contact with the surfactant solution.

The effect of salt on the precipitation of hemoglobin with AOT is shown in Figure 8.6. Unlike cytochrome c, the presence of salt did not have any noticeable effect on the percent precipitation of hemoglobin. The percent precipitation of hemoglobin was 100% at $R = 30$ in a salt concentration range from 0 to 0.1 M NaCl. However, further increase in the salt concentration to 0.6 M NaCl resulted a slight decrease in the formation of hemoglobin–AOT complex, and about 95% precipitation efficiency was obtained at $R = 30$. However, the percent precipitation of hemoglobin increased to 100% at 1 M NaCl, indicating that the salt concentration had little effect on the formation of hemoglobin–AOT water-insoluble complex.

8.3.3 Recovery of Cytochrome C and Hemoglobin

The recovery of the cytochrome c and hemoglobin from the protein–AOT complex was carried out using acetone as a polar organic solvent. The surfactant-free protein precipitated in the acetone was recovered and solubilized into a fresh aqueous solution. Table 8.4 summarizes the percent mass recovery of cytochrome c and hemoglobin using eq. (8.1). The percent recovery of the solid cytochrome c obtained from the cytochrome c–AOT complex was 88 ± 10%. The large standard deviation on the percent recovery was due to the mass loss during washing in the

Table 8.4: Percent mass recovery of cytochrome c and hemoglobin.

Protein	% mass precipitated from the initial protein solution	% mass recovered in the final aqueous phase
Cytochrome c	100	88 ± 10
Hemoglobin	100	37 ± 3

recovery process. As the samples are small, a small loss during washing represents a major change in the results. In addition, the percent recovery of cytochrome c was a strong function of the processing time used for the precipitation and the recovery process. As soon as the insoluble cytochrome c–AOT complex was formed, the precipitate was collected and dissolved in acetone. When the solid cytochrome c stays in the acetone phase for more than 10 min, the recovered solid presented a different conformational stability, which showed up as change in the shape of protein peak in the HPLC chromatogram. The cytochrome c recovered after 30 min showed a severely distorted peak shape, and the percent recovery was zero percent. When the precipitation and the recovery were conducted within 10 min, the recovered cytochrome c showed the original peak shape, and the percent recovery was about 90%. The AOT concentration in the aqueous solution containing recovered cytochrome c was below the detection limit of the HPLC. In comparison, the recovery of cytochrome c through back-extraction mechanism using a fresh aqueous phase required addition of alcohol [36] or counterionic surfactant [44] to obtain the same efficiency as our reported results.

The recovery of hemoglobin from the protein–surfactant complex was also conducted using acetone as a polar organic solvent. An overall recovery of 37 ± 3% was obtained for hemoglobin. The concentration of AOT in the recovered hemoglobin solution was below the detection limit, indicating that the recovered protein was free of surfactant. It is unclear whether the low percent recovery for hemoglobin, compared to cytochrome c, was due to protein denaturing that resulted in an insoluble protein precipitate state, either due to the direct contact with AOT or acetone polar solvent, or due to the final aqueous solution that was not optimized in terms of pH and ionic strength to enhance the recovered hemoglobin to be solubilized optimally.

8.3.4 Conclusions

The precipitation of two transport proteins, cytochrome c and hemoglobin, was successfully achieved using AOT as a precipitating ligand and acetone as a polar solvent. This method has clear advantages over a reverse micellar extraction method based on the less amount of surfactant and shorter processing time required to

achieve the similar purification efficiency as a reverse micellar extraction method. In addition, a direct addition of AOT to the aqueous phase eliminates the need for an organic phase such as isooctane to obtain a reverse micellar solution.

8.4 Precipitation and Recovery of α-Chymotrypsin and Ribonuclease Using AOT and Acetone

Following the successful results of protein purification using AOT as a direct precipitation agent using lysozyme, cytochrome c and hemoglobin rather than reverse micellar forming agent, our research continued to further examine the use of this technique to separate proteins from a protein mixture [45]. In this section, the use of AOT was tested for selective purification of two proteins that have similar pIs: α-chymotrypsin (pI = 8.5) and ribonuclease-A (pI = 7.8). These two proteins are often purified from bovine pancreases. The precipitation and recovery of these two proteins were studied and compared with the results obtained using reverse micellar extraction method.

8.4.1 Experimental Conditions

The experimental conditions used for the precipitation of proteins from the initial aqueous phase, the preparation of AOT solution, and the recovery of protein from the protein–surfactant complex were the same as provided in Section 8.2.1. For this study, enzymatic activities of α-chymotrypsin and ribonuclease-A were also measured in terms of protein concentration and the protein enzymatic activities before and after the formation of protein–surfactant complex. The enzymatic activity of α-chymotrypsin in the aqueous solution was determined at 25 °C according to Hummel [46]. The enzymatic activity of ribonuclease-A was measured following the method described by Crook et al. [47].

8.4.2 Precipitation of α-Chymotrypsin

Before testing for the selectivity of AOT to purify α-chymotrypsin and ribonuclease from the protein mixture, it was necessary to first understand the precipitation behavior of AOT–protein complex from a single-protein solution. An aqueous solution-containing α-chymotrypsin without pH or salt concentration adjustment was between 3.6 and 4.5. The α-chymotrypsin has an overall surface charge of +7 at a pH of 4.5 [43].

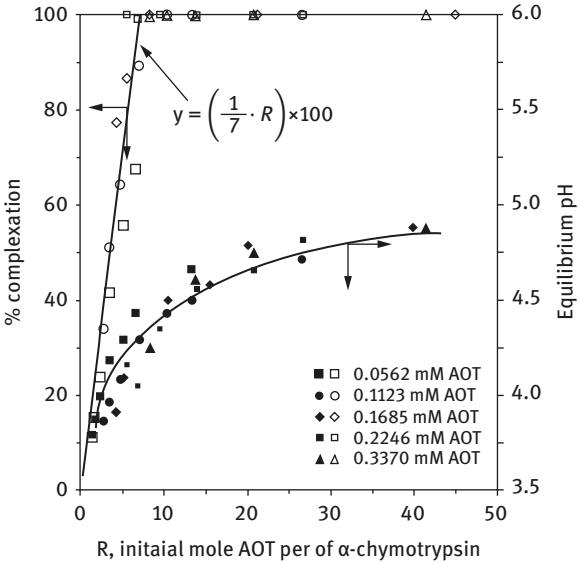

Figure 8.7: Percent precipitation of α-chymotrypsin as a function of the molar ratio R between AOT and protein: initial aqueous solution, 0.1 to 1.0 g/L α-chymotrypsin, no salt added, no pH adjustment.

Figure 8.7 shows the precipitation efficiency, as defined by eq. (8.1), plotted as a function of the molar ratio, R, between the AOT and the α-chymotrypsin initially present in the aqueous solution. The equilibrium pH after the formation of the insoluble α-chymotrypsin–AOT complex is also presented in this figure. The precipitation efficiency increased as R increased. At R = 7, a complete precipitation of α-chymotrypsin was obtained. When R was less than 7, the concentration of AOT remaining in the solution was below the detection limit of the HPLC, indicating that all the ligand added to the solution formed lysozyme–ligand complex and was removed from the aqueous phase. When R was greater than 7, as all protein was removed, excess ligand was detected in the aqueous phase. As the percent precipitation increased to 100%, the pH of the mixture increased to a value of about 5. Note that the percent precipitation line, shown in the figure, can be written as $y = (100 \div 7) \cdot x$. This indicates that the α-chymotrypsin and α-chymotrypsin–AOT complex intermediates containing less than seven moles of AOT per mole of protein stay soluble in water until they take up seven moles of AOT per mol of protein. The compound containing seven moles of AOT per mole of α-chymotrypsin is insoluble in water and thus precipitates out of the aqueous phase. For example, if 3.5 moles of AOT are added to the protein solution, not all the protein molecules share the AOTs equally, but it is 50% of the protein molecules that get all the AOT, at a 7:1 mole ratio between α-chymotrypsin and AOT, and precipitate. The other 50% of the protein molecules remain in the aqueous solution free of AOT. In comparison, the minimum number of AOTs required to extract α-chymotrypsin into an AOT reverse micellar phase was 57 moles of AOT per mole of protein [48]. Furthermore, the present method

has the additional advantage over the reverse micellar extraction that it does not require the contact with an organic phase containing reverse micelles.

Figure 8.8 shows the precipitation efficiency when NaCl was added to the initial protein solution. A decrease in the percent precipitation is observed as the salt concentration increased in the initial α-chymotrypsin solution. For example, at $R = 7$, the percent precipitation decreased from 100% to less than 80% when the salt concentration increased from 0 to 0.05 M NaCl. A further decrease in the percent precipitation was observed, and at 0.3 M NaCl, the percent precipitation was about 30%, independent of the molar ratio R.

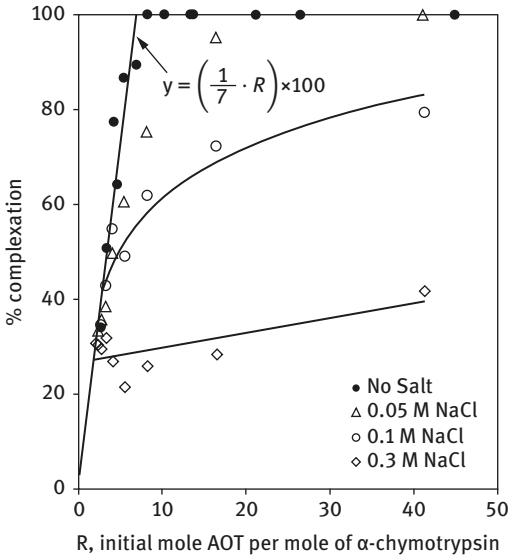

Figure 8.8: Effect of salt on the percent precipitation of α-chymotrypsin: initial aqueous solution, 0.1 to 1.0 g/L α-chymotrypsin, 0.1685 mM AOT, no pH adjustment.

8.4.3 Precipitation of Ribonuclease-A

Ribonuclease-A showed a similar precipitation behavior to α-chymotrypsin when contacted with AOT. The ribonuclease-A-containing solution without any pH adjustment ranged between 4.0 and 4.5. In this pH range, the ribonuclease-A has an overall surface charge from +13 to +10 [43].

Figure 8.9 shows the precipitation of ribonuclease-A upon the addition of AOT. The percent precipitation of ribonuclease-A increased as the molar ratio of AOT to protein increased. The equilibrium pH of the protein solution after the precipitation is also presented in this figure. As the percent precipitation increased to 100%, the pH of the aqueous solution reached a value of 6. An increase in the salt concentration in the initial protein solution resulted in a decrease in the percentage removal of protein

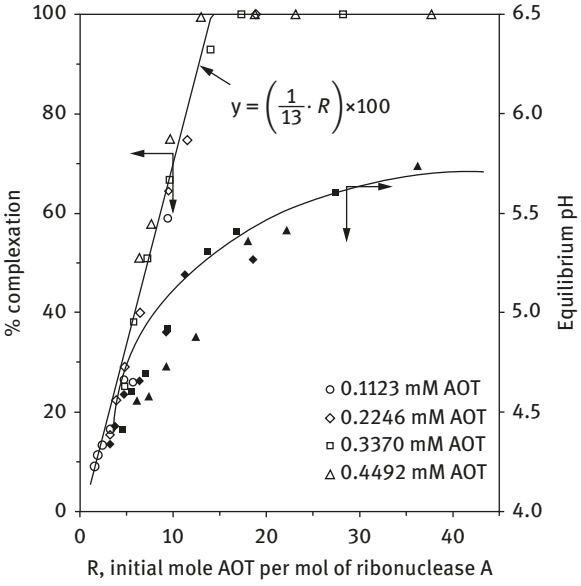

Figure 8.9: Percent precipitation of ribonuclease-A as a function of the molar ratio R between AOT and protein: initial aqueous solution, 0.1 to 1.0 g/L ribonuclease-A, no salt added, no pH adjustment.

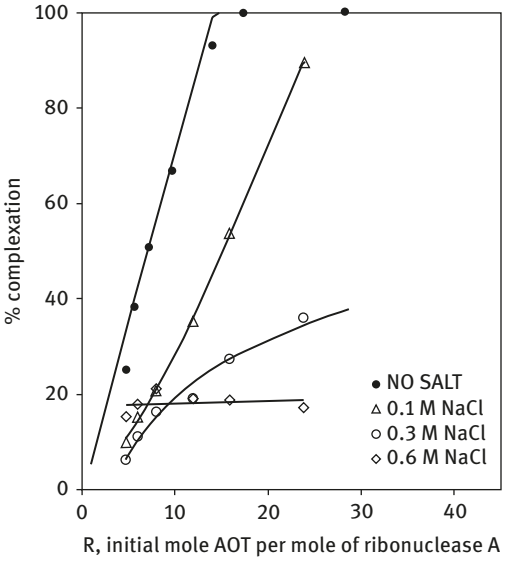

Figure 8.10: Effect of salt on the percent precipitation of ribonuclease-A: initial aqueous solution, 0.1 to 1.0 g/L ribonuclease-A, 0.3370 mM AOT, no pH adjustment.

at a given value of *R*. The slope of the precipitation line in Figure 8.9 is 100/13, indicating that the 100% removal of the protein was obtained at the molar ratio of 13 between AOT and the protein. In order words, the protein–AOT complex was a compound containing 13 moles of AOT per mol of ribonuclease-A which was

water insoluble, and no other intermediates were formed. In comparison, for α-chymotrypsin, the molar ratio of AOT to protein, required for a complete precipitation of the protein, was 7 (Figure 8.7). Even though the molecular weight of the ribonuclease-A was about half of that of α-chymotrypsin, the number of moles of AOT required to precipitate a mole of ribonuclease-A was almost twice as many as that required to precipitate one mole of α-chymotrypsin. This result clearly indicates that the formation of protein–AOT insoluble complex is a function of the surface charge of the protein and not of molecular weight. In comparison, when the reverse micellar method was used to extract ribonuclease-A from the initial aqueous phase, a minimum of 55 moles of AOT per protein was required [48].

Figure 8.10 shows the percent precipitation of ribonuclease-A as NaCl was added to the initial protein solution. As shown in this figure, at R = 22, the percentage removal of ribonuclease decreased to about 95% and 40% when the salt concentration was set at 0.1 M and 0.3 M NaCl, respectively. At 0.6 M NaCl, the percentage of ribonuclease precipitated was found to be around 20%, independent of the value of R. The results presented in this figure indicate that the precipitation of ribonuclease-A at an elevated salt concentration was due to the salt precipitation as a driving force rather than the formation of protein–AOT complexation.

8.4.4 Recovery of α-Chymotrypsin and Ribonuclease-A

After obtaining successful complexation of α-chymotrypsin and ribonuclease-A from a single protein containing aqueous phase, our research continued to examine the recovery of the protein from the protein–AOT complex using acetone as a polar organic solvent. The final aqueous solution used to solubilize the recovered protein was distilled water. Table 8.5 summarizes the recovery of α-chymotrypsin and ribonuclease-A. The α-chymotrypsin was recovered as a pure solid by dissolving protein–AOT complex using acetone. The percent overall recovery of the α-chymotrypsin using eq. (8.2) was 37 ± 18%. The percent recovery of the ribonuclease-A was 84 ± 33% with the maximum overall recovery of 100%. The recovered ribonuclease retained its original enzymatic activity indicating that the protein denaturing was low.

Table 8.5: Percent recovery of the enzymatic activities of α-chymotrypsin and ribonuclease-A after surfactant precipitation.

Protein	% protein activity recovered in the initial protein solution	% protein activity recovered in the final aqueous phase
α-chymotrypsin	100	37 ± 18
Ribonuclease-A	100	84 ± 33

8.4.5 Selective Precipitation and Recovery of α-Chymotrypsin and Ribonuclease-A

After obtaining successful complexation of α-chymotrypsin and ribonuclease-A from a single protein containing aqueous phase, our research continued to examine the selectivity of AOT to form a complex with each protein in the aqueous solution containing both proteins. An aqueous solution was prepared containing the equal molar ratio of α-chymotrypsin and ribonuclease-A. The pH of the protein solution was adjusted to 5.5 using HCl, and no salt concentration adjustment was made in the initial protein solution.

Figure 8.11 shows the percent precipitation of each protein as a function of the initial mole ratio between AOT and the particular protein, R. These ratios were calculated from the values of the concentration of AOT and the concentration of each protein in the solution. Even though values of R = 7 and 13 were sufficient to obtain 100% precipitation of α-chymotrypsin and ribonuclease-A in a single protein solution, when in a mixture, only 24% of initial α-chymotrypsin precipitated at R = 11. The precipitation efficiency of ribonuclease-A showed similar values as those of α-chymotrypsin at all range of R tested. At R = 16, the percent precipitation of α-chymotrypsin and ribonuclease-A was 60% and 50%, respectively, indicating that the AOT was distributed equally between the two proteins. In order to obtain the complete precipitation of two proteins, the molar ratio of 33 between AOT and the proteins was required.

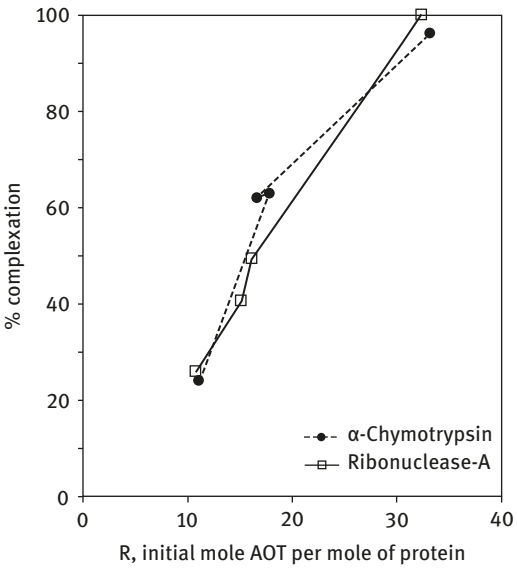

Figure 8.11: Precipitation of α-chymotrypsin and ribonuclease A from mixture: initial aqueous solution, 0.5 g/L α-chymotrypsin (0.02 mM) and 0.3 g/L ribonuclease A (0.02 mM), pH = 5.5 adjusted using HCl.

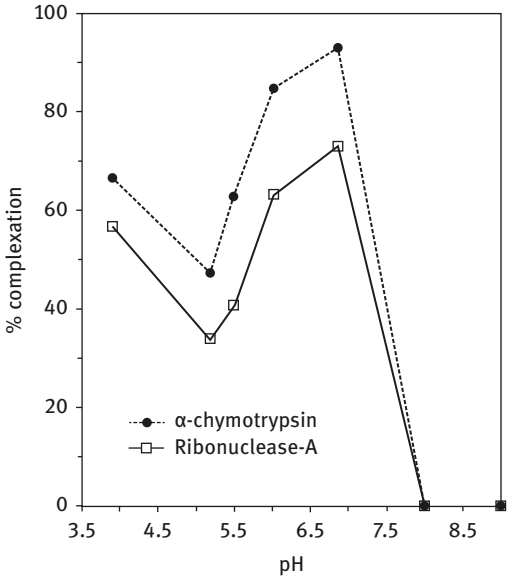

Figure 8.12: Selectivity of precipitation of α-chymotrypsin and ribonuclease-A from mixture: 0.5 g/L α-chymotrypsin and 0.3 g/L ribonuclease-A, 0.3370 mM AOT, pH adjusted using HCl or NaOH.

The selectivity of the AOT precipitation for the two enzymes was studied as a function of pH. As shown in Figure 8.12, the percent precipitation of α-chymotrypsin was slightly higher than that of ribonuclease-A. However, due to the close values of the p*I*s of these two enzymes (7.8 for α-chymotrypsin and 8.5 for ribonuclease-A), the precipitation resulted in a product containing a composition of α-chymotrypsin and ribonuclease-A similar to that in the initial sample.

8.4.6 Conclusions

The surfactant precipitation of enzymes using surfactant was successfully carried out using AOT. To precipitate the protein from a single protein containing aqueous solution, the stoichiometric ratios for the formation of insoluble protein–AOT complex were determined to be 7 for α-chymotrypsin and 13 for ribonuclease-A, which is about 25% of the amount of AOT required for a reverse micellar extraction. However, when the initial aqueous solution contained a mixture of two proteins, the amount of AOT needed to precipitate either protein increased more than the stoichiometric ratios required for both. The selectivity of proteins with its p*I* close to each other could not be achieved with a simple pH or salt concentration adjustment. This finding confirms that the precipitation mechanism is the electrostatic interaction between oppositely charged protein and the surfactant which is consistent with the findings in the literature related to ionic surfactant purification of proteins using reverse micellar phases.

8.5 Selective Precipitation of Lysozyme from Egg White Using AOT

In Sections 8.3 and 8.4, it was shown that an anionic surfactant, such as AOT, can be used directly as a precipitation reagent to precipitate the proteins from an aqueous solution. The protein can then be recovered from the protein–surfactant complex by using polar organic solvent without protein denaturing or loss of enzymatic activity. The selective precipitation for two proteins with similar p*I* showed that the separation of such proteins using simple pH adjustment was not possible. In the continuation of this work, our studies extended to a more complex mixture such as selective purification of lysozyme from the egg white mixture [49]. For this work, the recovery of lysozyme from the egg white mixture was used, and our objective was to selectively purify lysozyme from the egg white solution. The lysozyme purification from egg white was an attractive option to test the feasibility and selectivity of protein–surfactant complexation because the amount of lysozyme in the egg white mixture is low and because the p*I* of lysozyme is distinctively different from the p*I*s of other proteins present in the egg white mixture. For example, the main proteins in the egg white solution are ovalbumin (54%), ovotransferin (13%), and ovomucoid (11%), while lysozyme makes up of only 3.4% of the egg white protein; the p*I*s of those proteins range between 4.5 and 6, while the p*I* of lysozyme is 11 [50]. In this research, the effect of pH on the precipitation efficiency was studied, and the aim of our study was to recover lysozyme without loss of its enzymatic activity.

8.5.1 Experimental Conditions

The experiments were first carried out by using an initial aqueous solution with known amount of pure lysozyme and albumin mixed in together. The concentrations of lysozyme and albumin were chosen to simulate the natural concentrations of each of these proteins in the hen egg white. For the preparation of egg white solution, the hen egg white was separated from the yolk and diluted 50-fold with 0.02 M phosphate buffer solution. A dilution greater than 50-fold resulted in a lysozyme concentration close to the detection limit of HPLC, while a dilution of less than 50-fold resulted in an overloading of the HPLC column due to the large amount of albumin present in the sample. Furthermore, when the dilution was less than 50, the precipitation experiment showed a large standard deviation, indicating that the solution was too viscous to have a homogeneous contact of the proteins with AOT. It was critical to obtain fresh egg for each experiment, since the lysozyme concentration in the purchased egg white was found to decrease by more than 50% after a few days from the date of purchase.

The preparation of AOT solution, the protein solution, and the analytical methods for protein concentration and activity measurement followed the same procedures described in Section 8.2.1.

8.5.2 Selective Precipitation of Lysozyme from the Lysozyme–Albumin Mixture

Göklen and Hatton reported that a 100% extraction of lysozyme was obtained in the pH range between 4 and 11 using an AOT reverse micellar solution [10]. However, no literature was available on the albumin–surfactant interaction to select optimum conditions for albumin–AOT complex formation. As such, our research first started with testing the albumin–AOT complex formation behavior using a pure albumin solution. The natural pH of the albumin solution was between 6.25 and 6.42, and no precipitation of albumin in the presence of AOT was obtained at this pH. Since the p*I* of albumin was 4.6, the pH of the initial albumin solution was adjusted to pH = 4. At this pH, a 100% precipitation of albumin was obtained at a molar ratio of 14 moles of AOT per mole of albumin. The recovery of albumin from the albumin–AOT complex was tried using various polar organic solvents. Notably, the albumin–AOT insoluble complex was not solubilized in acetone. The percent recovery of albumin from the insoluble complex was 0%. Six other possible polar organic solvents were tested for the albumin recovery, including methanol, isopropanol, pentanol, methyl acetate, methyl ethyl ketone, and formaldehyde. However, the percent recovery of albumin remained at 0%. Since our objective was to selectively precipitate lysozyme from the egg white mixture which contains large amount of albumin, the fact that the precipitation and the recovery of albumin was low was not a concern for us, and the research continued to selectively precipitate lysozyme from an aqueous solution containing albumin and lysozyme mixture. This experiment was conducted prior to test the egg white solution which had many other proteins present because we wanted to better understand the complexation mechanism of the key proteins, lysozyme as our target protein and albumin as the main component of the egg white, before moving on to the egg white solution itself.

The selective precipitation of lysozyme from an aqueous solution containing a mixture of lysozyme and albumin was tested as a function of pH. In order to mimic the concentration of lysozyme and albumin in natural chicken egg white, the protein concentrations selected for the experiments were 0.15 g/L lysozyme and 1.0 g/L albumin.

Figure 8.13 shows the percent precipitation of lysozyme at different pH as a function of the molar ratio between AOT and lysozyme, denoted as *R*. The percent complexation plotted in this figure was calculated using the following equation:

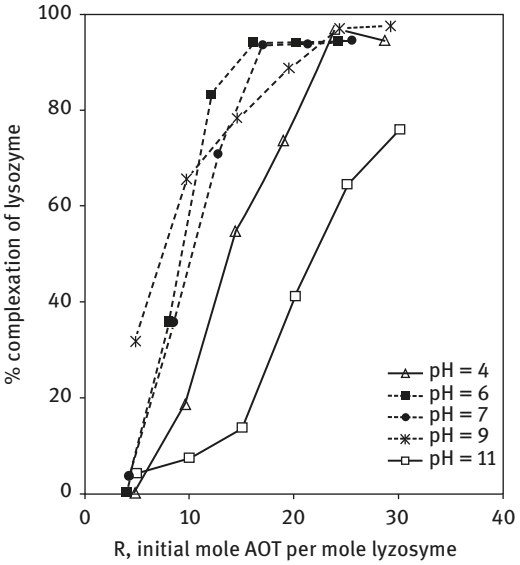

Figure 8.13: Percent precipitation of lysozyme from pure lysozyme-albumin mixture: initial aqueous solution, 0.15 g/L lysozyme and 1.0 albumin in phosphate buffer, pH adjusted with HCl or NaOH.

$$\% \text{ complexation} = \left(1 - \frac{C_e \cdot (V_i + V_s)}{C_i \cdot V_i}\right) \times 100 \tag{8.3}$$

where C_e refers to the protein concentration remaining in the initial aqueous phase after the surfactant solution was added and V_s refers to the volume of the surfactant solution added to the protein containing solution.

As shown in Figure 8.13, when the pH of the protein solution was at 4, a precipitation efficiency of 54% was obtained at R = 15, and about 95% at R = 25. An increase in the percent precipitation was obtained as the pH increased from 4 to 6. At pH = 6, about 95% precipitation of lysozyme was obtained at R = 15. Similar precipitation results were obtained at pH = 7. However, as the pH of the initial lysozyme–albumin solution was further increased to 9, less precipitation of lysozyme was obtained. At pH = 11, only 14% of lysozyme precipitation was obtained at R = 15. No albumin precipitated in the pH range from 6 to 11. At pH = 4, about 15% of albumin was precipitated. From these results, the optimum pH for lysozyme precipitation was selected to be between pH 6 and 7, which was consistent with the lysozyme–AOT insoluble complex formation mechanism reported in literature [32]. The only difference found in this study, compared to that reported in literature [32], is that the molar ratio of 11 was sufficient to obtain 100% extraction of lysozyme from a pure lysozyme solution, while the minimum amount of AOT used to obtain 100% lysozyme extraction from a lysozyme–albumin mixture was 15. This finding indicates that some AOTs bind to albumin without forming an insoluble complex at the pH tested.

8.5.3 Selective Precipitation of Lysozyme from Egg White Mixture

The selective precipitation of lysozyme from hen egg white was studied next using an egg white solution diluted by 50-fold using a phosphate buffer.

Figure 8.14 shows the percent precipitation of lysozyme measured in a pH range from 4 to 11 and calculated using eq. (8.3). The percent precipitation of lysozyme from the egg white solution shows similar pH dependence as that from the lysozyme–albumin mixture depicted in Figure 8.13. The percent precipitation increased with an increase in pH from 4 to 6 and decreased with an increase in pH from 9 to 11. Notably, the highest precipitation efficiency of lysozyme obtained from the egg sample was about 80%. The precipitation of other hen egg white proteins, such as ovalbumin, ovotransferin, and ovomucoid, measured using HPLC, was less than 3% of the initial mass of these proteins in the range of pH tested. The decrease in the percent precipitation of lysozyme from egg white, compared with the lysozyme–albumin solution, is believed to be due to the high viscosity of the egg white solution. This high viscosity makes it difficult to provide homogeneous contact of lysozyme with AOT in the buffer solution. The presence of other proteins in the aqueous egg white solution decreased the amount of free AOT to react with lysozyme to form an insoluble complex. Furthermore, it can to be due to the difference in the conformation of lysozyme in these two solutions. The purified lysozyme used in a synthetic lysozyme–albumin solution may have a different conformation from the native lysozyme found in the egg white. Furthermore, it is believed that the presence of other proteins in the aqueous solution decreased the amount of free AOT to bind with lysozyme to form an insoluble complex.

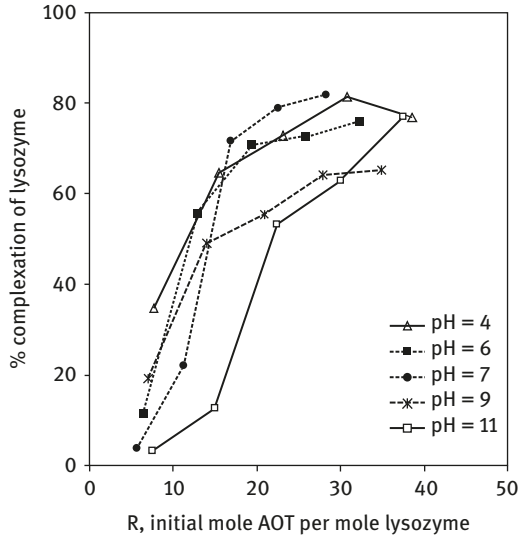

Figure 8.14: Percent precipitation of lysozyme from hen egg white: 2.5 mL egg white in 122.5 mL phosphate buffer, pH adjusted with HCl or NaOH.

8.5.4 Lysozyme Recovery from the Lysozyme–AOT Complex

The solid precipitates, obtained from either lysozyme–albumin or egg white solutions upon the addition of AOT, were then treated with acetone to recover the lysozyme from the lysozyme–AOT complex. The surfactant-free lysozyme obtained after adding acetone was solubilized into a fresh aqueous phase.

Figure 8.15 shows that the overall percent recovery of lysozyme was calculated using eq. (8.2). The percent recovery was examined as a function of pH of the initial protein solution prior to adding an AOT solution. The error bars indicate 95% confidence interval obtained using three replicates. As shown in Figure 8.15, the percent recovery was higher when the pH increased from 4 to 6, and then decreased as the pH was further increased from 9 to 11. The decrease in the overall percent recovery at pH 4 and after pH 7 was due to the low degree of precipitation of lysozyme as shown in Figures 8.13 and 8.14. From these results, it was concluded that the low recovery of the lysozyme was due to the mass of proteins not being recovered in the final aqueous solution, rather than the loss of enzymatic activity of the protein. Table 8.6 shows the activity of lysozyme before and after being contacted with AOT. As shown in this table, the recovery of lysozyme from the precipitate formed in a lysozyme–albumin solution showed higher efficiency than the values obtained from the egg sample. No other egg white proteins were detected when the aqueous solution containing the recovered lysozyme was analyzed with HPLC. Lysozyme precipitated from a hen egg white solution showed slightly less activity units than that precipitated from a lysozyme–albumin solution. Lysozyme from egg white showed the

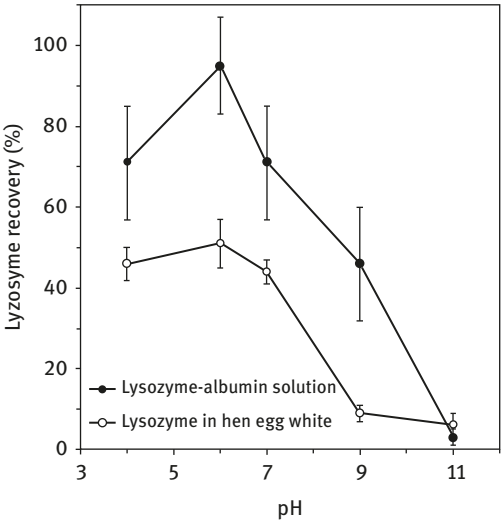

Figure 8.15: Overall percent recovery of lysozyme based on the initial amount of lysozyme from lysozyme-albumin mixture (closed symbols) and from hen egg white solution (open symbols).

Table 8.6: Specific activity (in 10^3 units/mg) of lysozyme in the lysozyme–albumin solution and in hen egg white measured before and after the purification.

pH	Specific activity (in 10^3 units/mg)			
	Standard lysozyme +albumin solution		Hen egg white	
	Initial	Final product	Initial	Final product
4	42.0 ± 1.3	44.7 ± 2.6	19.83 ± 0.62	20.6 ± 1.3
6	40.0 ± 5.4	43.2 ± 5.5	19.92 ± 0.27	21.0 ± 1.6
7	43.0 ± 1.3	42.6 ± 2.0	34.1 ± 1.6	28.5 ± 2.6
9	41.8 ± 1.6	40.4 ± 2.5	36.2 ± 2.9	32.6 ± 2.6
11	40.2 ± 1.9	–	32.4 ± 1.9	–

highest activity at a pH range between 7 and 9. At pH 4 or 11, a noticeable decrease in the lysozyme activity was observed. No change in the enzyme activity of lysozyme was observed when precipitated with AOT and recovered with acetone from hen egg white, confirming that the selective precipitation of lysozyme in a complex mixture, such as egg white, can provide an efficient purification result. With the method developed in this work, lysozyme was selectively precipitated and recovered, with a similar yield to the one obtained by reverse micellar extraction [26]. The advantages of the present method, compared with the reverse micellar extraction, are its simplicity of operation as it does not require organic phase to form a reverse micellar solution, and short processing time required as it does not require a long back-extraction processing step.

8.5.5 Conclusions

A selective purification of lysozyme from the egg white solution was obtained using AOT as a direct precipitation agent that formed an insoluble complex with lysozyme. Using an acetone solution to separate the precipitated lysozyme from the AOT insoluble complex provided an overall recovery efficiency of about 50% of the initial mass of lysozyme presented in the egg white solution. The lysozyme activity in the fresh aqueous solution after the lysozyme–AOT precipitation was maintained close to those obtained in the initial egg white solution indicating that this technique did not cause any denaturing of the protein. The results obtained from this research confirmed that an ionic surfactant can be used as a selective precipitation agent without having to be concerned about denaturing of the protein.

8.6 Selective Precipitation and Recovery of Xylanase Using Surfactant and Organic Solvent

The key finding from Sections 8.4 and 8.5 is that the ionic surfactant can be used to selectively purify proteins from the protein mixture if the target protein has the p*I* values that are distinctively different from the p*I* values of other proteins also present in the protein mixture. To continue with our research, our aim was to find practical use of ionic surfactants to purify proteins that had important commercial values, which were purified through lengthy purification processes [51]. In that regard, we collaborated with the Iogen Corporation (Ottawa, ON) to test the possibility of using an ionic surfactant to selectively purify cellulases and xylanases.

The fungus *Trichoderm*a secretes a range of enzymes including cellulases and xylanases that have high hydrolic activities against wood pulp, wheat, cotton, and other cellulose materials [52]. For large-scale biobleaching applications, xylanase can be made using *Trichoderma* [53]. However, xylanase must be separated from cellulase enzymes to prevent the degradation of cellulose fibers in the pulp. An economical and easily scalable method to selectively purify xylanase from solutions containing *Trichoderma* cellulase and xylanase was of interest.

In this work, we tested the use of different ionic surfactants to separate xylanase selectively from an industrial aqueous solution containing a mixture of cellulases and xylanase. Four surfactants were studied for the precipitation: sodium di-(2-ethylhexyl) sulfosuccinate (AOT), sodium di-(*n*-octyl) phosphinate, sodium di-(*n*-dodecyl) phosphinate, and dioctyl dimethyl ammonium chloride (DODAC). However, the use of sodium di-(*n*-octyl) phosphinate, sodium di-(*n*-dodecyl) phosphinate, and dioctyldimethyl ammonium chloride was unsuccessful in that no xylanase was recovered after the surfactant precipitation. Different precipitation and recovery conditions were tried, and those attempts were unsuccessful to yield any economical meaningful recovery of the protein of interest. As such, the results provided in this section focus on the results obtained using AOT as the precipitation agent.

8.6.1 Experimental Conditions

Industrial aqueous samples containing only xylanase, only cellulase, and a mixture of xylanase and cellulose, obtained from *Trichoderma* fermentation broth containing cellulase and over-expressed xylanase, were provided by Iogen Corporation. The cellulase product contained at least six different cellulases whose isoelectric points (p*I*) are around 6.0 or less. Azo-xylanase and cellulose, for the activity assays of xylanase and cellulase, were also provided by Iogen Corporation. In order to minimize the volume change of protein solution upon the addition of the surfactant solution, the surfactant concentrations used were the maximum possible as fixed

by the solubility limit of each surfactant in water. For AOT, the maximum concentration possible in an aqueous solution was 5 g/L. In order to ensure that experiments were conducted properly, the precipitation work was done with negative control in parallel, which contained the same protein solution but having the same volume of distilled water added during precipitation experiment instead of AOT-containing solution. Once the xylanase–AOT insoluble complex was formed, this solid was washed with distilled water to ensure that residual cellulose was fully removed prior to the addition of polar organic solvent. During the polar organic solvent precipitation step to separate xylanase from AOT, a small volume of a sodium acetate buffer (less than 1% of the polar organic solvent volume) was added to the polar organic solvent to accelerate the xylanase precipitation. Without this salt addition, xylanase precipitation was limited. Similar finding was also observed in an earlier study that a small amount of salt was required to neutralize the charges on the target protein in order to form pure-protein precipitate which could be easily solubilized into a fresh aqueous phase [33, 45]. Any xylanase remaining as solid in the final aqueous phase was filtered out of the solution before the analysis.

The concentration of xylanase and cellulase in the aqueous phase was measured using an UV spectrophotometer at 280 nm. The xylanase activity assay was carried out using a colorimetric assay from Megazyme International (Ireland), and cellulase activity was determined using carboxymethyl cellulose as a substrate and monitoring the release of reducing sugars using DNS [54]. In preliminary experiments, the protein concentration remaining in aqueous solutions after precipitation with the surfactant was measured using UV absorption. According to these experiments, about 50% of the xylanase remained in the solution after the precipitation step. However, measurements of the activity of the xylanase, before and after precipitation, indicated that only 1% of the original activity of the xylanase remained in the solution. This discrepancy was interpreted as the result of the presence of about 50% inactive xylanase in the original industrial sample, which was not removed by precipitation with the surfactant. As the important industrial parameter is the activity of the xylanase remaining in the solution, the results reported in our research were in terms of protein activity, instead of protein concentration values.

8.6.2 Effect of pH and Temperature on the Precipitation of Xylanase from Pure Xylanase Solution and Cellulase from Pure Cellulase Solution

Table 8.7 summarizes the percent removal of xylanase activity after the addition of AOT at pH 4.5 and at pH 8. The concentration of AOT in the initial protein solution before precipitation was below the critical micellar concentration value to avoid formation of micellar structures. At pH 4.5, more than 99% decrease in the xylanase

Table 8.7: Percent activity of xylanase removed with AOT. Initial enzyme concentration: 0.4 g/L xylanase, V_i = 10 mL, 1 mL of 5 g/L AOT solution, pH adjusted with NaOH.

	Activity (IU/mL) at pH 4.7	Activity (IU/mL) at pH 8.0
Initial	128.5 ± 1.5	182.2 ± 6.0
After AOT	<0.2	179.4 ± 2.9
% xylanase removed	>99.8	<1.5

activity was obtained upon the addition of AOT. The protein concentration measurement showed that the decrease in the xylanse activity was due to the decrease in the protein mass, not due to the decrease in the xylanase activity. This confirmed that the decrease in the xylanase activity was in fact due to complexation of xylanse with AOT to form an insoluble complex, not due to protein denaturing. The effect of temperature on xylanase precipitation was studied using 10 mL of 0.4 g/L xylanase solution and 1 mL of AOT (the molar ratio between AOT and xylanase = 54). Changing temperature from room temperature to 40 °C or 60 °C did not change the percent decrease in xylanase activity by precipitation with AOT.

8.6.3 Selective Precipitation of Xylanase from the Xylanse–Cellulase Mixture

The xylanase–cellulase mixture containing approximately 15–20% xylanase was used in the experiment.

Figure 8.16 presents the percent removal of xylanase and cellulase activities upon the addition of AOT as a function of the initial pH of the protein solution. At pH = 3, a total removal of xylanase activity was observed. As the pH increased, the percent removal of xylanase activity decreased. At pH 4.5, about 80% of the initial xylanase activity was removed, and it further decreased to about 18% at pH 5.8. No decrease in the xylanase activity was detected at pH 6.7. The removal of cellulase activity was less than 20% at pH = 4. At a pH of 4.5 or higher, essentially no decrease in the cellulase activity was observed.

Figure 8.17 shows the removal of xylanase activity as a function of the amount of AOT added to the 10 mL initial protein mixture at pH = 4.5. More xylanase precipitated as the volume of AOT solution increased; at 1.2 mL AOT addition, about 90% removal of xylanase activity was obtained. Larger AOT volumes did not change the percent activity removal of xylanase. In contrast, the percent precipitation of xylanase from a pure xylanase solution was 100% at 1 mL AOT addition. A similar phenomenon was observed in the purification of lysozyme from the hen egg white solution: less lysozyme was precipitated from a mixture of proteins than from a pure lysozyme solution (Figures 8.13 and 8.14).

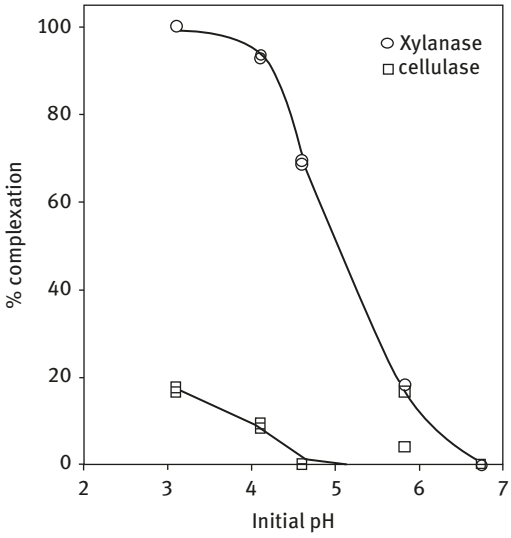

Figure 8.16: Effect of pH on the percent activity removal of xylanase and cellulase from a mixture upon the addition of AOT: initial protein solution volue = 10 mL at approximately 3.3 g/L cellulase and 0.7 g/L xylanase, 1 mL of 5 g/L AOT solution added for precipitation.

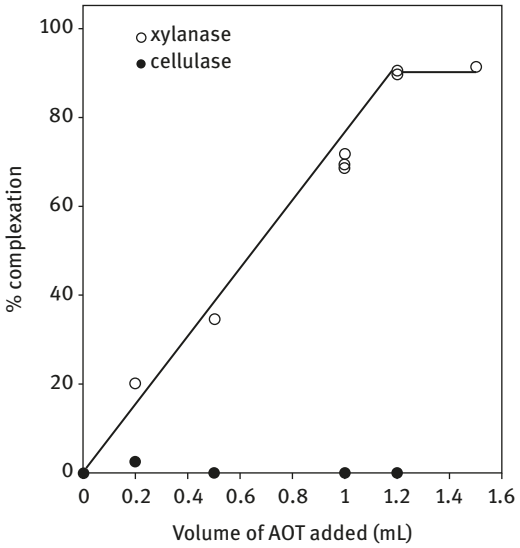

Figure 8.17: Effect of volume of 5 g/L AOT solution on the percent activity removal of xylanase: initial protein solution volume = 10 mL, initial pH = 4.5

8.6.4 Recovery of Xylanase from Xylanase–AOT Complex

Xylanase was recovered from the insoluble xylanase–AOT complex by adding either acetone or ethanol. During the experiments, it was found that xylanase was slightly soluble in the ethanol solution. Also, in order to improve the recovery efficiency, one or two washing steps were required to fully remove the attached AOT from the xylanase protein during the polar solvent recovery step. The xylanase concentration

Table 8.8: Effect of solvent volume, V_s, on the percent recovery of xylanase activity: initial protein solution, final aqueous phase = distilled water.

V_s/V_i	% xylanase activity recovered in the final aqueous phase	
	100% ethanol	50% (v/v) acetone/ethanol
1	33.4 ± 1.3	25.7 ± 0.5
2	33.9 ± 1.3	16.1 ± 0.9
4	25.2 ± 0.7	11.7 ± 1.5

in the washing solution was also measurable amount. In order to fully map the xylanase recovery in the ethanol and the washing solutions, the percent recovery of xylanase activity was calculated using the following equation:

$$\%\ \text{recovery} = \frac{a_f \cdot V_f}{a_i \cdot V_i - a_e \cdot Ve - a_w \cdot V_w} \times 100 \tag{8.4}$$

where a_f, a_i, a_e, and a_w are the xylanase activities in the final aqueous phase, in the initial solution, in the broth after precipitation, and in the washing solution used to remove any cellulase residual on the xylanase–AOT complex, respectively. The volumes of the final aqueous phase, the initial solution, the solution after addition of AOT, and the washing solution are denoted as V_f, V_i, V_p, and V_w, respectively. The percent recovery obtained from eq. (8.4) was compared with the overall xylanase recovery in the final aqueous solution obtained from eq. (8.2).

The recovery of xylanase was tested in terms of type and the volume of solvent used (either acetone or ethanol) and the effect of washing prior to being solubilized into the final aqueous solution. Table 8.8 shows the effect of the polar solvent volume, V_s, on the percent activity of xylanase recovered. Two solvents were used: 100% ethanol or 50% (v/v) ethanol/acetone mixture. For both solvents, the percent recovery of xylanase decreased as the volume ratio increased. The recovery was higher with ethanol than with the ethanol/acetone mixture. In a prior study for the lysozyme–AOT experiment, acetone gave the best recovery of lysozyme activity up to 100% with its original enzymatic activity [22]. However, for xylanase, the use of ethanol gave better recovery compared to acetone. This finding indicates that the protein stability can vary depending on the protein and the type of the solvents, and that the choice of right polar organic solvent to be used to recover surfactant-free protein must be evaluated on a case-by-case basis.

The cellulase activity in the recovered xylanase solution was measured using samples prepared without washing or with washing before the ethanol recovery step. The xylanase recovered without washing showed that about 6% of the initial cellulase accompanied the xylanase–AOT complex and was recovered in the final aqueous solution. This cellulase residual was removed from the complex by washing with

distilled water, and the xylanase in the final aqueous phase did not show any cellulase activity.

The effect of adding sodium acetate buffer to the ethanol phase on the percent recovery during the solvent recovery step was investigated. As previously observed, a small amount of salt solution was needed to be added to improve the surfactant-free protein in the polar organic solvent that could be easily solubilized into the final aqueous phase. Table 8.9 summarizes the xylanase activity solubilized in the ethanol phase and the xylanase recovered in the final aqueous phase of 0.5 M sodium acetate buffer.

Table 8.9: Effect of addition of sodium acetate buffer to the ethanol solvent phase during the recovery step: initial protein solution, pH = 4.1, initial and final aqueous solution volume = 10 mL, final aqueous phase = 10 mL 0.05 M pH 4.5 sodium acetate buffer.

	% xylanase in ethanol phase	% overall xylanase recovery (Equation 8.2)	% xylanase recovered (Equation 8.4)
No buffer added	0	0	0
0.05 mL, 0.5 M buffer	0	61.1	61.1
0.1 mL, 0.5 M buffer	9.6	46.4	56.0
0.1 mL, 2 M buffer	11.7	49.6	61.3
1 mL, 0.5 M buffer	24.3	47.0	71.3

When no sodium acetate buffer was added to the ethanol phase, no xylanase activity was recovered. Upon the addition of the buffer, the xylanase activity recovered in the final aqueous phase increased to about 61%. Although the amount or the concentration of the sodium acetate buffer had no effect on the total recovery efficiency, the percent xylanase solubilized in the ethanol phase increased as the volume of the buffer in the ethanol phase increased. For 1 mL buffer added to 10 mL ethanol, the xylanase activity in the ethanol phase reached 96 IU/mL, indicating that about 20% of the precipitated xylanase was solubilized in the ethanol phase. Also noted in this table is the loss of xylanase in the ethanol phase and during washing steps. The percent recovery was higher when the volume of sodium acetate buffer added to the ethanol phase was lower. However, the absence of sodium acetate buffer in the ethanol phase resulted in water-insoluble xylanase that could not be recovered in the final aqueous solution. This finding indicates that the amount of buffer solution added during solvent recovery step must be optimized carefully.

In order to study the effect of the final aqueous solution on the xylanase recovery, two different types of aqueous solutions were tested: distilled water and sodium acetate buffer. Figure 8.18 shows the percent of xylanase activity recovered in a 10 mL final aqueous solution at a different concentration of buffer

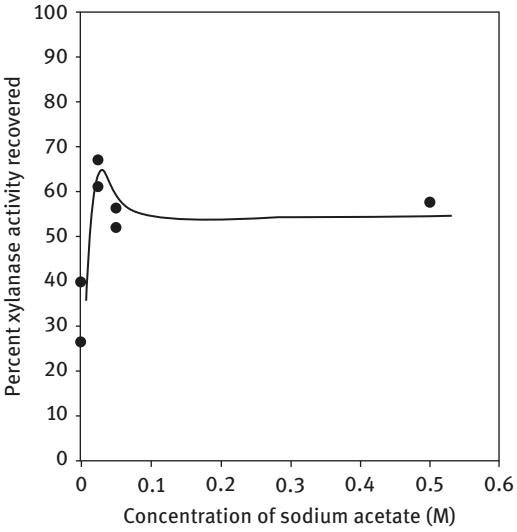

Figure 8.18: Percent xylanase activity recovered as a function of the concentration of sodium acetate buffer in the final aqueous solution: initial and final aqueous phase volume = 10 mL, ethanol as a recovery solvent.

composition. The lowest percent recovery of xylanase activity in distilled water was about 33%. The activity recovery increased to about 63% in a 0.025 M sodium acetate buffer but decreased to 58% at higher sodium acetate concentrations.

Finally, the effect of the final aqueous solution pH was examined to further optimize the xylanase recovery. Figure 8.19 shows the percent recovery of xylanase using 7 mL of ethanol as a recovery solvent and 10 mL 0.025 M pH 4.5 sodium acetate buffer as a final aqueous phase. The closed symbols indicate the overall protein recovery in the final aqueous phase calculated using eq. (8.2). The open symbols indicate the percent xylanase activity recovered from the precipitate calculated from eq. (8.4), accounting for the xylanase dissolved in the washing solution and the xylanase remaining in the initial protein mixture. As shown in Figure 8.19, the percent xylanase activity recovered was also higher at pH 4.5 than at pH 4.1. At pH 4.5, the xylanase activity in the final aqueous phase was 260 ± 30 IU/mL, about 67% of the initial xylanase activity value of 390 IU/mL. The cellulase activity in the recovered xylanase was 0.4 ± 0.2 IU/mL for the samples at pH = 4.1. The cellulase activity in the recovered xylanase at pH 4.5 was below the detection limit. Thus, by optimizing the pH of the initial protein solution, the composition and the volume of the polar solvent used to recover the precipitated xylanase, and the type of the final aqueous phase solubilizing the recovered xylanase in a solid form, a maximum of about 88% of selectively precipitated xylanase was recovered.

In comparison, xylanase was purified from a fermentation broth using ammonium sulfate precipitation method followed by a two-step size-exclusion chromatography at an overall activity recovery of about 10.3% [55]. In that

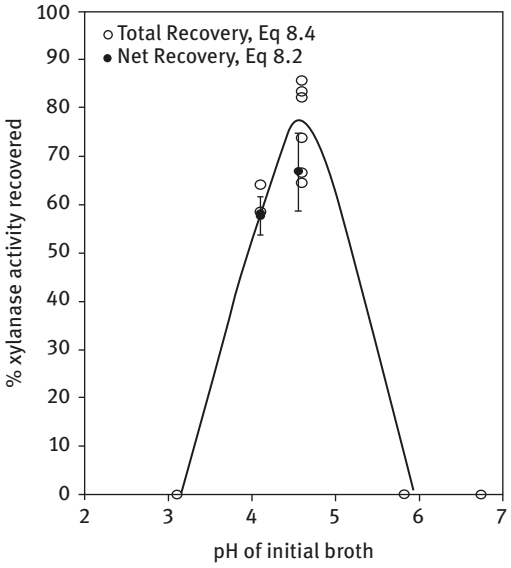

Figure 8.19: Effect of pH on the percent xylanase activity recovered using 0.025 M pH 4.5 sodium acetate buffer as a final aqueous phase: initial and final aqueous solution volume = 10 mL.

work, the salt precipitation method alone resulted in more than 70% impurities in the purified xylanase solution.

8.6.5 Conclusions

Selective precipitation and recovery of xylanase from an aqueous phase containing cellulase mixtures and xylanase was obtained using AOT as a precipitating ligand and ethanol as a recovery solvent. The recovered xylanase was free of contaminant cellulases and AOT. The cellulose activity in the initial broth remained unchanged after the xylanase precipitation with AOT. The percent xylanase recovery and purity in the final aqueous phase were highly depended on the amount of washing of xylanase–AOT insoluble complex, type of polar solvent used to separate xylanase from AOT, the amount of buffer added in the solvent, and the pH of the aqueous solutions. This study successfully demonstrated that the direct precipitation of proteins using ionic surfactant can be used as a cost-effective way to purify industrial proteins of interest. In order to further optimize the purification cost, the AOT and organic solvent such as ethanol could be easily recycled using simple distillation process.

8.7 Summary

The observation of white precipitate during the reverse micellar extraction of proteins from the initial protein solution into an organic phase, and to recover

the protein from the reverse micellar phase into a fresh aqueous phase lighted our insight that the ionic surfactants first form a complex with the appositively charged protein to form a water-insoluble moiety. The use of a polar organic solvent to separate the surfactant from the protein as surfactant-free particles which was subsequently recovered and solubilized into a fresh aqueous phase provided successful recovery of protein to its initial enzymatic activity. This technique was successfully used to separate lysozyme from egg white and xylanase from the xylanase–cellulase mixture.

Since our research, more research work has been carried out by various researchers to continue to examine the use of different surfactants as a protein-precipitating agent. The review paper by Wang et al. [56] summarized the extensive amount of work that has been carried out since our research. Among those studies, Cheng and Stuckey further examined the change of lysozyme structure in the aqueous phase after precipitation using circular dichroism spectroscopy and liquid chromatography and showed that there were no conformational changes in the lysozyme at different AOT concentrations tested [57]. For the proteins with low p*I*s, the use of cationic surfactant showed a successful complexation of proteins from the aqueous phase [58]. As an alternative to the widely used surfactants such as AOT or TOMAC, new biocompatible surfactants such as methyl ester sulphonate [59] and rhamnolipid and saponin [60] were developed for the protein–surfactant precipitation work and the results showed successful removal and recovery of proteins of interest. Instead of the polar solvent, some researchers successfully used counterionic surfactant to recover protein from the protein–surfactant complex [61, 62]. In their work, instead of using a polar aqueous solution, they have used a new aqueous solution to solubilize the protein–AOT complex which became water soluble upon the addition of TOMAC-containing solution. The AOT dissociated from the protein and bind with TOMAC to form water-insoluble complex allowing the AOT-free proteins remained in the solution. Kinugasa further simplified the protein recovery step by optimizing the salt concentration in the initial protein containing solution so that the addition of small amount of buffer solution during the solvent recovery step to separate protein from the protein–surfactant complex could be eliminated [63]. Wong and Stuckey successfully demonstrated the use of surfactant precipitation for bacteriocin which is an important peptide used as an antimicrobial agent in food [64], further demonstrating that this new technique does provide a new promise as a potential new way to purify protein effectively.

References

[1] Ladisch M. Wiley-Interscience, NY, USA, 2001.
[2] Dainiak MB, Izumrudov VA, Muronetz VI, Galaev IY, Mattiasson B. Bioseparation 1999, 7, 213.
[3] Galaev IY, Mattiasson B. Biochemistry 1997, 62, 571.
[4] Lali A, Balan S, John R, D'Souza F. Bioseparation 1999, 7, 195.
[5] Mattiasson B, Kumar A, Galaev IY. J Mol Recognit 1998, 11, 211.

[6] Vaidya AA, Lele BS, Deshmukh MV, Kulkarni MG. Chem Eng Sci 2001, 56, 5681.
[7] Luisi PL, Bonner FJ, Pellegrini A, Wiget P, Wolf R. Helv Chim Acta 1979, 62, 740.
[8] Marcozzi G, Domenico CD, Spreti N. Biotechnol Prog 1998, 14, 653.
[9] Naoe K, Nishino M, Ohsa T, Kawagoe M, Imai M. J Chem Technol Biotechnol 1999, 74, 221.
[10] Göklen KE, Hatton TA. Biotechnol Prog 1985, 1, 69.
[11] Dekker M, Van't Riet K, Weijers SR, Baltussen JWA, Laane C, Bijsterbosch BH. Chem Eng J 1986, 33, B27.
[12] Dungan SR, Bausch T, Hatton TA, Plucinski P, Nitsch W. J Colloid Interface Sci 1991, 145, 33.
[13] Sun Y, Ichikawa S, Sugiura S, Furusaki S. Biotechnol Bioeng 1998, 58, 58.
[14] Lye GJ, Asenjo JA, Pyle DL. Chem Eng Sci 1994, 49, 3195.
[15] Rahaman RS, Chee JY, Cabral JMS, Hatton TA. Biotechnol Prog 1988, 4, 218.
[16] Aires-Barros MR, Cabral JMS. Biotechnol Bioeng 1991, 38, 1302.
[17] Hagen AJ, Hatton TA, Wang DIC. Biotechnol Bioeng 1990, 35, 955.
[18] Lye GJ, Asenjo JA, Pyle DL. Biotechnol Bioeng 1995, 47, 509.
[19] Jarudilokkul S, Stuckey DC. Sep Sci Technol 2001, 36, 657.
[20] Kabanov AV, Nametkin SN, Evtushenko GN, Chernov NN, Klyachko NL, Levashov AV, Martinek K. Biochim Biophys Acta 1989, 996, 147.
[21] Goto M, Hashimoto Y, Fujita T, Ono T, Furusaki S. Biotechnol Prog 2000, 16, 1079.
[22] Shin Y-O, Weber ME, Vera JH. Sep Sci Technol 2003, 38, 1733.
[23] Davies RC, Neuberger A, Wilson BM. Biochim Biophys Acta 1969, 178, 294.
[24] Göklen KE, Hatton TA. Sep Sci Technol 1987, 22, 831.
[25] Choe J, VanderNoot VA, Linhardt RJ, Dordick JS. AIChE J 1998, 44(11),2542.
[26] Chou S-T, Chiang B-H. J Food Sci 1998, 63(3), 399.
[27] Paradkar VM, Dordick JS. Biotechnol Prog 1993, 9, 199.
[28] Chen JP, Jen JT. Sep Sci Technol 1994, 29, 1115.
[29] Kelly BD, Wang DIC, Hatton TA. Biotechnol Bioeng 1993, 42, 1199.
[30] Rabie HR, Helou D, Weber ME, Vera JH. J Colloid Interface Sci 1997, 189, 208.
[31] Luisi PL, Giomini M, Pileni MP, Robinson BH. Biochim Biophys Acta 1988, 947, 209.
[32] Shin Y-O, Weber ME, Vera JH. Biotechnol Prog 2003, 19, 928.
[33] Shin Y-O, Rodil E, Vera JH. Sep Sci Technol 2004, 39, 1005.
[34] Cassin G, Illy S, Pileni MP. Chem Phys Lett 1994, 221, 205.
[35] Jarudilokkul S, Poppenborg LH, Stuckey DC. Sep Sci Technol 2000, 35(4), 503.
[36] Ichikawa S, Imai M, Shimizu M. Biotechnol Bioeng 1992, 39, 20.
[37] Adachi M, Harada M. J Phys Chem 1993, 97, 3631.
[38] Ono T, Goto M, Nakashio F, Hatton TA. Biotechnol Prog 1996, 12, 793.
[39] Linfield WM. Marcel Dekker, New York, USA, 1976.
[40] Krei GA, Hustedt H. Chem Eng Sci 1992, 47(1), 99.
[41] Shield JW, Ferguson HD, Bommarius AS, Hatton TA. Ind Eng Chem Fundam 1986, 25, 603.
[42] Wolbert RBG, Hilhorst R, Voskuilen G, Nachtegaal H, Dekker M, Van't Riet K, Bijsterbosch BH. Eur J Biochem 1989, 184, 627.
[43] Horn D, Heuck C-C. J Biol Chem 1983, 10, 1665.
[44] Jarudilokkul S, Poppenborg LH, Stuckey DC. Biotechnol Bioeng 1999, 62, 593.
[45] Shin Y-O, Rodil E, Vera JH. Biochem Eng J 2004, 17, 91.
[46] Hummel BC, Canad J Biochem 1959, 37, 1393.
[47] Crook EM, Mathias AP, Robin BR. Biochem J 1960, 74, 234.
[48] Paradkar VM, Dordick JS. Biotechnol Bioeng 1994, 43, 529.
[49] Shin Y-O, Rodil E, Vera JH. J Food Science 2003, 68, 595.
[50] Gossett PW, Rizvi SSH, Baker RC. Food Tech 1984, 38(5),67.
[51] Shin Y-O, Wahnon D, Weber ME, Vera JH. Biotechnol Bioeng 2004, 86, 698.

[52] Foody B, Tolan JS. European Patent EP0866165, 1998.
[53] White T, Hindle C. US Patent US6015703, 2000.
[54] Ghose TK. Pure Appl Chem 1987, 59, 257.
[55] Li X-L, Zhang Z-Q, Dean JFD, Eriksson KEL, Ljungdahl LG. Appl Environ Microbiol 1993, 59, 3212.
[56] Wong FWF, Ariff AB, Stuckey DC. Crit Rev Biotechnol 2018, 38, 31.
[57] Cheng SL, Stuckey DC. Process Biochem 2012, 47, 712.
[58] Ward K, Cheng SL, Stuckey DC. J Chem Technol Biotechnol 2016, 91, 2563.
[59] Wong FWF, Ariff AB, Stuckey DC. Biochem Eng J 2017, 117, 30.
[60] Yuan X-Z, Peng X, Huang H-J, Wang H, Ma Y–J, Bao S, Liu H, Leng L-J, Cui K-L, Zeng G-M. Sep Sci Technol 2014, 49, 2249
[61] Cheng SL, Stuckey DC. Biotechnol Prog 2011, 27, 1614
[62] Cheng SL, Stuckey DC. Sep Sci Technol 2016, 51, 181.
[63] Kinugasa T, Okabe K, Jinno K, Uchida K, Nishii Y. Sep Sci Technol 2017, 52, 2918
[64] Wong FWF, Ariff AB, Stuckey DC. Food Chem 2017, 232, 245.

Maen M. Husein

9 The Use of Single Microemulsions for Nanoparticle Preparation

9.1 Introduction

Nanomaterials are organic and/or inorganic solid products with at least one dimension in the size range from 1 to 100 nm. Nanoparticles (NPs) may display different morphologies, for example, needle like, as long as one of their dimensions is in the size range from 1 to 100 nm [1], or less than 10 nm, as per some authors [2]. The physical, chemical, and electrical properties of NPs are size dependent. This fact inspired the preparation of different functional materials with desired properties through manipulating the size of NPs [3–7]. With properties superior to their bulk material counterparts, NPs find applications in catalysis [8, 9], environmental remediation [10], nanocomposites [11], nanofluids [12–14], medicine [15–17], imaging [18], magnetic resonance imaging [19], dip coating [20, 21], and so on. The higher efficiency of NPs reduces the requirement on the volume of materials needed and, hence, may lead to significant cost reduction, which justifies the cost of NP manufacturing. NP preparation techniques are broadly classified under physical or chemical routes. Physical processing involves extensive mechanical grinding of bulk materials into the nanosize domain, whereas chemical processing involves NP synthesis from nucleation and growth of precursor chemicals [22]. Figure 9.1 illustrates the top-down and the bottom-up approaches for NP synthesis using the two routes. Although common, physical processing typically produces NPs with large size distribution and high surface energy. Subsequently, the product particles may not meet the requirement for particles with specific properties. An NP synthesis technique must satisfy other criteria such as environmental footprint, availability of resources, energy requirements, and mass production. Depending on the degree they meet these criteria, many NP preparation routes have been limited to laboratory scale.

The chemical route for NP preparation spans six main techniques: (i) chemical co-precipitation, (ii) electrochemical, (iii) sonochemical, (iv) sol–gel processing, (v) phase transfer, and (vi) microemulsions. The presence of a stabilizing agent, often a surfactant, to protect against particle aggregation and growth is essential for these techniques. By virtue of their ability to dissolve wide variety of water-soluble precursors and limit particle growth and aggregation, water-in-oil (w/o) microemulsions enable the preparation of wide spectrum of inorganic NPs. The resultant NPs may be applied in the colloidal form or collected in the capped dry form for further consideration. In addition, highly homogenous core and shell NPs with controlled shape and size can be easily attained within w/o microemulsions

https://doi.org/10.1515/9783110564808-009

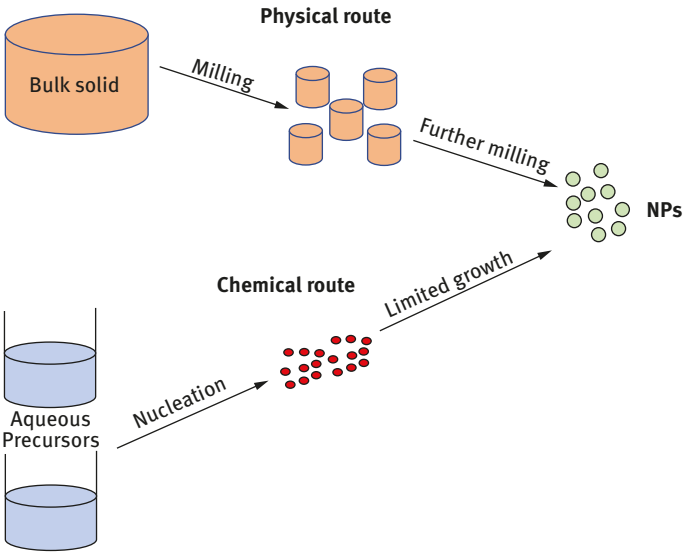

Figure 9.1: Schematic illustrating broad classification of NP preparation routes.

[23–27]. On the other hand, w/o microemulsions mainly suit NPs with water-soluble precursor(s) [28–32], can only dissolve small amount of reactants (especially given their low overall water content), and can only stabilize small amount of the product NPs. Husein recently summarized advantages of phase transfer route and their suitability for large-scale NP preparation [33].

Although w/o microemulsions are the prime microemulsions employed for inorganic NP preparation, microemulsion phase equilibria include other systems. Discussion of different microemulsion equilibria is given below. More details can be found in excellent reviews; including Shinoda and Lindman [34], Winsor [35], Schulman et al. [36], Schomacker et al. [37], Chhabra et al. [38], Chang et al. [39], Klier et al. [40], and Paul and Moulik [41].

9.2 Microemulsion Phase Equilibria

Microemulsions are thermodynamically stable single-phase mixtures (at the macroscopic level) of oil and water [35, 42]. The thermodynamic stability arises from the entropy of dispersion at the low surface energy brought forth by surfactant molecules assembling at the interface [36, 43, 44]. Thermodynamically stable w/o, oil-in-water (o/w), and/or bicontinuous microemulsions may be formed depending on the continuous phase. w/o Microemulsions with mole ratio of water to surfactant, R, below 15 are commonly called reverse micelles [6]. The single-phase microemulsions can

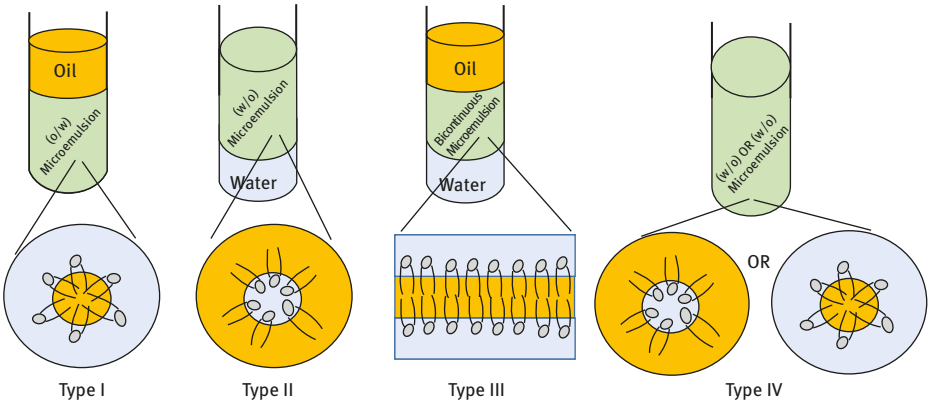

Figure 9.2: Winsor-type equilibria.

maintain thermodynamic equilibrium in a two-phase system having bulk aqueous or oil phase. Figure 9.2 illustrates single-, double-, or triple-phase Winsor equilibrium [34]. Type I is composed of a bulk oil phase in equilibrium with an o/w microemulsion, whereas type II consists of a bulk aqueous phase of certain ionic strength in equilibrium with w/o microemulsion. A three-phase system composed of bulk aqueous and oil phases in equilibrium with a bicontinuous-structured surfactant-rich middle phase is termed Winsor type III microemulsion. The w/o and o/w single-phase systems are known as Winsor type IV microemulsions. Kunieda et al. [45] proposed a fifth type composed of two microemulsion phases, one in contact with bulk water and another in contact with bulk oil, all simultaneously coexisting at equilibrium. In addition to the above equilibria, other single phases of surfactant aqueous solutions, such as liquid crystalline structures, lamellar structures, and chaotic structures, have been identified in the literature [42, 45, 46].

As noted earlier, a wide variety of inorganic NPs have been prepared in w/o microemulsions, or reverse micelles. At the microscopic level, most of these systems consist of spherically shaped water pools surrounded by surfactant and cosurfactant molecules dispersed in a continuous oil phase. The water pools are very dynamic and move under the effect of Brownian motion. The surfactant layer surrounding the water pools, depending on its rigidity, can also be very dynamic. Upon collision of the water pools, the sufficiently loose surfactant layer opens leading to exchange of content and reactions to proceed. Depending on the precursors, these reactions may lead to the formation of nuclei, which when preserved against excessive growth and aggregation by the surfactant layer remain within the nanodomain. Maintaining the colloidal stability of the particles is very important to keep their nanosize. Nevertheless, the size of the NPs can still be maintained, even of the particles are precipitated out of the colloidal system, by means of an effective protective surfactant layer [33]. A brief discussion of

colloidal stability and the role of major forces acting to stabilize/destabilize the particles are given below.

9.3 Colloidal Stability of NPs

Stability of colloids is associated with their resistance to aggregation. Particles move in a colloidal suspension under the influence of Brownian motion (or other external forces, e.g., electric field) as an outcome of their very small mass. Brownian motion disperses the colloidal particles down their concentration gradient against the forces of gravity and friction. Colloidal particles may aggregate and/or agglomerate as they approach one another under the action of attractive forces, for example, van der Waals and/or hydrophobic interactions. Once the particles aggregate/agglomerate, their mass becomes bigger and the effect of diffusion force diminishes. Subsequently, gravity dominates leading to precipitation and destabilization of the colloidal system [33]. Repulsive electrostatic and/or steric forces counteract the attractive forces and prevent particles from approaching close proximity where attractive forces dominate. It is constructive to note that van der Waals force attractive interactions are inversely proportional to the sixth power of the distance between the center of the particles and only dominate at short distances [47].

9.3.1 Electrostatic Stabilization

Electrostatic stabilization is a main colloidal particle stabilization mechanism within aqueous phases. Particles repel one another at a distance which extends through the electrical double layer. The repulsion force is proportional to the zeta potential, which is the electrical potential at the shear surface. The shear surface defines the boundary of the moving particles together with the attached water of hydration. The shear surface is located in between the fixed layer (Stern layer) and the diffuse layer (Guy-Chapman layer) and occurs closer to the fixed layer for a hydrophobic particle. The higher the charge on the colloidal particle, the higher its zeta potential. The diffuse layer extends to the bulk aqueous phase and is defined by an outer surface where the electrical potential reaches zero [48, 49]. Surface charges appear on colloidal particles because of defects in its crystalline structure, dissociation of surface functional groups, and/or adsorption of organic and/or inorganic ions. In addition to the charge density on a colloidal particle, zeta potential is dependent on the temperature of the mixture and the ionic strength of the aqueous phase. Figure 9.3 is a schematic representation of negatively charged colloidal particle and the potential surrounding it.

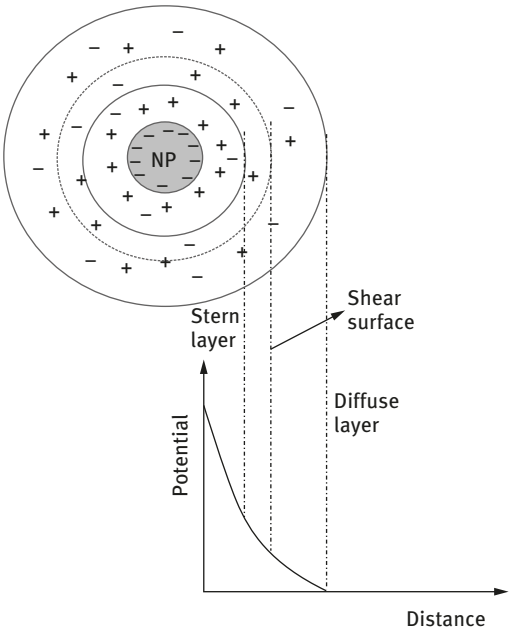

Figure 9.3: Charged colloidal NP and the surrounding potential.

9.3.2 Steric Stabilization

Steric stabilization can be effective in both polar and nonpolar phases. Stabilization pertains to hindering the particles from approaching close proximity beyond which attractive forces become dominant. Steric hindrance is associated with excluding a bigger region from the space surrounding a colloidal particle by means of adsorbed long-chain molecules, for example, surfactants and/or polymers. This region becomes off limit to other particles. Stabilization is highly boosted when the like interactions between the capping molecules are less than the unlike interactions between these molecules and the continuous phase. Otherwise, aggregation and destabilization of the colloidal system may occur. Nevertheless, there are cases where the identity of the capped particles is preserved. Stable NP suspensions of the capped particles may be attained upon redispersing the particles in a continuous phase with high affinity to the capping molecules. In addition to the like/unlike interactions, stabilization arises from the increase in Gibbs free energy as the capped particles approach one another. Within the region of overlap (see Figure 9.4), the entropy decreases as the movement of the molecules becomes more constrained. The extent of stabilization is determined from the change in free energy upon the interaction of the adsorbed layers [50]. Positive Gibbs free energy change is associated with stabilization.

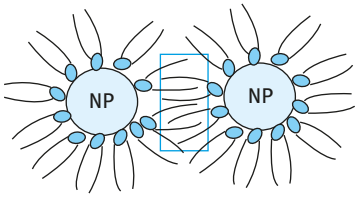

Figure 9.4: Steric stabilization of NPs in oil phase highlighting the region of configurational entropy.

Cross-linking and interdigitation [51] are associated with a decrease in the Gibbs free energy under isothermal conditions and result in aggregation of capped particles.

Steric stabilization of NPs prepared in w/o microemulsions in the form of adsorbed surfactant molecules is the main colloid stability mechanism. Details on NP formation in w/o microemulsions using two major preparation routes are given below. The role of the surfactant protective layer is also detailed.

9.4 Mixing of Two Microemulsions Scheme

Most literature pertaining NP preparation in w/o microemulsions employed the mixing of two identical microemulsions, each carrying one of the water-soluble precursors [3, 26, 28, 52–56]. Excellent reviews highlighted key concepts and advantages of this route of precursor addition [57–62]. Figure 9.5 is a schematic representation of major steps involved in NP formation under this scheme.

When the two w/o microemulsions are added, the water pools driven by Brownian motion and/or macromixing collide with one another. Some of the collisions result in opening of the surfactant protective layer, coalescence and fusion of the water pools, diffusion and eventually effective mixing of the water-soluble precursors. Subsequently, the reaction of NP formation proceeds at a rate dictated by the intrinsic rate of reaction subject to the compartmentalization effect [32]. Coalescence is followed by decoalescence, fission, into the original reverse micelles. For fast reaction kinetics, this time is sufficient to produce product monomers. The precursor in excess distributes itself among the reverse micelles following an overall Poissonian distribution [63–65]. Monomers below the critical nucleation number also distribute themselves among the product reverse micelles following Poissonian distribution [63–65]. Coalescence/decoalescence lead to more reaction and further populate the water pools with the product monomers. Nucleation proceeds whenever the population of the product monomers exceeds the critical nucleation number in a given water pool. The rate of nucleation is driven by the degree of supersaturation [63, 64, 66] and is resisted by the surface tension between the solid product and the surrounding water and/or surfactant molecules. Growth occurs instantaneously upon successful

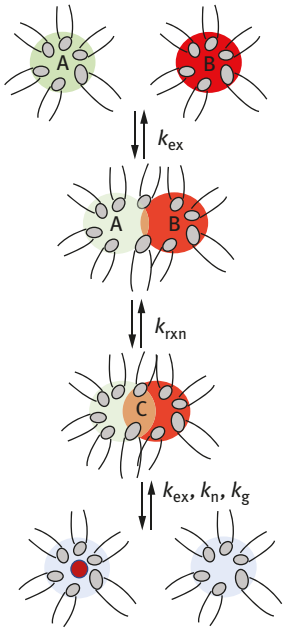

Figure 9.5: NP preparation using mixing of two microemulsions. k_{rxn}, intrinsic reaction rate constant; k_{ex}, rate constant for intermicellar exchange dynamics; k_n, nucleation rate constant; k_g, particle growth rate constant.

collision between a water pool carrying a nucleus and another one carrying the product monomers or carrying the different precursors [63, 65]. It is unlikely for two nuclei to form within a single reverse micelle. Even if this event occurs, Ostwald ripening rapidly eliminates the smaller nucleus [67]. Aggregation, on the other hand, may proceed upon successful collision between two NP-populated reverse micelles. This event is, however, dependent on the rigidity of the surfactant layer surrounding the water pools, which in turn may become more rigid upon NP formation.

For fast reactions, the rate of NP formation is limited by the rigidity of the surfactant layer, which governs the rate of successful collisions between reverse micelles carrying the different reactants [68–71]. This mechanism of NP formation is known as the intermicellar nucleation and growth. Intermicellar nucleation and growth dictates the rate of product formation for the two microemulsions scheme. When proceed slowly, reactions governed by intermicellar mechanism contribute to simultaneous nucleation and growth, which in turn leads to formation of large particles with wide size distribution [70].

Slow rate of intermicellar nucleation limits the ability to attain monodispersed particles, which defeats the purpose of NP design, and together with the need for large volumes of different chemicals, hinder the wide application of the mixing of two microemulsions scheme of NP preparation. The rigidity of the surfactant layer, the key to achieving fast intermicellar nucleation, can, nevertheless, be controlled by manipulating some microemulsion variables, including the water content, the

concentration of surfactant, cosurfactant and reactive species, and type of oil phase. In addition, some operating variables, including rate of mixing and temperature, can be used to control intermicellar nucleation. Eastoe et al. [57] reviewed the effect of these variables and reported some contradicting trends in the literature pertaining to the effect of these variables on particle size and monodispersity. Many researchers have identified the water to surfactant mole ratio, R, as the key variable to control the rigidity of the surfactant layer [68–70]. With an increase in R, the space between surfactant molecules at the reverse micelle interface increases. The interface becomes less curved, less rigid, and easily opens upon collision. The diffusivity of the water pools, on the other hand, decreases at higher R, as per Stokes–Einstein equation [72], leading to lower rate of collision. Accordingly, the effect of R depends on the net rate of successful collisions.

It is constructive to note that for slow reactions, the rate of NP formation depends on the statistical distribution of the precursors among the water pools. Pseudocontinuous-phase models sufficiently predict the rate of NP formation for slow reactions [66, 73, 74]. When the water content is low, accounting for reactant compartmentalization dramatically enhances the predictability of the pseudocontinuous-phase model [75]. Reactant compartmentalization is applicable for precursors residing in the core water pool and involves assigning precursor concentrations based on a volume which excludes the water of hydration associated with the fixed layer. Recall that the rate of NP formation significantly impacts their size distribution and monodispersity.

9.5 Single Microemulsion Scheme

As noted earlier, for fast reactions, surfactant layer opening limits intermicellar nucleation, which negatively impacts NP size controllability. Interestingly, the single microemulsion reactant addition scheme provides an alternative route, which limits the role of intermicellar nucleation. Early experiments on the formation of NPs in w/o microemulsions, in fact, employed the single microemulsion scheme. Boutonnet et al. [76] were the first to prepare 3–5 nm colloidal particles of Pt, Pd, Rh, and Ir in single microemulsions stabilized by hexadecyltrimethylammonium bromide (CTAB) or pentaethyleneglycole dodecyl ether. Prior to that attempt, all of these NPs, despite their role as effective catalysts for organic reactions, were synthesized in aqueous phases owing to precursor low solubility in oil. In Boutonnet et al.'s approach, both the water-soluble metal salt precursor and hydrazine or H_2 were added to/bubbled though the same microemulsion [76]. This study, however, did not investigate the role of different microemulsion variables on particle size distribution. Rather, the efficacy of nanocatalysts formed in organic media was the focus [77]. Despite the huge

surface area and the high population of active sites, the NPs formed in w/o microemulsions suffered from low selectivity owing to the absence of support material. Further work by Boutonnet-Kizling et al. [78] pursued supported catalyst preparation employing a sol–gel technique within single w/o microemulsions platform.

9.5.1 Particle Formation Steps

The formation of NPs in single w/o microemulsions in its most general form involves sequential addition of the two water-soluble precursors to the water pools. Subsequently, *intramicellar* nucleation and growth become important [7, 65]. Accordingly, trends in particle size and polydispersity different than those reported in the literature for the two microemulsions scheme should be expected upon a change in a given microemulsion or operating variable. In general, NP size and polydispersity within single microemulsions are controlled by one or more of the following mechanisms: reaction kinetics, *intramicellar* nucleation and growth, intermicellar nucleation and growth, and particle aggregation [79–81]. NP produced by slow reactions can still be fairly predicted using pseudocontinuous-phase models. For NPs obtained from fast reactions, on the other hand, the rate of particle formation is controlled by *intramicellar* and/or intermicellar nucleation and growth. Figure 9.6 represents particle formation steps within the single microemulsion scheme.

Intramicellar nucleation and growth dominates at high precursor occupancy numbers [7] coupled with rigid surfactant layer, whereas intermicellar nucleation and growth dominates at the reverse conditions [65]. At intermediate values of these variables, both *intramicellar* and intermicellar nucleation and growth govern particle size and polydispersity. Particle aggregation, on the other hand, influences NP size and polydispersity independent of the nucleation and growth mechanism and is less impactful for rigid surfactant layer [80, 81]. It should be noted, nevertheless, that rigid surfactant layers when coupled with low precursor occupancy numbers hinder intermicellar nucleation and contribute to simultaneous nucleation and growth [68–70]. Large NP with polydispersed sizes were formed when growth takes place over small number of nuclei.

Some researchers place preparation of NPs through gas bubbling into a single microemulsion in a separate category [82]. Nevertheless, in the absence of interphase mass transport, NP formation upon gas bubbling is governed by the same nucleation and growth mechanisms described above. With few exceptions in the literature [63], the reacting gas did not suffer from interphase mass transport limitations [64, 83–86]. Consequently, the discussion here also applies to NPs produced upon gas bubbling through single microemulsions.

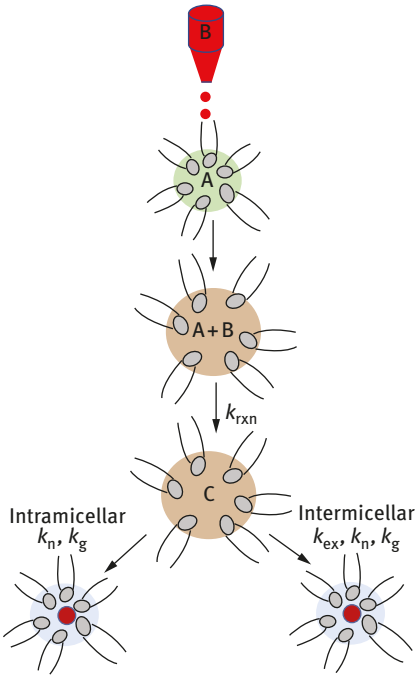

Figure 9.6: NP preparation in a single microemulsion. k_{rxn}, intrinsic reaction rate constant; k_{ex}, rate constant for intermicellar exchange dynamics; k_n, nucleation rate constant; k_g, particle growth rate constant.

9.5.2 Functionalized Surfactants

In the context of NP formation in microemulsions, functionalized surfactants refer to ionic surfactants with reactive counterions. NP preparation by means of adding water-soluble precursor to a microemulsion stabilized with a functionalized surfactant is more commonly encountered in the single microemulsion scheme. Reactive counterions contributed to a significant reduction in polydispersity [5, 80, 87]. Moreover, when functionalized surfactants are employed, the existence of one precursor is guaranteed in every reverse micelle [79–81, 88, 89]. This fact further promotes *intramicellar* nucleation and growth. Figure 9.7 is a schematic representation of NP formation in single microemulsions formed with functionalized surfactants. Sometimes a mixture of functionalized surfactants and unfunctionalized surfactants is used to ensure stability of the w/o microemulsion and the resultant NPs [4, 5, 7].

Husein et al. [29–31] exploited functionalized surfactants to prepare NPs starting from their bulk solid precursors. Their approach is based on the ability of the counterion to dissolve the solid at the very high concentrations of the counterion encountered when surfactant molecules adsorb onto the solid surface together with their water of hydration. The dynamic exchange of surfactant molecules between the

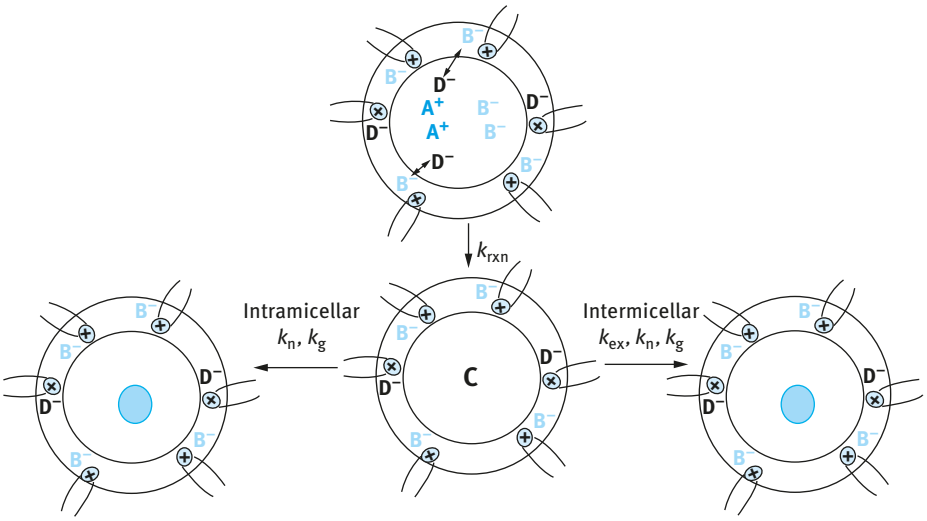

Figure 9.7: NP preparation in single microemulsion formed with functionalized surfactant. k_{rxn}, intrinsic reaction rate constant; k_{ex}, rate constant for intermicellar exchange dynamics; k_n, nucleation rate constant; k_g, particle growth rate constant.

surface of the solid and the reverse micelles helps carrying the dissolved solid to the reverse micellar interfacial region. The dissolved solid diffuses into the water pool, where it undergoes dilution and reprecipitated in form of NPs. The surfactant layer protects the NPs against further growth and aggregation. Even though Husein et al.'s work was limited to a specific combination of solid/counterion, it constituted a novel approach of forming inorganic NPs from their water-insoluble inorganic salts. In addition, the work of Husein et al. introduced the concept of NP uptake. This variable refers to the capacity of a microemulsion system to stabilize colloidal NPs [90, 91].

9.5.3 NP Uptake

Even though microemulsions are effective media for preparing wide variety of NPs, they can only support low amounts of reactants and products [29, 92, 93]. Maintaining the highest concentration of stabilized colloidal NPs is invincible for some applications, for example, large-scale production of NPs. NP uptake refers to the time-independent maximum possible concentration of colloidal NPs in the microemulsions for given values of microemulsion and operating variables.

The work of Nassar and Husein [90, 91] showed that NP uptake by AOT/isooctane/water w/o microemulsion is affected by the extent of interaction between the surfactant head groups and the NPs, the ionic strength of the water pools, and the water content of the microemulsions. Iron oxide NPs interacted with AOT head

groups to a higher extent than copper oxide and, hence, showed higher uptake at fixed values of the other variables [90, 91]. The ionic strength increased the NP uptake, up to a value where the microemulsions destabilized. Moreover, NP uptake varied linearly with the surfactant concentration and quadratically with the precursor salt concentration. Lastly, NP uptake showed a maximum w.r.t. *R*.

9.5.4 Trends in Particle Size and Polydispersity

Literature trends relating NP size and polydispersity to microemulsion and operating variables for the single microemulsion scheme of NP preparation are discussed below. The role of different NP formation mechanisms and their impact on NP size and size distribution are also discussed. The seemingly contradicting trends in the literature are explained in light of NP rate of formation controlling mechanism. Comparison with literature trends for the mixing of two microemulsions scheme can be made by referring to the excellent review by Eastoe et al. [57].

9.5.4.1 Effect of Water-to-Surfactant Mole Ratio, *R*

Even though it cannot be generalized, many investigations showed that the size of the NPs is chiefly controlled by the size of the reverse micellar water pools [26, 28, 30, 31, 62, 90, 91, 94–96]. In the context of single microemulsion scheme, an increase in *R*, fixing all other parameters, contributes to lower number of reverse micelles with larger water pools [68, 70, 73, 97]. This fact leads to two opposing effects on *intramicellar* nucleation. One effect increases the population of reverse micelles with minimum nucleation number of product monomers [68, 69]. This effect promotes *intramicellar* nucleation. The other effect dilutes the precursors and, hence, slows down the rate of *intramicellar* nucleation. In addition to the effects on *intramicellar* nucleation, high water content enhances the rate of intermicellar nucleation [68, 69, 73] as well as the rate of aggregation upon collision of NP-populated reverse micelles [90, 91] through reducing surfactant layer rigidity. Nevertheless, the adverse effect on intermicellar nucleation and growth pertaining to lowering the diffusivity of the reverse micelles as the water pools become larger should be kept in mind. Lastly, high water content smears the interaction between the surfactant head groups and the colloidal NPs [29–31], also promoting particle aggregation.

Three different trends for the effect of *R* on NP size and polydispersity are recorded in the literature for the single microemulsion technique. For partially functionalized surfactants, NP size increased followed by a plateau associated with a monotonic increase in polydispersity as *R* increased [6, 87, 98]. Pileni and coworkers attributed the increase in particle size to freeing more of the counterion reactant from the Stern layer with the abundance of water. This explanation

finds support in the fact that an increase in R beyond a given value could no longer contribute to the hydration of new ions and, hence had no significant effect on NP size. It appears that, at the conditions of the experiments, a rigid surfactant layer limited intermicellar nucleation and growth as well as particle aggregation, despite the increase in R. Accordingly, it is concluded that *Intramicellar* nucleation and growth most likely dominated NP rate of formation, and the counterions released from Stern layer probably contributed to local nucleation and growth.

Husein and coworkers reported a monotonic increase in particle size and polydispersity with R [79–81]. This trend was explained by simultaneous nucleation and growth coupled with particle aggregation. As the water content increased, the rate of *intramicellar* nucleation decreased, due to a dilution effect. On the other hand, the accompanying decrease in the rigidity of surfactant layer promoted intermicellar nucleation coupled with simultaneous growth. It is highly likely that the dilution effect slowed down the overall rate of nucleation via either mechanisms and contributed to simultaneous growth. Furthermore, aggregation increased as the surfactant layer became loose and the interaction between the surfactant molecules and the NPs decreased [29, 30]. The higher rate of successful collisions between NP-populated reverse micelles encountered at these conditions led to particle aggregation. It should be noted that in Pileni and coworkers investigations [6, 87, 98], the mole ratio of the reactants was close to the stoichiometric ratio. As such, counterion reactant release controlled the reaction rate and the final particle size, whereas Husein and coworkers employed a much higher ratio of the counterion reactant.

Sugih et al. [83] used CO_2 bubbling to prepare NPs of $CaCO_3$ within single microemulsions formed with the calcium form of AOT. Aqueous $Ca(OH)_2$ reactant was initially added to the water pools, or solid $Ca(OH)_2$ was dispersed in the continuous oil phase. Sugih et al. [83] reported an increase followed by a decrease in particle size and polydispersity with increasing R. This trend was explained by a decrease in the rate of successful collisions and, hence solubilizate exchange dynamics beyond a certain R. Consequently, nucleation commenced at very high rate via the *intramicellar* route; meanwhile, growth took place over a larger number of nuclei via the intermicellar route. This led to the formation of smaller particles beyond a certain R. Conversely, many researchers reported increasing rates of effective collisions and solubilizate exchange dynamics with R [68–70], especially given the effect of increased R on the rigidity of the surfactant surface layer. Sugih et al.'s explanation is, nevertheless, valid in light of the effect of R on the diffusivity of the water pools. Furthermore, since Sugih et al. used constant concentration of $Ca(OH)_2$ independent of R, the dilution effect reported by Husein and coworkers was not encountered. Accordingly, as R increased, the fraction of reverse micelles containing the critical nucleation number increased. Nucleation proceeded

via the *intramicellar* nucleation route in more reverse micelles, and growth also proceeded locally over larger number of nuclei resulting in smaller particle size and size distribution. It appears that particle aggregation was limited by rigid surfactant layer even at high values of R, which also limited intermicellar nucleation and growth. Lastly, the high interaction between the NPs and the head groups of the surfactant limited particle aggregation.

Lisiecki and Pileni [4] reported a decrease in copper NP size as R increased due to the formation of copper oxide layer, which impeded particle growth. Hence, this trend should not be generalized [5].

9.5.4.2 Effect of Polar Volume Fraction

Increasing the polar volume fraction involves increasing the surfactant concentration at constant R [4, 98]. Accordingly, higher polar volume fraction is equivalent to increasing the population of reverse micelles in the oil phase. Constant concentration of the aqueous precursors, under this scenario, translates into larger number of NP-populated reverse micelles, which in turn increases the probability of particle aggregation.

Results showed that, at constant ratio of the reactive versus nonreactive forms of the surfactant and constant surfactant to reactant ratio, no effect on particle size was observed as the polar volume fraction increased [5]. Meanwhile, NP concentration increased. These observations are explained in light of *intramicellar* nucleation and growth predominant mechanism coupled with rigid surfactant layer. Rigid surfactant layer limits intermicellar nucleation and growth as well as NP aggregation upon collision of NP-populated reverse micelles. This explanation finds further support in the fact that smaller particles were obtained when the polar volume fraction increased at fixed concentration of the reactive form of the surfactant [4]. The ion occupancy number of the reactive counterion decreased in this test. Similar observation was reported upon reducing a precursor ion occupancy number, by maintaining constant amount of sodium borohydride while increasing the polar volume fraction [5].

When the w/o microemulsions were entirely formed by functionalized surfactants, an increase in particle size was reported with the polar volume fraction [79–81]. In these experiments, as stated earlier, the mole ratio of the reactive counterion far exceeded the stoichiometric ratio and, under the conditions of the experiment, the mole ratio was allowed to increase further. The increase in particle size is explained based on intermicellar nucleation coupled with simultaneous growth. A decrease in silver occupancy number with increasing the polar volume fraction shifted the mechanism of nucleation from *intramicellar* to intermicellar dominated. Simultaneous intermicellar growth took place and large, polydispersed particles formed.

In Sugih et al.'s work [83] the particle size decreased with the polar volume fraction. This trend was explained by the decrease in the size of the reverse micellar water pools [99]. The authors, nevertheless, acknowledged that the sizes of the water pools and those of the NPs do not necessarily follow the same trend. The experiments of Sugih et al. also indirectly involved increase in NP concentration with the increased polar volume fraction. The ability to sustain smaller particle size at higher population of NPs suggests rigid surfactant layer surrounding the reverse micelles. With this in mind, coupled with the decrease in the micellar water pool size at higher surfactant concentration for a given R, reveal the following. The rate of *intramicellar* nucleation increased with the increase in supersaturation associated with smaller water pools. Intermicellar growth followed at a later stage owing to the high rigidity of the surfactant layer. Growth over large population of nuclei led to smaller particles [68–70]. Intermicellar nucleation, on the other hand, appears to have been kept to a minimum due to the highly rigid surfactant layer.

9.5.4.3 Effect of Reactant Concentrations

Reactant concentration within the single microemulsion addition scheme may be increased by adding more of the reactant to the microemulsion or increasing the polar volume fraction or R at constant reactant aqueous concentration. For functionalized surfactants, reactant concentration increases with the polar volume fraction, or with surfactant concentration at constant polar volume fraction.

High concentration of the functionalized $Cu(AOT)_2$ surfactant at constant mole ratio of copper to hydrazine increased copper NP size, independent of R [4]. Hydrazine concentration above 0.02 M, at constant $Cu(AOT)_2$ concentration, on the other hand, decreased NP size only at R = 3.0. Higher reactant occupancy number and the associated enhanced *intramicellar* nucleation and growth most likely led to larger NP size. Copper oxide layer formed on the surface of the NPs and prevented further NP growth at high R values. Subsequently, the results pertaining to increasing hydrazine concentration were inconclusive.

Increasing the concentration of sodium borohydride or hydrazine produced large, polydispersed silver particles [3]. It should be noted that very high mole ratio of the silver to the reducing agent was employed in these experiments. These observations may be explained by high rates of *intramicellar* nucleation and growth at the high occupancy number of the precursors. Polydispersity may be explained by potential aggregation of NP-populated reverse micelles. Conversely, Husein et al. [79–81] reported a decrease in NP size with silver ion concentration for functionalized surfactants. Higher silver

ion occupancy number enhanced the rate of *intramicellar* nucleation. Growth then commenced on larger number of nuclei leading to smaller particles.

9.5.4.4 Type of Reagent

For products that can be synthesized using different precursors, the choice of a precursor affects the intrinsic rate of product formation as well as the availability of the precursor in the reaction zone. Ohde et al. [100] prepared silver and copper colloidal NPs in single microemulsions based on supercritical CO_2. The sodium form of AOT was used as the surfactant and perfluoropolyether-phosphate as the cosurfactant. Aqueous silver or copper nitrate was used as the metal precursors. The reducing agents were supercritical CO_2-soluble species of sodium cyanoborohydride ($NaBH_3CN$) or *N,N,N',N'*-tetramethyl-*p*-phenylenediamine (TMPD). $NaBH_3CN$ contributed to a faster reaction rate, whereas mass transfer between the reaction zone and the CO_2 phase limited the migration of the oxidized form of the TMPD and, hence, the overall rate of NP formation. Surprisingly, NP size was not affected by the choice of the reducing agent. A rate-independent particle size is indicative of intrinsic kinetics-limited reaction. Solubilizate exchange dynamics proceeded at a faster rate, and a pseudocontinuous aqueous-phase model should sufficiently describe particle size for either of the reducing agents. Egorova and Revina [101] prepared silver and copper NPs in single microemulsions using a natural paint pigment as a reducing agent and silver nitrate as the source of silver. They compared copper nitrate and copper ammonium chloride, $Cu(NH_3)_4Cl_2$, as two different sources of the copper ions. Copper ammonium complexes contributed to slower reaction rate, and larger particles were obtained for $Cu(NH_3)_4Cl_2$. For copper nitrate precursor, on the other hand, the fast reaction kinetics exceeded the solubilizate exchange dynamics. *Intramicellar*/intermicellar nucleation supplied more seeds for growth and contributed to the formation of smaller particles.

CdS NPs prepared through bubbling $H_2S_{(g)}$ into a single microemulsion based on the functionalized $Cd(AOT)_2$ surfactant were larger compared with CdS prepared by the mixing of two microemulsions technique with $Na_2S_{(aq)}$ as the sulfide ion precursor [7]. This observation is attributed to a higher product yield as excess $H_2S_{(g)}$ was used. *Intramicellar* nucleation and growth probably dominated particle formation.

AOT functionalized with Ag^+ [5] or Cu^{2+} [6] was used to prepare the metallic NPs in single microemulsions. Two reducing agents were compared; namely sodium borohydride and hydrazine. Reduction of Ag^+ displayed slow kinetics, independent of the reagent. Accordingly, the rate of silver NP formation could be sufficiently described by a pseudocontinuous aqueous-phase

model. Only silver NP polydispersity increased when hydrazine was used, but the average size remained constant, since it contributed to a slower reaction rate. On the other hand, the reduction of Cu^{2+} commenced at a higher rate than the solubilizate exchange dynamics for sodium borohydride reagent, and smaller particles formed. The high intrinsic rate of copper reduction was rapid enough to promote *intramicellar*/intermicellar nucleation. More nuclei formed and, hence, smaller particles were obtained.

Much higher rates of reduction of silver and gold ions in single microemulsions were reported with sodium borohydride in comparison with photochemical or thermal reduction [102]. The study, however, did not focus on the role of the reduction mechanism on particle size or polydispersity. Nevertheless, as per above discussion, smaller particles with smaller size distribution are expected to form when the intrinsic kinetics is faster than the solubilizate exchange dynamics.

Husein et al. [29–31] obtained the same AgCl and AgBr particle size and distribution when compared bulk AgCl and AgBr powders with silver nitrate precursors. It should be noted that in their work, Husein et al. employed functionalized surfactants [79–81]. These findings were satisfactorily explained by *intramicellar* nucleation and growth as the controlling mechanism, independent of the nature of the precursor.

When forming $CaCO_3$ NPs upon bubbling CO_2 into single microemulsions and continuously supplying $Ca(OH)_2$ reactant, larger NPs were produced [83]. Dispersing calcium hydroxide into the oil phase provided continuous supply of the calcium ion upon diffusion into the water pools. *Intramicellar* nucleation and growth governed the mechanism of particle formation.

9.5.4.5 Type of Oil Phase

Some organic solvents are not suitable for the preparation of w/o microemulsions. For example, a combination of aromatic solvents and functionalized $Ca(AOT)_2$ surfactant produced turbidity even at low water content and, hence, the microemulsion could not be used to prepare $CaCO_3$ NPs [83]. In general, the continuous oil phase influences the viscosity of the w/o microemulsion system, therefore, affects the solubilizate exchange dynamics, as per Stoke–Einstein equation. In one investigation, when isooctane was replaced with cyclohexane, a 10-fold reduction in the rate of solubilizate exchange occurred without any effect on the size of the water pools [4]. Nevertheless, the NP size decreased, which suggests intermicellar nucleation and growth was minimal, since slower rate of solubilizate exchange dynamics leads to larger particles for intermicellar-dominated nucleation and growth mechanism [68–70]. It appears that *intramicellar* nucleation and growth dominated the rate of NP formation. Aggregation was limited at the slower rate of interparticle collisions associated with the higher viscosity oil.

9.5.4.6 Effect of Mixing

Mixing is important when solid or aqueous precursors are added to the single microemulsion system. In fact, mixing is indispensable when preparing w/o microemulsions following the titration method of w/o microemulsion [103]. Otherwise, phase separation and thermodynamically unstable separate bulk phases were formed. Gaseous reactants, on the other hand, provide their own mixing while bubbling through the microemulsion. Mixing becomes even lesser of an issue for highly soluble gases [64, 83]. Of course, for sparingly soluble gases, providing sufficient mixing is still important.

Barnickel and Wokaun [102] compared the efficacy of the aqueous form of the reducing agent sodium borohydride, $NaBH_4$, versus its solid form while preparing silver and gold NPs in single microemulsions. Although aqueous $NaBH_4$ was incorporated within the Ag^+-containing CTAB microemulsion and no bulk phase was formed, it induced particle aggregation as confirmed by UV-Vis spectroscopy. Temporal destabilization of the microemulsion while accommodating the added solution [80] coupled with relatively fast reaction kinetics most likely contributed to this aggregation. On the other hand, the solid $NaBH_4$ precursor under ultrasonic agitation produced very narrow particle size distribution. The authors explained the results by the effect of ultrasonication on the size distribution of the reverse micelles. Nevertheless, it is also important to refer to the effect of ultrasonication on distributing the precursors among the reverse micelles and on increasing the solubilizate exchange dynamics. Accordingly, the rate of both *intramicellar* and intermicellar nucleation increased leading to the formation of more nuclei.

Sugih et al. [83] attributed the increase in $CaCO_3$ NP size with stirring to an increase in the probability of successful interparticle collisions and the accompanying increase in the probability of NP aggregation. Husein et al. [29, 30], on the other hand, employed functionalized surfactants and reported no significant effect for mixing on particle size and polydispersity. This observation was explained by a rigid surfactant protective layer. The fact that mostly *intramicellar* nucleation and growth governed the rate of NP formation should also be noted here.

A quick comparison with the mixing of two microemulsions scheme shows that high mixing rates enhanced intermicellar nucleation and growth and contributed to smaller particle sizes for as more nuclei formed [104].

9.6 Conclusions

w/o Microemulsions, or reverse micelles, provide an attractive route for the preparation of wide variety of inorganic NPs with controlled sizes. The water pools accommodate the water-soluble precursor(s) and effectively mix the reactants, which provides highly

homogenous product. Careful control of microemulsion and/or operating variables provides the ability to design particles with predetermined sizes to serve certain application. Depending on the rigidity of the surfactant protective layer and the extent of interaction between the surfactant head groups and the NPs, microemulsions protect against particle aggregation and provide highly stable colloidal dispersions. There are two reactant addition schemes employed to prepare NPs within w/o microemulsion systems, namely the single microemulsion scheme and the mixing of two microemulsions scheme. The single microemulsion scheme is advantageous, since it requires much less volume of chemicals. The effect of a given microemulsion variable or an operating variable differs between the two schemes, primarily since *intramicellar* nucleation and growth is only encountered within the single microemulsion preparation route. On the other hand, solubilizate exchange dynamics and intermicellar nucleation and growth dominate the two microemulsions addition scheme. Rigid surfactant protective layer slows down solubilizate exchange rate and promotes simultaneous nucleation and growth, which limits the ability to control particle size. Functionalized surfactants can best be utilized within the single microemulsion scheme. Functionalized surfactants allowed NP preparation from aqueous as well as bulk solid precursors. The work on NP formation from bulk solid introduced the variable NP uptake, which refers to the time-independent maximum possible stable concentration of NPs within a w/o microemulsion. This variable is very important for large-scale application of microemulsions for preparing NPs.

Acknowledgements: The author is grateful to his former coworker Dr. Eva Rodil, now Professor Rodil, for her active participation in the five manuscripts that they published together on nanoparticles. The research work published in those manuscripts was the founding stone for the preparation of this chapter.

References

[1] Christian P, Kammer F, Baalousha M, Hofmann Th. Ecotoxicology 2008, 17, 326.
[2] Nagy JB. Colloids Surf 1989, 35, 201.
[3] Feltin N, Pileni MP. Langmuir 1997, 13, 3927.
[4] Lisiecki I, Pileni MP. J Phys Chem 1995, 99, 5077.
[5] Petit C, Lixon MP, Pileni MP. J Phys Chem 1993, 97, 12974.
[6] Pileni, MP. J Phys Chem, 1993, 97, 6961.
[7] Pileni MP, Motte L, Petit C. Chem Mater, 1992, 4, 338.
[8] Carnes CL, Klabunde KJ. J Molecular Catalysis A: Chem 2003, 194, 227.
[9] Ida T; Tsuiki H, Ueno A, Tohji K, Udagawa Y, Iwai K, Sano H. J Catalysis, 1987, 106, 428.
[10] Zhang W. J. Nanopart Res, 2003, *5*, 323.
[11] Utracki LA. Clay-containing polymeric nanocomposites, RAPRA: UK, 2004.

[12] Hwang, Y, Lee JK, Lee CH, Jung YM, Cheong SI, Lee CG, Ku BC, Jang SP. Thermochim Acta, 2007, *455*, 70.
[13] Keblinski P, Eastman JA, Cahill DG. Materials Today 2005, June, 36.
[14] Eastman JA, Choi SUS, Li S, Yu W, Thompson LJ. Appl Phys Lett 2001, 78, 718.
[15] Mirta SB, Wu D, Holmes BN. JADA 2003, 134, 1382.
[16] Tartaj P, Morales MP, Veintemillas-Verdauguer S, Gonzalez-Carreno T, Serna CJ. J Phys D: Appl Phys 2003, 36, R182.
[17] Brigger I, Dubernet C, Couvreur P. Adv Drug Deliv Rev 2002, 54, 631.
[18] Sametband M, Shweky I, Banin U, Mandler D, Almog, J Chem Comm 2007, 1142.
[19] Babes L, Benizot B, Tanguy G, Jeune JJL, Jallet P. J Coll Interfac Sci 1999, 212, 474.
[20] Yu J, Ho W, Lin J, Yip H, Wong P. Environ Sci Technol 2003, 37, 2296.
[21] Adachi M, Suzuki Y, Kashiwagi N, Isobe T, Senna M. Colloids Surf A 1998, 153, 617–623.
[22] Toshima N, Yonezawa T. New J Chem 1998, 22, 1179–1201.
[23] Filankembo M, Pileni MP. Appl surf Sci 2000, 164, 260–267.
[24] Zhang R, Liu J, Han B, He J, Liu Z, Zhang J. Langmuir 2003, 19, 8611–8614.
[25] Weidenkaff A, Ebbinghaus SG, Lippert T. Chem Mater 2002, 14, 1797–1805.
[26] Palla BJ, Shah DO, Garcia-Casillas P, Matutes-Aquino J. J Nanopart Res 1999, 1, 215–221.
[27] Tan W, Santra S, Zhang P, Tapec R, Dobson J. Method for identifying cells. U.S. Patent, Patent serial No. 010807, 2002.
[28] Debuigne F, Jeunieau L, Wiame M, Nagy JB. Langmuir 2000, 16, 7605–7611.
[29] Husein MM, Rodil E, Vera JH. WJChE 2007, 2007, 13–25.
[30] Husein MM, Rodil E, Vera JH. Langmuir 2006, 22, 2264–2272.
[31] Husein MM, Rodil E, Vera JH. J Colloid Interface Sci 2005, 288, 457–467.
[32] Husein MM, Nassar NN. Curr Nanosci 2008, 4, 370–380.
[33] Husein MM. J Nanopart Res 2017, 19, 405.
[34] Shinoda K, Lindman B. Langmuir 1987, 3, 135–149.
[35] Winsor PA. Trans Faraday Soc 1948, 44, 376–398.
[36] Schulman JH, Stoeckenius W, Prince LM. J Phys Chem 1959, 63, 1677–1680.
[37] Schomacker R, Schwuger M-J, Stickdorn K. Chem Rev 1995, 95, 849–864.
[38] Chhabra V, Free ML, Kang PK, Truesdail SE, Shah DO. Tenside Surfactants Deterg 1997, 34, 156–168.
[39] Chang GG, Huang TM, Hung HC. Proc Natl Sci Counc ROC (B) 2000, 24, 89–100.
[40] Klier J, Tucker CJ, Kalantar TH, Green DP. Adv Mater 2000, 12, 1751–1757.
[41] Paul BK, Moulik SP. Curr Science 2001, 80, 990–1001.
[42] Bourrel M, Schechter RS. Surfactant Science Series, Vol. 30. Dekker, New York (1998), pp. 15–21, 231–233.
[43] Schulman JH, Friend JA J Colloid Interface Sci 1949, 4, 497–509.
[44] Hoar TP, Schulman JH. Nature 1943, 152, 102–103.
[45] Kunieda H, Asaoka H, Shinoda KJ. J Phys Chem 1988, 92, 185–189.
[46] Ghosh O., Miller CA. J Phys Chem 1987, 91, 4528–4535.
[47] Roucoux A, Schulz J, Patin H. Chem Rev 2002, 102, 3757–3778.
[48] Stigter D. J Phys Chem 1964, 68, 3603–3611.
[49] Stigter D., Mysles K. J Phys Chem 1955, 59, 45–51.
[50] Dutta J., Hofmann H. Encyclopedia of Nanoscience and nanotechnology 2003, 10, 1.
[51] Manna A, Imae T, Iida M, Hisamatsu N. Langmuir 2001, 17, 6000–6004.
[52] Seip CT, Carpenter EE, O'Connor CJ. IEEE Trans Magn 1998, 34, 1111–1113.
[53] Santra S, Tapec R, Theodoropoulou N, Dobson J, Hebard A, Tan W. Langmuir 2001, 17, 2900–2906.

[54] Lopez-Perez JA, Lopez-Quintela MA, Mira J, Rivas J, Charles SW. J Phys Chem B 1997, 101, 8045–8047.
[55] Pillai V, Shah DO. J Mag Mag Mater 1996, 163, 243–248.
[56] Jeunieau L, Nagy JB. Colloids Surf A 1999, 151, 419–434.
[57] Eastoe J, Hollamby MJ, Hudson L. Adv Colloid Interface Sci 2006, 128–130, 5–15.
[58] Destrée C, Nagy JB. Adv Colloid Interface Sci 2006, 123–126, 353–367.
[59] Capek I. Adv Colloid Interface Sci 2004, 110, 49–74.
[60] Eriksson S, Nylén U, Rojas S, Boutonnet M. Appl Catal A: Gen 2004, 265, 207–219.
[61] Lopez-Quintela MA. Curr Opin Colloid Interface Sci 2003, 8,137–144.
[62] Pillai V, Kumar P, Hou M, Ayyub P, Shah DO. Adv Colloid Interface Sci 1995, 55, 241–269.
[63] Bandyopadhaya R, Kumar R, Gandhi KS. Langmuir 2000, 16, 7139–7149.
[64] Bandyopadhaya R, Kumar R, Gandhi KS, Ramkrishna D. Langmuir 1997, 13, 3610–3620.
[65] Natarajan U, Handique K, Mehra A, Bellare JR, Khilar KC. Langmuir 1996, 12, 2670–2678.
[66] Schmidt J, Guesdon C, Schomäcker R. J Nanopart Res 1999, 1, 267–276.
[67] Tojo C, Blanco MC, Lopez-Quintela MA. Langmuir 1997, 13, 4527–4534.
[68] Bagwe RP, Khilar KC. Langmuir 2000, 16, 905–910.
[69] Bagwe RP, Khilar KC. Langmuir 1997, 13, 6432–6438.
[70] Chew CH, Gan LM, Shah DO. J Dispersion Sci Technol 1990, 11, 593–609.
[71] Bommarius AS, Holzwarth JF, Wang DIC, Hatton TA. J Phys Chem 1990, 94, 7232–7239.
[72] Acharya A, Sanyal SK, Moulik SP. Curr Science 2001, 81, 362–370.
[73] Hirai T, Sato H, Komasawa I. Ind Eng Chem Res 1994, 33, 3262–3266.
[74] Hirai T, Sato H, Komasawa, I. Ind Eng Chem Res 1993, 32, 3014–3019.
[75] Holmberg K. Adv Colloid Interface Sci 1994, 51,137–174.
[76] Boutonnet M, Kizling J, Stenius P, Maire G. Colloids Surf 1982, 5, 209–225.
[77] Boutonnet M, Kizling J, Touroude R, Maire G, Stenius P. Appl Catal 1986, 20, 163–177.
[78] Boutonnet-Kizling M, Bigey C, Touroude R. Appl Catal A: Gen 1996, 135, L13–L17.
[79] Husein MM, Rodil E, Vera JH. J Nanopart Res 2007, 9, 787–796.
[80] Husein MM, Rodil E, Vera JH. J Colloid Interface Sci 2004, 273, 426–434.
[81] Husein MM, Rodil E, Vera JH. Langmuir 2003, 19, 8467–8474.
[82] Kumar AR, Hota G, Mehra A, Khilar KC. AICHE 2004, 50, 1556–1567.
[83] Sugih AK, Shukla D, Heeres HJ, Mehra A. Nanotechnology 2007, 18, 035607 (9pp).
[84] Sato H, Tsubaki Y, Hirai T, Komasawa I. Ind Eng Chem Res 1997, 36, 92–100.
[85] Karanikolos GN, Alexandridis P, Itskos G, Petrou A, Mountziaris TJ. Langmuir 2004, 20, 550–553.
[86] Kandori K, Kon-No K, Kitahara A. J Colloid Interface Sci 1988, 122, 78–82.
[87] Petit C, Lixon P, Pileni MP. J Phys Chem 1990, 94, 1598–1603.
[88] Lisiecki I, Pileni MP. Langmuir 2003, 19, 9486–9489.
[89] Germain V, Pileni MP. J Phys Chem B 2005, 109, 5548–5553.
[90] Nassar NN, Husein MM. Langmuir 2007, 23, 13093–13103.
[91] Nassar NN, Husein MM. J Colloid Interface Sci 2007, 316, 442–450.
[92] Husein MM, Weber M, Vera JH. Can J Chem Eng 2001, 79, 744–750.
[93] Siswanto C, Battal T, Schuss OE, Rathman JF. Langmuir 1997, 13, 6047–6052.
[94] Nassar NN, Husein MM. Phys Status Solidi A 2006, 203, 1324–1328.
[95] Lopez-Quintela MA, Rivas J. J Colloid Interface Sci 1993, 158, 446–451.
[96] Hingorani S, Pillai V, Kumar P, Multani MS, Shah DO. Mater Res Bull 1993, 28, 1303–1310.
[97] Curri ML, Agostiano A, Manna L, Monica MD, Catalano M, Chiavarone L, Spagnolo V, Lugara M. J Phys Chem B 2000, 104, 8391–8397.
[98] Pileni MP. Langmuir 1997, 13, 3266–3276.
[99] Kinugasa T, Kondo A, Nishimura S, Miyauchi Y, Nishii Y, Watanabe K, Takeuchi H. Colloids Surf A 2002, 204, 193–199.

[100] Ohde H, Hunt F, Wai CM. Chem Mater 2001, 13, 4130–4135.
[101] Egorova EM, Revina AA. Colloid Surf A 2000, 168, 87–96.
[102] Barnickel P, Wokaun A. Molecular Physics 1990, 69, 1–9.
[103] Rabie HR, Helou D, Weber ME, Vera JH. J Colloid Interface Sci 1997, 189, 208–215.
[104] Motte L, Petit C, Boulanger L, Lixon P, Pileni MP. Langmuir 1992, 8, 1049–1053.

Maen M. Husein

10 Reactions in Ionic Surfactant-Based Emulsions/Microemulsions

10.1 Introduction

Reactions between oil- and water-soluble compounds find applications in many industries. To attain appreciable reaction rates, a proper contact between the reactants must be granted. A phase transfer catalyst, such as a crown ether or a quaternary ammonium salt, is conventionally used to facilitate the transfer of one of the reactants between the immiscible phases [1–4]. This approach is referred to as liquid–liquid phase transfer catalysis (LLPTC). A solid–liquid phase transfer catalysis (SLPTC) provides the option of avoiding water migration into the organic phase by using the solid form of the water-soluble reagent [5, 6]. The need for an organic solvent as well as the many steps involved in LLPTC and SLPTC may pose major challenges. LLPTC and SLPTC are usually carried out with mixing to increase the rates of mass transfer [1, 5, 6].

Alternatively, reactions involving oil- and water-soluble compounds can be carried out in polar aprotic solvents, such as acetonitrile or dimethylformamide [5, 7], or a mixture of solvents, such as alcohol or acetone and water [8, 9], which can dissolve both reactants in one phase. This technique eliminates interphase mass transport, and thus the rate of product formation is kinetically controlled. However, the difficulty of separation of polar aprotic solvents, the need for an organic solvent, and the limits on the amounts of reactants that can be dissolved prevent the large-scale application of this technique.

Dispersed microphases (e.g., particles, droplets, or bubbles) with diameters smaller than the diffusion length of the solute also facilitate reactions between oil- and water-soluble compounds. The stability of the dispersion is key to attaining high rates of reactions. Micro- or nanosized droplets eliminate the diffusion within the dispersed phase and provide high surface area of contact between the phases and the reactants [10]. Sometimes microphases are coupled with phase transfer catalysis to improve the performance [5]. This technique still suffers from the multistep mechanism that can limit the overall rate of product formation. Micromixing through ultrasonic waves may also be used to attain small droplets and effective mixing between the phases. If one of the reagents is added in the solid form, in addition to increasing the interfacial area between the phases by creating microfragments of the solid in the oil phase, ultrasound may remove an unreactive coating from the surface of the solid [11, 12]. Ultrasound increases mass transfer rates by creating microscopic turbulence and reducing the boundary layer thickness at the solid–liquid interface. Ultrasonication can also be coupled with phase transfer catalysts [5, 13, 14].

https://doi.org/10.1515/9783110564808-010

Microemulsions are suitable media for reactions involving oil- and water-soluble compounds because they solubilize these compounds and provide a large contact surface between them [15, 16]. Microemulsions can also shift the equilibrium of some reversible reactions [17], promote the formation of one isomer over another [18], and enhance the activity of some enzymes [19, 20]. Water-in-oil microemulsions are exploited in the formation of ultrafine particles, where the particles size can be manipulated by adjusting the water-to-surfactant mole ratio [21–23]. Microemulsions are thermodynamically stable dispersions of oil and water. The thermodynamic stability arises from the entropy of mixing, provided sufficiently low interfacial tension is granted with the aid of a surfactant [24]. Microemulsions can be of two types, depending on the continuous and the dispersed phases: oil-in-water microemulsion (o/w) or water-in-oil microemulsion (w/o).

A major problem that restricts the industrial application of microemulsions is their low reactant loading [25, 26]. With large reactant concentrations, emulsions may form with bulk aqueous and oil phases, thus changing the reaction rate [25, 27–30]. In addition, emulsions need continuous mixing to maintain their stability. More effective mixing, hence more energy, is required in the absence of less effective surfactant. Selectivity and separation of the product are also of concern.

10.2 Nucleophilic Substitution Reactions

Nucleophilic substitution reactions are the reactions in which a nucleophile, a chemical species willing to share electrons, substitutes a functional group in an organic compound [31, 32]. Nucleophilic substitution reactions often involve an oil-soluble compound and a hydrophilic anion. Depending on the reactants and the solvent, these reactions can follow one of two mechanisms or a combination of both [31–34]. The first-order mechanism, S_N1, is a two-step reaction in which the first and the rate determining step is the formation of a carbocation upon the breakage of the carbon-functional group bond. In the second step, the nucleophile attacks the carbocation forming the product. The second-order mechanism, S_N2, is a one-step reaction in which the nucleophile attacks the polar bond between the carbon atom and the functional group from the side opposite to the functional group. A new bond between the nucleophile and the carbon atom forms, while the bond with the functional group breaks. The reaction rate for this mechanism depends on the concentrations of both reactants.

When cationic surfactants were employed to carry out nucleophilic substitution reactions, side products were formed as a result of the reaction between the surfactant counterion and the organic substrate [26]. Another disadvantage of cationic surfactants is that many of them are toxic [35]. Cationic surfactants, however, are the best choice for nucleophilic substitution reactions because they attract the

reacting nucleophile to the interface by electrostatic forces [36]. Some of the nonionic surfactants, on the other hand, are biodegradable, nontoxic, and easily separable [26, 29, 30]. To overcome the disadvantages of smaller interaction between the nucleophile and the nonionic microemulsion surface, micellar phase transfer catalysis was developed [25, 26, 28]. A phase transfer catalyst forms a complex with the reacting anion. This complex is more soluble in the oil core of the o/w microemulsion, and hence the reaction takes place in the organic core as well as at the interface. This technique improved the performance of nonionic and anionic surfactants, but not the performance of a cationic surfactant. Even with this technique, the rate of reaction was slower than that obtained with cationic surfactants [26].

10.3 Modeling Reactions in Microemulsions

The first kinetic model to describe reactions in micelles was proposed by Menger and Portnoy [37]. They treated micelles as enzymes, and the catalytic effect was attributed to changes in the activation energy of the reaction when carried out in micelles. The enzyme model failed to describe the effect on the reaction rate of increasing the surfactant concentration and the concentration of nonreacting salts. Berezin et al. [38] modeled reactions between organic compounds in a micellar system using the *Pseudophase Separation* (PS) model in which the micellar system consists of micellar and aqueous pseudophases separated by an interfacial region, the Stern layer. The Stern layer extends from the oil core to the shear surface containing the surfactant head groups and the counterions associated with the surfactant. For ionic or polar reactants, the interfacial region represents the micellar pseudophase. The rate of the reaction in the pseudophases is dictated by the reactant concentrations in each phase, which are determined by partition coefficients that are specific for each reactant. The results from the PS model showed that the reaction rate constants in micelles were equal to or less than the ones obtained in water, suggesting that micelles enhance reactions by concentrating reactants at the reaction site and not by affecting the activation energy of the reaction [15, 38–40].

Romsted [40] modified the PS model of Berezin et al. [38] to describe reactions between organic compounds and hydrophilic anions. Partition coefficients were used to calculate the concentration of the organic reactants in the micellar and the aqueous pseudophases, and the *Pseudophase Ion Exchange* (PIE) model was used to describe the distribution of the anions. Small amounts of the reactants were used to avoid changes in the critical micelle concentration and in the properties of the micellar phase. The ion exchange constant governs the concentration of the ions at the interface. The relative concentrations of the ions at the interface are controlled by their mole ratio in the aqueous phase and their specific interactions, which generally follow the Hofmeister series [41, 42]: large weakly hydrated, polarizable anions

displace strongly hydrated anions. Although the surface of the micelles is charged due to the dissociation of the ionic surfactant, coulombic interactions were neglected.

In some of the previous work, the degree of counterion association, β, that is, the fraction of the surfactant molecules at the interface that are not dissociated, was assumed to be constant, independent of the type of ions present at the interface [36, 40, 43]. The volume of the micellar pseudophase and the interfacial region were taken to be directly proportional to the number of surfactant molecules forming the micelles. This model described the maximum observed in the overall rate of bimolecular reactions as a function of surfactant concentration. It also accounted for the effect of salt added to the reaction mixture at low reactant and salt concentrations. The PIE model, however, failed to account for the increase in the reaction rate upon the addition of salt for very hydrophilic anions, such as OH^- and F^- [43, 44]. The assumption of constant degree of surfactant counterion association is not valid in this case. Two different approaches were followed to address this problem. In one approach, β was measured conductimetrically or electrochemically as a function of the surfactant concentration, and this variation was included in the model [45–47]. In the second approach, β was assumed to be constant and Langmuir isotherms were used to account for extra ions adsorbed on the surface of the micelle [36, 48–50].

An alternative description of the interaction between the charged micellar surface and the ions in the solution used the Poisson–Boltzmann equation (PBE) adjusted to account for the specific interaction [39, 51, 52]. In this model, the micellar system is divided into cells, each containing a surfactant aggregate surrounded by aqueous solution. The aggregates are assumed to have uniform distribution throughout the micellar system. Electroneutrality is assumed to be valid in each cell and the PBE is solved numerically in a coordinate system that corresponds to the shape of the surfactant aggregate. The solution of the PBE gives the distribution of the ions at the interface and in the diffuse electrical double layer, the Gouy–Chapman layer, created by thermal motion. Unlike the PIE model, the PBE model accounts for the size and shape of the micelles, the aggregation number, and the coulombic and the specific interactions. The PBE model succeeded where PIE model failed due to the assumption of constant β [51].

10.4 Nucleophilic Sulfonation of Organic Halides

Nucleophilic sulfonation of an organic halide involves the formation of C–S covalent bond upon substitution of the halide functional group with the sulfite anion, SO_3^{2-} [32, 53]. The halide is called the leaving group and the sulfite anion is called the nucleophile [31–34]. This work considers the nucleophilic sulfonation of decyl halides to produce sodium decyl sulfonate.

Industrial-scale production of primary alkane sulfonates uses sulfur trioxide as a reactant and yields alkene sulfonic acid as an intermediate that further reacts to give the final product [53, 54]. Alkane sulfonates are used in heavy- and light-duty powder detergents, all-purpose hard liquid cleaners, and industrial and domestic cleaners [54].

Gutfelt et al. [27], Holmberg et al. [28], and Oh et al. [29, 30] carried out the nucleophilic sulfonation, S_N2 reaction, of decyl bromide in w/o microemulsions formed with the nonionic surfactant penta(ethyl glycol)monododecyl ether with decyl bromide solubilized in dodecane forming the oil phase. The water phase consisted of an aqueous solution of sodium sulfite. The molar rate of product formation was governed by the type of microemulsion that, in turn, was affected by the reactant and the surfactant concentrations. The highest rate, approximately 5.5 mM/h, was obtained in w/o microemulsion and isotropic channels at relatively small concentration of the reactants, about 40 mM equimolar reaction mixture. Gutfelt et al. [27] and Holmberg et al. [28] studied the effect of adding a small amount of cationic surfactant to the microemulsion. The rate increased or decreased depending on the surfactant counterion. Bromide as a counterion decreased the rate, since it tends to remain at the interface, while acetate and chloride increased the rate. However, the possibility of side product formation upon reaction between the counterion of the cationic surfactant and the decyl bromide was not considered. Gutfelt et al. [27] compared the microemulsion route and the phase transfer route and found that phase transfer catalysis was much less efficient due to the formation of a strong ion pair between the decyl sulfonate product and the phase transfer catalyst.

10.5 Nucleophilic Sulfonation of Decyl Halides

The overall reaction to form sodium decyl sulfonate from decyl halides is

$$C_{10}H_{21}X + Na_2SO_3 \rightarrow C_{10}H_{21}SO_3{}^-Na^+ + NaX \qquad \text{(R10.1)}$$

where $C_{10}H_{21}X$ refers to any decyl halide reactant. For chloride as the surfactant counterion, and either decyl iodide or decyl bromide as reactant, decyl chloride formed according to

$$C_{10}H_{21}X + Cl^- \rightarrow C_{10}H_{21}Cl + X^- \qquad \text{(R10.2)}$$

Sodium decyl sulfonate was then formed through reaction (R10.1) by the further reaction of decyl chloride. The percent conversions to decyl chloride intermediate and sodium decyl sulfonate were calculated from

$$\%\ C_{10}H_{21}Cl = \frac{[C_{10}H_{21}Cl]}{[C_{10}H_{21}X]^{STD}} \times 100 \tag{10.1}$$

$$\%\ C_{10}H_{21}SO_3^-\ Na^+ = \frac{[C_{10}H_{21}X]^{STD} - [C_{10}H_{21}X] - [C_{10}H_{21}Cl]}{[C_{10}H_{21}X]^{STD}} \times 100 \tag{10.2}$$

where [i] is the total concentration (mM) of species i in the sample and the superscript STD refers to the concentration in the calibration solution. The decyl halide was always the limiting reactant in this work.

Initial attempts to carryout sulfonation of decyl iodide in dodecyltrimethylammonium chloride microemulsions were not successful. In this system, mixed surfactants formed and resulted in the formation of a highly viscous solution. The formation of the highly viscous solution limited mass transfer of reactants to the reaction site and thus resulted in low conversion. The formation of mixed surfactants can be minimized by increasing the steric hindrance of the alkyl groups of the cationic surfactant [55, 56]. Therefore, the two-tailed dioctyldimethylammonium halide surfactant was used.

10.5.1 Effect of Stirring and Preconditioning

To investigate the roles of mass transfer of the reactants to the interfacial region and equilibrium between the ions at the interface in the two-tailed surfactant system, the effects of stirring and preconditioning were studied. The concentrations of the components added to the reaction mixture were $[R_2(Me)_2N^+Cl^-]^a$ = 200 mM, $[C_{10}H_{21}Br]^a$ = 57 mM, with initial mole ratio $Na_2SO_3/C_{10}H_{21}Br$ = 6.0. It should be noted that at these conditions, a single phase was maintained for most of the reaction time. The results of two experiments, one stirred and the other unstirred, are shown in Figure 10.1. The differences in the conversion to $C_{10}H_{21}SO_3^-Na^+$ and $C_{10}H_{21}Cl$ between the stirred and unstirred runs fall within the 95% confidence interval shown in the figure. Mass transfer of the reactants occurs sufficiently rapidly so that the reaction rate is controlled by the reaction kinetics. This conclusion is supported by other studies [39, 40, 51].

The preconditioning experiment was also performed under the aforementioned conditions. In this experiment, $R_2(Me)_2N^+Cl^-$ and Na_2SO_3 were mixed in distilled water for 24 h prior to adding the decyl bromide to allow for the replacement of the surfactant counterion. For the run with no preconditioning $R_2(Me)_2N^+Cl^-$, Na_2SO_3, and $C_{10}H_{21}Br$ were added at almost the same time. The results, plotted in Figure 10.2, are similar and show that ion exchange equilibrium between the reacting nucleophile, SO_3^{2-}, and the surfactant counterions, $Cl^-$and Br^-, is attained rapidly.

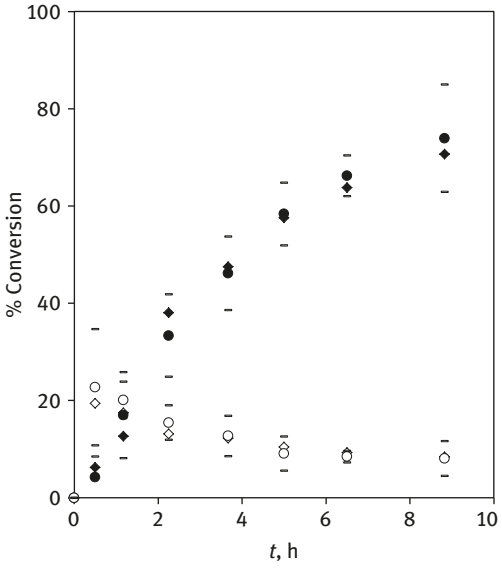

Figure 10.1: Effect of stirring on the conversion to sodium decyl sulfonate (solid symbols) and decyl chloride (open symbols). $[R_2(Me)_2N^+Cl^-]^a$ = 200 mM, $[C_{10}H_{21}Br]^a$ = 57 mM, mole ratio $Na_2SO_3/C_{10}H_{21}Br$ = 6.0. Stirring (◆,◇). No stirring (●,○).

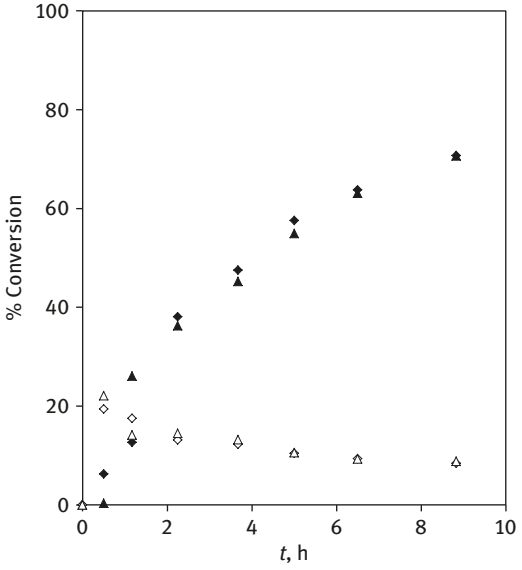

Figure 10.2: Effect of preconditioning on the conversion to sodium decyl sulfonate (solid symbols) and decyl chloride (open symbols). $[R_2(Me)_2N^+Cl^-]^a$ = 200 mM, $[C_{10}H_{21}Br]^a$ = 57 mM, mole ratio $Na_2SO_3/C_{10}H_{21}Br$ = 6.0. Preconditioning (▲,△). No preconditioning (◆,◇).

10.5.2 Effect of $R_2(Me)_2N^+Cl^-$ Concentration

The conversion to the intermediate and the final products, as calculated from eqs. (10.1) and (10.2), for $R_2(Me)_2N^+Cl^-$ concentrations from 50 to 800 mM were obtained. The concentration of $C_{10}H_{21}Br$ added to the reaction mixture was 57 mM and initial

mole ratio $Na_2SO_3/C_{10}H_{21}Br$ was 9.0. The conversion to sodium decyl sulfonate after 8.83 h of the reaction is plotted against the concentration of $R_2(Me)_2N^+Cl^-$ added to the reaction mixture as shown in Figure 10.3. The conversion versus time and the maximum conversion at each concentration could be described using a reaction model detailed later. The maximum conversion was inspired from experiments pertaining to varying $C_{10}H_{21}Br$ concentration, as explained below.

Figure 10.3 shows that without surfactant, $[R_2(Me)_2N^+Cl^-]^a = 0$, the conversion was almost zero because the solubility of $C_{10}H_{21}Br$ in water is low, 0.17 ± 0.04 mM. This indicates that the reaction takes place mainly at the interface between the phases in the microemulsion and/or emulsion. It should be noted that at the concentrations used in these experiments, emulsion was formed. Consistent mixing had to be ensured to obtain reproducible results.

The conversion to $C_{10}H_{21}SO_3^-Na^+$ and $C_{10}H_{21}Cl$ increased with increasing $R_2(Me)_2N^+Cl^-$ concentration, with the conversion to the final product reaching a broad maximum at $R_2(Me)_2N^+Cl^-$ concentrations between 200 and 400 mM. This behavior is typical of second-order reactions carried out in micelles [39, 40] and it can be explained as follows. As the $R_2(Me)_2N^+Cl^-$ concentration increased, more of the reactants, $C_{10}H_{21}Br$ and SO_3^{2-}, were bound to the interface, thus increasing the conversion to the final product. The conversion to $C_{10}H_{21}Cl$ also increased, because there was more Cl^- at the interface. Since the intermediate, $C_{10}H_{21}Cl$, reacted more slowly than the original reactant, $C_{10}H_{21}Br$, the conversion to the final product decreased. Another factor could

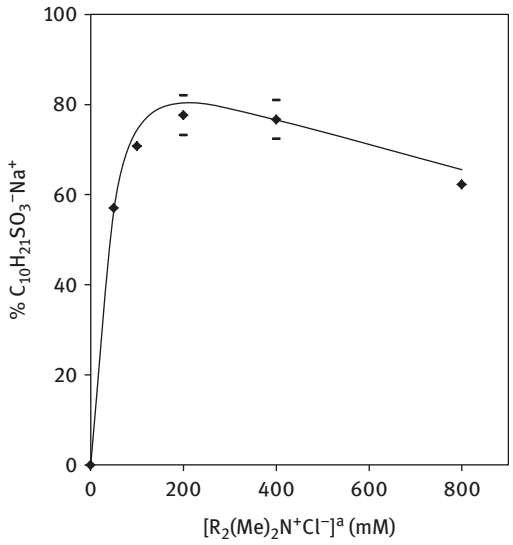

Figure 10.3: The conversion to sodium decyl sulfonate versus $[R_2(Me)_2N^+Cl^-]^a$ after 8.83 h. $[C_{10}H_{21}Br]^a$ = 57 mM; mole ratio $Na_2SO_3/C_{10}H_{21}Br$ = 9.0. Points, experiments; curve, model.

be the dilution caused by the increase in the volume of the interfacial region with increasing $R_2(Me)_2N^+Cl^-$ concentration [40].

10.5.3 Effect of $R_2(Me)_2N^+Br^-$ Concentration

To eliminate the formation of the intermediate and to examine the effect of the ion exchange between the reacting nucleophile and the surfactant counterion, $R_2(Me)_2N^+Br^-$ was used to form the emulsion with decyl bromide as the reactant. The concentration of $R_2(Me)_2N^+Br^-$ added to the reaction mixture, $[R_2(Me)_2N^+Br^-]^a$, was varied from 50 to 800 mM with the concentration of the decyl bromide added to the reaction mixture, $[C_{10}H_{21}Br]^a$, of 57 mM and an initial mole ratio $Na_2SO_3/C_{10}H_{21}Br$ of 6.0. The time variation of the conversion of decyl bromide to $C_{10}H_{21}SO_3^-Na^+$ and the maximum conversion were also captured by the model. Figure 10.4 shows the conversion to $C_{10}H_{21}SO_3^-Na^+$ after 8.83 h of reaction as a function of $[R_2(Me)_2N^+Br^-]^a$.

Figure 10.4 shows an increase in the conversion to $C_{10}H_{21}SO_3^-Na^+$ with increasing $R_2(Me)_2N^+Br^-$ concentration as larger amounts of reactants are bound to the interface. At a fixed time, the conversion decreased when the $R_2(Me)_2N^+Br^-$ concentration was increased to 800 mM, as shown in Figure 10.4. This trend is attributed to two factors: (1) the increase in the ratio of the nonreacting anion, Br^-, to the reacting nucleophile, SO_3^{2-}, at the interface and (2) the dilution effect at the interface due to the increase in the volume of the interfacial region [39, 40].

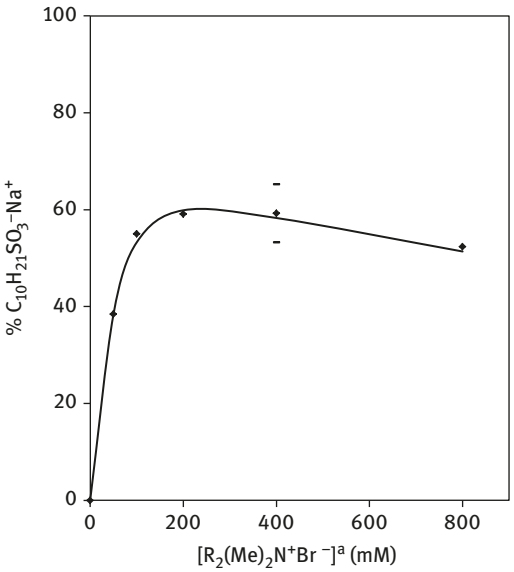

Figure 10.4: The conversion to sodium decyl sulfonate versus $[R_2(Me)_2N^+Cl^-]^a$ after 8.83 h. $[C_{10}H_{21}Br]^a$ = 57 mM; mole ratio $Na_2SO_3/C_{10}H_{21}Br$= 9.0. Points, experiments; curve, model.

Comparison of these results with those for the reaction of $C_{10}H_{21}Br$ in $R_2(Me)_2N^+Cl^-$ shows that at a fixed time the $R_2(Me)_2N^+Cl^-$ system gave higher conversion to $C_{10}H_{21}SO_3^-Na^+$, even though the $C_{10}H_{21}Cl$ intermediate, which reacted more slowly to the final product than $C_{10}H_{21}Br$, formed in $R_2(Me)_2N^+Cl^-$ system. This can be explained by the fact that SO_3^{2-} could replace Cl^- to a larger extent than Br^- following the Hofmeister series [41, 42], yielding higher SO_3^{2-} concentration at the $R_2(Me)_2N^+Cl^-$ microemulsion or emulsion interface.

10.5.4 Effect of Decyl Bromide Concentration

The objective of this experiment was to determine the effect of loading the system with the reactants. The $C_{10}H_{21}Br$ concentration was increased from 57 to 189 mM at a $R_2(Me)_2N^+Cl^-$ concentration of 400 mM and an initial mole ratio $Na_2SO_3/C_{10}H_{21}Br$ of 9.0. The results are shown in Figure 10.5(a)–(c).

The molar rate of formation of the final product increased upon increasing the amounts of reactants added, due to the increase in the amounts of reactants bound to the interface, while the conversion to sodium decyl sulfonate dropped. This drop in the conversion suggests that some of the $C_{10}H_{21}Br$ was unavailable for the reaction at the interface. Since the solubility of $C_{10}H_{21}Br$ in water is low, it seems likely that some decyl bromide remains in the oil core of the microemulsion or the emulsion. This amount will not react at the interface because the product, $C_{10}H_{21}SO_3^-Na^+$, is a surfactant that remains at the interface, thus blocking further $C_{10}H_{21}Br$ from approaching it to react. It may also be that the increase in the interfacial concentration of the product, which is an anionic surfactant, repels the reacting nucleophile from approaching the interface [26]. Another reason might be the formation of mixed surfactants of the cationic and the anionic surfactants. The neutralization of the cationic surfactant head groups reduces the attraction of the reacting nucleophile to the interface and thus lowers the conversion. The concentration of mixed surfactants was, however, limited by the steric hindrance of the octylammonium groups of the cationic surfactant.

10.5.5 Effect of the Initial Mole Ratio of Sodium Sulfite to Decyl Bromide

The effect of the initial mole ratio $Na_2SO_3/C_{10}H_{21}Br$ on the conversion to sodium decyl sulfonate and decyl chloride is shown in Figure 10.6(a)–(d). The concentration of $R_2(Me)_2N^+Cl^-$ added to the reaction mixture was 200 mM and that of $C_{10}H_{21}Br$ was 57 mM.

The conversion to $C_{10}H_{21}SO_3^-Na^+$ increased and the conversion to $C_{10}H_{21}Cl$ decreased with increasing mole ratio, with the mole ratio having less significance

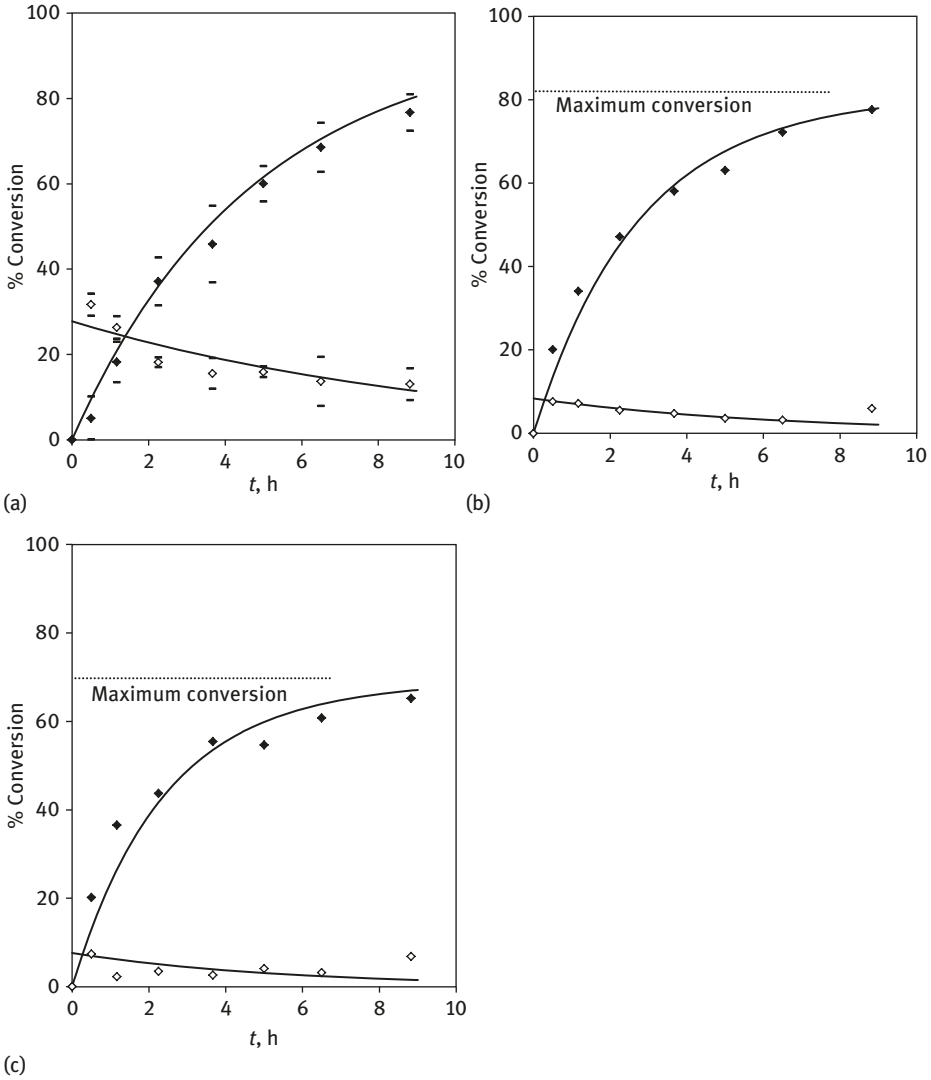

Figure 10.5: Effect of $[C_{10}H_{21}Br]^a$ on the conversion to sodium decyl sulfonate (solid symbols) and decyl chloride (open symbols). $[R_2(Me)_2N^+Cl^-]^a$ = 400 mM, mole ratio $Na_2SO_3/C_{10}H_{21}Br$ = 9.0. $[C_{10}H_{21}Br]^a$ = (a) 57 mM; (b) 142 mM; and (c) 189 mM. Points, experiments; curves, model.

at higher values. The increase in the conversion to $C_{10}H_{21}SO_3^-Na^+$ and the decrease in the conversion to $C_{10}H_{21}Cl$ suggest an ion exchange step between the reacting nucelophile and Cl^-. Increasing the bulk concentration of Na_2SO_3 increased the interfacial concentration of SO_3^{2-} at the expense of the interfacial concentration of Cl^-. The conversion to $C_{10}H_{21}SO_3^-Na^+$ was not directly proportional to the initial mole ratio since the reaction takes place at the interface and

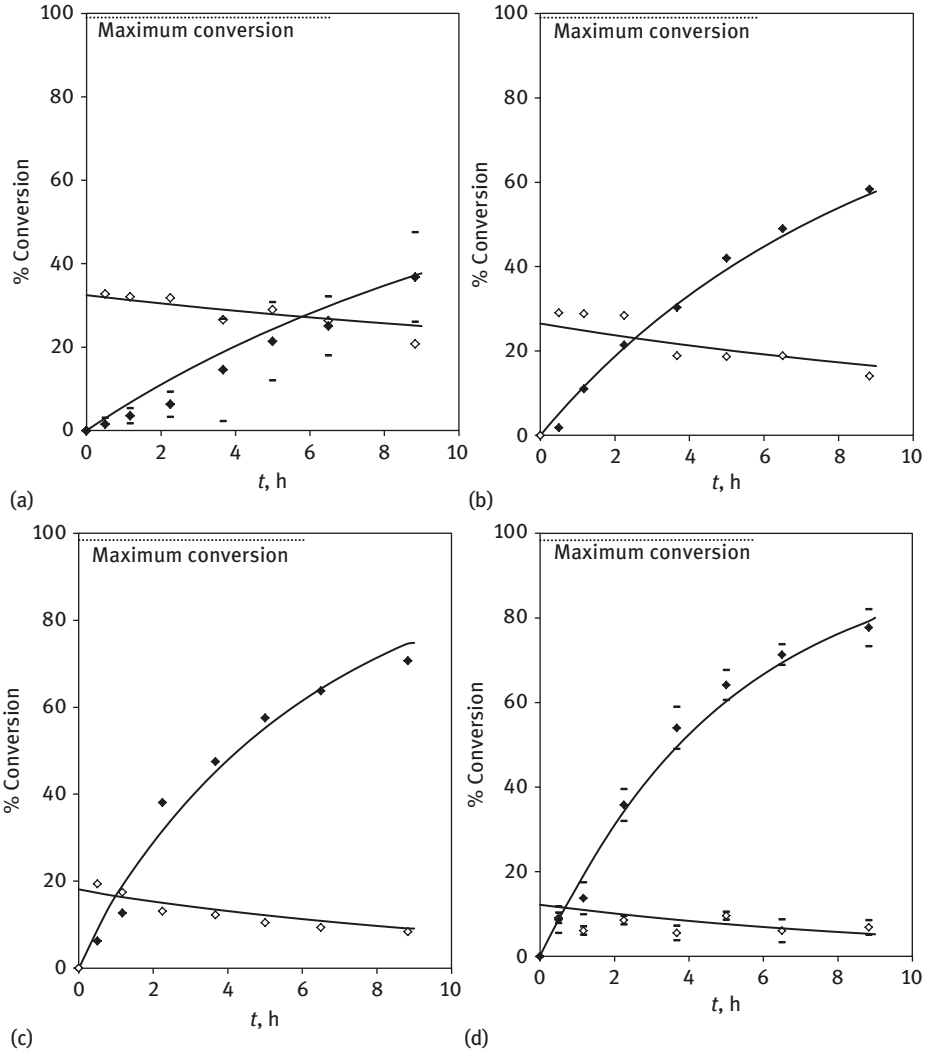

Figure 10.6: Effect of mole ratio $Na_2SO_3/C_{10}H_{21}Br$ on the conversion to sodium decyl sulfonate (solid symbols) and decyl chloride (open symbols). $[R_2(Me)_2N^+Cl^-]^a$ = 200 mM, $[C_{10}H_{21}Br]^a$ = 57 mM. Mole ratio $Na_2SO_3/C_{10}H_{21}Br$ = (a) 1.0; (b) 3.0; (c) 6.0; and (d) 9.0. Points, experiments; curves and maximum conversion, model.

the interfacial concentration of the reacting nucleophile is governed by the ion exchange step.

Despite the fact that phase separation occurred at different times depending on the mole ratio, the general trend of the conversion was not affected. This indicates that mass transfer of the reactants was not limited by phase separation for the degree of mixing provided.

10.5.6 Different Decyl Halides as Reactants

The reactivity of decyl halides, $C_{10}H_{21}X$, in nucleophilic substitution reactions of the second order, S_N2, increases from up to down in the periodic table. Iodide is a weaker base and thus it shares its electron with the carbon atom less than chloride [31, 33, 34]. To test the proposed mechanism of the kinetically controlled rate of product formation, the experimental conditions were $[R_2(Me)_2N^+Cl^-]^a$ = 400 mM, $[C_{10}H_{21}X]^a$ = 95 mM, and initial mole ratio $Na_2SO_3/C_{10}H_{21}X$ = 9.0.

Figure 10.7 shows the conversion to $C_{10}H_{21}SO_3^-Na^+$ and $C_{10}H_{21}Cl$ versus time for different decyl halides. With decyl chloride as reactant, no intermediate was formed. The comparison of the conversions to $C_{10}H_{21}SO_3^-Na^+$ and $C_{10}H_{21}Cl$ shows that decyl iodide reacted most rapidly, followed by decyl bromide and then decyl chloride. This suggests that the nucleophilic reaction was kinetically controlled during the time considered and that mass transfer of SO_3^{2-} or the decyl halide did not limit the rate of reaction.

The conversion to decyl chloride shows that it forms very rapidly and that its rate of consumption depends on the decyl halide reactant. More decyl chloride was formed and it was consumed more rapidly when decyl iodide was the reactant than when decyl bromide was used. This difference may be due to the presence of I^- at the interface since iodide is a catalyst for S_N2 reactions [29].

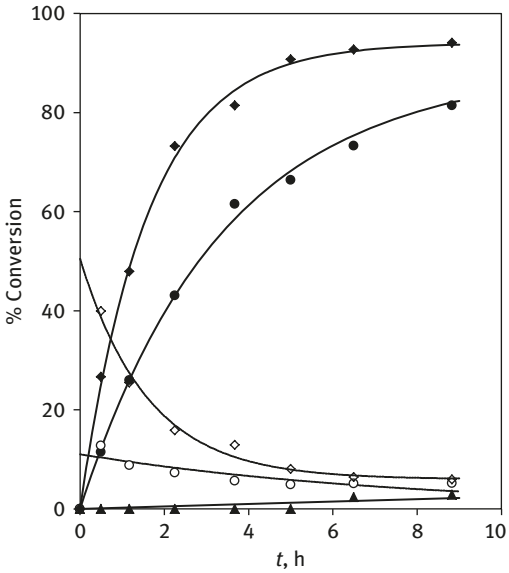

Figure 10.7: Effect of different decyl halide, $C_{10}H_{21}X$, reactants on the conversion to sodium decyl sulfonate (solid symbols) and decyl chloride (open symbols). $[R_2(Me)_2N^+Cl^-]^a$ = 400 mM, $[C_{10}H_{21}X]^a$ = 95 mM, initial mole ratio $Na_2SO_3/C_{10}H_{21}X$ = 9.0. $C_{10}H_{21}Cl$ (▲), $C_{10}H_{21}Br$ (●,○), $C_{10}H_{21}I$ (◆,◇). Points, experiments; curves, model.

10.5.7 Effect of Decyl Iodide Concentration

The nucleophilic substitution reaction was carried out with decyl iodide as the reactant. The concentration of decyl iodide was increased from 57 to 189 mM at a $R_2(Me)_2N^+Cl^-$ concentration of 400 mM and an initial mole ratio $Na_2SO_3/C_{10}H_{21}I$ of 9.0.

Figure 10.8(a)–(c) shows the time variation of the conversions to the final and the intermediate products. The molar rate of the formation of sodium decyl sulfonate increased, but the conversion at a fixed time decreased with increasing $C_{10}H_{21}I$ concentration. The rate increased because larger amounts of reactants were bound to the interface. The decreased final conversion, as shown in Figure 10.8(c), suggests that some $C_{10}H_{21}I$ and $C_{10}H_{21}Cl$ were unavailable for reaction at the interface. Since the solubility of these reagents in water is low (0.16 ± 0.04 mM for $C_{10}H_{21}I$ and 0.17 ± 0.05 mM for $C_{10}H_{21}Cl$), the amounts unavailable remain in the oil core of the emulsion. The presence at the interface of the product anionic surfactant ($C_{10}H_{21}SO_3^-Na^+$) blocks the interfacial region by creating a mass transfer barrier, by increasing the electrostatic repulsion of SO_3^{2-} from the interface [26], and by neutralizing the polar heads of the cationic surfactant [54, 57–59].

The behavior was similar to that of decyl bromide as the reactant, but with higher reaction rate and higher conversion. Higher reaction rate is due to the higher reactivity of decyl iodide, and higher conversion is due to the fact that decyl iodide has a greater tendency to remain at the interface because the polarity of the C–I bond is higher than that of the C–Br bond.

10.5.8 Use of High Concentrations of Surfactant and Reactants

To test the assumption that some $C_{10}H_{21}I$ and $C_{10}H_{21}Cl$ was unavailable for reaction, an experiment was performed with $[R_2(Me)_2N^+Cl^-]^a$ = $[C_{10}H_{21}I]^a$ = $[Na_2SO_3]^a$ = 800 mM. The results, shown in Figure 10.9, indicate that the conversions to $C_{10}H_{21}SO_3^-Na^+$ and $C_{10}H_{21}Cl$ reach plateau of about 37% and 20%, respectively. Thus, only 55% of the $C_{10}H_{21}I$ was available for the reaction and 46% of this amount reacted to form the $C_{10}H_{21}Cl$ intermediate. Only 40% of $C_{10}H_{21}Cl$ formed reacted to the final product. According to the hypothesis, the remaining 45% $C_{10}H_{21}I$ and 60% $C_{10}H_{21}Cl$ was trapped in the oil core (emulsified droplets) of the emulsion.

10.6 Summary of Experimental Observations

The single-tailed cationic surfactant dodecyltrimethylammonium chloride (o/w) microemulsion system was not suitable to prepare the anionic surfactant sodium decyl

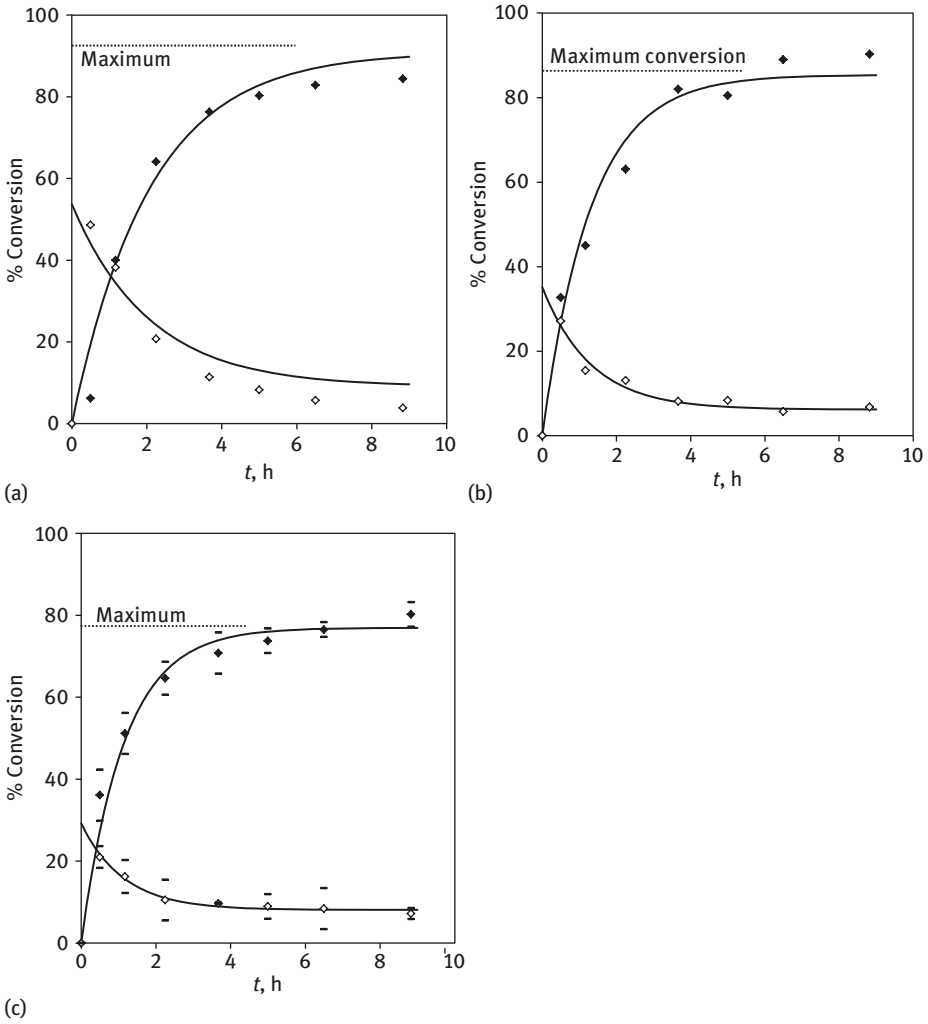

Figure 10.8: Effect of $[C_{10}H_{21}I]^a$ on the conversion to sodium decyl sulfonate (solid symbols) and decyl chloride (open symbols). $[R_2(Me)_2N^+Cl^-]^a$ = 400 mM, initial mole ratio $Na_2SO_3/C_{10}H_{21}I$ = 9.0: $[C_{10}H_{21}I]^a$ = (a) 57 mM; (b) 142 mM; and (c) 189 mM. Points, experiments; curves and maximum conversion, model.

sulfonate. Mixed surfactants of the cationic and the anionic surfactants formed and resulted in the formation of a highly viscous solution, which limited mass transfer of the reactants to the reaction site. In the two-tailed cationic surfactants system, the formation of mixed surfactants was not significant due to the steric hindrance of the alkylammonium groups. Microemulsions and emulsions formed with the two-tailed cationic surfactant dioctyldimethylammonium chloride, $R_2(Me)_2N^+Cl^-$, or bromide,

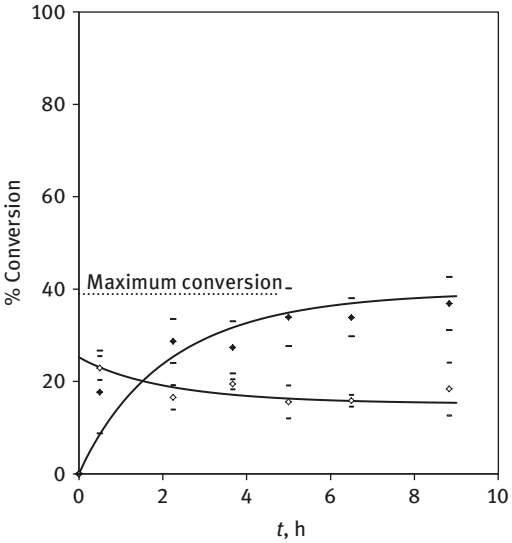

Figure 10.9: Effect of high concentrations of surfactant and reactants on the conversion to sodium decyl sulfonate (solid symbols) and decyl chloride (open symbols). $[R_2(Me)_2N^+Cl^-]^a = [C_{10}H_{21}I]^a = 800$ mM, initial mole ratio $Na_2SO_3/C_{10}H_{21}X = 1.0$. Points, experiments; curves and maximum conversion, model.

$R_2(Me)_2N^+Br^-$, were used to prepare sodium decyl sulfonate with high reactant loading. The effects of stirring, preconditioning, surfactant counterion, and surfactant and reactant concentrations were investigated. Stirring and preconditioning did not affect the conversion, suggesting that, in spite of phase separation, mass transfer of reactants to the interfacial region did not limit the reaction. Chloride as the surfactant counterion gave more conversion than bromide, since it is replaced by SO_3^{2-} to a larger extent than bromide. The product of the reaction between the surfactant counterion and the decyl halides, decyl chloride, was an intermediate rather than a side product. At a fixed time, maximum conversion was obtained at a concentration of the surfactant that is sufficient to bind all the organic substrate to the interface. Increasing the concentration of the reacting halide in the reaction mixture increased the molar rate of product formation and decreased the conversion. The highest reaction rate and 100% conversion can be obtained by finding the optimum concentration of $R_2(Me)_2N^+Cl^-$ in a reaction mixture containing sodium sulfite at the solubility limit and decyl iodide at the corresponding mole ratio. In comparison with previous studies [25, 27–30], concentrations of about 20 times higher and rates of about 18 times faster were obtained. A clearer description about the reaction steps was provided by accounting for the intermediate formation.

10.7 Modeling

This section includes the proposed reaction mechanism, the model assumptions and derivation, and the performance of the model in describing the nucleophilic sulfonation

of the decyl halides in the o/w microemulsion and emulsion. Preliminary modeling attempts showed that apparent second-order rate constants and total concentrations of Na_2SO_3 and decyl halide in the reaction mixture without considering ion exchange with the surfactant counterion failed to account for the effect of the initial mole ratio of reactants. The approach based on the solution of PBE was not pursued since it requires knowledge of the shape and size of aggregates [52, 60, 61]. For the high surfactant and reactant concentrations considered here, establishing the characteristics of the microemulsions and the emulsions is almost impossible because they change with time as the reaction proceeds. The PIE model does not require a description of the shape, size, and aggregation number of micelles; thus, it is potentially applicable to reactions in emulsions [51, 62]. However, the existing PIE models have failed to describe the kinetics of reactions involving more than two ions exchanging at the interface [44]. The PS model is used in this work in combination with the PIE model to describe the distribution of the anions between the bulk aqueous phase and the interfacial region with an assumption to account for more than two ions exchanging at the interface.

Romsted [40] used partition coefficients to calculate the concentration of the oil-soluble reactant in the oil and the aqueous pseudophases, and the PIE model to describe the distribution of ions between the phases. Da Rocha Pereira et al. [63] and Minero et al. [64] employed a three-pseudophase model consisting of water, interface, and oil to account for reactions carried out in microemulsions. Partition coefficients were used to calculate the reactant concentrations in each phase. Such partition coefficients are irrelevant to this work, since the solubility of decyl halides in water is low, the nucleophile is insoluble in the oil phase, and there is no reaction in the absence of the cationic surfactants. In light of the work of Menger et al. [65], it is unlikely that the cationic surfactant increases the solubility of the reacting anion in the oil phase by acting as a phase transfer catalyst. Hence, in this work, the interfacial region is assumed to be the main reaction site [29].

10.7.1 Proposed Reaction Mechanism

When decyl iodide was the reactant, less than 2.5% of the original Na_2SO_3 added oxidized to Na_2SO_4 after 6 h, and when decyl bromide was the reactant, only 1.0% oxidized. Thus, the oxidation reaction was not significant and can be neglected.

The mechanism is written for the reaction of $C_{10}H_{21}I$ in $R_2(Me)_2N^+Cl^-$ microemulsion or emulsion, where $C_{10}H_{21}Cl$ is the intermediate form. The reaction of $C_{10}H_{21}Br$ in $R_2(Me)_2N^+Cl^-$ microemulsion or emulsion follows a similar mechanism. For the reactions of $C_{10}H_{21}Br$ in $R_2(Me)_2N^+Br^-$ and $C_{10}H_{21}Cl$ in $R_2(Me)_2N^+Cl^-$, no intermediate forms and the ion exchange involves only two anions: the reacting nucleophile and the surfactant counterion, Br^- or Cl^-.

The experimental results presented earlier suggest the following sequence of reactions.

1. The surfactant counterion, Cl^-, reacts with some of the decyl iodide at the interface to form decyl chloride and some iodide replaces chloride as the surfactant counterion:

$$R_2(Me)_2N^+Cl^- + C_{10}H_{21}I \rightarrow C_{10}H_{21}Cl + R_2(Me)_2N^+I^- \quad \text{(R10.3)}$$

2. Sulfite anion, SO_3^{2-}, the predominant form of sulfite in the bulk aqueous phase at the solution pH of around 10, exchanges with the surfactant counterions forming the anionic complex $R_2(Me)_2N^+SO_3^{2-}$. This complex interacts immediately with Na^+ from the bulk aqueous phase. For simplicity, the overall reaction is written as sodium sulfite anion from the bulk aqueous phase exchanging with the surfactant counterions, Cl^- and I^-, as follows:

$$R_2(Me)_2N^+Cl^-/I^- + NaSO_3^- \overset{K}{\leftrightarrow} R_2(Me)_2N^+NaSO_3^- + Cl^-/I^- \quad \text{(R10.4)}$$

3. Sulfite as the surfactant counterion reacts with decyl iodide and decyl chloride to form $C_{10}H_{21}SO_3^-$, which attracts Na^+ at the interface forming the final product. For simplicity, the reaction is written as sodium sulfite anion reacting with decyl iodide and decyl chloride according to the following reaction:

$$R_2(Me)_2N^+NaSO_3^- + C_{10}H_{21}I \overset{k_1}{\rightarrow} C_{10}H_{21}SO_3^-Na^+ + R_2(Me)_2N^+I^- \quad \text{(R10.5)}$$

$$R_2(Me)_2N^+NaSO_3^- + C_{10}H_{21}Cl \overset{k_2}{\rightarrow} C_{10}H_{21}SO_3^-Na^+ + R_2(Me)_2N^+Cl^- \quad \text{(R10.6)}$$

Bruice [34] suggests that a difference of one or less between the pK_a of the conjugate acid of the leaving group and the pK_a of the conjugate acid of the nucleophile would result in a reversible nucleophilic substitution reaction. Hence, it is safe to assume that reactions (R10.3), (R10.5), and (R10.6) are irreversible since the pK_as of the conjugate acids of I^-, Cl^-, and SO_3^{2-} (–10.0, –7.0, and 1.9, respectively); create large enough differences to assume irreversibility [34, 66]. For decyl bromide reactant, the pK_a of the conjugate acid of Br^- (–9.0) also creates large enough differences to assume irreversibility [29]. According to the pK_a criterion, the reaction of intermediate formation (R10.3) has higher possibility of being reversible than the sulfonation reactions (R10.5) and (R10.6).

10.7.2 Model Assumptions

The remaining assumptions in the model are as follows:

1. All surfactant molecules are at the microemulsion or emulsion interface. The critical micelle concentrations (cmc's) of $R_2(Me)_2N^+Cl^-$ and $R_2(Me)_2N^+Br^-$ (2 and 4

mM, respectively) were neglected, since they are low compared with the concentrations employed.

2. The surfactant molecules at the interface are not dissociated, that is, $\beta = 1.0$. This assumption is justified, because phase separation indicates low charge density at the interface. Low charge density at the interface reduces the coulombic interaction; thus, the interfacial concentrations of ions are dictated by specific interactions following the Hofmeister series [41, 42]. This type of interaction favors the use of the PIE model [51].
3. The total volume of the reaction mixture and the volume of the interfacial region are constant throughout the reaction time. At a fixed total reaction mixture volume, the volume of the interfacial region varies only with the concentration of the surfactant added to the reaction mixture ($[R_2(Me)_2N^+Cl^-]^a$ or $[R_2(Me)_2N^+Br^-]^a$) [67, 68] and is independent of the surfactant counterion.
4. The microemulsion droplets or the emulsified droplets have the same size and shape, which does not vary with time as the reaction proceeds [39, 40]. This assumption is essential to obtain equal volumes of the interfacial region for all droplets and combine them in to one volume for the interfacial region.
5. Reaction (R10.3) takes place instantaneously at time zero ($t = 0$). This assumption is based solely on the experimental findings. The largest concentration of the decyl chloride intermediate was always measured shortly after the reaction started. Earlier work by Al-Lohedan et al. [43] showed that nucleophilic substitution reactions involving cationic surfactant counterions occurred readily due to the compartmentalization of the reactants in the micellar phase. At a fixed total reaction mixture volume, the moles of decyl chloride formed at $t = 0$ ($n^{o}_{C_{10}H_{21}Cl}$) vary with the total concentrations of dioctyldimethylammonium chloride ($[R_2(Me)_2N^+Cl^-]^a$), the decyl iodide ($[C_{10}H_{21}I]^a$), and sodium sulfite ($[Na_2SO_3]^a$) added to the reaction mixture.
6. At a fixed total reaction mixture volume, the moles of $C_{10}H_{21}I$ and $C_{10}H_{21}Cl$ trapped in the oil core of the microemulsion or the emulsion, $n^{e}_{C_{10}H_{21}I}$ and $n^{e}_{C_{10}H_{21}Cl}$, vary with $[R_2(Me)_2N^+Cl^-]^a$ and $[C_{10}H_{21}I]^a$. Some of the decyl chloride formed at $t = 0$ migrates to the oil core instantaneously to be replaced by decyl iodide. Decyl iodide has a greater tendency to remain at the interface since the polarity of the C–I bond is higher than that of the C–Cl bond. For the decyl bromide reactant, $n^{e}_{C_{10}H_{21}Cl}$ was zero. It should be noted that decyl halides partition themselves between the oil core and the interface at $t = 0$ and the amounts consumed in the reactions are not replaced from the oil core since the product surfactant ($C_{10}H_{21}SO_3^-Na^+$) acts as a mass transfer barrier.
7. The ion exchange reactions, represented by the overall reaction (R10.4), are instantaneous and the transfer of the anions to and from the interfacial region does not limit the reaction rate. The overall ion exchange equilibrium constant, K, is the same for the exchange of I^- and Cl^- in reaction (R10.4). Although, according to the Hofmeister series, Cl^- exchanges more readily than I^- [41, 42], this

simplifying assumption reduces the number of adjustable parameters. Following reaction (R10.4),

$$K_{Cl^-/I^-/NaSO_3^-} = \frac{[R_2(Me)_2N^+NaSO_3^-] \times [Cl^-/I^-]^w}{[R_2(Me)_2N^+Cl^-/I^-] \times [NaSO_3^-]^w} = \frac{n_{R_2(Me)_2N^+NaSO_3^-} \times n^w_{Cl^-/I^-}}{n_{R_2(Me)_2N^+Cl^-/I^-} \times n^w_{NaSO_3^-}} \quad (10.3)$$

where $[R_2(Me)_2N^+i^-]$ is the interfacial concentration of the surfactant counterion (mM), $[i^-]^w$ is the concentration of this ion in the bulk aqueous phase (mM), $n_{R_2(Me)_2N^+i^-}$ is the amount of the surfactant counterion in the interfacial region (mmol), and $n^w_{i^-}$ is the amount of this ion in the bulk aqueous phase (mmol) where i^- stands for Cl^-, I^-, or $NaSO_3^-$. Combining eq. (10.3) with the mass balance when only the reacting salt is added gives

$$K_{Cl^-/I^-/NaSO_3^-} = \frac{y^2}{(n^a_{Na_2SO_3} - y)(n^a_{R_2(Me)_2N^+Cl^-} - y)} \quad (10.4)$$

where $y = n_{R_2(Me)_2N^+NaSO_3^-}$ and $n^a_{Na_2SO_3}$ and $n^a_{R_2(Me)_2N^+Cl^-}$ are the amounts of Na_2SO_3 and $R_2(Me)_2N^+Cl^-$ added to the reaction mixture (mmol), respectively.

8. Reactions (R10.5) and (R10.6) are second order and also the rate determining steps.

10.7.3 Model Derivation

Since the reactions take place only at the interface, the second-order rate equations for reactions (R10.5) and (R10.6) can be written as

$$\frac{dx_1}{dt} = k_1 \frac{n_{R_2(Me)_2N^+NaSO_3^-}}{V^i} \times \frac{n^i_{C_{10}H_{21}I}}{V^i} \quad (10.5)$$

and

$$\frac{dx_2}{dt} = k_2 \frac{n_{R_2(Me)_2N^+NaSO_3^-}}{V^i} \times \frac{n^i_{C_{10}H_{21}Cl}}{V^i} \quad (10.6)$$

where x_1 and x_2 are the interfacial concentrations of $C_{10}H_{21}SO_3^-Na^+$ (mM) produced from reactions (R10.5) and (R10.6), respectively; $n^i_{C_{10}H_{21}I}$ and $n^i_{C_{10}H_{21}Cl}$ are the amounts of decyl iodide and decyl chloride at the interface at any time (mmol), and V^i is the volume of the interfacial region (l). Since the experimental measurements were based on the total volume of the reaction mixture, V^t, eqs. (10.5) and (10.6) are multiplied by V^i/V^t to obtain

$$\frac{dX_1}{dt} = k_1 \frac{n_{R_2(Me)_2N^+ NaSO_3^-}}{V^i} \times \frac{n^i_{C_{10}H_{21}I}}{V^t} \tag{10.7}$$

and

$$\frac{dX_2}{dt} = k_2 \frac{n_{R_2(Me)_2N^+ NaSO_3^-}}{V^i} \times \frac{n^i_{C_{10}H_{21}Cl}}{V^t} \tag{10.8}$$

where X_1 and X_2 are the total concentrations of $C_{10}H_{21}SO_3^-Na^+$ (mM).

When the initial mole ratio of sodium sulfite to decyl halide was 9.0, the pseudo first-order approximation was used. The value of $n_{R_2(Me)_2N^+ NaSO_3^-}$ was taken to be constant at the value obtained from eq. (10.3). Eqs. (10.7) and (10.8) were then integrated to give

$$X_1 = \frac{n^{i,o}_{C_{10}H_{21}I}}{V^t} \left\{1 - \exp\left(\frac{k_1}{V^i} \times n_{R_2(Me)_2N^+ NaSO_3^-} \times t\right)\right\} \tag{10.9}$$

and

$$X_2 = \frac{n^{i,o}_{C_{10}H_{21}Cl}}{V^t} \left\{1 - \exp\left(\frac{k_2}{V^i} \times n_{R_2(Me)_2N^+ NaSO_3^-} \times t\right)\right\} \tag{10.10}$$

where $n^{i,o}_{C_{10}H_{21}I}$ and $n^{i,o}_{C_{10}H_{21}Cl}$ are the amounts of decyl iodide and decyl chloride available for the reaction at the interface at $t = 0$ (mmol), calculated as follows:

$$n^{i,o}_{C_{10}H_{21}I} = n^a_{C_{10}H_{21}I} - n^o_{C_{10}H_{21}Cl} - n^e_{C_{10}H_{21}I} \tag{10.11}$$

$$n^{i,o}_{C_{10}H_{21}Cl} = n^o_{C_{10}H_{21}Cl} - n^e_{C_{10}H_{21}Cl} \tag{10.12}$$

where $n^a_{C_{10}H_{21}I}$ is the amount of $C_{10}H_{21}I$ added to the reaction mixture (mmol), and $n^e_{C_{10}H_{21}I}$ and $n^e_{C_{10}H_{21}Cl}$ are the amounts of $C_{10}H_{21}I$ and $C_{10}H_{21}Cl$ trapped in the oil core of the microemulsion or emulsion at $t = 0$ (mmol). The latter values are zero if there is sufficient surfactant to bind all of the decyl halide to the interface. For decyl bromide reactant, $n^e_{C_{10}H_{21}Cl}$ in eq. (10.12) was zero.

Equs. (10.4) and (10.9)–(10.12) were used to calculate X_1 and X_2 with K, k_1, and k_2 as fitted parameters. For the fixed total reaction mixture volume, the value of V^i was a fitted parameter, which varied only with the concentration of the surfactant added to the reaction mixture; the quantities $n^e_{C_{10}H_{21}I}$ and $n^e_{C_{10}H_{21}Cl}$ from eqs. (10.11) and (10.12) were fitted as functions of $[R_2(Me)_2N^+Cl^-]^a$ and $[C_{10}H_{21}I]^a$; and finally, $n^o_{C_{10}H_{21}Cl}$ was taken as a fitted parameter that varied with $[R_2(Me)_2N^+Cl^-]^a$, $[C_{10}H_{21}I]^a$, and $[Na_2SO_3]^a$. The parameters were fitted using Microsoft Excel Solver to minimize the average of

the sum of the root mean-squared deviations of the conversion to the final and intermediate products between the experimental and the model values.

When the mole ratio of the reactants was less than 9.0, eqs. (10.4), (10.7), (10.8), and (10.11)–(10.15) were solved simultaneously using a fourth-order Runge–Kutta method. The value of $n_{R_2(Me)_2N^+NaSO_3^-}$ was calculated from eq. (10.4), with $n_{Na_2SO_3}$ obtained as a function of time from

$$n_{Na_2SO_3} = n^a_{Na_2SO_3} - (X_1 + X_2) \times V^t \tag{10.13}$$

This quantity was substituted for $n^a_{Na_2SO_3}$ in eq. (10.4), while $n^i_{C_{10}H_{21}I}$ and $n^i_{C_{10}H_{21}Cl}$ in eqs. (10.7) and (10.8) were calculated from

$$n^i_{C_{10}H_{21}I} = n^{i,o}_{C_{10}H_{21}I} - X_1 \times V^t \tag{10.14}$$

$$n^i_{C_{10}H_{21}Cl} = n^{i,o}_{C_{10}H_{21}Cl} - X_2 \times V^t \tag{10.15}$$

The parameters k_1, k_2, V^i, and K were not fitted again, except for $K_{Br^-/NaSO_3^-}$, but were fixed at the values obtained for a mole ratio of 9.0.

The percent conversions to decyl chloride and sodium decyl sulfonate were calculated from

$$\%\, C_{10}H_{21}Cl = \frac{n^o_{C_{10}H_{21}Cl} - X_2 \times V^t}{n^a_{C_{10}H_{21}I}} \times 100 \tag{10.16}$$

and

$$\%\, C_{10}H_{21}SO_3^-Na^+ = \frac{(X_1 + X_2) \times V^t}{n^a_{C_{10}H_{21}I}} \times 100 \tag{10.17}$$

10.7.4 Performance of the Model

The ion exchange constants were different for the different surfactant counterions and the different decyl halide reactants, while the reaction rate constants for the decyl halide reactant and the intermediate were different for the different decyl halide reactants. The values of these parameters are listed in Tables 10.1 and 10.2. For example, for decyl bromide reacting in $R_2(Me)_2N^+Cl^-$ microemulsion or emulsion, the ion exchange constant between $NaSO_3^-$ and Cl^- and Br^-, $K_{Cl^-/Br^-/NaSO_3^-} = 1.0\times10^{-5}$; the decyl bromide sulfonation rate constant $k_{1,C_{10}H_{21}Br} = 2.0\times10^{-2}$ (mM/h); and the decyl chloride sulfonation rate constant with decyl bromide as reactant, $k_{2,C_{10}H_{21}Br} = 9.0\times10^{-3}$ (mM/h).

Table 10.1: Values of the ion exchange constants for the two surfactants and the three decyl halides.

Surfactant	$C_{10}H_{21}Cl$	$C_{10}H_{21}Br$	$C_{10}H_{21}I$
$R_2(Me)_2N^+Cl^-$	1.5×10^{-4}	1.0×10^{-5}	5.8×10^{-6}
$R_2(Me)_2N^+Br^-$	–	3.4×10^{-6}	–

Table 10.2: Values of the reaction rate constants for three decyl halides.

Reaction rate constants*	$C_{10}H_{21}Cl$	$C_{10}H_{21}Br$	$C_{10}H_{21}I$
k_1 (mM/h)	–	2.0×10^{-2}	6.1×10^{-2}
k_2 (mM/h)	7.5×10^{-5}	9.0×10^{-3}	6.1×10^{-2}

*Subscript 1 refers to sulfonation of decyl bromide or decyl iodide; and subscript 2 refers to sulfonation of decyl chloride.

The percentage of decyl chloride intermediate formed at $t = 0$, % $C_{10}H_{21}Cl^o$, and the percentage of decyl halide trapped in the oil core, % $C_{10}H_{21}X^e$, were calculated from the following equations:

$$\% C_{10}H_{21}Cl^o = \frac{n^o_{C_{10}H_{21}Cl}}{n^a_{C_{10}H_{21}X}} \times 100 \tag{10.18}$$

$$\% C_{10}H_{21}X^e = \frac{n^e_{C_{10}H_{21}X}}{n^a_{C_{10}H_{21}X}} \times 100 \tag{10.19}$$

where $n^a_{C_{10}H_{21}X}$ is the amount of decyl halide added to the reaction mixture (mmol). The maximum conversion obtained from the model, computed as (100– $\%C_{10}H_{21}X^e$), is shown in the figures.

10.7.4.1 Effect of $R_2(Me)_2N^+Cl^-$ Concentration

The model fit for experiments on the effect of $R_2(Me)_2N^+Cl^-$ concentration is compared with the experimental data shown in Figure 10.3. In these experiments, the concentration of $R_2(Me)_2N^+Cl^-$ added to the reaction mixture, $[R_2(Me)_2N^+Cl^-]^a$, was varied from 50 to 800 mM at a concentration of $C_{10}H_{21}Br$ added to the reaction mixture, $[C_{10}H_{21}Br]^a$, of 57 mM and an initial mole ratio $Na_2SO_3/C_{10}H_{21}Br$ of 9.0. The model curves were obtained using the values of the parameters listed in Tables 10.1 and 10.2, V^i/V^t values are listed in Table 10.3, and % $C_{10}H_{21}Cl^o$ and % $C_{10}H_{21}Br^e$ are calculated from eqs. (10.18) and (10.19) and are also listed in Table 10.3.

The model fitted well the conversion to the final and the intermediate products for the different concentrations. The model accounted for the maximum conversion

Table 10.3: The values of the ratio of the volume of the interfacial region to the total volume, the percentage of decyl chloride formed at $t = 0$, and the percentage of decyl bromide trapped in the oil core for different $[R_2(Me)_2N^+Cl^-]^a$. $[C_{10}H_{21}Br]^a$ = 57 mM; mole ratio $Na_2SO_3/C_{10}H_{21}Br$ = 9.0.

$[R_2(Me)_2N^+Cl^-]^a$ (mM)	V^i/V^t	% $C_{10}H_{21}Cl^o$	% $C_{10}H_{21}Br^e$
50	0.052	6.9	28.6
100	0.074	11.0	4.6
200	0.092	12.2	1.7
400	0.138	26.6	0
800	0.236	43.1	0

observed in Figure 10.3 between $R_2(Me)_2N^+Cl^-$ concentrations of 200 and 400 mM. As discussed earlier, this optimum is caused by two factors: the dilution effect and the increase in the conversion to $C_{10}H_{21}Cl$ intermediate as the $R_2(Me)_2N^+Cl^-$ concentration increases. Table 10.3 shows that a concentration of $R_2(Me)_2N^+Cl^-$ between 200 and 400 mM was sufficient to bind all of the decyl bromide to the interface, thus yielding the maximum conversion.

Table 10.3 also indicates that the volume of the interfacial region increased roughly linearly with surfactant concentration above 50 mM. In previous studies, where the surfactant and reactant concentrations were kept low to avoid changing the nature of the microemulsion, the volume of the interfacial region was assumed to vary directly with the amount of surfactant forming the micelles [39, 40, 51].

10.7.4.2 Effect of $R_2(Me)2N+Br^-$ Concentration

The model fit for the effect of $R_2(Me)_2N^+Br^-$ concentration is compared with the experimental results shown in Figure 10.4. The concentration of $R_2(Me)_2N^+Br^-$ added to the reaction mixture was varied from 50 to 800 mM, with the concentration of the decyl bromide added to the reaction mixture of 57 mM and an initial mole ratio $Na_2SO_3/C_{10}H_{21}Br$ of 6.0. The values of the parameters used in the model are listed in Tables 10.1, 10.2 and 10.4. The volume of the interfacial region was taken from Table 10.2. The only parameters adjusted in the fit were $K_{Br^-/NaSO_3^-}$ and % $C_{10}H_{21}Br^e$. No intermediate was formed in this case, and the model results were obtained by solving eqs. (10.4), (10.7), (10.11), (10.13), and (10.14) simultaneously, replacing the subscript $C_{10}H_{21}I$ with $C_{10}H_{21}Br$ and neglecting $n^o_{C_{10}H_{21}Cl}$ in eq. (10.11) and X_2 in eq. (10.13).

There is a good agreement between the model and the experimental results. The model described the broad maximum in the conversion with increasing $R_2(Me)_2N^+Br^-$ concentration as shown in Figure 10.4. This behavior is explained by the dilution effect and the increase in the ratio of the nonreacting to the reacting anion at the interface. Figure 10.4 and Table 10.4 suggest that the maximum binding occurred at the $R_2(Me)_2N^+Br^-$ concentration, which was sufficient to bind all the organic reactant to

Table 10.4: The values of the percentage decyl bromide trapped in the oil core for different $[R_2(Me)_2N^+Br^-]^a$ with $[C_{10}H_{21}Br]^a$ = 57 mM and initial mole ratio $Na_2SO_3/C_{10}H_{21}Br$ = 6.0.

$[R_2(Me)_2N^+Br^-]^a$ (mM)	% $C_{10}H_{21}Br^e$
50	31.5
100	3.4
200	0
400	0
800	0

the interface. Bunton et al. [51] argued that rate maxima observed for second-order reactions in micelles do not necessarily correspond to complete substrate binding, but form a balance between the increase in the rate due to binding more of the organic substrate and the decrease due to the increase of the volume of the interfacial region. However, for nuleophilic substitution reactions carried out in microemulsions or emulsions formed with cationic surfactants, the effect of the surfactant counterion, that is, side or intermediate product formation, on the overall reaction of product formation should also be considered.

10.7.4.3 Effect of Decyl Bromide Concentration

The model fit for the effect of $C_{10}H_{21}Br$ concentration is shown in Figure 10.5(a)–(c). The $C_{10}H_{21}Br$ concentration was increased from 57 to 189 mM at an $R_2(Me)_2N^+Cl^-$ concentration of 400 mM and an initial mole ratio $Na_2SO_3/C_{10}H_{21}Br$ of 9.0. The values of the ion exchange constant, the reaction constants, and V^i/V^t at $[R_2(Me)_2N^+Cl^-]^a$ = 400 mM were taken from the values listed Tables 10.1, 10.2 and 10.3. Table 10.5 lists the values of the parameters calculated from eqs. (10.18) and (10.19).

There is a good agreement between the model fit and the experimental results. Table 10.5 shows that an increasing percentage of the decyl bromide is trapped as the concentration of decyl bromide added increased.

10.7.4.4 Effect of the Initial Mole Ratio of Sodium Sulfite to Decyl Bromide

The initial mole ratio $Na_2SO_3/C_{10}H_{21}Br$ was increased from 1.0 to 9.0 at a concentration of $R_2(Me)_2N^+Cl^-$ added to the reaction mixture of 200 mM and constant concentration of $C_{10}H_{21}Br$ added to the reaction mixture of 57 mM. The model fit for this experiment was obtained using the parameters listed in Tables 10.1 and 10.2 for the reaction of decyl bromide in $R_2(Me)_2N^+Cl^-$ microemulsion or emulsion. The values of V^i/V^t and % $C_{10}H_{21}Br^e$ at $[R_2(Me)_2N^+Cl^-]^a$ = 200 mM were taken from Table 10.3. The data from this experiment were not included in the optimization of the parameters

Table 10.5: Values of the percentage of decyl chloride formed at $t = 0$, and the percentage of decyl bromide trapped in the oil core for different $[C_{10}H_{21}Br]^a$. $[R_2(Me)_2N^+Cl^-]^a$ = 400 mM and mole ratio $Na_2SO_3/C_{10}H_{21}Br$ = 10.0.

$[C_{10}H_{21}Br]^a$ (mM)	% $C_{10}H_{21}Cl^o$	% $C_{10}H_{21}Br^e$
57	27.9	0
142	8.4	17.6
189	7.6	30.2

Table 10.6: Values of the percentage decyl chloride formed at $t = 0$ for different mole ratios $Na_2SO_3/C_{10}H_{21}Br$. $[R_2(Me)_2N^+Cl^-]^a$ = 200 mM and $[C_{10}H_{21}Br]^a$ = 57 mM.

Mole ratio $Na_2SO_3/C_{10}H_{21}Br$	% $C_{10}H_{21}Cl^o$
1.0	32.5
3.0	26.5
6.0	18.1
9.0	12.2

except for the one result at a mole ratio of 9.0. The only adjustable parameter in this fit was % $C_{10}H_{21}Cl^o$, which is listed in Table 10.6. The model curves shown in Figure 10.7(a)–(d), including the one at mole ratio of 9.0, were obtained by simultaneously solving eqs. (10.4), (10.7), (10.8), and (10.11)–(10.15).

The difference between the pseudo first-order fit and the one shown in Figure 10.6 (c), mole ratio of reactants of 6, was less than 0.5%. Table 10.6 shows that % $C_{10}H_{21}Cl^o$ decreases as the mole ratio increases. There is more SO_3^{2-} at the interface replacing the Cl^-. The model fit agreed well with the experimental results for the different mole ratios. The difference between the experimental and the model results typically fell within the 95% confidence interval for the measured conversions.

10.7.4.5 Different Decyl Halides as Reactants

In the experiments with different decyl halides, the fixed conditions were $[R_2(Me)_2N^+Cl^-]^a$ = 400 mM, $[C_{10}H_{21}X]^a$ = 95 mM, and initial mole ratio $Na_2SO_3/C_{10}H_{21}X$ = 9.0. The model fit for these experiments is shown in Figure 10.7. With decyl chloride as a reactant, no intermediate was formed. The parameters fitted from the data are listed in Tables 10.1, 10.2 and 10.7.

The model fits the results well for the three different reactants. Decyl iodide reacted most rapidly, followed by decyl bromide and then decyl chloride ($k_{1,C_{10}H_{21}I} > k_{1,C_{10}H_{21}Br} > k_{2,C_{10}H_{21}Cl}$). The fact that $C_{10}H_{21}Cl$ reacts at different rates depending on the reacting decyl halide ($k_{2,C_{10}H_{21}I} > k_{2,C_{10}H_{21}Br} > k_{2,C_{10}H_{21}Cl}$) might be because of the catalytic effect of I^- and

Table 10.7: Values of the percentage of decyl chloride intermediate formed at t = 0, and the percentage of decyl chloride and the percentage of decyl halide trapped in the oil core for the different decyl halide reactants with $[R_2(Me)_2N^+Cl^-]^a$ = 400 mM, $[C_{10}H_{21}X]^a$ = 95 mM, and initial mole ratio $Na_2SO_3/C_{10}H_{21}X$ = 10.0.

	% $C_{10}H_{21}Cl^o$	% $C_{10}H_{21}Cl^e$	% $C_{10}H_{21}X^e$
$C_{10}H_{21}Cl$	–	0.0	–
$C_{10}H_{21}Br$	11.1	0.0	9.4
$C_{10}H_{21}I$	51.1	6.0	0

Br^- on the reaction or by the reversibility in the reaction for the formation of the intermediate (R10.3). With decyl iodide as the reactant, the sulfonation rate constants for decyl iodide and decyl chloride intermediate were the same, 6.1×10^{-2} (mM/h). The ion exchange constants decreased in the order $K_{Cl^-/NaSO_3^-} > K_{Cl^-/Br^-/NaSO_3^-} > K_{Cl^-/I^-/NaSO_3^-}$; and $K_{Cl^-/NaSO_3^-} > K_{Br^-/NaSO_3^-}$, in agreement with the Hofmeister series [41, 42], that is, higher charge density ions exchange more readily. The maximum conversion for $[C_{10}H_{21}Br]^a$ = 95 mM predicted by the model based on % $C_{10}H_{21}Br^e$ (90.4%) was compared to an experimental measurement after 24 h of reaction (86.5%). The model and experimental values differed by less than 5%. This difference is less than the 95% confidence interval for the measured value.

10.7.4.6 Effect of Decyl Iodide Concentration

In this experiment, the $C_{10}H_{21}I$ concentration was increased from 57 to 189 mM at an $R_2(Me)_2N^+Cl^-$ concentration of 400 mM and an initial mole ratio $Na_2SO_3/C_{10}H_{21}Br$ of 9.0. The model fit for the effect of $C_{10}H_{21}I$ is shown in Figure 10.8(a)–(c). The ion exchange constant between $NaSO_3^-$ and Cl^- and I^-, $K_{Cl^-/I^-/NaSO_3^-}$; the decyl iodide sulfonation rate constant, $k_{1,C_{10}H_{21}I}$; and the decyl chloride sulfonation rate constant with decyl iodide as reactant, $k_{2,C_{10}H_{21}I}$, are listed in Tables 10.1 and 10.2. The volume of the interfacial region was taken from Table 10.3. The parameters calculated from eqs. (10.18) and (10.19) are listed in Table 10.8.

The model does not fit the experiment at 57 mM $C_{10}H_{21}I$ (Figure 10.8a) as well as those at higher concentrations. This may be because the model neglects the effect of I^- interfacial concentration on $k_{2,C_{10}H_{21}I}$. Since I^- acts as a catalyst for the sulfonation of $C_{10}H_{21}Cl$, the sulfonation rate constant is expected to vary with I^- concentration [69, 71]. The model described the increase in the molar rate of the reaction and the decrease in the conversion as the concentration of the reactant increased. The reaction rate increased because larger amounts of the reactants were bound to the interface, while the conversion dropped because more $C_{10}H_{21}I$ and $C_{10}H_{21}Cl$ were trapped in the oil core of the emulsion for the same amount of $R_2(Me)_2N^+Cl^-$ added to the reaction mixture.

Table 10.8: Values of the percentage of decyl chloride formed at $t = 0$, and the percentage of decyl chloride and the percentage of decyl iodide trapped in the oil core for different $[C_{10}H_{21}I]^a$ with $[R_2(Me)_2N^+Cl^-]^a$ = 400 mM; initial mole ratio $Na_2SO_3/C_{10}H_{21}I$ = 9.0.

$[C_{10}H_{21}I]^a$ (mM)	% $C_{10}H_{21}Cl^o$	% $C_{10}H_{21}Cl^e$	% $C_{10}H_{21}I^e$
57	53.7	9.0	0.0
142	35.2	6.2	8.4
189	29.2	8.1	15.0

Comparing the percentage of decyl bromide trapped, listed in Table 10.5, and decyl iodide trapped, listed in Table 10.8, shows that more decyl iodide remained at the interface, as expected, because the polarity of the C–I bond is higher than the polarity of the C–Br bond.

10.7.4.7 Use of High Concentrations of Surfactant and Reactants

The parameter values fitted to the experimental results shown in Figure 10.9 are % $C_{10}H_{21}Cl^o$ = 25.2, % $C_{10}H_{21}Cl^e$ = 15.1, and % $C_{10}H_{21}I^e$ = 45.4. The values of $K_{Cl^-/I^-/NaSO_3^-}$, $k_{1,C_{10}H_{21}I}$ and $k_{2,C_{10}H_{21}I}$ were taken from Tables 10.1 and 10.2 and the volume of the interfacial region from Table 10.3. The model fits the experimental results within the 95% confidence intervals.

10.7.4.8 Assessing the Fit of the Model

Figure 10.10(a) and (b) shows the percentage residuals calculated as the difference between the conversions to sodium decyl sulfonate and decyl chloride obtained from the measured concentrations and the model values vs. the experimental ones for all the experiments. A total of 22 points at each value of time are shown for the conversion to sodium decyl sulfonate and 18 for the conversion to decyl chloride. For the conversion to sodium decyl sulfonate, 92% of the residuals fall within a ±5% interval, which is a typical 95% confidence interval for replicated data. For the conversion to decyl chloride, 94% of the residuals fall within the ±5% interval. Except for 0.5 h, the residuals in the conversion to the final and the intermediate products appear to be randomly distributed around zero. The residuals in the conversion to the final product are larger at t = 0.5 h than subsequently. At 0.5 h, 25% of the residuals exceed ±5%. Figure 10.11(a) and (b) shows histograms of the residuals in the conversion to the final and the intermediate products at t = 0.5 h. Residuals from the same experiments are aligned vertically. The experiments are separated horizontally, but the horizontal position has no significance. More residuals are positive than negative, indicating that the model underpredicts the results at small times of the reaction.

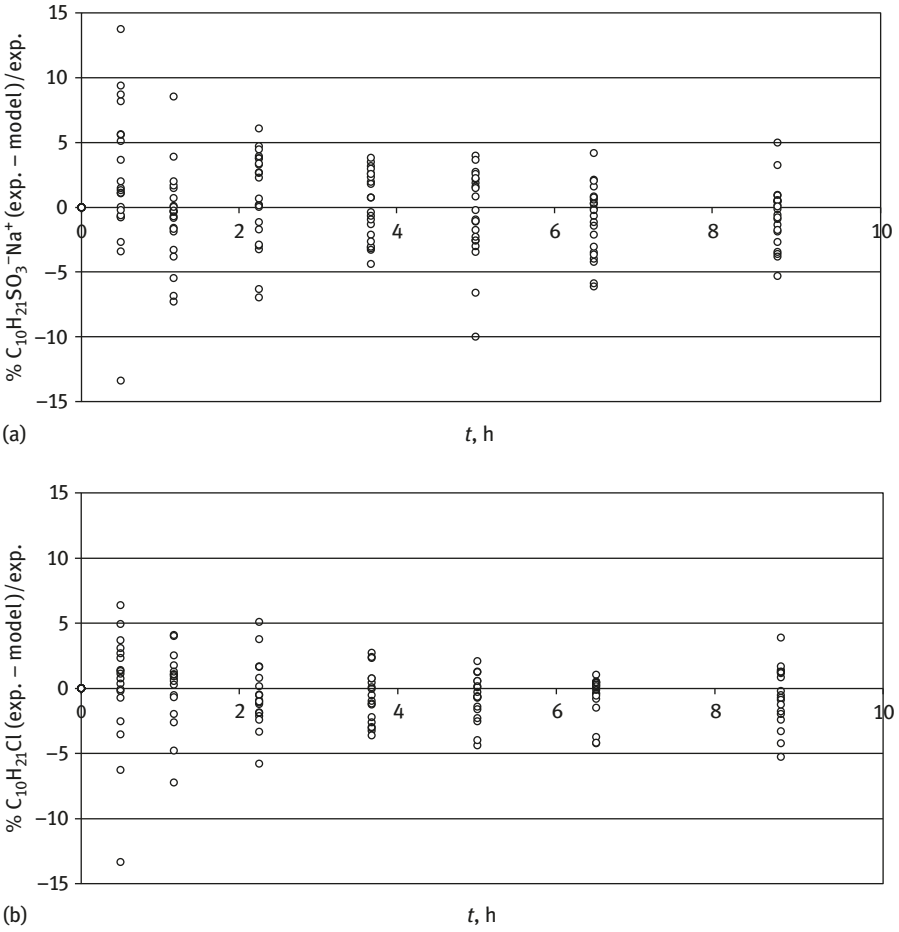

Figure 10.10: Time variation of the relative residuals calculated from the percentage conversion to (a) sodium decyl sulfonate and (b) decyl chloride.

Figures 10.12(a) and (b) and 10.13(a) and (b) are histograms showing the residuals in the conversion to the final and the intermediate products at 2.25 and 8.83 h, respectively. The numbers of positive and negative residuals are approximately the same. In these figures, only 10% of the residuals exceed ±5%.

10.7.4.9 The Thickness of the Interfacial Region

The thickness of the interfacial region may be estimated from the interfacial volume, which is a fitted parameter in the model. Assuming that the interfacial region is thin, its thickness, δ, is given by

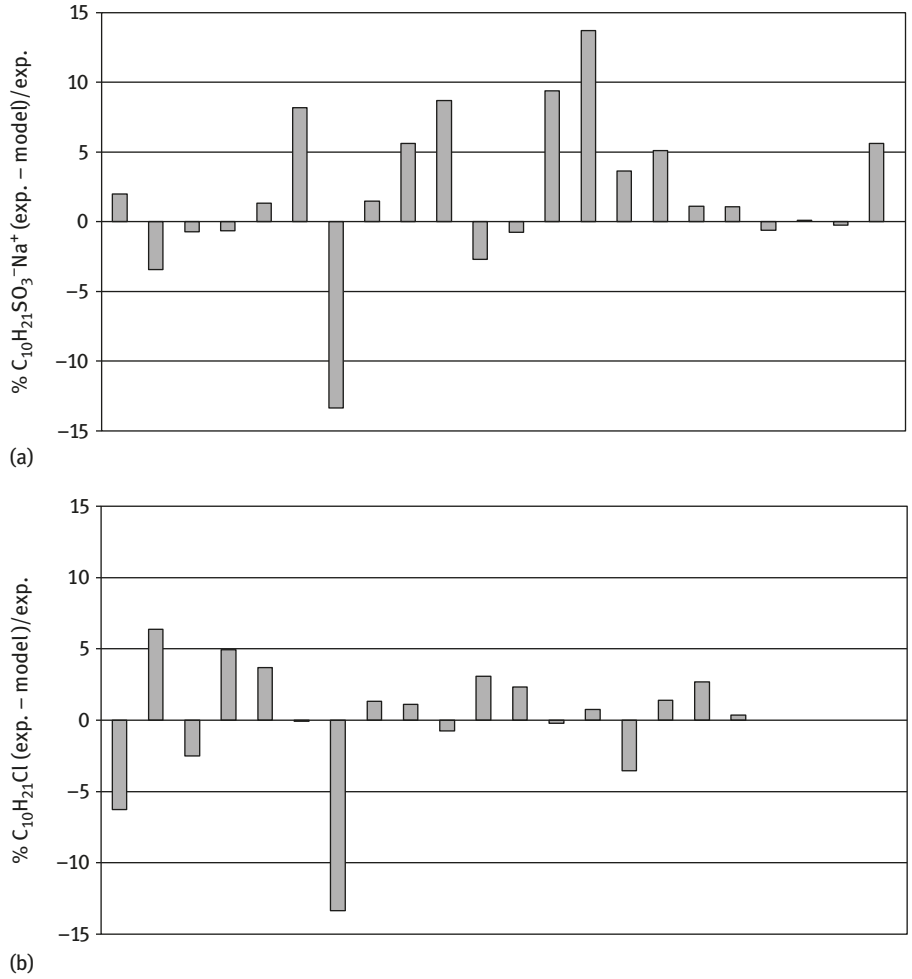

Figure 10.11: Relative residuals at $t = 0.5$ h calculated from the percentage conversion to (a) sodium decyl sulfonate and (b) decyl chloride.

$$\delta = \frac{V^{\mathrm{i}}}{A^{\mathrm{i}}} \tag{10.20}$$

where A^{i} is the area of the interfacial region (nm^2) and is calculated from

$$A^{\mathrm{i}} = n^i a \tag{10.21}$$

where n^{i} is the number of surfactant molecules at the interface and a is the interfacial area occupied by one surfactant molecule. Assuming that all surfactant molecules are at the interface,

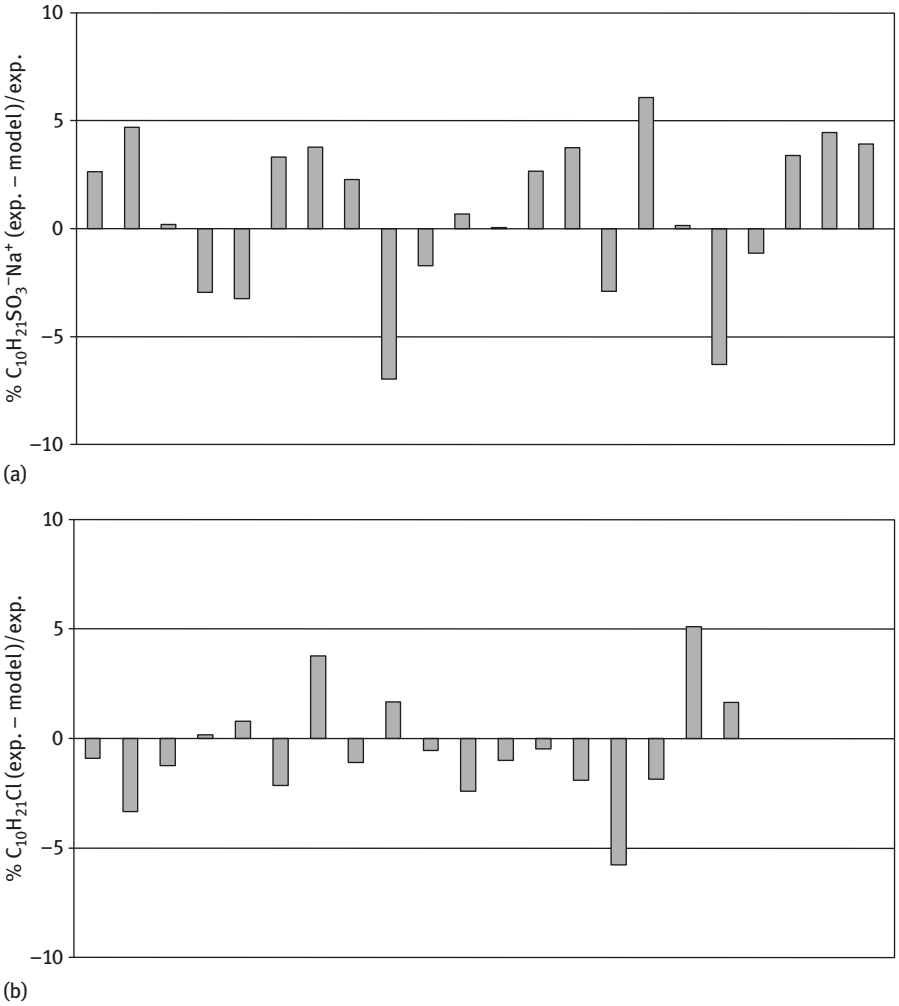

Figure 10.12: Residuals at t = 2.25 h calculated from the percentage conversion to (a) sodium decyl sulfonate and (b) decyl chloride.

$$n^i = \left[R_2(Me)_2N^+Cl^-\right]^a V^t \; N_A \tag{10.22}$$

where N_A is Avogadro's number. Combining eqs. (10.20)–(10.22) gives

$$\delta = \frac{1}{N_A a} \left(\frac{V^i/V^t}{[R_2(Me)_2N^+Cl^-]} \right) \tag{10.23}$$

The interfacial area occupied by one surfactant molecule, a, depends on the size of the surfactant head group, the number and length of surfactant hydrocarbon tails,

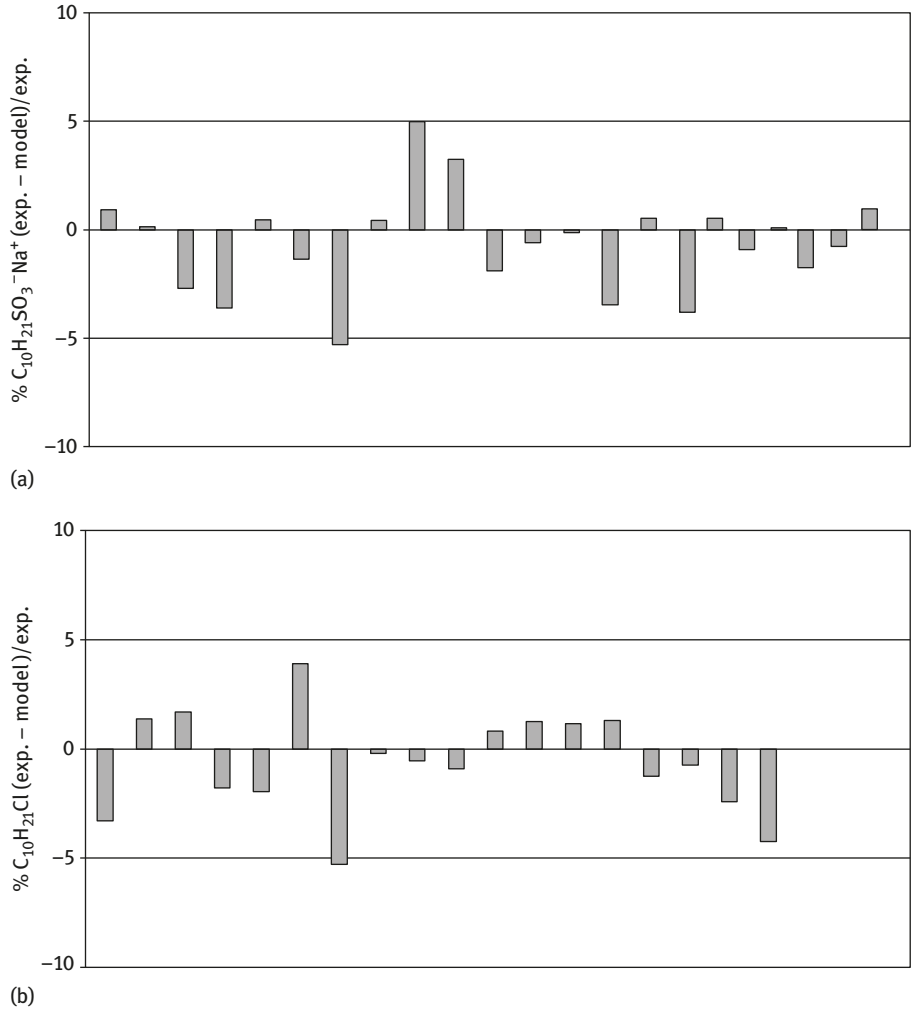

Figure 10.13: Residuals at t = 8.83 h calculated from the percentage conversion to (a) sodium decyl sulfonate and (b) decyl chloride.

and the type of surfactant aggregate [59, 72]. Durbut [73] reported values of a at water–air interfaces ranging from 0.38 to 0.87 nm^2. The values of a for the two-tailed cationic surfactants didodecyldimethylammonium bromide and dihexadecyldimethylammonium acetate in aqueous solutions are 0.68 and 0.70 nm^2, respectively [72]. Table 10.9 lists the values of δ; for values of a of 0.4, 0.6, and 0.9 nm^2 as estimates [61, 73]; and for surfactant concentrations between 50 and 800 mM. The values of δ range from about 0.5 to 4.3 nm, with the most likely values between 0.8 and 3 nm.

Table 10.9: The thickness of the interfacial region, δ, for different concentrations of the cationic surfactant for different values of a.

Concentration of surfactant (mM)	$\frac{1}{N_A}\left(\frac{V^i/V^t}{[R_2(Me)_2N^+Cl^-]}\right)$ (nm^3)	δ (nm) $a = 0.4$ nm^2	δ (nm) $a = 0.6$ nm^2	δ (nm) $a = 0.9$ nm^2
50	1.73	4.3	2.9	1.9
100	1.23	3.1	2.1	1.4
200	0.76	1.9	1.3	0.8
400	0.57	1.4	1.0	0.6
800	0.49	1.2	0.8	0.5

If the estimated thickness of the interfacial region is realistic, it satisfies two criteria. Following the rough-surfaced micelles model [40, 61], the fully hydrated counterions penetrate through the fully hydrated surfactant head groups in the interfacial region. The first of criterion is that the thickness of the interfacial region, δ, should be larger than the size of the hydrated surfactant head group and the size of the hydrated surfactant counterions. The second criterion is that δ should be of the same order of magnitude as the thickness of the double layer, which can be estimated by the capacitor model or the Debye length, k^{-1} [74].

Stigter [60] used a diameter of 0.46 nm for the hydrated sodium or the hydrated sulfate ions in the interfacial region of sodium dodecylsulfate micelle, and a diameter of 0.38 nm for the hydrated chloride or the hydrated ammonium ions in the interfacial region of dodecyltrimethylammonium chloride micelle. A comparison between the thickness of the interfacial region, δ values listed in Table 10.9, and the sizes of the hydrated ions shows that the computed thickness of the interfacial region is sufficient to accommodate the largest of the ions.

The thickness of the double layer surrounding a charged surface can be estimated using the capacitor model [74]. In the capacitor model, the charged surface is neutralized with a plate of opposite charge at a distance δ, the electrical double-layer thickness. The charge density of the surface is calculated with the assumption that charged monolayers obey the two-dimensional ideal gas law. For a potential drop across the double layer of 0.10 V, the double-layer thickness for a charged surface in water at 298.2 K is 4.4 nm [74]. This value is of the same order of magnitude as the values of δ listed in Table 10.9.

The Debye length is calculated from Debye–Hückel approximation [74]:

$$\kappa^{-1} = \left[\frac{\varepsilon\, k_B\, T}{1,000\, e^2\, N_A \sum_i z_i^2 M_i}\right]^{1/2} \tag{10.24}$$

Table 10.10: Debye length, k^{-1}, for 1:1 electrolyte solutions at 298 K.

Concentration of the salt (mM)	κ^{-1} (nm)
10	3.0
100	1.0

where ε is the dielectric constant of the medium, for water $\varepsilon = 6.95 \times 10^{-10}$ C^2/Jm; k_B is the Boltzmann constant = 1.38×10^{-23} J/K; T is the absolute temperature (K); z_i is the charge number; and M_i is the molar concentration of the ion. The Debye length calculated from eq. (10.24) for a 1:1 electrolyte in water at 298 K is listed in Table 10.10 for two concentrations. The 1:1 electrolyte is used merely to provide an estimate. Table 10.10 shows that k^{-1} is in the order of 1 nm. Comparing the thickness of the interfacial region, δ values listed in Table 10.9, with k^{-1} given in Table 10.10, shows that the two values are in the same order of magnitude.

The thickness of the interfacial region estimated from the capacitor model and from eq. (10.23) satisfied the aforementioned two criteria. This suggests that the physical picture employed in the model is reasonable.

10.8 Summary

A second-order model with apparent rate constants and reactant total concentrations without the ion exchange failed to describe the effect of the initial mole ratio of reactants. A single-pseudophase model in combination with the PIE model was used to describe S_N2 reactions in microemulsions and emulsions formed with cationic surfactants. The three new assumptions employed in the current model are as follows: (1) the volume of the interfacial region varies only with the amount of surfactant, but is not directly proportional to the surfactant concentration, (2) decyl halides may be trapped within the oil core and not participate in the reaction if there is insufficient surfactant to bind all of the organic substrate to the interface, and (3) a single ion exchange constant accounts for the exchange between the reacting nucleophile and the surfactant counterions. The first assumption was needed to handle high surfactant and reactant concentrations. The second assumption accounted for the retarding effect of an anionic surfactant, such as $C_{10}H_{21}SO_3^-Na^+$, on nucleophilic substitution reactions. The third assumption reduced the number of fitted parameters and accounted for a lower interfacial concentration of the reacting nucleophile in the presence of less hydrophilic anion, such as Br^-, together with a more hydrophilic anion, such as Cl^-, at the interface by giving an average value of the ion exchange constant. The model described well the experimental results over the wide range of concentrations employed for microemulsion and emulsion systems; for different surfactant counterions, Cl^- and Br^-; and for different decyl halide reactants. About

93% of the residuals fill within a ±5% interval, which is a typical 95% confidence interval. An estimate of the thickness of the interfacial region gave values that were physically realistic.

References

[1] Naik S, Doraiswamy L. AIChE J 1998, 44, 612.
[2] Dehmlow E. Russ Chem Bull 1995, 44, 1998.
[3] Wang ML., Chang SW. Ind Eng Chem Res 1995, 34, 3696.
[4] Aserin A, Gari N, Sasson Y. Ind Eng Chem Prod Res Dev 1984, 23, 452.
[5] Hagenson L, Naik S, Doraiswamy L. Chem Eng Sci 1994, 49, 4787.
[6] Pradhan N, Sharma M. Ind Eng Chem Res 1990, 29, 1103.
[7] Schomäcker R, Stickdorn K, Knoche W. J Chem Soc Faraday Trans 1991, 87, 847.
[8] Bunton C, Halevi E. J Chem Soc 1952, pt. 4, 4541.
[9] Evans E, Mabbott E, Turner E. J Chem Soc 1927, 1159.
[10] Janakiraman B, Sharma M. Chem Eng Sci 1985, 40, 235.
[11] Suslick K, Johnson R. J Amer Chem Soc 1984, 106, 6856.
[12] Ando T, Kimura T. Ultrasonic 1990, 28, 326.
[13] Berlan J, Mason T. Ultrasonics 1992, 30, 203.
[14] Davidson R, Safdar A, Spencer J, Robinson B. Ultrasonic 1987, 25, 35.
[15] Holmberg K. Adv Colloid Interface Sci 1994, 51, 137.
[16] Menger F, Elrington A. J Am Chem Soc 1991, 113, 9621.
[17] Martinek K, Yatsimirski A, Osipov A, Berezin I. Tetrahedron 1973, 29, 963.
[18] Chhatre A, Joshi R, Kulkarni B. J Colloid Interface Sci 1993, 158, 183.
[19] Karpe P, Ruckenstein E. J Colloid Interface Sci 1991, 141, 534.
[20] Kabanov A, Nametkin S, Evtushenko G, Chernov N, Klyachko N, Lavashove A, Martinek K. Biochem Biophys Acta 1989, 996, 147.
[21] Hirai T, Sato H, Kosmasawa I. Ind Eng Chem Res 1994, 33, 3262.
[22] Kumar P, Pillai V, Shah D. App Phys Lett 1993, 62, 765.
[23] Houyi N, Taichenc S, Ganzuo L. J Dispersion Sci Technol 1992, 13647.
[24] Langevin D. J Am Chem Soc 1988, 21, 255.
[25] Battal T, Siswanto C, Rathman J. Langmuir 1997, 13, 6053.
[26] Siswanto C, Battal T, Schuss O, Rathman J. Langmuir 1997, 13, 6047.
[27] Gutfelt S, Kizling J, Holmberg K. Colloid Surf A 1997, 128, 265.
[28] Holmberg K, Oh SG, Kizling J. Progr Colloid Polym Sci 1996, 100, 281.
[29] Oh SG, Kizling J, Holmberg K. Colloids Surf A 1995, 97, 169.
[30] Oh SG, Kizling J, Holmberg K. Colloids Surf A 1995, 104, 217.
[31] Carey F. Organic Chemistry, 2nd ed., McGraw-Hill, New York, 1992, 303–337.
[32] Solomon T. Fundamentals of Organic Chemistry, 3rd ed., John Wiley & Sons, New York, 1990, 363–369.
[33] Loudon G. Organic Chemistry, 2nd ed., Benjamin/Cummings Publishing Company, CA, 1988, 319–359.
[34] Bruice P. Organic Chemistry, 2nd ed., Prentice Hall: Upper Saddle River, 1998, 363–369.
[35] Drobeck H. In Cationic Surfactants: Analytical and Biological Evaluation; Surfactant Science Series; Vol. 53; Cross, J.; Singer, E., ed.; Marcel Dekker, New York, 1994, 61.
[36] Bunton C, Gan LH, Hamed F, Moffatt J. J Phys Chem 1983, 87, 336.

[37] Menger F, Portnoy C. J Am Chem Soc 1967, 89, 4698.
[38] Berezin I., Martinek K, Yatsimirski A. Russ Chem Rev 1973, 42, 787.
[39] Martinek K, Yatsimirski A, Levashov A, Berezin I. In Mittal K., ed. Micellization, Solubilization and Microemulsions; Plenum Press, New York, 1977, 489.
[40] Romsted L. Micellization, Solubilization and Microemulsions, Mittal, K., ed., Plenum Press, New York, 1977, 509.
[41] Thompson R, Allenmark S. J Colloid Interface Sci 1992, 148, 241.
[42] Bartet D, Gamboa C, Sepulveda L. J Phys Chem 1980, 84, 272.
[43] Al-Lohedan H, Bunton C, Moffatt J. J Phys Chem 1983, 87, 332.
[44] Quarti N, Marques A, Blagoeva I, Ruasse MF. Langmuir 2000, 16, 2157.
[45] Bertocini C, Nome F, Cerichelli G, Bunton C. J Phys Chem 1990, 94, 5875.
[46] Athanassakis V, Bunton C, Mckenzie D. J Phys Chem 1986, 90, 5858.
[47] Bunton C, Buzzaccarini F. J Phys Chem 1982, 86, 5010.
[48] Bacaloglu R, Blasko A, Bunton C, Cerichelli G, Ortega F. J Phys Chem 1990, 94, 5062.
[49] Bacaloglu R, Bunton C, Cerichelli G, Ortega F. J Phys Chem 1990, 94, 211.
[50] Mackay R. J Phys Chem 1982, 86, 4756.
[51] Bunton C, Nome F, Quina F, Romsted L. Acc Chem Res 1991, 24, 357.
[52] Gudmundur G, Jönsson B, Wennerström H. J Phys Chem 1980, 84, 3114.
[53] Othmer K. Encyclopedia of Chemical Technology, 4th ed., Vol. 23, John Wiley & Sons, New York, 1991, 146–185.
[54] Guertechin L. In Handbook of Detergents Part A: Properties; Surfactant Science Series, Vol. 82, Broze, G., ed., Marcel Dekker, New York, 1999, 7.
[55] Bhat M, Gaikar V. Langmuir 1999, 15, 4740.
[56] Kern F, Zana R, Candau S. Langmuir 1991, 7, 1344.
[57] Bhat M, Gaikar V. Langmuir 2000, 16, 1580.
[58] Jönsson B, Lindman B, Holmberg K, Kronberg B. Surfactants and Polymers in Aqueous Solution, John Wiley & Sons, New York, 1998, 57–63.
[59] Laughlin R. The Aqueous Phase Behavior of Surfactants, Academic Press, London, 1994,242–253.
[60] Stigter D. J Phys Chem 1964, 68, 3603.
[61] Stigter D, Mysels K. J Phys Chem 1955, 59, 45.
[62] Athanassakis V, Bunton C, Buzzaccarini F. J Phys Chem 1982, 86, 5002.
[63] Da Rocha Pereira R, Zanette D, Nome F. J Phys Chem 1990, 94, 356.
[64] Minero C, Pramauro E, Pelizzetti E. Langmuir 1988, 4, 101.
[65] Menger F, Rhee J, Rhee H. J Org Chem 1975, 40, 3803.
[66] Chang R. Chemistry, 3rd ed., Random House, New York, 1988, 661–662.
[67] Chen S, Evans D, Ninham B, Mitchell D, Blum F, Pickup S. J Phys Chem 1986, 90, 842.
[68] Blum F, Pickup S, Ninham B, Chen S, Evans D. J Phys Chem 1985, 89, 711.
[69] Berman S, Melnychuk A, Othmer D. Ind Eng Chem 1948, 40, 1312.
[70] Levesque C, Craig A. Ind Eng Chem 1948, 40, 96.
[71] Leyes C, Othmer D. Ind Eng Chem 1945, 37, 968.
[72] Dubois M, Zemb Th. Langmuir 1991, 7, 1352.
[73] Durbut, P. Handbook of Detergents Part A: Properties; Surfactant Science Series, Vol. 82; Broze, G., ed., Marcel Dekker, New York, 1999, 47.
[74] Hiemenz P, Rajagopalan R. Principles of Colloid and Surface Chemistry, 2nd ed., Marcel Dekker, New York, 1997, 499–533.

Epilogue, Patents and General Conclusions

An epilogue is a closing section, addressed to the readers about the work presented in this book. So, we can say that editing this book has been an extraordinarily enriching experience for us. While cats may have seven consecutive lives, academics have only three simultaneous ones: family, teaching and research. In this sense, this book has given us a fourth life, a consecutive addition to the one in research. Considering this perspective, we can say that for the authors it was a trip back to their youthful student years of high creativity and hope. Their thoughtful retrospective view to the work they did more than 20 years ago and also the knowledge acquired in all these years have resulted in this book.

Working in McGill University, a world-class university, helped producing high quality research. The fame and its location, Montreal – a multicultural city, with a large number of postgraduate schools, attract the best graduate students and visiting researchers. Our McGill research group was fortunate enough to collaborate closely with the research group directed by Professor Alberto Arce at yet another first-class university – Universidade de Santiago de Compostela, Spain. As its name suggests, this university is also located in a multicultural city and known around the world for the high intellectual level of its academics. This book is an effort to put forward an overview of the collaborative research work on aqueous systems and ionic surfactants done by the research groups at McGill and Santiago de Compostela. The research results have been published in peer-reviewed international journals in bits and pieces, which clearly lack the general perspective of the whole initiative.

The contributors of this book are the researchers who have worked on these topics years ago and now are either professors at universities (Maen Husein, Eva Rodil, and Ana Soto) or hold high industrial or research positions (Remy Dumortier, Mohammad Khoshkbarchi, Hamid Rabie, and Younok Dumortier Shin). When we were invited by De Gruyter to publish a comprehensive view of our research results, before coming to any decision we consulted the idea with all of them and, to our delight, they all responded positively with enthusiasm. Thus, we signed the contract for this book with De Gruyter. In spite of our best efforts, we could not reach Wayne Wang and Jamal Esalah, so the presentation of their work was taken by those with the closest research topics.

Dealing with busy active professionals we had to consider that, in addition to their family concerns, they all had other very demanding duties at work. Considering this, we, as editors, helped to the best of our ability in the coordination of the whole effort and, after a full year of pleasant work, we declare our complete satisfaction with the result that we proudly present here.

Our work on ionic surfactants and aqueous solutions of ions, or electrically charged biomolecules, started with studies on reverse micellar systems. These systems were interesting enough by themselves, without even considering their commercial applications. Chapter 2 gives a comprehensive view of the effect of

https://doi.org/10.1515/9783110564808-011

different experimental variables on the formation of reverse micelles and on their performance as ion exchangers. The chapter closes with the presentation of a universal model describing the behavior of these complex systems.

When we started studies with dioctyl dimethyl ammonium chloride, we were aware of some publications reporting reverse micellar studies with trioctyl methyl ammonium chloride, commonly known as TOMAC; and thus, we named dioctyl dimethyl ammonium chloride, DODMAC, and dioctyl dimethyl ammonium bromide, DODMAB. In recent years, however, we realized that in all chemical catalogs the name DODMAC was used for dimethyl dioctadecyl ammonium chloride (CAS 107-64-2) while dioctyl dimethyl ammonium chloride was called DODAC (CAS 76723-98-3). Thus, in this book, we have changed DODMAC and DODMAB, which appeared in all our previous publications, to DODAC and DODAB, respectively.

In parallel, with the understanding of the behavior of reverse micellar systems and the development of separation processes for metals and biomolecules in dilute aqueous solutions, we made progress in fundamental studies dealing with the activity coefficients and solubilities of amino acids in aqueous electrolyte solutions. Re-examining the results obtained in these two fields helped in deeper understanding, as reflected in Chapters 3 to 5. Comparing the values obtained for the activity coefficients of amino acids in aqueous electrolyte solutions by us with those reported by other researchers we found them to be in good agreement, irrespective of different experimental techniques being used.

In contrast, the comparison of solubilities of amino acids in aqueous electrolyte solutions reported by different authors showed a large dispersion of values. As shown previously, the activity coefficients of samples containing different optical isomers of amino acids in aqueous electrolyte solutions have the same values; therefore we concluded that the solid phase of different optical isomers had to have different solubility values. Thus, in future studies, there is a need to specify the proportion of the different optical isomers in a sample studied while determining the solubility of an amino acid. All these studies suggested the elaboration and discussion of thermodynamic models for activity coefficients in aqueous bio molecule-electrolyte solutions, discussed in Chapter 5. This is perhaps the strongest contribution to knowledge coming out from this project.

And this brings us to the history of two patents. Patenting research findings can be originated for two very different reasons: a commercial motive and an academic one. While the academic motivation looks only for recognition of generating new knowledge, the commercial motivation seeks economic remuneration for use of the idea. McGill University has a very active Office of Technology Transfer (OTT) that is always looking for patentable results appearing from research endeavors. So, when we found that heavy metals could be extracted from contaminated water using ionic surfactants especially synthesized for the purpose by us, OTT immediately obtained a patent in the United States. The patent was granted to J.H. Vera, M.E. Weber and J.O. Esalah under the number 6,165,427 A on December 26, 2000. It seems that there was

not sufficient industrial interest to continuing paying the costs of this patent because, after some time, OTT discontinued supporting it.

When we realized that the idea of extracting an electrically charged solute with an ionic surfactant could also be applied to recover biomolecules (amino acids, enzymes, etc.) from aqueous solutions at the appropriate pH, OTT also decided to protect the idea and applied for registration on behalf of J.H. Vera, M.E. Weber and Y. O. Shin with International Patent Protection. This had the International Publication number WO03//080651, which was published on October 2, 2003, and not followed afterward. Thus, at present we do not have any commercially protected patents, but both ideas were patentable, and, in academic terms, this is the recognition of their originality.

At this point, it is more interesting for us to understand to what extent these two ideas were really original. As detailed in Chapter 7, the extraction of metal ions from an aqueous phase into an organic solution using organophosphorus acids was a well-established concept. In fact, we started our studies using commercial products with the idea of extracting metals from aqueous solutions to the water pools of reverse micellar systems. This was the research topic of Dr Jamaladdin Esalah's PhD thesis. Then, he decided to synthesize his own ionic surfactants and designed them with the specific purpose for the formation of reverse micellar systems. Ionic surfactants with two hydrocarbon chains were known to form reverse micelles with larger water uptake. As branched hydrocarbons are more soluble in water than straight-chain hydrocarbons, in order to decrease the loss of surfactant, it was decided to have two long straight hydrocarbon chains attached to the polar phosphorous head. After some preliminary experiments, Esalah observed that by using specially synthesized ionic surfactants there was still a large loss of it, the material balance of metal ions failed to close, and there was formation of a crud at the organic–aqueous interface. In fact, we learned at the time of writing Chapter 7 that this formation of a crud was a major problem in the industrial recovery of metals from aqueous solutions because not only it caused loss of ionic surfactant but also plugged the recovery system of the surfactant and metal. The key step was that we decided to analyze the crud and realized that the lost ionic surfactant and the metal ions were concentrated there, so we considered ways of recovering the metals from it. That was what psychologists call "the AHA moment!" What if instead of using a reverse micellar system we would add the ionic surfactant directly to the aqueous solution containing metal and collect the floating crud to recover the metal and the ionic surfactant? The metal could be easily recovered by ion exchange of the complex metal–surfactant in contact with a concentrated aqueous solution of salt. The idea worked well and it was worth a US patent at the time. When an idea works, the sequence of studies following it works automatically. The study of the extraction of different metals and other cations showed that the ionic surfactants were quite selective in extracting ions and took them virtually on a one-by-one basis. This is more clearly shown in Figure E.1.

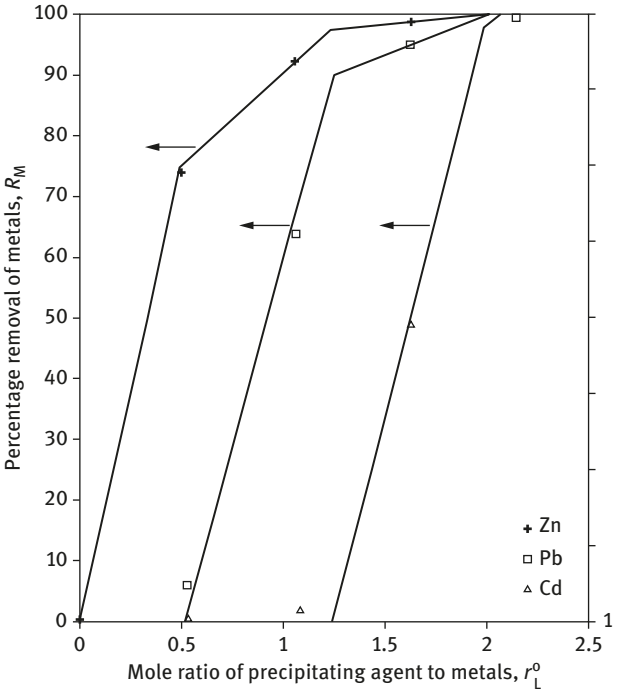

Figure E.1: Effect of mole ratio of sodium di-(*n*-octyl) phosphinate to mixture of Pb, Cd, and Zn on the removal of metals. The initial concentrations of Pb and Cd were 2.0 mM and that of Zn is 2.1 mM; the initial pH = 4.3.

Notably, at mole ratio of 2, precipitating agent to metals such as zinc, lead, and cadmium (in that order) has been quantitatively removed from water. Figure E.2 shows that calcium starts to be removed at almost exactly a mole ratio of 2, which means that after extracting the three heavy metals, the last ion picked up is calcium. This fact was seen as the main advantage for using the newly synthesized ionic surfactant to decontaminate water from heavy metal pollution. If any ionic surfactant was left in the water after the process, it could be eliminated from the treated water by the addition of calcium chloride.

As shown, the only residual problem before adopting this decontamination treatment of polluted water is its cost, and it may be that, unless there is legislation forcing it, there is no incentive to spend money in keeping the environment clean.

Over the years, studies for recovering electrically charged biomolecules using reverse micellar systems showed that there was a loss of ionic surfactant and the formation of a white crud in the organic–aqueous interface. The connection, although not immediate, was clear. Thus, the next step was to eliminate the reverse micellar system and add directly the ionic surfactant to the aqueous solution of the biomolecules at an appropriate pH. As a result, a white complex was formed and

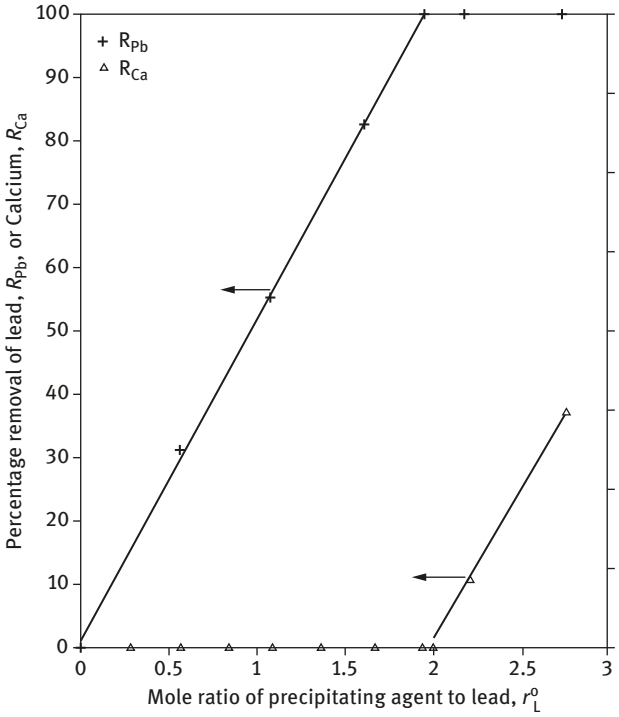

Figure E.2: Effect of mole ratio of sodium di-(*n*-octyl) phosphinate to lead on the removal of lead in the presence of calcium. Initial concentration of lead is 10 mM and initial pH is 4.3.

floated over the solution. The critical step in this case was the recovery of the biomolecule from the complex formed with the surfactant. It certainly was not advisable to contact the biomolecules, say lysozyme, with concentrated salt solutions, risking the loss of its enzymatic activity. Somehow, M.E. Weber recalled that acetone had been successfully used to recover enzymes from reverse micellar systems; therefore, acetone was tried and the recovery process worked as expected. Many other organic solvents were also tested but with limited success. The most important point was that the different enzymes were recovered without significant loss of their enzymatic activities. Thus, we consider this process of recovery of biomolecules from dilute aqueous solutions by complexation with an ionic surfactant and decomplexation with acetone, a quite innovative idea with a major potential of commercial use.

Revisiting our publications that report the complexation of biomolecules with ionic surfactants, we realized that in the earlier articles published we have failed to notice, and to report properly, an interesting relation between the molar ratio of AOT surfactant to biomolecule, "*R*", and the percentage "*y*" of biomolecule recovered from an aqueous solution in the absence of another electrolyte. In the figures

included in the publications, we put "$y = R_c\, x$" for the straight line instead of writing "$y(\%) = (R/R_c) \times 100$, for $R \leq R_c$," with y being the percentage of biomolecule complexed and R being the molar ratio of AOT to biomolecule in the initial aqueous solution. Here R_c is the value of R for which there is 100% recovery, that is, all molecules of a biocompound are forming an insoluble complex, each of them with R_c molecules of ionic surfactant. Although "x" was not clearly defined, it was implicit that it referred to the abscissa of the figure, that is, R. In fact, for all cases studied, when the molar ratio of AOT to biomolecule has a well-defined value R_c, or higher, the complexation is 100%. Notably, this relation is valid independently of the concentration of the solution of AOT added.

In all cases studied, the percent of biomolecule complexed by the ionic surfactant, y, was a linear function of the molar ratio, R, of surfactant to biomolecule in the solution. This is an extremely important observation as it indicates that when surfactant is added to the solution containing the biomolecule it does not distribute at random in the molecules of biocompound present, but it concentrated in a few molecules and when one of these molecules reaches a well-defined number "R_c" of surfactant molecules attached, say 10 for lysozyme, seven for α-chymotrypsin, or 13 for ribonuclease c, the complex floats as a solid over the aqueous solution. This behavior, which is independent of the concentration of the solution of AOT added, is more clearly seen considering that when the ratio of ionic surfactant added to biomolecule in the solution is equal to $R_c/2$, exactly 50% of the biomolecules in solution form the insoluble complex and not all biomolecules get half of the surfactant added and keep being in solution. This was an amazing finding. Figure E.3 illustrates the case of complexation of lysozyme with AOT surfactant.

Perhaps the most interesting point here is that this linear relation is valid for both the extraction of biomolecules with reverse micelles and the extraction by direct complexation with the ionic surfactant. The results presented in Figure E.3 are from the extraction of lysozyme with reverse micelles, and the model is the one presented in Chapter 6,where the results for complexation fall in the same straight line as the one shown in Figure E.3, which clearly indicate that the product of the interaction between the ionic surfactant with the biomolecule is always in the same stoichiometric relation.

Unfortunately, as stated earlier, in the original manuscripts publishing the results of these studies, the wrong formula was entered in the figures, so this important observation was not immediately evident. Looking in retrospect, we have tried to find the cause of entering a wrong equation in the figures of the original publications. The reason seems to be that as the first biomolecule that we extracted forming an insoluble complex with AOT surfactant was lysozyme, and for this biomolecule R_c is equal to 10, the correct equation gives

$$y\,(\%) = (R/10) \times 100, \;\; for\, R \leq 10$$

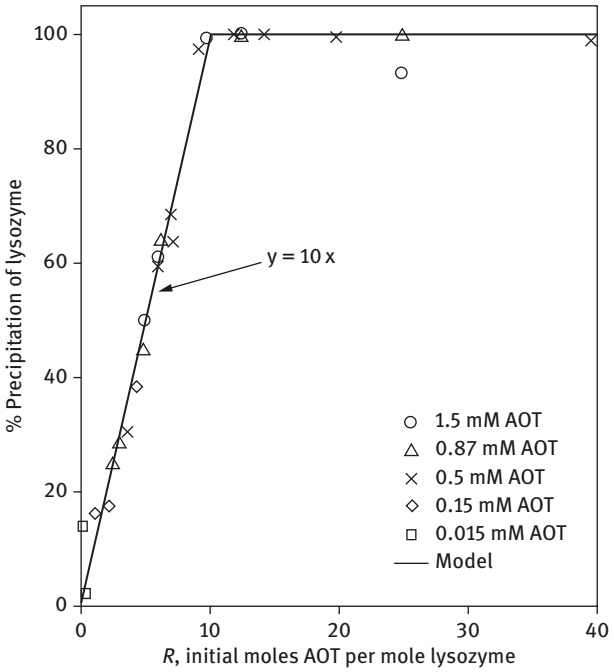

Figure E.3: Precipitation of lysozyme as a function of the amount of AOT added.

or

$$y\,(\%) = 10\,R, \quad for\, R \leq 10$$

Thus, identifying R with x, the abscissa, and knowing that for this compound $R_c = 10$, the equation for other biocompounds were wrongly written as

$$y = R_c x$$

Doing research is difficult because, in true research, we do not know what results we are supposed to obtain. Reporting research results is even more difficult because we have to translate into words and equations of those facts that we had never seen before and, sometimes, we do not exactly understand their meaning. This case is a good example of an honest mistake: "Errare humanum est, sed in errare perseverare diabolicum.[1]" The important step however is to be ready to admit errors and correct them as soon as they are detected. There is no shame on this. Consequently, we have promptly sent notes to the journals involved [1-3], calling the attention to these mistakes.

1 Attributed to Seneca, which translates to: "To err is human, but to persist in error (out of pride) is diabolical."

As in the cases of the activity coefficients and solubility of amino acids presented in Chapters 3 and 4, respectively, the writing of this book gave us an overview of the experimental results that generated a new perspective of the complexation of an ionic surfactant and biomolecules.

Followed by the idea that the ionic surfactant molecules "reacted" with biomolecules to form insoluble complexes came the idea of using ionic surfactants as reactants in other different situations. It was an accidental discovery that when an organic phase containing a reverse micellar solution of an ionic surfactant was left overnight in contact with an aqueous solution of an insoluble inorganic salt, the following day it was noticed that the bulk solid salt "dissolved" completely in the reverse micellar phase. The detailed study of the exchange of the counterion of the ionic surfactant with the corresponding ion of the inorganic salt followed. This naturally widened the understanding of the new approach to form inorganic nanoparticles, that is, particles of nanosizes from aqueous insoluble salts. As shown in the concluding section of this Epilogue, the number of studies related to nanoparticle formation is showing viral propagation in recent years.

Once the idea of using ionic surfactant as reactants for ion exchange reactions was established, it was natural to think about new applications. As it happens sometimes in research, even bright ideas do not give the desired results. A study was found in the literature of an esterification reaction of long hydrocarbon chain fatty acids with short hydrocarbon chain alcohols to produce lubricant esters for industrial use. As the long-chain fatty acids are insoluble in water and the short-chain alcohols are insoluble in an organic phase, the idea was to use a reverse micellar system to produce the contact of both reactants. As cosmetics are much more valuable than industrial lubricants, it seemed more attractive to use the same idea to contact a long hydrocarbon chain alcohol with a short hydrocarbon chain organic acid to produce perfumes. After some preliminary experiments, it became evident that the direct reaction of acid and alcohol in an emulsion system was faster and easier to work with than using the microemulsion; therefore, the idea was not followed further.

Looking in retrospect, there was no advantage in combining the chemicals in a reverse micellar phase in which the ionic surfactant was not participating in the reaction, so the attention was focused on the study of micellar phase transfer catalysis for nucleophilic substitution reactions. This study turned out to be one of the most outreaching adventures of this research as it put us in the field of chemistry. Thermodynamics deals with equilibrium and the rate at which a process occurs is not a relevant variable. Knowing that the ionic head of the surfactant participated directly in the reactions, we entered the field of chemical kinetics with all its enriching aspects. The results of these studies were quite successful as it was possible to work with higher concentrations of the reactants and obtain rates 20 times higher than that obtained in previous studies. The modeling of these systems that forced us to get out of our comfort zone was quite successful too.

Details of the studies that followed us in recent years have been discussed in each chapter.

We present here a visual perspective of results.

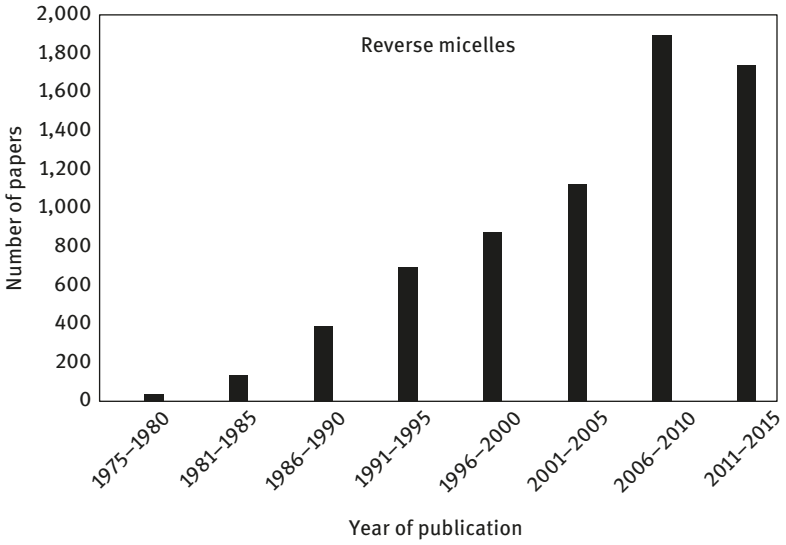

Figure E.4: Number of publications on the topic "Reverse Micelles" as searched by the SciFinder in January 2018.

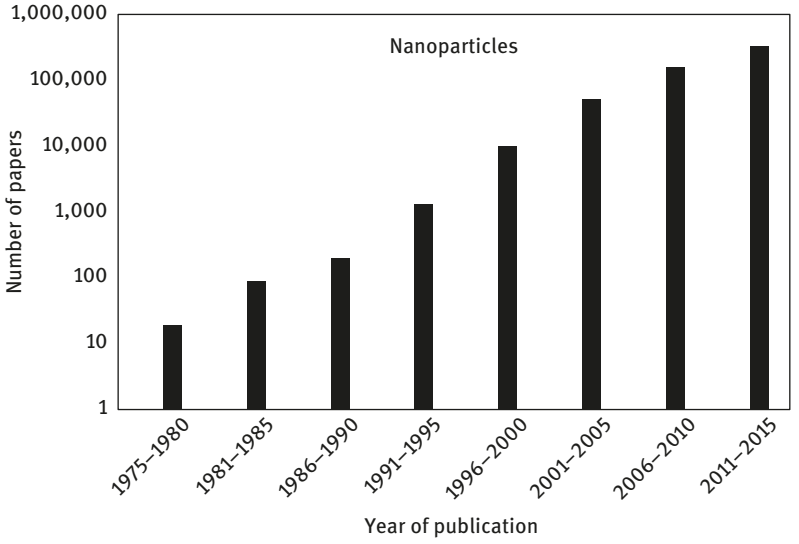

Figure E.5: Number of publications in the topic "Nanoparticles" as searched by the SciFinder in January 2018.

Figures E.4 and E.5 show that with the passing years the interest in reverse micellar studies continued and it seems to reach a plateau now. On the other hand, there is considerable increase in in nanoparticle studies. Note that the "Number of Papers" published needs to be plotted on the logarithmic scale in Figure E.5.

Martin Edmund Weber, our colleague and friend, is no more with us to see the continuation and recapitulation of this long research adventure. This book is dedicated to him.

Grazyna Wilczek-Vera and Juan H. Vera

References

[1] Wilczek-Vera G, Dumortier Shin YO, Rodil E, Vera JH. "Corrigendum to Biochem.Eng.J., 17 (2004) 91-97 by Y.O. Shin, E. Rodil and J.H. Vera", Biochem Eng J 2018, 134, 57–59. https://doi.org/10.1016/j.bej.2018.02.013

[2] Wilczek-Vera G, Dumortier Shin YO, Rodil E, Vera JH. "Corrigendum to Biotechnology Progress 2003, 19, 928-935 by Y.O. Shin, M.E. Weber and J.H. Vera", Biotechnology Progress 2018, 34(2), 552. DOI 10.1002/btpr.2621

[3] Wilczek-Vera G, Dumortier Shin YO, Rodil E, Vera JH. "Corrigendum to Separation Sci. & Technology, 39:5 (2004) 1005-1019 by Y.O. Shin, E. Rodil and J.H. Vera.", Separation Sci. & Technology 2018, 53(14).

Appendix

List of Peer-Reviewed Publications on Which Different Chapters Are Based

Chapter 1: Some Exploratory Studies

J. H. Vera and G. Wilczek-Vera

Ashrafizadeh SN, Weber ME, Vera JH. "Cation Exchange with Reverse-Micelles", Ind Eng Chem Res, 1993, 32, 125–132.

Rabie HR, Helou D, Weber ME, Vera JH. "A Comparison of the Titration and the Contact Methods for the Water Solubilization Capacity of AOT Reverse Micelles in the Presence of a Cosurfactant", J Coll Interf Sci, 1997, 189, 208–215.

Khoshkbarchi MK, Vera JH. "Formation of Water in Oil Microemulsions with Three Dialkyl Sodium Phosphinates in Alcohol/Isooctane Mixtures", J Coll Interf Sci, 1995, 170, 562–568.

Esalah JO, Weber ME, Vera JH. "Reverse Micelle Formation Using Sodium Di(n-Octyl) Phosphinate Surfactant", J Coll Interf Sci, 1999, 218, 344–346. Refereed Note.

Wang W, Weber ME, Vera JH. "Effect of Alcohol and Salt on the Water Uptake of Reverse Micelles Formed by Dioctyldimethyl Ammonium Chloride (DODMAC) in Isooctane", J Coll Interf Sci, 1994, 168, 422–427.

Rabie HR, Vera JH. "Effects of Volume Ratio and of Surfactant, Salt, and Alcohol Concentration on the Ion Distribution of Dioctyldimethyl Ammonium Chloride Reverse Micelles in Isooctane", Langmuir, 1996, 12, 3580–3584.

Zabaloy MS, Vera JH. "Water Uptake and Dioctyldimethyl Ammonium Chloride Distribution in Water + Hydrocarbon Microemulsions Containing an Alcohol and Sodium Chloride at 296.1 K", J Chem Eng Data, 1996,41, 1499–1504.

Rabie HR, Weber ME, Vera JH. "Effect of Surfactant Purity and Concentration, of Surfactant Counterion and of Different Ions on the Water Uptake of Dioctyldimethyl Ammonium Chloride-Salt-Decanol-Isooctane Reverse Micellar Systems", J Coll Interf Sci, 1995, 174, 1–9.

Chapter 2: Reverse Micellar Studies

H. R. Rabie

Rabie HR, Vera JH. "A Chemical Theory for Ion Distribution Equilibria in Reverse Micellar Systems. New Experimental Data for Aerosol-OT-Isooctane-Water-Salt Systems", Langmuir, 1995, 11, 1162–1169.

Rabie HR, Vera JH. "Generalized Water Uptake Modelling of Water-in-Oil Microemulsions. New Experimental Results for Aerosol-OT-Isooctane-Water-Salts Systems", Fluid Phase Equilib, 1996, 122, 169–186.

Rabie HR, Vera JH. "Counterion Binding to Ionic Reverse Micellar Aggregates and its Effect on Water Uptake", J. Phys Chem. B, 1997, 101, 10295–10302.

Rabie HR, Vera JH. "Counterion Effect of Amino Acids in Reverse Micelles", Fluid Phase Equilib, 1997, 135, 269–278.

Rabie HR, Vera JH. "A Simple Model for Reverse Micellar Extraction of Proteins", Sep Sci Technol, 1998, 33, 1181–1193.

Rabie HR, Vera JH. "A Chemical Theory for Ion Distribution Equilibria in Reverse Micellar Systems. New Experimental Data for Aerosol-OT-Isooctane-Water-Salt Systems", Langmuir, 1995, 11, 1162–1169.

https://doi.org/10.1515/ 9783110564808-012

Chapter 3: Solubilities of Amino Acids in Aqueous Electrolyte Solutions
M. K. Khoshkbarchi and A. Soto

Khoshkbarchi MK, Vera JH. “Effect of NaCl and KCl on the Solubility of Amino Acids in Aqueous Solutions at 298.2 K”, Ind Eng Chem Res, 1997, 36, 2245–2451.

Soto A, Arce A, Khoshkbarchi MK, Vera JH. “Measurements and Modelling of the Solubility of a Mixture of Two Amino Acids in Aqueous Solutions”, Fluid Phase Equilib, 1999, 158–160, 893–901.

Soto A, Arce A, Khoshkbarchi MK, Vera JH. “Effect of the Cation and the Anion of an Electrolyte on the Solubility of DL-Aminobutyric Acid in Aqueous Solutions. Measurements and Modelling”, Biophys Chem, 1998, 73, 77–83.

Pradhan A, Vera JH. “Effect of Acids and Bases on the Solubility of Amino Acids”, Fluid Phase Equilib, 1998, 152, 121–132.

Pradhan A, Vera JH. “Effect of Anions on the Solubility of Zwitterionic Amino Acids”, J Chem Eng Data, 2000, 45, 140–143.

Chapter 4: Activity Coefficients of Biomolecules in Aqueous Electrolyte Solutions
M.K. Khoskbarchi and A. Soto

Khoshkbarchi MK, Soto-Campos AM, Vera JH. “Interactions of DL- and L- Serine with NaCl and KCl in Aqueous Solutions”, J Sol Chem, 1997, 26, 941–955.

Soto-Campos AM, Khoshkbarchi MK, Vera JH. “Interaction of DL-Threonine with NaCl and $NaNO_3$ in Aqueous Solutions: e.m.f. Measurements with Ion Selective Electrodes”, J Chem Thermod, 1997, 29, 609–622.

Khoshkbarchi MK, Vera JH. “Measurement of Activity Coefficients of Amino Acids in Aqueous Electrolyte Solutions: Experimental Data for the Systems H_2O + NaCl + Glycine and H_2O + NaCl + DL-Alanine at 25 °C”, Ind Eng Chem Res, 1996, 35, 2735–2742.

Khoshkbarchi MK, Vera JH. “Activity Coefficients of DL-Valine in Aqueous Solutions of KCl at 25 ºC. Measurement with Ion Selective Electrodes and Modelling”, J Sol Chem, 1996,25, 865–875.

Khoshkbarchi MK, Vera JH. “Measurement and Modelling of Activities of Amino Acids in Aqueous Salt Systems”, AIChE J, 1996, 42, 2354–2364.

Soto-Campos AM, Khoshkbarchi MK, Vera JH. “Activity Coefficients of the Electrolyte and Amino Acid in Water+$NaNO_3$+Glycine and Water+NaCl+DL-Methionine Systems at 298.15K”, Biophys Chem1997, 67, 95–105.

Soto-Campos AM, Khoshkbarchi MK, Vera JH. “Effect of the Anion and the Cation of an Electrolyte on the Activity Coefficient of DL-Alanine in Aqueous Solutions”, Fluid Phase Equilib, 1998, 142, 193–204.

Chung YM, Vera JH. “Activity Coefficients of the Peptide and the Electrolyte in Ternary Systems Water + Glycylglycine + NaCl, + NaBr, + KCl, + KBr at 298.2 K”, Biophys Chem, 2001, 92, 77–88.

Gao C, Vera JH. “The Activity Coefficients of Glycine, DL-Serine and DL-Valine in Aqueous Solutions Containing Nitrates at 298.15 K”, Can J Chem Eng, 2001, 79, 392–401.

Chung YM, Vera JH. “Activity Coefficients of the Electrolyte and the Amino Acid in the Systems Water + DL, α-Aminobutyric Acid + NaCl, + NaBr, + KCl, + KBr at 298.2 K”, Fluid Phase Equilib, 2002, 203, 99–110.

Hamelink JM, Rudolph ESJ, van der Wielen LAM, Vera JH. “Activity Coefficients of Antibiotics in Aqueous NaCl Solutions at 298.2 K”, Biophys Chem, 2002,95, 97–108.

Chapter 5: Modelling of Activity Coefficients of Biomolecules in Aqueous Electrolyte Solutions

M. K. Khoskbarchi

Khoshkbarchi MK, Vera JH. “A Perturbed Hard Sphere Model with Mean Spherical Approximation for the Activity Coefficients of Amino Acids in Aqueous Electrolyte Solutions”, Ind Eng Chem Res, 1996, 35, 4755–4766.

Khoshkbarchi MK, Vera JH. “A Simplified Perturbed Hard-Sphere Model for the Activity Coefficients of Amino Acids and Peptides in Aqueous Solutions”, Ind Eng Chem Res, 1996, 35, 4319–4327.

Khoshkbarchi MK, Vera JH. “A Theoretically Improved Perturbation Model for Activity Coefficients of Amino Acids and Peptides”, Ind Eng Chem Res, 1998, 37, 3052–3057.

Chapter 6: Extraction of Biomolecules from Aqueous Solutions by Reverse Micelles

Y.-O. Dumortier Shin

Wang W, Weber ME, Vera JH. “Reverse Micellar Extraction of Amino Acids Using Dioctyldimethylammonium Chloride”, Ind Eng Chem Res, 1995, 34, 599–606.

Wang W, Weber ME, Vera JH. “Effect of the Concentration of DODMAC and 1–Decanol on the Behavior of Reverse Micelles in the Extraction of Amino Acids”, Biotech Bioeng, 1995,46, 343–350.

Khoshkbarchi MK, Vera JH. “Reverse Micellar Extraction and Back-Extraction of L-lysine with Three Dialkyl Sodium Phosphinates in Pentanol/Isooctane Mixtures”, Sep Sci Technol, 1995, 30, 2301–2314.

Rabie HR, Vera JH. “Extraction of Zwitterionic Amino Acids with Reverse Micelles in the Presence of Different Ions”, Ind Eng Chem Res, 1996, 35, 3665–3672.

Rabie HR, Suyyagh T, Vera JH. “Reverse Micellar Extraction of Proteins Using Dioctyldimethyl Ammonium Chloride”, Sep SciTechnol,1998,33, 241–257.

Shin YO, Vera JH. “Solubilization Limit of Lysozyme into DODMAC Reverse Micelles”, Biotech Bioeng, 2002, 80, 538–543.

Shin YO, Weber ME, Vera JH. “Reverse Micellar Extraction and Precipitation of Lysozyme Using Sodium di-(ethylhexyl) Sulfosuccinate”, Biotechnol. Progr, 2003, 19, 928–935.

Shin YO, Vera JH. “Reverse Micellar Extraction of Lysozyme Using Two Dialkyl Phosphinates”, Can J Chem Eng, 2004, 82, 349–357.

Chapter 7: Removal of Metals from aqueous Solutions by Complexation using Surfactants

R. Dumortier and E. Rodil

Esalah JO, Weber ME, Vera JH. “Removal of Lead, Cadmium and Zinc from Aqueous Solutions by Precipitation with Sodium Di-(n-octyl) Phosphinate”, Can J Chem Eng, 2000, 78, 948–954.

Esalah JO, Weber ME, Vera JH. “Removal of Lead from Aqueous Solutions by Precipitation with Sodium di-(n-octyl) Phosphinate”, Sep Pur Technol, 2000,18 25–36.

Husein MM, Vera JH. and Weber ME, “Removal of Lead from Aqueous Solutions with Sodium Caprate”, Sep Sci Technol, 1998, 33, 1889–1904.

Dumortier R, Rodil E, Weber ME, Vera JH. "Selective Removal of Gallium (III) from Aqueous Solutions Containing Zinc or Aluminium Using Sodium Di-(n-octyl) Phosphinate", Water Res, 2004, 38, 1745–1752.
Rodil E, Dumortier R, Vera JH. "Removal of Aluminium from Aqueous Solutions Using Sodium di-(n-octyl) Phosphinate", Chem Eng J 2004, 97, 225–232.
Dumortier R, Weber ME, Vera JH. "Removal and Recovery of Gallium from Aqueous Solutions by Complexation with Sodium Di-(n-Octyl) Phosphinate", Hydrometallurgy, 2005, 76, 207–215.

Chapter 8: Extraction of Biomolecules from Aqueous Solutions by Complexation using Surfactants

Y.O. Dumortier Shin and E. Rodil

Shin YO, Rodil E, Vera JH. "Selective Precipitation of Lysozyme from Egg White Using AOT", J. Food. Sci 2003, 68, 595–599.
Shin YO, Weber ME, Vera JH. "Comparison of two Methods to Recover Proteins from Reverse Micellar Phases", Sep Sci Technol, 2003, 38, 1733–1748.
Shin YO, Rodil E, Vera JH. "Surfactant precipitation and polar solvent recovery of α-chymotrypsin and ribonuclease-A", Biochem Eng J, 2004, 17, 91–97.
Shin YO, Rodil E, Vera JH. "Precipitation and Recovery of Cytochrome C and Hemoglobin Using AOT and Acetone", Sep Sci Technol, 2004, 39, 1005–1019.
Shin YO, Wahnon D, Weber ME, Vera JH. "Selective Precipitation and Recovery of Xylanase Using Surfactant and Organic Solvent", Biotechnol Bioeng 2004,86, 698–705.

Chapter 9: Formation of Nanoparticles using Surfactants

M.M. Husein

Husein M, Rodil E, Vera JH. "Formation of Silver Chloride Nanoparticles in Microemulsions by Direct Precipitation with the Surfactant Counterion", Langmuir, 2003, 19, 8467–8474.
Husein MM, Rodil E, Vera JH. "Formation of Silver Bromide Precipitate of Nanoparticles in a Single Microemulsion Utilizing the Surfactant Counterion", J. Coll. Interf Sci, 2004, 273, 426–434.
Husein MM, Rodil E, Vera JH. "A Novel Method for the Preparation of Silver Chloride Nanoparticles Starting from Their Solid Powder Using Microemulsions", J Coll Interf Sci, 2005, 288, 457–467.
Husein MM, Rodil E, Vera JH. "A Novel Approach for Preparation of AgBr Nanoparticles from their Bulk Solid Precursor Using CTAB Microemulsions", Langmuir, 2006, 22, 2264–2272.
Husein MM, Rodil E, Vera JH. "Preparation of AgBr Nanoparticles in Microemulsions Via Reaction of $AgNO_3$ with CTAB Counterion", J Nanopart Res., 2007,9, 787–796.

Chapter 10: Sulfonation in Emulsions

M. M. Husein

Husein MM, Weber ME, Vera JH. "Nucleophilic Substitution Sulfonation in Microemulsions and Emulsions", Langmuir, 2000, 16, 9159–9167.

Husein MM, Weber ME, Vera JH. “Nucleophilic Substitution Sulfonation in Emulsions: Formation of Sodium Benzyl Sulfonate”, Can J Chem Eng, 2001, 79, 744–750.
Husein MM, Vera JH. and Weber ME, “Nucleophilic Substitution Sulfonation in Emulsions: Effect of the Surfactant Counterion and Different Decyl Halide Reactants”, Coll Surf A, 2001, 191, 241–252.

Index of Chemical Compounds

https://doi.org/10.1515/9783110564808-013

Index of Subjects

https://doi.org/10.1515/9783110564808-014